Gasification of wood, urban wastewood (Altholz) and other wastes in a fluidised bed reactor

Diss. ETH Nr. 14207

Gasification of Wood, Urban Wastewood (Altholz) and other Wastes in a Fluidised Bed Reactor

A disseration submited to the
Swiss Federal Institute of Technology Zürich

for the degree of
Doctor of the Technical Sciences

presented by
Luiz Carlos Reichenbach de Sousa
Dipl. Chem.-Ing. ETH
born 27 October 1966
from Brazil and Portugal

accepted on the recomendation of
Prof. Dr. A. Wokaun (ETHZ), examiner
Prof. Dr. H. Hofbauer (TU-Wien), co-examiner
Dr. S. Stucki (PSI), co-examiner

Zürich June 2001

Aos meus pais e à Claudia.

Acknowledgements

The present work was carried out at the Laboratory for Energy and Materials Cycles of the General Energy Research Department of the Paul Scherrer Institute in Villigen, Switzerland. It was funded by the Swiss Federal Office for Energy (BfE) to whom I whish to express my gartitude. I would like to thank all the persons who have through their co-operation contributed to the achievement of my thesis. Specially I would like to thank:

- Professor A. Wokaun, head of the General Energy Research Department and Professor at the Laboratory of Technical Chemistry of the ETH Zürich, for accepting to be the advisor of my thesis and for the scientific guidance, valuable discussions and continued support of my work;
- Professor H. Hofbauer head of the Institute of Chemical Engineering, Fuel and Environmental Technology of the University of Technology Vienna, for accepting the co-chair of my thesis and his interest in my research;
- Dr. Samuel Stucki, head of the Laboratory for Energy and Materials Cycles, for countless dicussions on the results and problems, practical orientation of my work, unreserved support and confidence throughout my stay at PSI;
- Mr. T. Marti, for the friendship and collaboration in the technical and practical area of the present work;
- Mr. M. Fankhauser, Mr. H. Nonaka and Mr. K. Nikolajsen, IAESTE exchange students, for their collaboration in different stages of this thesis;
- Mr. R. Schaubhut and Mr. D. Notter for the help in the scope of their “Semesterarbeiten”;
- The technical staff of the workshops at PSI for many practical hints;
- All my colleagues of the Laboratory for Energy and Materials Cycles and other research laboratories at PSI for their help and the friendly atmosphere the PSI;
- Ms. C. von Scala for her unconditional support throughout the thesis.

Zürich, December 2000

TABLE OF CONTENTS

Summary v
Zusammenfassung vii
Nomenclature ix

1 INTRODUCTION 1
1.1 Biomass, a renewable energy resource 1
1.2 The Biometh project 2
1.3 Definition of the present thesis 4
1.4 References 7

2 FLUIDISED BED GASIFICATION PLANT 11
2.1 Introduction 11
2.2 Gas Feeding 13
2.3 The biomass feeding system 16
2.4 The Reactor 19
2.5 The off gas section 26
2.6 The plant's periphery 29
2.6.1 Data acquisition and control 29
2.6.2 On-line gas analysis 30
2.7 Bed material 34
2.8 Fuels studied 37
2.9 Operating procedure of the plant 43
2.10 References 52

3 PYROLYSIS, THE ORIGIN OF TARS IN GASIFICATION 55
3.1 Biomass pyrolysis 55
3.1.1 The chemical composition of wood 56
3.1.2 Pyrolysis behaviour of wood and its constituents 61
3.1.3 Evolution of pyrolysis products 66
3.1.4 The tars of a biomass gasifier 68
3.2 Pyrolysis of plastics 69
3.2.1 Chemical structure of polyethylene and polystyrene 70
3.2.2 Pyrolysis of polyethylene 71
3.2.3 Pyrolysis of polystyrene 74
3.2.4 Plastics Mixtures 76
3.2.5 Tars from plastics gasification 76
3.3 References 77

4 TAR SAMPLING AND ANALYSIS METHODS 85
4.1 Introduction 85
4.2 Tar sampling methods 87
4.3 PSI's Tar sampling and analysis method 90
4.3.1 The sampling train 90
4.3.2 Tar sampling procedure 96
4.3.3 Sample treatment procedures 98
4.3.4 GC/MSD analysis method 105
4.3.5 Laboratory tests of the sampling train 117
4.4 References 118

5 EXPERIMENTAL RESULTS 123
5.1 Experimental plan 123
5.1.1 Fractional factorial experimental plan 123
5.1.2 Final experimental plan 128
5.2 Treatment of experimental data 132
5.3 References 158

6 DISCUSSION 161
6.1 Reproducibility of results 161
6.1.1 Gas composition 162
6.1.2 Tar composition 166
6.2 Influence of fuels 169
6.2.1 Standard clean wood (SCW) and Altholz (AH) in air 169
6.2.2 SCW/AH in steam/oxygen 185
6.2.3 Altholz and Altholz+Polyethylene in steam/oxygen 200
6.2.4 Altholz and Altholz+Polystyrene in steam/oxygen 217
6.2.5 Effect of ageing on SCW 231
6.2.6 Effect of fuel particle size in the gasification of SCW 236
6.3 Influence of operational parameters 243
6.3.1 The gasification agent 243
6.3.2 Steam to biomass ratio 254
6.3.3 Reactor load 265
6.4 References 274

7 CONCLUSIONS 279
7.1 Summary of conclusions 279
7.1.1 General 279
7.1.2 Tar measurement method 281
7.1.3 SCW versus AH as fuel 281
7.1.4 Gasification agent 282
7.1.5 Steam to biomass ratio 282
7.1.6 Plastics admixture to the AH fuel 283
7.1.7 Effect of aging/particle size 283
7.2 Recommendations for further research 285

APPENDIX A: TAR DATA A-1

APPENDIX B: EXPERIMENTAL DATA B-1

Summary

Alternative, environmentally sound and renewable energy resources are becoming increasingly important in view of the world's ever increasing population and energy demand and the consequences of the usage of fossil fuels. A possible resource are waste materials such as waste wood and waste plastics. The conversion of these waste fuels into the clean energy carrier methanol may be accomplished by thermochemical gasification as proposed in the BIOMETH project. The waste wood does however contain exobiotic contaminants such as heavy metals and chlorine not found in untreated forest wood. The behaviour of this contaminated fuel in a gasifier has so far not been studied systematically. Also the co-gasification of biomass and plastics has received little attention. The aim of the present thesis is therefore to shed light on the gasification behaviour of the above mentioned fuels and mixtures thereof, with special emphasis on differences in the yield and composition of the product gases and tar by-products.

For this purpose, a stationary fluidised bed gasification reactor facility was built at the Paul Scherrer Institute. With this installation, the gasification process occuring in industrial sized reactors has successfully been simulated and the differences in the gasification behaviour of different fuels under well-defined operational conditions can be established. The operational parameters studied were temperature or equivalence ratio (which are equivalent in an autothermal gasifier for a given fuel humidity), gasification agent (air or steam/oxygen mixtures), steam to biomass ratio and reactor load. The fuels used in the tests were uncontaminated wood in the form of saw dust ("standard clean wood" SCW), urban waste wood ("Altholz" AH) pre-treated for combustion in a cement kiln (i.e. free of metals, stones and milled), mixtures of Altholz with polyethylene (AH+PE) and mixtures of Altholz with polystyrene (AH+PS). The polymers were chosen as they represent the largest fraction of waste plastics and their fraction in the total fuel was also varied. Another fuel parameter studied was the particle size of the unconatminated wood fuel. Data on the gas composition obtained under different conditions as well as tar amount and detailed information on the tar composition was gathered as well as mass flow information enabling for the establishment of mass balances. The analysis of the gas composition has been performed on-line with a process mass spectrometer capable of simultaneous analysis of seven gas components at different loactions in the reactor.

Tars are products from the thermolysis reactions of biomass. This thermolysis is usually named pyrolysis. As gasification is carried out at relatively high temperatures, the pyrolysis step(s) will occur and consequently the tars will always be present in the gasification products. The pyrolysis of biomass has been extensively studied and some insight in the conditions leading to a certain tar has been achieved. Still, the composition and amount of the tars in a particular gasification system has to be experimentally determined. In the case of plastics the situtation is similar.

A tar sampling and analysis method was adapted and extensively tested in the course of the experiments. The sampling is based on the absorption of the tar constituents in organic solvents. The quantitative analysis of the tar components was made using gas chromatography coupled with mass selective detection (GC/MSD). A series of 40 compounds, representing the typical composition of the tars of fluidised bed gasifiers, is quantified by this method yielding the tar amount and composition.

Altholz and clean wood yield gases of comparable composition. However, the contaminants in Altholz exhibit catalytic effects on the gas composition, especially when gasifying in steam/oxygen mixtures. Significantly lower tar concentrations have been detected for the gasification of waste wood. The tar composition is very similar for both biomasses. In the range of parameters studied, the gasification agent seems to play only a minor role in determining the tar amount and composition. The particle size is seen to have an influence on the amount but not on the composition of the tars. A finer fuel produces larger tar amounts in the gas.

The admixture of plastics yields a different thermal behaviour of the fuel, leading to higher gasification temperatures under otherwise identical conditions. Both plastics studied cause a marked increase in the tar amount in the gas, especially at low equivalence ratios. The tar amounts may however be lowered by increasing the equivalence ratio. The effects observed are clearly dependent on the amount of plastics added to the waste wood.

Zusammenfassung

Alternative, umweltverträgliche und erneuerbare Energiequellen werden zunehmend wichtiger in einer Welt, in der Bevölkerung und Energieverbrauch immer wachsen und eine verstärkte Nutzung fossiler Energiequellen unabschätzbare Folgegefahren birgt. Eine interessante solche Quelle sind Abfälle wie Altholz und Abfallkunststoffe. Die Umwandlung dieser Ressourcen in den sauberen Energieträger Methanol kann via thermochemische Vergasung erzielt werden, wie im Projekt BIOMETH vorgeschlagen. Altholz enthält aber im Gegensatz zu naturbelassenem Holz Schadstoffe wie Schwermetalle und Chlor. Das Verhalten dieser Schadstoffe in einem Vergaser wurde bislang nicht systematisch untersucht. Co-vergasung von Biomasse und Kunsstoffen wurde ebenfalls bisher nur unzulänglich studiert. Das Ziel der vorliegenden Arbeit ist also, das Vergasungsverhalten dieser Brennstoffe und deren Gemische zu untersuchen, wobei besonders auf Unterschiede in der Gas- und Teerzusammensetzung sowie der Teermenge eingegangen wird.

Für diesen Zweck wurde am Paul Scherrer Institut eine Anlage nach dem Prinzip der stationären Wirbeschicht aufgebaut. Diese Versuchsanlage erlaubt die Simulation der Vergasungsprozesse, wie sie in grösseren Anlagen stattfinden. Unterschiede im Vergasungsverhalten verschiedener Brennstoffe können damit unter kontrollierbaren Prozessbedingungen festgestellt werden. Die Parameter, welche mit dieser Anlage untersucht wurden, sind die Temperatur oder das Verhältnis von Sauerstoff zu Brennstoff (welche in einen autothermen Vergaser bei gegebene Brennstofffeuchte equivalent sind), das Vergasungsmittel (Luft oder gemische aus Sauerstoff und Wasserdampf), das Verhältnis von Dampf zu Biomasse und die Reaktorleistung. Zum Einsatz kamen folgende Brennstoffe: naturbelassenes Holz in Form von Sägemehl (“standard clean wood”, SCW), Altholz (AH), welches in einen Zementwerk aufbereitet wurde (d.h. frei von Metallen, Steinen und fein zerkleinert), Gemische aus Altholz und Polyethylen (AH+PE) und Gemische aus Altholz und Polystyrol (AH+PS). Diese Kunststoffe wurden ausgewählt, weil sie die Hauptbestandteile von Kunststoffabfällen sind. Der Effekt des Anteils Kunststoff im Brennstoff wurde auch untersucht. Weiter wurde der Einfluss der Brennstoffpartikelgrösse anhand von zerkleinertem, naturbelassenem Holz studiert. Die Materialflüsse, die Gaszusammensetzungen, die Teermengen und -zusammensetzungen, welche unter verschiedenen Bedingungen resultierten, wurden gemessen, um Massenbilanzen der Anlage zu erstellen. Die Gasanalyse erfolgte durch ein on-line Massenspektrometer, welches pa-

rallel die Konzentration von sieben gasförmigen Komponenten an verschiedenen Orten des Vergasers misst.

Teere sind Produkte der Thermolyse von Biomasse, auch Pyrolyse genannt. Pyrolyse ist ein integraler Bestandteil der Vergasung, da der Brennstoff auf vergleichsweise hohe Temperaturen gebracht werden muss, um zu vergasen. Deshalb sind Teere immer Bestandteil der Vergasungsprodukte. Die Pyrolyse von Biomasse wurde eingehend studiert, und qualitative Aussagen können in Bezug auf die zu erwartenden Teerkomponenten in einem Vergasungssystem gemacht werden. Allerdings muss die genaue Menge und Zusammensetzung der Teere experimentell ermittelt werden. Für Kunststoffe ist die Situation ähnlich.

Eine Teermessmethode wurde entwickelt und in den Versuchen eingehend getestet. Die Teerprobenahme basiert auf der Absorption der Teerkomponenten in organischen Lösungsmitteln. Eine Reihe von 40 Subtanzen, charakteristisch für die Teere von Wirbelschichtvergasern, wurde mittels Gaschromatographie mit massenspektrometrischem Detektor (GC/MS) quantifiziert und daraus die Teermenge und Zusammensetzung ermittelt.

Altholz und naturbelassenes Holz ergeben vergleichbare Gaszusammensetzungen. Die Schadstoffe im Altholz zeigen allerdings einen katalytischen Effekt auf die Gaszusammensetzung, besonders bei der Vergasung in Sauerstoff/Dampf-Gemischen. Die Teermenge ist bei Einsatz von Altholz merklich tiefer als bei naturbelassenem Holz, auch wenn die Teerzusammensetzung sehr ähnlich ist. Im untersuchten Parameterbereich konnte kein Einfluss des Vergasungsmediums auf Teermenge und -zusammensetzung festgestellt werden. Die Partikelgrösse des Brennstoffes hat einen merklichen Einfluss auf die Teermenge: je feiner der Brennstoff, umso grösser ist die Teerkonzentration im Gas.

Die Altholz/Kunststoff Gemische zeigen ein anderes thermisches Verhalten als “reines” Altholz: die Vergasungstemperaturen waren merklich höher bei den Kunststoffgemischen unter sonst identischen Bedingungen. Beide Kunststoffsorten verursachten eine deutliche Zunahme der Teermengen. Diese Unterschiede waren besonderst ausgeprägt bei tiefen Sauerstoff/Brennstoff-Verhältnissen und nahmen mit zunehmenden Sauerstoff/Brennstoff-Verhältnissen ab. Die beobachteten Effekte waren ferner von der zugegebenen Menge Kunststoff abhängig.

Nomenclature

AH	Altholz.
BFB	Bubbling fluidised bed.
CFB	Circulating fluidised bed.
DAF	Dry, ash-free.
d_p	Particle diameter.
$d_{p,max}$	Largest particle diameter of a particle size distribution.
$\bar{d}_p$	Mean particle diameter.
$d_{p,i}$	Upper particle diameter of class *i* (discrete particle size distribution).
$\Delta d_{p,i}$	Width of class *i* (discrete particle size distribution).
$\bar{d}_{p,\,i}$	Mean patricle size of class *i* (discrete particle size distribution).
EMPA	Swiss Federal Laboratories for Materials Testing and Research.
ER	Equivalence ratio.
IGCC	Integrated gasification/combined cycle.
LDPE	Low density polyethylene.
LLDPE	Linear low density polyethylene.
HDPE	High density polyethylene.
HIPS	High-impact polystyrene.
LHV	Lower heating value. Energy released in the combustion to gaseous CO_2 and gaseous H_2O (water vapour).
N	Particle size classes in a discrete particle size distribution.
$\dot{m}_i$	Mass flow of component *i*.
M_i	Molecular mass of component *i*.
m/z	Mass to charge ratio.
PAH	Polycyclic aromatic hydrocarbons.
PE	Polyethylene.

PC	Personal computer.
PSI	Paul Scherrer Institut.
PS	Polystyrene.
PTFE	Polytetrafluorethylene (Teflon).
on-line MS	On-line mass spectrometer.
GC	Gas chromatograph.
GC/FID	Gas chromatograph with flame ionisation detector.
GC/MSD	Gas chromatograph with mass selective detector.
RPM	Revolutions per minute.
u_{mf}	Minimum fluidisation velocity.
u_0	Superficial gas velocity.
$q_3(d_p)$	Particle size distribution density.
$q_{3,i}$	Discrete particle size distribution density.
$Q_3(d_p)$	Mass or volume fraction of particles with a diameter smaller than d_p, cumulative mass distribution (continuous particle size distribution).
$Q_{3,i}$	Mass or volume fraction of particles with a diameter smaller than $d_{p,i}$, cumulative mass distribution (discrete particle size distribution).
$\Delta Q_{3,i}$	Mass or volume fraction of particles in the class *i* (discrete particle size distribution).
$w_{i,daf}$	Mass fraction of element/compound *i* in fuel on dry, ash-free basis.
SCW	Standard clean wood.
T_{Bed}	Bed temperature.
T_{FB}	Freeboard temperature.
X_i	Normalised variable *i*.
Y_i	Result or response of experiment *i*.
$\hat{Y}$	Model prediction for the response or result Y.
m^3_N	Normal cubic meter (1013.25 mbar, 273.15 K).

Subscripts

DIF	Dry, inert-free gas data.
DTF	Dry, tar free basis gas data.
mf	At minimum fluidisation.
N	Gas data at normal conditions: p=1013.25mbar, T= 273.15K.
PG	Product gas.
RAW	"Raw" or "as used" fuel data.
S	Solid.
TF	Tar-free basis gas data.
th	Thermal power corresponding to the enegy released by the combustion of the fuel.

Greek Symbols

ε	Voidage.
Φ	Sphericity.
ρ	Density.
γ	Freeboard temperature gradient.
ζ	Fuel humidity (mass water/mass wet fuel).

1 INTRODUCTION

1.1 Biomass, a renewable energy resource

On the background of an ever increasing population, the accompanying rise in energy demand and the fear of climate change associated with anthropogenic emissions, the search for effective, new and environmentally sound energy sources is more important than ever [1.1]. Biomass is the oldest energy resource used by mankind as firewood, an energy resource still in use in many developing countries nowadays. It has regained interest in the early 70's as the first oil shock triggered a large number of research and development activities in biomass conversion, aimed primarily at the replacement of fossil fuels. Biomass is predicted to play an important role in the world's future energy supply [1.2] and the large number of still ongoing research projects in this area ([1.3] - [1.5]) reflects the current interest of the scientific community worldwide in this particular energy resource. The future contribution of biomass to the world's energy demand is still a matter

of controversial studies and discussions [1.6]. Biomass is however still the only truly renewable carbon source on the planet, and on the background of increasing world wide concern for anthropogenic CO_2 emissions its use as an energy resource in the future is unavoidable.

Among the possible conversion technologies, gasification represents an interesting and cost effective route ([1.8] - [1.11]). In this process the solid biomass is transformed into a combustible gas at temperatures in the range of 600 to 1000°C using substoichiometric amounts of an oxidant (air, oxygen, steam and mixtures thereof). The main components of this product gas are CO, CO_2, H_2 and H_2O and small amounts of CH_4. This conversion process allows for a flexible and varied usage of the gas generated from the original fuel by, e.g.:

- subsequent synthesis/production of clean fuels such as methanol, methane, Fischer-Tropsch gasoline or hydrogen, in which case the gasification must be carried out without nitrogen (i.e. in steam/oxygen mixtures);
- combustion in advanced systems such as integrated gasification/combined cycle (IGCC) with high fuel to energy conversion efficiencies.

1.2 The BIOMETH project

The conversion of biomass, waste biomass and selected industrial plastic wastes to methanol by the gasification route has been studied for the special case of Switzerland in the BIOMETH project ([1.12]-[1.15]). The goal of the project was to demonstrate the feasibility of a plant for the conversion of 100 tons per day of waste biomass to methanol. A scheme of the proposed conversion process is given in Figure 1.1.

In this study, the availability of waste fuels to be converted using state-of-the-art technology and the opportunities for the usage of the product methanol have been evaluated. Due to the size of the installation envisaged, fluidised bed gasification technology would have to be employed.

Figure 1.1: Schematic flow sheet of the BIOMETH process [1.15].

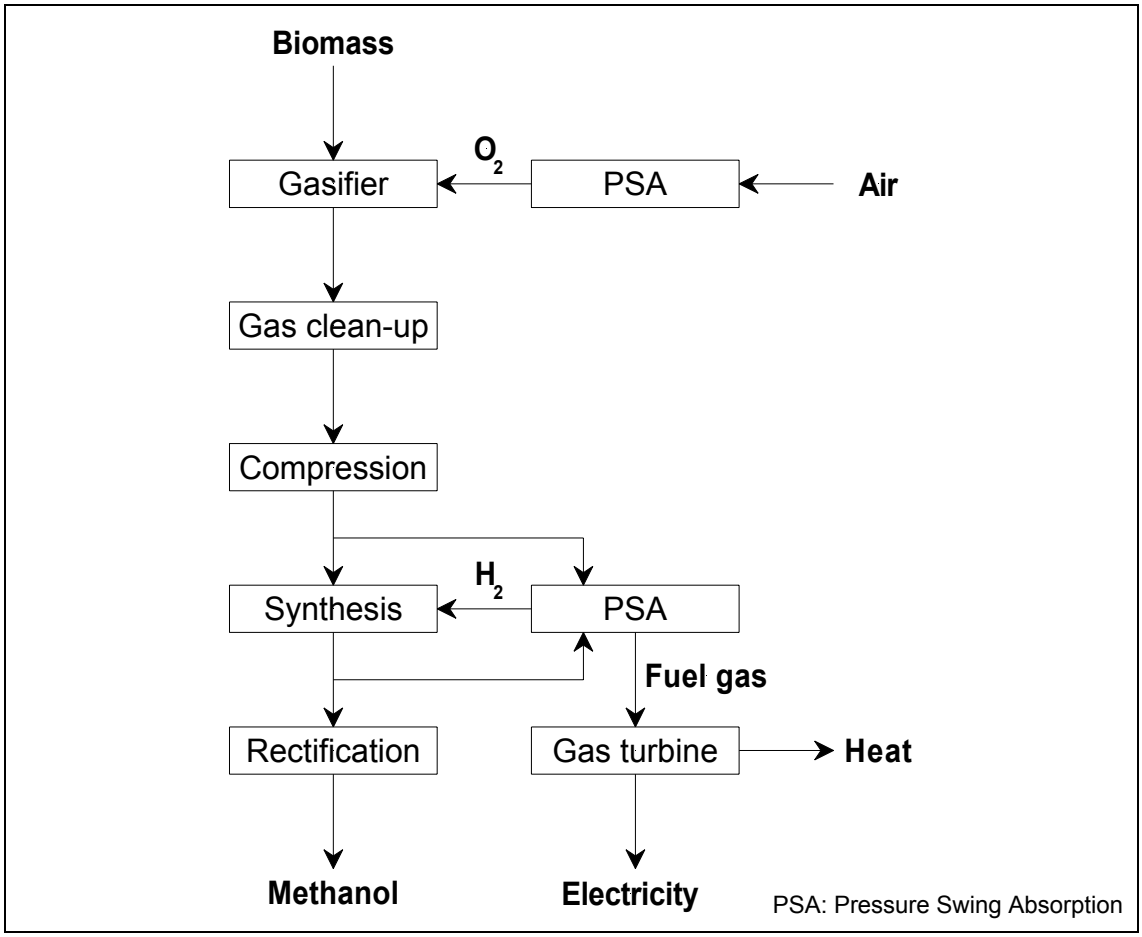

The cost of the biomass fuel is one of the important factors influencing the overall economic aspects of the conversion process. Therefore, waste biomass represents an interesting resource since wastes have a low or even negative cost (disposal fees). The proposed fuel composition for the BIOMETH process is given in Table 1.1, showing the important share of waste fuels for this process.

Table 1.1: Fuel composition for the BIOMETH process [1.16].

Fuel	**Fraction [mass-%]**
Urban waste wood "Altholz"	>70
Packaging wastes: mixture of paper, cardboard, wood and plastics	<20
Plastic wastes	<10
Uncontaminated waste wood	<5

The main conclusion of the BIOMETH project was that methanol can be produced from waste fuels in Switzerland using state-of-the-art technology to be used as transportation fuel:

- from an environmental point of view a positive effect is achieved by the proposed conversion process;
- waste fuels are available in sufficient quantity in Switzerland;
- the product methanol may be inserted into the existing fuel market in several ways;
- no return on 50% of the investment costs would have to be accepted if a fuel competitive to regular gasoline would be produced;
- some technical aspects of the conversion process could not thoroughly be studied as little practical experience was available on the gasification of waste fuels.

1.3 Definition of the present thesis

The main fuel considered in the BIOMETH study is urban waste wood or "Altholz" as it is known by its german denomination. This fuel is issued mainly from (de)construction activities but may also originate from e.g. packaging wastes or used furniture. This waste fuel is very inhomogeneous in its composition [1.17]. An important feature of this fuel is that, even though the main elemental composition (C, H, O) is similar to clean wood, it contains a significantly higher amount of ash, chlorine and heavy metals, as shown in Table 1.2. The behaviour of this fuel in gasification is yet poorly studied. In particular the impact of the exobiotic contaminants (heavy metals, chlorine etc.) on the quality of the gas and on the quantity and nature of the by-products (tars) has not been studied systematically. An impact of these contaminants on the gasification reactivities of the wood chars resulting from wood pyrolysis has been established [1.18]. It is therefore likely that these contaminants will have an effect on the operation of a gasifier fed with this particular fuel. Especially the gasification by-products, the tars, will have a major impact on the design and operation of gas cleaning equipment downstream of the gasification reactor.

Table 1.2: Elemental composition of Altholz and clean wood [1.15].

Element		Fuel				
		Altholz			Clean wood	
		Average	min.	max.	Sawdust	Bark
C	[mass-%]	44.3	41.4	45.9	49.9	50.9
H	[mass-%]	5.7	5.3	6.1	6.1	6.2
O	[mass-%]	43.8	-	-	43.5	39.4
N	[mg/kg]	7900	5600	12000	1500	2900
S	[mg/kg]	1385	20	5800	60	400
P	[mg/kg]	200	120	320	-	-
Cl	[mg/kg]	849	20	4400	50	200
F	[mg/kg]	42	0.01	140	-	-
Ash	[mass-%]	5.3	1.6	11.1	0.35-0.45	3.2-7.0
Hg	[mg/kg]	0.3	0.005	0.7	0.01	0.04
As	[mg/kg]	4.1	0.7	22.0	0.1	0.4
Cd	[mg/kg]	3.4	0.4	24.0	0.1	0.6
Co	[mg/kg]	1	1	3	0.1	0.8
Cr	[mg/kg]	32	14	93	2.4	4.8
Pb	[mg/kg]	314	43	690	0.4	4.4
Cu	[mg/kg]	27	11	85	1.2	4.4
Ni	[mg/kg]	6	2	12	0.3	2.4
Sn	[mg/kg]	6	0.04	12	-	-
Zn	[mg/kg]	535	170	960	11.1	89.7
Ca	[mg/kg]	15000	9000	25000	1210	10300
Al	[mg/kg]	840	390	1500	64	470
Fe	[mg/kg]	2100	1000	5200	50	500
K	[mg/kg]	890	740	1300	380	1480
Mg	[mg/kg]	1060	540	1900	300	1230
Si	[mg/kg]	750	270	1800	470	3270

The pyrolysis behaviour of plastics has been extensively studied (see Chapter 3), but little attention has been given to the gasification of this valuable waste fuel. The literature on co-gasification of plastics and biomass is also very sparse, especially with respect to the tar by-products.

The aim of the present thesis is therefore to assess, both qualitatively and quantitatively, the influence of the above mentioned contaminants in the gasification process.

Furthermore, the effect of co-gasification of waste biomass and plastics should be systematically studied. Through a better understanding of the phenomena occurring in the gasifier we expect to predict the gasification parameters yielding an optimum gas composition for a given fuel or mixture of fuels. Also questions such as the quality and possibilities for disposal of the processes residues (e.g. ashes) are of interest, as well as the size and type of downstream gas cleaning equipment.

Finally, the type and quantity of the gasification reaction by-products (tars) is expected to be strongly influenced by the type of fuel used. These tars are the main source of complications in any further utilisation scheme for the produced gas. Many methods have been used to quantify and analyse the tars issued from biomass gasification (see Chapter 4). The results reported in the literature are not easily comparable since the sampling and analysis method employed is known to influence the results. By the use of one consistent and reproducible tar measurement method a database for the comparison of the gasification fuels considered in the BIOMETH study should be established.

1.4 References

[1.1] A. Wokaun, *Erneuerbare Energien*, Teubner Studienbücher Chemie, B.G. Teubner, Stuttgart, Leipzig, 1999

[1.2] D.O. Hall, *Will Biomass be the Environmentally Friendly Fuel of the Future?*, in Making a Business from Biomass in Energy, Environment, Chemicals, Fibers and Materials Proceedings of the 3rd Biomass Conference of the Americas, Montreal, Quebec Canada, August 24-29, R.P. Overend and E. Chornet (eds.), Elsevier Science, 1997, pp.1-2

[1.3] *Developments in Thermochemical Biomass Conversion*, A.V. Bridgwater and D.G.B. Boocock (eds.), Blackie Academic & Professional, London, 1997

[1.4] *Biomass for Energy and Industry*, H. Kopetz et. al. (eds.), Proceedings of the 10th European Conference and Technology Exhibition, Würzburg 8-11 June 1998, CARMEN, Rimpar, Germany, 1998

[1.5] Proceedings of the 1st World Conference on Biomass for Energy and Industry, June 5-9, Seville, Spain, 2000

[1.6] M. Hoogwijk, R. van den Broeck, A. Faaij, *A Review of Assessments on the Future Global Contribution of Biomass Energy*, Presented at the 1st World Conference on Biomass for Energy and Industry, June 5-9, Seville, Spain, 2000

[1.7] *Biomass Gasification: Principles and Technology*, T.B. Reed (ed.), Noyes Data Corporation, Park Ridge, 1981

[1.8] A. Faaij, B. Meuleman, *Long Term Perspectives of Biomass Integrated Gasification/Combined Cycle Technology and a Comparison with Combustion*, Presented at the 1st World Conference on Biomass for Energy and Industry, June 5-9, Seville, Spain, 2000

[1.9] A. Faaij, C. Hamelinck, E. Larson, T. Kreuz, *Production of Methanol and Hydrogen from Biomass via Advanced Conversion Concepts - Preliminary Results*, Presented at the 1st World Conference on Biomass for Energy and Industry, June 5-9, Seville, Spain, 2000

[1.10] K. D. Owens, *Trigeneration: Flexible, Competitive Production of Biofuels and Power*, Presented at the 1st World Conference on Biomass for Energy and Industry, June 5-9, Seville, Spain, 2000

[1.11] S. Biollaz, M. Sturzenegger, S. Stucki, *Redox Process for the Production of Clean Hydrogen from Biomass*, Presented at the Progress in Thermochemical Biomass Conversion conference, 17-22 September, Tyrol, Austria, 2000

[1.12] S. Stucki, *Production of Methanol from Waste Biomass*, R'95 Recovery, Recycling, Re-integration Congress, 1-3 February, Geneva, Switzerland, 1995

[1.13] R. Bühler, P. Hasler, L. C. de Sousa, S. Stucki, *BIOMETH - Methanol Production from Waste Biomass in Switzerland*, Presented at the Seminar on Power Production from Biomass II, 27-28 March, Espoo, Finland, 1995

[1.14] S. Stucki, R. Bühler, P. Hasler, B. Covelli, M. Müller, W. Vock, *BIOMETH - Feasibility of Methanol Production from Waste Biomass and it's USe as a Fuel in Switzerland*, Proceedings of the 11th International Symposium on Alcohol Fuels, ISAF, Sun City, South Africa, 1996, pp.466-467

[1.15] P. Hasler, T. Nussbaumer, R. Bühler, *Vergasung von belasteten Brennstoffen zu Synthesegas, Schlussbericht im Sektor Technik Projekt BIOMETH,* Bundesamt für Energiewirtschaft, Bern, 1995

[1.16] S. Stucki, *BIOMETH - Methanolproduktion aus Biomasse-Abfällen in der Schweiz. Phase 1: Machbarkeitsstudie, Schlussbericht*, Bundesamt für Energiewirtschaft, Bern, Switzerland, 1996

[1.17] T. Nussbaumer, P. Hasler, A. Jenni, M. Erni, W. Vock, *Emissionsarme Altholznutzung in 1-10MW Anlagen*, Bundesamt für Energie, Bern, Switzerland, 1994

[1.18] C. von Scala, *The Influence of Contaminants on the Gasification of Waste Wood*, ETH Dissertation Nr. 12665, Zürich, Switzerland, 1998

2 FLUIDISED BED GASIFICATION PLANT

2.1 Introduction

To study the behaviour of waste fuels a gasification plant was built at the Paul Scherrer Institute. The goal of this installation was to simulate large fluidised bed gasifiers as the one planned for the demonstration phase of the BIOMETH project. The size of the latter demonstration installation ($20MW_{th}$) implies, that circulating fluidised bed (CFB) technology would have been used [2.1]. It was nevertheless decided to build a bubbling stationary fluidised bed (BFB) as this type of reactor is simpler to operate than a CFB (for example no loop seals for the bed material are required in a BFB) and the behaviour of both reactor types is similar.

The two reactor principles have however distinct characteristics [2.2]. First of all, the relative velocity between particles and gases is higher in CFBs than in BFBs, influencing thus the heat and mass transfer between particles and gases. The solids profile

found in the freeboard of CFBs is absent in BFBs. The temperature in CFBs is more homogeneous than in BFBs and the residence time of the solids is different for the two systems. These differences may have an influence on the gasification process. For example gas composition ranges reported in the literature ([2.3],[2.4]) for CFB and BFB gasification of wood with air are presented in Table 2.1. CFB gasifiers exhibit higher hydrogen contents in the gas as well as a lower methane and light hydrocarbons concentration.

Table 2.1: Gas composition for air blown gasification in CFB and BFB gasifiers.

Concentration of component (vol.-% dry gas)	**BFB**	**CFB**
CO_2	13 - 17	13 -15
CO	12 -17	13 - 15
H_2	7.5 - 11.5	15 -22
CH_4	3 - 5	2 - 4
C_nH_m	0.5 - 2.5	0.1 - 1.2

Regarding the tar contents of the gases no comparative study using the same sampling and analysis method, the same fuel and comparable operational conditions was made so far on both reactor types. In the literature ranges of the tar concentration in the product gases are reported for the two kinds of fluidised beds, see [2.5]. CFB reactors seem to lie at the lower end of the ranges reported, but it is not clear whether this difference comes from the reactor principle or from differences in the operating conditions or sampling and analysis methods. The goal of this study was to compare results when different fuels were processed. Thus an exact reproduction of the operation principle of the gasifier is not of prime importance as it is expected that the observed trends can be transferred to CFB systems.

A simplified scheme of the gasification plant is given in Figure 2.1. It is composed of 5 main sub systems: the gas feeding, the biomass feeding, the reactor itself, the off-gas and the periphery of the installation. These parts are described in detail in the following sections.

Figure 2.1: Scheme of the gasification plant.

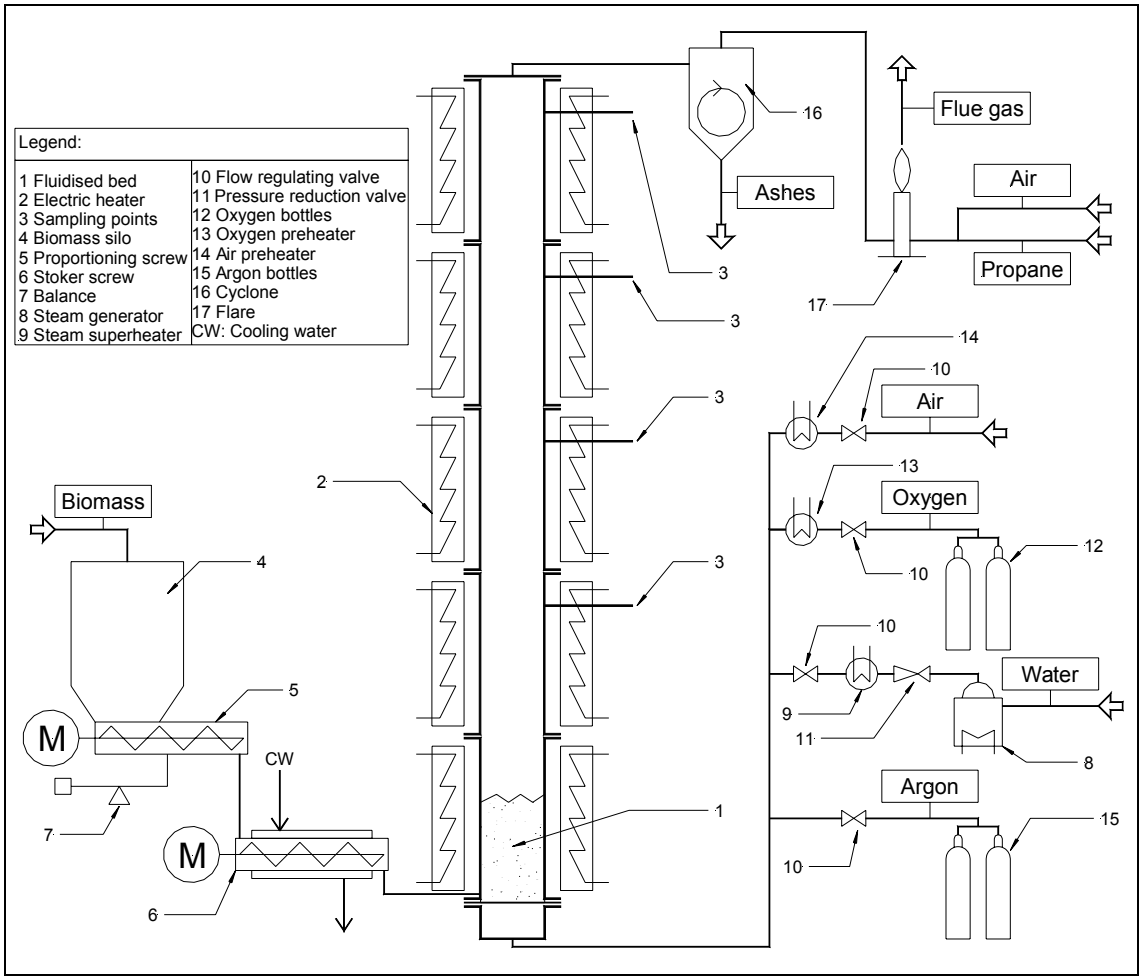

2.2 Gas Feeding

The reactor was designed so that both air or steam and oxygen mixtures could be used as gasification agents. A scheme of the gas feeding section is given in Figure 2.2. The air is provided by oil and water-free compressed air from PSI's compressed air network. It first passes a filter and then a pressure reduction valve where its pressure is reduced from 12 to 4bar. The air throughput is measured and regulated by a mass flow controller. The maximum air throughput is $36 m^3_N/h$. A pneumatically operated shut-off valve is provided after the mass flow controller so that the air flow to the reactor can be interrupted at any time. The air then passes through an electrical pre-heater of 7.5kW pow-

er. With this pre-heater the air temperature can be set to a desired value (max. 650°C). Before being mixed with other gases and entering the reactor the air finally passes through a check valve.

Figure 2.2: Scheme of the gas feeding.

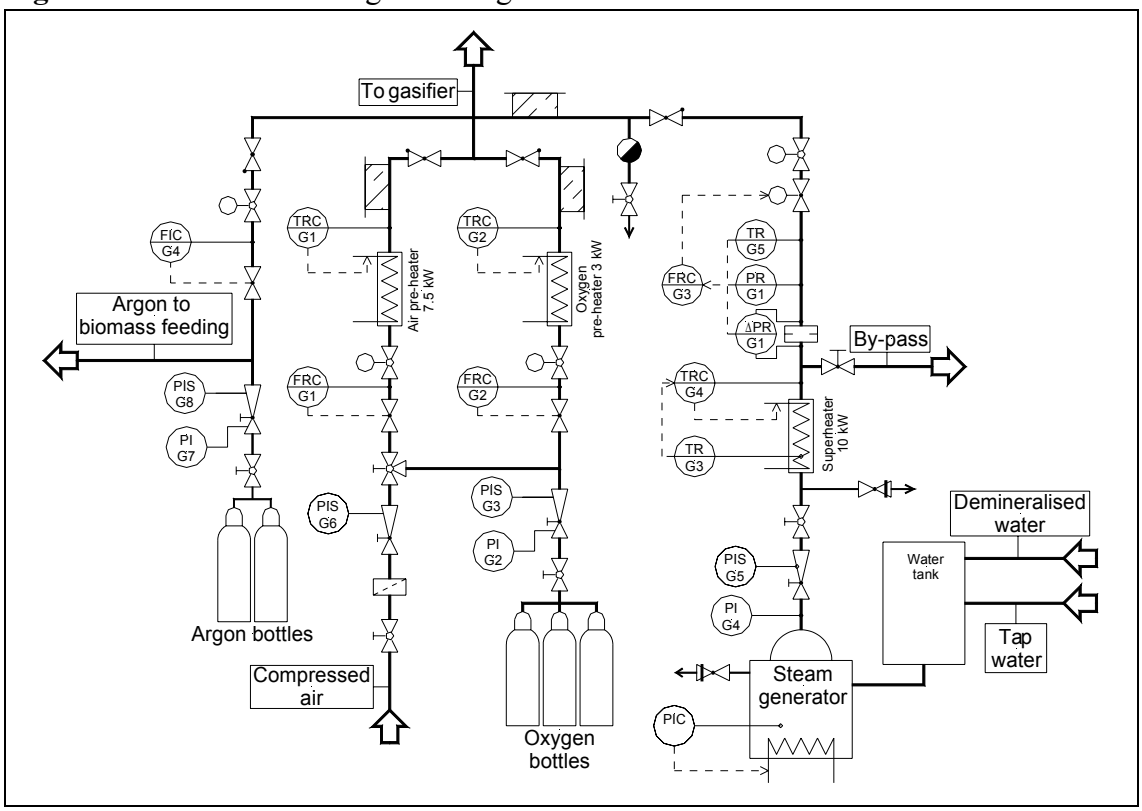

Oxygen is drawn from bundles of 12 bottles with 50 litres volume each under 200 bar pressure. The oxygen used is of 99.5% purity and the installation can be operated for 10 hours at maximum throughput with one filling. The oxygen flow path is analogous to the air flow path. The mass flow controller has a smaller maximum throughput of $12 m^3_N/h$ and the pre-heater has a smaller power (3.5kW). Also here a shut-off valve as well as a check valve are provided. A connection is fitted between the air and oxygen flow paths. This allows for the oxygen flow path and the reactor to be heated to operating temperature with air, saving the costly oxygen for the experiment.

Steam is generated in an electrically heated, commercially available steam generator with a maximum steam output of 36kg/h. The water used in this generator is premixed from 1/3 tap water and 2/3 deminearlised water in a tank. This precaution is taken to minimise depositions in the steam drum and at the same time provide the minimal con-

ductivity required for the operation of a water level sensor inside the steam drum. The electrical power for heating of the steam generator is controlled by the pressure inside the steam drum. The heating rods are switched in two independent groups providing smoother operation at low throughputs. Saturated steam leaves the generator at about 3.5bar, passes through a manual pressure reduction valve where the pressure is adjusted to less than 3 bar before entering the steam superheater. With this superheater the steam temperature can be increased up to a maximum of 400°C. The steam temperature at the outlet of the superheater is electronically controlled. After the superheater the steam path is divided in to two. A by-pass is provided for the heat-up and shut-down phase of the installation. In start-up the steam is simply flown through the superheater to the by-pass allowing this apparatus to heat-up under a flow of steam. The by-pass is fitted with a manual shut-off valve which is closed when steam is to be admitted to the reactor. At shut-down the steam flow is interrupted and this manual shut-off valve opened before the steam generator is switched off. The steam flow path leading to the reactor is made of an orifice plate flow meter, pressure and temperature sensors, pneumatically operated regulating valve, a pneumatic shut-off valve and again a check valve. The orifice plate and the flow regulating valve can both be exchanged, according to the steam throughput to be used. The pressure drop generated by this orifice plate is measured by a differential pressure transducer. Together with the temperature and absolute pressure after the plate the steam flow is calculated by a dedicated flow computer. This value is then used by a controller to set the position of the steam regulating valve.

Argon of 99.9% purity is drawn from two 50 litre bottles under 200bar and is primarily used to create an inert atmosphere in the biomass feeding. Argon can also be fed to the reactor if gasification has to be stopped abruptly (safety). This flow path is composed of a mass flow controller of 20.4m^3_N/h troughput, a pneumatically operated valve and a check valve.

Finally the gas flow path is equipped with a steam trap to allow for the evacuation of water coming from the steam flow path when it is cold or from the cold reactor inlet at start-up. The main properties of the gas supply system are summarised in Table 2.2.

Table 2.2: Gas feeding system main characteristics.

Gas	max. flow	max. temperature	pre-heater power
Air	$36m^3_N/h$	650°C	7.5kW
Oxygen	$12m^3_N/h$	650°C	3.5kW
Steam	10 (50)* kg/h	400°C	10 kW
Argon	$20.4m^3_N/h$	20°C	-

*: Depending on orifice plate/control valve installed

2.3 The biomass feeding system

The biomass feeding is composed of a lock hopper, a feeding screw or feeder with a biomass reservoir and a stoker screw, see Figure 2.3. The biomass feeding system is under an inert argon atmosphere to prevent dust explosions and to minimise the flow of gases from the hot reactor into the feeding system.

Figure 2.3: Scheme of the biomass feeding.

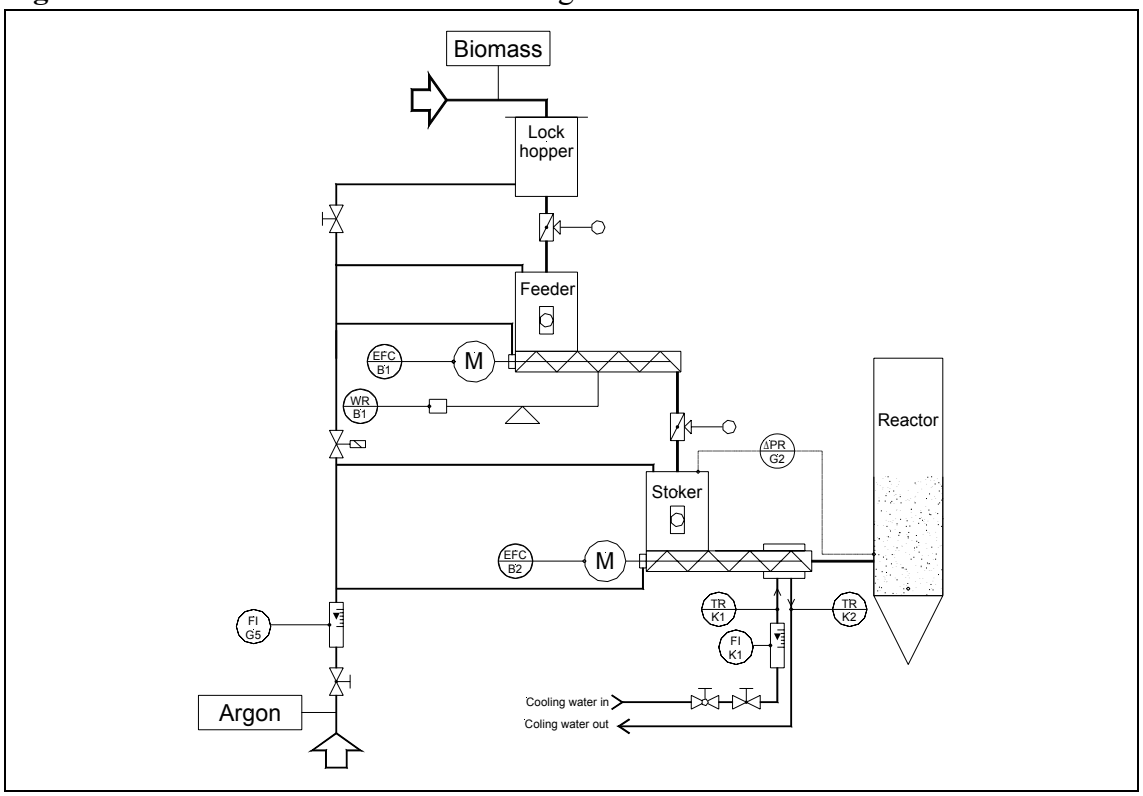

The lock hopper has a volume of approximately 60 litres and a gas tight lid on its top. It is placed above the feeder and is separated from it by a pneumatically operated butterfly valve. The biomass in the lock hopper is discontinuously discharged by opening the butterfly valve as the biomass inside the feeder's reservoir reaches a minimum level. The feeder's reservoir may be refilled approximately two times before the lock hopper has to be opened and refilled with fresh biomass. At this time and during normal operation in between refills the butterfly valve is in the closed position. The feeder is placed on a balance. With this balance the decrease of the fuel mass in the feeder's reservoir in time can be measured and from it the biomass flow rate can be calculated. This semi-continuous mode of operation is illustrated in Figure 2.4. To avoid bridging of the biomass inside the feeder a slowly rotating mixer is placed co-axially to the feeder's screw.

Figure 2.4: Weight loss of feeder during an experiment (000215A).

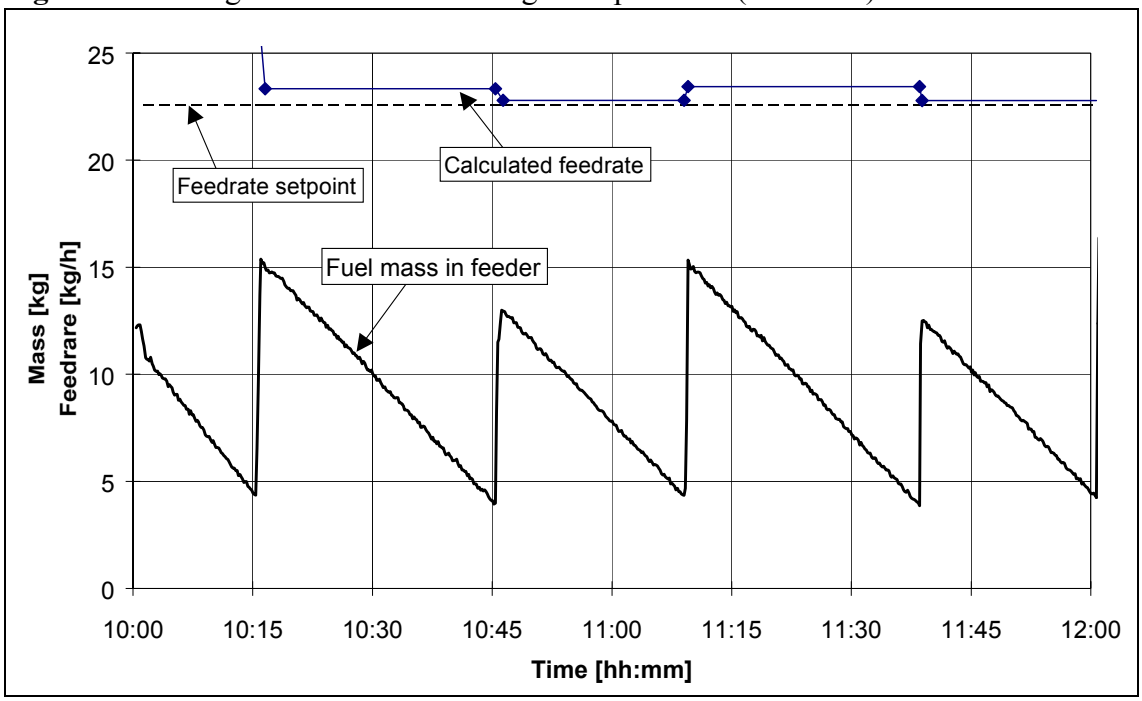

The feeder's connections to the lock hopper and to the tube leading to the stoker are made of flexible latex sleeves so that the feeder is "floating" on the balance and the correct weight of the feeder's content can be measured. Between the feeder and the stoker a connection pipe is fitted with another pneumatically operated butterfly valve. This valve isolates the feeder and lock hopper from the reactor during start-up and shut-down of the plant. The stoker was modified from its original design by placing the screw inside a steel

tube with roughly the same inner diameter as the stoker's screw and by fitting a transparent plexiglas tube from the biomass inlet to the tube surrounding the screw. With these modifications all biomass coming out of the feeder is readily fed into the reactor. The screw of the stoker ends inside the reactor, ca. 5mm of this screw are inside the fluidised bed. The tube connecting the stoker to the reactor is made of special heat resisting steel (Inconel 600) and its end is fitted with a water cooled jacket, to minimise thermal decomposition of the biomass in the stoker. Screws and outlet pipes of both feeder and stoker can easily be changed to allow for different ranges of biomass throughput. Both feeding devices are driven by motors with a variable speed control. By changing the rotation speed of the feeder screw the biomass feed rate can be set to a desired value. Figure 2.5 shows feed rates as a function of the feeder's rotation speed for different fuels.

Figure 2.5: Biomass feed rates as a function of the feeder's speed for different fuels (for details on the fuels see section 2.8).

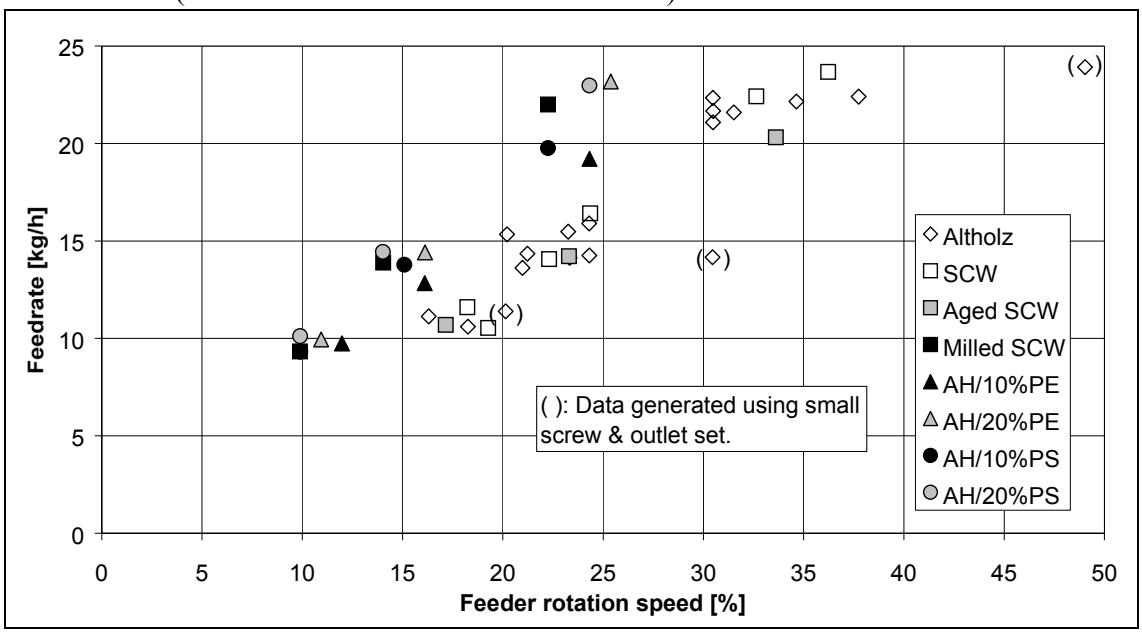

The feed rate is primarily dependent on fuel parameters and differs somewhat from batch to batch of fuel. For a given fuel the dependency between feed rate and rotation speed is linear. The rotation speed of the stoker screw is adjusted to a slightly higher value than that of the feeder so that no accumulation of biomass is observed in the plexiglas tube. The pressure difference between the stoker and the reactor is monitored. By adjusting the flow of argon to the feeding system the pressure in the feeding system is kept at a slightly higher value than the pressure in the reactor. The front end of the stoker is mount-

ed on springs to follow the thermal expansion of the lower part of the reactor (see page 22).

2.4 The Reactor

The gasifier has a modular design and is essentially a tall column with 213mm inner diameter and a total height (distributor to exit) of 5.1m. The column is made of a special heat and corrosion resisting alloy, Inconel 625. Corrosion resistance of the construction material is important as some of the fuels to be studied will contain chlorine. The whole reactor is enclosed in electrical heaters. These heaters are divided in 10 sections of approximately 0.5m length, which have each an independent temperature control. The biomass feeding is at the lowest possible position in the bed. This configuration is known to allow higher heating rates of the fresh biomass particles entering the reactor. Therefore higher gas and lower tar amounts are achieved, see [2.6].

Figure 2.6: The inlet section and the distributor plate holder.

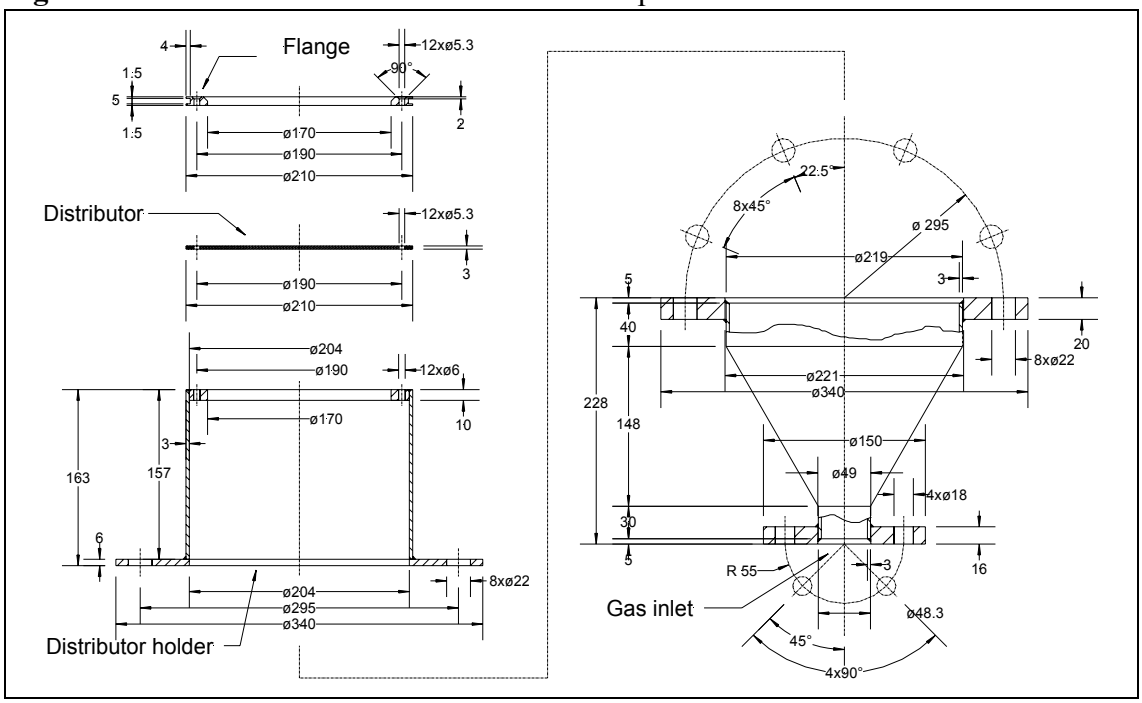

The gases enter the reactor from the bottom by a conical inlet section, see Figure 2.6. Pressure and temperature of the gases are measured at this point, before the gases pass through a gas distributor on which the fluidised bed rests. As gas distributor a sintered metal plate made of Hastelloy X with 15μm average pore size is used. The plate itself is located on a plate holder, so that the biomass inlet to the reactor is at the same level as the gas distributor. Note that since clean gases (compressed air from the distribution network at PSI, oxygen from pressurised bottles etc.) are used as fluidisation agents no problems with plugging of the distributor where ever observed.

The tubular section containing the fluidised bed is called the bed module and is 1124mm long. It is depicted in Figure 2.7. This section is fitted with a horizontal pipe by which the biomass is fed into the reactor. The end of the stoker outlet tube fits tightly in this pipe. The stoker tube and the reactor's inlet for biomass are connected by a flange and the inlet is large enough to accommodate the different diameter outlets of the stoker. At the opposite side of the inlet, an outlet tube looking 60° down from the horizontal is fitted. Through this outlet the bed material can be drawn from the reactor. Just above this outlet the first of a series of 5 access pipes is located. Through 4 of these pipes thermocouples are inserted into the reactor, enabling temperature measurements at the centre (or by using shorter thermocouples at another radial location) of the reactor. The first three are placed at 110, 320 and 530mm from the distributor plate. This arrangement allows for different bed heights (corresponding to 1,2 and 3 times the diameter of the reactor) to be used and still have at least one thermocouple inside the bed. The last thermocouple is at 125mm from the top flange of the bed module. On the outer surface of the bed module's tube, pockets are provided in which thermocouples are inserted to measure the outer wall temperature of the bed module. These pockets provide that the thermocouples at the outside will be at the same level of those inside the reactor and at the opposite side. Finally, an access port is provided below the last thermocouple tube (195mm from the top flange). The access pipes are required to protect the thermocouples from breaking by moving the heating shells (see page 24), the same reason making protecting tubes for the outer thermocouples necessary.

Figure 2.7: The bed module.

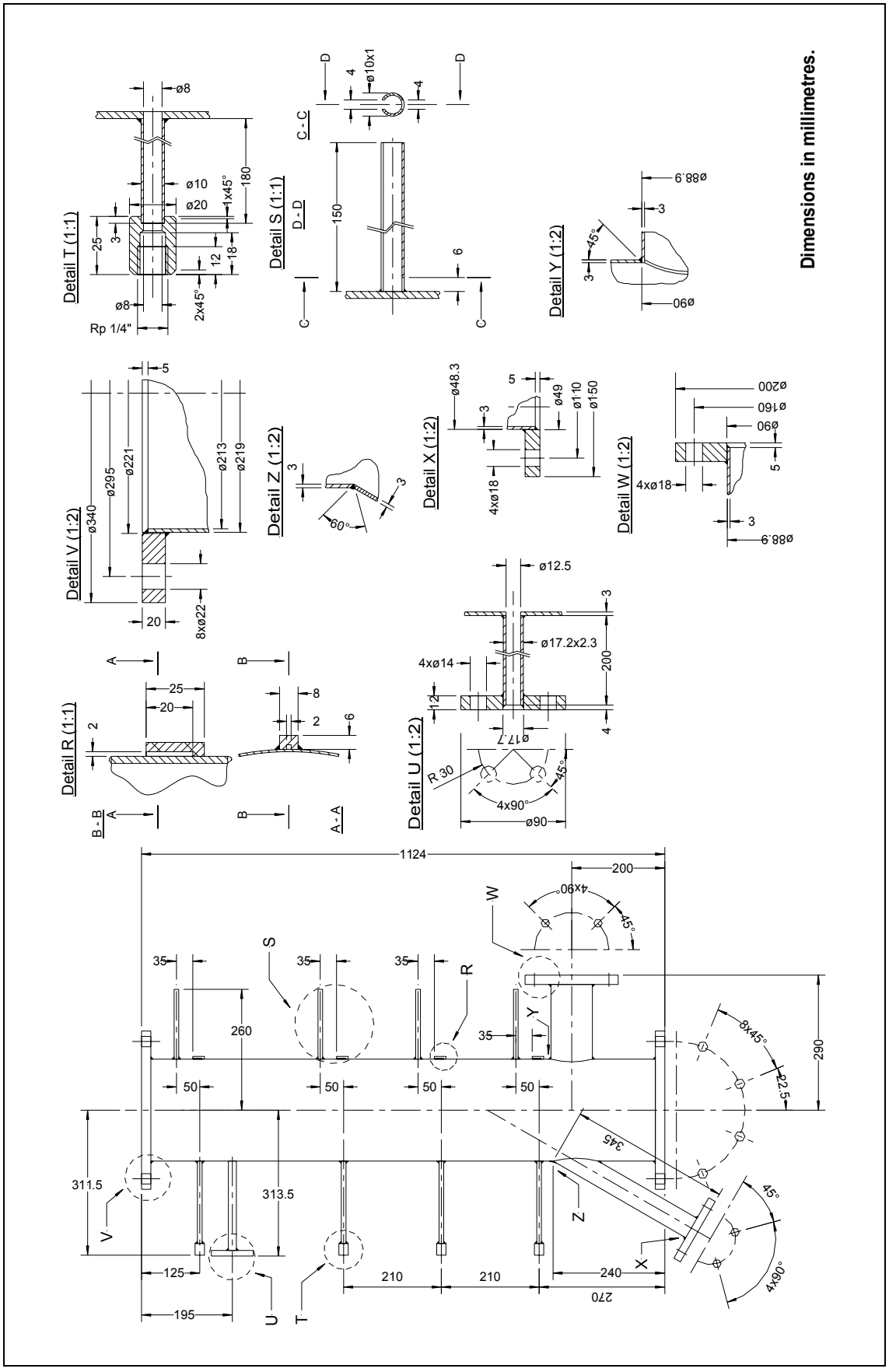

The bed module and gas inlet to the reactor are hanging from a short sustaining module, which connects the reactor to the supporting structure surrounding it. The bed module will therefore expand downwards when hot by about 10-20mm. This sustaining module is not enclosed by electrical heaters but only insulated. A drawing of this sustaining module is given in Figure 2.8.

Figure 2.8: The sustaining module.

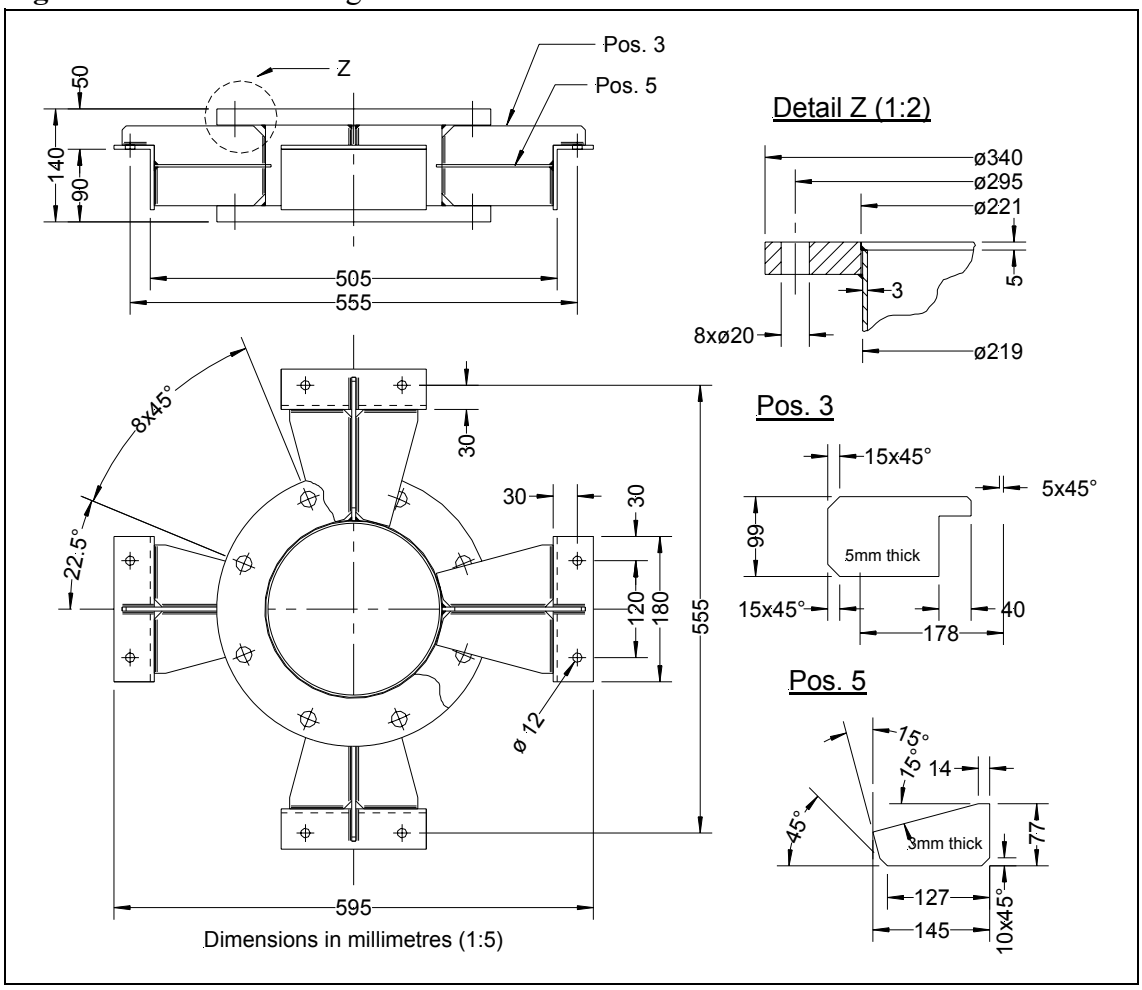

Resting on top this first sustaining module, four identical tubular modules form the reactor's freeboard. The freeboard modules are each 1'000mm long. They are fitted with two access tubes for thermocouples at 270 and 730mm from the bottom flange. As in the bed module pockets for outer thermocouples are fitted at the same height. The position of these thermocouples place them at the axial centre of the heater shells surrounding the reactor. Two further access openings by tubes are provided the lowest of both (50mm from the lower flange) being a reserve access. The access at 660mm from the lower flange is dedicated to sampling gases or tars from the reactor.

Figure 2.9: The freeboard module.

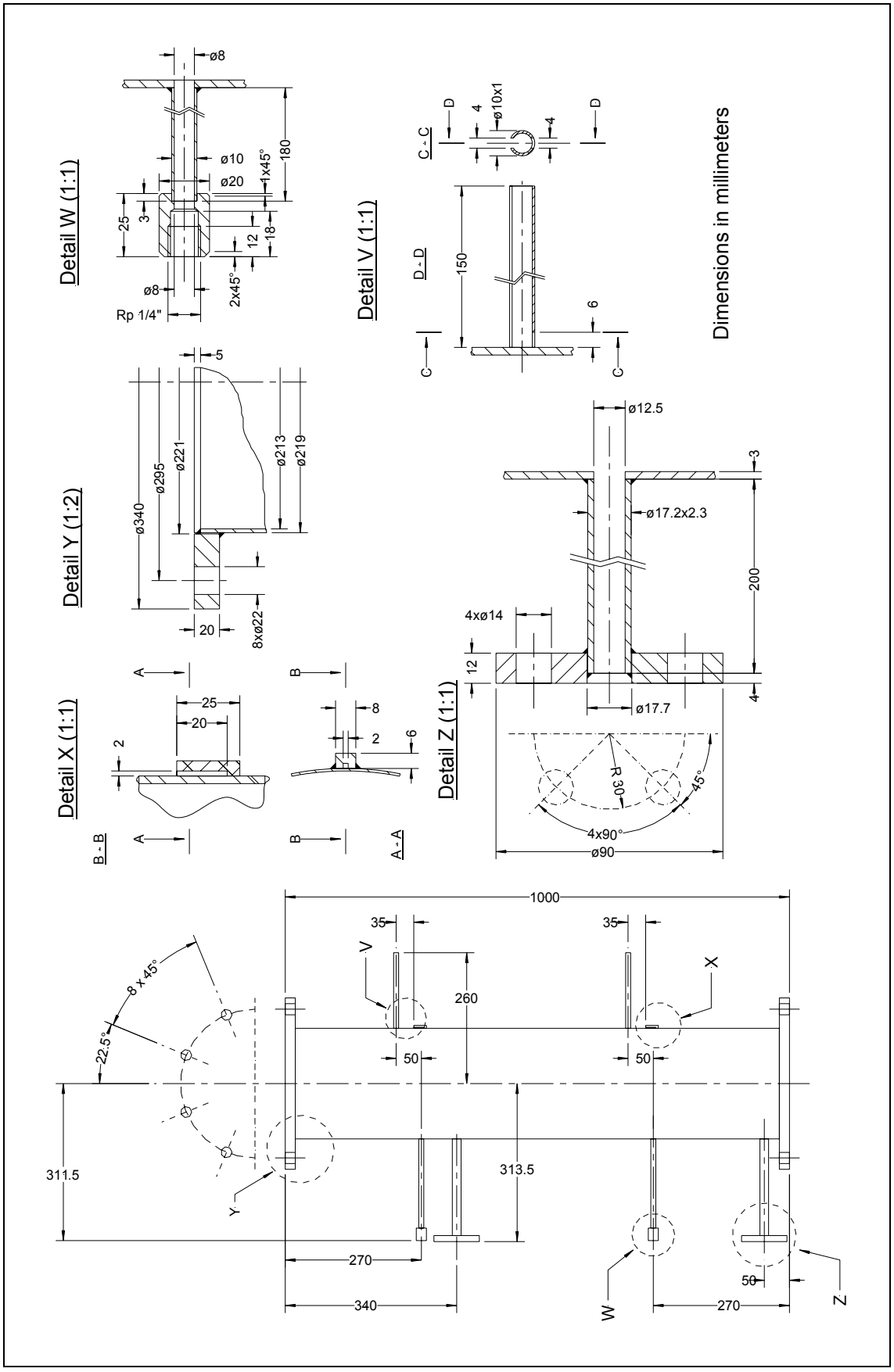

Above the last freeboard module a metallic expansion joint (metal bellow) is fitted. This joint compensates for the thermal expansion of the freeboard modules, which can expand upwards by some 40mm when at 900°C. Another sustaining module is placed above the expansion joint and holds the reactor at the top of the supporting structure. Finally the gases and particles from the reactor pass a large 90° bow before entering a cyclone.

The whole reactor (bed and freeboard modules) is enclosed in metallic shells containing the electrical heating. These shells are divided in the longitudinal axis forming half cylinders. When put together they enclose the reactor tube completely. The shells are mounted on skids which rest on rails fixed to the supporting structure of the reactor. The half-cylinders join at the plane in which the thermocouple tubes exiting the reactor are located. The heating modules are half cylinders of light ceramic material with an inner diameter of 250mm, an outer diameter of 450mm and a length of 400mm. The heating is provided by Kanthal coils embedded in the ceramic material. The maximum operating temperature of these heaters is 1150°C and their power is 2.5kW. The shells are mounted such, that the flanges of the tubular modules of the reactor are just between two sets of shells. A drawing showing the heater shells is given in Figure 2.10.

Figure 2.10: The heater shells.

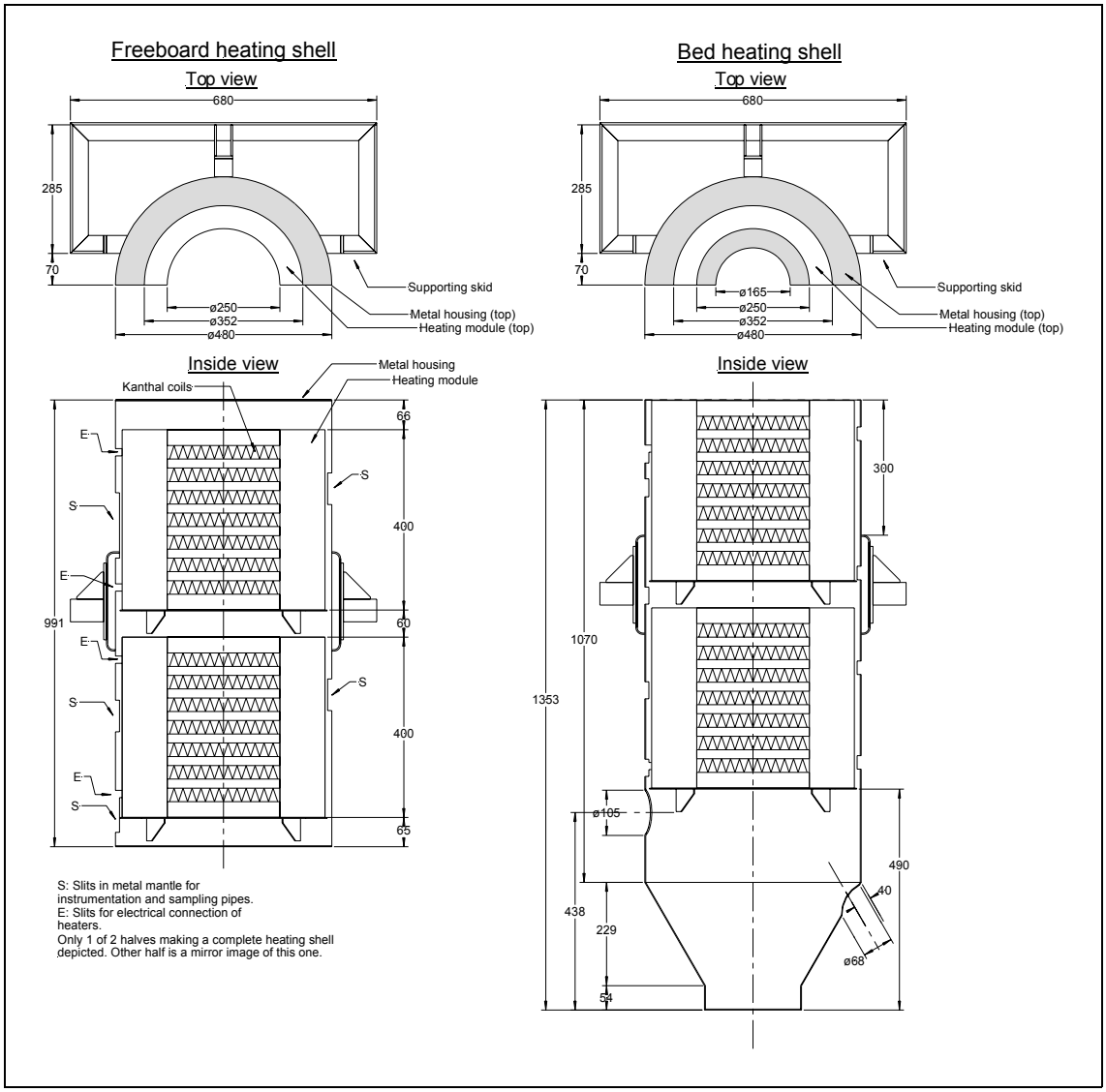

The reactor is fitted with several thermocouples and pressure difference sensors to monitor both the pressure drop across the distributor and across the bed. A scheme of the reactor's instrumentation is given in Figure 2.11.

Figure 2.11: Instrumentation scheme of the reactor.

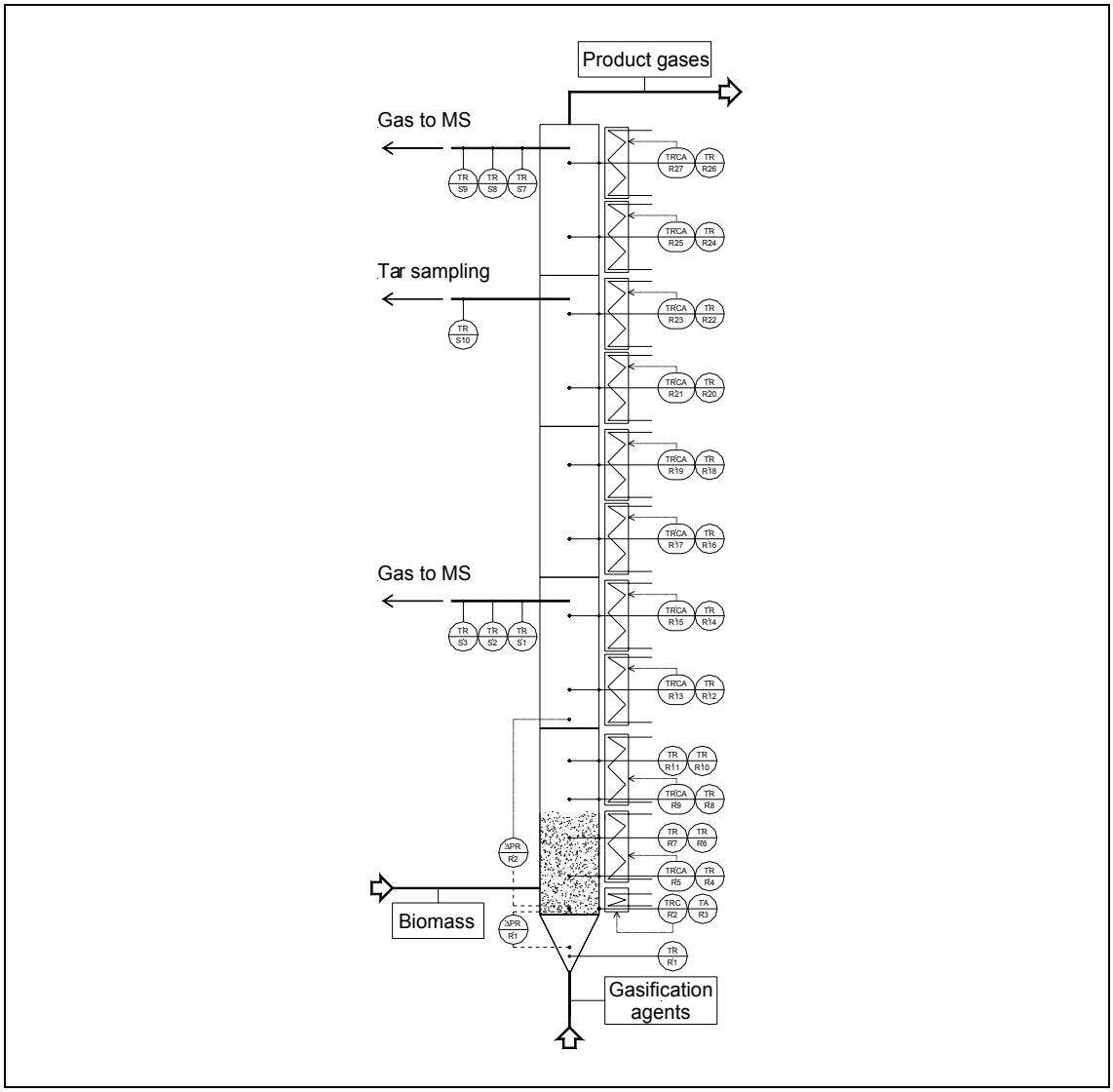

2.5 The off gas section

The off gas section is shown in Figure 2.12. The gases and particles leaving the reactor enter a high efficiency cyclone. This unit was designed with an exchangeable outlet to provide proper separation characteristics in a large range of gas throughputs. A schematic drawing of the cyclone is given in Figure 2.13. Particles separated in the cyclone fall into a container. Between the container and the cyclone a butterfly valve is provided. This valve seals off the cyclone allowing to exchange the container during operation of

the gasifier. A flow meter based on the impact pressure principle (pitot tube) is placed in the pipe leading the product gases to the flare. Together with the temperature and the absolute pressure of the gas inside the outlet tube the flow of product gases can be calculated. It was however found, that this device does not work properly due to depositions in the flow meter's sensor and in the outlet pipe.

Figure 2.12: Scheme of the off gas section.

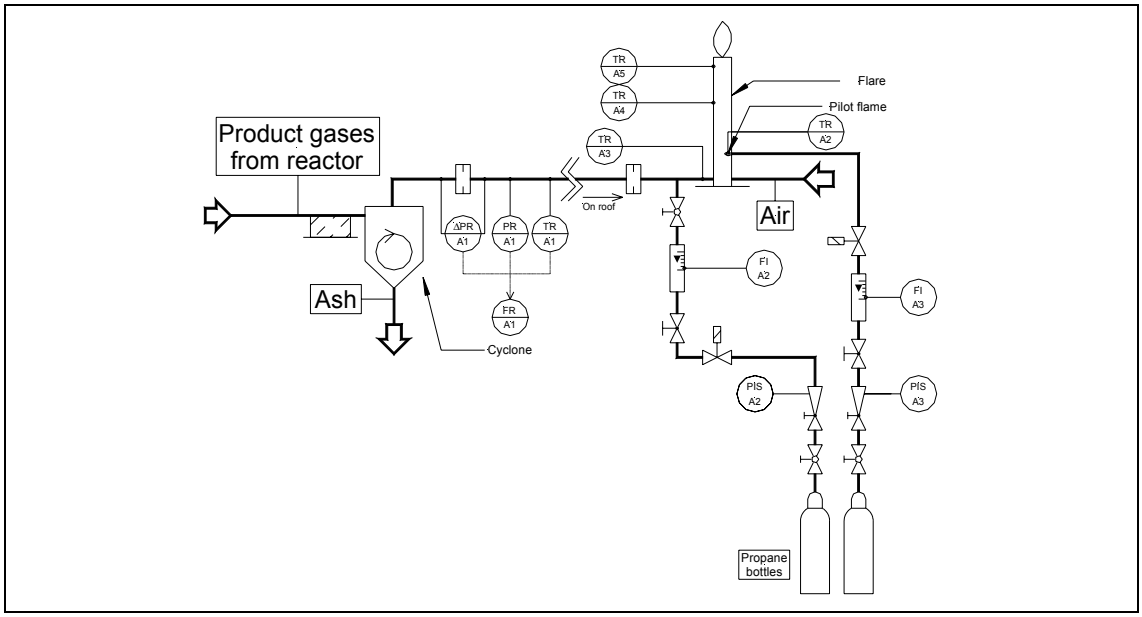

Figure 2.13: The cyclone.

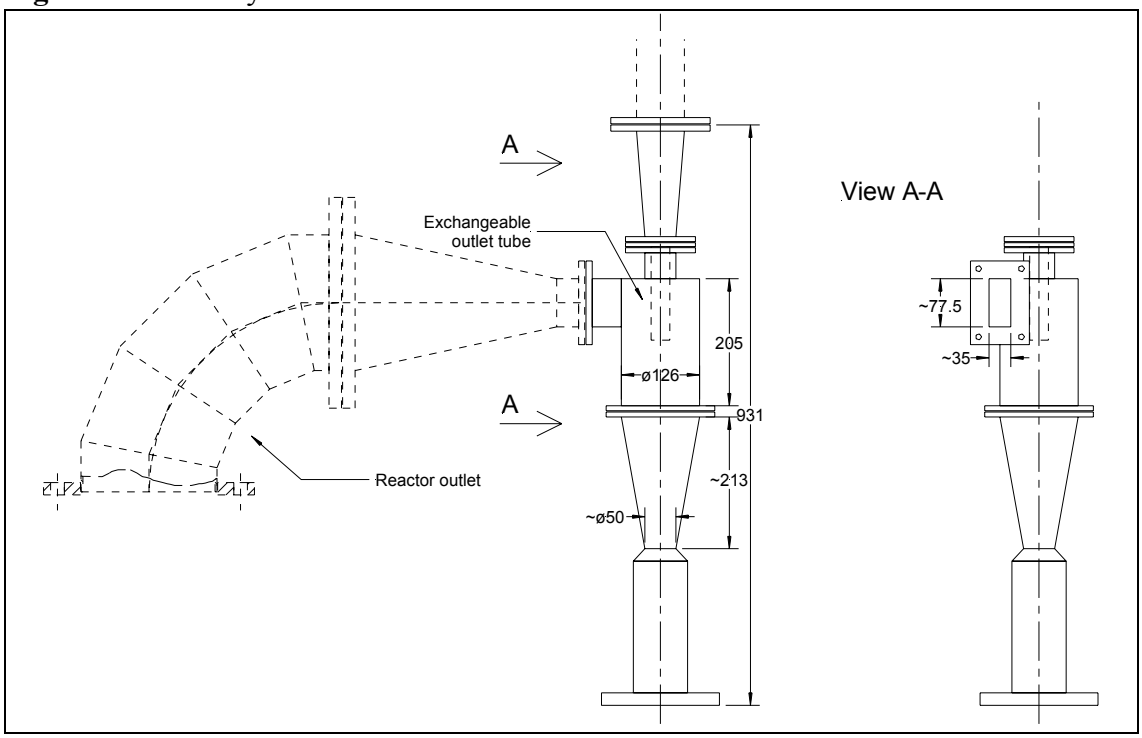

The de-dusted gases flow then through an insulated pipe to a flare at the top of the building where the gasifier is located. Before the flare a metal disc with an orifice is fitted inside the tube to prevent backfiring of the gases into the reactor. The flare is basically a diffusion flame burner where the gases burn inside an insulated tube. A schematic drawing of the flare is given in Figure 2.14. Propane can be added to the gases should these be too lean to burn properly. The flare has a pilot burner fuelled by propane gas which burns continuously during an experiment.

Figure 2.14: The flare.

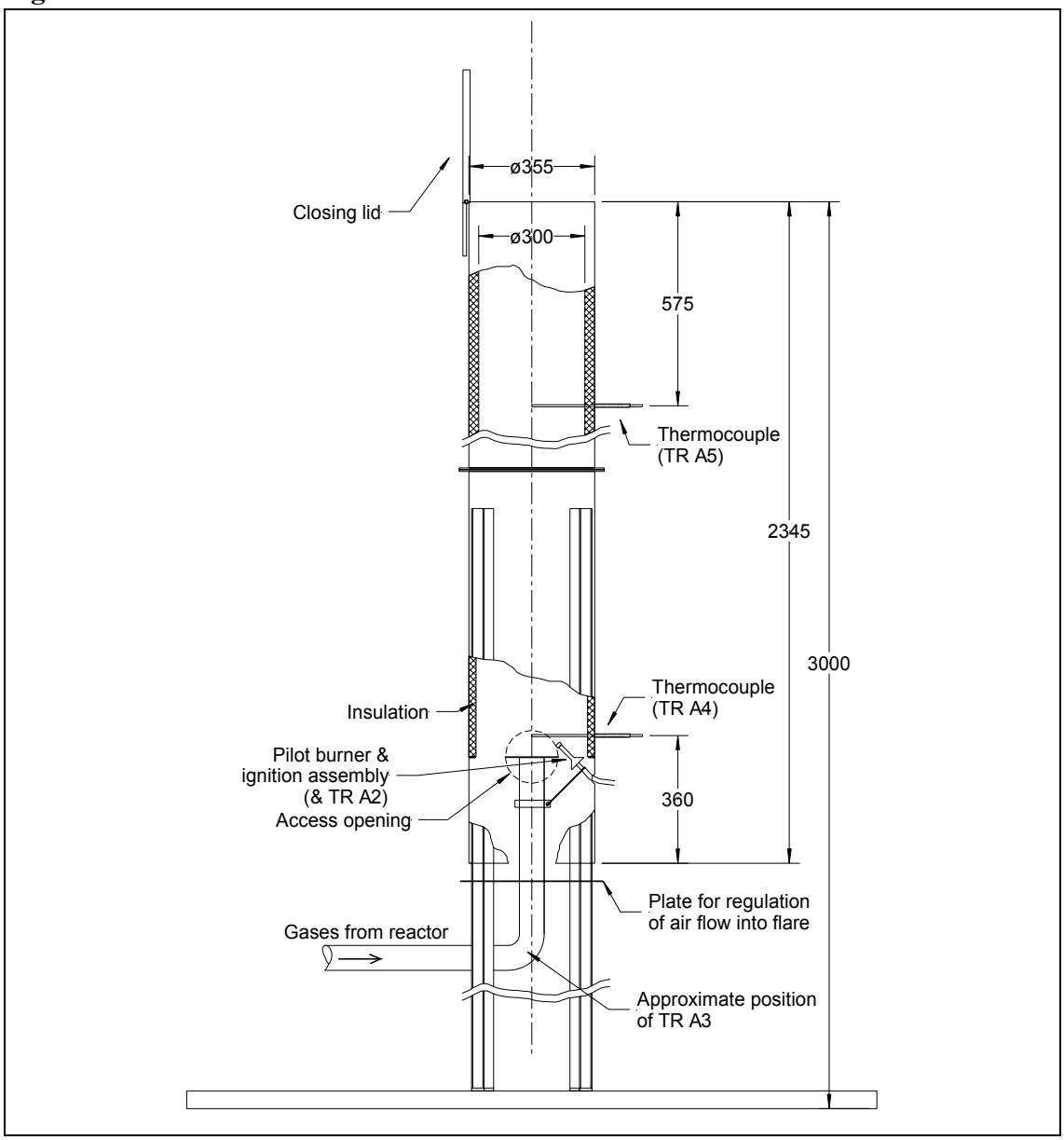

2.6 The plant's periphery

2.6.1 Data acquisition and control

The installation is equipped with an array of various sensors (temperatures, pressure differences, flows etc.) producing data on the current operational conditions of the installation. This data is acquired, visualised and saved for later analysis on a dedicated personal computer (PC). This computer runs a program written in the LabView data acquisition environment. The electrical signals from the transducers are processed (filtered and averaged) by multiplexers before being transmitted to a data acquisition card on the PC. Some instruments of the installation (for example the balance below the biomass feeder) communicate directly with the PC via digital interfaces (RS-232 and RS-485). This communication is also managed by the data acquisition program. New data is acquired about every 2 seconds. The data is saved to a file on the hard disk of the PC at regular time intervals, generally 10 seconds. The same data is displayed on the visualisation screen representing a scheme of the plant shown in Figure 2.15. The visualisation is updated at about the same rate of the acquisition. Data can further be shown as time series on separate screens. The visualisation screen allows the operator of the installation to enter set-points for different control loops of the installation. These set-points are then transmitted from the data acquisition card on the PC via dedicated signal output modules to the controllers of the specific loops. The data acquisition program performs calculations on the data acquired, for example the biomass feed rate is calculated from the weight signal of the balance below the biomass feeder and displayed.

All control loops of the installation have dedicated controllers which are not depending on the PC for operation. As already mentioned, most of the set-point values can be transmitted to the controllers from the PC. Still, all controllers can operate using local set-points. This precaution is taken for safety, enabling to continue the operation or to safely shut down the plant in the case of a PC failure.

Figure 2.15: Data visualisation screen.

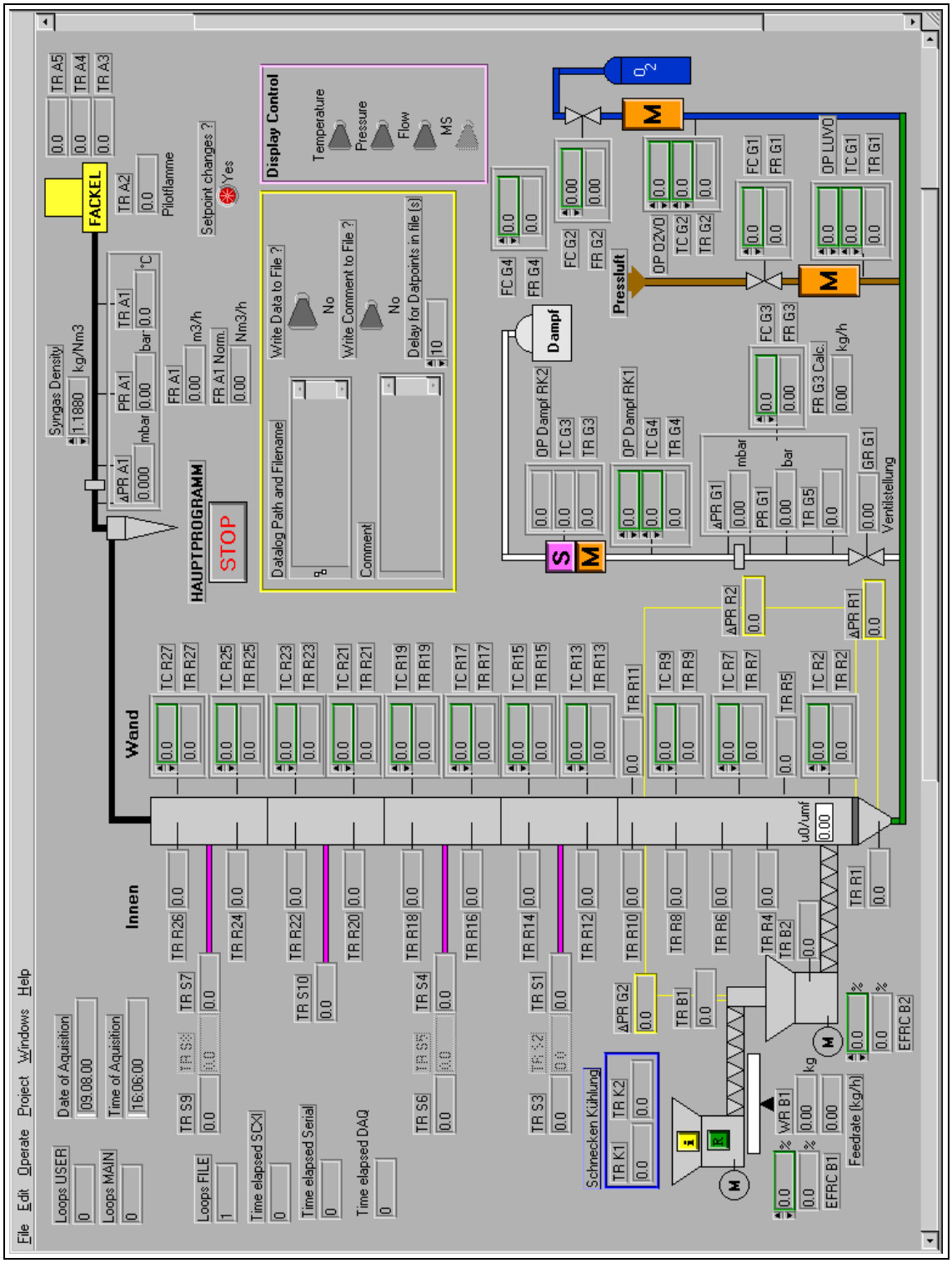

2.6.2 On-line gas analysis

Product gases are sampled in 2 locations of the gasifier's freeboard, at the first and at the last freeboard element (1760 and 4760mm above the gas distributor). The raw

gas is filtered and conditioned before it is sent to an on-line mass spectrometer (on-line MS) for analysis of its composition. The gas conditioning used is shown in Figure 2.16. The hot gases first pass a particle filter made of a sintered steel tube enclosed in a heating shell. The filter is kept at 300°C to minimise tar deposition. It was dimensioned to allow for several hours of operation and to be easily removed for cleaning.

Figure 2.16: Scheme of the gas conditioning.

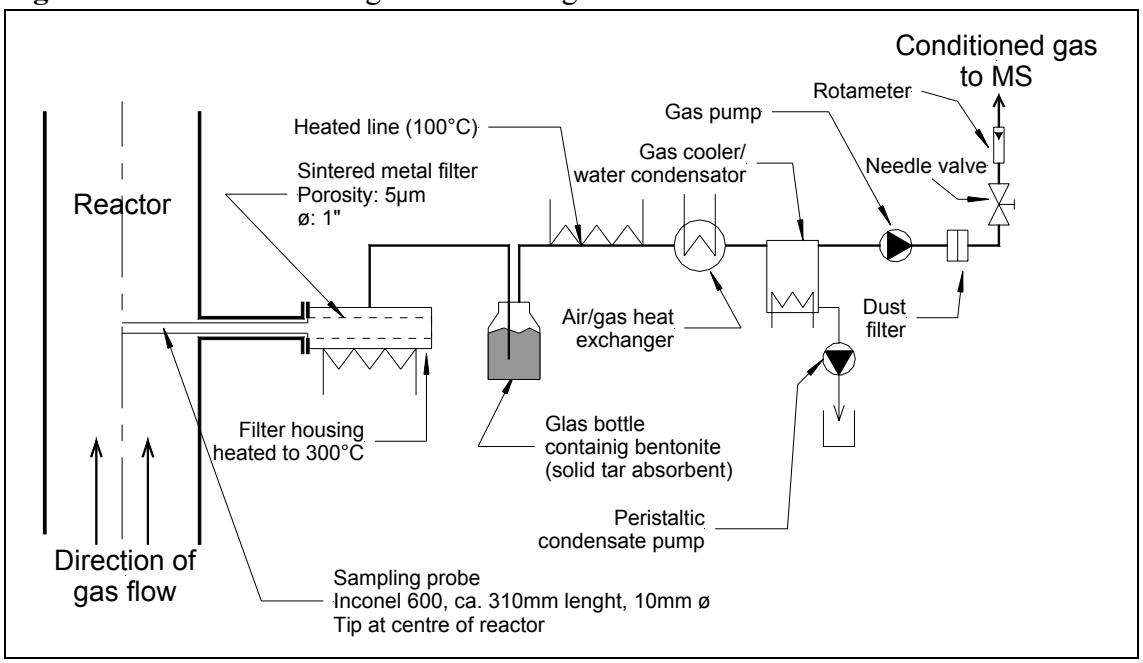

The filtered gas is then led to a glass bottle containing bentonite for tar absorption. This material shows excellent tar trapping capabilities even with very wet gases and is easily disposed of after an experiment. The gases are led by a heated PTFE pipe (100°C) to a heat exchanger and a cooler. The cooler is fitted with a Peltier element and cools the gases to 4°C so that the water in the gas condenses. The condensed water is drawn out of the cooler by a peristaltic pump into a proper reservoir. The cool dry gas is then drawn by a diaphragm pump, passes a dust filter and then a needle valve with which the gas throughput is set. The gases pass a rotameter which indicates the actual flow and from there they are led by teflon tubes to the mass spectrometer.

The on-line MS used is a magnetic sector device. It has a special sampling interface which allows for the sequential survey of 32 different gas sources. The on-line MS is calibrated using the gases shown in Table 2.3 before each experiment.

The measurement principle is straightforward, i.e. a certain mass to charge ratio (m/z) is selected as being representative for a given compound in the gas and the intensity of the signal from the detector is directly proportional to the concentration of the compound in the gas mixture. The m/z usually chosen is the so called molecular ion, that is the ionized gas molecule since this is where the strongest signal is achieved. When complex gas mixtures are analysed by on-line MS some compounds yield strong signals at the same m/z as is for example the case at m/z = 28 for nitrogen and carbon monoxide, two

Table 2.3: Concentrations (vol.-%) of the calibration gases used for the on-line MS. *: Gas Nr. 0 is used to determine background levels of analysed species.

Gas Nr.	0*	1	2	3	4	5	6	7
N_2	0	100	0	0	0	45.17	0	94.92
CO_2	0	0	100	0	0	15.0	0	0
CO	0	0	0	100	0	15.18	0	0
H_2	0	0	0	0	0	19.71	0	0
CH_4	0	0	0	0	100	4.94	0	0
Ar	0	0	0	0	0	0	100	0
O_2	0	0	0	0	0	0	0	5.08
He	100	0	0	0	0	0	0	0

species present in our product gases. This difficulty is overcome by assigning other m/z to these compounds. Nevertheless overlapping of peaks can still occur at the m/z ratios and is corrected using the so called cracking pattern of the compounds in the gas. The cracking pattern is composed of the relative intensities at selected m/z for a specific substance based on a assigned base peak. The overlapping signals can then be corrected by the MS software. An example of a cracking pattern matrix is shown in Table 2.4. The cracking pattern matrix is determined during the calibration procedure performed before each experiment. In our case, corrections are made for carbon monoxide (overlapping at m/z=12 caused by carbon dioxide and methane) and nitrogen (overlapping at m/z=14 caused by carbon monoxide and methane). This measurement technique presupposes that all compounds in the gas are known and specified for proper correction of their overlapping peaks. In the present case a small error is expected for nitrogen, as the gases issued of biomass gasification are known to contain low levels (less than 2% by volume) of C_2-

isomers (ethane, ethene and ethine) and these hydrocarbons have peaks at m/z=14. The MS offers the possibility of including these (and other) compounds in the analysis method, but the effort required would be quite substantial (see [2.7]). It was thus decided to leave them out of the analysis method.

Table 2.4: Cracking pattern matrix for experiment 991214.

m/z	N_2	CO_2	CO	H_2	CH_4	Ar	O_2
2	0	0	0	100	0	0	0
12	0	0.868	100	0	0.970	0	0
14	100	0	80.369	0	8.522	0	0
15	0	0	0	0	100	0	0
32	0	0	0	0	0	0	100
40	0	0	0	0	0	100	0
44	0	100	0	0	0	0	0

The MS has a dedicated PC which controls the instrument and saves the gas composition data for later analysis. The gas composition is displayed on the PC's screen as time series or in tabular form. An example of the gas composition for an experiment measured with this instrument is given in Figure 2.17.

Figure 2.17: Gas composition evolution for experiment 000125.

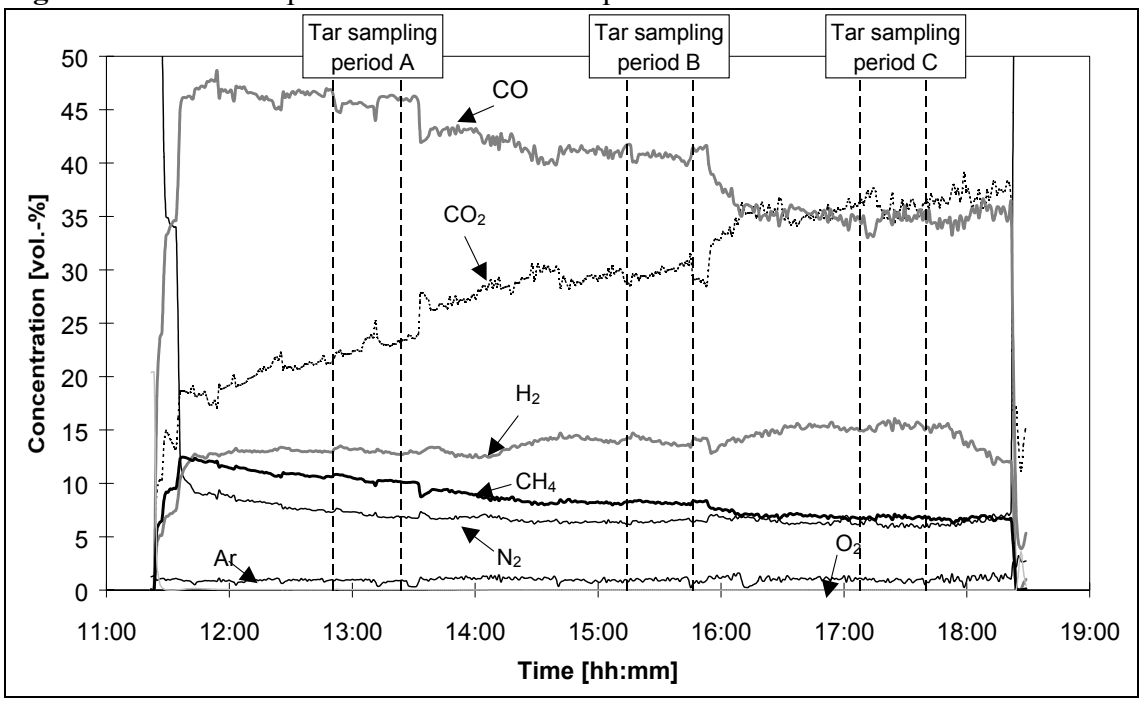

2.7 Bed material

The bed materials used in the present study are silica/alumina sands (calcined kaolins) with the commercial name "Molochite 16-30DD" and "Molochite 22-60DD". These sands are normally used in the ceramics industry for different applications both in the household and technical sector. They were chosen since practical experience was available from a previous fluidised bed combustion project at PSI, showing good stability both mechanically (low attrition loss) and thermally (sintering above 1400°C). The chemical composition of these bed materials is given in Table 2.5.

Table 2.5: Chemical composition of the bed material [2.8].

Compound	Mass-%
SiO_2	54.5
Al_2O_3	42.0
K_2O	2.0
Fe_2O_3	1.1
MgO	0.31
Na_2O	0.1
TiO_2	0.07
CaO	0.06

The difference between the bed materials is the particle size. Molochite 16-30DD being the coarser of the two. The particle size distribution was measured by sieve analysis and is shown in Figure 2.18. From this particle size distribution, the mean particle diameter $\bar{d}_p$ is calculated from the particle size distribution according to the following equation [2.2]:

$$\bar{d}_p = \left(\int_0^{d_{p,max}} \frac{q_3(d_p)}{d_p} \cdot d(d_p) \right)^{-1} \quad \text{where} \tag{2.1}$$

$$q_3(d_p) = \frac{d}{d(d_p)} Q_3(d_p) \quad \text{with} \tag{2.2}$$

$Q_3(d_p)$ being the mass fraction of particles with a diameter smaller than d_p and $d_{p,max}$ being the largest particle diameter present.

Figure 2.18: Particle size distribution of the bed materials.

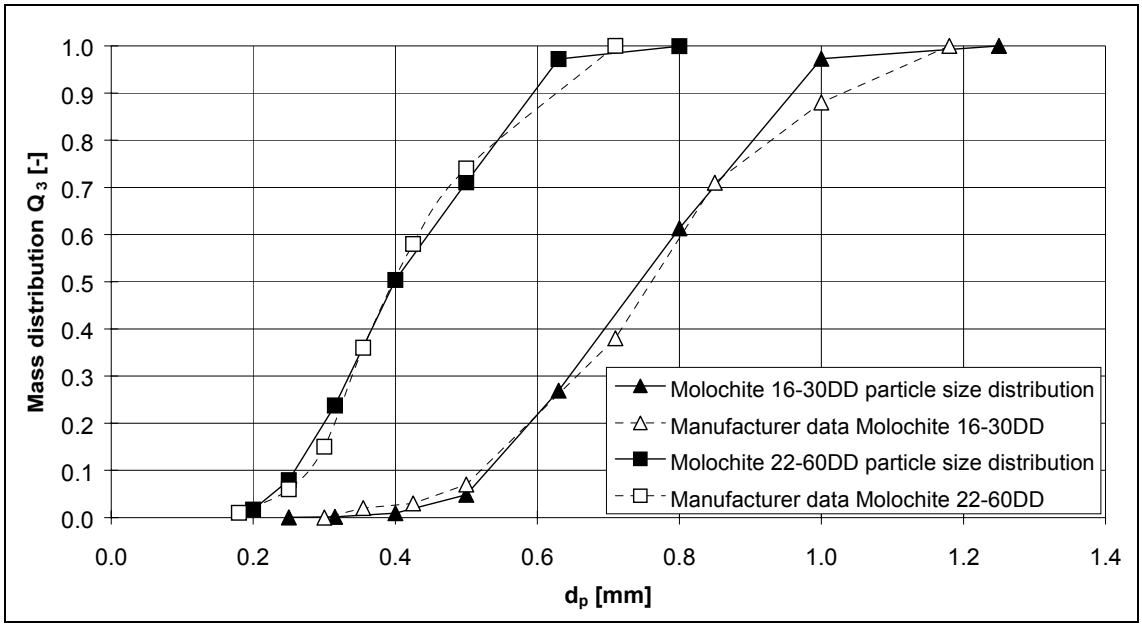

For a discrete particle size distribution as measured by sieve analysis with N particle size classes, the above set of equations reads:

$$\bar{d}_p = \left(\sum_{n=1}^{N} \frac{q_{3,i} \cdot \Delta d_{p,i}}{\bar{d}_{p,i}} \right)^{-1} \quad \text{where} \tag{2.3}$$

$$q_{3,i} = \frac{\Delta Q_{3,i}}{\Delta d_{p,i}} \quad \text{yielding} \tag{2.4}$$

$$\bar{d}_p = \left(\sum_{n=1}^{N} \frac{\Delta Q_{3,i}}{\bar{d}_{p,i}} \right)^{-1} \quad \text{with} \tag{2.5}$$

$$\Delta Q_{3,i} = Q_{3,i} - Q_{3,(i-1)} \quad \text{being the mass fraction of particles in the class i,} \tag{2.6}$$

$$\Delta d_{p,i} = d_{p,i} - d_{p,(i-1)} \quad \text{the width of the class i and} \tag{2.7}$$

$$\bar{d}_{p,i} = \frac{d_{p,i} - d_{p,(i-1)}}{2} \quad \text{the mean particle size of the class i.}$$

This mean diameter definition is used to characterise particles in fluidised bed applications. It relates the average projected surface area of the particles to their average volume. The projected surface area in turn determines the pressure drop of the bed, an important engineering aspect when dealing with fluidised or fixed beds.

The fluidisation-relevant characteristics of these materials, the minimum fluidisation velocity u_{mf}, the voidage at minimum fluidisation ε_{mf} and the particles' sphericity Φ_S have been determined experimentally by using transparent fluidisation columns of circular cross section and are summarised in Table 2.6.

Table 2.6: Fluidisation-relevant data of bed materials.

Molochite type	**22-60DD (fine)**	**16-30DD (coarse)**
Mean Particle diameter $\bar{d}_p$	385µm	708µm
Minimum fluidisation velocity u_{mf} (air, 20°C)	0.133m/s	0.325m/s
Voidage at minimum fluidisation ε_{mf}	0.5390	0.5557
Particles' sphericity Φ_S	0.5540	0.4709
Particle density ρ_s [2.8]	2500kg/m^3	2500kg/m^3

The fluidisation columns used are equipped with pressure difference meters allowing the determination of the pressure drop over the bed for different air flows through the bed. The exact procedure for obtaining the fluidisation parameters is described in detail in reference [2.2] and will not be discussed here. Note, however, that instead of using the theoretical pressure drop at minimum fluidisation (given by the bed's weight divided by the cross sectional area of the fluidisation column) the average of the measured pressure drop above the (optically determined) minimum fluidisation was used. The reason for this procedure was the poor agreement between the theoretical values for the pressure drop with the observed average values. The differences might originate from systematic (for example incorrect column diameter) as well as experimental (for example non-ideal gas distribution in the set-up used, incorrect material mass) errors which may lead to large errors in the calculation of the theoretical pressure drop. Note also that the relatively low sphericity values obtained agree with the observed unspherical form of the fresh Molochite particles.

Figure 2.19 shows the results of the experiment for the determination of the characteristics of the coarser bed material, in which 11.9kg of bed material and a fluidisation column with an internal diameter of 0.2m where used.

Figure 2.19: Fluidisation experiment for the estimation of coarse bed material fluidisation characteristics.

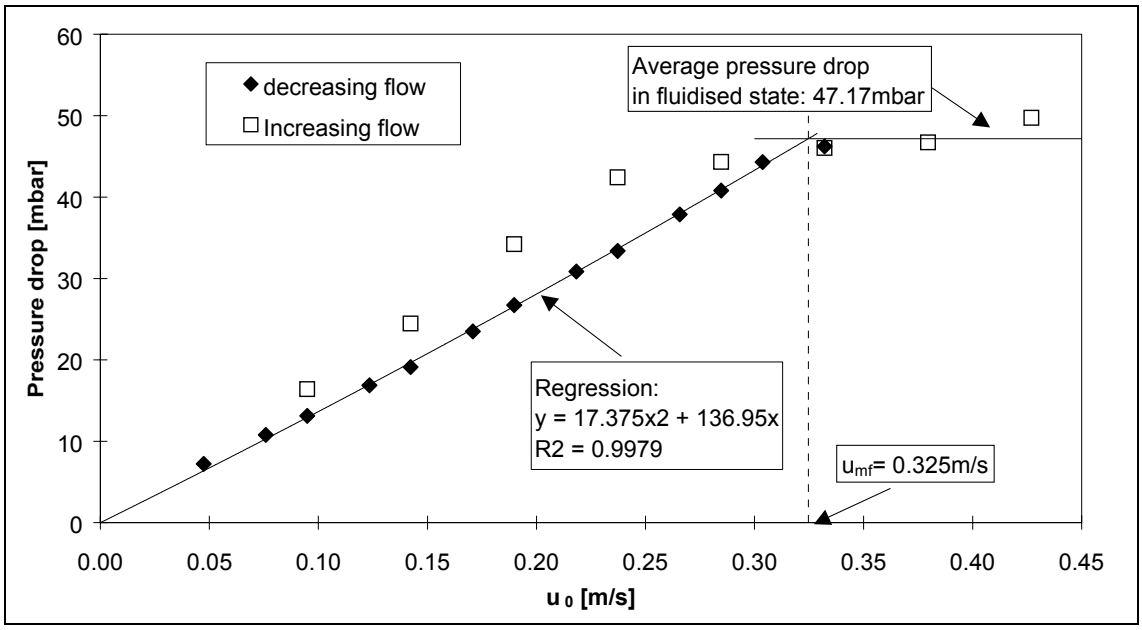

2.8 Fuels studied

Six fuels were used in the present study. As "clean" i.e. contaminant-free wood, a mixture of fir and spruce sawdust was used. This standard clean wood (SCW) is a saw-mill residue, chosen as reference fuel because its composition in terms of the wood types present is constant, it is bark-free and readily available in large quantities from a saw mill near-by PSI. This fuel is recovered from the log cutting at the saw mill and has an original humidity of 30-45% (kg water/kg raw fuel). It is dried in an oven at 60°C to ca. 5-10% humidity before it is used in the gasification experiments. The elemental composition of this fuel was measured in the Swiss Federal Laboratories for Materials Testing and Research (EMPA Dübendorf) and is shown in Table 2.7. The lower heating value (LHV) of the fuel was calculated based on the average elemental composition using to the following equation [2.9]:

$$LHV = 34.8 \cdot w_{C,daf} + 93.9 \cdot w_{H,daf} + 10.5 \cdot w_{S,daf} + 6.3 \cdot w_{N,daf} - 10.8 \cdot w_{O,daf} \quad (2.8)$$

yielding the LHV in MJ/kg dry, ash-free (DAF) fuel and where $w_{i,\,daf}$ are the contents of the elements on a DAF basis.

Table 2.7: Elemental composition of SCW in mass-% on DAF basis. Ash and chlorine contents in mass-% respectively in mg/kg on raw basis.

Element	Sample 1	Sample 2	Mean
C	51.00	50.28	50.64
H	6.54	6.37	6.46
N	0.08	0.05	0.06
S	0.02	0.02	0.02
O (by difference)	42.37	43.27	42.82
Ash	0.27	0.35	0.31
Cl	<500	<500	<500
LHV [MJ/kg$_{DAF}$]			19.068

The particle size distribution was measured by sieve analysis for the dried and the raw, wet fuel. The curves are displayed in Figure 2.20. The mean particle diameter calculated from these distributions are 430µm for the dry fuel and 620µm for the raw, wet fuel.

Figure 2.20: Particle size distribution of SCW and of milled SCW.

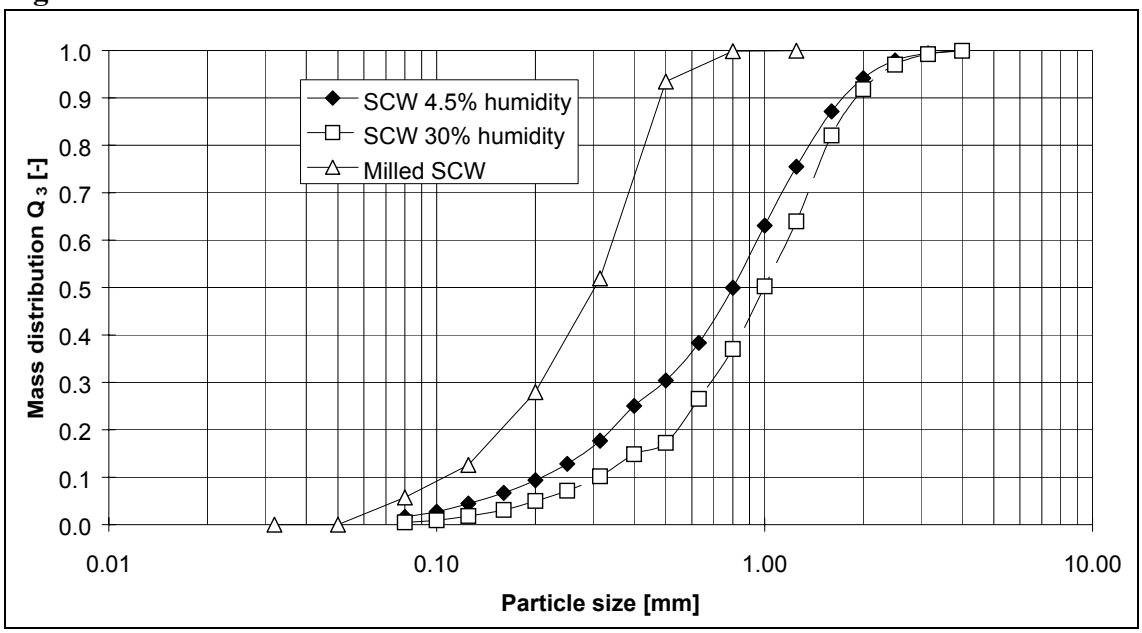

The second fuel used was made by milling the SCW in a high-speed cross beater mill. This fuel was prepared from SCW to study the influence of particle size on gasifica-

tion. It is important to point out that, by this procedure, other fuel parameters namely the humidity and the composition can be regarded as identical to those of SCW enabling a unique base of comparison for the influence of particle size on gasification products. The resulting particle size distribution is shown in Figure 2.20 and the corresponding mean diameter is 220 μm.

The third fuel was again a modification of the SCW. To test for the effect of "aging" of the fuel, a batch of SCW was placed in the drying oven and heated to 100°C for approximately 190 hours. By this procedure it was hoped that chemical changes happening in the aging process of the wood could be accelerated. Particle size and composition are assumed to be the same as those of SCW. The humidity of the aged SCW was adjusted to 5-10% by mixing a suitable but small amount of fresh, raw SCW with the artificially aged fuel. This mixture was placed in plastic bags and allowed to equilibrate its humidity over several weeks.

The fourth fuel used is scrap or waste wood, which will be referred henceforth by its German denomination "Altholz" (AH). This particular Altholz was obtained from a cement plant which was using it to replace part of the coal burned in the cement kiln. To burn this fuel with the existing burner equipment, pre-treatment steps were required. The bulk Altholz was delivered to the cement factory where is was first crushed to splinters of approximately 1 x 5cm. It was then separated from ferrous as well as non-ferrous metals, from stones and finally milled to a size suitable for the pulverised coal burner. Prior to milling, the splinters would be transferred to large storage bins not only for logistic purposes but also to mix different day batches achieving a certain degree of homogeneity of the fuel. It is not possible to establish the exact origin of this material. It can however be assumed, that most of it comes from the activities in the building industry. A simple elemental analysis from this fuel was performed by EMPA Dübendorf and is shown in Table 2.8. The Altholz exhibits a similar composition to SCW in terms of the main elements carbon, hydrogen and oxygen. Higher amounts of nitrogen, sulphur and chlorine as well as a higher ash contents are however observed for Altholz. No detailed analysis on the trace elements was performed, but literature data for other Altholz sources reported in Chapter 1 (see Table 1.2 on page 5) showing further differences between the two fuels.

Table 2.8: Elemental composition of Altholz in mass-% on DAF basis. Ash and chlorine contents in mass-% respectively in mg/kg on raw basis.

Element	Sample 1	Sample 2	Mean Altholz	Mean SCW
C	51.07	52.53	51.80	50.64
H	6.53	6.54	6.54	6.46
N	0.64	1.04	0.84	0.06
S	0.09	0.14	0.12	0.02
O (by difference)	41.67	39.75	40.71	42.82
Ash	4.36	10.55	7.46	0.31
Cl	1240	1580	1410	<500
LHV [MJ/kg$_{DAF}$]			19.812	19.068

The particle size distribution was measured by sieve analysis for 11 samples of this fuel taken from three different production batches. Typical results are given in Table 2.21. The particle size distribution of the samples analysed does not vary largely, a consequence of the pre-treatment procedure applied at the cement plant. This fuel has a larger fraction of fines compared to SCW, its mean particle size is 330µm with a standard deviation of 25µm. From a detailed analysis of the particle sizes of these 11 samples it was however found, that segregation may occur during the transportation of the fuel. The particle size determination for the sample taken from the topmost layer of one of the transportation containers revealed a coarser distribution than all other samples ($\bar{d}_p$ = 512µm). Caution must be thus used when a sample is taken from these transportation containers.

The ash contents and the humidity was also determined for these 11 samples. As another consequence of the pre-treatment procedure, the humidity was found to be very consistent from sample to sample: 6.7 mass-% (on wet fuel basis) with a standard deviation of 0.2 mass-%. On the other hand, the ash contents is subject to larger variations, indicating the heterogeneous nature of this fuel. The mean ash contents of the 3 batches was 7.8 mass-% (on wet fuel basis) and the standard deviation 1.8 mass-%. The heterogeneicity is clearer when this standard deviation is put in relation to the mean value, yielding a relative standard deviation of 22.4% of the ash contents.

Figure 2.21: Particle size distribution of Altholz.

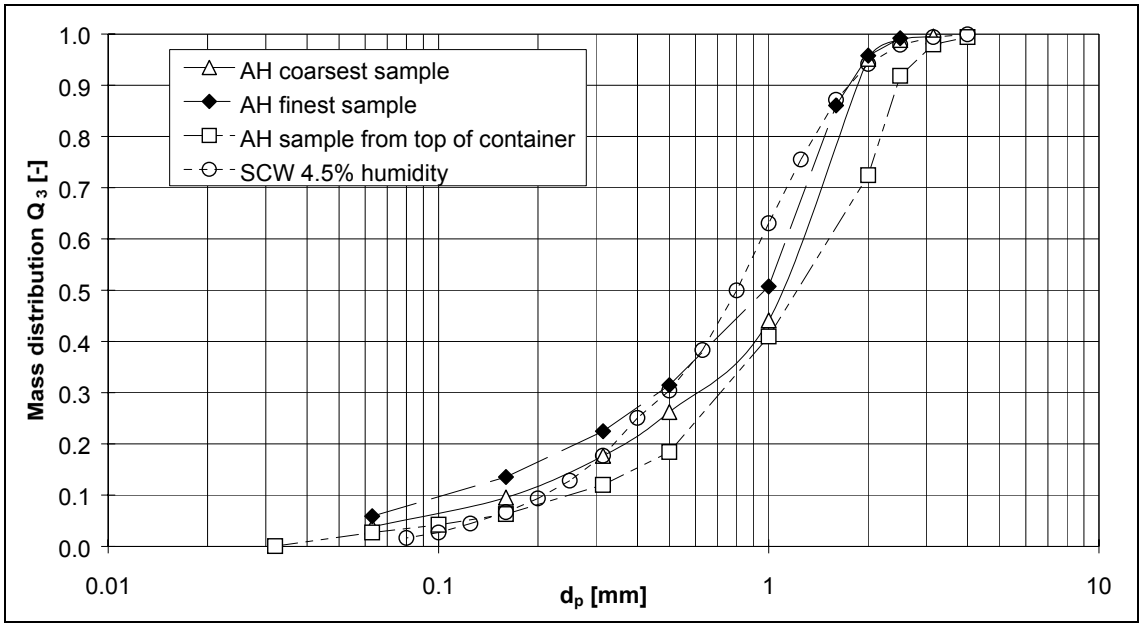

Finally the fifth and sixth fuels studied are mixtures of Altholz with high density polyethylene granules and mixtures of Altholz with polystyrene granules. The plastics used have the properties shown in Table 2.9 and the particle size distribution given in Figure 2.21. The LHV was calculated using Equation 2.8 and is in good agreement with literature data. For an account on the reasons for the choice of these polymers and the mounts mixed with Altholz see the discussion on the experimental plan on page 129.

Table 2.9: Characteristics of the plastics used.

Property	**Polyethylene**	**Polystyrene**
Commercial name	Rigidex HD 5502GA (BP Chemicals)	Standard polystyrene HH 111 (BP Chemicals)
Density [kg/m^3]	954	1050
Mean diameter [mm]	3.5	2.8
Composition [mass%]		
C	85.6	92.3
H	14.4	7.7
LHV [MJ/kg$_{DAF}$] by Equation 2.8	43.294	39.376
LHV (literature data)	[2.11] 46.412	[2.12] 41

Two mixtures were prepared with each plastic to study the influence of the amount of plastics in the fuel. 10% and 20% plastics were mixed by weight with Altholz

using a rotary mixer. These mixture levels were chosen to simulate extremes in the plastics composition of the fuel for a large-scale gasification system.

Figure 2.22: Particle size distribution of plastics used.

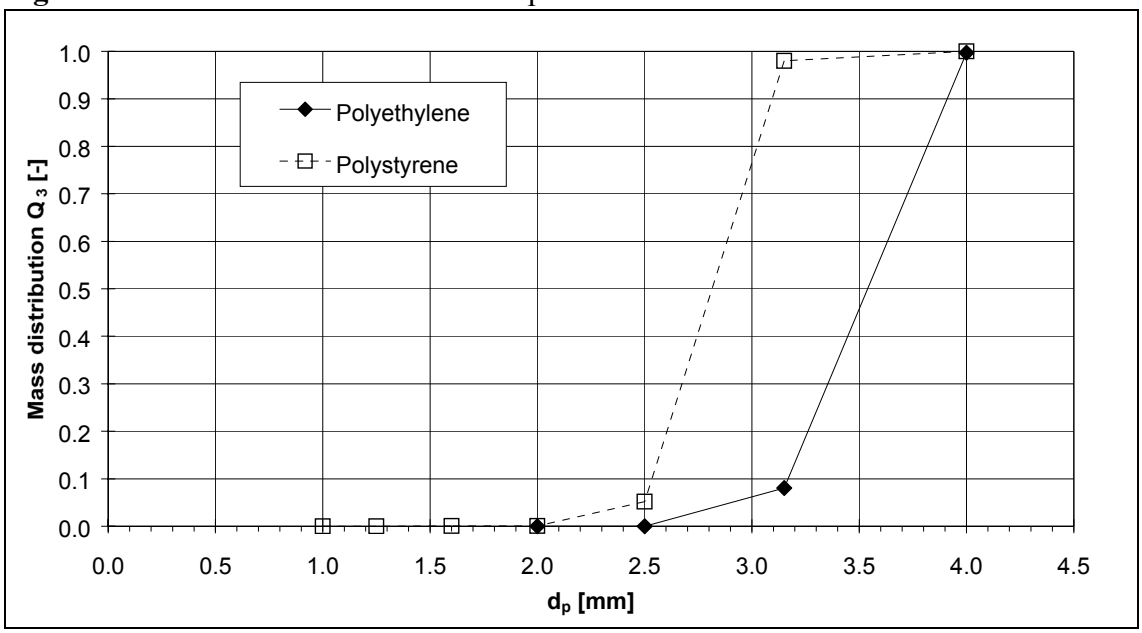

The elemental composition of the resulting fuels was calculated using the average values from the elemental analysis for Altholz. The ash contents and the humidity were measured in samples taken after the mixing process. The LHV was calculated using Equation 2.8 based on the resulting fuel composition, see Table 2.10.

Table 2.10: Elemental composition of Altholz/plastics mixtures on DAF-basis. Ash and humidity on wet fuel basis.

Element	**Altholz/Polyethylene**		**Altholz/Polystyrene**		**Altholz**
	10%	**20%**	**10%**	**20%**	
C	55.1	58.5	55.8	59.9	51.8
H	7.3	8.1	6.7	6.8	6.5
N	0.7	0.7	0.7	0.7	0.8
S	0.1	0.1	0.1	0.1	0.1
O	36.7	32.6	36.7	32.6	40.7
Ash	5.09	5.58	7.72	4.73	7.8
Humidity	6.50	5.79	5.53	5.75	6.7
LHV [MJ/kg$_{DAF}$]	22.161	24.509	21.769	23.725	19.812

2.9 Operating procedure of the plant

The gasifier was first operated on a one-experiment-per-day strategy. This strategy was changed as the experimental plan was modified (see section 5.1 on page 123). For the experiments according to the fractional factorial design only one set of operational conditions was planned for a daily run, whereas for the final experimental plan three operational conditions were studied in one daily run. As the results from the experiments according to the fractional experimental plan will not be reported, only operational procedures corresponding to the final experimental plan will be described in this section.

Three operational phases are required to run the gasification plant: a start-up phase, the actual experimental phase and a shut-down phase. Additionally, between experiments, several parts of the installation such as the particle and tar filters of the on-line gas sampling have to be cleaned and prepared for the next run. A maximum of 2 operating days in a week is possible with PSI's gasification plant.

Start-up

In the start-up phase, parts of the installation such as the gas pre-heaters, the steam superheater and the corresponding pipes are heated to their steady-state operational temperature.

Figure 2.23: Temperature evolution of air pre-heater and steam superheater (991005).

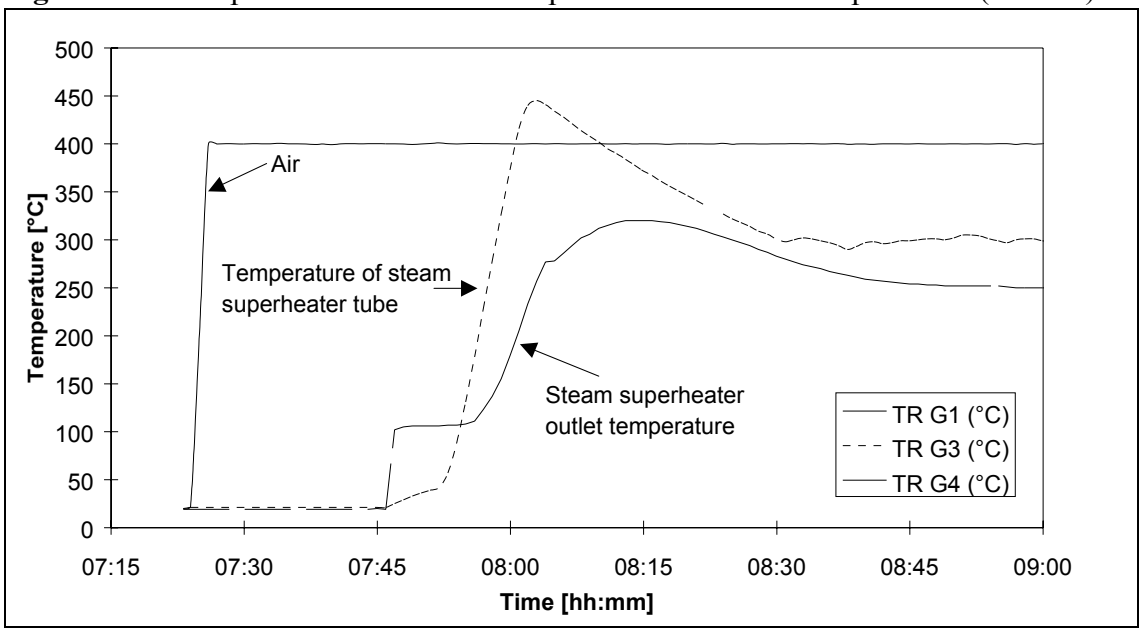

In all experiments reported in this thesis, air is always pre-heated to 400°C, and the steam is superheated to 250°C. Note that the steam superheater outlet temperature is controlled using a cascade control loop which uses the temperature of the outer surface of the tube inside the superheater as input, see Figure 2.23. This configuration allows for smoother temperature control and prevents overheating of the tube.

The bed is heated to 450-500°C, a temperature high enough to allow ignition of the fuel when it enters the bed. The bed is allowed to heat-up using primarily the heating shells surrounding the bed module as heat source. Efficient heat transfer from the bed module's walls to the bed is achieved by keeping the bed fluidised. At low bed temperatures (<150°C) this procedure requires air to be admitted by the oxygen flow path to ensure fluidisation. As the bed temperature rises, the minimum fluidisation velocity decreases. The gas flow is thus slowly decreased over time, always keeping the velocity ratio of superficial inlet velocity to minimum fluidisation velocity, u_0/u_{mf}, at a value between a minimum of 2 and a maximum of 5. The lower limit was chosen to ensure good fluidisation and thus sufficient heat transfer and mixing of the particles in the bed. The upper limit is chosen to keep the particles from being entrained out of the bed. Figure 2.24 illustrates the bed heat-up procedure.

Figure 2.24: Bed temperature evolution and gas flows during start-up (991005).

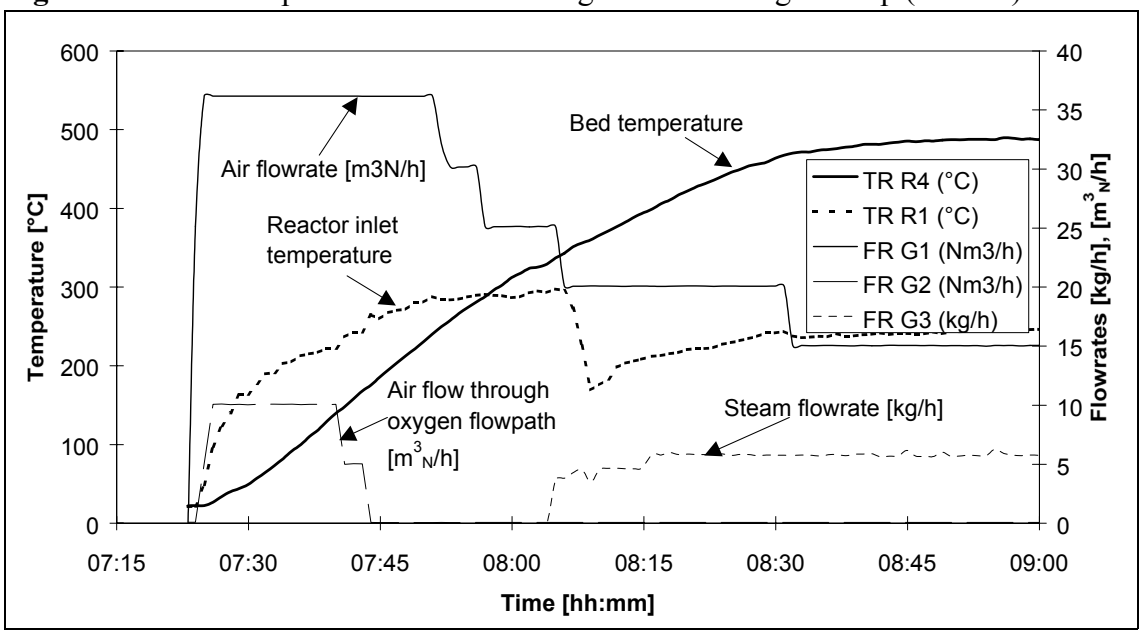

The minimum fluidisation velocity, the actual superficial velocity, the velocity ratio u_0/u_{mf}, and the transport velocity of the solids are calculated by a sub-program of the

data acquisition program using the measured gas flows and the bed temperature. u_0/u_{mf} is displayed on the visualisation screen. Parallel to the heat-up procedure of the bed, the reactor's freeboard is allowed to reach steady state temperature. The heat in the freeboard is also provided by the external heater shells of this part of the set- up.

To minimise tar deposition inside the exhaust piping it is allowed to reach 350-400°C before gasification is started. To accelerate the heat transport out of the reactor into the exhaust section, air is injected in the freeboard of the reactor. By this procedure the gas velocity in the bed is kept at acceptably low values and the gas mass flow out of the reactor is increased. This "secondary air" is of course turned off before the actual gasification experiment. Temperature evolution for the freeboard and exhaust gas section are presented in Figure 2.25.

In parallel to the plant's main components the filters of the gas sampling are allowed to reach their operational temperature of ca. 300°C.

Figure 2.25: Evolution of freeboard and exhaust section temperatures (991005).

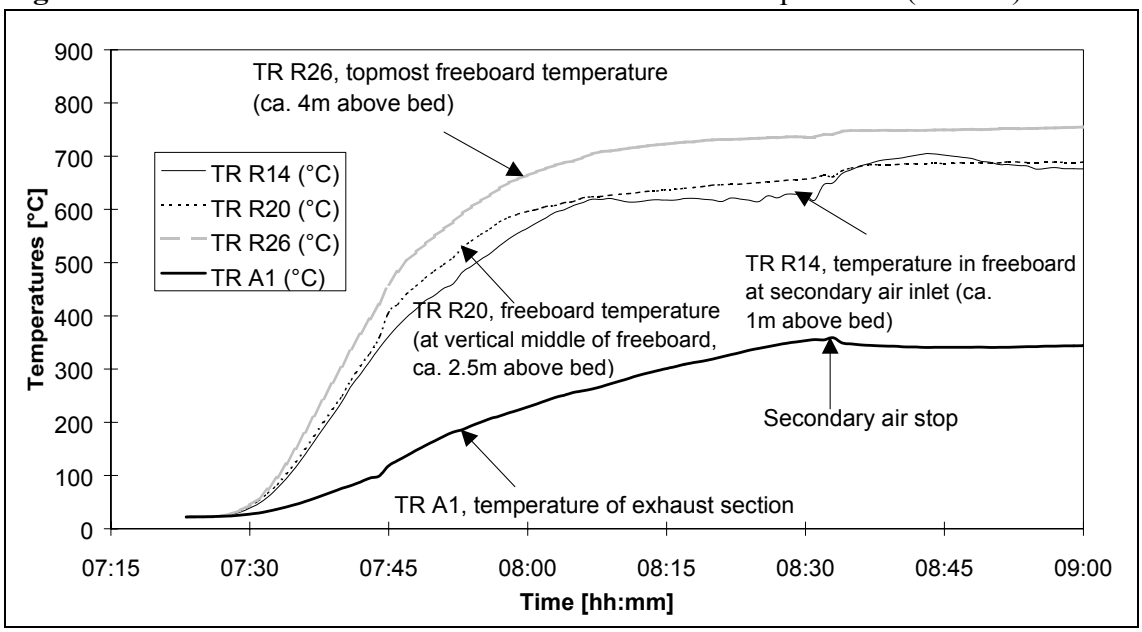

If an experiment with steam/oxygen as gasification agent is planned, steam is allowed to flow to the reactor as soon as the slower heating bed reaches a temperature of 300°C. By this precaution the condensation of water inside the reactor is avoided. Nevertheless, condensation occurs as steam is first fed through the still cold steam flow path to the reactor and the temperature in the reactor inlet drops, see Figure 2.24. The condensate

accumulated here is allowed to exit by the steam trap provided. The start-up procedure is completed in about 1.5 to 2 hours when all temperatures of the installation are stable. During the whole start-up procedure argon is blown into the stoker to prevent an exit of gases from the reactor and the connection between feeder and stoker is closed.

Experimental phase

In all experiments reported in this thesis, it was planned to run three different steady-state conditions with the same fuel in one day. The experimental conditions differed in the equivalence ratio (ER) used. ER is defined by the following equation:

$$ER = \frac{\dot{m}_{\mathrm{O}} / \dot{m}_{\mathrm{Fuel,daf}}}{(\dot{m}_{\mathrm{O}} / \dot{m}_{\mathrm{Fuel,daf}})_{min}} \text{ with} \tag{2.9}$$

$\dot{m}_{\mathrm{O}} / \dot{m}_{\mathrm{Fuel,daf}}$ being the ratio of the oxygen mass flow to the DAF fuel mass flow in the experiment and $(\dot{m}_{\mathrm{O}} / \dot{m}_{\mathrm{Fuel,daf}})_{min}$ being the ratio of the oxygen mass flow to the DAF fuel mass flow required for the stoichiometric combustion of the fuel. Note that in this calculation only the mass flows of oxygen supplied by either air or oxygen being fed to the reactor are taken into account, disregarding the oxygen input by steam in the case of a steam/oxygen experiment.

The stoichiometric oxygen to fuel ratio is calculated by the following equation [2.10] using the DAF elemental composition of the fuel to be gasified:

$$(\dot{m}_{\mathrm{O}} / \dot{m}_{\mathrm{Fuel,daf}})_{min} = \frac{M_{O_2}}{M_C} \cdot w_{\mathrm{C,daf}} + \frac{M_{O_2}}{2 \cdot M_{H_2}} \cdot w_{\mathrm{H,daf}} + \frac{M_{O_2}}{M_S} \cdot w_{\mathrm{S,daf}} - w_{\mathrm{O,daf}} \tag{2.10}$$

where M_i is the molecular mass of the element i.

The ER's chosen were 0.2, 0.3 and 0.4, covering the range of ER's usually applied in gasification systems. Furthermore, all experiments are carried out in autothermal mode, meaning that the heaters in the bed section are switched off as soon as gasification is started. Changing the equivalence ratio under these conditions brings about a change in bed temperature, roughly equating the above ER's to 700, 800 and 900°C in the bed. It was further decided to keep the freeboard at the above mentioned temperatures at each ER condition run. This experimental method was chosen, as the temperature in the freeboard of a gasifier will be either close to or lower than that of the bed (if no secondary oxidant inlet is provided in the freeboard zone). The variation in ER during an experiment is al-

ways performed by increasing the ER, meaning that the reactor's temperature will also increase as the experiment proceeds. This approach was chosen as it is faster to heat-up the installation than it is to allow it to cool down, since no other cooling means than natural convection and radiation are provided. The variations of ER were achieved by adjusting (decreasing) the fuel feed rate while keeping the flow of gasification agents constant. The flow of gasification agents was selected to yield a u_0/u_{mf} value of 2 at the lowest expected bed temperature of 700°C in the experiments to ensure a good mixing of the bed contents.

For air as gasification agent and the bed particles used in the present study, the above criterion immediately translates to an input flow of 24.4kg/h. In the case of steam/oxygen mixtures as gasification agent the total amount of oxygen fed to the reactor is kept constant and thus the DAF fuel input will be the same as in the air gasification experiments. The amount of steam was adjusted to meet the u_0/u_{mf} criterion yielding a steam flow of 5.8kg/h. Note that for balance calculation purposes (see page 143) a small flow of air of $1m^3_N/h$ (1.3kg/h) was also used in the steam/oxygen experiments. Using Equation 2.10 and the set-point ER's the fuel input mass flow can be calculated, based on the elemental analysis of the fuel to be used. Tables 2.11 and 2.12 summarise the set-points of the input mass flows used in this study.

Table 2.11: Set-points for fuel input mass flows (for all gasification agents used).

Fuel	Input fuel mass flow [kg_{DAF}/h] at		
	ER=0.2	**ER=0.3**	**ER=0.4**
SCW	19.7	13.1	9.9
AH	18.9	12.6	9.5
AH/10% PE	16.8	11.2	8.4
AH/20% PE	15.0	10.0	7.5
AH/10% PS	17.1	11.4	8.6
AH/20% PS	15.6	10.4	7.8

Table 2.12: Set-points for gas input mass flows.

Gasification agent	Input gas stream	Flow [kg/h]
Air	Air	24.4
Steam/Oxygen	Air	1.3
	Oxygen	5.4
	Steam	5.8

Shortly before starting the gasification experiment the MS is calibrated, the heavy tar filter (see page 91) is installed and its heating is started and the pilot flame of the flare is ignited. Argon is allowed to flow into the feeder and the pressure in both, feeder and stoker, is allowed to equilibrate. The connection between the two parts of the feeding system is then opened and argon is allowed to flow through the feeding system for at least 15 minutes before the feeding of biomass is started, sweeping out any air present to prevent dust explosions. The stoker screw is then set in motion and, shortly after, the feeder screw is turned on. The initial rotation speed of the feeder is chosen according to previously observed RPM/biomass feed rate relationship.

For an experiment with air as gasification agent, the air flow is adjusted to the set-point value prior to the start of the biomass feeding. When steam/oxygen mixtures are used, the reactor contains a steam/air atmosphere before starting of the fuel feed. In this case, as soon as no oxygen is detected by the on-line MS in the product gases at the topmost sampling point the flow of air is gradually reduced and at the same time the flow of oxygen is increased to the set-point value. This precaution is taken to prevent the dangerous mixing of an oxygen rich atmosphere in the hot freeboard with combustible gases sweeping out of the bed as the reaction is started.

Figure 2.26: Start of an experiment (991214).

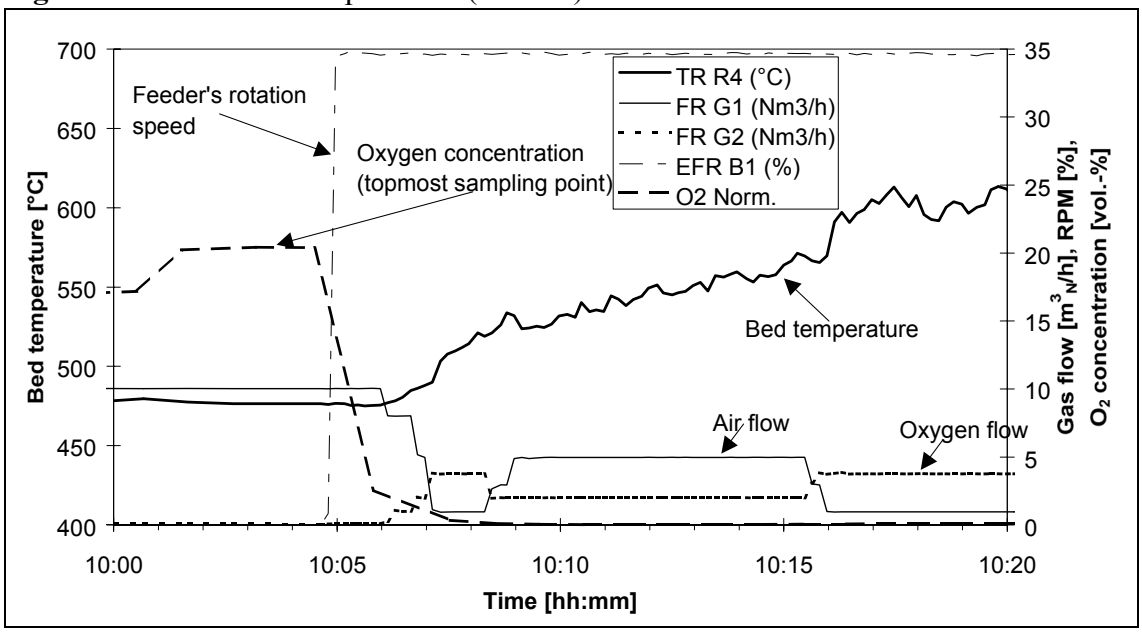

An example of the evolution of important operating parameters in this delicate start phase is shown in Figure 2.26. Note that in this specific experiment the air input had to be increased for a short period of time as defluidisation of the bed was observed.

When the biomass feed has been started and the gas flows have been brought to their set-point values, the reactor is allowed to reach steady-state. During this period, the biomass flow rate is constantly checked and if deviations from the set-point larger than ±0.5kg/h are observed the rotation speed of the feeder is adjusted.

Once the desired fuel mass flow is attained and the bed temperature is stable, the reactor is run for at least 30 minutes under the same conditions to make certain that the system is fully in steady state. Tar and ash sampling are then performed. As soon as sampling procedures are complete the operation conditions of the reactor are changed to the next (ER) set-point by reducing the fuel feed rate. At the same time the set-points for the freeboard heaters are increased and the heavy tar filter's heating is turned off. As before, the fuel feed rate is corrected and the installation is allowed to stabilise before sampling is repeated under the new conditions. This procedure is repeated a third time, completing the experiment. An example of the evolution of temperatures and gas composition during an experiment is shown in Figures 2.27 and 2.28.

Figure 2.27: Example of temperature evolution during an experiment. (991214).

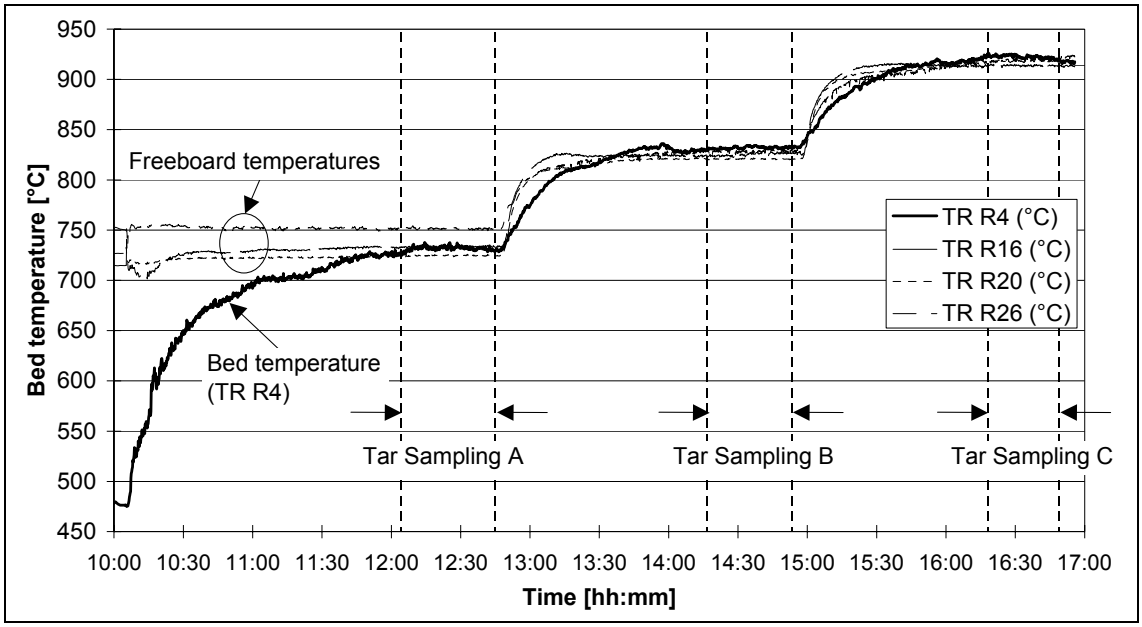

Figure 2.28: Example of gas composition evolution in an experiment. (991214)

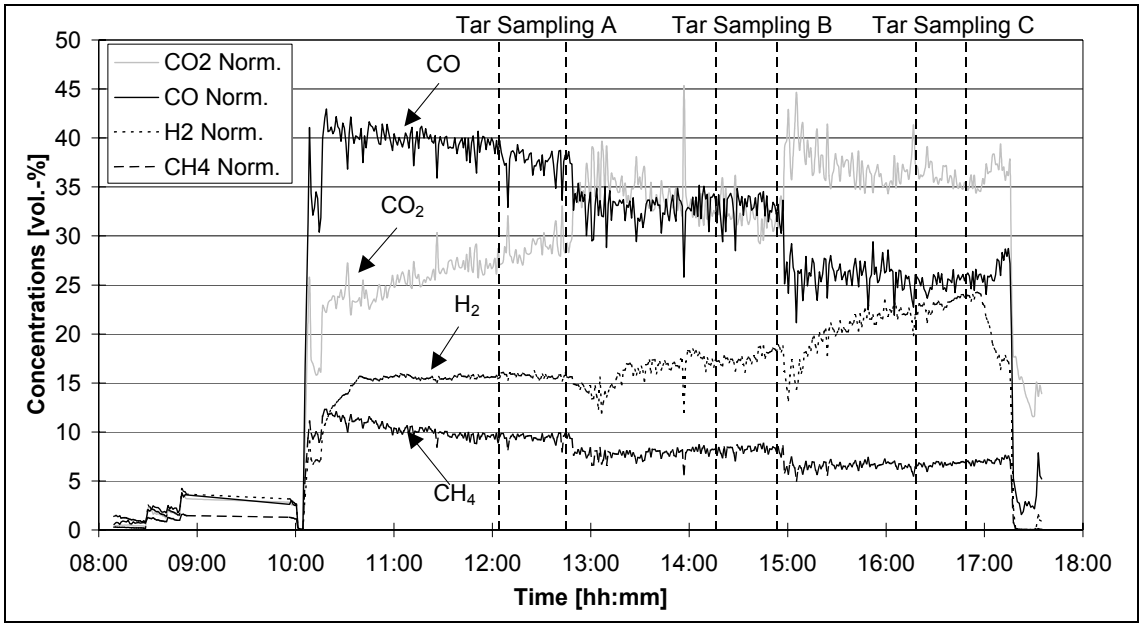

Shut-down

As soon as the last sampling is complete the freeboard heaters are turned off. Similarly to the start of the experimental phase, the oxygen is replaced by air for safety purposes when steam/oxygen is used as gasification agent. Shutting down the reactor is accomplished by turning off the fuel supply. This procedure takes the system through a short period of combustion, which might yield a short increase in the temperature of the bed. If this temperature is already high (>950°C) it must first be brought down by e.g. replacing some of the gasification agent by argon before the fuel feed is interrupted. In general, however, gasification is stopped almost instantly and the temperature of the bed starts to fall. As soon as this decrease is observed, steam input is stopped and the reactor is allowed to cool down under a small flow of air. An example of the shut-down is shown in Figure 2.29. The whole plant is then allowed to slowly cool over night before preparation tasks for the next run are executed.

Figure 2.29: Example of shut-down. (991214)

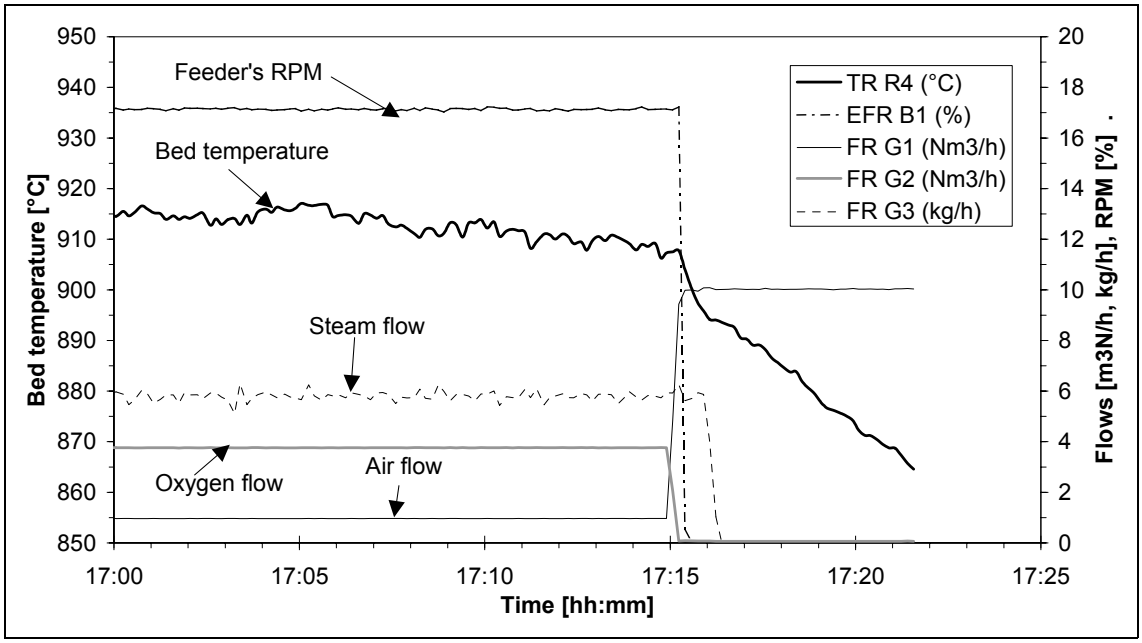

2.10 References

[2.1] Ph. Hasler, Th. Nussbaumer, R. Bühler, *Vergasung von belasteten Brennstoffen zu Synthesegas, Schlussbericht im Sektor Technik Projekt Biometh,* Bundesamt für Energiewirtschaft, Bern, 1995

[2.2] D. Kunii, O. Levenspiel, *Fluidization Engineering,* 2nd edition, Butterworth-Heinemann, 1991

[2.3] I. Navárez, A. Orio, M.P. Aznar, J. Corella, *Biomass Gasification with Air in an Atmospheric Bubbling Fluidized Bed. Effect of Six Operational Variables on the Quality of the Produced Raw Gas,* Industrial Engineering Chemistry Research, 1996, **35** (7), pp. 2110-2120

[2.4] Ph. Hasler, R. Bühler, Th. Nussbaumer, *Evaluation of Gas cleaning Technologies for Biomass Gasification,* in Biomass for Energy and Industry, Proceedings of the International Conference, Würzburg, Germany, 8-11 June 1998, pp.272-275

[2.5] T.A. Milne, N. Abatzoglou, R.J. Evans, *Biomass Gasifier "Tars": Their Nature, Formation and Conversion*, National Renewable Energy Laboratory, Report Number NREL/TP-570-25357, 1998

[2.6] J. Corella, J. Herguido, F.J. Alday, *Pyrolysis and Steam Gasification of Biomass in Fluidized Beds: Influence of the Type and Location of the Biomass Feeding Point on the Product Distribution,* in Research in Thermochemical Biomass Conversion, Proceedings of the International conference, Phoenix, Arizona, 1988, pp.384-398

[2.7] R.G. Wright, *On-Line Analysis of Complex Gas Mixtures by Mass Spectrometry*, Process Analytical Chemistry, 1998, **4**, pp.71-78

[2.8] Technical data sheets on Molochite, English China Clay plc., England

[2.9] R. Marutzky, *Erkenntnisse zur Schadstoffbilding bei der Verbrennung von Holz und Spannplatten*, Professorial dissertation, Wilhelm-Klauditz-Institut, Fraunhofer-Arbeitsgruppe für Holzforschung, Braunschweig, 1991

[2.10] H.D. Baehr, *Thermodynamik*, 7. Auflage, Springer-Verlag, Berlin, 1989

[2.11] *Polymer Handbook*, J. Brandrup, E.H. Immergut, E.A. Gulke (eds.), John Wiley & Sons Inc., 1999, pp.V/9

[2.12] *Ullmann's Encyclopedia of Industrial Chemistry*, B. Elvers et. al. (eds.), VCH Verlagsgesellschaft, Weinheim, Germany, 1992

3 PYROLYSIS, THE ORIGIN OF TARS IN GASIFICATION

3.1 Biomass pyrolysis

Gasification can be defined as the process in which organic materials are degraded by thermal reactions in the presence of sub-stoichiometric amounts of oxidising agents such as oxygen, carbon dioxide or water. This process ideally yields a gaseous phase composed of carbon monoxide, carbon dioxide, methane, hydrogen and water and a solid inorganic residue, the ash. Gasification of biomass is typically carried out at temperatures in the range of 700 to 1000°C. If the same biomass is heated in the absence of oxidising agents, it will thermally degrade and yield a complex mixture of organic compounds, gases and a solid carbonaceous residue named char containing also the inorganic compounds. This thermolysis process is called pyrolysis. The organic compounds formed in this pyrolysis step are referred to as primary tars. Gasification of biomass always includes a pyrolitic stage [3.1]. Fresh biomass particles entering a gasification reactor will be heated

and will first loose their moisture. As the temperature of the dry particles continues to rise pyrolysis occurs yielding the above mentioned products. The carbon in the residual solid char will finally react with the gasification agents, producing gases and leaving behind the inorganic constituents in the biomass, the ashes. A simplified scheme of these processes is shown in Figure 3.1 for a wood particle.

Figure 3.1: Simplified reaction scheme for a wood particle.

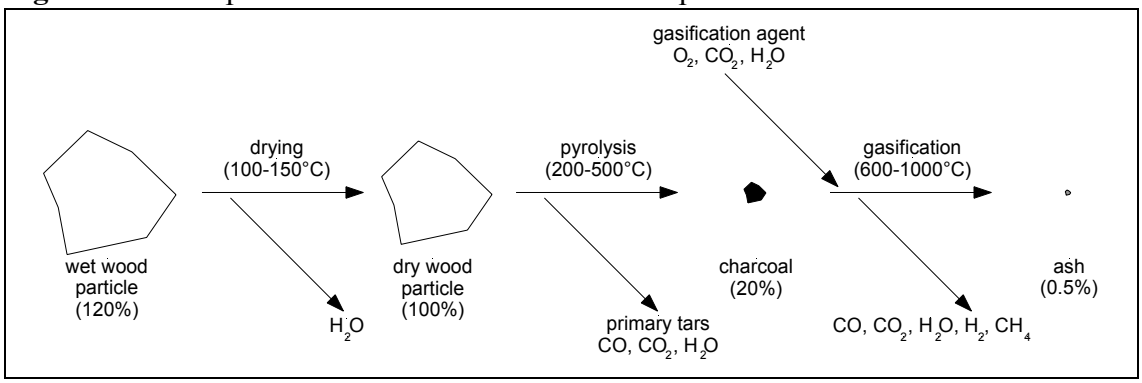

The primary tars formed in the pyrolysis step are at the origin of the tars in the gas exiting the gasifier. Biomass is not a single, chemically pure substance. It is composed of distinct fractions with dissimilar chemical reactivity and a more or less clearly identifiable chemical structure. The primary tars are the sum of the products of the thermolysis of the different biomass constituents. To understand the origin and properties of the tars at the exit of a thermochemical reactor a considerable amount of research has been carried out on the pyrolysis reactions of the single biomass constituents. The pyrolysis behaviour of biomass is not identical but only similar to the behaviour of its constituents [3.2]. Nevertheless characteristic products of the pyrolysis of these constituents are found in the primary tars.

3.1.1 The chemical composition of wood

Woody biomass can be separated into three fractions [3.3]: the cell wall components, components which may be extracted by solvents (then called extractables) and the ash. The cell wall components represent the bulk of the wood, and can in turn be further divided into cellulose, hemicellulose and lignin. Values for the contents of these 5 components in woods and different biomass are given in Table 3.1.

Table 3.1: Approximate composition in mass-% of different biomass species [3.4]. [1)]: sum of water and solvent extractables.

Species	Ash	Extrac-tables	Lignin	Hemicel-lulose	Cellulose
Softwood	0.4	2.0 [1)]	27.8	24.0	41.0
Hardwood	0.3	3.1	19.5	35.0	39.0
Wheat straw	6.6	11.1	16.7	28.2	39.9
Rice straw	16.1	17.9	11.9	24.5	30.2
Bagasse	1.6	0.3	20.2	38.5	38.1

The inorganic constituents or ashes represent less than 1% of the wood by mass but as shown above are much higher in herbaceous biomass. The ash is composed mainly of CaO, K_2O, Na_2O, MgO, SiO_2, Fe_2O_3, P_2O_5, SO_3 and Cl [3.3]. The first five oxides are the main compounds found in wood ashes with CaO as the most abundant of them. Traces of heavy metals are also present in wood ashes (see for example [3.6]).

Table 3.2: Compounds found in the extractable fraction of woods [3.3].

Volatile Oils (removed by steam or ether soluble)	
	Terpenes
	Sesquiterpenes and their oxygenated derivatives
Resins and fatty acids (soluble in ether)	
	Resin acids
	Fatty acids (oleic, linoleic and palmitic)
	Glyceryl esthers of fatty acids
	Waxes (esthers of monohydroxy alcohols and fatty acids)
	Phytosterols (high molecular weight cyclic alcohols)
Pigments (soluble in alcohol)	
	Flavonols, Pyrones, Anthranols (multi-ring naphthalenic and aromatic alcohols, chlorides, ketones and acids)
	Tannins (amorphous polyhydroxylic phenols)
Carbohydrate components (water soluble)	
	Starch
	Simple sugars
	Organic acids

The extractables consist of materials derived from the living cells in wood and make up 4 to 20% of the wood mass. The composition of the extractables varies widely. Some typical components of the extractable fraction are listed in Table 3.2.

Cellulose is the most abundant single component present in wood, representing some 40-50% by mass of the dry wood. Cellulose is a polymer of D-glucose monomers (i.e. a polysaccharide) bound together by ether-type linkages called glycosidic bonds. Its structure is shown in Figure 3.2.

Figure 3.2: Chemical structure of cellulose [3.7].

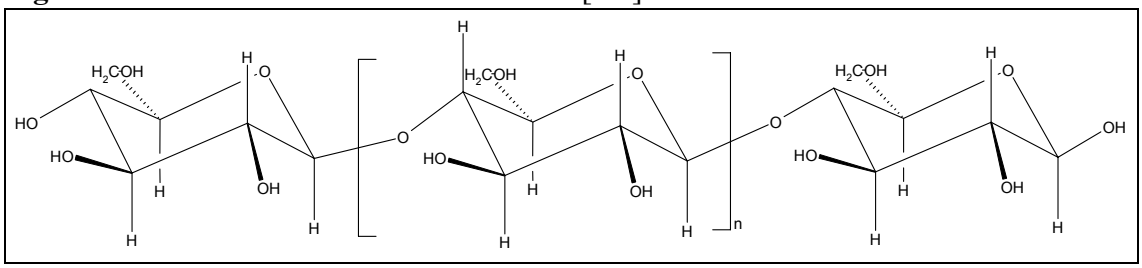

Cellulose is found in all biomass species. The degree of polymerisation (chain length) is however distinct in different biomass. The principal physical characteristic of cellulose is its extreme insolubility. It can only be dissolved by hydrolysis into sugars using strong mineral acids or enzymes. The long cellulose molecules may form both amorphous and crystalline agglomerates.

Hemicelluloses are also polysaccharides. They show however a large variation in their composition among the different biomass species. The name is somewhat misleading as hemicelluloses are not related to cellulose but distinct compounds of low and high molecular weight that contain neutral and acidic molecules. Most hemicelluloses are composed of two to four simpler sugars. The most important hemicelluloses are xylans, polymers of D-xylose, and mannans, co-polymers of D-glucose, D-mannose and D-gallactose. Their structure is shown in Figure 3.3. Hemicellulose constitutes some 25-30% by weight of most woods.

Figure 3.3: Hemicellulose structures [3.3], [3.7], [3.8].

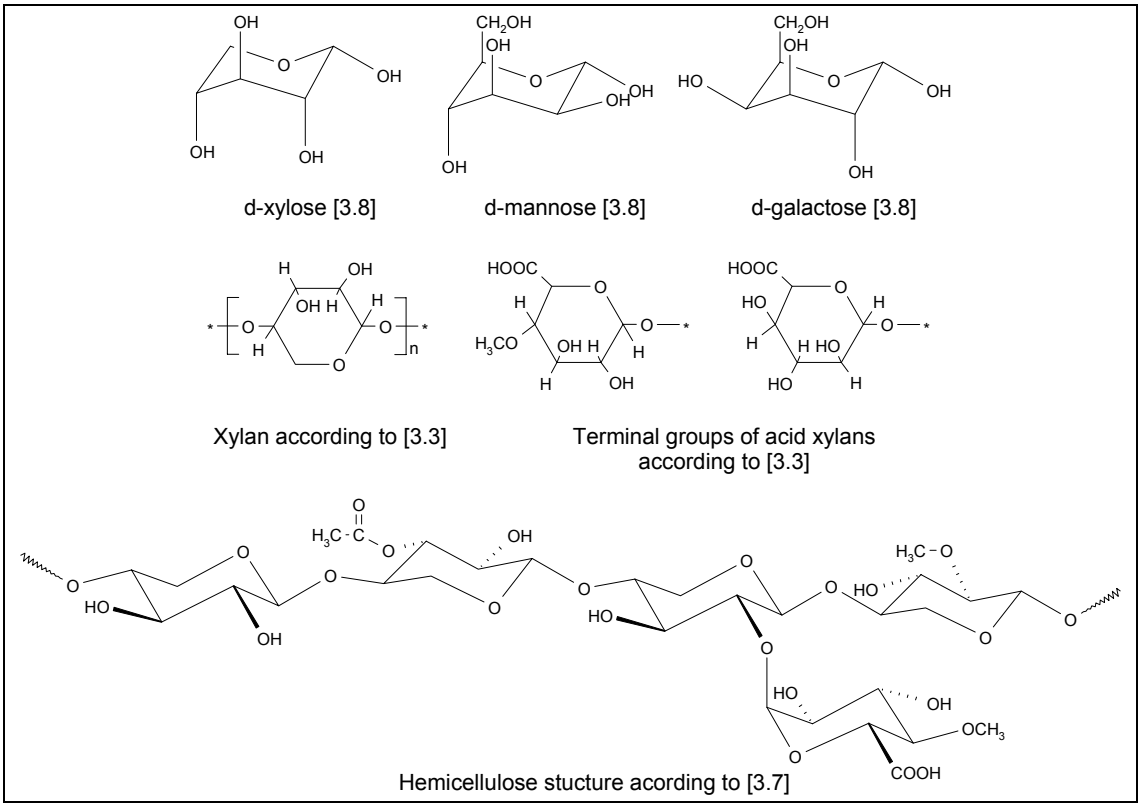

Lignin is the non carbohydrate component of the cell walls accounting for some 15-30% by mass of most woods. It is a complex three-dimensional polymer based on the phenyl-propane units shown in Figure 3.4. The exact structure of lignin is unknown but its composition is known to vary significantly between biomass species. A proposed structure for lignin is shown in Figure 3.5. One of the main problems when studying lignin is the impossibility of extracting it from the biomass without chemically modifying it.

Figure 3.4: Monomer units of lignin [3.3].

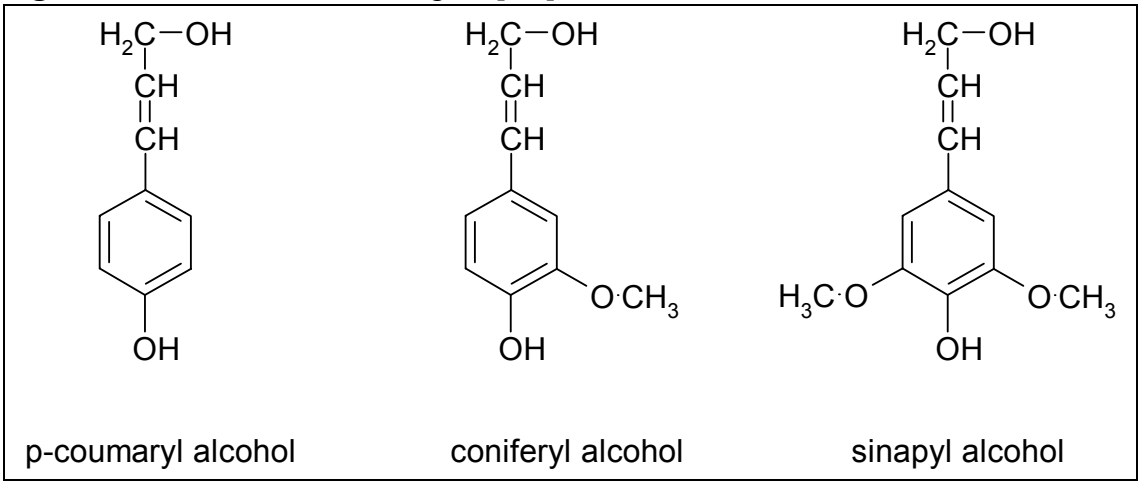

Figure 3.5: Representative structure of coniferous lignin [3.3].

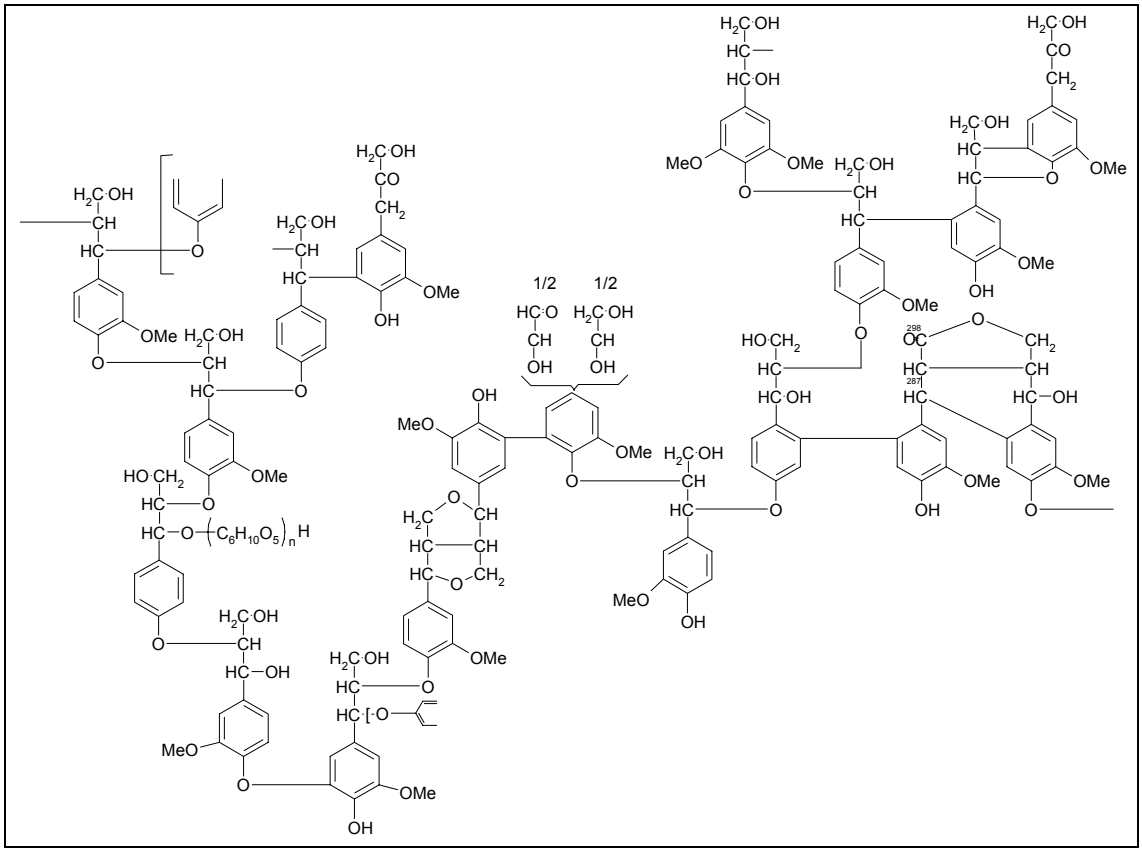

As already shown in Table 3.1, the proportions of the three main components of wood (cellulose, lignin and hemicellulose) vary between softwoods (coniferous woods) and hardwoods (deciduous woods). According to [3.9] the cellulose contents varies little between these wood categories (41-43%), more lignin is found in softwoods (27-28% versus 22-24% in hardwoods) and accordingly more hemicelluloses are present in hardwood (30-35% versus 25-30% in softwoods). Also within these wood categories as well as in the different parts of the tree the relative amounts of the main chemical constituents may vary: compression wood contains more lignin (ca. 40%) and tension wood more cellulose (> 50%). The main characteristic differentiating the two wood types is the structure of the woods. Softwoods exhibit a simpler structure made up of elongated (2-5mm) tracheids disposed mainly in the axial direction. The evolutionary more advanced hardwoods posses a functionally and morphologically more diversified structure, in which the most distinctive feature is the occurrence of vessels or pores.

The density of pure wood cell wall substance is close to 1500kg/m^3. However the apparent density of a piece of wood may vary widely (from 170kg/m^3 for balsa wood

to 1200 kg/m^3 for pock wood). This range results from the different volume fraction occupied by cell walls in each species (11% in balsa versus 80% in pock wood) the remainder of the volume being pores filled by air (in dry wood, water in wet wood). Physical properties of the wood such as its modulus of elasticity, strength, abrasion resistance, hardness and thermal conductivity are a function of the amount of cell material rather than of the chemical composition of the wood, and thus correlate well with the wood's density as shown in Figure 3.6.

Figure 3.6: Physical properties of different woods against wood apparent density [3.9].

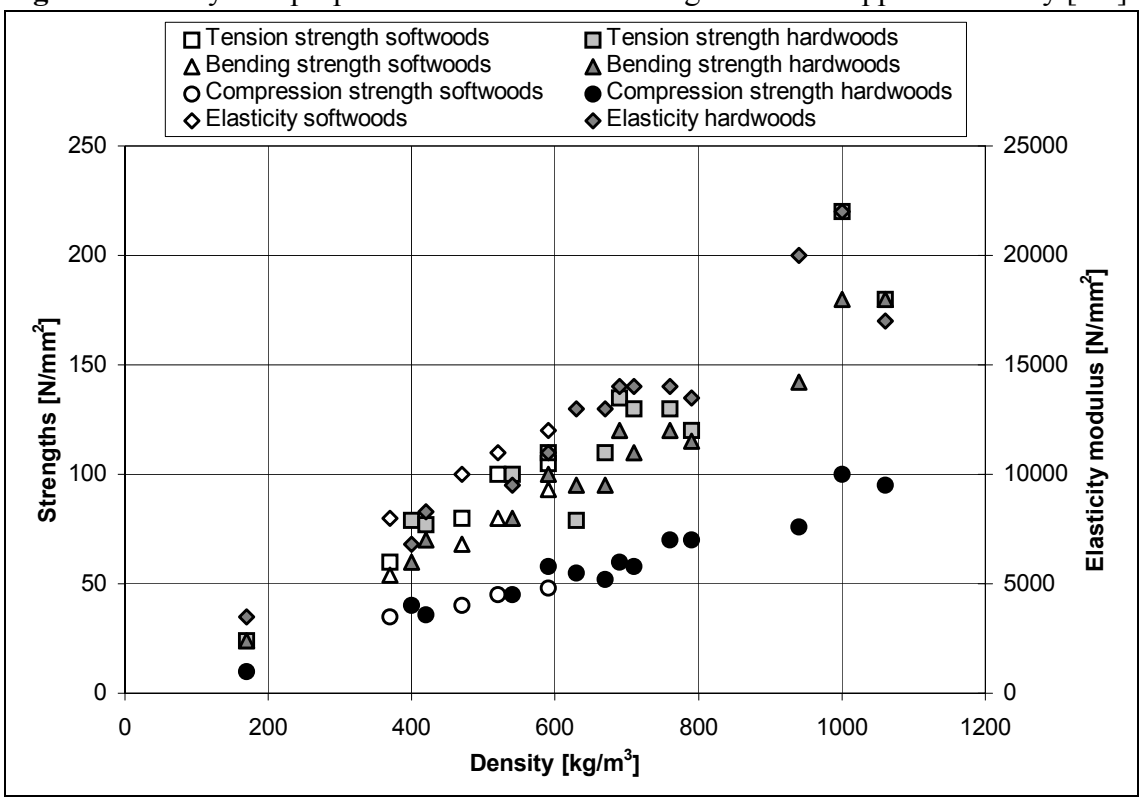

3.1.2 Pyrolysis behaviour of wood and its constituents

The literature on the pyrolysis behaviour of biomass and its constituents is vast. The different experimental techniques employed, the large number of biomass species studied and the distinct preparation methods for the single biomass constituents make a systematic review of this field very difficult. Such a review would definitely lie beyond the scope of this thesis. Detailed reviews of the chemistry and kinetics involved in the pyrolysis process of each component have been published (see for example [3.2], [3.10], [3.11] and [3.12]).

Pyrolysis of biomass leads to three major product groups: gases (composed mainly of CO, CO_2, CH_4, H_2 and lesser amounts of C_2-C_3 hydrocarbons), tars and char. The gross pyrolysis behaviour of the wood components may be summarised as follows [3.13] and has been confirmed by more recent studies [3.14], [3.15]:

1. Hemicelluloses are the most reactive compounds and pyrolyse between 225 and 325°C.
2. Lignins are the most thermally stable compounds and decompose progressively between 250 and 500°C.
3. Cellulose shows an intermediate reactivity and pyrolyses between 325 and 375°C. Cellulose depoymerisation starts at higher temperatures than lignin but proceeds faster and therefore in a narrower temperature range.

Parameters influencing the relative amounts of gases, tars and char are listed below:

Temperature: the pyrolysis process is a complex network of chemical reactions. At different temperatures, distinct chemical reactions may become rate determining yielding thus a different pyrolysis products distribution. The following models have been proposed for the pyrolysis of cellulose and solid biomass and illustrate this situation.

Figure 3.7: Proposed reaction mechanisms for cellulose pyrolysis [3.16], [3.17], [3.18].

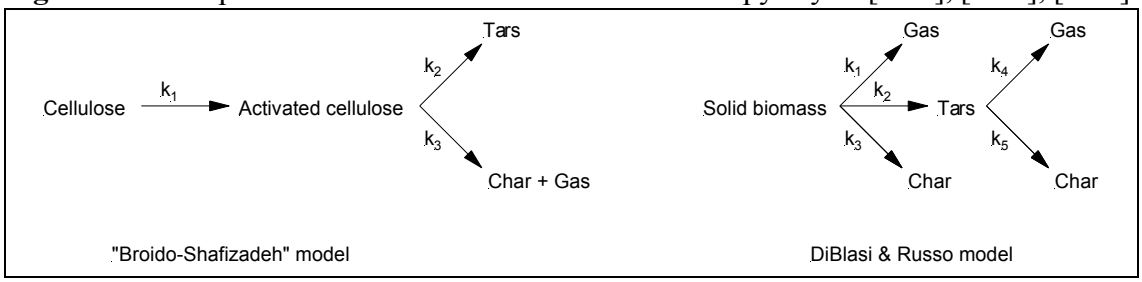

Heating rate: pyrolysis of biomass is an endothermic process. Biomass has a low thermal conductivity and thus the temperature in a pyrolysing particle may differ from that of the surrounding medium and temperature profiles can exist inside the particle [3.19]. This in turn will affect the distribution of pyrolysis products.

Size of the particles: this parameter influences the process in two ways. First it determines heat and mass transfer rates, and may thus change the temperatures inside the particle influencing thus the scope of pyrolysis products. Second, when primary pyrolysis

products evolve from the biomass matrix they may react with the solid or with other pyrolysis products inside the pores of the particle, again yielding different products [3.20].

Gaseous environment: heat transfer may be influenced by the properties of the surrounding gas. Also, differences in the relative yields of char, tars and gases are observed when pyrolysis is carried out in vacuum. Primary pyrolysis products may react with the gases once released from the pyrolysing particle.

Pretreatment of the materials studied: pretreatment procedures may extract inorganic [3.21] and organic compounds from the biomass or even modify the chemical structure of the biomass sample [3.22].

The extent of inorganic impurities/presence of catalysts: the presence of K, Li and Ca in woods is known to promote the formation of char at the expense of tars. Fe and Cu on the other hand increase the yield of levoglucosan and char in the pyrolysis of wood [3.23]. The presence of heavy metals, as studied in [3.24], seems to influence the composition but not the relative amount of the pyrolysis products char and volatiles (tar and gas).

The first two parameters, temperature and heating rate, are the most important ones. With respect to the heating rate it is usual to distinguish between [3.25] slow pyrolysis when heating rates smaller than 2°C/s are applied, and fast pyrolysis with heating rates in (large) excess of 2°C/s. Slow pyrolysis is known to achieve high char yields whereas fast pyrolysis leads to larger gas and tar yields. In fluidised bed systems, heat transfer rates are high, in the order of 50°C/s or larger depending on the size of the particles [3.2]. The temperatures in gasification systems are also high (700 to 1000°C) narrowing the conditions of interest for the discussion of the pyrolysis process to fast pyrolysis at high temperatures. Many authors discussed the influence of the above parameters on the three product groups, gas, tar and char without specifying or analysing the tar fraction in detail. Only a few have concentrated on the composition and nature of the tar generated by primary pyrolysis reactions. In fact it is a difficult task to accurately sample primary pyrolysis products as these may interact not only with the pyrolysing substrate but also with other primary pyrolysis products.

Under the conditions mentioned above, the primary tar products for the wood constituents are of rather low molecular weight, representing characteristic monomers of the biopolymers and fragments of these monomers [3.26]. Cellulose pyrolysis yields one

primary tar product, levoglucosan (see Figure 3.8), due to its structural homogeneity. Hemicelluloses will undergo a similar depolymerisation of the glycosidic units with of course a broader range of possible products due to the range of monomers present (see page 58). The authors of the mentioned study also show, how primary pyrolysis products of the carbohydrates are affected by the presence of even small amounts of inorganics such as potassium. This element, present in most biomass, catalyses a different reaction path yielding low levels of levoglucosan in primary biomass tars. This catalysis effect is one of the reasons why pyrolysis products from biomass are not identical to those of the pure constituents.

Figure 3.8: Structure of levoglucosan and suggested depolymerisation mechanisms of cellulose [3.26].

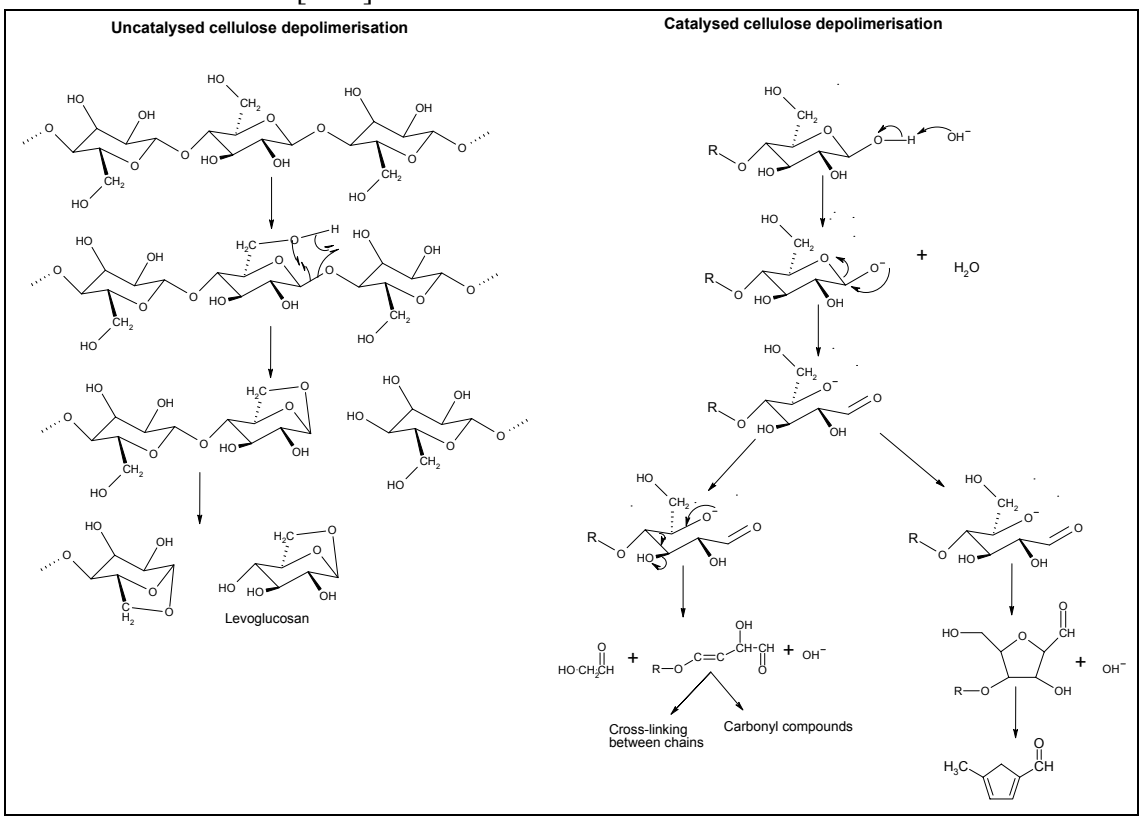

Lignin pyrolysis proceeds also through structurally controlled depolymerisation, but also involves significant homolysis yielding derivatives of the monomers [3.32] shown in Figure 3.9.

Figure 3.9: Tar constituents derived from lignin according to [3.32].

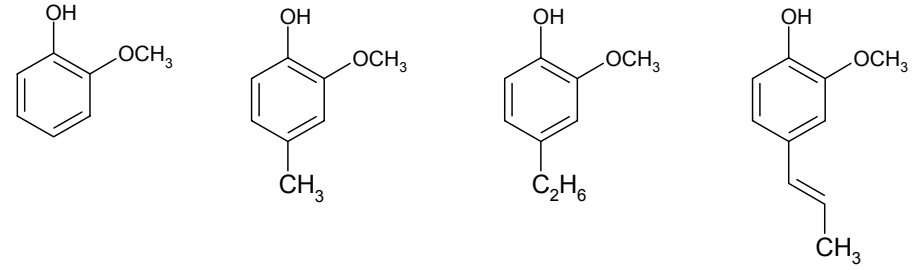

An evolution of different products can be clearly detected as pyrolysis progresses, relating the observed range of temperatures for complete pyrolysis of lignin to the complex structure of this biopolymer (see page 62) and the diverse types of bonding between the monomers (C-O-C but also C-C bonds).

However, in another publication [3.27], evidence is presented that the primary products of biomass pyrolysis are not strongly affected by temperature (400-900°C) or heating rate (in the range 0.5 to 50°C/s). This apparent contradiction is explained by the authors as follows. The sampling of pyrolysis products was carried out very closely to the pyrolysing particle. Therefore the products had little or no time to react once they have been released from the substarte. The temperature in the particle is buffered by the endothermic fast pyrolysis reactions minimising the effect of changes in the temperature of the surrounding gas on the particle itself. The particles used for the study of these parameters were of relatively small size (<6mm), so that the products had little chance of interacting with the solid carbon matrix after devolatilisation. The heating rate affected the relative amounts of gaseous/liquid and solid products, but the composition of the former was not greatly altered by this parameter. As the particle size was increased, secondary reactions are observed to alter the products detected. The water in the particles is driven away from them before pyrolysis reactions start, explaining why the moisture contents has little influence on the products detected.

This article shows the importance of precise knowledge on the conditions existing in a particle in pyrolysis experiments. Many of the deviations observed in the study of pyrolysis may be attributed to imprecise definition of the conditions in which the reactions occur. Only very carefully conducted experiments such as in [3.27] allow the observation of true primary pyrolysis products. In general experimental results will show secondary

besides primary reaction products as secondary reactions start almost instantly as soon as the primary products are released from the biopolymer.

3.1.3 Evolution of pyrolysis products

Hundreds of different chemical species have been identified in the tars from different pyrolysis processes [3.31]. This large number is partially explained by the variety of conditions of the pyrolysis experiments performed and by the diversity of biomass studied. The primary tars released from the pyrolysing particle will undergo further reactions once released from the pyrolysing substrate. These so called secondary reactions are far from being completely understood and are the object of ongoing research [3.32]. The tar composition at the exit of a gasifier will show characteristics deriving from their thermal history, their environment and of the type of biomass being processed. The changes in the composition of the primary tars have been studied both in the absence and in the presence of oxidising agents [3.26], [3.27], [3.28], [3.29], [3.30].

Thermal cracking of primary tars

An early characterisation of the evolution of primary tars is shown in Figure 3.10. The chemical groups reported in this progression are representative of the type of components found in tars from the short residence time processing of wood at the given temperature. These groups give an insight into the type of reactions involved: dehydrogenation, condensation (aromatisation), dealkylation and deoxygenation.

Figure 3.10: Progression of tars with temperature according to [3.30]. PAH: Polycyclic aromatic hydrocarbons.

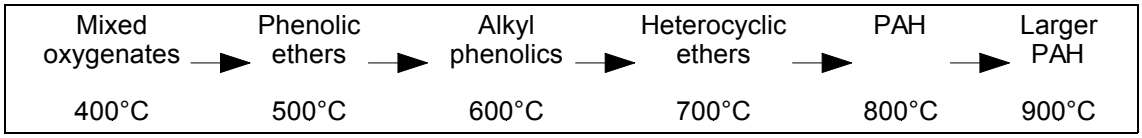

When primary tars are allowed to react at temperatures above 500°C, a steady decrease in the amount of resulting tars is observed while the amount of gas produced increases. Also both char and tar composition change as indicated by the observed dramatic changes in their oxygen contents. As temperature increases, the highly oxygenated pyrolysates are converted to thermally stable oxygenated compounds. Eventually these inter-

mediates are further deoxygenated forming highly aromatic structures. Additionally, alkylated aromatics gradually loose their side chains at high temperatures [3.30].

A similar progression was observed [3.26], [3.27] for the pyrolysis of both, biomass and its constituents. When primary pyrolysis products were allowed to react at high temperatures, a continuous change in the nature of the products was observed. Depending on the temperature, characteristic products were observed to form by gas-phase thermal cracking from the primary pyrolysis tars. As a result a systematic classification of pyrolysis products can be made:

1. Primary pyrolysis products characterised by levoglucosan, hydroxyacetaldehyde, and furfurals derived from cellulose, analogous products for hemicellulose and methoxyphenols derived from lignin.
2. Secondary products formed between 500 and 700°C characterised by phenolics and olefins.
3. Alkylated aromatic tertiary products formed between 700 and 850°C composed of methyl derivates of aromatics such as toluene or methyl naphthalenes as well as indene and phenols.
4. Condensed aromatic tertiary products formed above 850°C characterised by aromatic compounds without substituents (i.e. benzene, naphthalene etc.).

Figure 3.11: Distribution of the four tar component classes as a function of temperature [3.28]

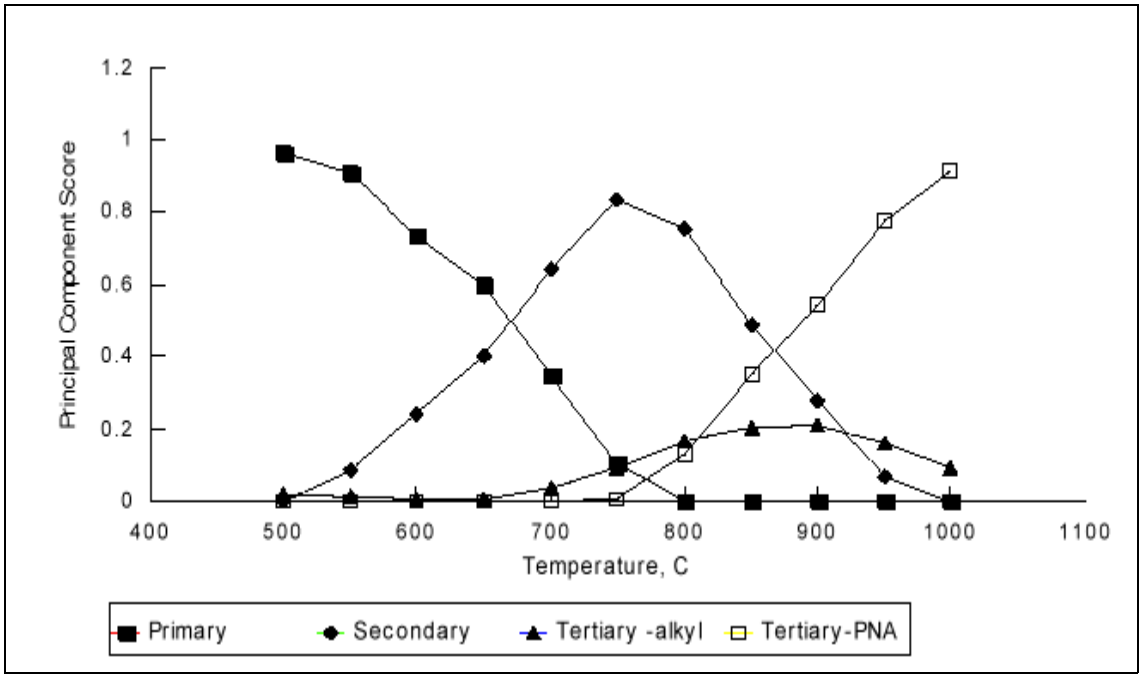

The evolution of these products with temperature is shown in Figure 3.11. Note that in this plot tar composition and not yields at a given temperature are shown (i.e. the numbers always sum to 1) thus no direct conclusion regarding total tar cracking can be made. Primary tars are completely transformed into secondary products before the aromatics and polyaromatics form.

In a recent study [3.32], the mechanisms involved in the transformation of phenolic compounds to low molecular weight aromatics such as naphthalene and indene were elucidated. The high molecular weight PAHs were shown to derive from oligomers of the primary tar constituents shown in Figure 3.9.

The influence of oxidising agents

Early studies with a secondary tar cracking reactor [3.33] showed that the addition of steam and steam/oxygen mixtures at high temperatures (950-1250°C) reduces the amount of tar. The modifications of the tar composition were studied in more recent papers [3.28], [3.29] under milder conditions (600-800°C) with oxygen. The presence of oxygen accelerates both the destruction of primary tar products from the carbohydrates through specific oxidation reactions and the formation of aromatic compounds from the lignin derived phenolic compounds. The amount of aromatics formed by thermal cracking is shown to even increase in the presence of low amounts (less than 10%) of oxygen in the gas as presented in [3.28] for naphthalene. Only above 10% a decrease in the amount of naphthalene was observed. A net increase in the CO level could also be observed as the product from the oxidative cracking of tars. A further important result from this study is that benzene levels where not affected by the presence of oxygen.

3.1.4 The tars of a biomass gasifier

From the previous exposition on reactions involving the pyrolysis products, a complex mixture of compounds of largely aromatic nature must be expected in the tars of a gasifier. Gasifiers operate at temperatures ranging from 700 to 1000°C and oxygen levels of 20 to 40% of the oxygen required for complete oxidation of the fuel are present. The exact composition of these tars will be a function of the "severity" of the gasification or in other words of the thermal history of and the availability of oxidising compounds to the pyrolysis products. High temperatures and high oxygen levels will yield a tar largely

formed of PAHs. The amount of tars is expected to be lower at high oxygen levels. Low temperatures and low oxygen levels will produce a more complex tar, composed partially of PAHs but also containing secondary pyrolysis products, i.e. phenolic compounds.

3.2 Pyrolysis of plastics

As pointed out in Chapter 1, plastics were also considered in the BIOMETH study as interesting fuels for the gasification to methanol process demonstration in Switzerland. The plastic types considered in the present study are polyethylene and polystyrene. Just as the biopolymers in biomass, these synthetic polymers also display characteristic pyrolysis properties and products. These products may lead to the formation of tars in the gasification process. An overview of the pyrolysis of these two compounds is given in the following sub-sections.

In the case of synthetic polymers the structure and the mode of thermal decomposition are intimately related [3.7]. As with biomass the resulting yields of products of pyrolysis are dependent on various parameters. Particle size, heating rate and temperature have an impact on the heat and mass transfer and affect potential secondary reactions in the bulk of the sample or in the gas phase leading to variations in the composition of the volatiles. Environmental factors such as the surrounding gas and the presence of a catalyst may bring a change in decomposition pathway and lead to a distinct products distribution. Moreover, the numerous additives present in commercial plastics (fire retardants, fillers etc.) may have an impact on the resulting products. The product distribution in a pyrolysis process has to be derived experimentally, with the operating temperature, heating rate, catalytic effects, residence time of feed material and reaction products, reaction pressure, possible supply of reactive gases (such as oxygen, hydrogen) and, of course, the chemical constitution and structure of the original plastics as major factors [3.34]. The composition of tars from a gasifier operating on plastics as input will thus also have to be derived experimentally.

3.2.1 Chemical structure of polyethylene and polystyrene

Polyethylene is the major tonnage plastics material worldwide, in 1990 the production capacity of polyethylene was 34 million tons [3.35]. Polyethylene is made from the monomer ethylene by different processes yielding a polymer with the simplified chemical formula $-(-CH_2-)_n-$. Depending on the process used in the production basically three types of polyethylene can be produced. The differences in the structures of these polymers is shown in Figure 3.12.

Figure 3.12: Schematic molecular structure of polyethylenes [3.35].

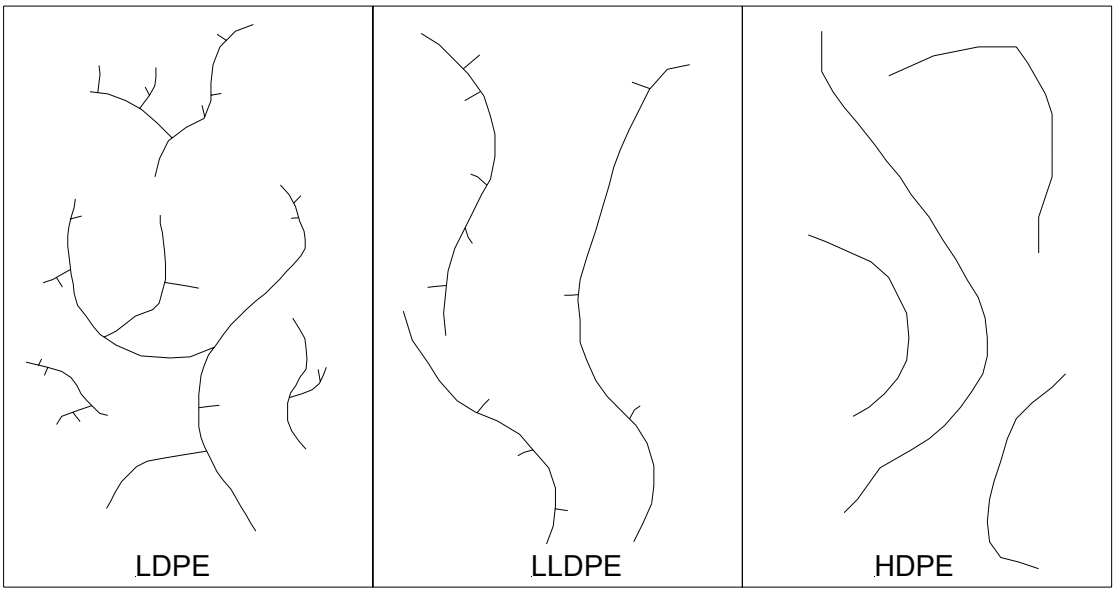

The older production process employing high pressures (above 100 MPa) and occurring through free-radical polymerisation yields a product of high density (in the order of 960 kg/m^3) called high density polyethylene (HDPE). HDPE is essentially free of both long and short branching. Its molecular mass distribution is dependent on the catalyst used but is typically of medium width.

A more recent process for the production of polyethylene is carried out at lower pressures in the presence of so called coordination catalysts yielding a polymer of lower density (around 920 kg/m^3) accordingly called low density polyethylene (LDPE). LDPE has a random long branching structure with branches on branches. The molecular mass distribution of LDPE (i.e. the chain length of the polymer) is moderately broad.

Further refinement of the catalysts employed in LDPE production allowed for the production of a low density polymer with less branching called linear low density pol-

yethylene (LLDPE). LLDPE has branching of uniform length which is randomly distributed along a given chain.

Polystyrene belongs to the group of standard thermoplastics that also includes polyethylene, polypropylene and polyvinyl chloride. Because of its special properties, polystyrene can be used in an extremely wide range of applications. The annual consumption worldwide in 1990 was ca. 6.7 million tons. Polystyrene molding materials are transparent, hard and brittle plastics. The mechanical properties can be improved by the use of mixtures of polystyrene with rubber-like materials such as polybutadiene yielding the so called high-impact polystyrene (HIPS). The rubber particles in HIPS scatter visible light, thus making the material loose its transparency.

Polystyrene is produced from styrene monomer by a free-radical polymerisation mechanism yielding products with a molecular mass in the range of 100000 to 400000 Da. The polymer obtained is a linear hydrocarbon chain with phenyl side groups linked, on average, to every second carbon atom in the main chain. The chemical structure of polystyrene is thus $-(-CH_2-CH(C_6H_5)-)_n-$.

The exact composition of a specific polyethylene or polystyrene is further determined by additives such as antioxidants, stabilizers, pigments etc. present in virtually all commercial polymers.

3.2.2 Pyrolysis of polyethylene

The primary mechanism of polyethylene thermal decomposition has been established as the a random chain scission mechanism exemplified in Figure 3.13.

The product distribution is dependent on the reactivity and possible reactions of the various radicals produced [3.47]. Experimental investigations of the pyrolysis products of polyethylene are reported by a large number of authors in the literature. The main goals of these studies have been either the determination of the thermal degradation mechanism of polyethylene or the ascertainment the of optimal conditions for recovery of specific valuable products from plastic wastes via special pyrolysis process. Again as in biomass pyrolysis a large variety of reactor types (fluidised beds, fixed beds, thermogravimetric reactors and isothermal reactors), reaction conditions (temperature, heating rates, residence time of products, gaseous environments) and sampling/analysis (condensation, absorption in solvents, direct mass spectrometry, gas chromatography with various detec-

tors) methods have been used, making comparison of results difficult. From these experimental studies, it can however be said that the product distribution form the pyrolysis of polyethylene is largely dependent on the temperature of the pyrolysis process.

The random scission mechanism mentioned above theoretically yields a broad spectrum of alkanes and alkenes of varying chain length. This product distribution is found in low temperature (300-600°C) degradation studies ([3.37], [3.38], [3.39], [3.40], [3.41]). The products reported are mainly alkenes and alkanes with chain lengths up to C_{60} (although this limit can be related to the analytical methods used) often referred to as "waxes". In this temperature range only a minor part of the polymer is converted to gaseous C_1-C_4 alkanes and alkenes. The amount of solid residue reported (char or unconverted polymer) is always very low (< 1% of the original polymer). No aromatic hydrocarbons are observed in the products from low temperature pyrolysis of polyethylene.

Figure 3.13: Degradation mechanism of PE [3.36].

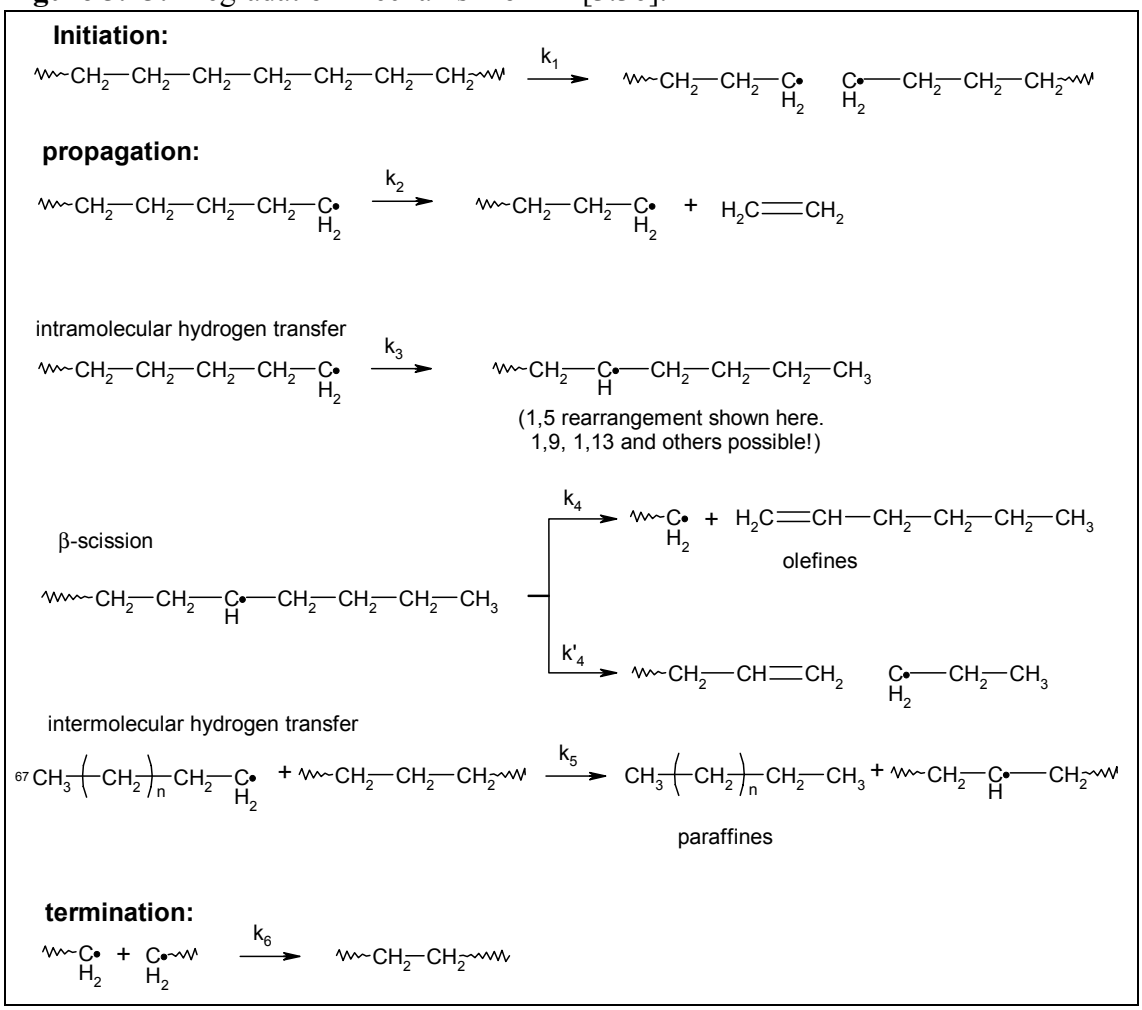

At high temperatures (600-900°C), dramatic changes in product distribution are observed ([3.42], [3.43], [3.44]). Solid residues disappear completely. The amount of condensible alkanes and alkenes decreases steadily with the temperature and the amount of gases produced increases. The amount of alkenes and methane in the gases increase as temperature is raised. Also the composition of the condensible products changes. The size of the alkenes/alkanes in this "oil" or "wax" product decreases. Aromatic compounds ranging from benzene to phenanthrene and larger polyaromatics as well as alkylated aromatic compounds are observed already at 650°C. The amount of these aromatic products increases with increasing temperature but the number of aromatic compounds present decreases as suggested by size exclusion analysis. PAHs are also reported in pyrolysis experiments conducted under steam atmospheres [3.45].

The role of the residence time on secondary reactions at high temperatures is not clear. The product distribution resulting from different experiments with short residence time (0.4-0.6s) [3.46] and (0.1-1s) [3.52] show inconclusive results regarding the presence of aromatic compounds. Experiments with a "pyroprobe" pyrolyser [3.43] where residence time of primary or secondary products at high temperatures should be almost nil show the presence of aromatic hydrocarbons.

Similarly to biomass pyrolysis the series of reactions shown in Figure 3.14 has been proposed and is supported by the experimental evidence discussed above.

Figure 3.14: Reaction scheme for PE pyrolysis (adapted from [3.52]).

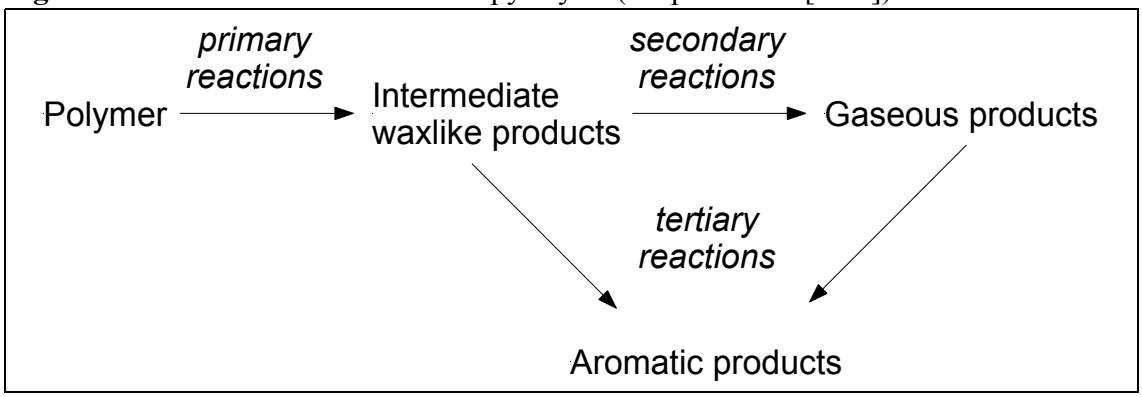

Primary reactions of the polymer yields a series of alkenes and alkanes. The secondary reactions in this scheme lead, by cracking of the primary wax like products, to the higher yields of gaseous products observed. These gaseous products (mainly ethylene and propylene) may undergo cyclisation reactions either by carbonium ion addition to double

bonds or Diels-Alder type of reactions. The light fraction of the aromatics formed may be assigned to reactions involving the gaseous products. The PAHs may be formed by interactions of these aromatic products with the gaseous products present. This reaction mechanism has been suggested for the thermal degradation of n-alkanes ([3.48], [3.49], [3.50], [3.51]).

Regarding the type of polyethylene, experimental studies of LDPE and HDPE ([3.52], [3.63]) show only little difference in products distribution. Also the mixture of polyethylene with polypropylene, another common polyene in waste plastics, was shown to yield only minor changes in products distribution. However, the use of waste polyethylenes, probably contaminated by other polymers or containing impurities which may act as catalysts show deviations in the pyrolysis products [3.53].

3.2.3 Pyrolysis of polystyrene

The pyrolysis of polystyrene has also received some attention as it is an important component of waste streams which may be treated by thermochemical methods. The mechanism involved in this thermolysis is shown in Figure 3.15.

The primary products from the pyrolysis of polystyrene have been confirmed by several studies to be the monomer styrene and lower amounts of the dimer and the trimer ([3.54], [3.55], [3.56], [3.57]). Almost no solid residue (char) is formed (less than 0.2% of the original polymer mass) in the pyrolysis of polystyrene. The amount of gases produced is also very low (less than 1-2%) below 600°C. Above this temperature the amount of gases evolved increases (up to 3.5%) but the gases remain a minor product. The main compounds reported in the gases are ethylene and propylene. On increasing the temperature from 450 to 900°C the amount of styrene oligomers decreases with an increase in temperature, some authors reporting a sharp decline around 600°C. The monomer amount also declines at higher temperatures.

Simple aromatic compounds such as benzene, toluene and other alkylated aromatics are reported to form already at 500°C. Polyaromatic compounds such as naphthalene, phenanthrene and larger ring PAHs have also been identified in the pyrolysis products already at 550°C. The amount of these two product classes and the number of compounds in them is reported to increase as temperature rises.

The presence of small amounts of oxygen in the pyrolysis atmosphere ([3.58], [3.59]) has a net increase in the amount of PAHs found in the products. The presence of alkaline earth metals such as calcium or manganese, which are also found in the inorganic constituents of biomass, increases the amount of PAHs formed at low temperatures (600°C) and reduces them at high temperatures.

Figure 3.15: Thermal degradation mechanisms of polystyrene [3.54].

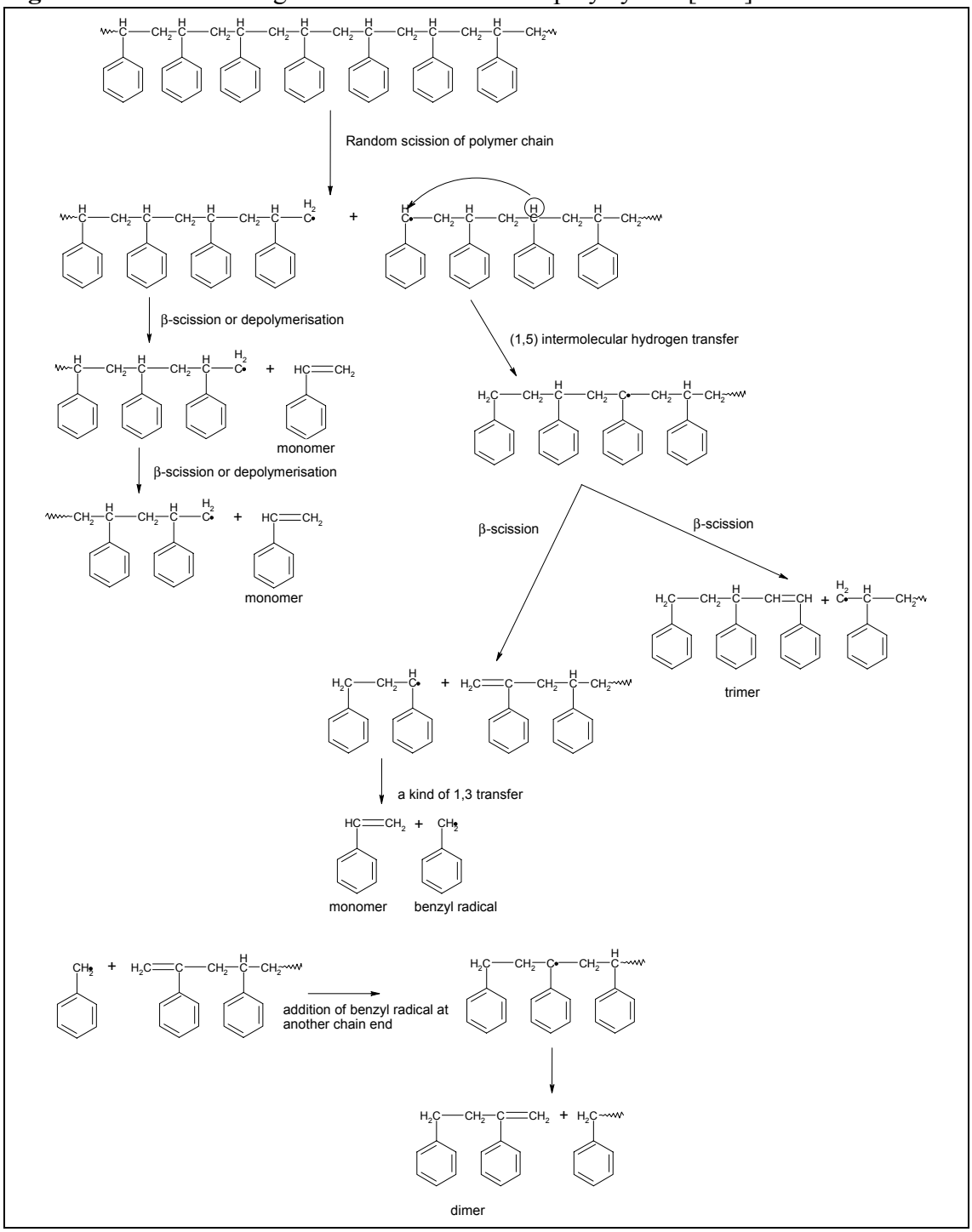

3.2.4 Plastics Mixtures

Although mixtures of the polymers where not examined in this study, some effects reported in the literature are worth of a comment. Numerous authors have studied mixtures representative of plastic blends encountered for example in municipal solid wastes in fluidised bed systems ([3.60], [3.61], [3.62], [3.63]). The temperature range of these studies is 500-740°C. All authors report high amounts of benzene, toluene and xylene in the product oils. One possible explanation for this experimental finding, is the high residence time of the primary products at high temperatures in some of the reactors used.

A systematic comparison of polyethylene, polystyrene and their mixtures [3.63] in the same experimental set-up and conditions shows that when these two polymers are pyrolysed as a mixture, much higher concentrations of aromatic compounds are found in the products than when the polymers are pyrolysed alone. The composition of the aromatic fraction of these products also seems to be influenced by the presence of a second polymer as indicated by differences observed in the amounts of some of the aromatic compounds detected.

3.2.5 Tars from plastics gasification

As seen before in the sections dealing with the biopolymers from biomass, polyethylene and polystyrene also present a characteristic behaviour when pyrolysed. Both synthetic polymers have distinct primary pyrolysis products. These primary products are also distinct from those found in biomass pyrolysis. As the primary pyrolysis products from biomass further reactions have been observed transforming these primary products when they are exposed to high temperatures. Products from these secondary reactions are similar to those expected in the case of biomass, it is they include aromatic, alkylated aromatic and polycyclic aromatic hydrocarbons. Certainly the composition of the tars will be different when biomass is gasified with plastics, but the scope of compounds making up the tars is similar if not identical.

3.3 References

[3.1] D.L. Brink, Chapter 4 in Organic Chemicals from Biomass, I.S. Goldstein (ed.), CRC Press Inc., Boca Raton, 1981, pp.46-62

[3.2] R. Graham, M. Bergougnou, R.P. Overend, *Fast Pyrolysis of Biomass*, Journal of Analytical and Applied Pyrolysis, 1984, **6**, pp.95-135

[3.3] *Biomass Gasification: Principles and Technology*, T.B. Reed (ed.), Noyes Data Corporation, Park Ridge, 1981

[3.4] F. Shafizadeh, *Introduction to Pyrolysis of Biomass*, Journal of Analytical and Applied Pyrolysis, 1982, **3**, pp.283-305

[3.5] *Concise Encyclopedia of Chemical Technology*, R.E. Kirk, D.F. Othmer (eds.), 4th edition, John Wiley & Sons, New York, 1999. get newest data in 1999 edition.

[3.6] P. Ruckenbauer, I. Obernberger, H. Holzner, *Erforschung der Verwendungsmöglichkeiten von Aschen aus Hackgut- und Rindenfeuereungen*, Endbericht der Phase I (1992/1993), Forschungsbericht StU 48 der Bund-Bundesländer Kooperation, Wien, 1993

[3.7] M.A. Serio, M.A. Wójtowicz, S. Charpenay, *Pyrolysis*, in Encyclopedia of Energy Technology and the Environment, A. Bisio and S. Boots (eds.), John Wiley & Sons, New York, 1999, (vol. 3), pp.2281-2308

[3.8] J.D. Roberts, M.C. Caserio, *Basic Principles of Organic Chemistry*, 2nd edition, W.A. Benjamin, Inc., Menlo Park, 1981

[3.9] *Ullmann's Encyclopedia of Industrial Chemistry*, B. Elvers et. al (eds.), VCH Verlagsgesellschaft, Weinheim, Germany, 1996

[3.10] M.J. Antal, G. Varhegyi, *Cellulose Pyrolysis Kinetics: The Current state of Knowledge,* Industrial Engineering Chemistry Research, 1995, **34**, (3), pp.703-717

[3.11] M.G. Grønli, *A Theoretical and Experimental Study of the Thermal Degradation of Biomass*, PhD thesis, Norvegian University of Science and Technology, Trondheim, 1996

[3.12] P. Morf, T. Nussbaumer, *Grundlagen zur Teerbildung bei der Holzvergasung*, Bundesamt für Energie, Bern, 1998

[3.13] F. Shafizadeh, P.S. Chin, in *Proceedings 172nd National ACS Meeting*, August 30-September 6, Washington DC, 1976

[3.14] S. Gaur, T.B. Reed, *An Atlas of Thermal Data for Biomass and other Fuels*, National Renewable Energy Laboratory Report Nr. NREL/TP-4337963, Golden, 1995

[3.15] P.T. Williams S. Besler, *The Influence of Temperature and Heating Rate on the Slow Pyrolysis of Biomass*, Renewable Energy, 1995, **7**, (3), pp.233-250

[3.16] A.G.W. Bradbury, Y. Sakay, F. Shafizadeh, *A Kinetic Model for Pyrolysis of Cellulose*, Journal of Applied Polymer Science, 1979, **23**, pp.3271-3280

[3.17] A. Broido, *Kinetics of Solid-Phase Cellulose Pyrolysis*, in Thermal Uses and Properties of Carbohydrates and Lignins, 172nd National Meeting ACS, F. Shafizadeh, K.V. Sarkanen and D.A. Tillmann (eds.), Academic Press, 1976, p. 19-36

[3.18] C. Di Blasi, *Numerical Simulation of Cellulose Pyrolysis, Biomass and Bioenergy*, 1994, **7**, (1-6), pp.87-98

[3.19] R. Bilbao, M.B. Murillo, A. Millera, *Angular and Radial Temperature Profiles in the Thermal Decomposition of Wood*, Themochimica Acta, 1992, **200**, pp.401-411

[3.20] M.J. Antal, C. DeAlmeida, W.S. Mok, S. Sinha, *A New Technology for Manufacturing Charcoal from Biomass*, in Proceedings of the IGT Conference on Energy from Biomass and Wastes XV, D.L. Klass (ed.), Institute of Gas Tecnology, 1991

[3.21] S.Q. Turn, C.M Kinoshita, D.M. Ishimura, B.M Jenkins, *Removal of Inorganic Constituents of Fresh Herbaceous Fuels: Process and Costs*, in Making a Business from Biomass in Energy, Environment, Chemicals, Fibers and Materials Proceedings of the 3rd Biomass Conference of the Americas, Montreal, Quebec Canada, August 24-29, R.P. Overend and E. Chornet (eds.), Elsevier Science, 1997, pp.401-414

[3.22] G. Varhegyi, P. Szabo, M.J. Antal, *Kinetics of the Thermal Decomposition of Cellulose and Hemicellulose in Biomass Materials*, in Advances in Thermochemical Biomass Conversion, A.V. Bridgwater (ed.), Blackie Academic & Professional, Glasgow, 1994, (Vol. 2), pp.760-770

[3.23] G.N. Richards, *Influence of Metal Ions and of Salts on Products from Pyrolysis of Wood Applications to Thermochemical Processing of Newsprint and Biomass*, Journal of Analytical and Applied Pyrolysis, 1991, **21**, pp.133-146.

[3.24] C. von Scala, *The Influence of Contaminants on the Gasification of Waste Wood*, ETH Dissertation Nr. 12'665, Zürich, Switzerland, 1998

[3.25] R.G. Graham, M.A. Bregougnou, L.K.S. Mok, H.I. de Lasa, *Fast Pyrolysis (Ultrapyrolysis) of Biomass Using Solid Heat Carriers*, in Fundamentals of Thermochemical Biomass Conversion, R.P. Overend, T.A. Milne and L.K. Mudge (eds.), Elsevier Applied Science Publishers Ltd., London, 1985, pp.397-410

[3.26] R.J. Evans, T.A. Milne, *Molecular Characterisation of the Pyrolysis of Biomass. 1. Fundamentals*, Energy and Fuels, 1987, **1**, (2), pp.123-137

[3.27] R.J. Evans, T.A. Milne, *Molecular Characterisation of the Pyrolysis of Biomass. 2. Applications*, Energy and Fuels, 1987, **1**, (4), pp.311-319

[3.28] R.J. Evans, T.A. Milne, *Chemistry of Tar Formation and Maturation in the Thermochemical Conversion of Biomass*, in Developments in Thermochemical Biomass Conversion, A.V. Bridgwater and D.G.B. Boocock (eds.), Blackie Academic & Professional, London, 1997, Volume 2, pp.803-816

[3.29] R.J. Evans, C.C. Elam, M. Looker, M. Nimlos, *Formation of Aromatic Hydrocarbons due to Partial Oxidation Reactions in Biomass Gasification*, Preprints of the Division of Fuel Chemistry of the American Chemical Society, 1999, vol. 4, issue 2, pp.256-260

[3.30] D.C. Eliott, *Relation of Reaction Time and Temperature to Chemical Composition of Pyrolysis Oils*, Chapter 6 in Pyrolysis Oils from Biomass: Producing, Analyzing, and Upgrading: ACS Symposium Series, Nr. 376, E.J. Soltes and T.A. Milne (eds.), 1988

[3.31] E.J. Soltes, T.J. Elder, in Organic Chemicals from Biomass, I.S. Goldstein (ed.), CRC Inc., Boca Raton, 1981, pp.64-99

[3.32] H. Egsgaard, E. Larsen, *Thermal Transformation of Light Tar - Specific Routes to Aromatic Aldehydes and PAH*, Presented at the 1st World Conference on Biomass for Energy and Industry, June 5-9, Seville, Spain, 2000

[3.33] O. Jönsson, *Thermal Cracking of Tars and Hydrocarbons by Addition of Steam and Oxygen in the Cracking Zone*, in Fundamentals of Thermochemical Biomass Conversion, R.P. Overend, T.A. Milne and L.K. Mudge (eds.), Elsevier Applied Science Publishers Ltd., London, 1985,pp.733-746

[3.34] A.G. Buekens, J.G. Schoeters, *Technical Methods in Plastics Pyrolysis*, Macromolecular Symposia, 1998, **135**, pp.63-81

[3.35] *Ullmann's Encyclopedia of Industrial Chemistry*, B. Elvers et. al (eds.), VCH Verlagsgesellschaft, Weinheim, Germany, 1992

[3.36] H. Bockhorn, A. Hornung, U. Hornung, *Mechanisms and Kinetics of Thermal Decomposition of Plastics from Isothermal and Dynamic Measurements*, Journal of Analytical and Applied Pyrolysis, 1999, **50**, (2), pp.77-101

[3.37] N.I. Maksimova, O.P. Krivoruchko, V.N.A Sidel'nikov, *A Study of Composition of Liquid and Solid Products of Thermal and Thermocatalytic Decomposition of Polyethylene, Polyvinyl Alcohol, and Polystyrene*, Russian Journal of Applied Chemistry, 1998, 71, (8), pp.1386-1392

[3.38] H. Bockhorn, A. Hornung, U. Hornung, D. Schwaller, *Kinetic Study on the Thermal Degradation of Polypropylene and Polyethylene*, Journal of Analytical and Applied Pyrolysis, 1999, 48, (2),pp.93-10

[3.39] H. Bockhorn, A. Hornung, U. Hornung, *Mechanisms and Kinetics of Thermal Decomposition of Plastics from Isothermal and Dynamic Measurements*, Journal of Analytical and Applied Pyrolysis, 1999, 50, (2), pp.77-101

[3.40] J. Liggat, *Products of Thermal Degradation of Polymers*, in Polymer Handbook, J. Brandrup, E.H. Immergut, E.A. Gulke (eds.), John Wiley & Sons Inc., 1999, pp.II/451-II/480

[3.41] N. Horvat, F.T.T. Ng, *Tertiary Polymer Recycling: Study of Polyethylene Thermolysis As A First Step To Synthetic Diesel Fue*l, Fuel, 1999, 78, pp.459-470

[3.42] P.T. Williams, E.A. Williams, *Fluidised Bed Pyrolysis of Low Density Polyethylene to Produce Petrochemical Feedstock*, Journal of Analytical And Applied Pyrolysis, 1999, 51, (1-2), pp.107-126

[3.43] J.A. Conesa, R. Font, A. Marcilla, A.N. Garcia, *Pyrolysis of Polyethylene in a Fluidized Bed Reactor*, Energy & Fuels, 1994, 8, pp.1238-1246

[3.44] J.A. Condesa, R. Font, A. Marcilla, J.A. Caballero, *Kinetic Model for the Continuous Pyrolysis of Two Types of Polyethylene in a Fluidized Bed Reactor*, Journal of Analytical and Applied Pyrolysis, 1997, 40-41, pp.419-431

[3.45] J.G. Schoeters, A.G. Buekens, *Pyrolysis of Plastics in a Steam Fluidised Bed*, in Recycling Berlin '79, J. Thomé-Kozmiensky (ed.), Freitag, Berlin, 1979

[3.46] B.J. Milne, L.A. Behie, F. Berruti, *Recycling of Waste Plastics by Ultrapyrolysis Using an Internally Circulating Fluidized Bed Reactor*, Journal of Analytical and Applied Pyrolysis, 1999, 51, (1-2), pp.157-166

[3.47] I.C. McNeill, *Thermal Degradation*, in Comprehensive Polymer Science, G. Allen, J.C. Bevington (eds.), Pergamon Press, Oxford, 1989, (vol. 6), pp.451-500

[3.48] L.F. Hatch, S. Matar, *Chemistry of Petrochemical Processes*, Gulf Publishing Company, Houston, 1994

[3.49] R. Cypres, Fuel Processing Technology, 1987, **15**, (1)

[3.50] D. Depeyre, C. Flicoteaux, C. Chandaire, *Pure n-Hexane Thermal Steam Cracking*, Industrial & Engineering Chemistry. Process Design and Development, 1985, **24**, pp.1251 ff.

[3.51] J.A. Fairburn, L.A. Behie, Y. Svrcek, Fuel, 1990, **96**, pp.1537 ff.

[3.52] R.W.J. Westerhout, J.A.M. Kuipers, W.P.M van Swaaij, *Experimental Determination of the Yield of Pyrolysis Products of Polyethene and Polypropene. Influence of Reaction Conditions*, Industrial and Engineering Chemistry Research, 1998, **37**, (3), pp.841-847

[3.53] N. Kiran, E. Ekinci, C.E. Snape, *Recycling of Plastic Wastes Via Pyrolysis*, Resources Conservation and Recycling, 2000, 29, (4), pp.273-283

[3.54] M. Yang, Y. Shibasaki, *Mechanisms of Thermal Degradation of Polystyrene, Polymethacrylonitrile and Their Copolymers on Flash Pyrolysis*, Journal of Polymer Science: Part A: Polymer Chemistry, 1998, **36**, pp.2315-2330

[3.55] C. Bouster, P. Vermande, J. Veron, *Evolution of the Product Yield with Temperature and Molecular Weight in the Pyrolysis of Polystyrene*, Journal of Applied and Analytical Pyrolysis, 1989, **15**, pp.249-259

[3.56] P.T. Williams, E.A. Williams, *Product Composition From the Fast Pyrolysis of Polystyrene*, Environemental Technlogy, 1999, **20**, pp.1109-1118

[3.57] Y. Liu, J. Quian, J. Wang, *Pyrolysis of Polystyrene Waste in a Fluidized-Bed to Obtain Styrene Monomer and Gasoline Fraction*, Fuel Processing Technology, 2000, **63**, pp.45-55

[3.58] Y.-L.Wei, J.-H. Lee, *Formation of Priority PAHs from Polystyrene Pyrolysis with addition of Calcium Oxide*, The Science of The Total Environment, 1998, **212**, pp.173-181

[3.59] Y.-L.Wei, J.-H. Lee, *Manganese Sulfate Effect on PAH formation from Polystyrene Pyrolysis*, The Science of The Total Environment, 1999, **228**, pp.59-66

[3.60] J.-S. Kim, W. Kaminsky, B. Schlesselmann, *Pyrolysis of a fraction of mixed plastic wastes depleted in PVC*, Journal of Analytical and Applied Pyrolysis, 1997, **40-41**, pp.365-372

[3.61] E.A. Williams, P.T. Williams, *Analysis of Products Derived from the Fast Pyrolysis of Plastic Waste*, Journal of Analytical and Applied Pyrolysis, 1997, **40-41**, pp.347-363

[3.62] W. Kaminsky, J.-S. Kim, *Pyrolysis of Mixed Plastics into Aromatics*, Journal of Analytical and Applied Pyrolysis, 1999, **51**, pp.127-134

[3.63] P.T. Williams, E.A. Williams, *Interaction of Plastics in Mixed-Plastics Pyrolysis*, Energy & Fuels, 1999, **13**, pp.188-196

4 TAR SAMPLING AND ANALYSIS METHODS

4.1 Introduction

The unavoidable tars formed in the process of biomass gasification are a major obstacle for the further use of the produced gas. For example, when the gas is to be converted into electricity in a gas engine or a gas turbine the tars can create deposits in the ducts transporting the gas or in the conversion device itself. Such deposits were also observed in cold spots along the gas flow path and gas sampling system of our experimental set-up. The deposits were soluble in acetone, indicating that they probably consist of condensed tars which are not polymerised as the presence of phenolic compounds may suggest. Their composition was however not studied systematically and may include char, soot or other solid particles.

The requirements for the use of the gas in a synthesis process are even more stringent as can be seen in Table 4.1. In consequence considerable effort has been spent in the

past and in recent years in the development of biomass gasification processes with low tar levels and gas cleaning systems. In these research activities different tar sampling methods have been and still are employed. A few of them will be described in the next section of this chapter.

Table 4.1: Gas quality requirements for different power generation systems and methanol synthesis [4.1]. n.l.: not limited

Contaminant	Units	IC Engine	Gas turbine	Methanol synthesis
Particles	mg/m^3_N	<50	<30	<0.02
Particle size	µm	<10	<5	
Tars	mg/m^3_N	<100		<0.1
alkali metals	mg/m^3_N		0.24	
NH_3	mg/m^3_N			<0.1
S components (H_2S, COS)	mg/m^3_N			<1
Cl components	mg/m^3_N			<0.1
CO_2	Vol.-%	n.l	n.l	<12, n.l.

Up to this date, there still is no consensus among researchers in what compounds found in the product gases of a gasifier make up tars or not. This lack of agreement is not surprising. The term tar is generically used to designate residues produced in the thermochemical conversion of organic materials. In the context of biomass gasification, tars have often been operationally defined as the condensates deposited in equipment downstream of the gasifier. Tars could thus be identified as those compounds that make difficult the usage and handling of the producer or synthesis gas. In this line of reasoning, it is not surprising that for example benzene or other low molecular weight aromatics will not qualify as tar to researchers involved in the development of gasification for power production via combustion devices (motors or gas turbines). These compounds will not disturb the operation of a motor since they will not deposit in the lines transporting the gas to the combustion chamber and will readily burn.

Another problem encountered when trying to investigate tars, is the absence of standards regarding the methods for sampling and analysis. Not only have a large number of different tar sampling methods been developed, also different quantification methods

have been used. Since 1998 the members of the IEA Bioenergy Gasification Task have tried to bring some standardisation in this field. In the beginning of the year 2000 the IEA Bioenergy Gasification Task published their definition of relevant tars in gasification and sampling and analysis methods ([4.2]-[4.4]). These might in the future attain the status of internationally accepted standard methods.

4.2 Tar sampling methods

A wide number of tar sampling and analysis methods has been reported in the literature and a complete review lies beyond the scope of this thesis. Only a short overview of some methods described will be given here to illustrate the scope of procedures used.

Probably the simplest way to obtain information on the tar load of a gas is to cool down the gas and allow the tars to deposit in a vessel or on an appropriate substrate. Once the sampling is complete the vessel or substrate's contents may be treated and the weight of the deposited condensates is taken as a measure of the tar contents of the gas. Examples of this kind of method are given in references [4.5], [4.6] and [4.7]. This kind of simple sampling procedure certainly has advantages with respect to cost and to the time required to deliver results. However, the amount of condensate deposited will unavoidably be a function of the cooling conditions (e.g. temperature, gas flow rate) used. Furthermore, the most volatile of the tar compounds will most probably not be retained by this simple collection technique. The condensate may be treated and analysed for its composition by appropriate techniques such as gas chromatography with a flame ionisation detector (GC/FID) or gas chromatography with a mass selective detector (GC/MSD) resulting in detailed tar composition data.

The next step in refinement of tar sampling will thus be to try to capture the compounds not held back by a cooling stage alone. One popular method is to lead the cooled gas into an appropriate organic solvent scrubbing the gases from the remaining tar components. A number of solvents has been used in this kind of sampling method ranging

from the volatile dichloromethane [4.8], [4.9] over acetone [4.10] to toluene [4.11], anisole [4.12] and 1-methoxy-2-propanol [4.13]. The solvent is usually placed in a cooling bath and again here the temperature used is different from method to method influencing the results obtained. The treatment of the liquid samples is diverse ranging from simple gravimetric determination of a tar residue after solvent evaporation (again at dissimilar temperatures for different procedures) to sophisticated analysis of the solutions via GC/FID, GC/MSD or size exclusion chromatography [4.14].

This analysis of solutions via appropriate methods for the identification of single compounds yields the most detailed results. It has however the big disadvantage of producing data with a large time lag as the analysis methods as well as sample preparation procedures are time consuming. Another disadvantage of these sophisticated analytical methods is clearly the cost involved in their execution.

Tar trapping techniques using solid phase adsorbent have also been proposed [4.17], [4.16]. They are advantageous for sampling what the authors call "phenolic fraction" of tars and allow rapid sampling. However these adsorption method is found not to be suitable for polycyclic aromatic hydrocarbons or light aromatic compounds, major components of biomass gasification tars. Also large errors arise due to the low sampled volume which induces low compound concentrations for the subsequent GC/MSD analysis.

Besides the condensation/absorption methods listed above other techniques have been proposed. For example the use of flame ionisation detectors (FID) [4.15] measuring the tars contained in the gas as the difference between the signals of two FIDs. The gas delivered to one of the FIDs is cleaned of its tars by condensing these in filter placed inside a Peltier element. The temperature at which the condensation takes place will probably influence the results obtained by this system. The advantages of this measurement technique is the speed at which tar concentration changes may be detected. It does not however deliver information on the composition of the tars.

Probably the most sophisticated technique used in the determination of tars is molecular beam mass spectrometry (MBMS) [3.26]-[3.29], [4.18]. This technique directly samples the gases from a gasifier without prior condensation or separation of the tars. It yields quantitative as well as qualitative information not only on tars but on all gas components. The research group at the National Renewable Energy Laboratory employing

this very sophisticated technique has been able to build a more compact transportable MBMS and has tested this method on a demonstration scale gasification unit [4.19]. The disadvantage of this procedure is the complexity and size of the MBMS making it possibly the most expensive alternative for tar analysis thus limiting its use.

Just very recently have different conventional tar sampling and analysis methods been compared in parallel sampling runs on both an up-draft and on a down-draft fixed bed gasifier [4.21]. In these test runs not only tars but also the content of particles in the gas was measured. The results obtained by the diverse methods are quite different from each other. Most of the deviations can be explained by the dissimilarities in the sampling and analysis procedures. The need for standardisation not only of the sampling procedures and equipment but also of the analysis and definitions used herein is another important conclusion of these test runs.

As stated in [4.9] "different levels of information on tars are required for different purposes. Most detailed information, including all compounds, is needed in scientific research and often also in order to calculate accurate elemental material balances for gasifiers. On the other hand only the concentrations of the heaviest tar compounds have to be determined when evaluating potential problems in using product gas in applications which do not require cold gas cleaning steps". The aims of a specific research goal thus determine the level of detail required in the tar sampling and analysis procedure.

The aims and applicability of tar sampling methods vary greatly. Also the operating parameters of a gasifier as well as the fuel processed have an impact on the amount and quality of the tars produced. Even if large efforts are being done in the sense of standardisation of tar sampling methods it might well be that there will never exist one single tar sampling and analysis method to cover the whole range of applications possible.

At the time when the method used in the present thesis was developed, only scarce information on precise sampling and analysis procedures was available from the literature. The method which was best described then was the one employed by the Technical Research Centre of Finland, VTT [4.8], [4.9], [4.20]. It appeared thus that this method would supply the best information on tar levels and composition and therefore it was decided to use a similar system.

4.3 PSI's Tar sampling and analysis method

The sampling and analysis method employed in this work is based on the method developed in Finland by VTT [4.20], of which a complete and detailed description has only recently become available [4.9]. The goal pursued was to correctly sample and analyse as many compounds as possible, yielding precise information about the tar amount present in the gases as well as detailed information on the tar composition. The method used in the present thesis has been first set-up in 1994 and has since been continuously refined as more experience in its use was accumulated. Especially the analysis method has been changed from a GC/FID system to a GC/MSD. The reason for this change was mainly the problems in the identification of compounds on the GC/FID system. Another advantage of the GC/MSD system is, that certain co-eluting compounds (i.e. substances exiting the capillary column at the same time) can be discerned when their masses are different, allowing for a larger number of compounds to be identified with a simpler chromatographic method.

4.3.1 The sampling train

The sampling train used in this work was designed to separate "heavy" and "light" tars and to allow for the measurement of the water content of the gas. It is composed of three sections: a heavy tar filter, a series of bottles connected by PTFE tubing, containing water and organic solvents to absorb the tars and a cold trap to retain evaporated solvent and compounds not absorbed in the solvents of the preceding bottles. The tar sampling train is outlined in Figure 4.1.

Gas is drawn from the reactor by an Inconel 600 sampling tube of 10 x 8 mm (outer x inner Ø) and ca. 500mm length. The tip of the sampling tube is at the center of the reactor. At the outer end of this tube a temperature resistant ball valve is fitted to interrupt gas flow. Directly after the ball valve a heated filter containing ca. 2.5g of glass wool is fitted. Both the ball valve and the filter housing are heated. The temperature of this part of the sampling train is set and controlled to 300ºC (exterior temperature) during sampling. A thermocouple is fitted into the center of the glass wool allowing to monitor its temperature during sampling, see Figure 4.2.

Figure 4.1: Scheme of the tar sampling train.

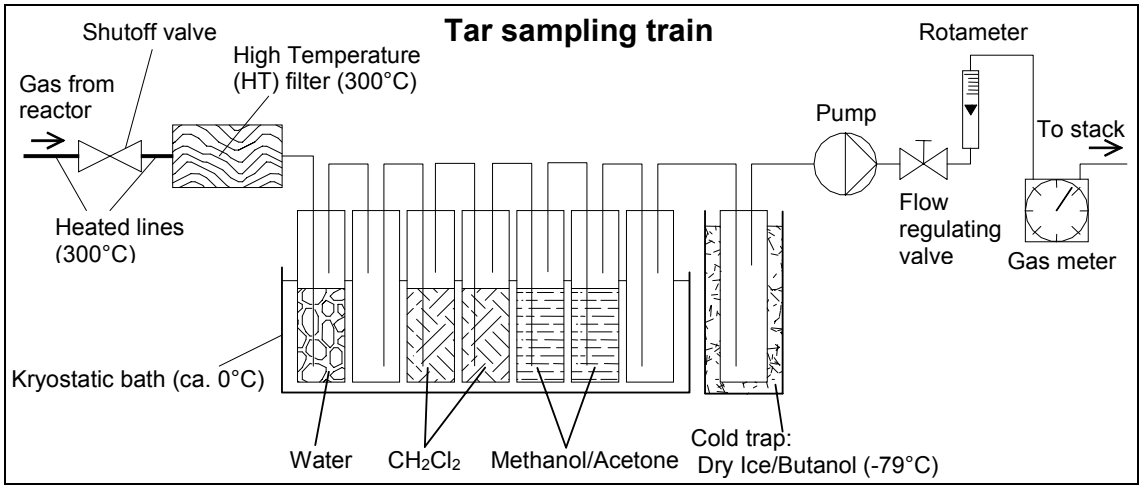

Figure 4.2: Temperature evolution measured in the heavy tar filter (991214). For an explanation on the meaning of "Run A, B, C" see page 132.

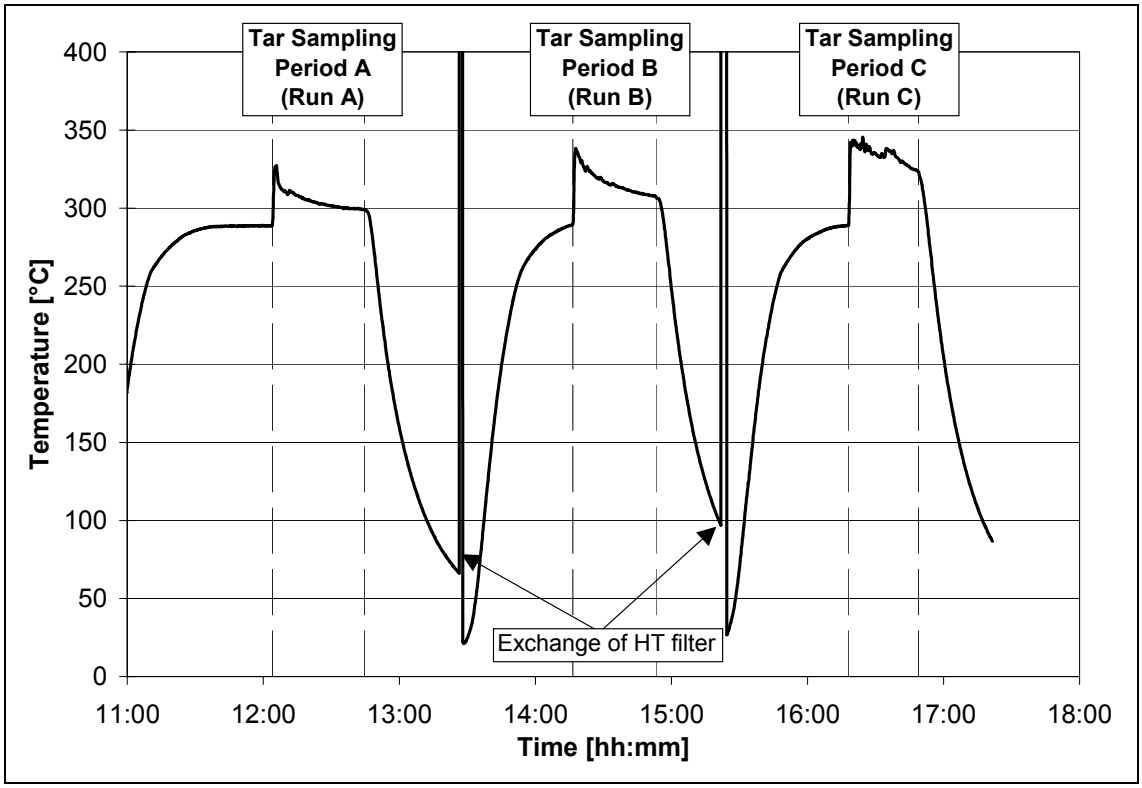

The assembly containing the glass wool is called the heavy tar filter, as it is designed to trap mainly compounds with a high boiling point and accordingly high molecular mass. The temperature of 300°C was chosen to allow only the heaviest compounds to deposit in the filter, minimising the risk of plugging during sampling. In fact, as seen in a test run where the heavy tar filter was only heated to 150°C neither the operation of the sampling train nor the results are affected by this temperature set-point. The details of this

filter are given in Figure 4.3. The design used allows for a leak-free sampling: the tension springs between in the cap force the tip of the interior filter housing into the inlet tube of the exterior housing and a labyrinth-type gasket between interior filter housing and cap ensure tightness at this point. No tar deposition could ever be detected on the outside walls of the interior filter housing or on the inner walls of the exterior filter housing. Also it allows to easily change the filter so that more than one sampling during an experiment is possible.

Figure 4.3: Scheme of the heavy tar filter.

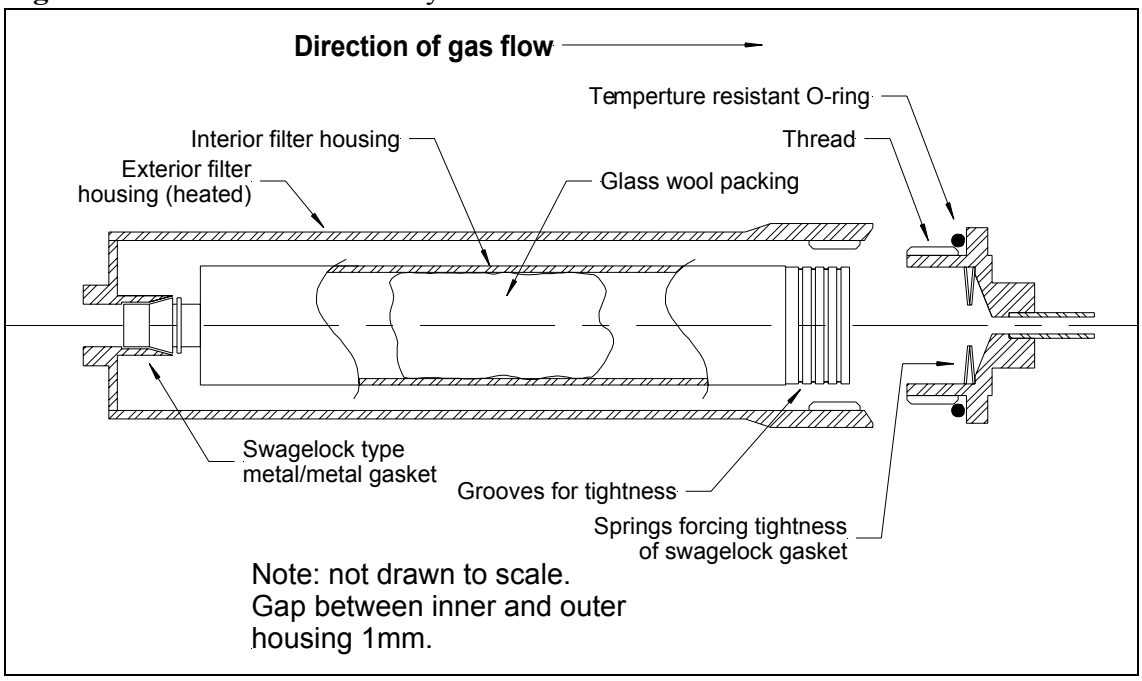

After the gas passes the heavy tar filter it is led by a stainless steel tube (inner diameter 4mm) to the first bottle of the absorption section. The dimensions of the bottles used are shown in Figure 4.4.

These are commercially available glass bottles (Schott laboratory bottles with DIN thread, ISO 4796) with a volume of 250ml and are made of relatively thick glass, allowing for moderate pressure differences between sampling train and the atmosphere. All bottles are immersed in a cooling bath connected to a cryostat which circulates the cooling fluid (water and polyethylene glycol) and controls its temperature to 0°C.

The first bottle is filled with 150ml of deionised water and the gas is led into the water by an impinger made of stainless steel depicted in Figure 4.5. In this first bottle,

mostly water as well as tar compounds with an intermediate molecular mass are condensed, and the polar compounds like phenol are dissolved in the water.

Figure 4.4: Tar sampling train bottle.

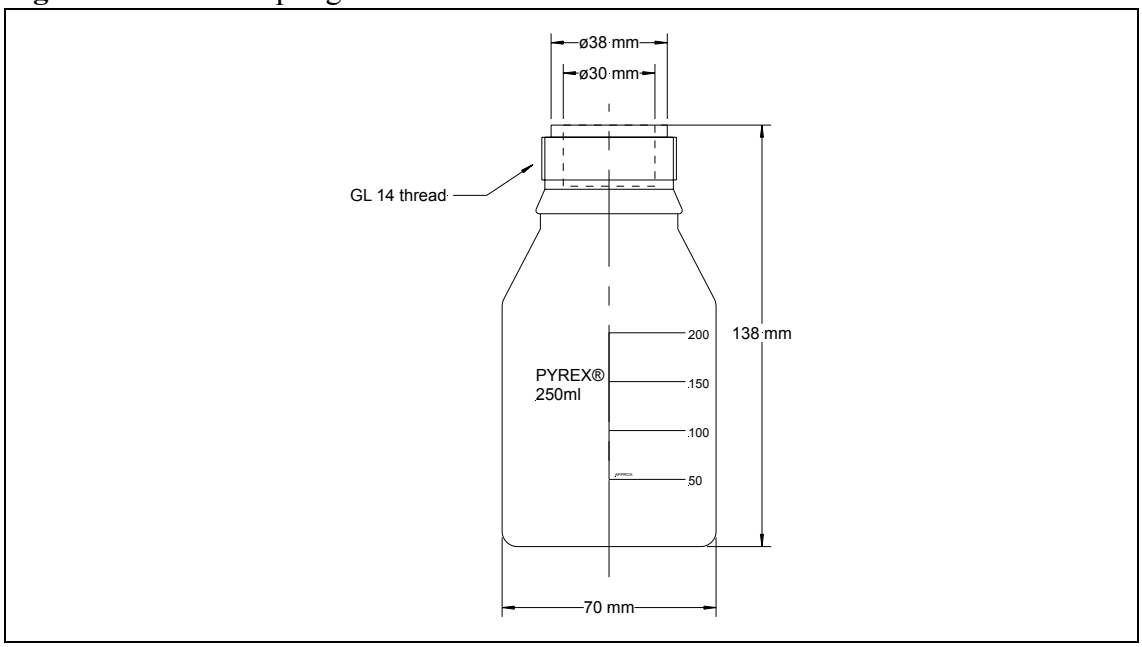

Figure 4.5: Impingers used in the sampling train.

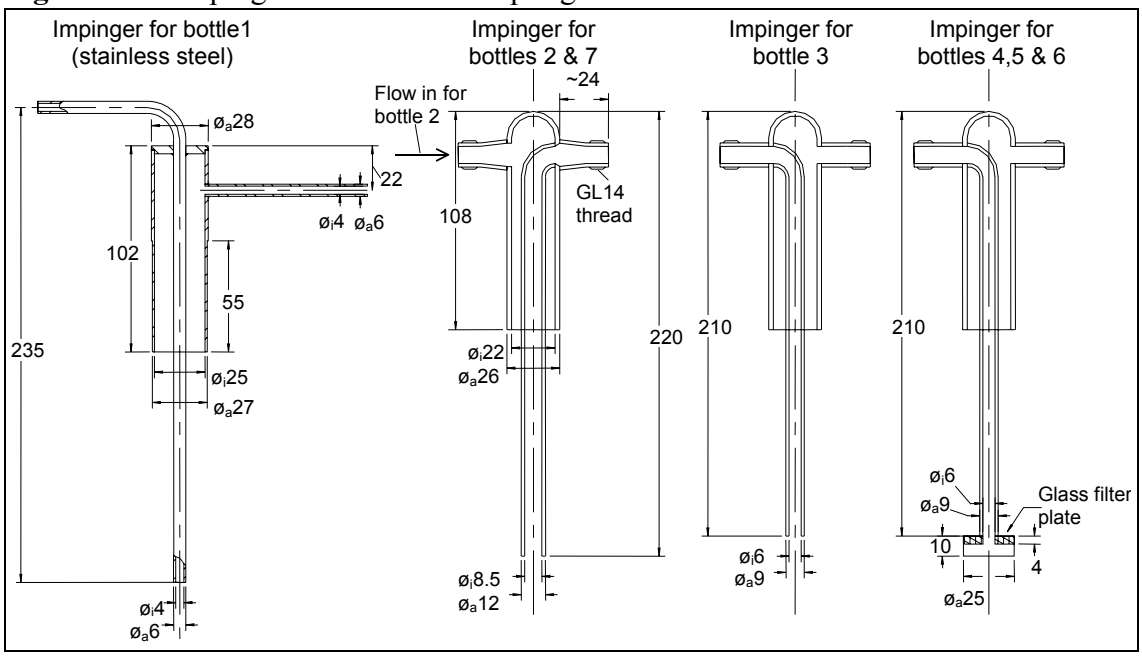

The gases are then led into the second bottle, which is empty and has its impinger reversed, meaning that the impinger is connected such, that the gases will enter the bottle by the top of the impinger and exit through the impinger pipe (see Figure 4.5). This bottle serves primarily as safety device to prevent the organic solvent from the third bottle to

flush into the water phase of the first bottle. In this bottle again mainly water is condensed and only little tar deposition is observed. The third bottle in the series is filled with 150ml of dichloromethane CH_2Cl_2 (DCM). A tube impinger of slightly smaller diameter than the second forces the gases into the solvent. DCM was chosen as solvent because it is known to dissolve all tar compounds well. The fourth bottle of the series is also filled with 150ml of DCM, but its impinger has a porous glass filter plate of porosity 1 (ø of pores 100-160µm) at its end. This filter plate allows for the formation of small gas bubbles in the solvent, enhancing the absorption process. A glass filter plate cannot be used in bottle 3, as it was seen to plug during sampling with small particles and water. The next two bottles, the 5^{th} and 6^{th}, in the series are filled with 150ml of a mixture of methanol and acetone (1:1 by volume) and have the same impingers as bottle 4. The reason for this different solvent is, that it might trap polar compounds not retained by the DCM in the preceding bottles. Also, the volatile DCM from the 3^{rd} and 4^{th} bottles is trapped by the less volatile solvent present, diminishing solvent loss during sampling. The last bottle in the series is again an empty safety bottle.

The last component of the sampling train is a cold trap (CT), depicted in Figure 4.6, which is immersed in an insulating Dewar vessel containing a dry ice/2-propanol mixture. This mixture cools the cold trap to ca. -78°C and allows for solvent evaporated and tar compounds not trapped by the preceding bottles to be held back.

Figure 4.6: The cold trap.

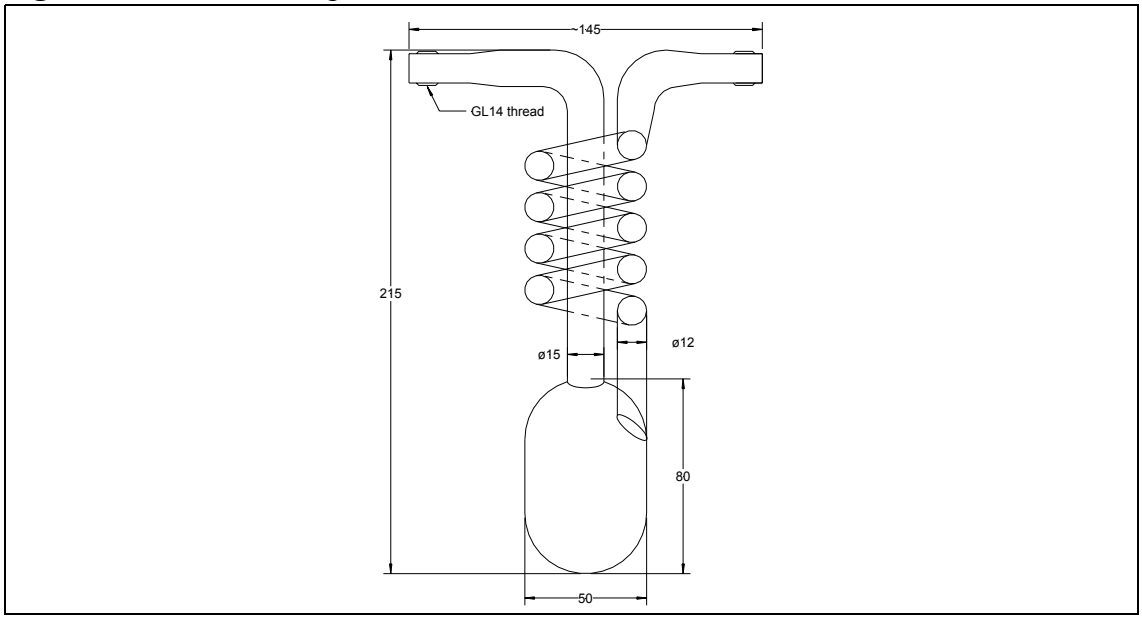

All bottles are connected by PTFE tubes of 6 x 4mm and ca. 50-70mm length. The PTFE tubes are connected to the glassware by caps with an inner GL14 thread and tightness is ensured by the use of silicone ring gaskets. All solvents used are of 99.9% purity.

After the sampling train, the gas passes by the same type of gas conditioning device used for gas sampling (see chapter 2, page 31) composed of a gas cooler with a Peltier element for water condensation, a diaphragm gas pump, a dust filter, a needle valve for setting the gas throughput and a rotameter. The gas flows then to a total gas volume meter with which the volume of gas sampled is accurately measured. This device is fitted with a thermometer and a u-tube manometer to measure the gas temperature and pressure. A typical example of the gas volume, pressure difference and temperature evolution during sampling is shown in Figure 4.7.

Figure 4.7: Gas volume sampled, pressure difference to atmosphere and gas temperature for experiment 991214B.

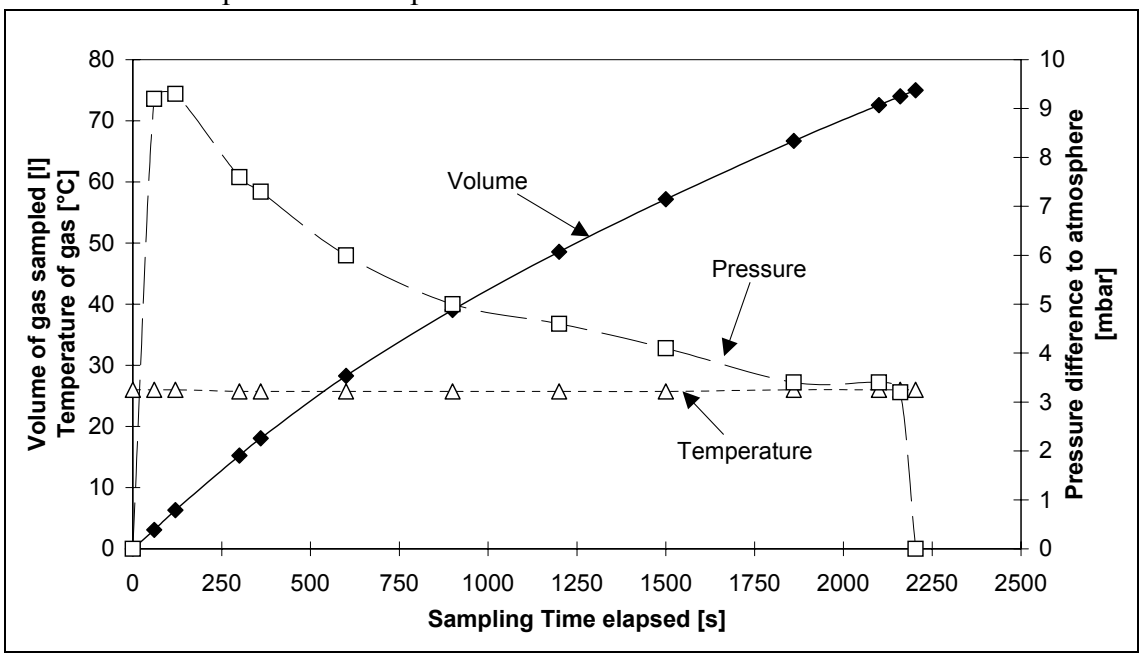

The gases are then led by PTFE tubes to the mass spectrometer, enabling the measurement of the gas composition during sampling. An example of the gas composition measured during a tar sampling is shown in Figure 4.8. The observed initial peak of N_2 and O_2 is due to the air in the bottles being sucked out and very rapidly the gas composition becomes equal to that before sampling. The lack of oxygen in the gases shows well the tightness of the sampling train.

Figure 4.8: Gas composition evolution during tar sampling. (991214B)

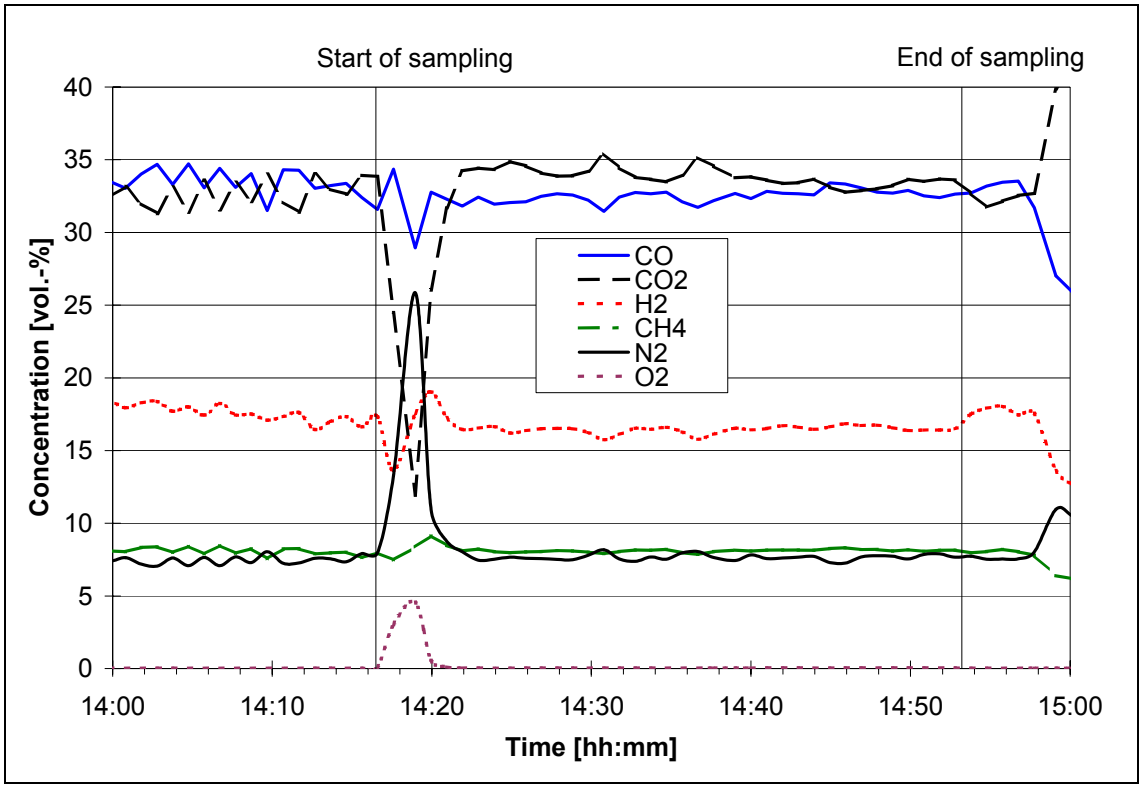

4.3.2 Tar sampling procedure

Before sampling, the glass wool in the heavy tar filter is weighted and inserted into the filter, forming a plug approximately at the centre of the filter and leaving enough space at the filter inlet for particles which are sucked with the gases and deposited there. A small cavity is made in the glass wool to accommodate the tip of the thermocouple. Special attention is given not to pierce through the glass wool. The heavy tar filter is the assembled (i.e. the tension springs inserted into the cap and the cap placed carefully on the tight fitting inner filter housing) and the steel tubes which connect the HT filter to the bottles fitted loosely. All bottles of the sampling train are tared with their caps and respective impingers. The water and the solvents are filled in and their weight is also noted and the bottles are loosely connected together by the PTFE tubes. A transportation rack is fitted which fixes the bottles allowing their transportation as a single unit to the tar sampling point of the reactor. The cold trap is flushed with argon to prevent water condensation when it is immersed in the dry ice/2-propanol mixture and its weight is also written down. On the installation the heavy tar filter is mounted in its housing and its heaters are turned on. The sampling train bottles are immersed into the cooling bath for thermal equilibra-

tion. When the heavy tar filter reaches its operational temperature the connecting tubes are fastened, the sampling bottles are connected to the cold trap and the cold trap to the gas conditioning device. The exact volume displayed by the gas volume meter is noted on a tar sampling protocol. Tar sampling can then be performed.

Sampling is begun by starting the pump in the gas conditioning device and then opening the ball valve before the heavy tar filter. The gas flow is initially set to $200 l_N/h$ using the needle valve and the rotameter on the gas conditioning device. The volume indicated by the volume meter, the gas temperature and pressure as well as the approximate gas flow indicated by the rotameter are noted on a tar sampling protocol at regular time intervals during sampling (at 1, at 5 and then at every 5^{th} minute after the start). Sampling is complete when a total gas volume of at least 75 litres (in general 100 litres are sampled) has flown through the sampling train. This volume has been set as a practical value yielding appropriate concentrations of the tar compounds in the solutions and a sampling time of 30-40 minutes. It is assumed, that the gas volume measured is that of dry gas. The sampled gases pass through the cold trap at -78°C and the gas cooler/water condenser at 4°C before reaching the gas volume meter. This assumption was experimentally confirmed, as no condensate was ever seen to exit the gas cooler.

The sampling is stopped by closing the ball valve and shutting down the pump of the gas conditioning device. This procedure creates a slight vacuum in the sampling train. The total volume sampled and the duration of the sampling are noted on the protocol. The heater of the heavy tar filter is turned down and allowed to cool to 100°C before it is taken out of its housing. The connection between the heavy tar filter and the first bottle is immediately opened after stopping the sampling pump and a cap is placed on the steel tube which remains connected to the heavy tar filter to prevent compounds from escaping from the heavy tar filter. The connections between the sampling bottles are then opened sequentially from the first bottle in the direction of flow of the gas to prevent back flushing of the solvents between bottles. The cold trap is disconnected from the sampling train, plugged and removed from the dry ice/2-propanol mixture to slowly heat-up to room temperature. The sampling bottles are then taken out of the cooling bath, thoroughly

dried and taken to the laboratory as soon as possible for weighting and processing of the solutions. An example of a mass balance for the sampling train is shown in Table 4.2.

Table 4.2: Mass balance of tar sampling train. (990729A)

Bottle Nr.	Contents	Tara [g]	Mass of liquid added [g]	Bottle's weight [g] before sampling	Bottle's weight [g] after sampling	Balance [g]
1	150ml H_2O	405.85	147.3	553.15	606.83	+53.68
2	-	322.85	0	322.85	324.2	+1.35
3	150ml DCM	316.89	191.8	508.69	426.16	-82.53
4	150ml DCM	316.81	195.66	512.47	496.41	-16.06
5	150ml Acetone/MeOH	316.35	116.03	432.38	500.16	+67.78
6	150ml Acetone/MeOH	306.98	118.25	425.23	439.13	+13.9
7	-	306.93	0	306.93	307.17	+0.24
CT	-	163.95	0	163.95	180.98	+17.03
Water accumulated [g]						55.03
Solvent lost [g]						0.36
Solvent lost [% of total mass of solvent used]						0.06

4.3.3 Sample treatment procedures

The heavy tar filter, the water phase in bottles 1 and 2 and the organic phases of bottles 3 to 7 and the cold trap are prepared by different procedures prior to the determination of the tar contents by GC/MSD.

Handling of heavy tar filter

The tars deposited in the heavy tar filter are extracted from the glass wool by soxhlet liquid/solid extraction. This extraction method allows for high recovery of compounds in the solid sample while keeping the volume of solvent employed low. A scheme of the extraction apparatus is shown in Figure 4.9.

The metal body containing the glass wool and the tension springs are directly placed in a cellulose extraction thimble of 33mmø and 205mm length and covered with some fresh glass wool. The filter cap and the steel connection tubes are immersed respectively filled with fresh acetone and put in an ultrasonic bath for 15 minutes. They are then

thoroughly washed with more fresh acetone. The thermocouple is also rinsed with acetone and all the solvent used is added to the extraction apparatus.

Figure 4.9: Soxhlet extraction apparatus.

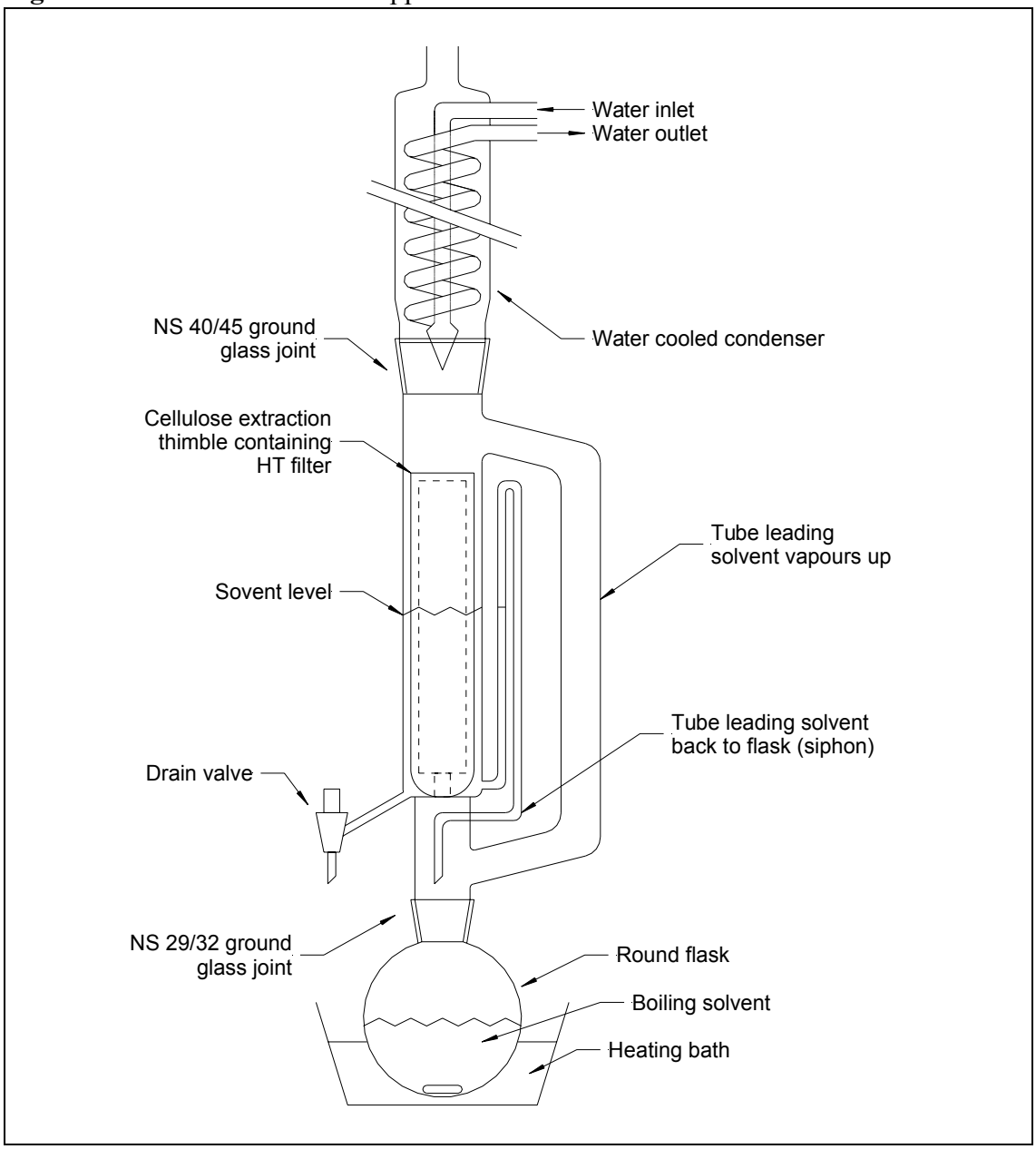

The glass wool filter is first extracted for 24 hours with 300ml acetone. The heating bath is kept at 90°C and both bath and solvent reservoir are vigorously stirred. At the end of this period, the acetone extract volume is reduced to below 100ml by evaporating the solvent and removing the excess through the outlet of the extraction apparatus. The concentrated acetone extract is allowed to cool to room temperature. The round flask is then removed and set aside. A fresh round flask is attached to the extraction apparatus and

250ml toluene are added. Extraction is then continued for another 24 hours with the heating bath kept at 150°C. At the end of this second extraction period the toluene extract is again concentrated, allowed to cool and set aside. Under the conditions used the thimble is flushed with a fresh batch of distilled solvent ca. every 10-15 minutes, resulting in ca. 100-140 extraction cycles per solvent.

Both the acetone and the toluene extracts are then transferred into 100ml volumetric flasks. The volumetric flasks are then filled with the corresponding solvent. From these solutions with known volume, fractions of 8ml are drawn and transferred into 10ml volumetric flasks. Internal standard (see page 102) is added and the flasks filled to 10ml. These solutions are then ready to be injected into the GC/MSD.

The excess solvent reclaimed at the end of the extraction is filled in 200 or 250ml volumetric flasks. Internal standard is added and the flasks are filled with fresh solvent. These samples can also be analysed by GC/MSD to test for the completeness of the extraction. Even if the second extraction with toluene yields a dark coloured extract, no tar compounds could be detected in significant amounts in both excess solvent samples. For this reason the analysis and preparation of the excess solvent samples was discontinued.

Handling of the water phase (sampling bottles 1&2)

Compounds dissolved in the water phase are extracted by liquid/liquid extraction with DCM. The water and tar condensate in sampling bottle 1 is transferred into the continuous extraction apparatus shown in Figure 4.10. This apparatus allows for the extraction of the water phase with a relatively small amount of solvent. The glass insert with porous sintered glass plate enables the distribution of the freshly distilled solvent coming from the condenser as fine droplets into the aqueous phase, enhancing the extraction process. The sampling bottles 1 and 2 as well as the impingers are carefully washed with little water, then with DCM and finally with acetone. The water and the DCM used in this washing procedure are also transferred into the extraction apparatus. The acetone solution obtained in the washing of the bottles is incorporated to the extract after the extraction procedure. A total volume of 250ml of DCM is used in this extraction procedure, which also runs for 24 hours with the heating bath set to 50°C. After this period, the DCM extract is concentrated and the excess solvent reclaimed. The extract and the acetone washing are

then filled into a 100ml volumetric flask and internal standard added. This solution is then ready for analysis on the GC/MSD.

Figure 4.10: Liquid/liquid extraction aparatus.

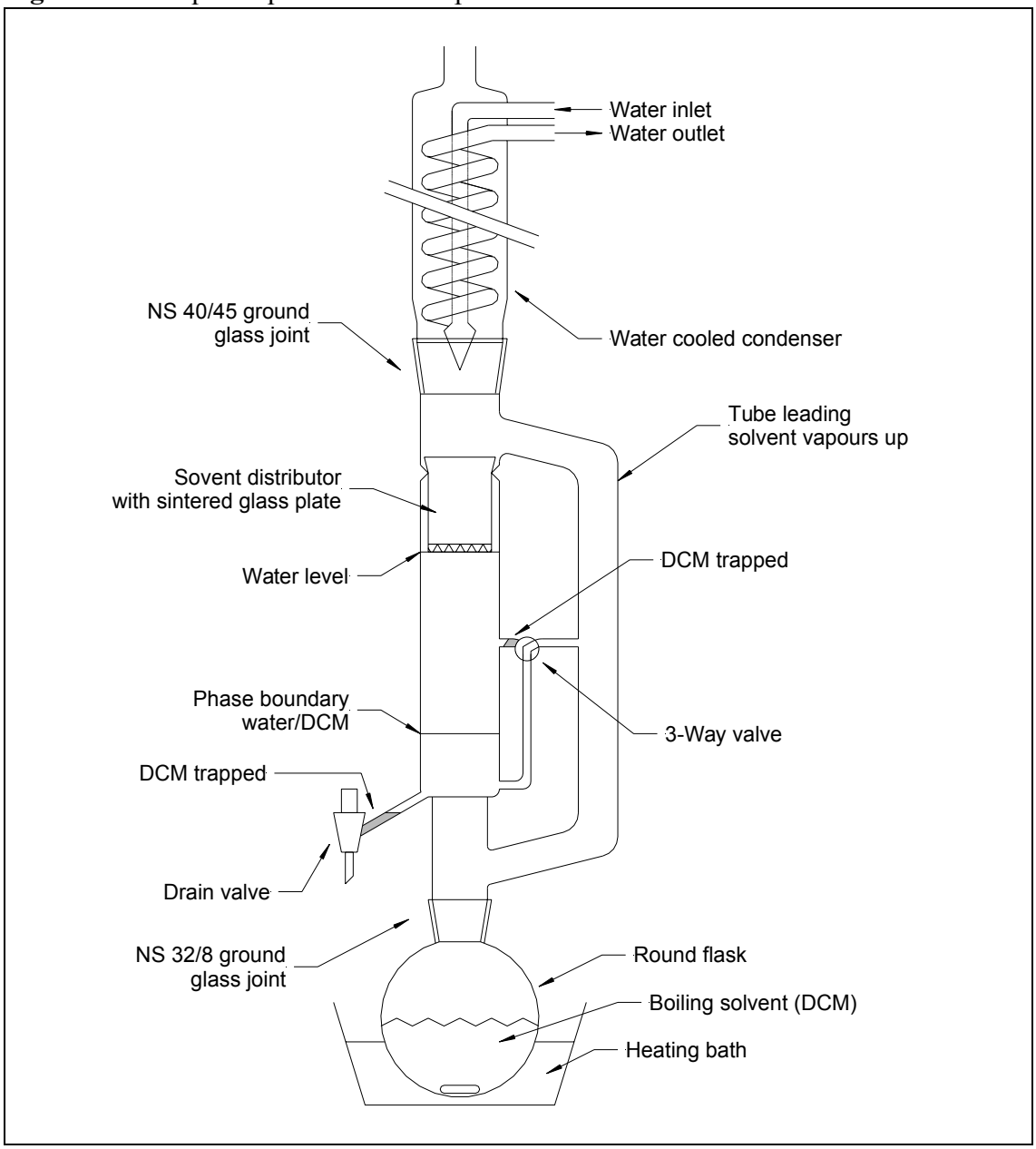

The excess solvent is filled into a 250ml volumetric flask, internal standard is added and the flask filled to the mark with acetone to prevent phase separation of the water saturated DCM. This excess solvent is analysed by GC/MSD as it has been found that it contains minute amounts of tar compounds. These traces of tar compounds probably coming from deposits of DCM with a high tar content which are trapped especially in the drain

valve and in the upper connection to the 3-way valve (see Figure 4.10) as the content of the bottles is transferred into the apparatus.

The thoroughness of the extraction procedure was tested by performing a second extraction for 24 hours with fresh solvent in some samples. The results showed that only negligibly small amounts of tar compounds were still present in the water phase after the first extraction. Also the influence of the acidity of the aqueous phase was tested. The water coming from the sampling procedure is quite alkaline, as it is exposed in the sampling procedure to a gas containing high levels of CO_2. Especially phenolic compounds may be deprotonated if the pH of the aqueous phase is high (pK_A of phenol ≈ 10) making their transfer into the organic phase difficult. Lowering the pH of the water in the extractor by adding acid from approximately 10 to 4 and performing a second 24-hour extraction again showed negligible increase in the amounts of tars extracted. Therefore a single 24 hour extraction is sufficient to remove all tar compounds from the aqueous phase.

Handling of the organic phases (sampling bottles 3-7 and cold trap)

The organic solution in the bottles/cold trap is transferred into appropriate volumetric flasks. In practice, the volumes shown in Table 4.3 were found to be suitable for almost all experiments. The bottles, the impingers and the connecting tubes leading the gas to each bottle are thoroughly rinsed with acetone and the washing solutions added to the corresponding organic phase. Internal standard is added and the volumetric flasks are filled. The solutions are ready for GC/MSD analysis.

Table 4.3: Volumes of the organic solutions.

Bottle Nr.	**3**	**4**	**5**	**6**	**7**	**CT**
Volume [ml]	200	200	250	200	25	50

All samples analysed by the GC/MSD contain the same internal standard (ISTD), 1,2,3,4-tetrahydronaphthalene at a concentration of 100±5µg/ml. This substance was chosen as internal standard for the following reasons:

- it is absent in the gasification tars;
- it has aromatic character and will thus behave similarly to the aromatic tar compounds in the chromatographic system;

- it has an intermediate boiling point relative to the tar compounds analysed. It will thus elute approximately in the middle of the chormatogram making it suitable for the characterisation of all of the tar compounds;
- it is readily available at high purity and modest cost.

The use of an internal standard for GC/MSD quantitative analysis is necessary to eliminate inaccuracies derived from unequal volumes of sample injected. An appropriate volume of internal standard stock solution is added to the samples prior to their dilution to final volume. The exact concentration of ISTD is noted for each sample for later correction of the concentrations.

The result of this preparation procedure are the 10 liquid samples listed in Table 4.4 for each run which are then analysed on the GC/MSD The handling procedures of the tar samples are summarised in Figure 4.11.

Table 4.4: Samples for GC/MSD analysis. YYMMDD: experiment number; X: run in experiment.

Sample name	Origin
YYMMDD X HT Ac	Liquid/solid extract of HT filter with acetone
YYMMDD X HT Tol	Liquid/solid extract of HT filter with toluene
YYMMDD X OE	Liquid/liquid extract of water in bottles 1 and 2
YYMMDD X OER	Excess solvent from liquid/liquid extraction
YYMMDD X 3	Bottle 3
YYMMDD X 4	Bottle 4
YYMMDD X 5	Bottle 5
YYMMDD X 6	Bottle 6
YYMMDD X 7	Bottle 7
YYMMDD X CT	Cold trap

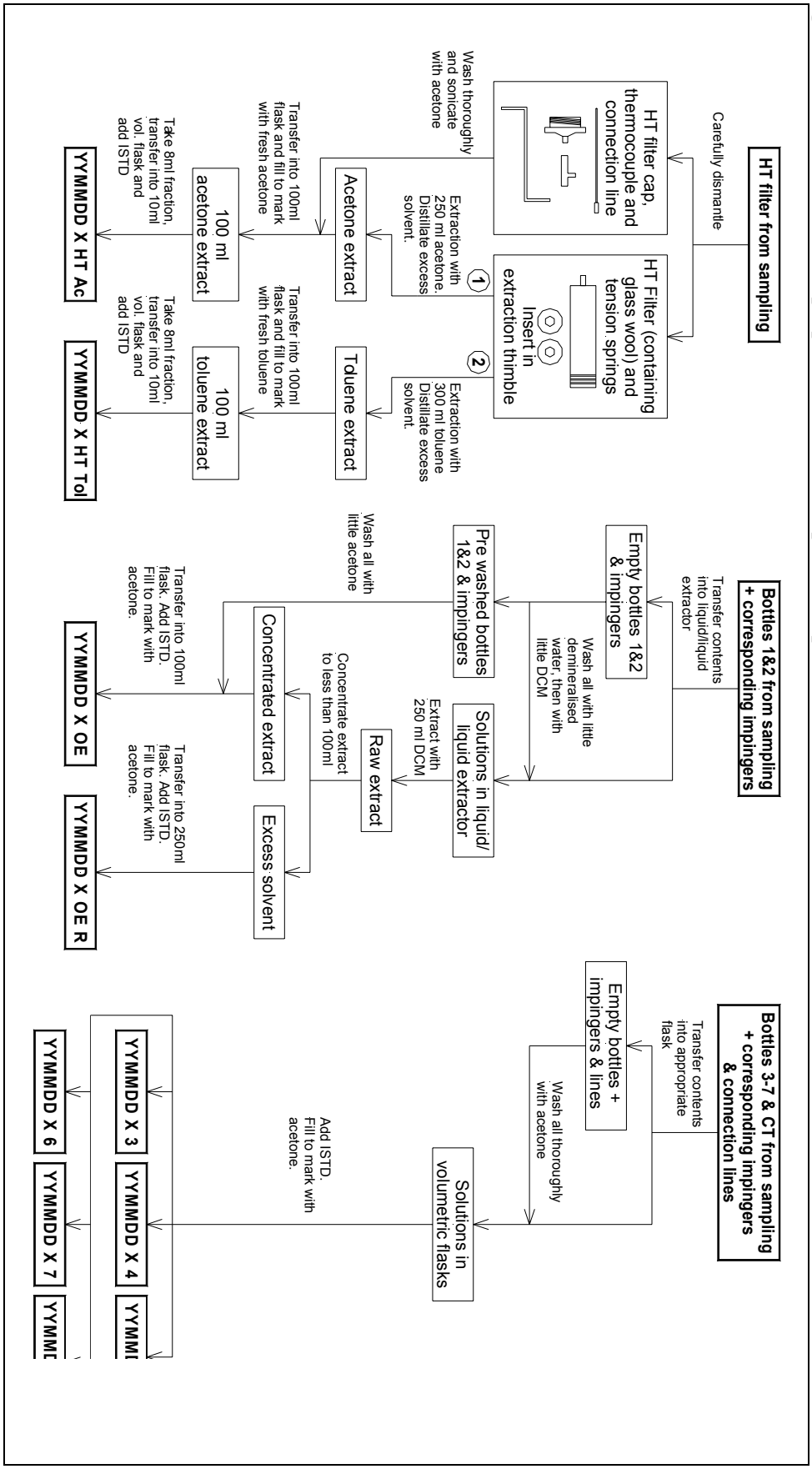

Figure 4.11: Scheme for the preparation of tar samples of experiment YYMMDD run X.

4.3.4 GC/MSD analysis method

Samples prepared according to the last section are analysed for their contents on the 41 compounds listed in Table 4.5. These compounds where selected according the information in references[4.10], [4.24], [4.20], [4.25] and [4.26]. The compounds reported in large concentrations in more than one of the above references where chosen for our GC/MSD analysis method. Also the 16 priority polycyclic aromatic hydrocarbon (PAH) compounds defined by the US environmental protection agency were included.

Table 4.5: Compounds measured by GC/MSD method (BP: Boiling point [4.22], [4.23])

Compound	Formula	Mol. mass [kg/kmole]	BP [°C]	CAS Nr.
Benzene	C_6H_6	78.11	79.9	71-43-2
Toluene	C_7H_8	92.14	110.7	108-88-3
Ethylbenzene	C_8H_{10}	106.17	136.3	100-41-4
p-Xylene	C_8H_{10}	106.17	138.4	106-42-3
m-Xylene	C_8H_{10}	106.17	139.2	108-38-3
o-Xylene	C_8H_{10}	106.17	144.5	95-47-6
Styrene	C_8H_8	104.15	145.3	100-42-5
3-Ethyltoluene	C_9H_{12}	120.19	161.4	620-14-4
4-Ethyltoluene	C_9H_{12}	120.19	162.1	622-96-8
2-Ethyltoluene	C_9H_{12}	120.19	165.3	611-14-3
Phenol	C_6H_6O	94.11	181.8	108-95-2
α-Methylstyrene	C_9H_{10}	118.18	165.5	98-83-9
2-Methylstyrene	C_9H_{10}	118.18	-	611-15-4
3-Methylstyrene	C_9H_{10}	118.18	171.7	100-80-1
4-Methylstyrene	C_9H_{10}	118.18	172.9	622-97-9
2,3-Benzofuran	C_8H_6O	118.14	174.1	271-89-6
o-Cresol	C_7H_8O	108.14	191.1	95-48-7
Indene	C_9H_8	116.16	182.7	95-13-6
p-Cresol	C_7H_8O	108.14	202.0	106-44-5
m-Cresol	C_7H_8O	108.14	202.3	95-48-7
Naphthalene	$C_{10}H_8$	128.17	218.0	91-20-3
2-Methylnaphthalene	$C_{11}H_{10}$	142.20	241.1	91-57-6
1-Methylnaphthalene	$C_{11}H_{10}$	142.20	245.1	90-12-0
Biphenyl	$C_{12}H_{10}$	154.21	256.0	92-52-4
Acenaphthylene	$C_{12}H_8$	152.20	280.1	208-96-8

Table 4.5: Compounds measured by GC/MSD method (BP: Boiling point [4.22], [4.23])

Compound	Formula	Mol. mass [kg/kmole]	BP [°C]	CAS Nr.
Acenaphthene	$C_{12}H_{10}$	154.21	279.1	83-32-9
Dibenzofuran	$C_{12}H_8O$	168.19	287.1	132-64-9
Fluorene	$C_{13}H_{10}$	166.22	294.1	86-73-7
Phenanthrene	$C_{14}H_{10}$	178.23	340.1	85-01-8
Anthracene	$C_{14}H_{10}$	178.23	340.1	120-12-7
Fluoranthene	$C_{16}H_{10}$	202.26	385.8	206-44-0
Pyrene	$C_{16}H_{10}$	202.26	394.2	129-00-0
Benz[a]anthracene	$C_{18}H_{12}$	228.29	437.7	56-55-3
Chrysene	$C_{18}H_{12}$	228.29	448.1	218-01-9
Benz[e]acephenanthrylene	$C_{20}H_{12}$	252.32	-	205-99-2
Benzo[k]fluoranthene	$C_{20}H_{12}$	252.32	480.1	207-08-9
Benzo[a]pyrene	$C_{20}H_{12}$	252.32	495.1	50-32-8
Perylene	$C_{20}H_{12}$	252.32	497	198-55-0
Dibenzo[ah]anthracene	$C_{22}H_{14}$	278.35	524.1	53-70-3
Indeno[1,2,3-cd]pyrene	$C_{22}H_{12}$	276.34	536.0	193-39-5
Benzo[ghi]perylene	$C_{22}H_{12}$	276.34	542	191-24-2

The analysis is carried out on an HP6890 Series gas chromatograph equipped with an HP5973 mass selective detector and an HP6890 Series auto sampler/liquid injector. The column used is an "optima δ-3" capillary column from the company Macherey Nagel. Its dimensions are 60m length, 250µm diameter and a stationary film thickness of 0.25µm. The stationary phase is similar to the popular 5%-phenyl-methyl-siloxane phase used in many capillary GC applications and by some research groups in the analysis of tar compounds. The stationary phase has been modified by the manufacturer to allow for dipole-dipole interactions between the stationary phase and the analytes, enhancing its separation capabilities. This property allows for the proper separation and analysis of compounds with a wider range of polarities. The thermal stability of this particular phase is also very high, allowing for oven temperatures up to 340°C without damage to the costly column. Furthermore this column exhibits low bleeding (i.e. loss of stationary phase when heated), an advantage when performing both quantitative as well as qualitative ("scan") measurements.

The inlet used is a split mode inlet heated to 340°C to minimise deposition of tar compounds. A deactivated glass liner of "reverse cup" design with a silanised glass wool insert is placed into the inlet. This particular liner is used as it exhibits better evaporation characteristics for mixtures of compounds with large range of molecular weights. Furthermore the glass wool prevents fine particles from entering and damaging the column. The carrier gas used is helium and the inlet pressure is automatically corrected to yield a constant gas flow rate of 3 ml/min. throughout the chromatographic analysis run. Two split ratios are used, according to the concentration range to be covered. For analysis of compounds in low concentrations a split of 1:9 is used. For analysis of high concentrations the split used is 1:90. This procedure allows for the coverage of a very wide range of concentrations spanning over four decades (1:1000). This procedure requires however separate calibrations for each split ratio used.

The GC oven is programmed to start analysis at 40°C and then heat up with 10°C/min. to 340°C and hold this temperature for 5 to 10 minutes. This hold time at the end of the chromatographic run depends on the retention time of the last component eluted, Benzo[ghi]perylene. This retention time becomes shorter as the column slowly deteriorates by losing its stationary phase and is adapted as required.

The transfer line between GC and MSD is kept at 340°C. The MSD is in the so-called select ion monitoring mode (SIM) for quantitative analysis of the samples. This technique is important to ensure that the abundance registered by the MSD's detector is proportional to the amount of substance eluted from the column. In SIM mode the MSD is set to retrieve only the abundances of selected ions which are characteristic of the substance exiting the column. This in turn means, that both the characteristic ions as well as the retention time of the substances to be analysed must be known. Both parameters were established by running chromatograms of solutions of the single substances with the MSD in scan mode. In contrast to SIM mode, when in scan mode the MSD is set to sweep through a range of m/z ratios. Therefore a complete mass spectrum is generated at all points of the chormatogram. From these single analyte scan chromatograms, the list of characteristic ions for each substance given in Table 4.6 was established. The chormatogram of the strongest ion of a substance is used for the quantification and is called the target ion. The other ions are merely used to control if the peak registered is truly the substance expected. This control is made by comparing the ratio of responses of these so

called qualifier ions to the target ion. Due to limitations in the hardware it is not possible to switch between groups of ions fast enough if the substances elute too closely. This problem is overcome by allowing for the simultaneous measurement of the characteristic ions of more than one compound. A limit of 9 simultaneously measured ions is used throughout the method to ensure high sensitivity.

Table 4.6: Characteristic ions for GC/MSD SIM mode.

Compound	Target ion	Qualifier ions	
		1st	2nd
1,2,3,4-Tetrahydronaphthalene (ISTD)	104	132	91
Benzene	78	77	52
Toluene	91	92	65
Ethylbenzene	91	106	92
p-Xylene	91	106	105
m-Xylene	91	106	105
o-Xylene	91	106	105
Styrene	104	103	78
3-Ethyltoluene	105	120	91
4-Ethyltoluene	105	120	91
2-Ethyltoluene	105	120	91
Phenol	94	66	65
α-Methylstyrene	118	117	103
2-Methylstyrene	117	118	115
3-Methylstyrene	117	118	115
4-Methylstyrene	117	118	115
2,3-Benzofuran	118	89	90
o-Cresol	108	107	77
Indene	115	116	89
p-Cresol	107	108	77
m-Cresol	108	107	77
Naphthalene	128	129	127
2-Methylnaphthalene	142	141	115
1-Methylnaphthalene	142	141	115
Biphenyl	154	153	152
Acenaphthylene	152	151	150
Acenaphthene	154	153	152
Dibenzofuran	168	139	169
Fluorene	166	165	163
Phenanthrene	178	179	176
Anthracene	178	179	176

Table 4.6: Characteristic ions for GC/MSD SIM mode.

Compound	Target ion	Qualifier ions	
		1st	2nd
Fluoranthene	202	203	200
Pyrene	202	203	200
Benz[a]anthracene	228	226	229
Chrysene	228	226	229
Benz[e]acephenanthrylene	252	250	126
Benzo[k]fluoranthene	252	250	126
Benzo[a]pyrene	252	250	126
Perylene	252	250	126
Dibenzo[ah]anthracene	278	279	139
Indeno[1,2,3-cd]pyrene	276	277	274
Benzo[ghi]perylene	276	277	274

To calibrate the GC/MSD four solutions are used. The concentrations of the analytes in these solutions is given in Table 4.7. The concentration of internal standard (1,2,3,4-Tetrahydronaphthalene) is 101.04µg/ml for all calibration solutions. Note that the method using the lower split ratio is calibrated using only the 3 solutions with the lowest concentration (CS2 to CS4) whereas the method with the high split ratio uses the three solutions with higher analyte concentrations (CS1 to CS3). The calibration procedure involves three-fold injection of each solution and averaging of the measured peak areas. In all 18 runs are necessary to calibrate both methods, a time consuming procedure which offers the advantage of only having to run a single analysis of each sample, as the reproducibility of the analysis results is excellent. The variation of the results generated by the GC/MSD is smaller than 5% about the mean. Note that some isomers among the compounds, namely p- and m-xylene, 2- and 3-methylstyrene could not be separated by the chromatographic method employed and are treated as single compounds.

Table 4.7: Concentrations [µg/ml] of calibration solutions (CS) used.

Compound	CS1	CS2	CS3	CS4
Benzene	10106	1010.6	101.06	10.106
Toluene	5025	502.5	50.25	5.25
Ethylbenzene	5089	508.9	50.89	5.089
p&m-Xylene	10528	1052.8	105.28	10.528
o-Xylene	5002	500.2	50.02	5.002
Styrene	4997	499.7	49.97	4.997
3-Ethyltoluene	1034	103.4	10.34	1.034
4-Ethyltoluene	1020	102	10.2	1.02
2-Ethyltoluene	1034	103.4	10.34	1.034
Phenol	1021	102.1	10.21	1.021
α-Methylstyrene	1039	103.9	10.39	1.039
3&2-Methylstyrene	2070	207	20.7	2.07
4-Methylstyrene	1041	104.1	10.41	1.041
2,3-Benzofuran	1095	109.5	10.95	1.095
o-Cresol	1198	119.8	11.98	1.198
Indene	1033	103.3	10.33	1.033
p-Cresol	1316	131.6	13.16	1.316
m-Cresol	1033	103.3	10.33	1.033
Naphthalene	1126	112.6	11.26	1.126
2-Methylnaphthalene	1039	103.9	10.39	1.039
1-Methylnaphthalene	1049	104.9	10.49	1.049
Biphenyl	1008	100.8	10.08	1.008
Acenaphthylene	437	43.7	4.37	0.437
Acenaphthene	1060	106	10.6	1.06
Dibenzofuran	1180	118	11.8	1.18
Fluorene	1017	101.7	10.17	1.017
Phenanthrene	1050	105	10.5	1.05
Anthracene	1000	100	10	1
Fluoranthene	1010	101	10.1	1.01
Pyrene	1040	104	10.4	1.04
Benz[a]anthracene	420	42	4.2	0.42
Chrysene	500	50	5	0.5
Benz[e]acephenanthrylene	205	20.5	2.05	0.205
Benzo[k]fluoranthene	152	15.2	1.52	0.152
Benzo[a]pyrene	420	42	4.2	0.42
Perylene	504	50.4	5.04	0.504
Dibenzo[ah]anthracene	539	53.9	5.39	0.539
Indeno[1,2,3-cd]pyrene	498	49.8	4.98	0.498
Benzo[ghi]perylene	505	50.5	5.05	0.505

The results of each injection are peak areas for each compound as well as for the ISTD. In the quantification method using internal standards it is assumed that the ratio of the peak area of a compound (A_i) to the peak area of the ISTD (A_{ISTD}) are proportional to the ratio of the concentrations:

$$\frac{A_i}{A_{ISTD}} = f_i \cdot \frac{c_i}{c_{ISTD}} \tag{4.1}$$

In reality this proportionality is only valid in a narrow range of concentrations. Therefore a polynomial curve is fitted for each compound yielding calibration functions of the form:

$$\frac{A_i}{A_{ISTD}} = \alpha_i \cdot \left(\frac{c_i}{c_{ISTD}}\right)^2 + \beta_i \cdot \left(\frac{c_i}{c_{ISTD}}\right) + \gamma_i \tag{4.2}$$

The GC/MSD software allows for the calculation of 7 types of calibration curves using weighted linear regression. Weighted linear regressions are required when the variances are not identical for all data points. In the case of our GC/MSD measurements extensive repeated measurements would be required to yield the variances of the complex set of data points generated. However, in the case of GC/MSD data, the variances can be approximated by using the factors $\frac{1}{\left(\frac{c_i}{c_{ISTD}}\right)}$ or $\frac{1}{\left(\frac{c_i}{c_{ISTD}}\right)^2}$ [4.27]. The regressions for the results obtained from each calibration is checked and the best fitting curve is selected for each compound separately. The best fit is defined as the smallest sum of deviations between the predicted and the actual concentrations in the calibration samples. Note that this choice was made as there is no unique statistical procedure for selecting the best regression equation [4.28].

Additionally to the quantitative analysis the samples are qualitatively analysed using the MSD in scan mode to check for unknown substances present in high concentrations. These scan runs were performed with the MS scanning the range of 18 to 400 amu. Examples of quantitative SIM and qualitative scan chromatograms are shown in Figures 4.12 and 4.13.

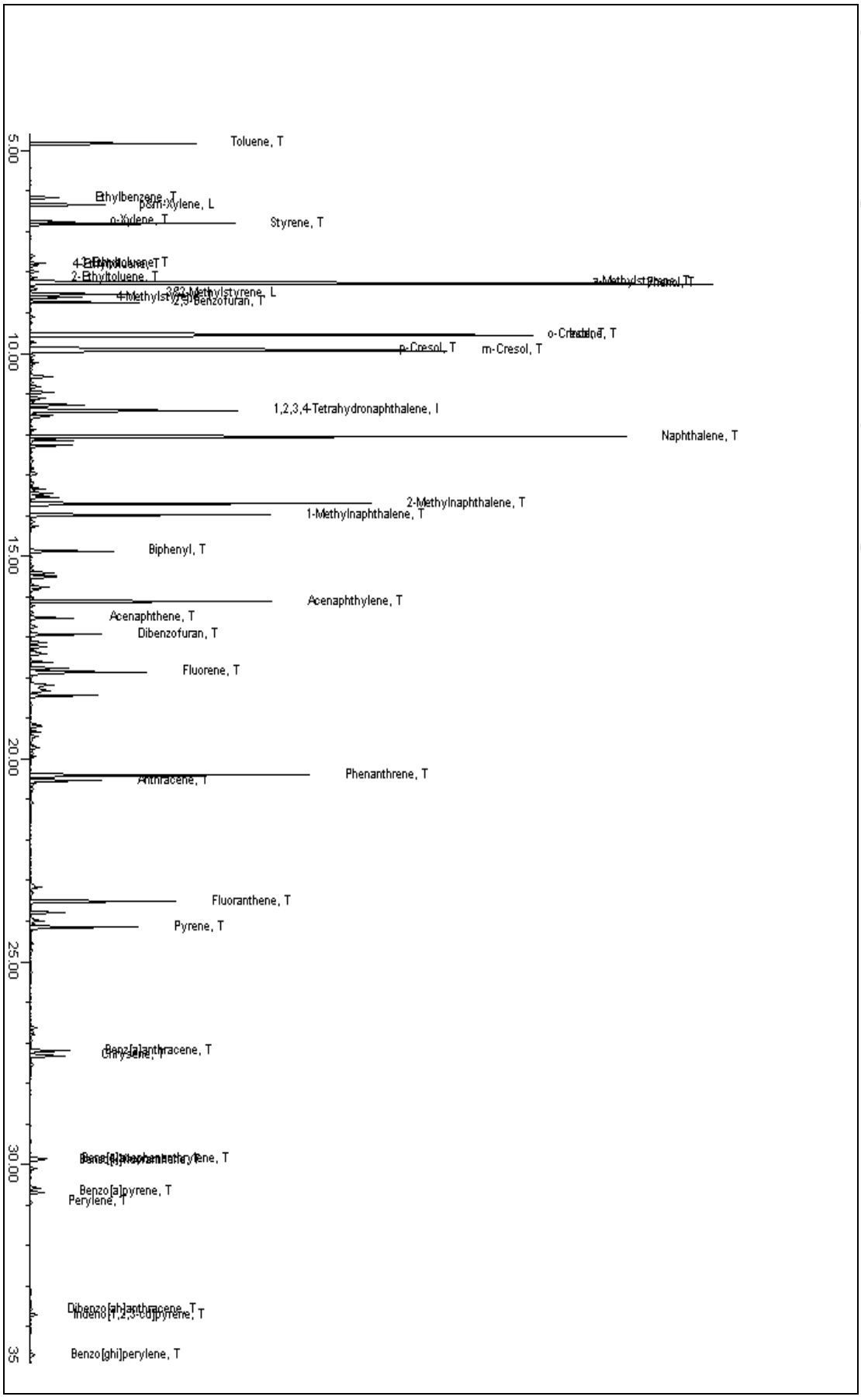

Figure 4.12: SIM (quantitative) chromatogram of sample 991005 A OE.

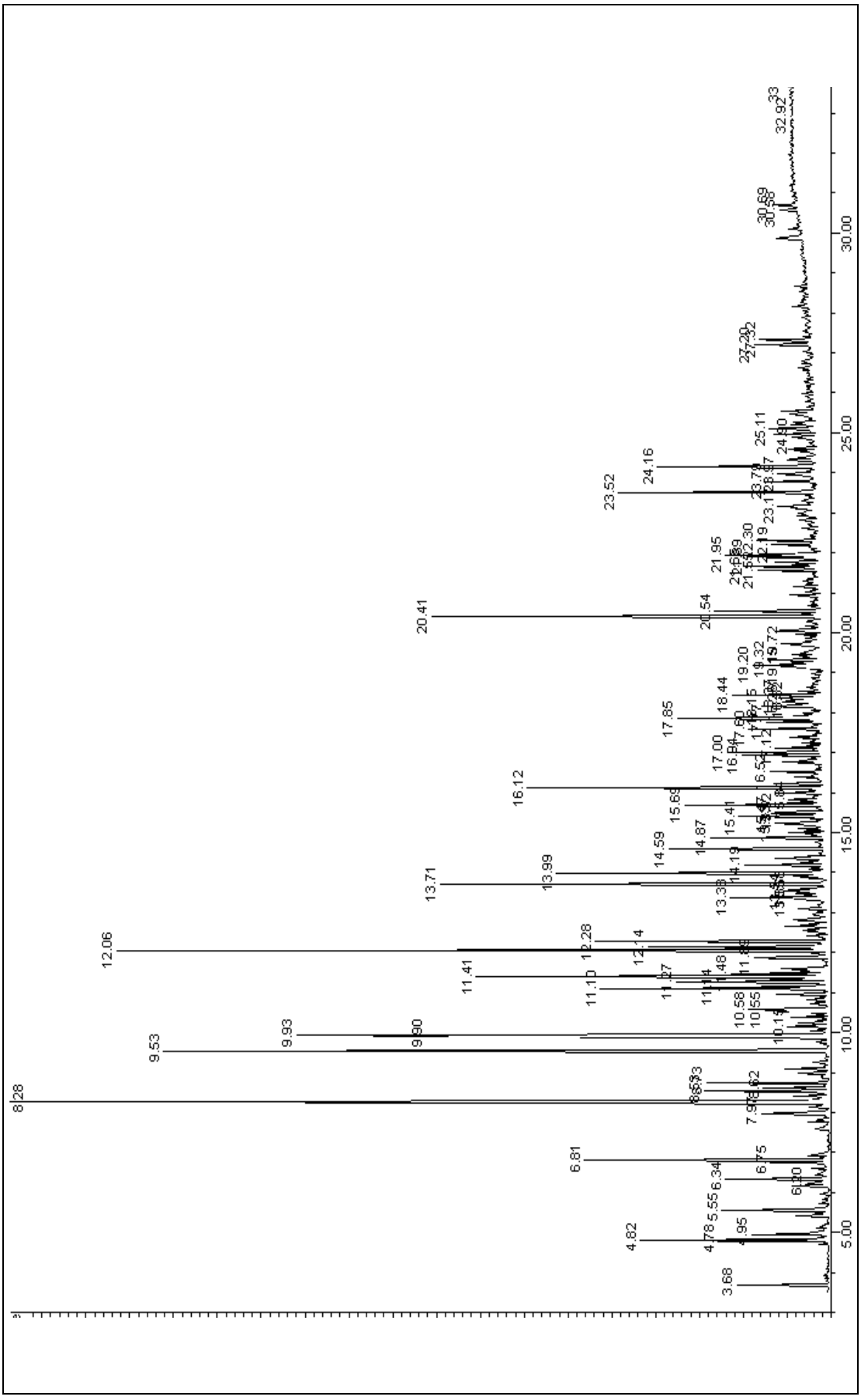

Figure 4.13: Scan (qualitative) chromatogram of sample 991005 A OE.

In the analysis of the toluene extract of the heavy tar filter, all compounds eluting before 2,3-bezofurane with the exception of phenol are ignored. The reason for this is, that many of these compounds are substituted toluenes already present in the toluene solvent used in amounts detectable by the analysis method.

The results from the GC/MSD qualitative analysis are concentrations of the single compounds in each sample. These concentrations are multiplied by the sample volume, yielding the compounds masses in each sample. The masses in the acetone and toluene extract are further multiplied by a factor (volume of raw extract/volume of fraction used in GC sample preparation, generally 100ml/8ml see page 100) to yield the correct mass of the compounds found in the original HT filter extracts. The masses of each sample are added yielding the total mass of a given component sampled in a particular run.

Finally, the concentrations of the compounds in the gas is obtained by simply dividing the mass of compound by the volume of gas sampled at normal or standard (1013.25mbar, 237.15K) conditions. As an example the tar masses in the samples of run 991005A is given in Table 4.8. Note that the concentrations of tar compounds calculated are tar concentrations per volume of dry, tar-free gas. To obtain the correct concentration of tar compounds in the gas as it exits the reactor allowance must be made for the tar and water amount in the gases.

Table 4.8: Tar compound masses [µg] for tar samples and total mass of compounds [mg] for run 991005A.

	Sample										Total
Compound	**HT Ac**	**HT Tol**	**OE**	**OER**	**3**	**4**	**5**	**6**	**7**	**CT**	**[mg]**
Benzene	63	0	8145	825	412880	37932	1213	63	5	4	461.1
Toluene	97	0	13732	126	242178	31319	216	0	10	0	287.7
Ethylbenzene	74	0	2588	7	11419	4711	18	0	0	0	18.8
p&m-Xylene	89	0	14033	41	52406	24027	100	0	0	0	90.7
o-Xylene	16	0	3918	3	9927	5792	7	0	0	0	19.7
Styrene	148	0	20310	133	40591	25565	151	62	8	16	87.0
3-Ethyltoluene	24	0	1422	12	1453	1671	30	0	0	0	4.6
4-Ethyltoluene	9	0	685	0	673	773	0	0	0	0	2.1
2-Ethyltoluene	4	0	561	1	463	611	1	0	0	0	1.6
Phenol	9932	169	244057	117	13301	37995	110	36	4	9	305.7
α-Methylstyrene	31	0	2858	11	2005	2860	25	0	0	0	7.8
3&2-Methylstyrene	101	0	10256	30	5669	9144	71	0	0	0	25.3
4-Methylstyrene	47	0	4094	16	2202	3654	38	0	0	0	10.0
2,3-Benzofuran	128	41	10624	14	5047	7580	18	0	0	0	23.5
o-Cresol	3270	63	88659	26	5307	14008	77	0	0	0	111.4
Indene	472	1	39758	19	13888	27987	40	0	0	0	82.2
p-Cresol	4712	124	79969	62	5331	15024	172	0	0	0	105.4
m-Cresol	5187	50	84761	0	5764	16869	31	0	0	0	112.7
Naphthalene	1745	63	57914	23	8253	24712	105	0	0	0	92.8
2-Methylnaphthalene	1483	24	20784	33	3045	10110	70	16	2	4	35.6

Table 4.8: Tar compound masses [µg] for tar samples and total mass of compounds [mg] for run 991005A.

	Sample										Total
Compound	**HT Ac**	**HT Tol**	**OE**	**OER**	**3**	**4**	**5**	**6**	**7**	**CT**	**[mg]**
1-Methylnaphthalene	1176	10	15301	23	2143	7221	50	12	0	0	25.9
Biphenyl	577	24	5256	16	693	2359	48	0	0	0	9.0
Acenaphthylene	2706	13	21246	12	2220	7090	50	0	0	0	33.3
Acenaphthene	360	0	2355	0	289	975	35	0	0	0	4.0
Dibenzofuran	744	30	4230	21	521	1757	58	0	0	0	7.4
Fluorene	1335	28	6658	23	759	2686	65	0	0	0	11.6
Phenanthrene	4516	44	15987	33	1909	6658	103	0	0	0	29.2
Anthracene	1295	0	4628	51	545	1901	130	0	0	0	8.5
Fluoranthene	2607	31	7022	27	813	2955	73	0	0	0	13.5
Pyrene	2010	29	5139	25	589	2131	65	0	0	0	10.0
Benz[a]anthracene	1062	20	2170	16	238	869	43	0	0	0	4.4
Chrysene	868	15	1728	12	201	694	33	0	0	0	3.6
Benz[e]acephenanthrylene	430	0	741	0	82	283	10	0	0	0	1.5
Benzo[k]fluoranthene	325	0	576	0	57	219	0	0	0	0	1.2
Benzo[a]pyrene	516	0	870	0	91	324	16	0	0	0	1.8
Perylene	88	0	151	0	24	59	15	0	0	0	0.3
Dibenzo[ah]anthracene	84	0	127	0	18	50	0	0	0	0	0.3
Indeno[1,2,3-cd]pyrene	248	4	375	0	41	138	0	0	0	0	0.8
Benzo[ghi]perylene	180	0	259	0	22	93	0	0	0	0	0.6
										Total tar mass detected by GC/MSD [mg]:	2052.6

Throughout the analysis of the tar samples it was noted that not all 10 solutions had to be analysed. An average of 99.9% of the tars are found in the samples coming from bottles 3 to 5, the acetone extraction of the HT filter, the liquid/liquid extract of the water phase and the excess solvent from this extraction. Accordingly the analysis of the samples issued from bottles 6 and 7 and from the cold trap was discontinued. This reduction in the number of analysed samples represents substantial time saving as each analysis requires over 40 minutes to complete.

Another point which allows some time to be saved is, that due to the splitting of the calibration in two ranges only one analysis per sample and concentration range is required. The samples containing high concentration if tars (usually OE, 3 and 4) are however analysed using both concentration range methods.

4.3.5 Laboratory tests of the sampling train

The trapping capability of the tar sampling train used was tested under laboratory conditions [4.29]. In these tests only three tar compounds, namely toluene, phenol and naphthalene were used, to represent roughly the types of compounds present in the gas. Also, the tests were carried out without the HT filter in an attempt to truly identify weather tar compounds could pass through the sampling train's absorption part. The tests were conducted by evaporating or sublimating the compounds from a glass container in a thermostat and flushing this container with nitrogen. The gas containing the compounds was then led to the series of 7 bottles used in the tar sampling train and the solutions obtained were prepared as explained in Section 4.3.3 and analysed by GC/MSD.

The results of these tests showed, that 99.9% of the compounds masses were always trapped in bottles 1 to 4. This excellent trapping capability was not affected by gas flow or by the concentration of the compounds in the gas phase. Additionally, an experiment were mass balances were carried out for all three compounds showed that this tar trapping set-up is able to quantitatively retain tar compounds.

4.4 References

[4.1] P. Hasler, R. Buehler, T. Nussbaumer, *Evaluation of Gas Cleaning Technologies for Biomass Gasification*, in Biomass for Energy and Industry, Proceedings of the 10th European Conference and Technology Exhibition, Würzburg 8-11 June 1998, H. Kopetz et. al. (eds.), CARMEN, Rimpar, Germany, 1998, pp.272-275

[4.2] K. Maniatis, A.A.C.M. Beenackers, *Tar Protocols. IEA Bioenergy Gasification Task*, Biomass and Bioenergy, 2000, **18**, (1), pp.1-4

[4.3] N. Abatzoglou, N. Barker, P. Hasler, H. Knoef, *The Development of a Draft Protocol for the Sampling and Analysis of Particulate and Organic Contaminants in the Gas from Small Biomass Gasifiers*, Biomass and Bioenergy, 2000, **18**, (1), pp.5-17

[4.4] P. Simell, P. Ståhlberg, E. Kurkela, J. Albrecht, S. Deutsch, K. Sjöström, *Provisional Protocol for the Sampling and Analysis of Tar and Particulates in the gas from Large-Scale Biomass Gasifiers. Version 1988*, 2000, **18**, (1), pp.19-38

[4.5] A. Das, *Contaminant Testing For Gasifier Engine Systems*, Biomass Energy Foundation, 1989 (Available through http:\www.webpan.com/bef)

[4.6] H.A.M. Knoef, T. Lautenschlaeger, A. Hollingdale, *Development of a Standard Procedure for Gas Quality Testing in Biomass Gasifier Plant/Power Generation Systems*, Final Report for the European Commission, Joule Programme, Report Nr. JOU2-CT93-0408, BTG Biomass Technology Group, Twente, 1995

[4.7] H. Hofbauer, T.F. Veronik, R. Rauch, H. Mackinger, E. Fercher, *The FIBC-Gasification Process*, in Developments in Thermochemical Biomass Conversion, A.V. Bridgwater, D.G.B. Boocock (eds.), Blackie Academic & Professional, London, 1997, Volume 2, pp.1016-1193

[4.8] P. Ståhlberg, E. Kurkela, *Sampling and Analytical Methods for Product gases from Solid Fuel Gasifiers*, Paper presented at the IEA/Biomass Thermal Gasification meeting in Neuchâtel, Switzerland, 1990

[4.9] P. Ståhlberg, M. Lappi, E. Kurkela, P. Simell, P. Oesch, M. Nieminen, *Sampling of Contaminants from Product Gases of Biomass Gasifiers*, Technical Research Centre of Finland, VTT Research Notes 1903, Espoo, 1998

[4.10] C.M. Kinoshita, Y. Wang, J. Zhou, *Tar Formation under Different Biomass Gasification Conditions*, Journal of Analytical and Applied Pyrolysis, 1994, **29**, pp.169-181

[4.11] E. Fercher, H. Hofbauer, T. Fleck, R. Rauch, G. Veronik, *Two Years Experience with the FIBC-Gasification Process*, in Biomass for Energy and Industry, Proceedings of the 10th European Conference and Technology Exhibition, Würzburg 8-11 June 1998, H. Kopetz et. al. (eds.),CARMEN, Rimpar, Germany, 1998 pp.280-283

[4.12] P. Hasler, R. Salzmann, H.P. Kaufmann, T. Nussbaumer, *Method for the Sampling and Analysis of Particles and Tars from Biomass Gasifiers*, in Biomass for Energy and Industry, Proceedings of the 10th European Conference and Technology Exhibition, Würzburg 8-11 June 1998, H. Kopetz et. al. (eds.),CARMEN, Rimpar, Germany, 1998 pp.1600-1603

[4.13] P. Hasler, P. Morf, T. Nussbaumer, *Testing of a Sampling Train with a Liquid Quench System for Tar and Particles from Biomass Gasifiers*, Test Report for the Swiss federal Office of Energy, Bern, 2000

[4.14] P. Morf, P. Hasler, T. Nussbaumer, *Mechanisms of Tar Conversion During Fixed-Bed Gasification*, Presented at the 1st World Conference on Biomass for Energy and Industry, June 5-9, Seville, Spain, 2000

[4.15] O. Moersch, H. Spliethoff, K.R.G. Hein, *Quasi Continuous Tar Quantification with a new Online Analyzing Method*, in Biomass for Energy and Industry, Pro-

ceedings of the 10th European Conference and Technology Exhibition, Würzburg 8-11 June 1998, H. Kopetz et. al. (eds.),CARMEN, Rimpar, Germany, 1998 pp.1638-1641

[4.16] C. Barge, Q. Yu, G. Chen, K. Sjöström, *Use of Amino Phase Adsorbent for Biomass Tar Sampling and Separation*, Fuel, 1997, **2**, pp.137-142.

[4.17] N. Padban, W. Wang, Z. Ye, I. Bjerle, I. Odenbrand, *Tar Formation in Pressurised Fluidized Bed Air Gasification of Woody Biomass*, Energy and Fuels, 2000, **14**, pp.603-611

[4.18] D.C. Dayton, R.J. Evans, *Laboratory Gasification Studies via Partial Oxidation of Biomass Pyrolysis Vapors*, in Making a Business from Biomass in Energy, Environment, Chemicals, Fibers and Materials Proceedings of the 3rd Biomass Conference of the Americas, Montreal, Quebec, Canada, August 24-29 1997, R.P. Overend, E. Chornet (eds.), Elsevier Science, 1997, pp.673-682

[4.19] http://www.nrel.gov/research/industrial_tech/tmbms.html

[4.20] E. Kukela, P. Ståhlberg, J. Laatikainen, *Pressurized fluidized-bed gasification experiments with wood, peat and coal at VTT in 1991-1992. Part 1. Test facilities and gasification experiments with sawdust*, Technical research centre of Finland, VTT-Report 161, 1993

[4.21] U. Zielke, P.D. Kellberg, *Parallel measurement of tar and particulates*, Test Report for the Danish Energy Agency, DEA Journal No. 51166/99-0004, Danish Technological Institute, 1999

[4.22] http://webbook.nist.gov/chemistry/

[4.23] http://chrom.tutms.tut.ac.jp/JINNO/DATABASE/00alphabet.html

[4.24] H.Aldén, B.G. Espenäs, E. Rensfelt, *Conversion of tar in pyrolysis gas from wood using a fixed dolomite bed*, Research in thermochemical biomass conversion, 1988, pp.987-1001

[4.25] P. Simell, E. Kurkela, P. Ståhlberg, *Formation and catalytic decomposition of tars from fluidized-bed gasification*, in Advances in Thermochemical Biomass Conversion, A.V. Bridgwater (ed.), Blackie Academic & Professional, Glasgow, 1994, (Vol. 1), pp.160-174

[4.26] R.J. Evans, R.A. Knight, M.Oniscak, S.P. Babu, *Process performance and environmental assessment of the Renugas® process*, in Energy from biomass and wastes X, D.L. Klass (ed.), Institute of Gas Technology, Chicago, 1987

[4.27] H.T. Karnes, G. Shiu, V.P. Shah, *Validation of Bioanalytical Methods*, Pharmaceutical Research, 1991, **8**, (4)

[4.28] N. Draper, H. Smith, *Applied Regression Analysis*, 2nd edition, John Wiley & Sons, New York, 1981

[4.29] R. Schaubhut, *Überprüfung der Apparatur zur Teerprobenahme bei der Wirbelschichtvergasungsanlage MARTHA mittels den Mustersubstanzen Toluol, Phenol und Naphthalin*, Praktische Semesterarbeit im Block Umwelttechnik, ETH Zürich, 2000

5 EXPERIMENTAL RESULTS

5.1 Experimental plan

5.1.1 Fractional factorial experimental plan

The study of gasification was started with an experimental plan based on the fractional factorial design method using SCW as fuel and air as gasification agent. For an in-depth discussion of this experimental design method see references [5.1] and [5.2]. Experimental design methods are used in the study of complex systems to yield a maximum of information on the system's behaviour with a minimum number of experiments. Design methods prescribe the values of the variables for a series of experiments to meet the above criterion. By this procedure, I expected to gather information on which operational parameters had the strongest influence on the gasification products, especially the tar amount and composition. Once these most important parameters where established, fur-

ther experiments with other fuels and gasification agents would focus only on a smaller number of variables.

The variables to be studied using the factorial method must be independent. In preliminary or screening experiments (such as those envisaged at the beginning of the study) it is usual to select the values for the variables as the maximum and minimum values of the range considered. The variables are normalised for the mathematical treatment of the design. For example if a temperature T is to be studied between T_{min} and T_{max} the normalised variable X_T assigned to the temperature is calculated as follows:

$$X_T = \frac{T - \left(\frac{T_{max} + T_{min}}{2}\right)}{\left(\frac{T_{max} - T_{min}}{2}\right)} \tag{5.1}$$

X_T will therefore assume the values of +1 and -1 when the temperature T is set to T_{max} respectively to T_{min}. In a full factorial design, all the n variables of interest are combined at both levels, yielding a total of 2^n experiments to be preformed. With this design it is possible to fit an empiric linear model to the data generated by the experiments in which the combined interactions of more than one variable may be determined. It is also possible to design experiments at more than two levels for the variables, allowing for more complexity in the models to be fitted. The number of experiments required does however grow rapidly (for example 3^n for three levels and n variables) making such designs impractical at the beginning of an investigation. Table 5.1 shows an example of a

Table 5.1: Full factorial design for three variables.

Experiment number	X_1	X_2	X_3	Result
4	-1	-1	-1	Y_4
7	+1	-1	-1	Y_7
5	-1	+1	-1	Y_5
1	+1	+1	-1	Y_1
6	-1	-1	+1	Y_6
3	+1	-1	+1	Y_3
8	-1	+1	+1	Y_8
2	+1	+1	+1	Y_2

full factorial design for three variables in which a quantity Y is measured as a result (or response) of each experiment. To minimise the effect of systematic errors the order in which the experiments are carried out is chosen randomly.

The results data set ($Y_1, Y_2, ..., Y_8$) obtained by the experiments allows the calculation of 8 fit parameters θ_i, yielding the following linear model:

$$\hat{Y} = \theta_0 + \theta_1 X_1 + \theta_2 X_2 + \theta_3 X_3 + \theta_{12} X_1 X_2 + \theta_{13} X_1 X_3 + \theta_{23} X_2 X_3 + \theta_{123} X_1 X_2 X_3 \qquad (5.2)$$

The *fractional* factorial design method allows for a reduction in the number of experiments by using the combination of values of arbitrarily chosen variables to assign values to the remaining variables. The assignment relations are called "generators of the design". This procedure also reduces the number of parameters which can be predicted accurately. However proper selection of the combination procedure still allows to estimate the parameters θ_i for the single variables and some of the combined influences of more than one variable. This loss of information is compensated by the fact, that the combined influence of more than two variables is generally small and may be disregarded.

Using this method it was planned to establish the influence of the 6 variables listed in Table 5.2, with only 16 experiments in a so called 2^{6-2} design with the "generators" 5=123 and 6=234.

Table 5.2: Operational variables for fractional factorial design.

Variable	Normalised variable	Level		
		Low (-1)	Mid (0)	High (+1)
Bed temperature (T_{bed})	X_1	700°C	800°C	900°C
Freeboard temperature gradient (γ)	X_2	0°C	-50°C	-100°C
Equivalence ratio (ER)	X_3	0.2	0.3	0.4
Fuel humidity (ζ)	X_4	0%	15%	30%
Bed particle size ($d_{p,bed}$)	X_5	0.4mm	0.4mm	0.7mm
Bed aspect ratio (H/D)	X_6	1	2	3

This design would allow for the precise estimation of the parameters for the single variables X_1-X_4. The parameters for the variables X_5 and X_6 can however not be estimated alone. Only a combination of these parameters with the parameter for the combined influence of the variables X_1, X_2, X_3 and X_2, X_3, X_4 respectively can be calculated. This

drawback was accepted, as the first four variables where expected to be those with the major influence. To estimate the variance of the results, repeated experiments were planed at the so-called central point (X_i=0).

The bed temperature was to be set and controlled with the aid of the heater shells surrounding the bed module. The freeboard temperature gradient to be used was defined as the difference of the bed temperature to the topmost temperature in the reactor. The fuel humidity values are on a wet basis and would be set by drying the fuel in an oven as required. The bed particle size corresponds to the mean particle diameters of two types of Molochite available (see page 34). The central point value for this parameter could not properly be set and it was decided to run the central point experiment using the smaller bed particles. The bed aspect ratio is defined as the height of the bed at minimum fluidisation conditions to the reactor's inner diameter (0.213m). To simplify the operation of the set-up is was further decided to perform first all experiments with the fine bed material and then change the bed's inventory to the coarser material. The complete set of planned experimental conditions is shown in Table 5.3.

Table 5.3: Experiments planned by the fractional factorial method.

Exp. Nr.	T_{bed} [°C]	γ [°C]	ER [-]	ζ [%]	$d_{p,bed}$ [mm]	H/D [-]
1	700	0	0.2	0	0.4	1
2	900	0	0.4	30	0.4	1
3	700	-100	0.4	30	0.4	3
4	900	0	0.4	0	0.4	3
5	900	-100	0.2	0	0.4	3
6	700	0	0.2	30	0.4	3
7	900	-100	0.2	30	0.4	1
8	700	-100	0.4	0	0.4	1
9	700	-100	0.2	0	0.7	3
10	900	-100	0.4	30	0.7	3
11	700	-100	0.2	30	0.7	1
12	900	0	0.2	0	0.7	1
13	900	-100	0.4	0	0.7	1
14	900	0	0.2	30	0.7	3
15	700	0	0.4	30	0.7	1
16	700	0	0.4	0	0.7	3
R1	800	-50	0.3	15	0.4	2
R2	800	-50	0.3	15	0.4	2

This experimental plan could however not be carried out fully, only the experiments 1 to 13 were performed and not in all experiments could the planned conditions, especially the bed temperature, be maintained. Problems arose as the second part of the design with coarser bed material was started and experiments with "extreme" combinations of the parameters temperature, fuel humidity and ER were performed. In these experiments it was not possible to keep the bed temperature within the self-imposed limits of ±10°C and in some experiments the bed temperature rose slowly but constantly over the whole experiment. With the coarser material higher air flows are required to meet the $u_0/u_{mf} = 2$ criterion (see page 44). Larger fuel flows are thus required for a given ER and therefore larger heat production or demand arise. This heat demand respectively cooling requirements could not be met. The heat input to the bed is limited by the heating shells' heating power and no special means for cooling the bed (as for example a heat exchanger) are provided.

The clear result from these experiments is the unequivocal dependence of the parameters bed temperature, ER and fuel humidity. This relationship was clear before the experiments were started, but still it was expected that these variables could be changed within certain limits using the present gasification test rig. Results from other authors (see for example [5.3] and [5.4]) state, that these variables can be treated independently in experimental studies. One conclusion from these experiments is, that the range of operational conditions chosen was too broad to be realised with the existing installation.

At about the same time as these operational problems were first encountered, a major change in the tar analysis procedure took place. The GC/FID instrument used so far was replaced by a GC/MSD instrument. A series of tar samples already analysed by GC/FID were re-analysed by GC/MSD, revealing that the results produced by the two instruments were too different to allow comparison. This discrepancy in the results may be explained by inaccuracies in the calibration procedure and maintenance of the analysis method for the GC/FID instrument and by improper peak assignment in the GC/FID chromatograms, where the substances could only be identified by their retention time. Re-analysis of all samples was not possible, since many of the back-up samples clearly showed loss of substance even if kept in a refrigerator and since too much time would be required in the re-analysis process.

Additionally, the data gathered in these experiments could not be properly treated, as the experimental plan was not completed. An attempt was made to analyse the data from the first half of the factorial plan (experiments with smaller bed material) without success. Only a complete set of data allows for correct analysis when using the factorial method, a clear disadvantage of this experimental design procedure.

A complete abandon of the experimental plan executed so far was thus decided and a new one was designed. The results obtained in these experiments will not be presented or discussed here. Even if useful scientific information could not be gathered by this long series of tests, valuable knowledge on the operation of the set-up and on tar sampling and analysis procedures was gathered throughout this period.

5.1.2 Final experimental plan

A new series of experiments all performed under autothermal conditions at three different ERs (0.2, 0.3 and 0.4, see page 46) was planned to study the aspects described in the next sub-sections.

In all experiments the bed aspect ratio used was H/D=3 equating to a bed height at minimum fluidisation of ca. 640mm or a bed material mass of ca. 25.8 kg. The bed material used was the coarse Molochite ($\bar{d}_p$ = 708μm). No temperature gradient was applied to the freeboard meaning that corresponding to the ER's of 0.2, 0.3 and 0.4 the freeboard temperature was set uniformly at 700, 800 and 900°C respectively. Even though the fuel humidity is an operational parameter for a large scale gasifier, it was not studied here. The fuel humidity of the Altholz used cannot be changed, and preliminary experiments showed that it was not possible to gasify very wet SCW. Thus the humidity of the SCW was always set at 5-10% to match the humidity of the Altholz.

The influence of the fuel type and gasification agent.

SCW and altholz would be tested using both, air and steam/oxygen as gasification agents. These experiments would allow the comparison of the behaviour of the same fuel with different gasification agents as well as the comparison of different fuels with the same gasification agent.

From preliminary experiments it was already known that Altholz yields a lower tar amount in the gases and some experiments were planned to test whether some characteristics of the Altholz used were responsible for this reduction.

The Altholz used had a smaller particle size than the SCW and thus milled SCW would be used to test for the influence of the particle size.

Altholz originates to a large extent from demolition activities. This in turn means, that the Altholz is made of "old" wood. The aging process could modify the structure or composition of the wood. For example, some of the volatile compounds found in fresh wood might not be present in Altholz and this could have an influence on the behaviour of this fuel. To test this hypothesis a batch of SCW would be artificially aged (see page 39) and gasified.

Finally, Altholz contains higher amounts of chlorine and heavy metals than wood. Experiments were planned in which SCW would be mixed with salts or impregnated with solutions containing these contaminants. Due to lack of time, these contaminant experiments could however not be carried out.

The influence of plastics admixture.

The admixture of plastics would be studied only with steam/oxygen as these fuel mixtures would only be used in gasification for the production of nitrogen-free synthesis gas. The amount of plastics to be mixed would be varied at two levels to gain information on the influence of this parameter, the levels chosen being 10 and 20% by weight of plastics in the mixture. The upper limit was regarded as a practical maximum both from an operational point of view (possible clogging of feeding devices at high plastics levels) as well as from a materials availability point of view for a large scale operation of a gasification plant in Switzerland. It was decided to use single plastics rather than plastics mixtures even if mixtures would invariably be present in large scale operation. By this method clearer results were expected as effects arising from different relative amounts of the single plastics in a blend are excluded.

The plastics chosen were polyethylene and polystyrene. Data available on the composition of plastics wastes and on the consumption of plastics (see references [5.5] to [5.10]) shows that the largest portion of plastic wastes is composed of the polyolefins polyethylene and polypropylene. Polystyrene forms another large fraction of plastics wastes

in Switzerland as well as elsewhere in Europe see Figure 5.1. Polyvinyl chloride is also an important part of the waste plastics, but was ruled out in the BIOMETH study and will therefore not be considered here.

Figure 5.1: Plastics wastes composition according to different sources. (N.D.: not determined)

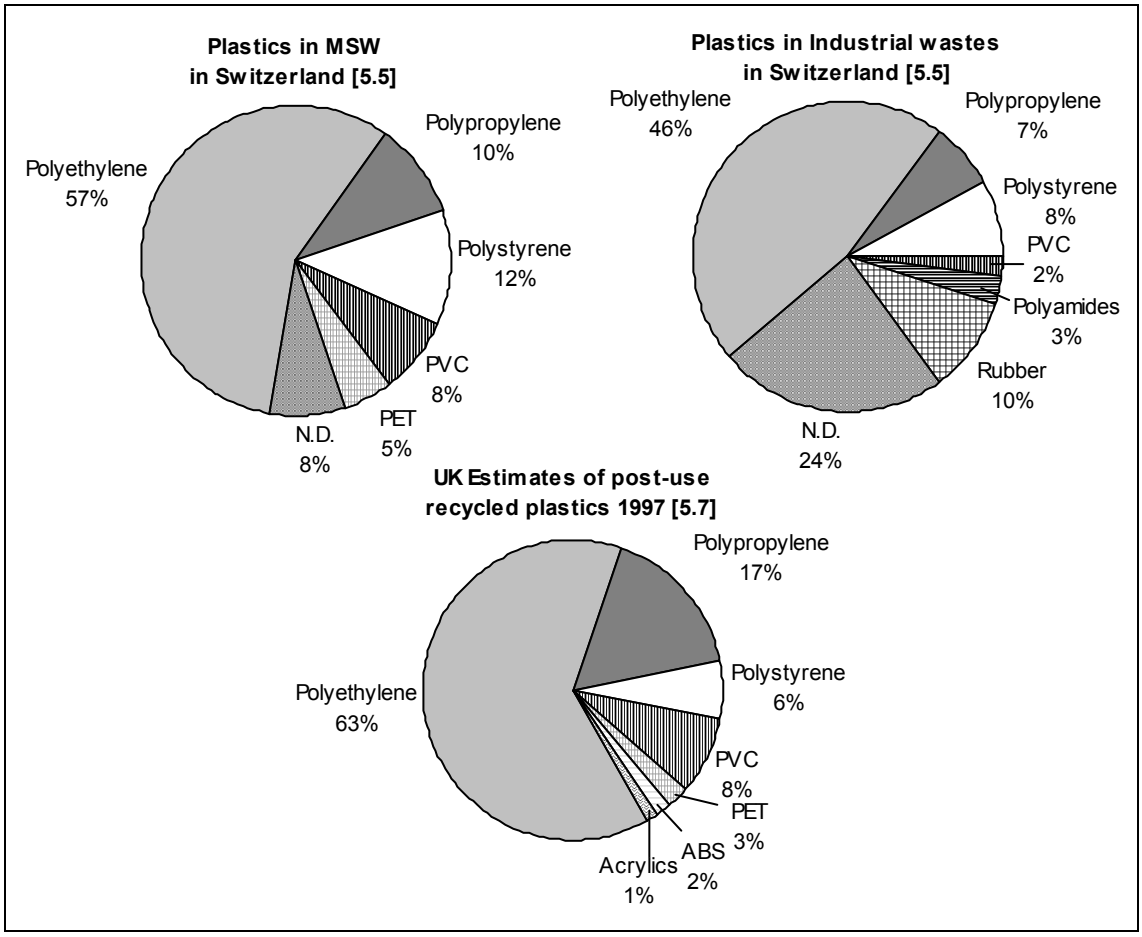

It was assumed, that the polyolefins would exhibit similar behaviour in the gasifier as they are chemically very similar long aliphatic molecules. Therefore only one of them, polyethylene, was selected for the experiments. Polystyrene displays a chemical structure in which aromatic sub-structures are present. These aromatic constituents were expected to have a strong impact on the tars in the gas, making this particular polymer an interesting study object.

The influence of operational parameters.

Besides the variation of the ER, it was decided to test the influence of the steam to biomass ratio by performing experiments where a higher steam input would be admit-

ted to the reactor with otherwise constant parameters. Also, the influence of the reactor load would be studied in an experiment where the biomass feedrate would be kept constant and the input of oxygen would be adjusted to yield the desired ER.

Finally, to ascertain to what extent systematic errors arising from the continued use of the set-up would influence the results obtained, a series of repetition experiments was planned.

Table 5.4 lists the experiments performed grouped with respect to the fuel used. The repetition experiments are marked with "RE" in the comments column of this table. Due to lack of time only one such repetition experiment could be carried out using Altholz as fuel and steam/oxygen as gasification agent.

Table 5.4: Experiments performed according to final experimental plan.

Experiment Nr.	Fuel	Gasification agent	ER set-points	Comments
990903	SCW	air	0.2;0.3;0.4	
000125	SCW	steam/O_2	0.2;0.3;0.4	
000201	Aged SCW	steam/O_2	0.2;0.3;0.4	Aged SCW
000330	Milled SCW	steam/O_2	0.2;0.3;0.4	Milled SCW
981029	AH	air	0.2;0.3;0.4	
990615	AH	steam/O_2	0.2;0.2	
990722	AH	steam/O_2	0.3;0.4	
991214	AH	steam/O_2	0.2;0.3;0.4	RE
990729	AH	steam/O_2	0.2,0.3,0.4	2x steam
990706	AH	steam/O_2	0.2;0.3	2x steam
991005	AH	steam/O_2	0.2;0.3;0.4	m^*_{Fuel}=¢
991123	AH+10%PE	steam/O_2	0.2;0.3;0.4	
000215	AH+20%PE	steam/O_2	0.15;0.25;0.35	
991126	AH+10%PS	steam/O_2	0.2;0.3;0.4	
991207	AH+20%PS	steam/O_2	0.15;0.25;0.35	

The treatment procedure of the results from these experiments will be shown in the following section using data from experiment 990903. Note that the results presented refer to gasifier data gathered in the time period in which tar sampling was performed. In this time interval the reactor is assumed to be in steady-state.

5.2 Treatment of experimental data

An example of how the data gathered in an experiment is treated will be given in this section for the experiment 990903, where standard clean wood (SCW) was gasified with air. The different ER conditions are designated with the roman literals A, B and C and will henceforth be referred to as "runs". The run parameters are listed in Table 5.5, as well as the set-point and achieved ER and the measured bed temperature (T_{Bed}). The

Table 5.5: Parameters of run 990903.

Parameter			**990903A**	**990903B**	**990903C**
Fuel flow rate		**[kg/h]**	22.402	16.407	11.602
Fuel composition	**C**	**[wt.-%$_{DAF}$]**	50.6	50.6	50.6
	H		6.5	6.5	6.5
	O		42.8	42.8	42.8
Fuel humidity		**[wt.-%]**	5.1	5.5	5.5
Fuel ash contents		**[wt.-%]**	0.22	0.30	0.30
Air		**[kg/h]**	24.513	24.513	24.492
ER achieved		**[-]**	0.19	0.25	0.36
ER set-point		**[-]**	0.2	0.3	0.4
T_{Bed} achieved		**[°C]**	708	810	911
T_{Bed} expected		**[°C]**	700	800	900

achieved ER is slightly below the set-point in all runs. The T_{Bed} attained lies at the upper end of the envisaged ±10°C range from the expected values. The relationship between T_{Bed} and ER was established in preliminary experiments. T_{Bed} is determined by the energy balance of the system, i.e. by the energy inputs by the fuel and gasification agents, by the energy generated and consumed by combustion respectively by gasification reactions and by the energy output in the product gases and by the heat losses of the system. Roughly, when ER is set at 0.2, 0.3 and 0.4 a T_{Bed} of roughly 700, 800 and 900°C is attained.

The dry, tar-free (DTF) gas composition measured with the on-line MS is shown in Table 5.6, and from it the normalised density of the DTF gas may be directly calculated. Notice that this gas composition is normalised, i.e. the sum of the 7 compounds listed is always 100%. This normalising procedure was chosen as the gas entering the MS may still

contain water, light hydrocarbons or even tars in unknown amounts. These amounts may vary according to the operational conditions of the gas cleaning system and would thus lead to wrong trends in the gas composition if not eliminated by the normalising procedure.

Table 5.6: Measured gas composition of run 990903 in vol.-%$_{DTF}$ and normal density ρ_N of dry, tar-free gas.

Species	990903A	990903B	990903C
N_2	50.5	52.8	58.4
CO_2	13.9	13.5	14.4
CO	19.4	19.1	14.7
H_2	9.4	8.9	8.1
CH_4	6.1	5.2	3.7
Ar	0.8	0.7	0.7
O_2	0.0	0.0	0.0
ρ_N **[kg/m$^3_{N,DFT}$]**	1.211	1.219	1.242

The gas composition for experiment 990903 does roughly follow the expected pattern of increasing CO_2 and decreasing CO concentrations with increasing ER. H_2 and CH_4 concentrations decrease as expected when the ER increases and more N_2 is detected in the product gases as a consequence of the decreasing fuel mass flow generating a smaller amount of product gases.

The water content of the gas was determined from a balance of the weights of the tar sampling bottles 1 and 2, assuming that the mass of water deposited in these bottles is much larger than the mass of tar compounds. The mass balance of the tar sampling bottles for run 990903A is shown in Table 5.7. Note the comparatively small loss of solvent also detected by a balance on the solvent containing bottles.

The total gas volume sampled as well as the pressure and temperature of the sampled gas are noted during tar sampling, enabling the normalised volume of sampled gas to be calculated. Using the previously calculated normalised gas density of the DTF gas the water contents can be calculated (see Table 5.8)

Table 5.7: Mass balances of tar sampling bottles for run 990903A.

Bottle Nr.	Contents	Tara [g]	Mass of liquid added [g]	Bottle's weight [g] before sampling	Bottle's weight [g] after sampling	Balance [g]
1	150ml H_2O	414.58	149.56	564.14	576.64	+12.5
2	-	320.8	0	320.8	321.95	+1.15
3	150ml DCM	324.7	199.22	523.92	444.8	-79.12
4	150ml DCM	319.48	197.01	516.49	516.64	+0.15
5	150ml Acetone/MeOH	323.69	120.04	443.73	497.86	+54.13
6	150ml Acetone/MeOH	325.5	120.55	446.05	457.62	+11.57
7	-	334.43	0	334.43	334.93	+0.5
CT	-	163.87	0	163.87	178.68	+14.81
Water accumulated [g]						13.65
Solvent lost [g]						2.04
Solvent lost [% of total mass of solvent used]						0.32

Table 5.8: Tar sampling details for experiment 990903A. TF: tar-free.

Parameter	Units	Value
Sampled volume	[l]	100.18
Gas temperature	[°C]	25.6
Gas pressure	[mbar]	984
Normalised sampled volume	[l_N]	89.0
Water contents of gas	[$g/m^3_{N,DTF}$]	153.4
	[$wt.-\%_{DTF}$]	12.7
	[$wt.-\%_{TF}$]	11.2

The tar sampling solutions are analysed on the GC/MSD, yielding the concentrations of individual tar components in the product gas shown in Table 5.9. The tar concentration values are reported as mg tar compound (or tar class or total tar, see below) per m^3_N of product gas on a wet, tar-containing basis expressing the conditions at the exit of the gasifier.

Table 5.9: Concentrations of tar compounds for run 990903 in mg/m^3_N.

Tar compound	990903A	990903B	990903C
Benzene	4228	8281	9584
Toluene	2632	2360	328
Ethylbenzene	214	9	1
p&m-Xylene	860	387	10
o-Xylene	202	66	1
Styrene	863	1030	300
3-Ethyltoluene	54	2	0
4-Ethyltoluene	27	1	0
2-Ethyltoluene	23	0	0
Phenol	3348	1590	13
α-Methylstyrene	72	15	1
3&2-Methylstyrene	246	117	7
4-Methylstyrene	117	55	4
2,3-Benzofuran	255	272	8
o-Cresol	1029	52	0
Indene	823	1443	358
p-Cresol	1240	77	0
m-Cresol	1102	159	0
Naphthalene	673	2445	2804
2-Methylnaphthalene	308	368	58
1-Methylnaphthalene	221	251	35
Biphenyl	58	173	137
Acenaphthylene	216	807	874
Acenaphthene	38	33	11
Dibenzofuran	43	153	115
Fluorene	75	307	163
Phenanthrene	101	478	690
Anthracene	50	209	186
Fluoranthene	30	160	308
Pyrene	33	162	288
Benz[a]anthracene	16	74	87
Chrysene	10	56	95
Benz[e]acephenanthrylene	5	24	39
Benzo[k]fluoranthene	4	32	53
Benzo[a]pyrene	9	48	79
Perylene	2	6	13
Dibenzo[ah]anthracene	2	6	12
Indeno[1,2,3-cd]pyrene	5	18	40
Benzo[ghi]perylene	3	14	34

From the detailed tar composition the tar characteristics shown in Table 5.10 may be calculated based on the properties of the single compounds. These characteristics are:

- the lower heating value (LHV), a measure of the chemical energy contents of the tars, needed for example in energy balance calculations;
- the elemental composition, necessary in elemental balance determination;
- an average molecular mass (normalised to a molecular formula of the form $C_1H_xO_y$), useful for transformations between mass and volume (or mole) based concentration data.

Table 5.10: Tar characteristics for run 990903.

Property			**990903A**	**990903B**	**990903C**
Lower heating value		**[MJ/kg]**	37.107	38.906	39.524
Elemental composition	**C**	**[wt.-%]**	86.7	91.0	92.7
	H		7.5	7.2	7.0
	O		5.8	1.7	0.2
Molecular mass		**[kg/kmole]**	13.854	13.195	12.950

The large number of compounds identified by the tar sampling and analysis method makes comparison of the gas composition with respect to its tar content difficult. The tar composition and concentration data has been simplified by:

- calculating the total tar content of a run by summing up the concentrations of all compounds identified;
- ordering the compounds into classes of similar substances and reporting the concentrations of these classes. The definition of the nine tar classes used in this study is shown in Table 5.11.

The resulting simplified tar data for experiment 990903 is shown in Table 5.12. For all subsequent experiments, only this simplified version of the tar concentrations will be shown in this chapter, the full data sets can be found in Appendix A: Tar data.

Table 5.11: Tar classes definition.

Tar class	Compounds in class
Benzene	Benzene
1 ring aromatics (1 ring)	Toluene, Ethylbenzene, Xylenes, Styrene, Ethyltoluenes, α-Methylstyrene, Methylstyrenes
Naphthalene	Naphthalene
2 ring aromatics (2 ring)	Indene, Methylnaphthalenes, Biphenyl
3 ring aromatics (3 ring)	Acenaphthylene, Acenaphthene, Fluorene, Phenanthrene, Anthracene
4 and 5 ring aromatics (4+ ring)	Fluoranthene, Pyrene, Benz[a]anthracene, Chrysene, Benz[e]acephenanthrylene, Benzo[k]fluoranthene, Benzo[a]pyrene, Perylene, Dibenzo[ah]anthracene, Indeno[1,2,3-cd]pyrene, Benzo[ghi]perylene
Phenol	Phenol
Cresols	o-, m- and p-Cresol
Oxygen containing heteroaromatics (O-heteroar.)	2,3-Benzofuran, Dibenzofuran

Table 5.12: Simplified tar composition for experiment 990903.

Concentration of class [mg/m^3_N]	**990903A**	**990903B**	**990903C**
Benzene	4228	8281	9584
1 ring	5311	4041	652
Naphthalene	673	2445	2804
2 ring	1409	2235	588
3 ring	479	1835	1924
4+ ring	119	601	1048
Phenol	3348	1590	13
Cresols	3371	287	0
O-heteroar.	298	425	123
Total tar concentration [mg/m^3_N]	19235	21740	16735

The tar composition data shows that the tar composition becomes less complex i.e. a smaller number of compounds is detected as the ER is increased. This trend is in good agreement with data reported in the literature, see [5.4] and [5.11]. Also in line with these reported observations is the decrease of oxygen containing compounds and the increase in the aromatic character of the tars, reflected by the increase in the concentrations of benzene, naphthalene and the higher ring systems. The total tar concentration does

however not follow the expected decrease trend with increasing ER. A maximum in tar concentration is observed at ER=0.26. One possible explanation is that during the sampling of tars for run A the sampling train was not tight. The registered gas sample volume would be higher than the actual gas volume sampled from the reactor, and therefore a too low tar concentration will result. From this run onward, the output of the tar sampling train was connected to the on-line MS as a means of identifying leaks during tar sampling. Note that the water content of the gas calculated will be too low as well.

Both tar and water concentration are expected to decrease gradually with increasing ER. An attempt to test whether a leakage can be detected by interpolating the tar or water concentration data of the extreme ERs and calculating the data for the intermediate ER yields inconclusive results. The tar concentration calculated by interpolation would be lower than the one measured implying that the sample volume measured during the sampling in run B is too small. This is a physical impossibility since the tar sampling train 's pressure is below atmospheric and no leakages of sampled gas out of it are possible. If the water concentration is taken as basis for interpolation, the result is an even higher tar concentration for the intermediate ER. Testing by using the data of the higher ER runs and extrapolating for the lower ER run leads to similar inconclusive results, and thus the source of the discrepancies observed in this experiment can not be tracked on basis of available data.

The composition of the gas exiting the gasifier is calculated taking into account all of the data related to gas composition of the experiment and the tar/water sampling results. This composition is shown in Table 5.13 for experiment 990903, and only these final values will be reported for the subsequent experiments.

The unusual trends already noticed when the DTF gas composition data was presented are still visible in the final gas composition data.

This composition data allows for the calculation of the LHV of the gas shown in Table 5.13, based on the LHVs of its constituents. The LHV is reported on a wet, tar containing basis. Also the gas density required for transformation of volume based data to mass based data is calculated using this composition data. The LHV decreases as the ER increases, a consequence of the larger amount of biomass burnt as the supply of oxygen increases leaving thus less fuel to be converted into gas. Also the dilution by the higher amount of nitrogen at high ER's decreases the gas' calorific power.

Table 5.13: Gas composition and gas properties for run 990903.

Run	990903A	990903B	990903C	990903A	990903B	990903C
Gas species	**Volume fraction, $y_{i,PG}$ [%]**			**Mass fraction, $w_{i,PG}$ [%]**		
N_2	41.1	44.7	49.7	45.4	48.7	53.1
CO_2	11.3	11.4	12.3	19.6	19.5	20.6
CO	15.8	16.2	12.5	17.5	17.6	13.3
H_2	7.6	7.5	6.9	0.6	0.6	0.5
CH_4	5.0	4.4	3.1	3.2	2.7	1.9
Ar	0.6	0.6	0.6	1.0	0.9	0.9
O_2	0.0	0.0	0.0	0.0	0.0	0.0
H_2O	15.5	11.6	11.9	11.1	8.1	8.2
Tar	3.1	3.7	2.9	1.7	1.9	1.4
LHV	**[kJ/m^3_N]**			**[kJ/kg]**		
	4599	4421	3451	4071	3852	2948
Normalised density [kg/m^3_N]				1.130	1.148	1.171

In parallel to the tar sampling, the amount of solids retained by the cyclone is determined. A clean solids container of known weight is installed at the (lower) cyclone outlet and the solids collected into it for a known period of time. Before the reactor's conditions are changed the container is exchanged and the mass of its contents is determined. A sample is taken for later analysis of its humidity and carbon content in the laboratory. The humidity is determined by drying part of the sample at 105°C and the carbon contents is determined by annealing another fraction in an oven in air at 815°C. The results for experiment 990903 are shown in Table 5.14.

Table 5.14: Solids properties for run 990903.

Solids properties		990903A	990903B	990903C
Solids mass flow	**[kg/h]**	0.514	0.287	0.187
Solids carbon contents	**[wt.-%]**	77.7	48.6	56.1
Solids humidity	**[wt.-%]**	0.9	0.6	1.5

The decrease in solids mass flow reflects the reduction of fuel input to the reactor at high ERs. The cyclone separation efficiency might decrease somewhat as a lower total mass flow through the set-up is used at higher ERs, a consequence of the experimental

procedure employed. On the other hand gas temperatures are higher at high ER, yielding higher gas volume flow rates. The exact consequence of these two parameters on the cyclone separation efficiency is difficult to predict. They have an opposite effect on the gas velocities in the cyclone, the main parameter influencing the separation efficiency of this unit. The solids contain less carbon at high ER, indicating a better conversion of the fuel particles as conditions become more oxidising in the reactor.

It is questionable whether the determined weight loss upon heating to 105°C may be assigned to water, the solids exiting the reactor at high temperature may certainly be assumed to be dry. Also, when this property was determined, a strong smell emanated from the samples, making the presence of tars on the recovered solids evident. An attempt to quantify these tars by solvent extraction of the solids revealed however only negligible amounts of tar compounds. The measured humidity is thus not taken into account for further calculations, with the exception of some solids samples from steam/oxygen gasification experiments in which water probably originating from steam condensing in the cyclone was observed to deposit in the container. For these easily identifiable samples (both optically as well as by their high weight loss upon exposure to 105°C), the humidity is deducted for the carbon contents determination and the solids assumed to be dry when they exit the reactor. Evidently not all solids are retained by the cyclone. The flame in the flare always showed a yellow colour indicating the presence of either carbon particles or gaseous hydrocarbons in the gas. Nevertheless the measured output of solids particles is used in the balance calculations.

With the data gathered on the streams exiting the set-up and the knowledge of the amount and composition of the input streams it is possible to calculate mass balances for the runs of an experiment, assuming that the system is in steady state. The only possibility for the verification of this assumption is to check whether experimental data such as the bed temperature or the gas composition does not change over a given time span. During an experiment the most reliable parameter for ascertaining if steady-state is reached is the bed temperature. The gas composition tends to react slower to changes in the system as there is a time lag due to the "scanning" of the different sampling ports. Also I have observed that the bed temperature will change in response to very small fluctuations of the biomass feed rate during the experiment. These fluctuations occur as the top screw feeder's reservoir gets empty thus changing the pressure on the fuel at the screw

level and so its bulk density. Since the screw feeders of the set-up are volumetric devices the instantaneous feed rate will become lower at this point and the bed temperature will rise. Inversely, when the reservoir is filled, the instantaneous feed rate increases slightly and the bed temperature decreases. Figure 5.2 illustrates such bed temperature fluctuations in function of the variation of the mass in the reservoir of the top feeder.

To make certain that the reactor was in steady state, every time the conditions were changed the reactor was allowed to stabilise for about 30 minutes before sampling was performed. Note however, that the biomass feed rate could not always be maintained at exactly the same level. If steady-state can be assumed there are different methods for the calculation of a mass balance.

Figure 5.2: Bed temperature, fuel weight in feeder and fuel feed rate for beginning of experiment 990903.

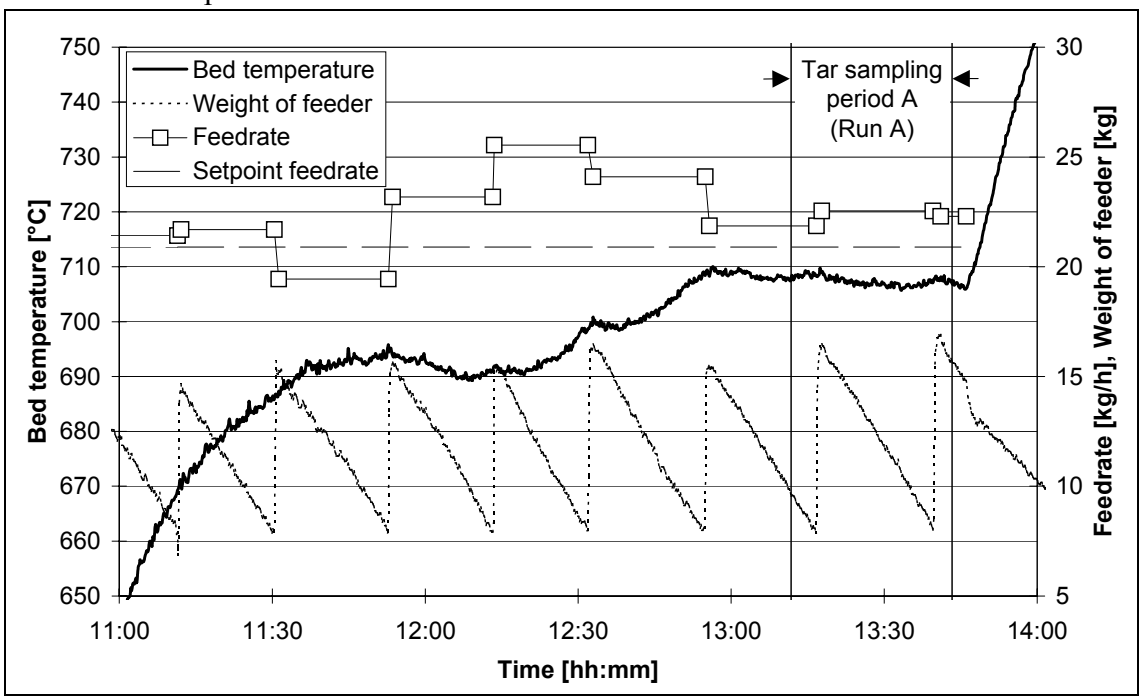

Mass balances by tracer elements

A straightforward method to determine the mass balance would be to use a given element as tracer. This means that the input of the chosen element must be known very accurately. Also the relative amounts (concentrations) of all components exiting the reactor which contain this element must be known. In the set-up used this equates to at least 4 alternatives given the 4 (main) elements present carbon, oxygen, hydrogen and nitrogen. These alternatives are discussed below.

Carbon: The only input of carbon is the fuel. The accurate elemental composition of the fuel was however not determined for every single experiment. Furthermore, not all carbon containing species leaving the set-up can be properly measured. For example, light hydrocarbons such as acetylene, ethylene and ethane are known to be present in the gas in concentrations of a few volume percent (see [5.11] and [5.12]), but have not been accounted for. Additionally, fine carbon containing particles might slip through the cyclone. The tars are another source of errors, especially when using low ERs where probably not all tar species present in the gas are accounted for by the sampling and analysis method used. Carbon is therefore inappropriate as a tracer element.

Hydrogen: Hydrogen is not appropriate either when performing air or steam/oxygen gasification since the mass flows present are very small. For air as gasification agent the main source of hydrogen is the fuel. For steam/oxygen as gasification agent the hydrogen input by the fuel was at least the same as by the steam, with the exception of those runs where steam to biomass ratio was deliberately set higher. Figure 5.3 shows the ratio of hydrogen input by steam to the hydrogen input by the fuel. Since the exact composition of the fuel is not known and it is the largest source of hydrogen, large errors may arise when using this element as a tracer.

Figure 5.3: Ratio of hydrogen input mass flows (steam/fuel) for all runs.

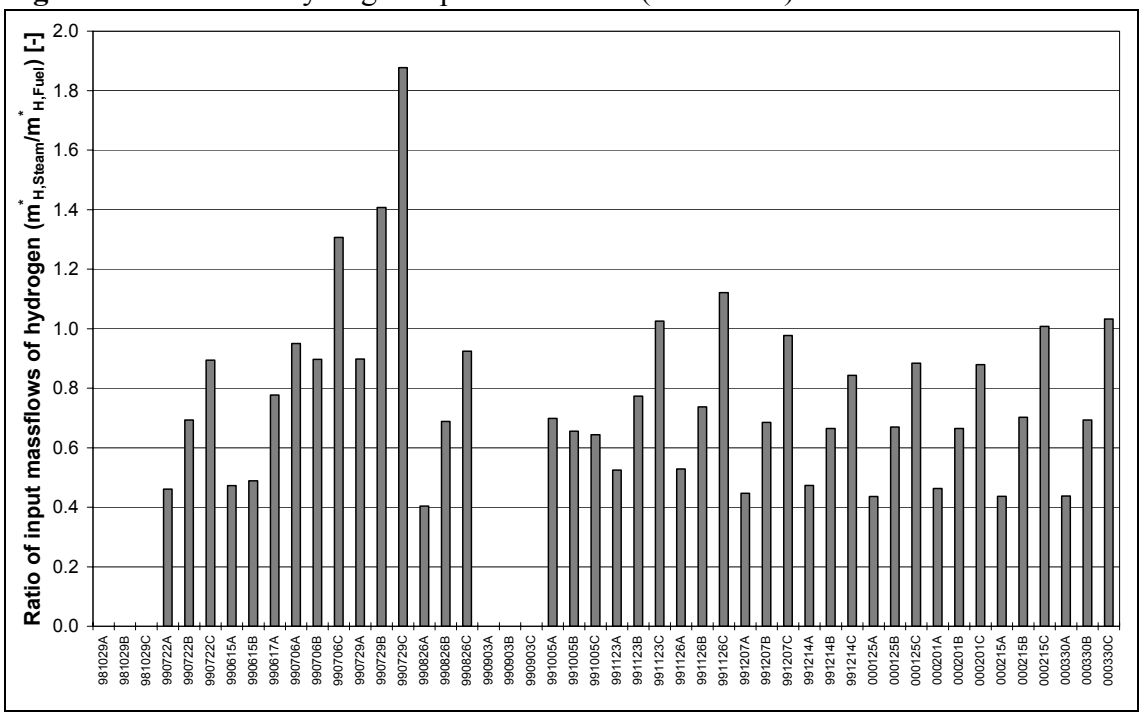

Oxygen: For air gasification experiments oxygen is not suitable as the main source of oxygen is the fuel, see Figure 5.4. In the case of steam/oxygen gasification oxygen is a slightly better tracer as its input by the gases is generally greater than by the fuel alone and thus less subject to errors arising from the unknown exact composition of the fuel. Still, in some experiments the influence of the inaccuracies in the fuel composition will interfere with the mass balance calculations and thus oxygen will not be used as tracer element.

Nitrogen: Nitrogen is at first sight an ideal tracer candidate. It might be looked at as an inert component, which simply passes the system without reacting. Oxidation reactions are not likely to occur, as the temperature in the gasification experiments is low (<1000ºC) and the environment in the reactor is strongly reducing. Research on the fate of fuel bound nitrogen [5.13] shows, that the main product of this nitrogen is ammonia (NH_3) and that in the gasification of wood concentrations in the order of some 1000 ppm ammonia may be expected.

Figure 5.4: Ratio of oxygen input mass flows (gases/fuel) for all runs.

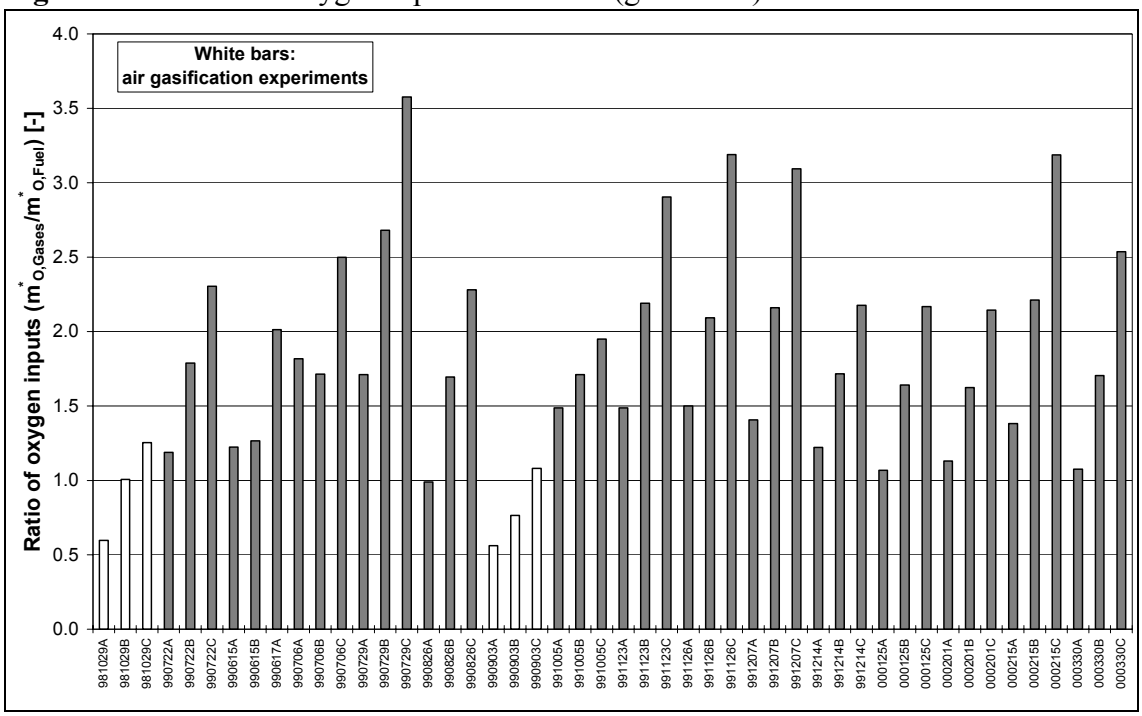

In the beginning of my experimentation, emphasis was on air gasification and the mass balance was calculated using nitrogen as tracer element. The main source of nitrogen in air gasification experiments is the air input to the reactor, measured accurately by the air mass flow controller.

This method has however a serious drawback when gasification experiments with steam/oxygen mixtures are to be analysed: the nitrogen input is only via the fuel-bound nitrogen and therefore extremely small and subject to the uncertainties arising from the lack of knowledge on the exact fuel composition. An opportunity for overcoming this difficulty is to replace some of the oxygen by air, allowing for higher nitrogen input to the reactor. The amount of air had however to be very small to avoid masking the effects of the steam/oxygen environment. To achieve this, the air mass flow controller will be operating below the optimum range of 20 to 80% of the maximum flow. Hence the precision of the measurement of the air mass flow will be poor. The result is that an incorrect or rather uncertain nitrogen input to the reactor will be used in the calculations, yielding poor mass balances. Also, errors may be expected in the gas composition measurement (see page 32) due to the presence of comparatively high concentrations of C_2 hydrocarbons as the N_2 concentration will be small.

Since the choice of not using nitrogen as tracer element was made after several steam/oxygen experiments had already been done, the small air input of ca. 1kg/h was kept for all subsequent experiments to yield experiments with as comparable conditions as possible.

"Total" mass balances

The alternative to the tracer element method is establishing a total mass balance for the whole system, see Figure 5.5. This simple method was chosen for the present thesis as the use of tracer elements is not satisfactory (see above). It includes only the assumption that at a given time in steady-state the total mass flow of inputs to the reactor is equal to the total mass flow of outputs of the reactor. The overall balance equation is:

$$\dot{m}_{Total,\,input} = \dot{m}_{Total,\,output} \quad \text{where} \tag{5.3}$$

$$\dot{m}_{Total,\,input} = \dot{m}_{Fuel} + \dot{m}_{Gasification\ agents} + \dot{m}_{Ar\ to\ feeders} \quad \text{and} \tag{5.4}$$

$$\dot{m}_{Total,\,output} = \dot{m}_{Product\ gas} + \dot{m}_{Solids} + \dot{m}_{Ar\ losses} \tag{5.5}$$

The mass flows of all the streams entering the system are known. The mass flows of the product gases $\dot{m}_{Product\ gas}$ and of the argon losses in the feeding system, $\dot{m}_{Ar\ losses}$ are unknown.

Figure 5.5: Balance boundaries.

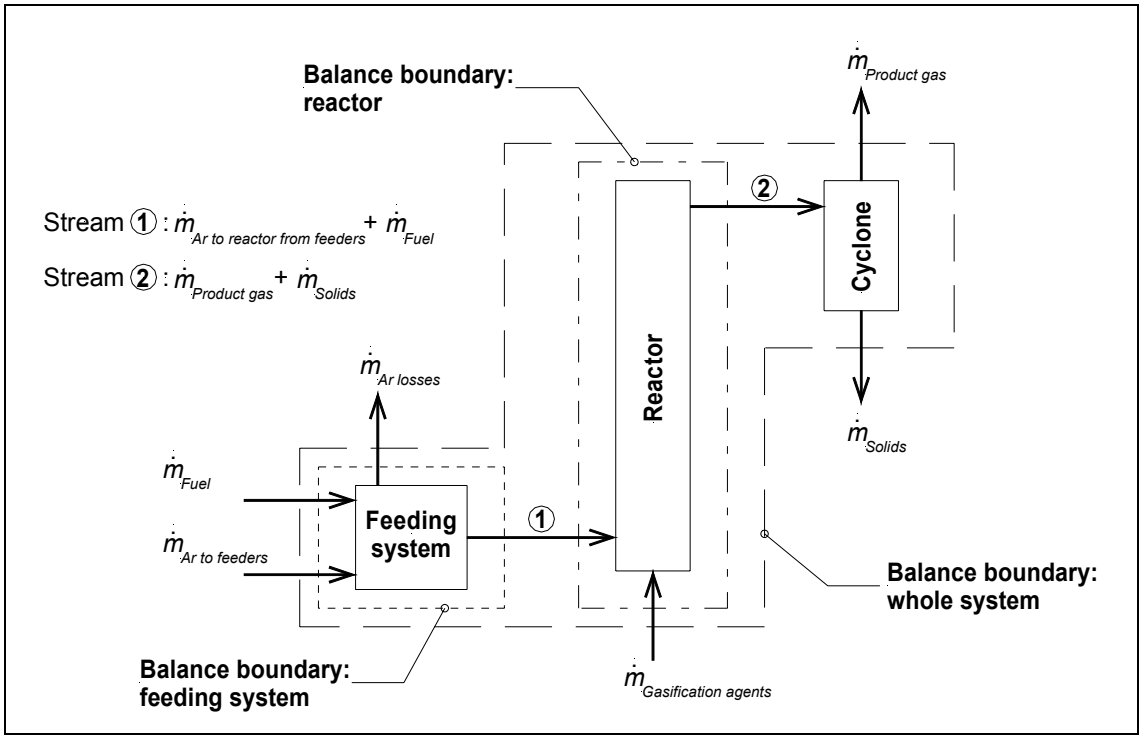

The solution for the above mentioned problem is to start by establishing the mass balance for the reactor alone on an argon-free basis. This calculation can be carried out as argon is an inert component in the reaction system studied. If the argon-free mass flow of gases exiting the reactor is known, the mass flow of argon in the output can be calculated using the known amount of argon in the product gas. Finally, as argon is an inert component, the argon input to the reactor is equal to the output. By using the mass balance for the feeding system the argon losses may be calculated. The mass balance for the reactor is:

$$\dot{m}_{Total\ input\ to\ reactor} = \dot{m}_{Total\ output\ from\ reactor} \quad \text{or} \tag{5.6}$$

$$\dot{m}_{Fuel} + \dot{m}_{Ar\ to\ reactor\ from\ feeders} + \dot{m}_{Gasification\ agents} = \dot{m}_{Product\ gas} + \dot{m}_{Solids} \tag{5.7}$$

The input mass flow of gasification agents will always consist at least partially of air (see page 144) and is given by:

$$\dot{m}_{Gasification\ agents} = \dot{m}_{Steam} + \dot{m}_{Oxygen} + \dot{m}_{Air} \tag{5.8}$$

The quantities on the right hand side of Equation 5.8 are all (directly or indirectly) measured during the experiment.

Table 5.15: Composition and normal density of air [5.14].

Component *i*	Volume fraction $y_{i,Air}$ [%]	Mass fraction $w_{i,Air}$ [%]
N_2	78.1	75.5
O_2	20.9	23.1
Ar	1.0	1.3
ρ_N [kg/m^3_N]		1.298

Using the air composition data given in Table 5.15, the amount of the components N_2, O_2 and Ar in air can be calculated yielding:

$$\dot{m}_{Gasification\ agents} = \dot{m}_{Steam} + \dot{m}_{Oxygen} + \dot{m}_{N_2,\,Air} + \dot{m}_{O_2,\,Air} + \dot{m}_{Ar,\,Air} \tag{5.9}$$

The product gas mass flow may also be written as the sum of its components yielding:

$$\dot{m}_{Product\ gas} = \dot{m}_{N_2,\,PG} + \dot{m}_{CO_2,\,PG} + \dot{m}_{CO,\,PG} + \dot{m}_{H_2,\,PG} + \dot{m}_{CH_4,\,PG} + \dot{m}_{Ar,\,PG} + \dot{m}_{O_2,\,PG} + \dot{m}_{H_2O,\,PG} + \dot{m}_{Tar,\,PG} \tag{5.10}$$

where the subscript PG stands for "in product gas". The argon-free balance over the reactor is given by:

$$\dot{m}_{Reactor\ input,\,Ar\text{-}free} = \dot{m}_{Reactor\ output,\,Ar\text{-}free} \text{ with} \tag{5.11}$$

$$\dot{m}_{Reactor\ input,\,Ar\text{-}free} = \dot{m}_{Fuel} + \dot{m}_{Steam} + \dot{m}_{Oxygen} + \dot{m}_{O_2,\,Air} + \dot{m}_{N_2,\,Air} \text{ and with} \tag{5.12}$$

$$\dot{m}_{Reactor\ output,\,Ar\text{-}free} = \dot{m}_{Product\ gas,\,Ar\text{-}free} + \dot{m}_{Solids} \text{ where} \tag{5.13}$$

$$\dot{m}_{Product\ gas,\,Ar\text{-}free} = \sum_i \dot{m}_{i,\,PG} \text{ with } i = N_2,\ CO_2,\ CO,\ H_2,\ CH_4,\ O_2,\ H_2O,\ Tar \tag{5.14}$$

and finally

$$\dot{m}_{i,\,PG} = w_{i,\,Ar\text{-}free,\,PG} \cdot \dot{m}_{Product\ gas,\,Ar\text{-}free} \text{ or}$$

$$\dot{m}_{i,\,PG} = w_{i,\,Ar\text{-}free,\,PG} \cdot [\dot{m}_{Fuel} + \dot{m}_{Steam} + \dot{m}_{Oxygen} + \dot{m}_{O_2,\,Air} + \dot{m}_{N_2,\,Air} - \dot{m}_{Solids}] \tag{5.15}$$

The term in parenthesis is calculated using the measured mass flows. The argon-free mass fractions of the compounds in the gas $w_{i,Ar\text{-}free,PG}$ are obtained from the measured gas composition according to Equation 5.16 and the argon-free mass balances of the reactor are calculated as shown for experiment 990903 in Table 5.16.

$$w_{i,\,Ar\text{-}free,\,PG} = \frac{w_{i,\,PG}}{1 - w_{Ar,\,PG}} \text{ with } i \neq \text{Ar} \tag{5.16}$$

Table 5.16: Argon-free reactor mass balances for experiment 990903. Stream mass flows in [kg/h].

Input streams		**990903A**	**990903B**	**990903C**
Fuel		22.402	16.407	11.602
Air	total	24.513	24.513	24.492
	N_2 by air	18.512	18.513	18.497
	O_2 by air	5.673	5.673	5.668
Total input argon-free		46.587	40.593	35.767
Output streams				
Solids		0.514	0.287	0.187
Total gases argon-free		46.073	40.306	35.580
Gas components	N_2	21.130	19.796	19.061
	CO_2	9.128	7.936	7.389
	CO	8.133	7.151	4.794
	H_2	0.282	0.239	0.192
	CH_4	1.467	1.114	0.690
	O_2	0	0	0
	H_2O	5.141	3.299	2.942
	Tar	0.792	0.770	0.513
Total output argon-free		46.587	40.593	35.767

Using the measured composition of the product gas, the output mass flow of argon is calculated. Since argon is an inert component, the mass flow of argon entering the reactor (from the feeders and by air) equals the flow at the exit:

$$\dot{m}_{Ar,\,PG} = \dot{m}_{Product\ gas,\,Ar\text{-}free} \cdot \frac{w_{Ar,\,PG}}{1 - w_{Ar,\,PG}} = \dot{m}_{Ar\ to\ reactor\ from\ feeders} + \dot{m}_{Ar,\,Air} \quad (5.17)$$

A balance over the feeding system yields:

$$\dot{m}_{Ar\ to\ feeders} + \dot{m}_{Fuel} = \dot{m}_{Ar\ to\ reactor\ from\ feeders} + \dot{m}_{Fuel} + \dot{m}_{Ar\ losses} \text{ or} \quad (5.18)$$

$$\dot{m}_{Ar\ to\ feeders} = \dot{m}_{Ar\ to\ reactor\ from\ feeders} + \dot{m}_{Ar\ losses} \quad (5.19)$$

finally providing the argon losses from the feeders. The complete mass balances of experiment 990903 are shown in Table 5.17.

Table 5.17: Mass balances for experiment 990903. Stream mass flows in [kg/h].

Input streams		**990903A**	**990903B**	**990903C**
Fuel		22.402	16.407	11.602
Air		24.513	24.513	24.492
Argon to feeders		0.304	0.304	0.304
Total input		47.218	41.224	36.398
Output streams				
Solids		0.514	0.287	0.187
Argon losses		0.183	0.279	0.295
Total product gas		46.521	40.658	35.916
Product gas components	N_2	21.130	19.796	19.061
	CO_2	9.128	7.936	7.389
	CO	8.133	7.151	4.794
	H_2	0.282	0.239	0.192
	CH_4	1.467	1.114	0.690
	Ar	0.448	0.352	0.337
	O_2	0	0	0
	H_2O	5.141	3.299	2.942
	Tar	0.792	0.770	0.513
Total output		47.218	41.224	36.398

Once all the mass flows have been determined the elemental balances can be established. The detailed calculations are shown in Table 5.18 for the single runs of experiment 990903.

From these balances a large deficit of the elements carbon and hydrogen is seen in the reactor output. This deficit decreases as the ER is increased. The oxygen balance is within reasonable limits ±10% for a set-up of the size used here and taking into consideration that the main source of oxygen is the fuel and that the contents of this element in the fuel is not known precisely. The nitrogen mass flow out of the set-up is clearly over-estimated, possibly from measurement errors due to overlapping intensities in the on-line MS. The argon balance is always perfect, as required by the calculations. In further data presentation only a simplified version of the elemental balance will be shown, excluding the elemental mass flows per stream and the argon balance which is always closed due to the calculation procedure.

Table 5.18: Detailed elemental mass flows ([kg/h]) and balances for experiment 990903. EMS: Element's mass flow in stream.

Element	Input							Output							Balance [%]		
		990903A		990903B		990903C			990903A		990903B		990903C		A	B	C
	Stream	EMS	Total	EMS	Total	EMS	Total	Stream	EMS	Total	EMS	Total	EMS	Total			
C	Fuel	10.741	**10.741**	7.828	**7.828**	5.535	**5.535**	CO_2	2.491	**8.163**	2.166	**6.907**	2.016	**5.169**	**76.0**	**88.2**	**93.4**
								CO	3.487		3.066		2.056				
								CH_4	1.098		0.834		0.516				
								Solids	0.399		0.140		0.105				
								Tars	0.687		0.701		0.476				
H	Fuel	1.497	**1.497**	1.099	**1.099**	0.777	**0.777**	H_2	0.282	**1.286**	0.239	**0.944**	0.192	**0.730**	**85.9**	**85.9**	**94.0**
	Steam	0.000		0.000		0.000		CH_4	0.369		0.280		0.173				
								H_2O	0.575		0.369		0.329				
								Tars	0.060		0.056		0.036				
O	Fuel	10.095	**15.768**	7.824	**13.497**	5.245	**10.913**	CO_2	6.637	**15.893**	5.770	**12.798**	5.372	**10.724**	**100.8**	**94.8**	**98.3**
	Air	5.673		5.673		5.668		CO	4.645		4.084		2.738				
	Oxygen	0.000		0.000		0.000		O_2	0.000		0.000		0.000				
	Steam	0.000		0.000		0.000		H2O	4.565		2.930		2.612				
								Tars	0.046		0.013		0.001				
N	Fuel	0.014	**18.526**	0.010	**18.522**	0.007	**18.504**	N_2	21.130	**21.130**	19.796	**19.796**	19.061	**19.061**	**114.1**	**106.9**	**103.0**
	Air	18.512		18.512		18.497											
Ar	Air	0.327	**0.631**	0.327	**0.631**	0.327	**0.631**	Ar	0.448	**0.631**	0.352	**0.631**	0.337	**0.631**	**100.0**	**100.0**	**100.0**
	Feeders	0.304		0.304		0.304		Losses	0.183		0.279		0.295				

The lack of carbon and hydrogen may be explained by C_2-hydrocarbons in the gas not detected with the on-line MS. In an attempt to estimate the concentration of these hydrocarbons the balances for experiment 990903 have been modified to allow for the presence of compounds with a formula C_2H_Z. The reason for this peculiar formulation is, that all three C_2 isomers are known to be present in the effluents of wood gasifiers but data on the relative amounts of these hydrocarbons for specific conditions is inconclusive. The main C_2-hydrocarbon present according to literature data is C_2H_4. The modification to the balance calculations consists in setting up and solving the equations for the carbon and hydrogen balances, yielding the composition ($C_2H_{\boldsymbol{Z}}$) and mass flow of C_2 hydrocarbons. The results of this correction are shown in Tables 5.19 and 5.20, the argon balance being omitted in the latter as it is always 100%.

Table 5.19: Corrected gas composition for run 990903.

Run	**990903A**	**990903B**	**990903C**	**990903A**	**990903B**	**990903C**
Gas species	**Volume fraction, $y_{i,PG}$ [%]**			**Mass fraction, $w_{i,PG}$ [%]**		
N_2	38.1	43.4	49.1	42.0	47.1	52.3
CO_2	10.5	11.1	12.1	18.2	18.9	20.3
CO	14.7	15.7	12.3	16.2	17.0	13.2
H_2	7.1	7.3	6.8	0.6	0.6	0.5
CH_4	4.6	4.3	3.1	2.9	2.6	1.9
Ar	0.6	0.5	0.6	0.9	0.8	0.9
O_2	0.0	0.0	0.0	0.0	0.0	0.0
H_2O	14.4	11.2	11.8	10.2	7.8	8.1
Tar	2.9	3.6	2.9	1.6	1.8	1.4
C_2H_Z	7.2	3.0	1.3	7.5	3.3	1.4
Z [mole]	2.32	3.88	3.12			

The above correction calculations show clearly, that small amounts of C_2-hydrocarbons in the gas have a dramatic influence on the closure of the carbon and hydrogen elemental balances. These compounds should be added to the on-line gas analysis method for any future experimental activities at PSI's gasification test rig.

Table 5.20: Corrected elemental mass flows ([kg/h]) and balances for experiment 990903.EMS: Element's mass flow in stream.

Element	Input							Output							Balance [%]		
		990903A		990903B		990903C			990903A		990903B		990903C		A	B	C
	Stream	EMS	Total	EMS	Total	EMS	Total	Stream	EMS	Total	EMS	Total	EMS	Total			
C	Fuel	10.741	**10.741**	7.828	**7.828**	5.535	**5.535**	CO_2	2.304	**10.741**	2.094	**7.828**	1.989	**5.535**	**100.0**	**100.0**	**100.0**
								CO	3.225		2.965		2.027				
								CH_4	1.016		0.806		0.509				
								Solids	0.399		0.140		0.105				
								Tars	0.635		0.678		0.470				
								C_2H_Z	3.163		1.145		0.436				
H	Fuel	1.497	**1.497**	1.099	**1.099**	0.777	**0.777**	H_2	0.261	**1.497**	0.231	**1.099**	0.189	**0.777**	**100.0**	**100.0**	**100.0**
	Steam	0		0		0		CH_4	0.341		0.271		0.171				
								H_2O	0.532		0.357		0.325				
								Tars	0.055		0.054		0.036				
								C_2H_Z	0.308		0.186		0.057				
O	Fuel	10.095	**15.768**	7.824	**13.497**	5.245	**10.913**	CO_2	6.137	**14.696**	5.580	**12.376**	5.298	**10.575**	**93.2**	**91.7**	**96.9**
	Air	5.673		5.673		5.668		CO	4.295		3.950		2.700				
	Oxygen	0		0		0		O_2	0		0		0				
	Steam	0		0		0		H2O	4.221		2.833		2.576				
								Tars	0.042		0.013		0.001				
N	Fuel	0.014	**18.526**	0.010	**18.522**	0.007	**18.504**	N_2	19.537	**19.537**	19.143	**19.143**	18.788	**18.788**	**105.5**	**103.3**	**101.5**
	Air	18.512		18.512		18.497											

The concentrations calculated by this correction lie well within the reported range for C_2-hydrocarbons with the exception of run 990903A where too high concentrations are predicted. The value of the composition parameter Z in this particular run (2.32) indicates that other carbon containing species must be involved if the carbon balance is to be closed and the concentration of light hydrocarbons in the gas is to stay within reasonable levels.

Another possibility to account for lacking carbon in the balances is a higher solids flux out of the reactor than is measured by the solids sampling procedure. This higher output could explain the low Z value of run 990903A.

An interesting feature of this correction procedure is, that it has a positive influence on the balances of both oxygen and nitrogen, allowing them to stay within the limits I regard as legitimate (±10%) for the set-up used.

As neither the C_2 hydrocarbons nor the missing carbon in the solids can be properly assessed during the experiments, the data will be treated without these values and errors in the carbon or hydrogen mass balances will not further be corrected for.

Using the gas flow rates displayed in Table 5.17 the energy output from the reactor may be calculated. With the lower heating value of the tars, of the gas and of the fuel and the corresponding flow rates the energy flows can be determined and the cold gas efficiency (η_{CG}), the ratio of the lower heating value of the fuel to the lower heating value of the gas (a measure of the conversion efficiency of the energy from the fuel into the gases) can be calculated. Similarly the ratio of energy contained in the tars to that of the fuel η_{Tars} may be calculated. Both The values are shown in Table 5.21.

Table 5.21: Energy flows for experiment 990903

Run		**990903A**	**990903B**	**990903C**
Fuel power	**[kW]**	111.83	81.52	57.64
Gas power	**[kW]**	51.67	42.66	28.98
Tars power	**[kW]**	8.16	8.32	5.64
η_{CG}	**[%]**	46.2	52.3	50.3
η_{Tars}	**[%]**	7.3	9.8	10.2

Two interesting points may be read from the above data. First, against the expectation that more energy should be transferred to the gases at low ERs (less biomass is be-

ing burnt) the cold gas efficiency of run 990903A lies well below that of the other runs in this experiment. This trend is however in agreement with literature data [5.16]. Second, the energy transferred from the fuel to the tars seems to increase with increasing ER. Less tars are found in the gas but their constitution (see Table 5.10), especially the oxygen contents drops as ER increases, resulting in a higher calorific power of the tars. The latter effect seems to dominate over the former.

The gas and tar yields (Y_{Gas} and Y_{Tars}) may finally be calculated using the data from the mass balances. To allow comparison with data from experiments using steam/oxygen as gasification agent the gas yield is calculated on a dry, inert-free basis. The values are shown in Table 5.22

Table 5.22: Specific gas and tar flow rates for experiment 990903.

Yields	**990903A**	**990903B**	**990903C**
$\mathbf{Y_{Gas}\ [m^3_{NGas,DIF}/kg_{Fuel,DAF}]}$	0.983	1.191	1.340
$\mathbf{Y_{Tars}\ [g_{Tar}/kg_{Fuel,DAF}]}$	37.34	49.83	46.97

The gas yield increases as the ER is increased following the trends reported in the literature [5.15], [5.16]. The tar yield data follows the same trend and is in accordance to [5.16]. The results presented in [5.15] show considerable scatter for air gasification and no clear trend can be seen there.

Throughout the presentation and discussion of the results of experiment 990903 shortcomings in the behaviour of the reactor when going from low to high ER become apparent. As this is the first data set presented in this thesis, the discussion was carried out for the complete three runs, illustrating the wealth and complexity of data generated by the experiments. The data from run 990903A will however be used for further comparison, even though the reactor probably was not in steady-state. A comparison of the gas composition evolution at the top and lower sampling port shown in Figure 5.6 illustrates this circumstance. The transients observed in the gas concentrations at the lower sampling location during run A might be attributed to a change in the reaction regime. Note how the ER changed from ca. 0.16-0.17 to 0.185-0.19 shortly before sampling period A. It is likely, that this change in ER had a large effect on the production of solid carbon. From thermodynamic calculations it is known, that a limit in ER exists below which solid carbon is formed. This solid carbon might accumulate in the bed and might react with any of

the oxidising gases present. O_2, the most reactive oxidising species, is probably totally consumed shortly after entering the bed, leaving CO_2 and H_2O as possible reaction partners for the solid carbon accumulated in the bed. The products CO and H_2 would result, explaining the gas composition evolution observed. Notice also, that the gas composition evolution is quite steady at the top sampling point and differs strongly from the one observed in the lower sampling point. Apparently further reactions are taking place in the freeboard of the reactor.

Figure 5.6: Gas composition evolution at top and lower gas sampling point for experiment 990903 (N_2, O_2, and Ar deliberately omitted).

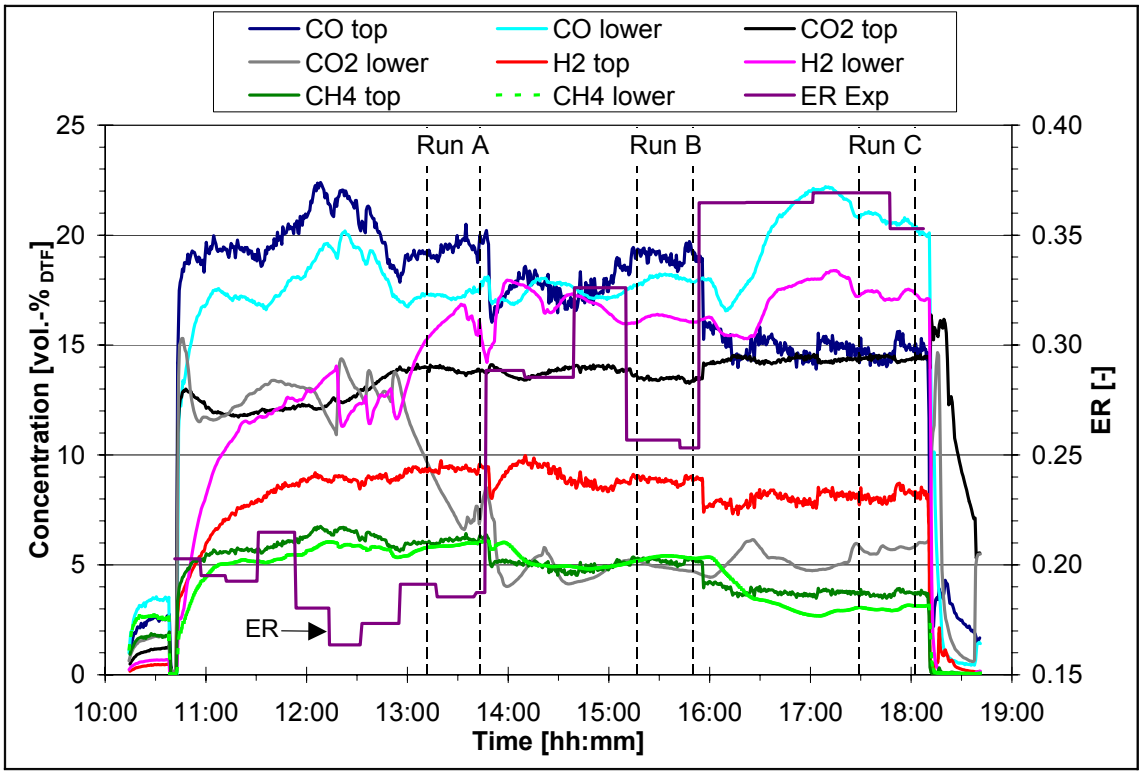

The differences between top and lower sampling point continue throughout the experiment. During run B the concentration of CO and CH_4 becomes almost identical for both sampling points. As the ER is further increased the differences for CO are reversed and a higher concentration is detected at the lower sampling point. Apparently, oxidative reactions are occurring in the freeboard lowering both CO and H_2 concentrations as the gases travel along this part of the reactor.

The data gathered in this experiment is summarised in Table 5.23. The data for all further experiments is given in Appendix B: Experimental data in the same form to en-

hance its readability. Note that the DAF fuel composition is not included in these tables as the values used for the calculations are always those reported in Tables 2.7, 2.8 and 2.10 on pages 38, 40 and 42 of Chapter 2. In addition to the already presented data the steam to fuel ratio is included in the summary table, as it is an important parameter for gasification with steam/oxygen. Further discussion on specific points of other experiments will be made in the next Chapter.

Table 5.23: Summary of data for experiment 990903.

Fuel: SCW		**Gasification agent: Air**		
Run		**990903A**	**990903B**	**990903C**
Input				
Fuel	[kg/h]	22.402	16.407	11.602
$w_{H2O,Fuel}$	[mass-%$_{Raw}$]	5.1	5.5	5.5
$w_{Ash,Fuel}$	[mass-%$_{Raw}$]	0.22	0.30	0.30
LHV_{Fuel}	[kJ/kg$_{Raw}$]	17.971	17.886	17.886
Air	[kg/h]	24.513	24.513	24.492
Oxygen	[kg/h]	0	0	0
Steam	[kg/h]	0	0	0
Argon	[kg/h]	0.304	0.304	0.304
ER	[-]	0.19	0.25	0.36
S/F	[kg/kg$_{Fuel,DAF}$]	0.05	0.06	0.06
T_{Bed}	[°C]	708	810	911
T_{FB}	[°C]	700	800	900
Output				
Solids	[kg/h]	0.514	0.287	0.187
$w_{C,Solids}$	[mass-%$_{Raw}$]	77.7	48.6	56.1
$w_{H2O,Solids}$	[mass-%$_{Raw}$]	0.9	0.6	1.5
Argon loss	[kg/h]	0.183	0.279	0.295
Gas + Tars	[kg/h]	46.521	40.658	35.916
Gas composition $y_{i,PG}$ [vol.-%]				
N_2		41.1	44.7	49.7
CO_2		11.3	11.4	12.3
CO		15.8	16.2	12.5
H_2		7.6	7.5	6.9
CH_4		5.0	4.4	3.1
Ar		0.6	0.6	0.6
H_2O		15.5	11.6	11.9
Tars		3.1	3.7	2.9
ρ_N	[kg/m^3_N]	1.130	1.148	1.171
Y_{Gas}	[m$^3_{N,DIF}$/kg$_{Fuel,DAF}$]	0.983	1.191	1.340
LHV_{Gas}	[kJ/m^3_N]	4599	4421	3451

Table 5.23: Summary of data for experiment 990903.

Fuel: SCW		**Gasification agent: Air**		
Run		**990903A**	**990903B**	**990903C**
$C_{Tar\ class}$	[mg/m^3_N]			
Benzene		4228	8281	9584
1 ring		5311	4041	652
Naphthalene		673	2445	2804
2 ring		1409	2235	588
3 ring		479	1835	1924
4+ ring		119	601	1048
Phenol		3348	1590	13
Cresols		3371	287	0
O-heteroar.		298	425	123
$C_{Tars,Total}$	[mg/m^3_N]	19235	21740	16735
Y_{Tar}	[$g/kg_{Fuel,DAF}$]	37.34	49.83	46.97
LHV_{Tars}	[kJ/kg]	37.107	38.906	39.524
M_{Tars}	[kg/kmol]	13.854	13.195	12.950
Tar elemental composition [mass-%]				
C		86.7	91.0	92.7
H		7.5	7.2	7.0
O		5.8	1.7	0.2
η_{CG}	[%]	46.2	52.4	50.3
η_{Tars}	[%]	7.3	10.2	9.8
Balances	[%]			
C		76.0	88.2	93.4
H		85.9	85.9	94.0
O		100.8	94.8	98.3
N		114.1	106.9	103.0

5.3 References

[5.1] N.R. Draper, H. Smith, *Applied regression analysis*, 3rd edition, Wiley, New York, 1998

[5.2] G.E.P. Box, W.G. Hunter, J.S. Hunter, *Statistics for experimenters: an introduction to design, data analysis, and model buildings*, Wiley, New York, 1978

[5.3] I. Navárez, A. Orío, M.P. Aznar, J. Corella, *Biomass Gasification with Air in an Atmospheric Bubbling Fluidized Bed. Effect of Six Operational Variables on the Quality of the Produced Raw Gas*, Industrial and Engineering Chemistry Research, 1996, **35**, pp.2110-2120

[5.4] C.M. Kinoshita, Y. Wang, J. Zhou, *Tar Formation under different Biomass Gasification Conditions*, Journal of Analytical and Applied Pyrolysis, 1994, **29**, pp.169-181

[5.5] K. Stumpf, *Kunststoffrecycling in der Schweiz: eine naturwissenschaftliche, technolgische und ökonomische Betrachtung*, Dissertation, Universität Zürich 1994

[5.6] *Kunststoff-Statistik 1998*, Kunststoff-Verband Schweiz, Aarau, 1998

[5.7] *http://www.wastewatch.org.uk/informtn/plastics.htm*

[5.8] *http://www.apme.org/*, Association of plastics manufacturers in Europe, APME, Brussels, Belgium

[5.9] *http://www.spmp.proplast.org/*, Syndicat des Producteurs de Matières Plastiques, SPMP, Puteaux, Fance

[5.10] *Produktions- und Verbrauchsdaten für Kunststoffe in Deutschland unter Einbeziehung der Verwertung 1997-Ergebinsse einer Umfrage*, ausgearbeitet für Verband Kunststofferzeugende Industrie e.V., Frankfurt, Germany, 1998

[5.11] E. Kurkela, P. Ståhlberg, *Air gasification of peat, wood and brow coal in a pressurized fluidized-bed reactor. I. Carbon conversion, gas yields and tar formation*, Fuel processing technology, 1992, **31**, pp.1-21

[5.12] M.P. Aznar, J. Corella, J. Gil, J.A. Martín, M.A. Cabllero, A. Olivares, P.Pérez, *Biomass gasification with steam and oxygen mixtures at pilot scale and with catalytic gas upgrading. Part I: Performance of the gasifier*, in Developments in Thermochemical Biomass Conversion, A.V. Bridgwater, D.G.B. Boocock (eds.), Blackie Academic & Professional, London, 1997, Volume 2, pp.1194-1208

[5.13] E. Kurkela P. Ståhlberg, *Air gasification of peat, wood and brow coal in a pressurized fluidized-bed reactor. II. Formation of nitrogen compounds*, Fuel processing technology, 1992, **31**, pp.23-32

[5.14] H.D. Baehr, *Thermodynamik*, 7. Auflage, Springer-Verlag, Berlin, 1989

[5.15] J. Gil, J. Corella, M.P. Aznar, M.A. Caballero, *Biomass Gasification in Atmospheric Bubbling Fluidized Bed: Effect of Type of Gasifying agent on the Product Distribution*, Biomass and Bioenergy, 1999, **17**, pp.389-403

[5.16] O. Moersch, H. Spliethoff, K.R.G. Hein, *Influence of Temperature and Stoichiometry on Gas Quality and Conversion Rate in Fluidized Bed Gasification of Biomass*, in Biomass for Energy and the Environment, Proceedings of the 9th European Bioenergy Conference, Copenhagen, Denmark 24-27 June 1996, P. Chartier et. al. (eds.), Elsevier Science, Oxford, 1996, Volume 2, pp.1398-1403

6 DISCUSSION

6.1 Reproducibility of results

To judge differences observed in the results with respect to their origin, i.e. if the effects observed are meaningful and may be assigned to alterations of parameters from experiment to experiment or if they are just experimental errors, an estimation of these errors must be first made. From a series of experiments using the same fuel and performed under (almost) identical conditions, it is possible to estimate the margin of errors in the results.

The results discussed in this chapter will focus on gas and tar composition differences observed when fuels or operational conditions are changed. Therefore, the gas and tar composition results of experiments involving Altholz (AH) and steam/oxygen as gasification agent performed at standard conditions, i.e. the results from experiments 991615, 990722 and 991214, will be discussed with respect to their reproducibility. In these experiments very similar operating conditions were achieved using the same fuel.

Some explanation is needed as not all runs in the experiments 990615 and 990722 will be used. In experiment 990615 it was planned to run through all three ERs. From run A to run B a different batch of Altholz had to be used, and it was decided to keep the run conditions constant to obtain data showing the reproducibility of the results with two different batches of AH. During the tar sampling of run 990722A leaks were observed. As the water content of the gas is measured in parallel to the tar sampling it is also incorrect and so the gas composition data cannot be used. The data from run 990722A had consequently to be discarded. In experiment 991214 all 3 ER conditions could be successfully be completed.

6.1.1 Gas composition

The temperatures obtained at the different ER set-points for these experiments are shown in Table 6.1. This data reveals that the discussion of data may be made for either ER or bed temperature as they are equivalent.

Table 6.1: Equivalence ratio and bed temperature for experiments with AH and steam/oxygen.

Run	ER	T_{Bed} [°C]
990615A	0.2	732
991214A	0.21	732
990615B	0.21	734
991214B	0.29	832
990722B	0.3	828
991214C	0.37	922
990722C	0.39	923

The gas composition for all runs using AH as fuel with steam/oxygen as gasification agent is shown in Figure 6.1 as a function of the equivalence ratio. Even though the temperatures and ERs of the partial runs in these experiments are almost identical, relatively large scatter is observed in the concentrations of the main reaction products CO_2, CO and H_2. The concentrations of all other gas compounds exhibit small scatter with the exception of argon. The scatter in the argon concentration may be explained by the very small argon concentrations measured. The average gas composition, the standard deviations and the ratio of both, the relative standard deviation are shown in Table 6.2.

Figure 6.1: Gas composition for experiments with AH and steam/oxygen.

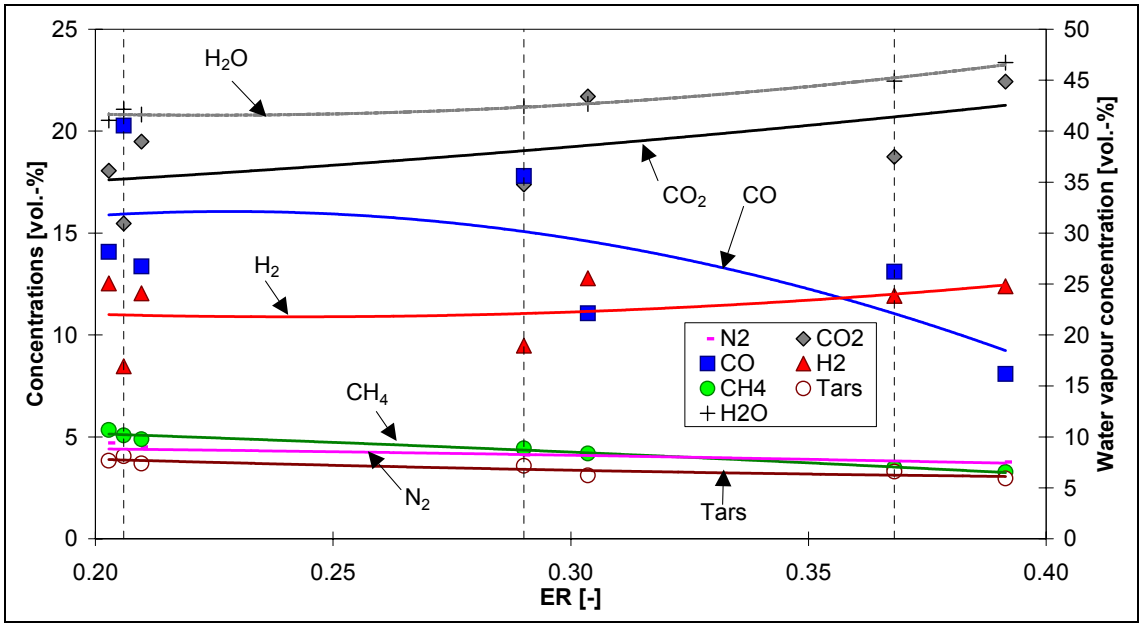

Table 6.2: Average ER, bed temperature and gas composition [vol.-%], absolute (STDEV) and relative standard deviations (RSD) [%].

	Averages			STDEV [%]			RSD [%]		
ER set-point [-]	**0.2**	**0.3**	**0.4**	**0.2**	**0.3**	**0.4**	**0.2**	**0.3**	**0.4**
ER [-]	0.21	0.30	0.38	0.0	0.01	0.02	1.7	3.2	4.3
T_{Bed} [°C]	733	830	923	1.4	2.8	0.22	0.2	0.3	0.0
N_2	4.4	4.1	3.7	0.4	0.04	0.02	8.6	1.0	0.6
CO_2	17.7	19.5	20.6	2.0	3.1	2.6	11.5	15.6	12.7
CO	15.9	14.4	10.6	3.8	4.8	3.6	23.9	33.0	33.5
H_2	11.0	11.1	12.2	2.2	2.3	0.3	20.2	21.0	2.7
CH_4	5.1	4.3	3.4	0.2	0.2	0.2	4.5	4.0	4.3
Ar	0.4	0.5	0.6	0.1	0.3	0.3	18.9	55.7	53.3
H_2O	41.6	42.6	45.8	0.6	0.2	1.3	1.3	0.3	2.8
Tars	3.9	3.3	3.1	0.2	0.3	0.2	4.7	10.1	7.6

The absolute standard deviations do not seem to follow a trend in function of the ER. The differences are better shown by the use of the relative standard deviation. The variations in the CO, CO_2 and H_2 concentrations could be attributed to various factors, such as differences in the fuel composition, not being in steady-state during the sampling period of the experiments and imprecisions in the gas composition measurement.

The on-line MS is calibrated before every experiment to ensure accurate measurement of the gas composition. The scatter in the concentrations of CH_4 and N_2 is small and comparable to the scatter of H_2O and tars which are measured by a different method, independent of the on-line MS. From the above considerations it seems that the data from the on-line MS is correct.

The RSD of raw gas composition data gathered in function of time during these experiments lies in the order of 5 to 7%. This small RSD indicates that the reactor was delivering gas of constant quality over the sampling periods. The RSD of the bed temperatures for these experiments is below 0.5%, another indication that the reactor was operating under stationary conditions. The hypothesis that the reactor was not operating in steady state can therefore be rejected.

A trend can be observed for certain points in the gas composition data of Figure 6.1, marked by vertical dotted lines, all issued form the same experiment, 991214. Notice how for comparable ER the CO concentrations are higher and at the same time CO_2 and H_2 concentrations are lower for this particular set of measurements.

The scatter of the data and the trend mentioned above may be explained by the presence of catalytically active substances in the Altholz. For example the metals Fe, Ni, Cr, Cu or Zn, known to be present in this fuel, are catalysts for reactions altering the gas composition as well as tar decomposition reactions, see Table 6.3, [6.1] - [6.6]. Especially the homogeneous water-gas shift reaction seems to exert a different influence on the gas composition issued form experiments using diverse batches of AH. The amount of the catalysts is certainly going to vary in a wide range for this very inhomogeneous fuel. These changes in the amounts of active species could well explain the observed scatter in the gas composition issued from AH gasification in air.

Table 6.3: Gas phase reactions catalysed in biomass gasification.

Reaction	**Catalysts**
Homogeneous water-gas shift $CO + H_2O \rightarrow CO_2 + H_2$	Fe, Cr, Cu, Zn
Hydrocarbon reforming $CH_4 + H_2O \rightarrow CO + 3\ H_2$ $C_nH_m + n\ H_2O \rightarrow n\ CO + (n+m/2)\ H_2$	Ni, Fe, $CaCO_3/MgCO_3$
Cracking	Ni, Fe, $CaCO_3/MgCO_3$

The above assumption is sustained by the observation that the scatter of the sums of the concentrations of CO and CO_2 and of CO and H_2, shown in Figure 6.2 on a dry, inert-free basis, are smaller than the scatter of the concentrations of the individual gas components. The smaller scatter of the sum $[CO]+[CO_2]$ compared to the sum $[CO]+[H_2]$ further suggests, that not only the homogeneous water-gas shift reaction, but also heterogeneous reactions such as the Boudouard reaction ($C_{(s)} + CO_2 \rightarrow 2\ CO$) or the steam gasification of carbon ($C_{(s)} + H_2O \rightarrow CO + H_2$) are affected by the catalytically active substances present in the Altholz.

Figure 6.2: Relative standard deviation of CO, CO_2 and H_2 concentrations and of the sums $[CO]+[CO_2]$ and $[CO]+[H_2]$.

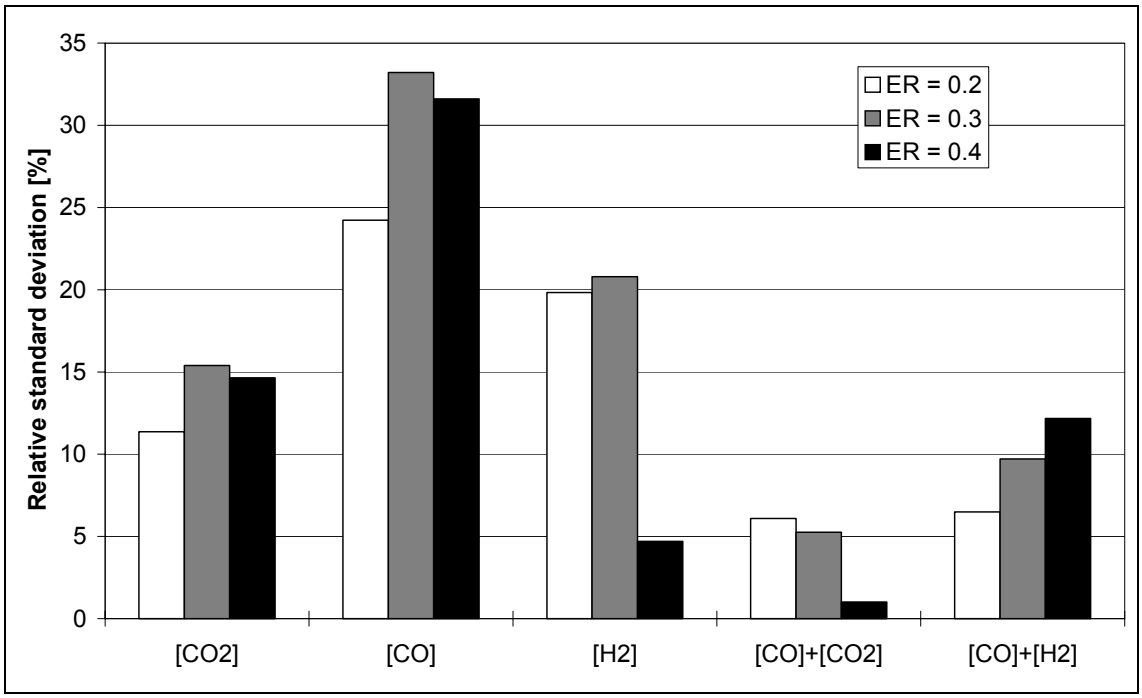

These catalysts also seem to have an influence on the amount of tars produced as Figure 6.3 shows. The total tar concentration is higher for those experiments where the reverse water-gas shift reaction ($CO_2 + H_2 \rightarrow CO + H_2O$) is observed to increase CO and to decrease the CO_2 and H_2 concentrations. The differences are however very small and might be attributed to errors in the complicated tar measurement procedure. This effect is taken as no more than a hint and will be neglected in further discussion.

Figure 6.3: Total tar concentration for experiments involving AH and steam/oxygen.

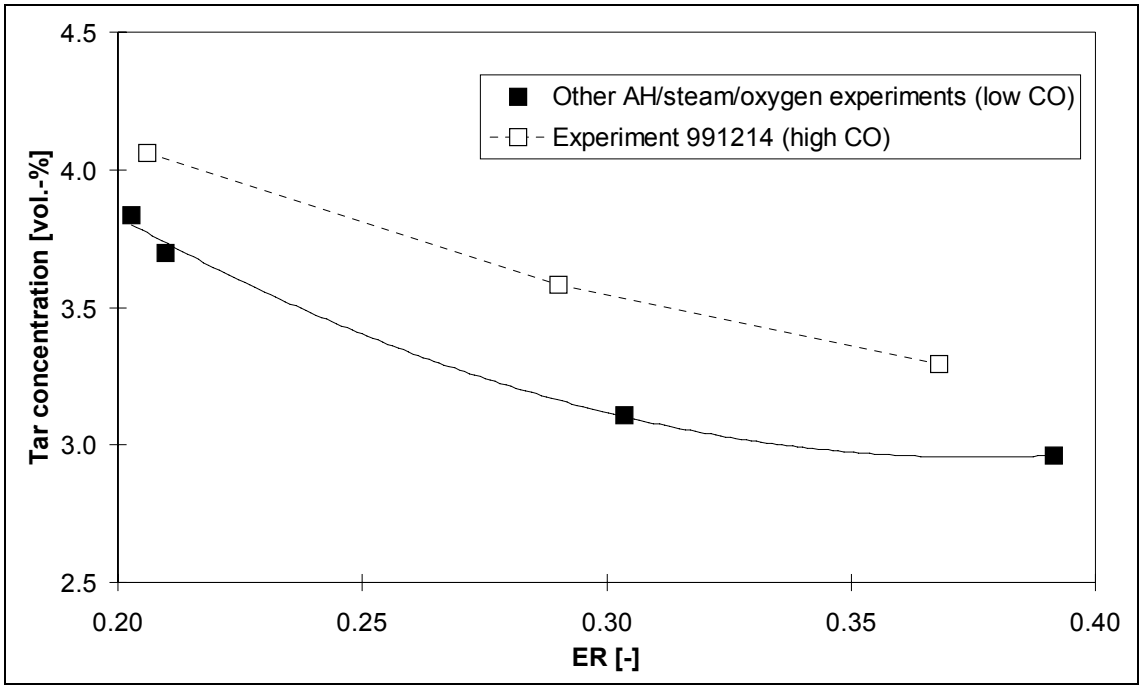

A fuel with more homogeneous composition should have been used for determining the scatter in the experimental data. This was intended by the use of SCW, but not enough data could be gathered with this fuel to allow a discussion of the dispersion of the data. Discussion of gas composition data, especially from AH runs, must therefore be made with caution, allowing for relatively large deviations such as shown in Table 6.2.

Notice however, that even with the large scatter in the AH data, trends may still be clearly read from it. In particular, notice how the trend lines shown in Figure 6.1 undoubtedly indicate the dependence between CO, CO_2 and H_2 concentrations as a function of ER (or T_{Bed}) for this fuel. As T_{Bed} or ER are raised, CO is seen to decrease, reacting probably with H_2O yielding the observed larger concentrations of CO_2 and H_2. Again, the homogeneous water-gas shift reaction $CO + H_2O \rightarrow CO_2 + H_2$ could account for these transformations.

6.1.2 Tar composition

The concentrations of single tar species for the runs involving AH and steam/oxygen are shown in Figures 6.4, 6.5 and 6.6. These charts show how well comparable the tar composition and the concentrations of individual species is in different runs. The results are consistent for the different tar compounds and for all the ERs studied. Tar com-

position and concentration data may therefore be well compared between runs, and only little allowance must be made for errors in this data.

Figure 6.4: Tar species concentrations for AH gasification with steam/oxygen at ER≈0.2.

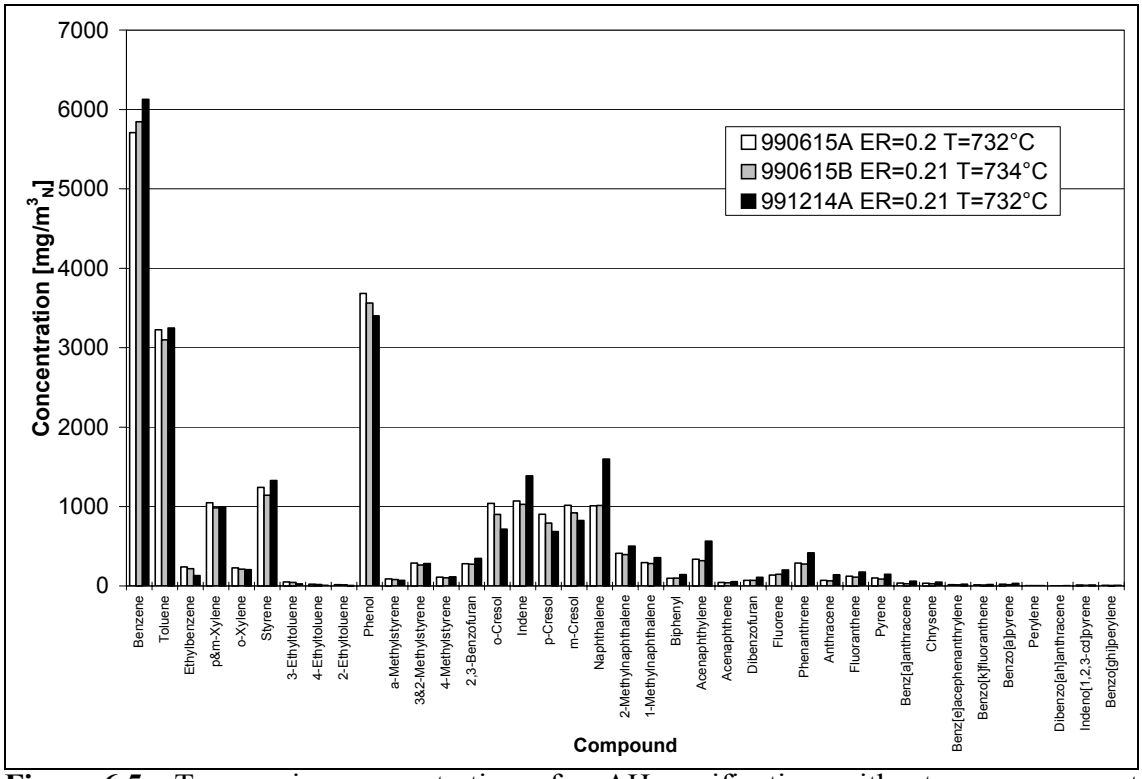

Figure 6.5: Tar species concentrations for AH gasification with steam oxygen at ER≈0.3.

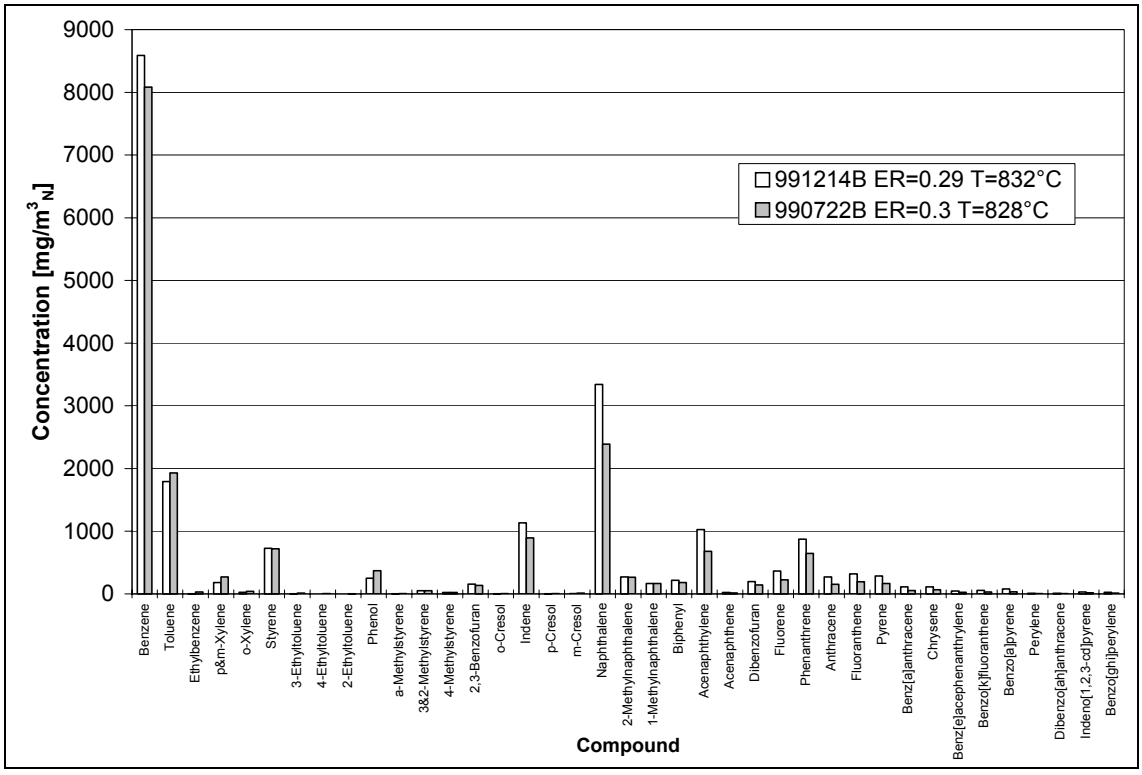

Figure 6.6: Tar species concentrations for AH gasification with steam/oxygen at ER≈0.4.

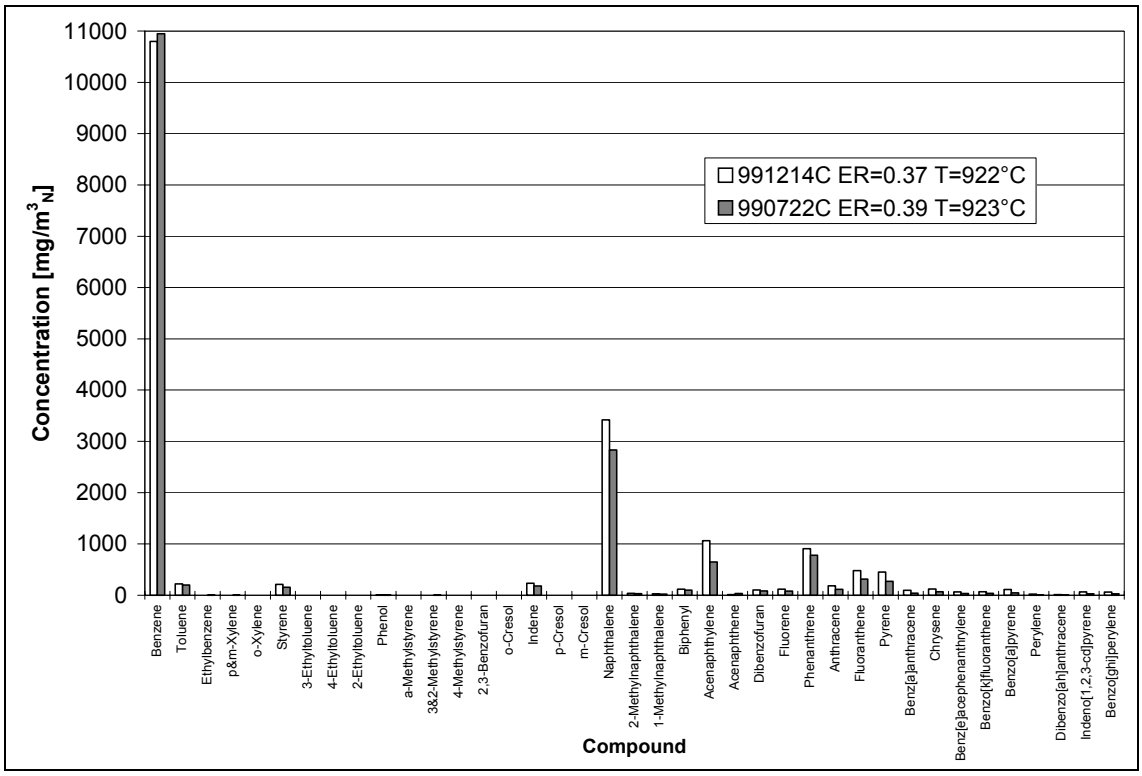

A dramatic change in the composition of the tars is observed in these charts as ER is increased. At ER ≈ 0.2 (or T_{Bed} ≈ 730°C) the tars are a complex mixture of aromatic and small amounts of polycyclic aromatic compounds (benzene making 25% of the tars by mass, naphthalene 5.1%, indene 4.9%, acenaphthylene 1.7% and phenanthrene 1.4%), alkylated aromatic compounds (toluene 13.6%, styrene 5.3% and xylenes 5.2%) and phenolic compounds (phenol 15.1%, cresols 11.1%).

At ER ≈ 0.3 (or T_{Bed} ≈ 830°C) the composition becomes less complex with larger amounts of aromatic and polycyclic aromatic compounds (benzene 42.9%, naphthalene 14.7%, indene 5.2%, acenaphthylene 4.4% and phenanthrene 3.9%). The concentrations of alkylated aromatic compounds decrease strongly (toluene 9.6%, styrene 3.7% and xylenes 1.4%). The cresols disappear completely and only small amounts of phenol (1.6%) are detected.

At ER ≈ 0.4 (or T_{Bed} ≈ 920°C) the tars are composed almost exclusively of benzene (60% of the tars by mass), naphthalene (17%) and of the 3 and 4 ringed polycyclic aromatic hydrocarbons phenanthrene (4.7%), acenaphthylene (4.7%), fluoranthene (2.2%), pyrene (2.0%) and anthracene (0.8%). Of the alkylated aromatic compounds only

small amounts of toluene (1.2%) and styrene (1%) subsist and phenol disappears almost completely (0.04%) at this ER.

Since the composition is almost identical for all runs discussed here, the data might be averaged to allow clearer recognition of trends. The evolution of the average of the tar classes (see page 136) for these Altholz steam/oxygen experiments with the ER is shown in Figure 6.7 illustrating the trends discussed above.

Figure 6.7: Averaged evolution of tar classes with ER for AH gasification in steam/ oxygen. Benzene on left abscissa, all other classes on right abscissa! Dashed lines designate alkylated aromatic compounds.

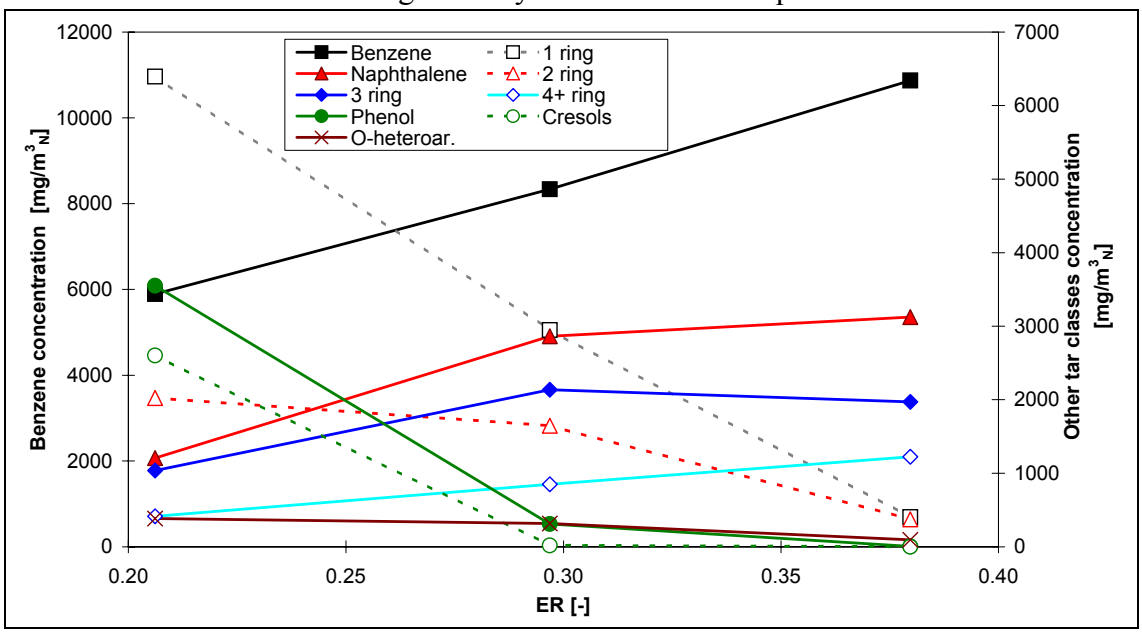

6.2 Influence of fuels

6.2.1 Standard clean wood (SCW) and Altholz (AH) in air

The data from experiments 990903 (SCW/air) and 991029 (AH/air) show that for the same ER the thermal behaviour of both fuels is similar, yielding comparable gasification temperatures as shown in Figure 6.8. The heating values of both fuels being very close, 18.22 and 17.94 MJ/kg respectively for AH and SCW, explains this behaviour. As in the preceding section a discussion of the variations in function of ER or T_{Bed} is therefore equivalent.

Figure 6.8: Bed temperatures and fuel input power for SCW and AH in air.

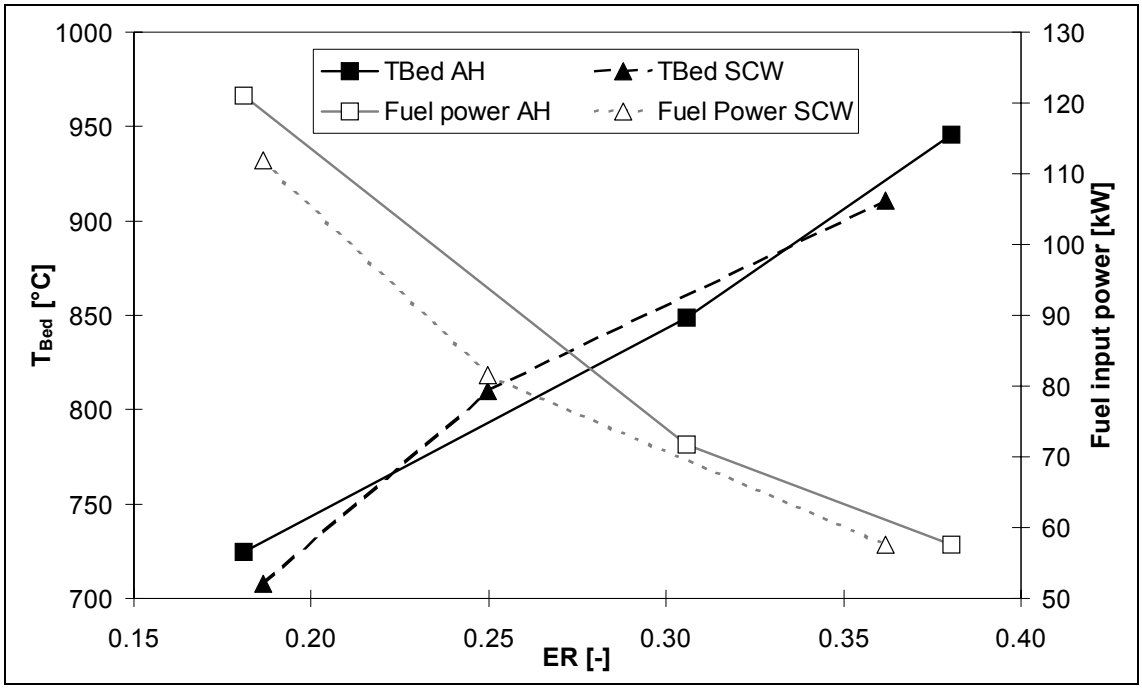

Figure 6.9: Gas composition evolution at top and lower gas sampling point for experiment 981029 (N_2, O_2, and Ar deliberately omitted).

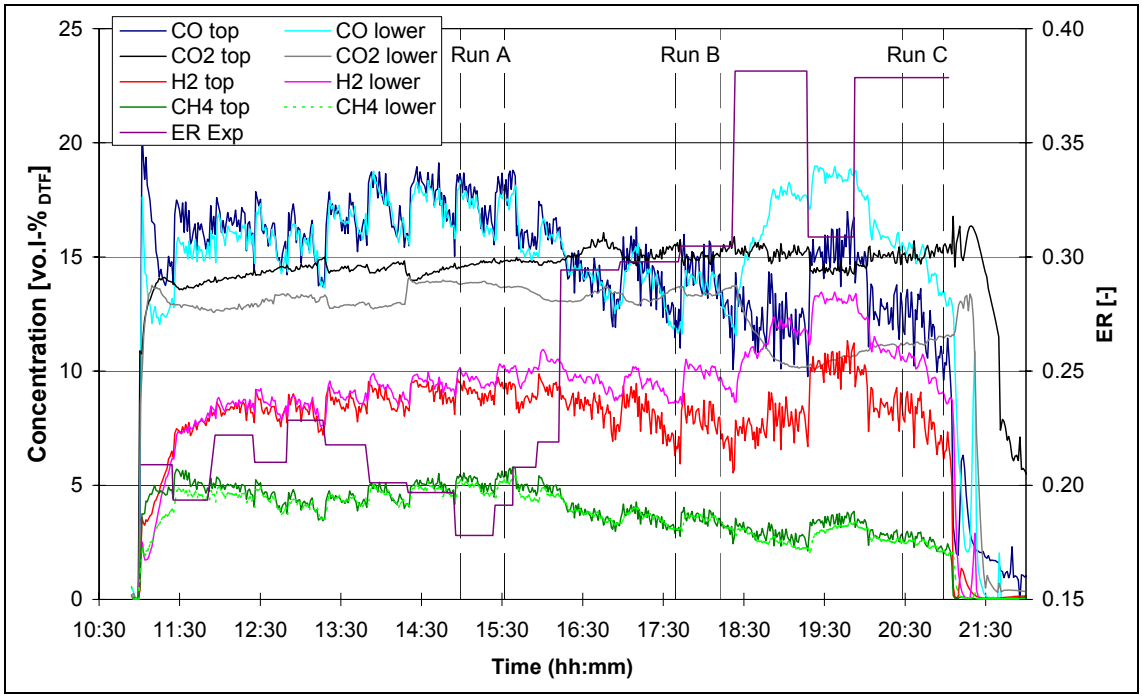

The gas composition evolution for experiment 990903 has been presented and discussed previously (see Figure 5.6 on page 154). The gas composition evolution for experiment 981029 is shown in Figure 6.9.

This plot shows that the gas composition is influenced in a stronger manner by the instantaneous fuel feed rate in the case of AH, yielding concentration evolution lines with a more "jiggy" pattern than was the case with SCW. Still, the reactor conditions were more stable during the measurements as can be deduced from this gas composition evolution plot. Also, the differences observed between top and lower gas sampling point for run 990903A (see Figure 5.6 on page 154) are absent in the low ER part of the experiment with AH. As with SCW the differences between top and lower sampling point persist throughout the experiment but are less marked. Again a reversal of differences is observed for CO as the ER is raised to around 0.4 (or T_{Bed} to ca. 946°C). This reversal could be attributed to the reverse Boudouard reaction ($2CO \rightarrow CO_2 + C_{(s)}$) also explaining the raise in CO_2 concentration observed between both sampling points.

Figure 6.10: Dry gas composition (main reaction products, N_2 deliberately omitted) for SCW and AH in air.

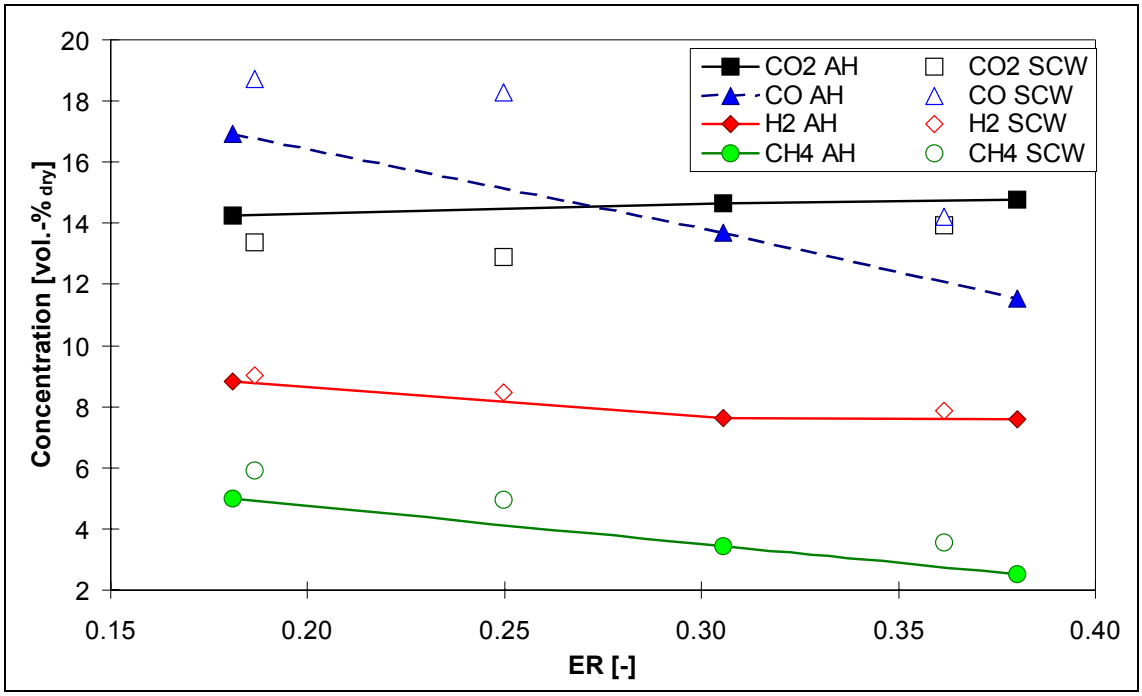

The concentration of the main gas compounds on a dry basis for these two fuels as a function of ER is shown in Figure 6.10. The product gas for SCW exhibits lower CO_2 and higher concentrations of all other compounds than that of AH. The differences between the two fuels are however quite small.

The dry gas composition for both fuels lies in the range reported in the literature for atmospheric, bubbling fluidised bed gasification of wood, as shown in Figure 6.11. CH_4 and H_2 concentrations seem to lie at the lower end of the results reported.

Figure 6.11: Comparison of gas composition with literature data (open symbols, [6.7], [6.8], [6.9]).

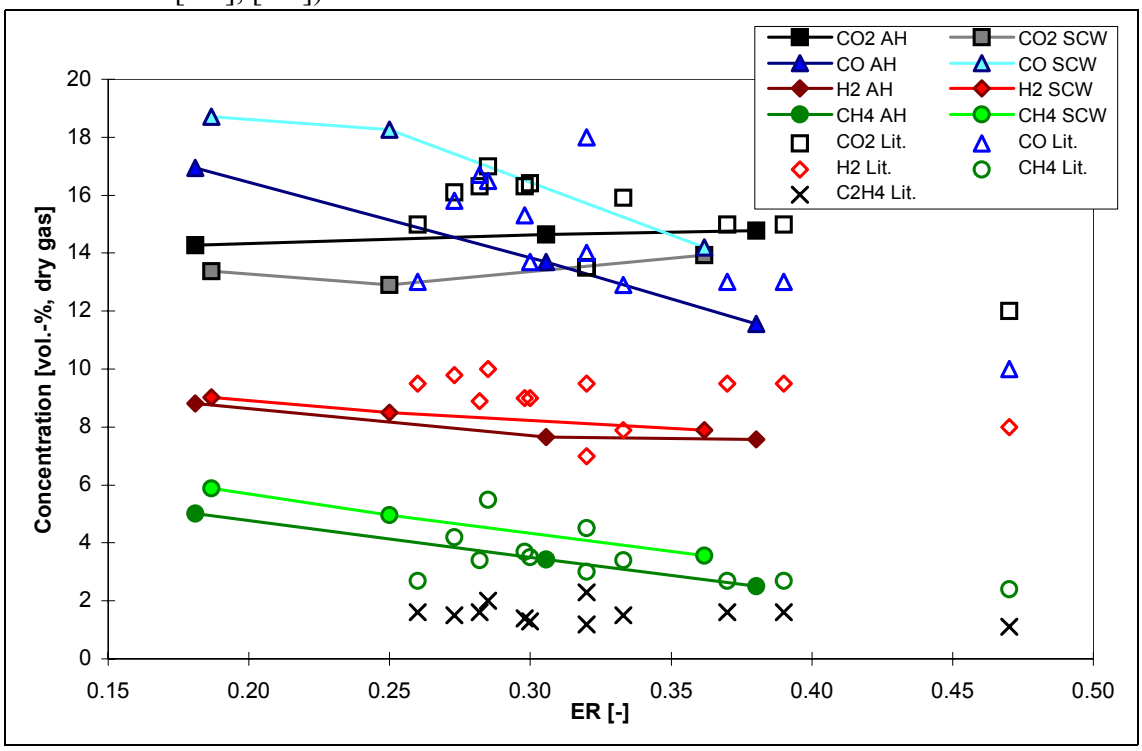

The trends of the gas composition, decreasing CO, H_2 and CH_4 and increasing CO_2 with increasing ER, are in agreement with those reported in the literature. Notice, that ER and T_{Bed} have distinct influences on gas composition. If ER is kept constant and T_{Bed} is increased, H_2 and CO concentrations are seen to increase, CO_2 will decrease and CH_4 will not change [6.9]. This distinct influence is of interest in a real (autothermal) gasifier since higher bed temperatures may be achieved by for example lowering the fuel humidity by drying or improving the thermal insulation of the reactor. As a result a gas with higher CO and H_2 concentrations and of higher calorific value is obtained. However drying of the fuel requires energy and a compromise will have to be made between gas quality and drying requirements, as the energy for drying will have to be derived from the fuel used.

Even though differences in concentrations of the main gas compounds are noted when the two fuels are gasified, these are small compared to the scatter not only in the present study but also in literature data. Both fuels yield a gas with comparable composition when gasified in air.

The gas composition for the thermodynamic equilibrium at the same temperature as the single runs has been calculated and the results are shown in Figure 6.12. The calculations have been performed using the NASA computation code described in [6.10]. This program calculates the equilibrium by minimising the total free enthalpy of a system with given chemical composition. This allows for the fuel to be replaced in the calculations by its composing elements C, H, and O. For the lowest ER in both fuels, the equilibrium computations yield a small fraction of solid carbon as product, 4.2 and 3.6 mol-% of the total products for SCW and AH respectively. The plots clearly show that the reactor was operating far from equilibrium at all experiments with both fuels. This situation has already been observed by other research groups (e.g [6.11]). The measured CO_2, H_2O, CH_4 and tar concentrations are higher than those predicted by the calculations. Tars are not predicted by the thermodynamic calculation and only minor amounts of methane are forecasted at the lowest ER. CO and H_2 are found in lower concentration than would be expected from thermodynamics. In relation to the thermodynamic equilibrium both fuels behave similarly.

In an attempt to understand the origin of the deviations from thermodynamic equilibrium, the measured gas composition has been recalculated with the premise that tars and methane would be steam reformed, yielding a gas with the same methane and tar content as predicted by the thermodynamical equilibrium calculations. The result of this procedure is also shown in Figure 6.12 as “reformed” gas composition. The resulting gas composition is closer to that predicted by the equilibrium calculations. The differences are smaller for SCW and decrease for both fuels when ER is increased.

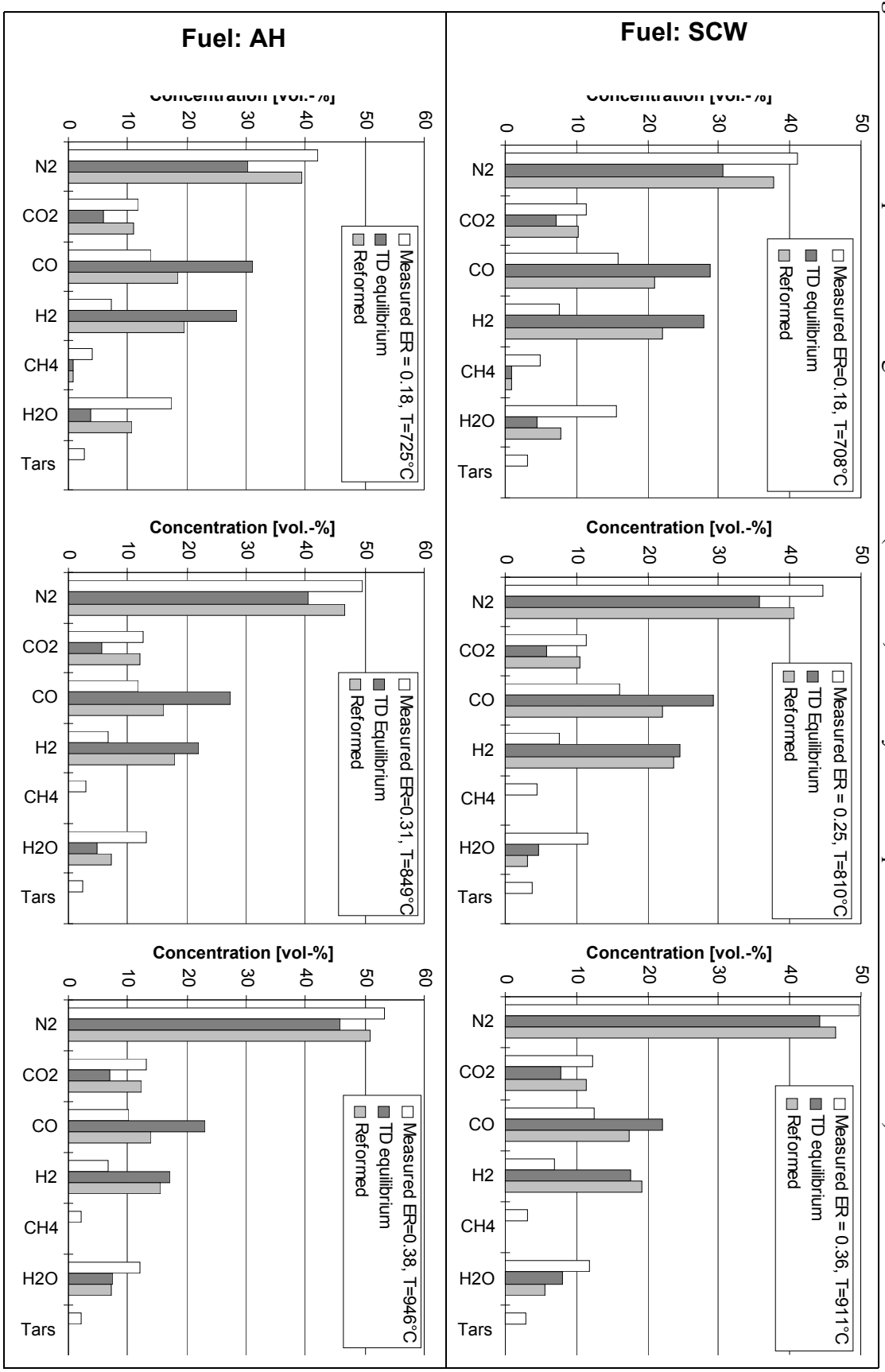

Figure 6.12: Gas composition for air gasification runs (measured, thermodynamical equilibrium and "reformed").

Notice also, that H_2 concentrations could be brought to better agreement between theory and experiment if more H_2O would be converted using CO, but the disagreement in the concentration of the latter compound would be even worse. Apparently, reducing components are missing in the gas composition. These are probably the light hydrocarbons not identified by the gas measurement method.

The gas yield for both fuels in air is shown in Figure 6.13, along with data found in the literature [6.7],[6.9], [6.12] and [6.13].

Figure 6.13: Gas yields for SCW and AH gasification in air and literature data.

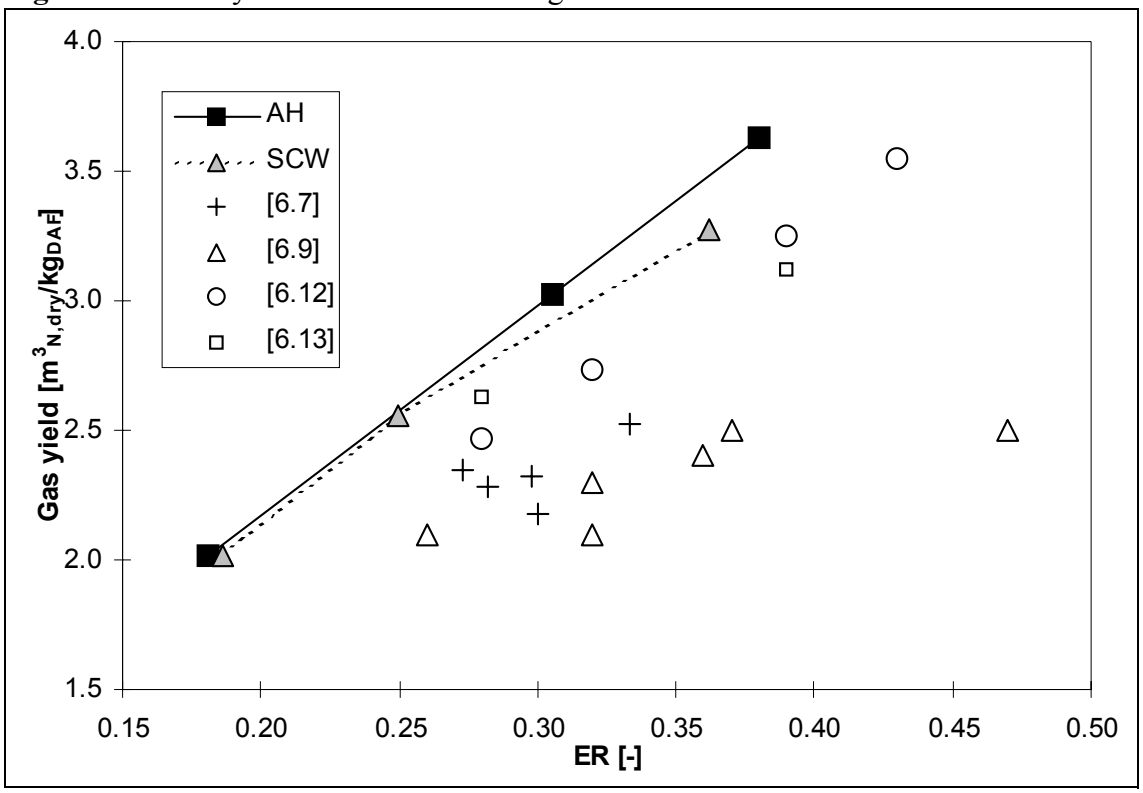

Both fuels essentially yield the same gas volumes when gasified in air. The observed increase in gas yield with increasing ER is in agreement with the literature data. The values in the present study are somewhat higher than the data published.

When gasifying SCW the tar concentration in the gas is clearly higher than when AH is used, as shown in Figure 6.14. The lower tar concentrations are definitely an advantage when gasifying AH in air. For AH the total tar concentration decline as ER is increased as expected. For SCW a maximum is observed at ER = 0.25. The low tar concentration for SCW at ER 0.18 seems unexpectedly low as a continuous increase in tar concentration is expected as ER is lowered (e.g. [6.9], [6.14]).

Figure 6.14: Total tar concentration for SCW and AH gasification in air.

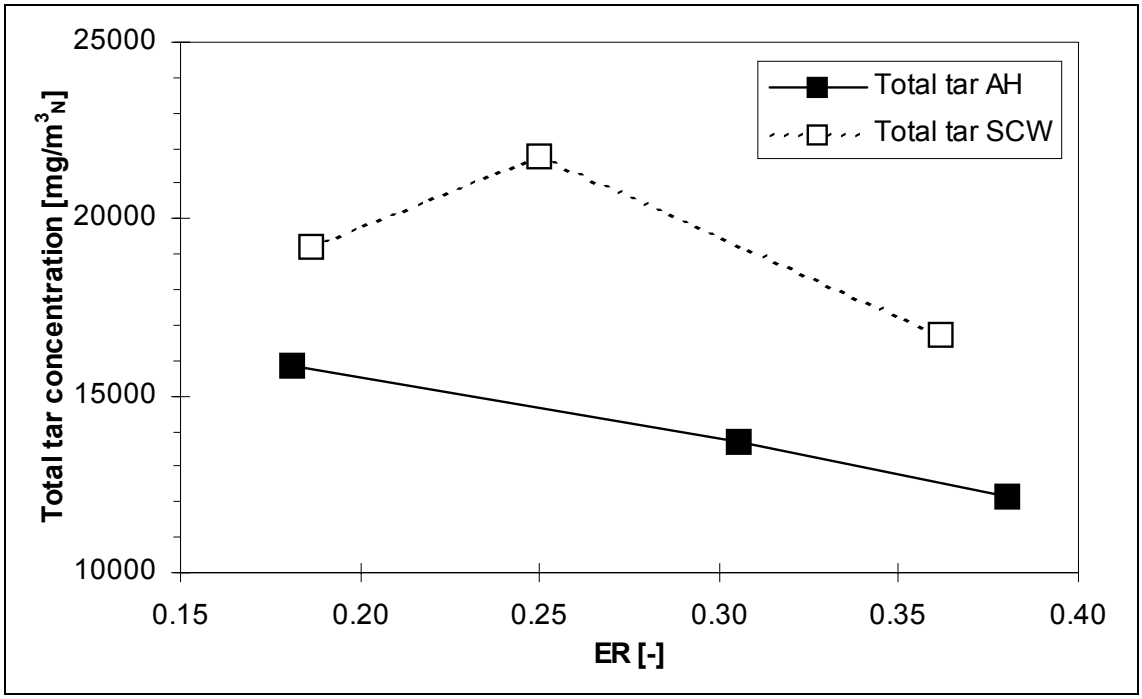

The evolution of the tar classes in function of the ER is shown in Figures 6.15, 6.16 and 6.17.

Figure 6.15: Tar classes (major aromatics) evolution for AH and SCW gasification in air.

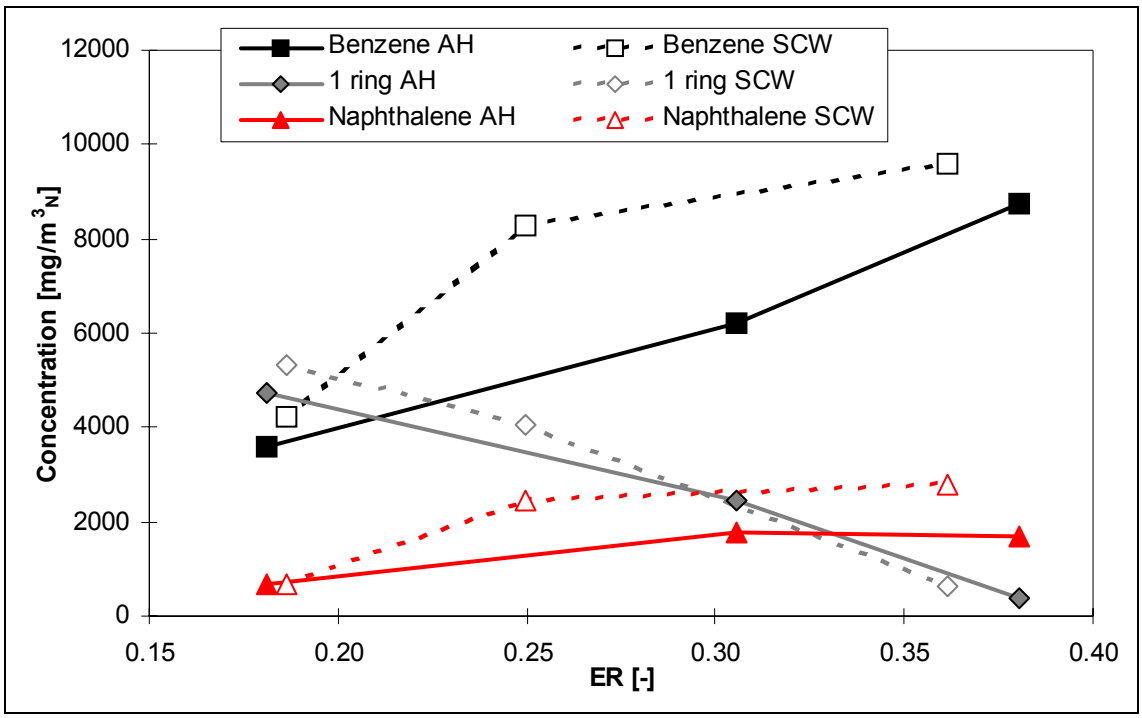

Figure 6.16: Tar classes (oxygenates) evolution for AH and SCW gasification in air.

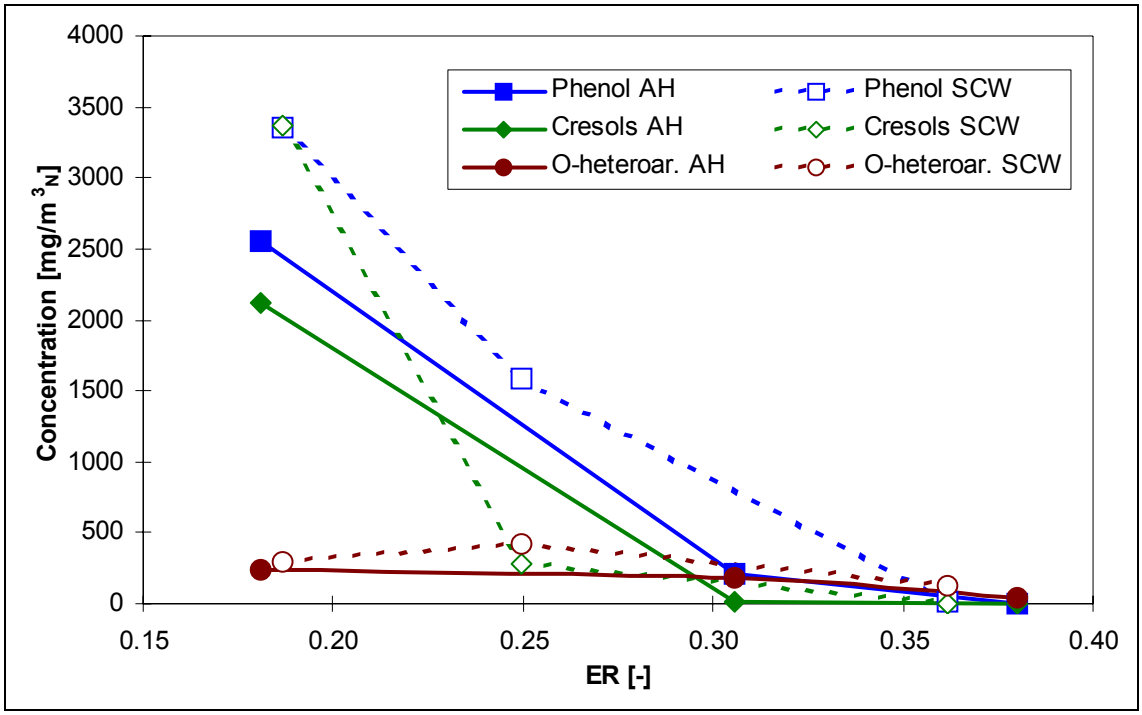

Figure 6.17: Tar classes (minor aromatics) evolution for AH and SCW in air.

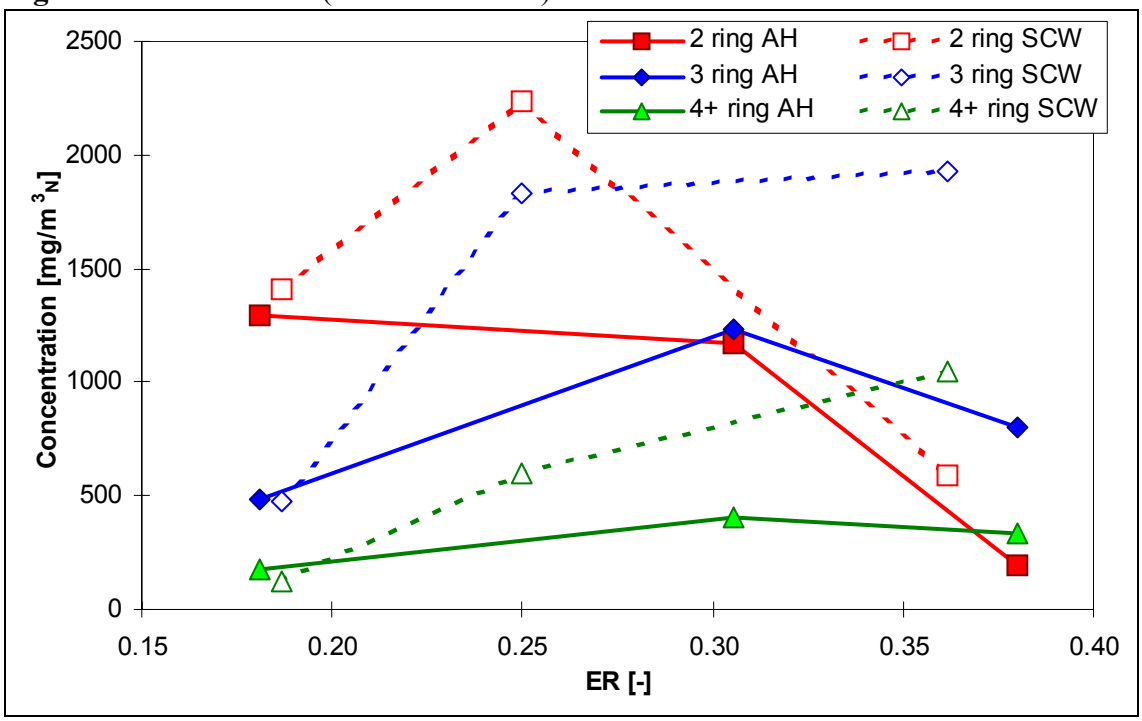

For AH, benzene concentrations increase steadily with ER. Naphthalene and the largest aromatic compounds increase up to ER ≈ 0.3 and seem to stabilise at higher ER. For this fuel the 3 ring compounds exhibit a maximum at the intermediate ER. All other

classes have decreasing concentrations as ER increases and phenolic compounds virtually disappear as ER is increased over 0.3.

For SCW the concentrations of all the tar classes are higher at ER > 0.25, with the exception of 1 ring aromatics. At high ER the concentration of this class is virtually identical for both fuels. The classes Benzene, 1 ring, Naphthalene, Phenols and Cresols follow similar trends in function of the ER as for AH. For the ER range 0.25 - 0.38 the evolution of the tar classes is as expected (see Chapter 3) not only for SCW but also for AH.

For SCW all aromatic compounds but the 1 ring class show a marked decrease at ER < 0.25. Their concentrations are approximately the same for both fuels at this low ER. For phenol and cresols on the other hand the concentrations at ER ≈ 0.2 are significantly higher in the case of SCW. A possibility for the explanation of these trends is that the tars issued from SCW gasification at low ER are composed of only partially converted pyrolysis products, i.e. they are secondary tars (see page 66). Indeed the reactor was operating under transient conditions as this measurement was performed (see page 153). These secondary tars are not quantified by the GC/MSD method employed, and thus the measured total tar concentration is lower than the actual concentration in the gas. As a matter of fact the qualitative or scan chromatograms of the samples issued form the low ER runs show a large number of relatively small peaks. The mass spectra corresponding to the apexes of these small peaks have been compared to a mass spectral database. This comparison reveals the presence of a large number of substances such as alkylated aromatics (various isomers of methyl, ethyl, ethenyl, ethinyl, propyl and propenyl substituted benzenes but also naphthalenes, phenanthrenes, anthracenes and larger PAHs), alkylated phenols and dihydroxybenzenes, hydroxy-PAHs, PAH isomers not present in the quantification method and also nitrogen containing species such as pyridine. The individual peaks are very small, indicating that these unquantified tar species are present only in low concentrations. Their number is especially high in the samples issued from low ER runs and decreases as ER is increased.

An estimation of the fraction of the tar compounds identified by the GC/MSD method was made using the tar analysis results of these air gasification runs. For this estimation the quantitative or scan chromatograms (see page 111) were used. The estimation was made by computing the sum of the areas of peaks in the scan chormatogram which

correspond to substances identified by the quantification method. Then the ratio of this sum to the total area of peaks present in the chromatogram, including identified and unknown substances, is calculated. This area ratio is assumed to be roughly proportional to the mass ratio of identified to total tar compounds. The area ratios have been calculated only for the samples 3, 4, OE ad HT Ac of the above runs as these samples are known to contain the main mass fraction (>95%) of the compounds identified. The mass of tar compounds identified in a sample is assumed to be proportional to the total mass of tars (identified and unknown) deposited in this sample. The area ratios are multiplied with the mass fractions of tar compounds found in each sample. This multiplication allows to take into account the distribution of tar compounds in the sampling train. Finally the products obtained for each sample (area ratio x mass fraction of identified tars in sample) are added to yield the mass fraction of tars identified. It is thus assumed that the fraction of unidentified compounds in the sample will be proportional to the total mass of tars deposited in this sample. The results of this computation are shown in Figure 6.18.

Figure 6.18: Estimated mass fraction of tars identified versus ER for SCW and AH gasification in air.

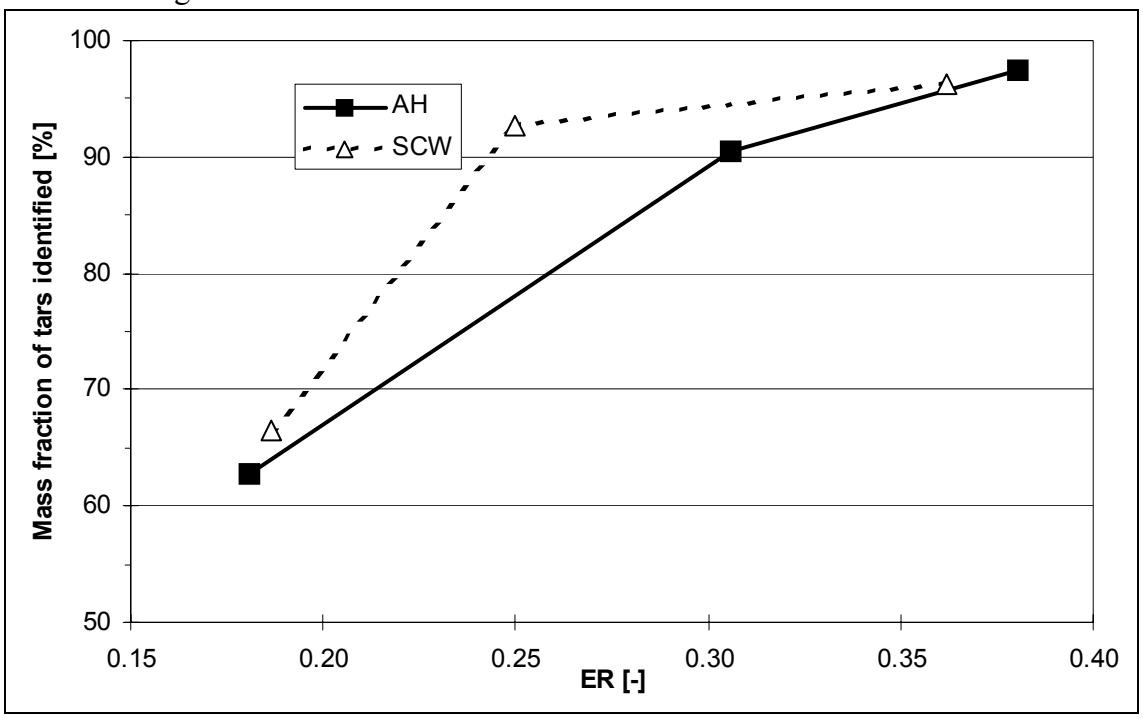

In [6.15] a similar estimation was made for air gasification of sawdust in an ER range of 0.22 to 0.32 and a temperature range of 700 to 900°C. The fraction of tars identified by the method used in this reference was 70 to 90% of the total tars present in the

samples collected. The trend described in function of the ER was the same as in the present study: an increase in the fraction identified with increasing ER. The present results for ER > 0.25 agree well with this literature data. The results for lower ER are however lower than those reported in the named reference and seem to fall out of the trend observed for higher ERs in the present study. The conclusion is, that the low tar amount observed when gasifying both fuels at low ER is due to the presence of large amounts of partially converted pyrolysis products or secondary tars. These secondary tars are not quantified by the tar measurement procedure used in the present study. This is a serious limitation of the tar analysis method used when low ERs are to be studied. The number of species present in these low ER tars is very high. An analysis method which would allow the exact quantification of such a high number of compounds requires analytical and manpower capabilities which were not available for the present study. As the method was designed a choice was made with respect to what compounds should be quantified or not. The results show, that these are the major tar constituents even at low ER, and therefore the goal pursued with the measurement method has been achieved. Furthermore to lower the total tar content in the gas most gasifiers are operated at high temperatures. The tars generated by high temperature gasification are accurately quantified by the employed method.

Even with the limitation of the tar analysis method the trends observed for the tar composition in function of the ER agree with the results found in the literature ([6.14], [6.15]). It is noteworthy, that the authors of [6.15] also report a decrease of the tar concentration as temperature is lowered below 750°C at a constant ER of 0.22. These results point out how complex the nature of the tar conversion reactions is. They are influenced by both, temperature and ER in similar but not identical manner.

If the tar content measured in the gas is corrected using the estimated fractions of tars identified, the evolution of tar concentrations shown in Figure 6.19 is obtained. The concentrations are higher especially for the low ERs, but still the AH is seen to yield lower tar concentrations.

Figure 6.19: Corrected total tar concentrations versus ER for air gasification of SCW and AH.

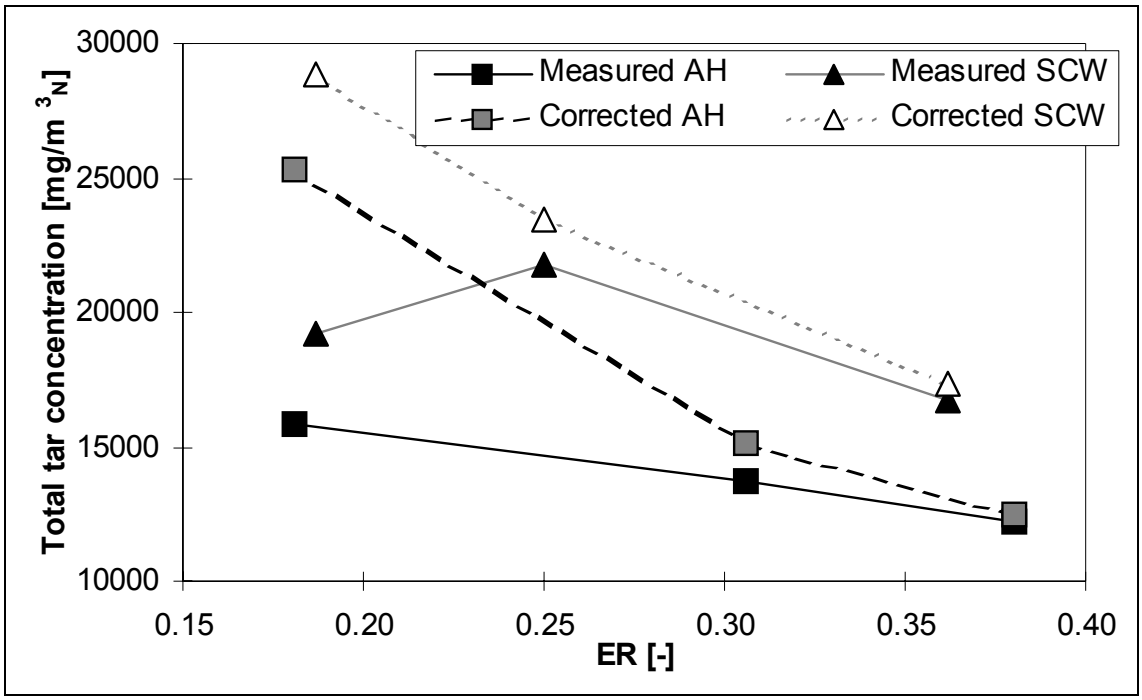

Figure 6.20 presents a comparison of the detailed tar composition for SCW with data from reference [6.12] where pine sawdust was gasified with air in a pressurised bubbling fluidised bed.

Figure 6.20: Comparison of SCW detailed tar data with literature data [6.12].

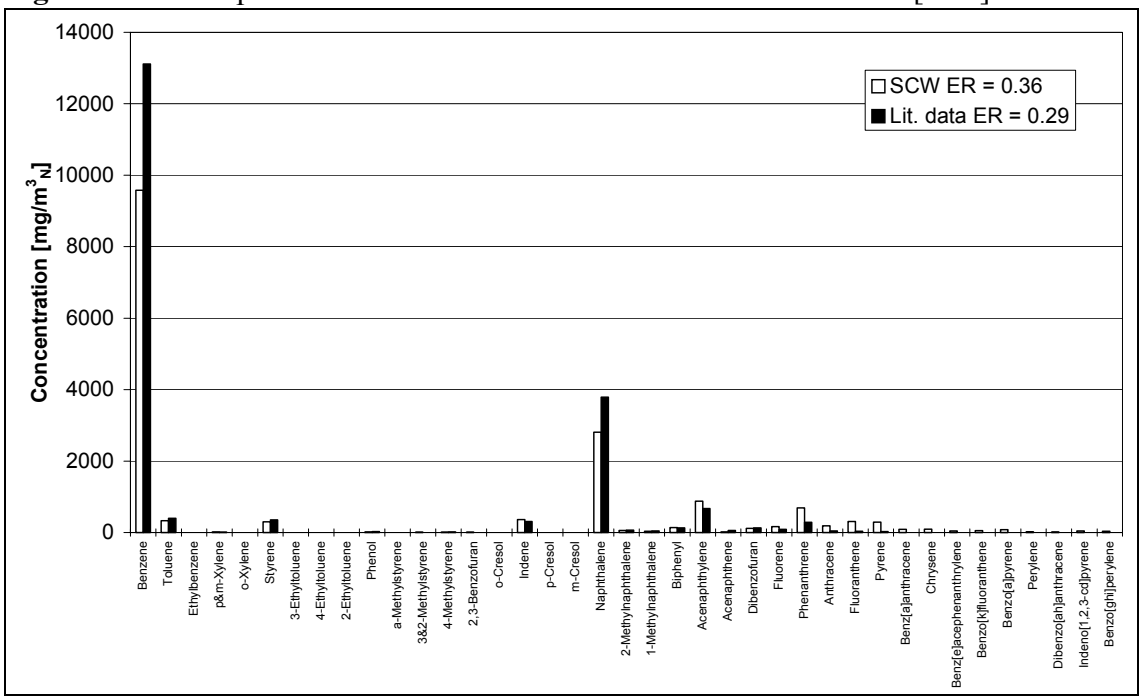

This literature data must be compared to the results from SCW gasification at high ER, as the temperature in this reported experiment was 900°C. The concentrations of individual compounds detected in the present study are lower than the literature data. In agreement with data reported in [6.12], the total tar concentrations drop as temperature (in the present case equivalent to ER!) increases. In contrast to this reference is the rising benzene concentration detected with an increase in temperature/ER in the present study and also reported by other authors ([6.14], [6.15]). The data from [6.12] does cover a higher range of temperatures than was possible to study with the installation used in the present study. Also, as stated before, this data was measured under pressure (4 bar), which according to [6.16] should lower the tar amount in the gases. This discrepancy can have a number of origins from diverse tar sampling methods used (in [6.16]) to different fuels or reactor conditions and will not be further commented here as no experiments under pressure could be carried out in the plant used in the present study. The method used in the present study is quite comparable to that in reference [6.12], as is the fuel. The total tar concentration reported in [6.12], 19556mg/m^3_N, lies in between those measured in the present study at comparable conditions, 21740 and 16735mg/m^3_N for ER = 0.25 and 0.36 respectively.

A comparison of the tar composition issued from both fuels is shown in Figures 6.21, 6.22 and 6.23. The tars issued from the two fuels are quite diverse. At low ER the tars from SCW have a higher content of phenolic compounds and all other tar classes are lower in this fuel than in the tars of AH. At the intermediate ER SCW exhibits lower benzene content but the phenolic compounds are present in higher fractions than in AH. At high ER the benzene content in the tars of SCW is lower, but the fraction of PAHs is higher than in AH.

Figure 6.21: Normalised tar composition of SCW and AH gasification in air at low ER.

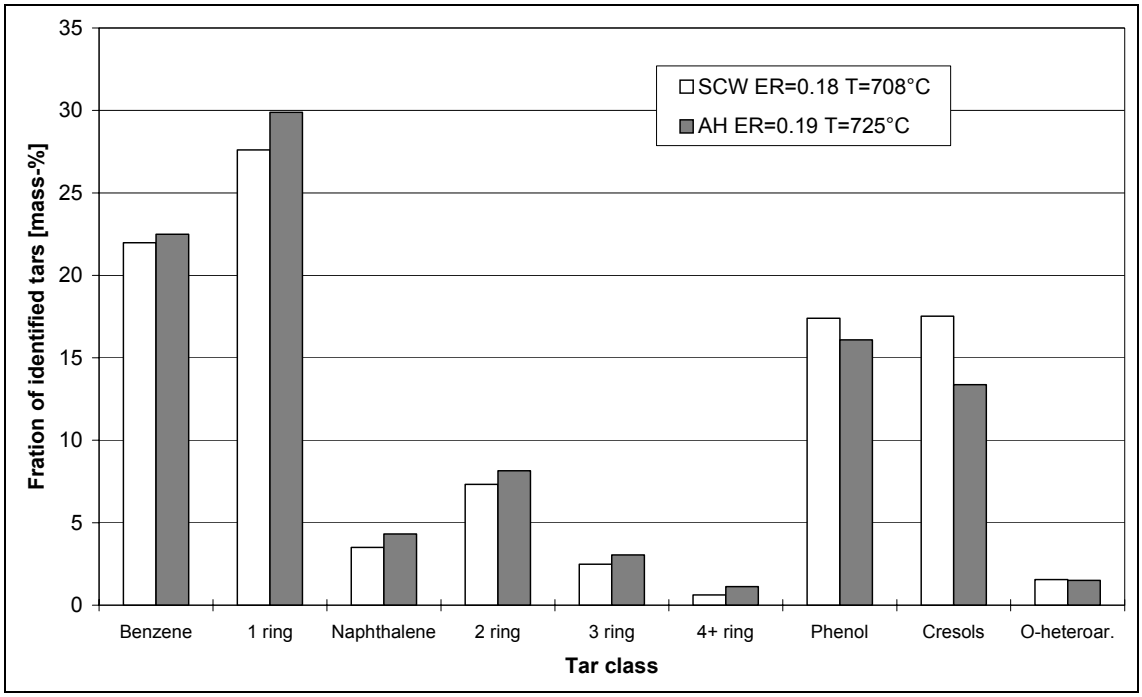

Figure 6.22: Tar composition of SCW and AH gasification in air at intermediate ER.

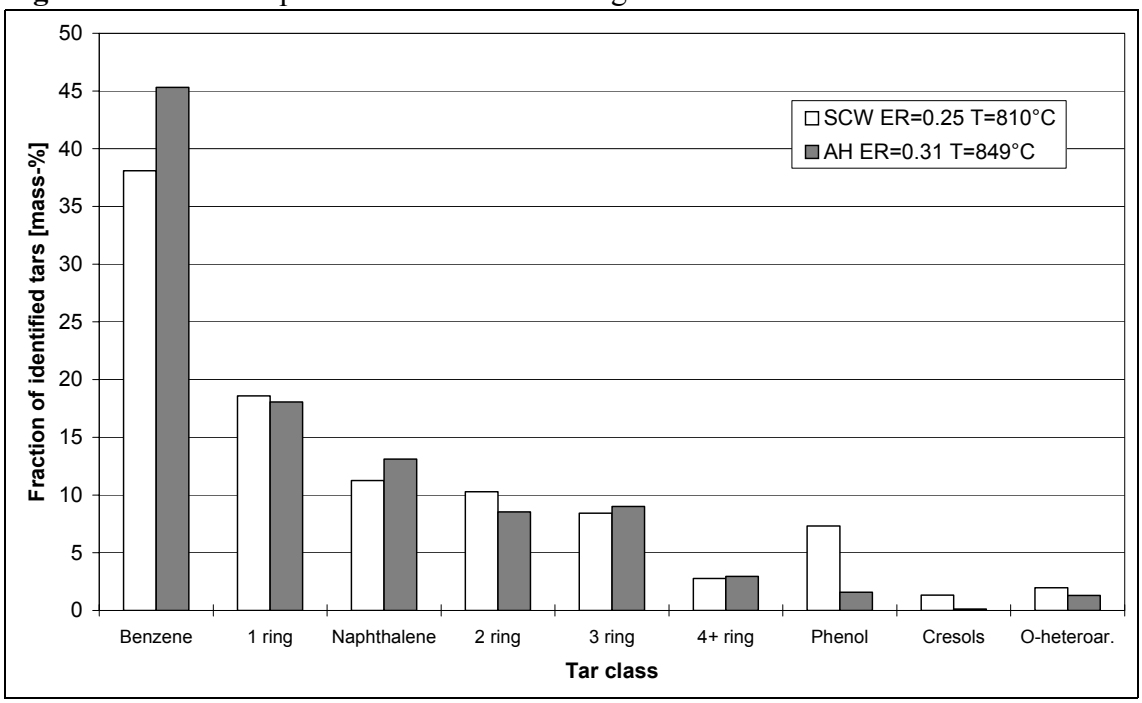

Figure 6.23: Tar composition of SCW and AH gasification in air at high ER.

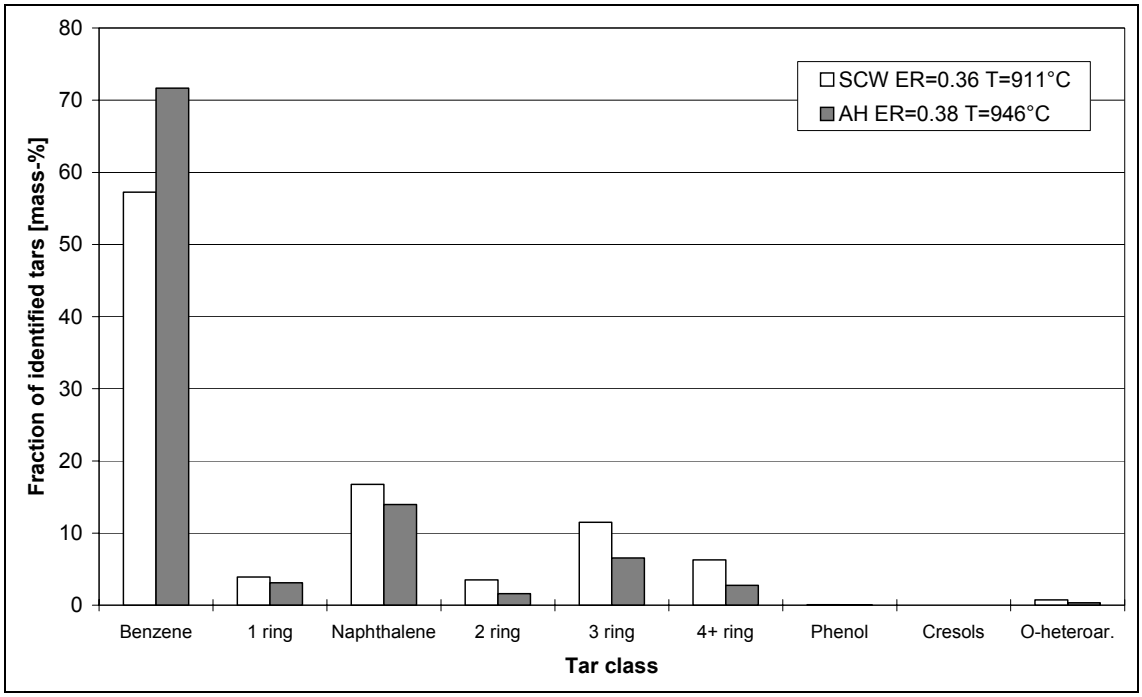

The tar composition is clearly affected by the type of fuel gasified. Also the total tar amount is lowered when AH is gasified. These effects may be attributed to the metals present in AH. It is noteworthy that even though the AH has been pre-treated and that this pre-treatment procedure largely removed metal particles from the fuel, the bed was always found to contain molten or sintered metal particles after an AH experiment. The composition of these particles was not studied. The particles were however found to be magnetic, indicating the presence of iron, a metal which might catalyse several important reactions in gasification and especially reforming and cracking reactions which in turn could explain the lower tar amount observed.

6.2.2 SCW/AH in steam/oxygen

The bed temperatures for both fuels in the case of steam/oxygen as gasification agent are almost identical for the same ER, and therefore discussion with respect to these parameters is equivalent, see Table 6.4.

Table 6.4: ER and bed temperatures for SCW and AH (averaged values) gasification in steam/oxygen.

AH		SCW	
ER [-]	T_{Bed} [°C]	ER [-]	T_{Bed} [°C]
0.21	733	0.20	707
0.30	830	0.30	841
0.38	923	0.40	932

The gas composition evolution for the experiments with AH as fuel are shown in Figures 6.24 to 6.26. The corresponding plot for the experiment involving SCW is given in Figure 6.27.

Figure 6.24: Gas composition evolution for experiment 990615: AH gasified in steam/oxygen (N_2 and Ar deliberately omitted, dry, tar-free basis).

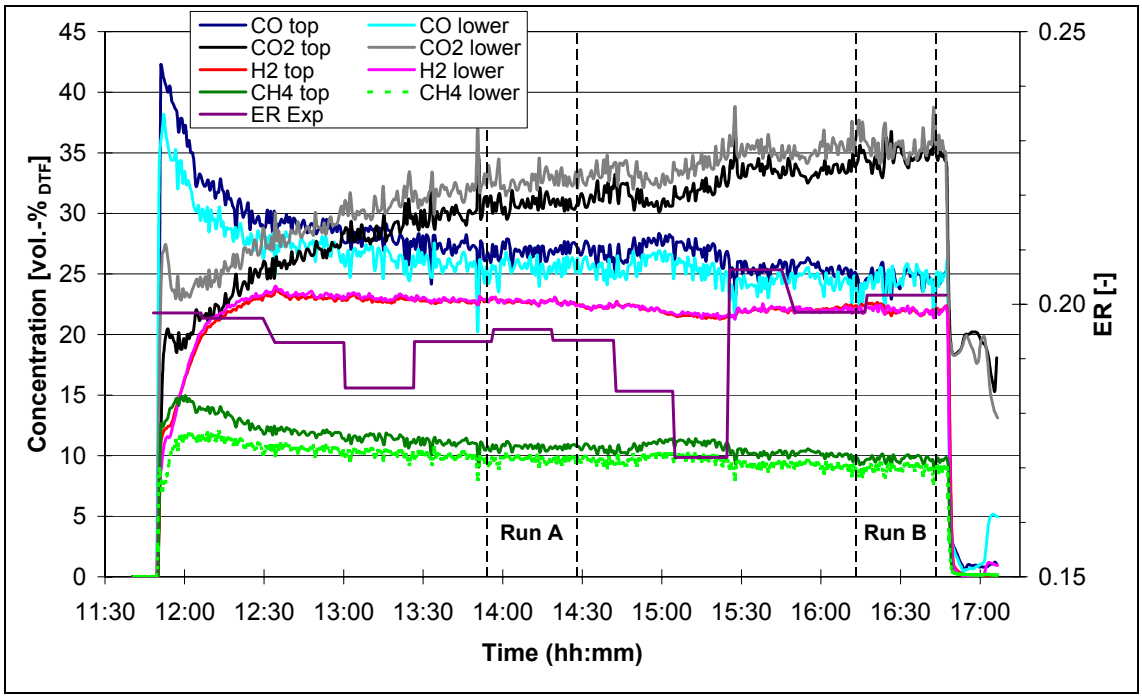

Figure 6.25: Gas composition evolution for experiment 990722: AH gasified in steam/ oxygen (N_2, O_2 and Ar deliberately omitted, dry, tar-free basis. data for run A discarded.).

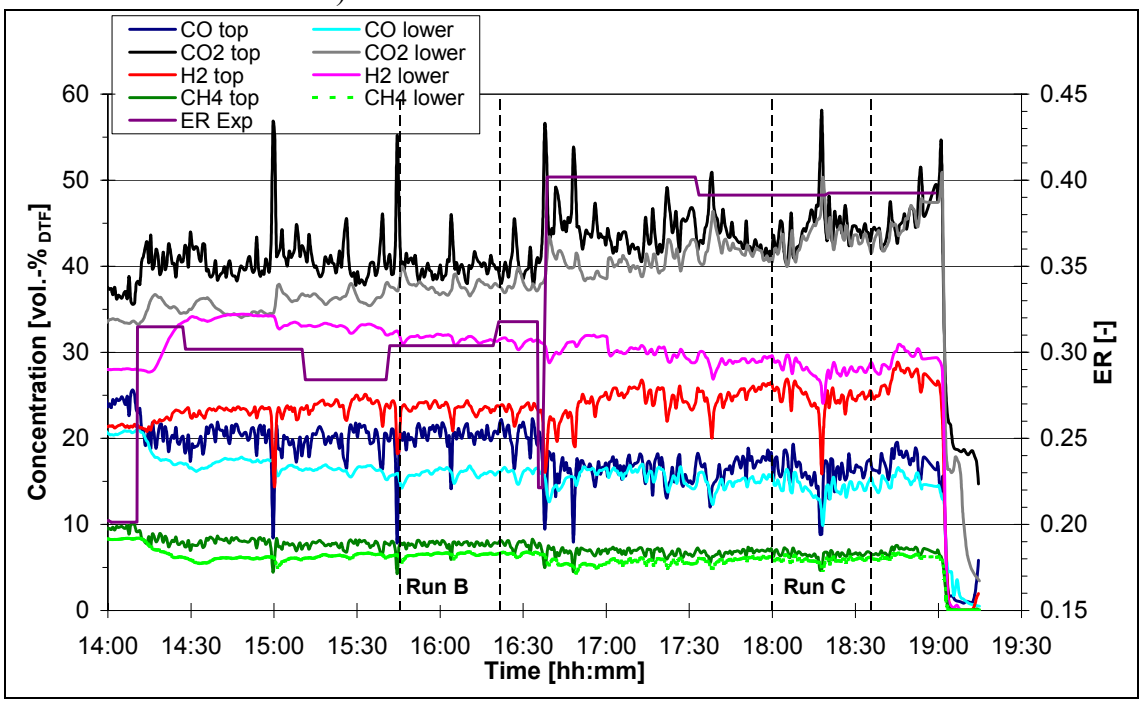

Figure 6.26: Gas composition evolution for experiment 991214: AH gasified in steam/ oxygen (N_2, O_2 and Ar deliberately omitted, dry, tar-free basis).

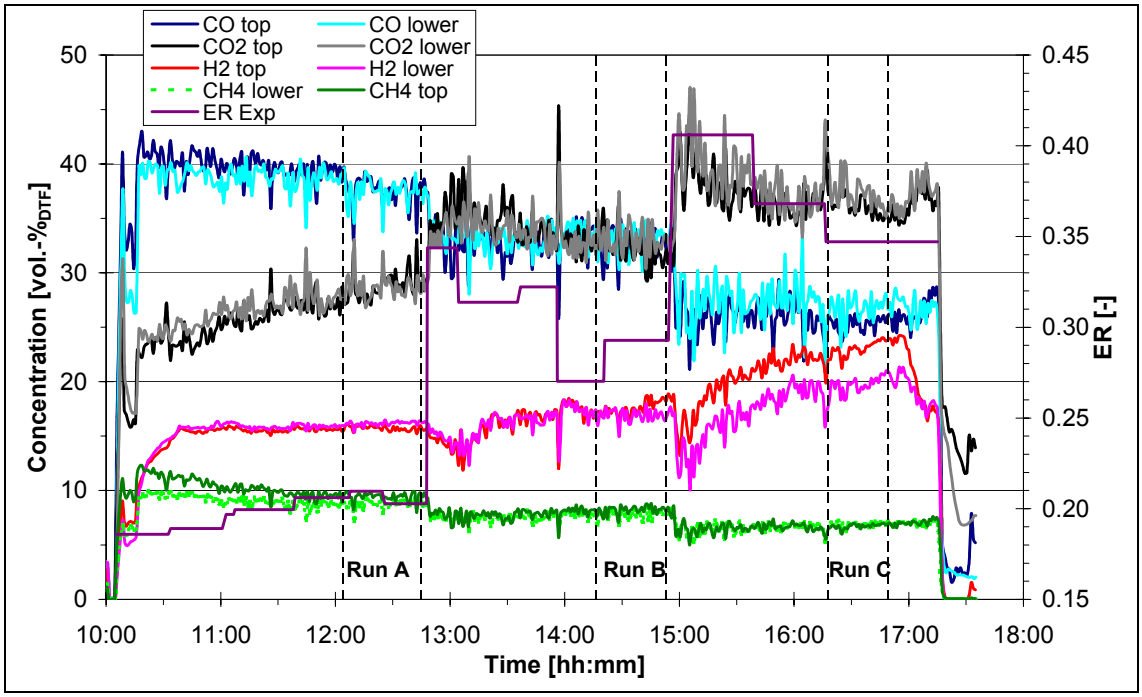

Figure 6.27: Gas composition evolution for experiment 000125: SCW gasified in steam/ oxygen (N_2, O_2 and Ar deliberately omitted).

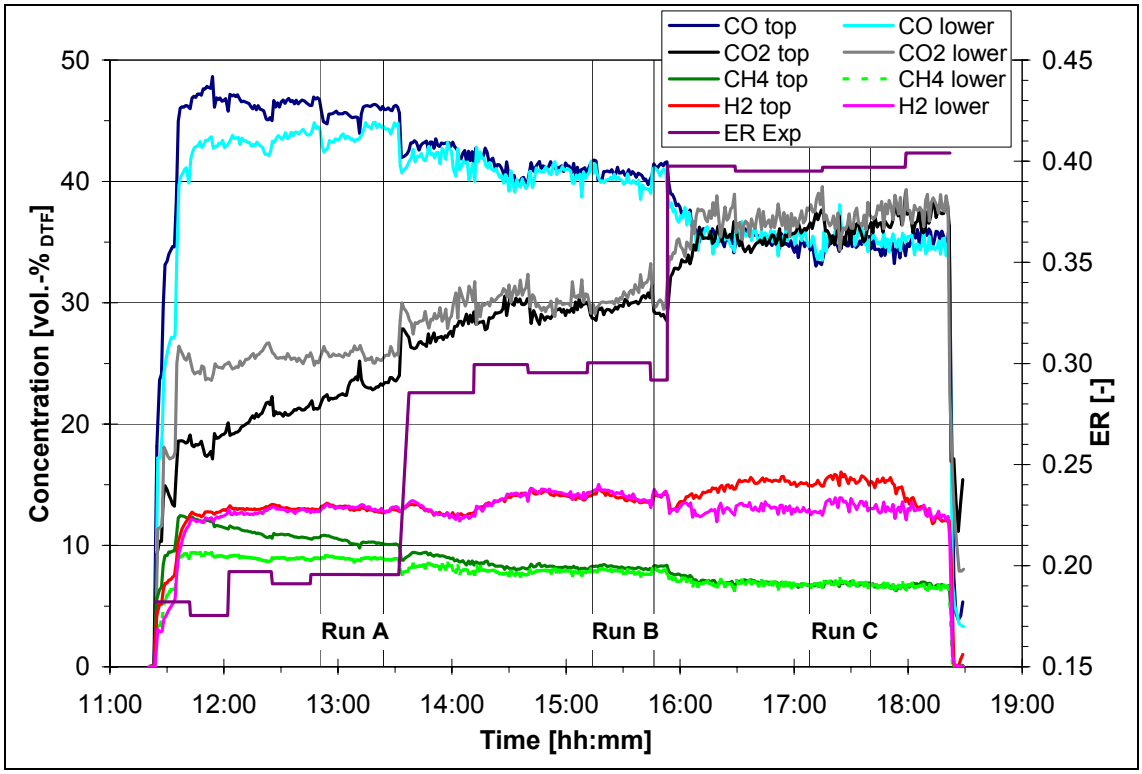

These plots show some interesting differences between top and bottom sampling point. In those runs, where the ER was below 0.2 and the reactor temperature around 700°C, differences between the concentrations of the carbon containing species CO, CO_2 and CH_4 as well as small differences in the H_2 concentrations are observed between the top and the lower sampling point. These are especially large in the experiment where SCW is gasified (experiment 000125, Figure 6.27).

The CO_2 concentration is higher in the lower zone of the reactor and the other gases show higher concentrations at the top of the installation. A hypothesis to explain this behaviour is that, under the strongly reductive conditions in these runs, the concentration of hydrocarbons and tars in the gas is high. CO_2 could react with these species yielding CO, smaller hydrocarbons and H_2. This hypothesis could only be confirmed if tar and hydrocarbons concentrations had been measured at the lower sampling point. Some experimental evidence however supports this hypothesis. The tar filter of the lower gas sampling port exhibited a darker colour and tended to plug faster than the similar filter at the top gas sampling point indicating that higher tar concentrations are present in this part of the re-

actor. From this observation we can conclude that reactions reducing the tar concentration (and possibly influencing its composition) occur in the reactor's freeboard.

At the intermediate ER setting, no notable differences are seen in the gas composition measured at both locations.

At high ER, where the temperature of the freeboard was around 900°C, a marked increase in H_2 concentration is observed as the gas travels along the reactor for the runs 991214C and 000125C. The increase in hydrogen could be assigned to reactions involving the unconverted char elutriated from the bed and water vapour. To test this hypothesis, measurements of the carbon load of the gases at different levels of the reactor would be necessary and have unfortunately not been performed in the current study. In run 990722C the H_2 concentration is seen to decrease as the gas travels through the reactor. This situation could be explained by the presence of substances inhibiting the heterogeneous reactions in the fuel used for this particular run.

These effects on the gas concentration as a function of the height of the reactor clearly show that reactions involving the unconverted chars elutriated from the bed occur in the freeboard of the installation and that these reactions have an important influence on the gas composition at the exit of the reactor.

The evolution of the gas composition as a function of ER obtained when gasifying AH and SCW in steam/oxygen is shown in Figure 6.28. The main gas components are seen to follow the same trends in function of the ER for both fuels. Differences in gas composition for the two fuels are however more evident than when using air as gasification agent. At all ERs studied, the AH shows lower CO and higher CO_2 and H_2 concentrations. This effect could be explained by the homogeneous water-gas shift reaction ($CO + H_2O \rightarrow CO_2 + H_2$) being catalysed by compounds present in the AH fuel. A large number of metals is known to be present in this fuel (even if in small amounts) and these could account for this effect (see page 164). As was the case with air as gasification agent CH_4 concentrations in the gas are higher when SCW is used as fuel, but differences are smaller when steam/oxygen is used as gasification agent.

Figure 6.28: Concentration of main reaction products for SCW and AH gasification in steam/oxygen.

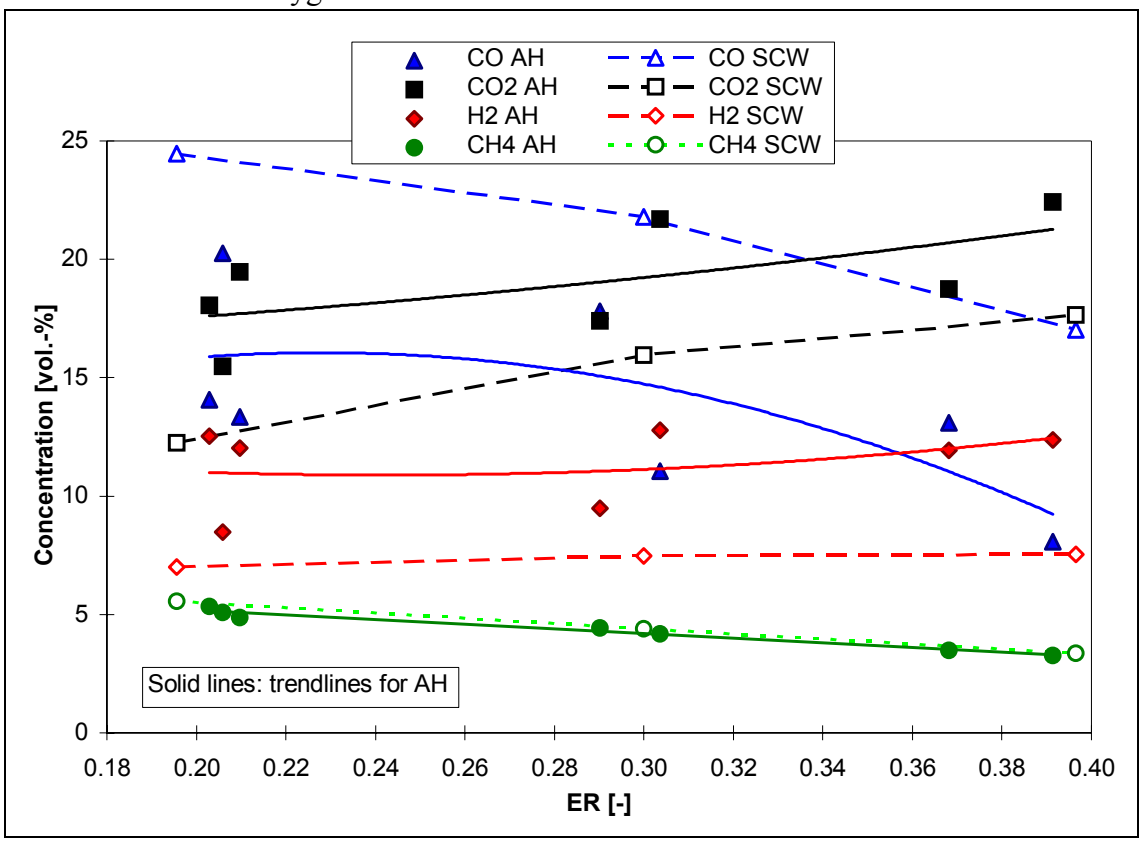

A comparison of the obtained gas composition with literature data [6.17] is shown in Table 6.5.

Table 6.5: Comparison of gas composition [vol.-% dry, nitrogen-free gas] with literature data [6.17] for steam/oxygen gasification. S/B: steam to biomass ratio [kg/kg$_{DAF}$].

	Literature data		AH (average)			SCW		
	min.	max.						
ER [-]	0.24	0.51	0.21	0.30	0.38	0.20	0.30	0.40
S/B	0.48	1.11	0.39	0.54	0.67	0.37	0.53	0.67
CO_2	14.4	36.3	33.0	37.0	41.3	23.0	29.6	35.9
CO	42.5	52.0	29.7	27.4	21.3	45.9	40.5	34.6
H_2	13.8	31.7	20.6	21.1	24.4	13.1	13.9	15.3
CH_4	6.0	7.5	9.5	8.2	6.8	10.4	8.2	6.8
C_2H_n	2.5	3.6	not measured			not measured		
H_2O [vol.% wet gas]	38	61	43.6	44.5	46.1	44.3	43.9	49.1

This data, obtained in an atmospheric bubbling fluidised bed using pine sawdust, a fuel comparable to SCW, reveals that the SCW results lie well in the range reported with the exception of CH_4 which is higher in the present study. Also the H_2 concentration measured in the present study lies at the lower end of the range reported.

AH on the other hand clearly shows lower CO and higher CO_2 concentrations than the literature data and the CH_4 and H_2 concentrations within the range reported.

A comparison of the measured data with the gas composition from thermodynamic equilibrium calculations and a "reformed" gas composition (see page 173) is depicted in Figure 6.29.

As was the case for air gasification the reactor does not deliver a gas with a composition close to the thermodynamic equilibrium. This situation is already documented in the literature [6.18]. In contrast to the similar calculations for air as gasification agent, no solid carbon is predicted for the low ER set-points by the calculations for neither fuel. A small concentration of CH_4 is however still forecasted by the calculations for these conditions.

For SCW CO_2 concentrations are almost identical and CO concentrations only slightly smaller than those predicted by the equilibrium calculations, the latter becoming smaller as ER (or T_{Bed}) is increased. Large differences are seen in the H_2 and H_2O concentrations. The former is too low and the later too high in the experiments. As for air gasification, no CH_4 above ER = 0.3 or tars at all ERs are predicted by the equilibrium computations. "Reforming" of the CH_4 and tars still leaves large differences for ER < 0.3. At high ER however the reformed and equilibrium gas composition is almost identical for SCW.

The data for AH exhibits larger CO_2 concentrations than calculated for the thermodynamic equilibrium at all ERs. Both CO and H_2 are lower in the experimental data and again H_2O concentrations largely exceeding the thermodynamic predictions are observed. Notice how the difference in the concentrations between measurement and equilibrium forecast of CO and CO_2 is smaller in the data marked with an * when compared to data at the same ER from other runs. This marked data corresponds to the results from experiment 991214. "Reforming" of the gas for AH does bring the gas composition closer to the equilibrium, but differences are still substantial.

Figure 6.29: Measured, thermodynamical equilibrium and "reformed" gas composition for steam/oxygen gasification experiments with SCW and AH.

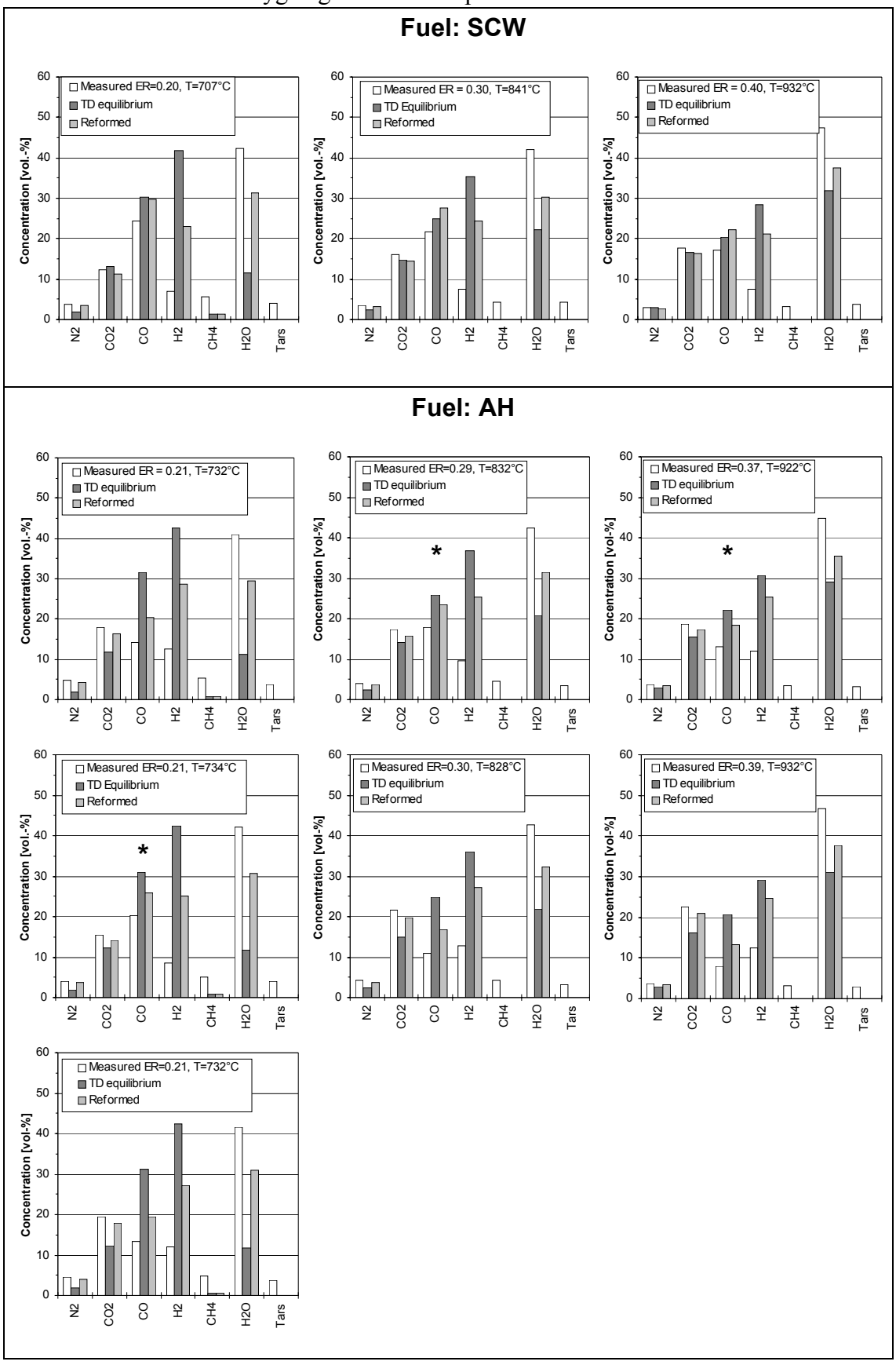

The gas yield of the experiments with AH and SCW in steam/oxygen is shown in Figure 6.30, compared to data published in the literature [6.19].

Figure 6.30: Gas yield for AH and SCW gasification in steam/oxygen.

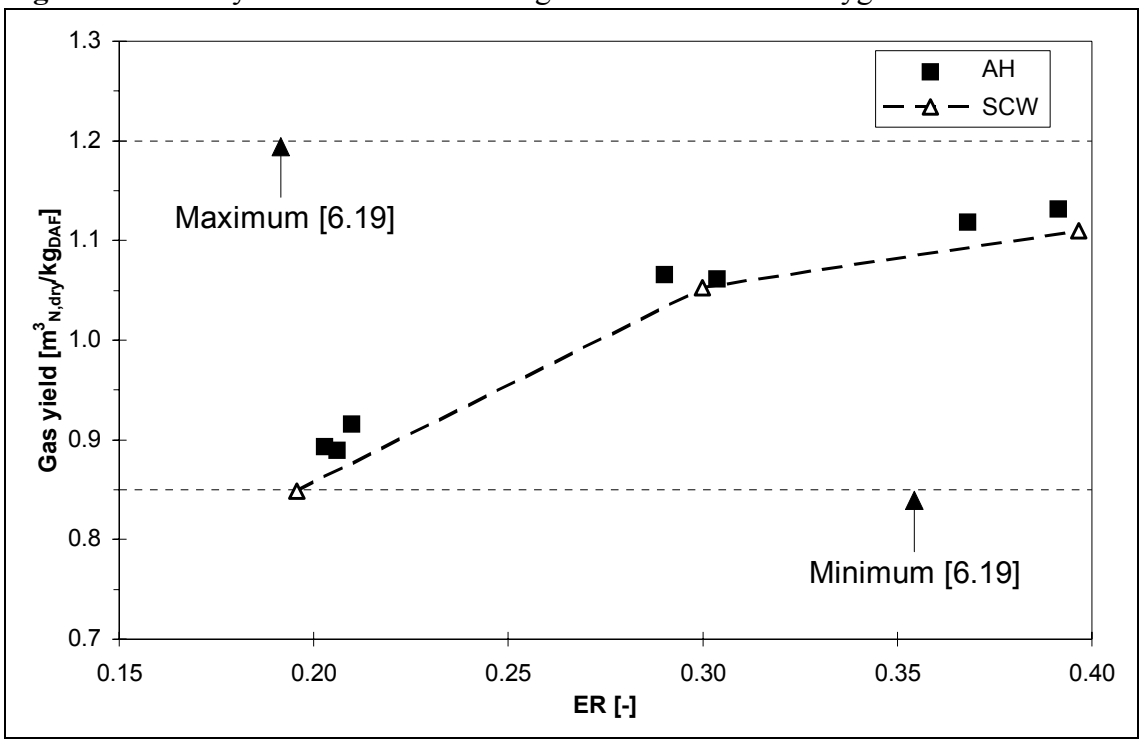

The gas volume yielded by the gasification of SCW in steam/oxygen is slightly lower than that of AH. Both fuels produce gas amounts comparable to literature data, and the observed increase of gas yield with ER in the present study further agrees with the results published in [6.19].

The tar yield data from the present study is somewhat higher than that reported in the literature, see Table 6.6. This difference is certainly due to diverse tar sampling and analysis methods and should not be regarded as significant. Only trends should be compared with literature data as it is known that diverging tar sampling and analysis methods yield incompatible quantitative results. The decrease of tar concentration observed in the present experiments does follow the trends described in the literature. When ER is increased the steam to biomass ratio (S/B) is also increased due to the experimental procedure employed. Both parameters influence the tar concentration (see [6.17]) and by

increasing either parameter a decrease in tar concentration results, as observed in the present study.

Table 6.6: Comparison of tar yields with literature data [6.17] for steam/oxygen gasification. S/B: steam to biomass ratio.

	Literature data		**AH (average)**			**SCW**		
	min.	**max.**						
ER [-]	0.24	0.51	0.21	0.30	0.38	0.20	0.30	0.40
S/B [kg/kg $Fuel_{DAF}$]	0.48	1.11	0.39	0.54	0.67	0.37	0.53	0.67
Tar yield [g/kg $Fuel_{DAF}$]	2.2	46	41.5	39.6	42.2	41.3	48.8	47.5

The total tar concentration measured in these steam/oxygen experiments is shown in Figure 6.31.

Figure 6.31: Total tar concentration for SCW and AH gasification in steam/oxygen.

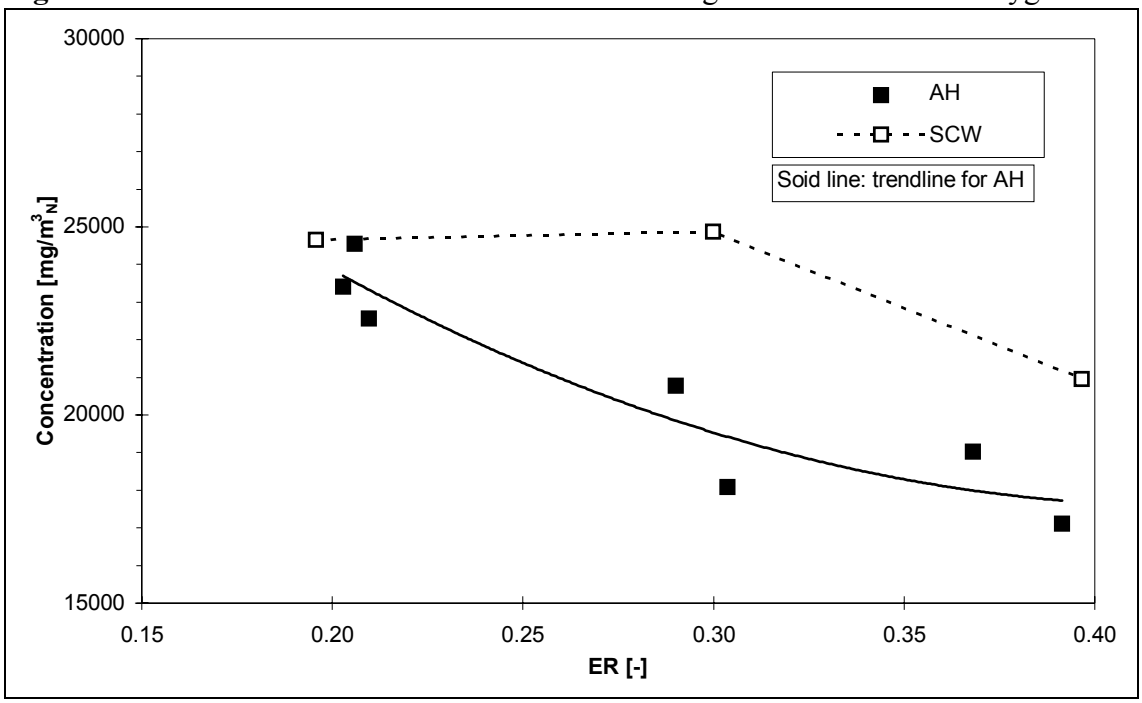

At ER > 0.3, SCW yields larger tar concentrations than AH. At low ER the measured total tar concentrations for both fuels seem to be almost identical. As was the case in air gasification, at low ER the SCW data clearly lies below what would be expected from the trend observed at higher ER for this fuel or from the trend observed for AH in steam/oxygen. In addition to the reasons for the same deviation observed in the case of air as

gasification agent, an effect of the steam on the concentration of the less stable tar compounds (reforming reactions) could account for the lower tar concentrations observed for SCW at low ER. As reported in [6.17], the tar composition is affected when steam/oxygen is used as gasification agent.

The tar composition evolution is shown in Figures 6.32 to 6.34 in function of the ER. The tar classes are altered in approximately identical manner for both fuels as ER is increased. The concentrations of individual classes are slightly higher for SCW, with the exception of benzene at ER ≈ 0.2. The measured concentration of this compound for SCW is lower than for AH. Phenols disappear from the gas issued from both fuels at ER > 0.3. As with air as gasification agent, benzene concentrations as well as those of unsubstituted aromatic compounds are seen to increase with rising ER for both fuels. The 3 ringed aromatics seem again to exhibit a maximum in concentration for AH at ER ≈ 0.3. An exception to this increase are the 2 ringed aromatics, which decrease with increasing ER.

Figure 6.32: Tar evolution (major aromatics) for SCW and AH gasification in steam/oxygen.

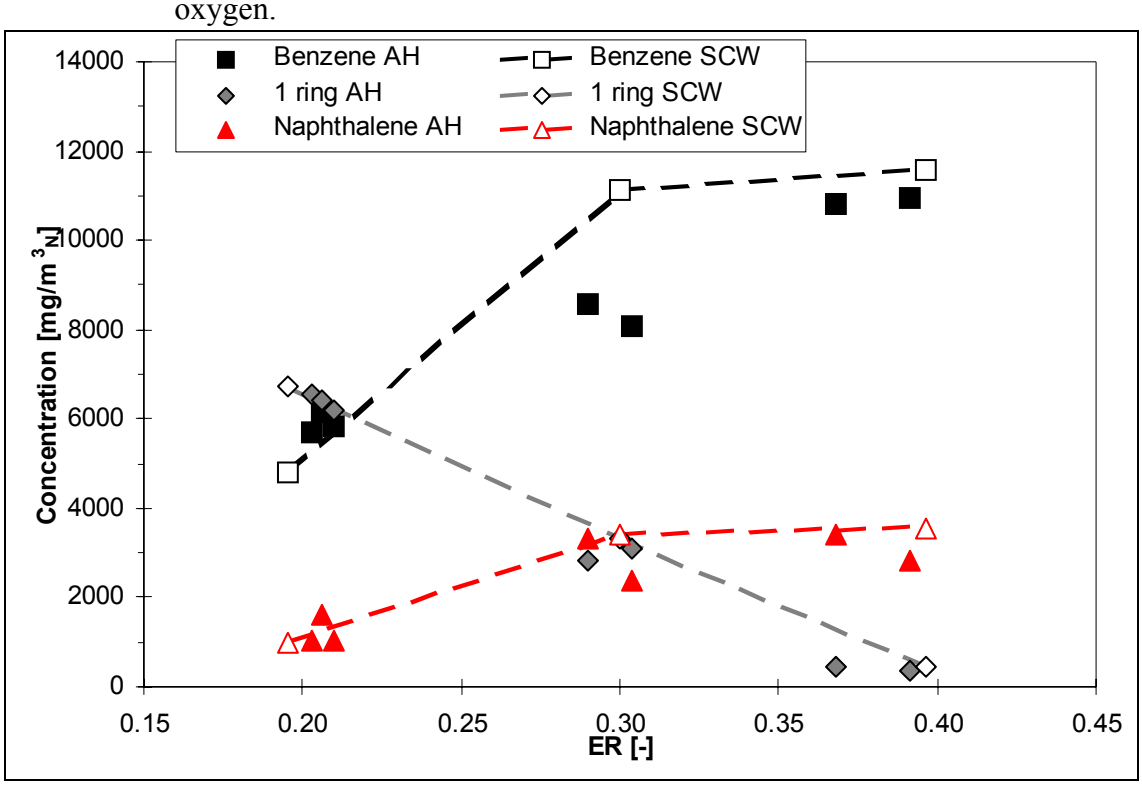

Figure 6.33: Tar classes (oxygenates) evolution for AH and SCW in steam/oxygen.

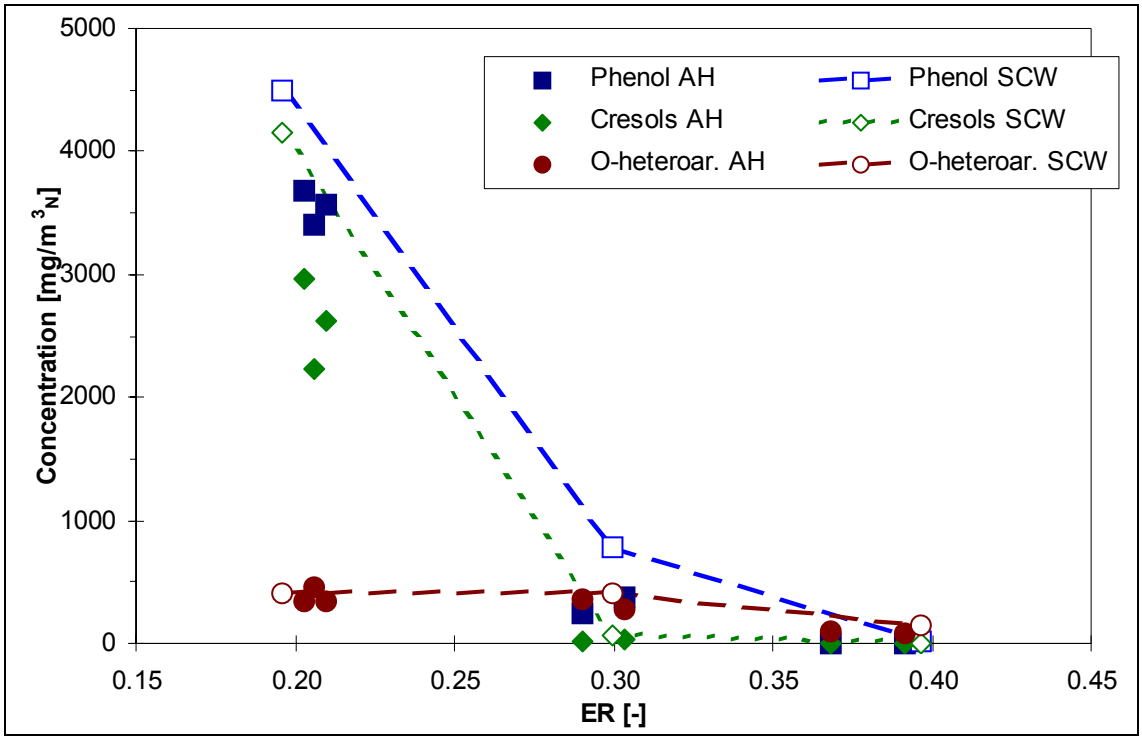

Figure 6.34: Tar classes (minor aromatics) evolution for AH and SCW in steam/oxygen.

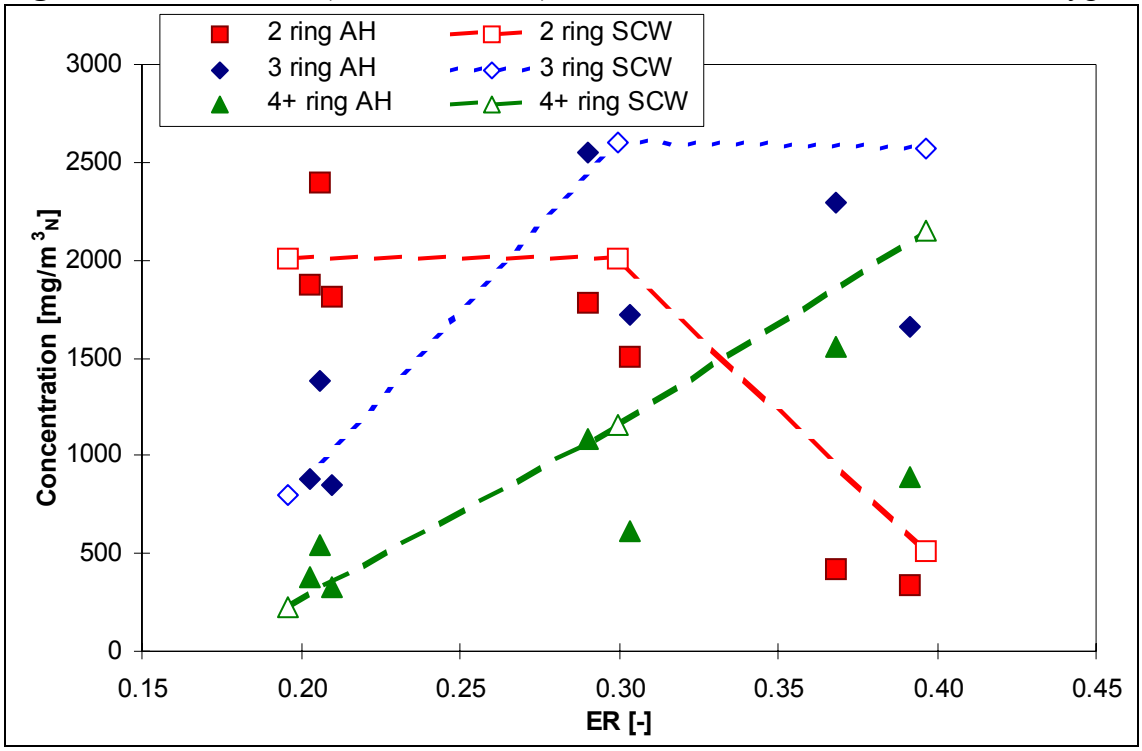

From the above data it is not possible to confirm the influence of steam on specific tar compounds to explain the low total tar concentration observed for SCW at low ER. Only the benzene concentration is remarkably low for SCW and clearly lies out of the

trend observed for this fuel at higher ER. No diverging trends in function of the ER are observed for other compounds in the tars for SCW gasification in steam/oxygen. The explanation for the observed low total tar concentration at low ER for SCW might be that either the benzene concentration measured is incorrect and too low, or that under these specific conditions other tar compounds not detected by the method used here make up a significant amount of the tars.

As in the case of air gasification, an estimation of the fraction of the tar compounds identified by the GC/MSD method was made and the results of this computation are shown in Figure 6.35.

Figure 6.35: Estimated mass fraction of tars identified versus ER for SCW and AH gasification in steam/oxygen and in air.

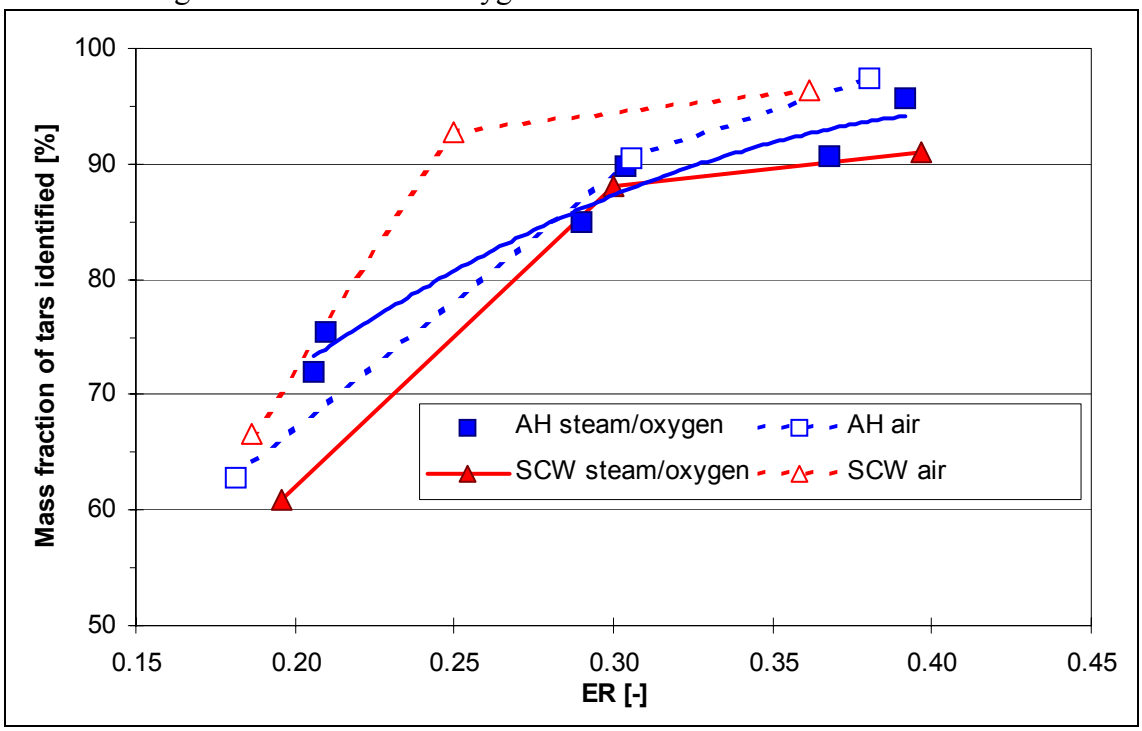

The trend of the fraction of tar identified with the ER is similar to the one obtained in air gasification for both fuels at ER > 0.3. At ER ≈ 0.2 however a larger fraction of the tars is correctly quantified for AH in steam/oxygen. This difference suggests, that the conversion of secondary tars produced at ER ≈ 0.2 to tars identifiable by the tar measurement method used in the present study is dependent on the presence of steam and on the type of fuel. The chemistry involved in the reduction of tars when AH is used, both in air and in steam/oxygen, could therefore be a reforming type of reaction, which may be

catalysed by the metals present in this fuel and absent in SCW. The presence or absence of these catalysts may explain the differences in the fraction of tars identified between the two fuels in the case of steam/oxygen as gasification agent.

The resulting corrected total tar concentrations are shown in Figure 6.36. Even with the higher tar concentrations issued from this correction, AH is seen to still yield lower tar concentrations than SCW when gasified in steam/oxygen at all ERs. As stated before for the case of air gasification this lower tar concentration is an advantage when this fuel is used.

Figure 6.36: Measured and corrected total tar concentrations for AH and SCW gasification in steam/oxygen.

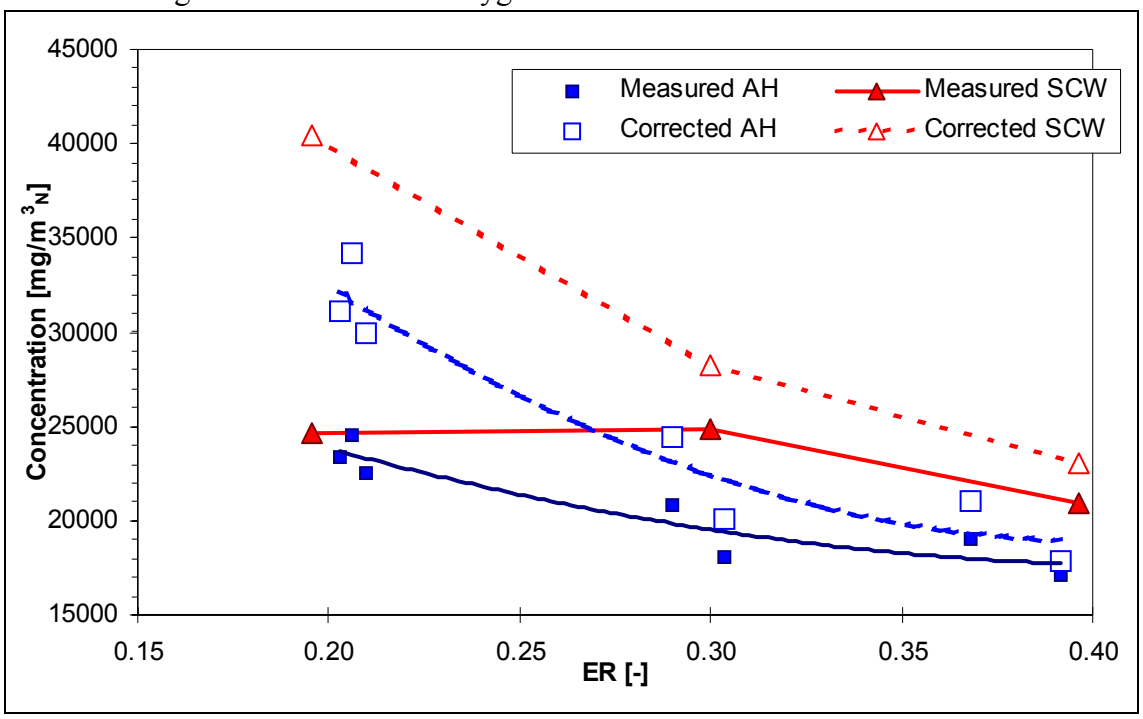

A comparison of the detailed tar composition issued of these two fuels in steam/oxygen for the different ERs is given in Figures 6.37 to 6.39.

Figure 6.37: Normalised tar composition for steam/oxygen gasification of SCW and AH at ER≈0.2.

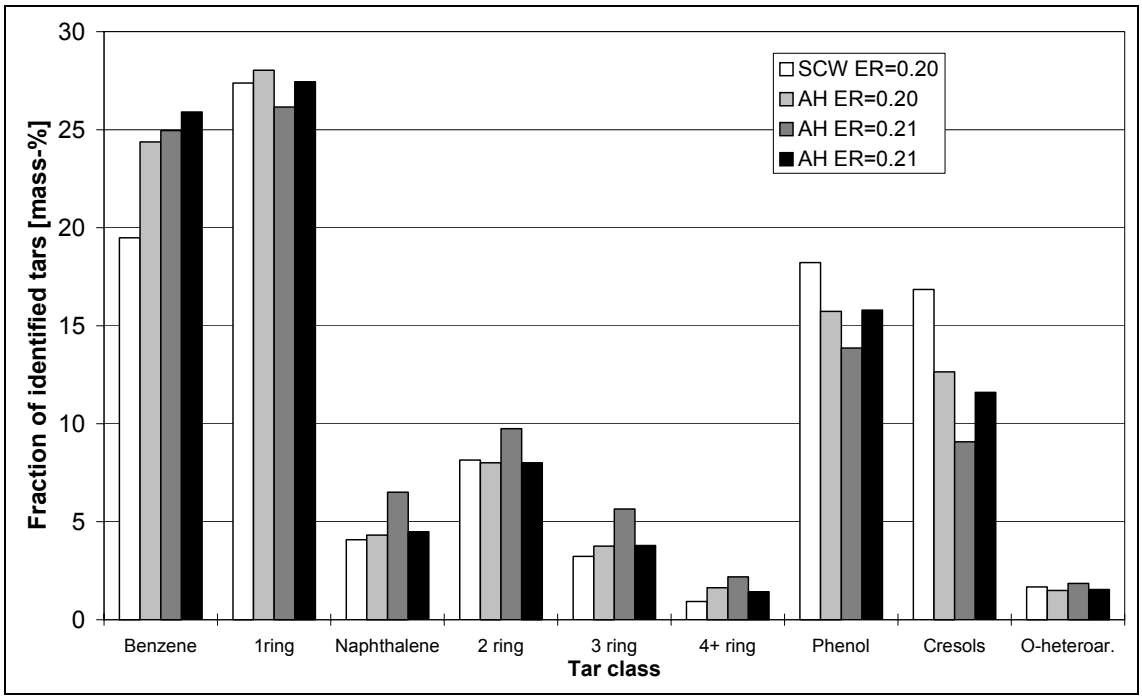

Figure 6.38: Normalised tar composition for steam/oxygen gasification of SCW and AH at ER≈0.3.

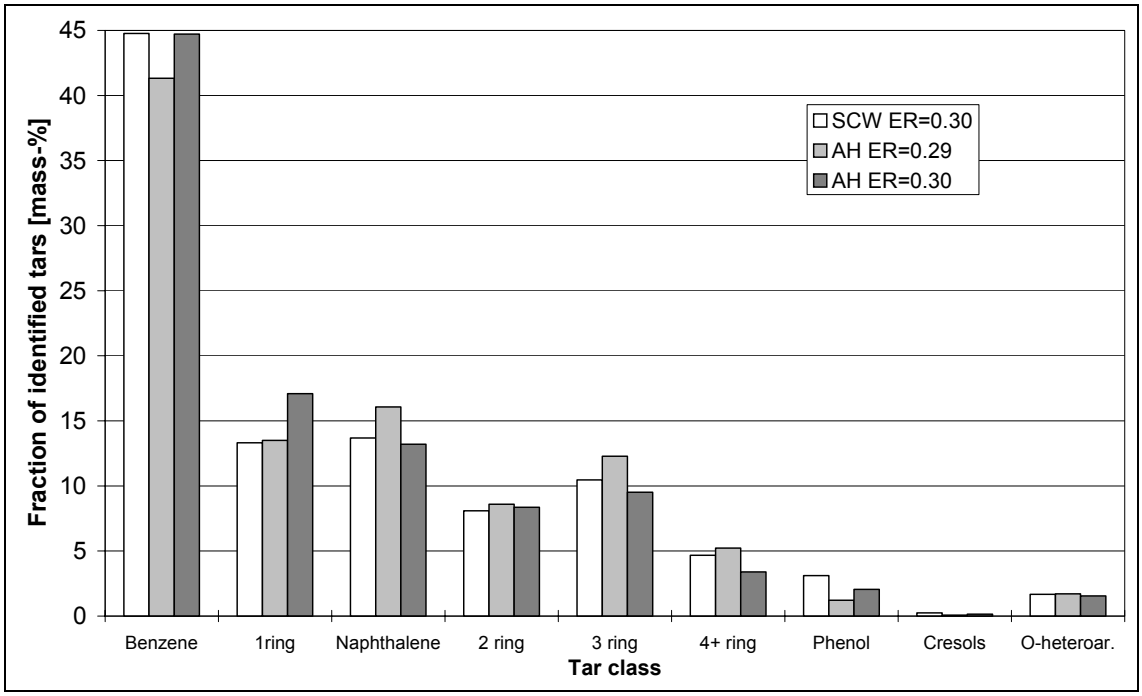

Figure 6.39: Normalised tar composition for steam/oxygen gasification of SCW and AH at ER≈0.4.

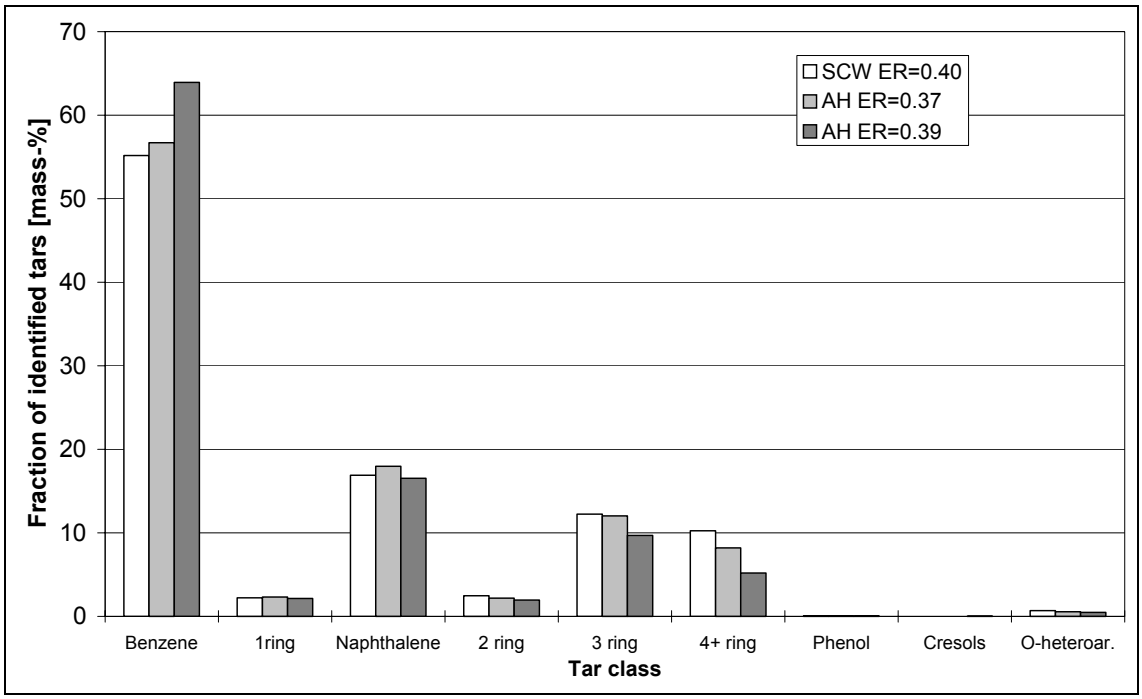

For ER ≈ 0.3 and ER ≈ 0.4 the tars issued from both fuels are almost identical. At ER ≈ 0.2 however, the tars from SCW display a larger amount of phenolic compounds than AH. This difference is another indicator that the tars issued from SCW in steam/oxygen gasification are of a more secondary nature than those from AH, as already seen in the estimation of the tar fraction identified by GC/MSD. This means that in comparison to the tars issued from AH gasification in this medium, the tars of SCW are composed to a larger extent of partially converted pyrolysis products. At the same ER the benzene amount in the tars of SCW is smaller than for AH. This observation leads to the hypothesis, that the conversion of the secondary tars observed when AH is gasified in steam/oxygen leads to the formation of benzene. This hypothesis is further sustained by the increasing amount of benzene in the tars observed as ER is increased for either fuel or gasification agent.

6.2.3 Altholz and Altholz+Polyethylene in steam/oxygen

The results from the AH experiments presented in last sub-section will be compared to the results of experiments 991123 and 000215 where mixtures of 10 and 20% by weight of polyethylene (PE) with Altholz were gasified in steam/oxygen. The bed temperatures for these experiments are shown in Figure 6.40.

Figure 6.40: Bed temperatures for AH+PE runs.

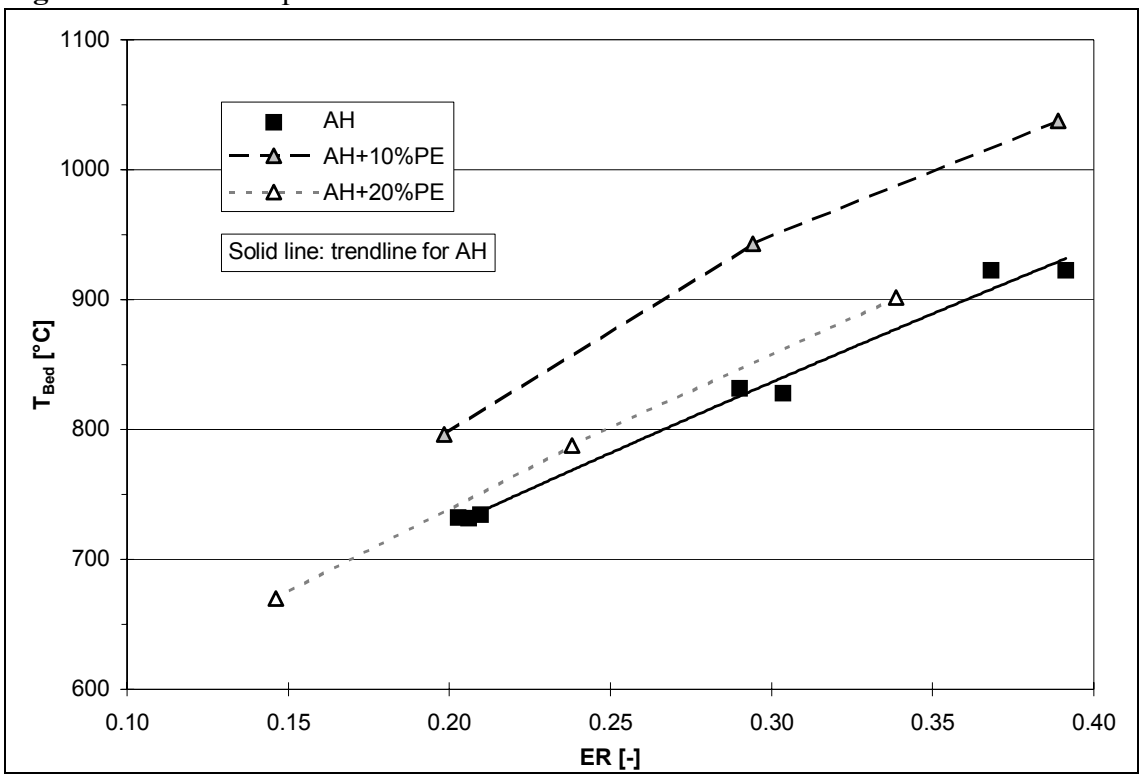

The experiment using the 10% PE mixture was performed as the first experiment with plastics blends and the standard ER set-points were applied. The bed temperature measured during this particular experiment was markedly higher than when AH was gasified alone. At the highest ER set-point the reactor was operating above its maximal temperature of 1000°C, but fortunately no damage to the reactor resulted. It was therefore decided, that for the experiment where the 20% PE mixture would be gasified, lower ER set-points would be used to avoid too high temperatures in the reactor. The experiment where the 20% PE mixture was used again show temperatures comparable to the AH experiments but clearly diverging from those of the 10% PE mixture.

The deviation in the temperatures cannot be explained by the higher LHV of the PE mixtures. By selecting an ER and the same oxygen input via the gasification agent, the

total energy input to the reactor by the fuel and thus the heat released by combustion is fixed. As Figure 6.41 shows, the fuel input power for the PE mixtures and the AH were practically the same at comparable ER set-points.

Figure 6.41: Fuel input power as a function of ER for AH, AH+PE and AH+PS experiments at fixed oxygen input.

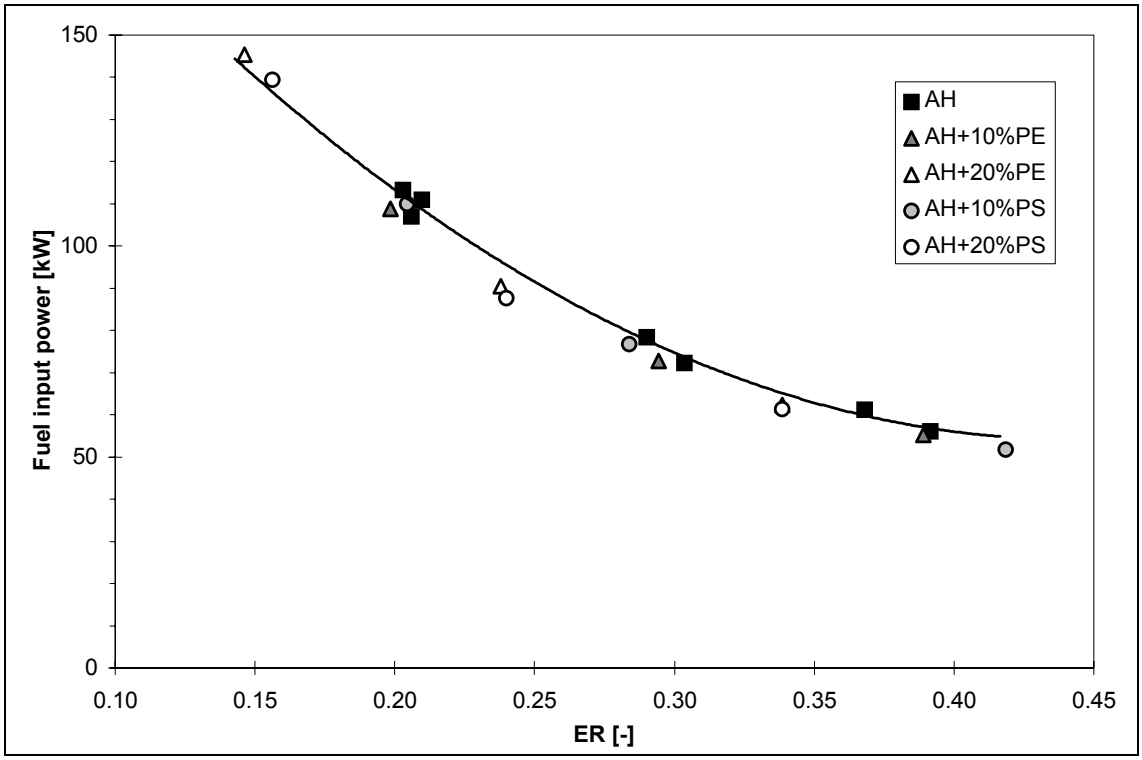

The (theoretical) energy released by combustion of the fuel is obtained by multiplying the total fuel energy input (in kW) by the ER (= fraction of fuel burnt). For all experiments in this study (with the exception of those at constant fuel input) ca. 21.5kW have been released by combustion. An analysis of further reactor data reveals no differences in operational set-points between the runs with AH and with the PE mixture.

Another hypothesis to explain the differences in the reactor temperature is a diverse thermochemistry of the PE mixtures in gasification. PE pyrolysis is known to yield a variety of alkanes and alkenes (see section 3.2.2). These carbohydrates could undergo steam reforming reactions, known to be endothermic. For example in [6.21] a heat of reaction of +151kJ/mol is given for the steam reforming of a CH_2 group according to $-CH_2- + H_2O \rightarrow CO + 2H_2$. This steam reforming of hydrocarbons should yield higher CO and H_2 concentrations in the gas of the PE mixtures. However the experimental data (see later in this chapter) does not support this hypothesis, as CO concentrations are al-

most identical and H_2 concentrations even lower when the results of AH/PE mixtures gasification are compared to those of AH gasification.

The reason for the observed temperature deviation remains unclear. Further discussion of the results will be made using the ER as in the previous sections. Bear however in mind that the temperatures for the AH experiments and those of the 10% PE experiment are not the same.

The evolution of the gas components as a function of the ER is shown in Figure 6.42. The gas components are seen to follow the same trends in function of the ER for all three fuels: CO and CH_4 decrease, H_2 and CO_2 increase as ER is raised.

The deviations of the concentrations of CO and CO_2 as PE is added to AH lie in the range of the scatter observed when gasifying only AH. A raise in the PE content of the fuel increases the CO concentration but does only slightly decreases the CO_2 concentration in the range of PE mixture levels studied.

For the 10% mixture at low ER, the H_2 concentration is comparable to that resulting from the gasification of AH. At higher ER more H_2 is present in the gas for this 10% PE fuel. Raising the PE fraction in the fuel clearly lowers the H_2 concentration. This decrease could be due to an increase in the fraction of light hydrocarbons in the gas. Unfortunately these species were not monitored in the present study to confirm this hypothesis.

CH_4 concentration is raised slightly by PE admixture. The difference does however diminish as ER is raised. The amount of PE added has only a small influence on the CH_4 concentration in the range of PE mixture levels studied.

In [6.22] results of the gasification of pine wood/PE mixtures in an allothermal atmospheric fluidised bed are presented. These authors report an increase in H_2 and a decrease in the concentration of hydrocarbons as the temperature is raised. These findings agree with the data of this study. No influence of the temperature was detected by this research group on the concentrations of CO or CO_2, possibly reflecting the lack of oxygen in the gasification agent used in this reference. The concentrations of H_2, CO and CO_2 displayed in this reference (on a dry, inert-free basis) do differ from those measured here, see Table 6.7.

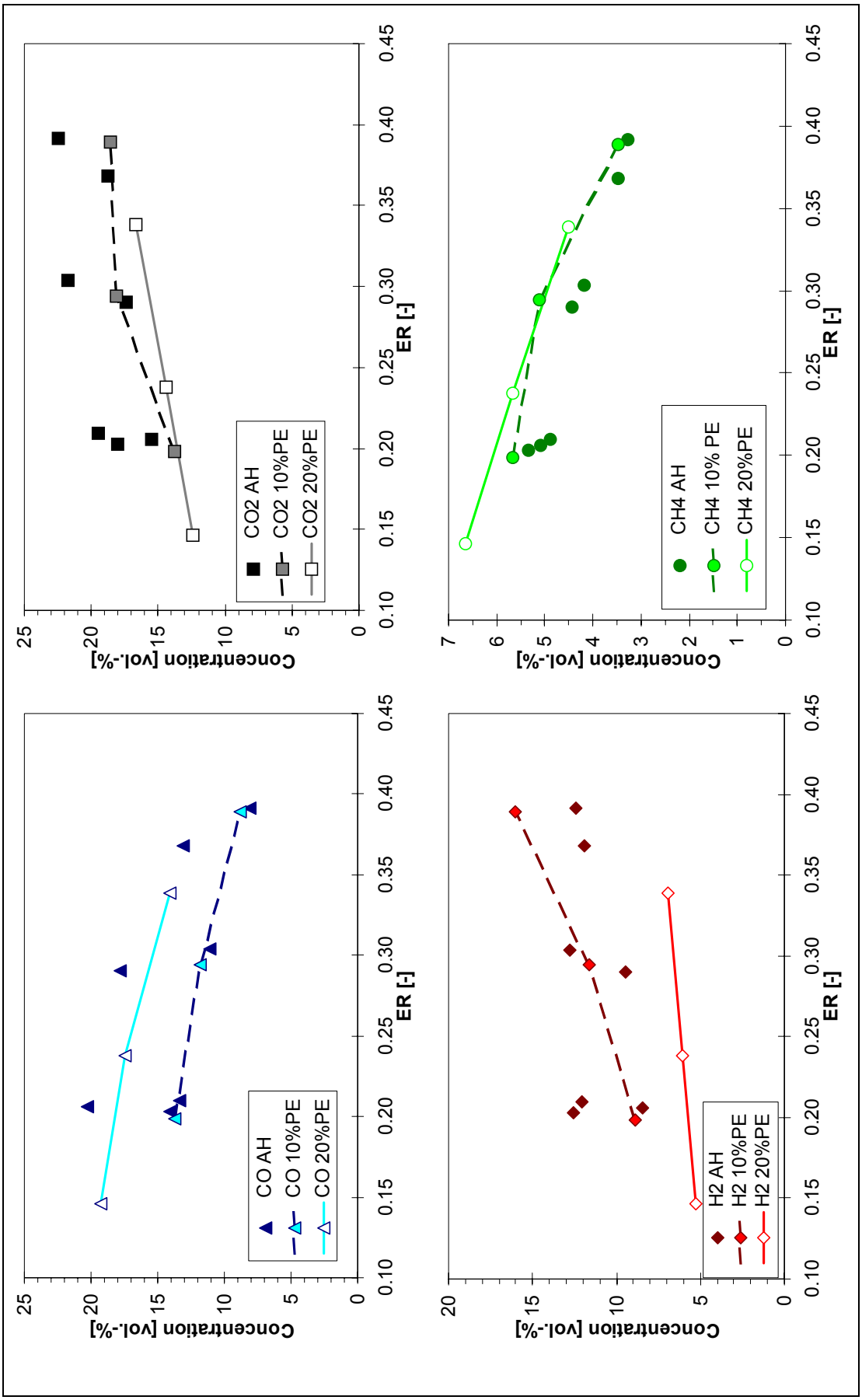

Figure 6.42: Gas composition evolution for AH and AH+PE mixtures.

Table 6.7: Comparison of dry, inert-free gas data for AH+PE runs with literature data.

Data from	**[6.22]**	**Present Study**	
PE fraction in fuel [%]	**20**	**10**	**20**
ER [-]	0	0.20 - 0.39	0.15 - 0.34
Temperature [°C]	730 - 880	796 - 1038	670 - 901
CO_2 [vol.-%$_{DIF}$]	10 - 11	29 - 37	25 - 35
CO [vol.-%$_{DIF}$]	29 - 30	18 - 29	30 - 40
H_2 [vol.-%$_{DIF}$]	36 - 53	19 - 32	11 - 15
CH_4 [vol.-%$_{DIF}$]	9 - 12	7 - 12	10 - 14
C_nH_m [vol.-%$_{DIF}$]	3 - 10	not measured	

CO_2 and H_2 concentrations are lower in the present study but CO and CH_4 are higher for the same PE amount in the fuel.

As for previously presented fuel/gasification agent combinations, thermodynamical equilibrium computations have been carried out. The results of this calculation are shown in Figure 6.43.

For the lowest ER/T_{Bed} combination in the experiments (0.15 and 670°C) the thermodynamic equilibrium products contain a large fraction of solid carbon (11.2 mol-% of the total products). Again large differences are observed between measurement and equilibrium composition. Reforming of CH_4 and tars does not yield much better agreement between theory and measurement, suggesting the presence of further carbon and hydrogen containing species.

This hypothesis is further sustained by the poor elemental balance for C and H in the experiments 991123 and 000215, see Tables B.12 and B.13 in Appendix B. From the results of pyrolysis experiments with polyethylene (see page 71), a large fraction of the polymer is expected to convert to C_2 and C_3 hydrocarbons. Also from the data of [6.22] an amount of hydrocarbons in the same order of magnitude as CH_4 can be expected to be present in the gases of the AH+PE mixtures.

In [6.7] the results of air gasification of a wood wastes and mixtures thereof with 10% polyethylene have been reported. The concentration of the above hydrocarbons is larger when the polymers are present, see Table 6.8, further sustaining this hypothesis.

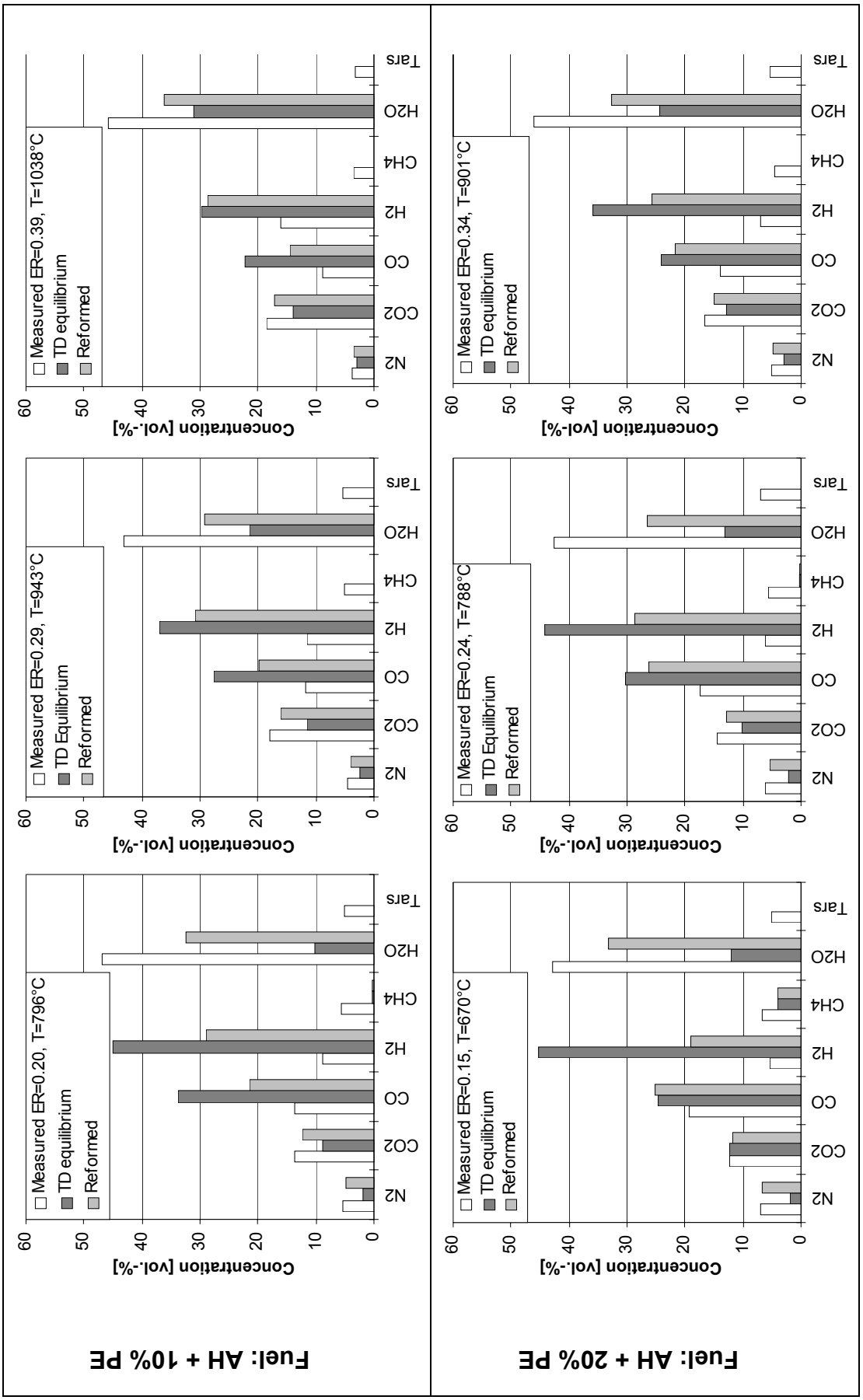

Figure 6.43: Gas composition for AH/PE mixtures gasification in steam/oxygen (measured, thermodynamical equilibrium and "reformed").

Table 6.8: Hydrocarbons concentration ranges in air gasification of wood and wood/ plastics mixtures [6.7].

Fuel	Wood wastes	Wood wastes + 10% PE
ER [-]	0.27 - 0.33	0.31 - 0.32
Temperature [°C]	743 - 857	740 - 843
CH_4 [vol.-%, dry]	3.4 - 4.2	3.5 - 4.6
C_2H_4 [vol.-%, dry]	1.3 - 1.6	1.9 - 3.1
C_2H_6 [vol.-%, dry]	0.1 - 0.2	0.2 - 0.3
C_3H_6 [vol.-%, dry]	0.1 -0.2	0.3 - 0.5

The gas yields for the experiments involving AH+PE mixtures are shown in Figure 6.44. The addition of PE has only a small effect on the gas yields when compared to AH. For the lower mixture level of 10% the gas yield is seen to decrease a little at low ER. Remember however, that no hydrocarbons could be measured, and that these are known to exist in the gas in a level of a few %. The gas yields could therefore be higher for the AH+PE mixtures than reported here.

Figure 6.44: Gas yields for AH and AH+PE gasification in steam/oxygen.

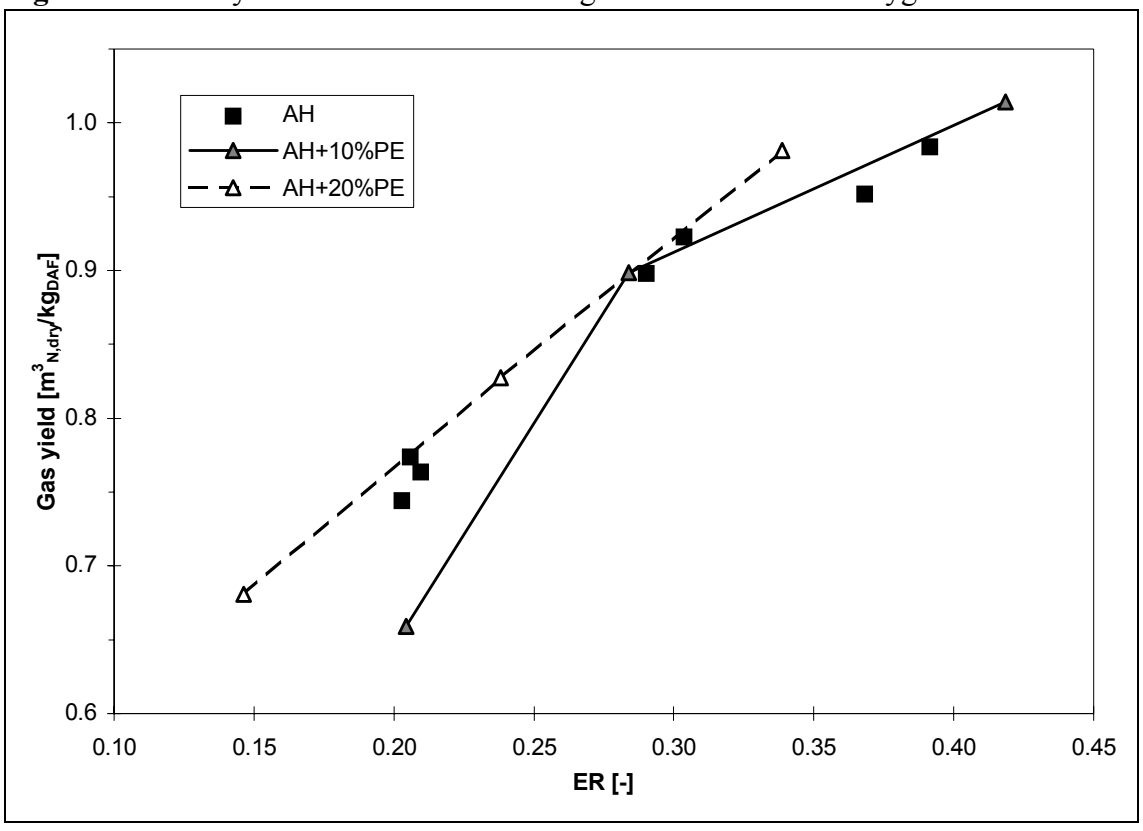

The tar concentration evolution with ER for the PE experiments is shown in Figure 6.45. The total tar concentrations in the gas from the gasification of PE mixtures is higher than for the gasification of AH alone. At high ER (and low PE level) the tar concentrations do however become identical. The amount of PE added to the AH does influence the tar concentration. At the higher PE level a higher tar concentration is observed. It is interesting to note that the results obtained for the 10% PE mixture were determined in runs where the temperatures were higher than in the runs with either the "pure" AH or the 20% PE mixture. The effect of the temperature seems to be smaller than the effect caused by changes in the ER or by the amount of plastics mixed into the AH. Again, at low ERs, the total tar concentrations evolution for the AH+PE mixtures is seen to remain constant or even to fall below the levels for higher ER.

Figure 6.45: Measured tar concentrations in function of ER for AH and AH+PE experiments.

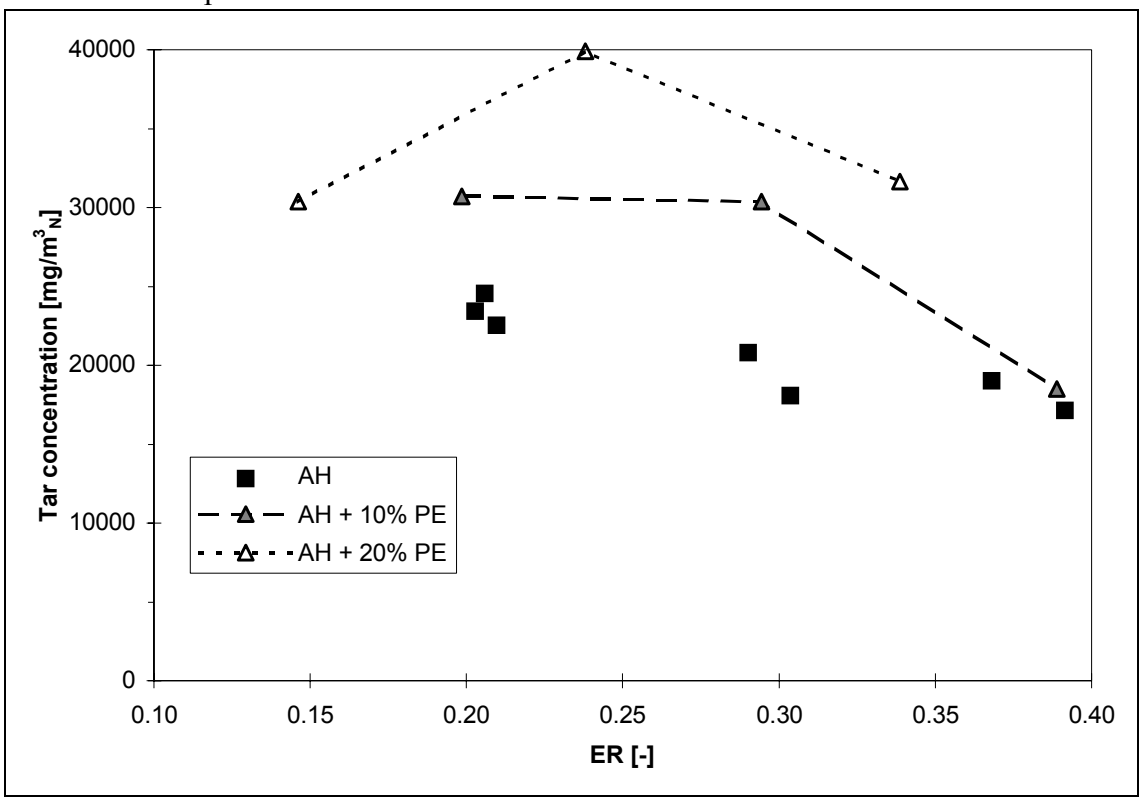

The previously described estimation of the fraction of tars identified by the GC/MSD (see page 178 for details) has also been performed for these AH+PE runs and the results are shown in Figure 6.46. The evolution of the fraction of tar identified is similar for all three fuels. At high ERs the presence of PE has no influence on the fraction of tars

identified. At low ERs the presence of PE does reduce somewhat the amount of unknown compounds in the tars.

Figure 6.46: Fraction of tars identified by GC/MSD for AH and AH+PE runs in function of ER.

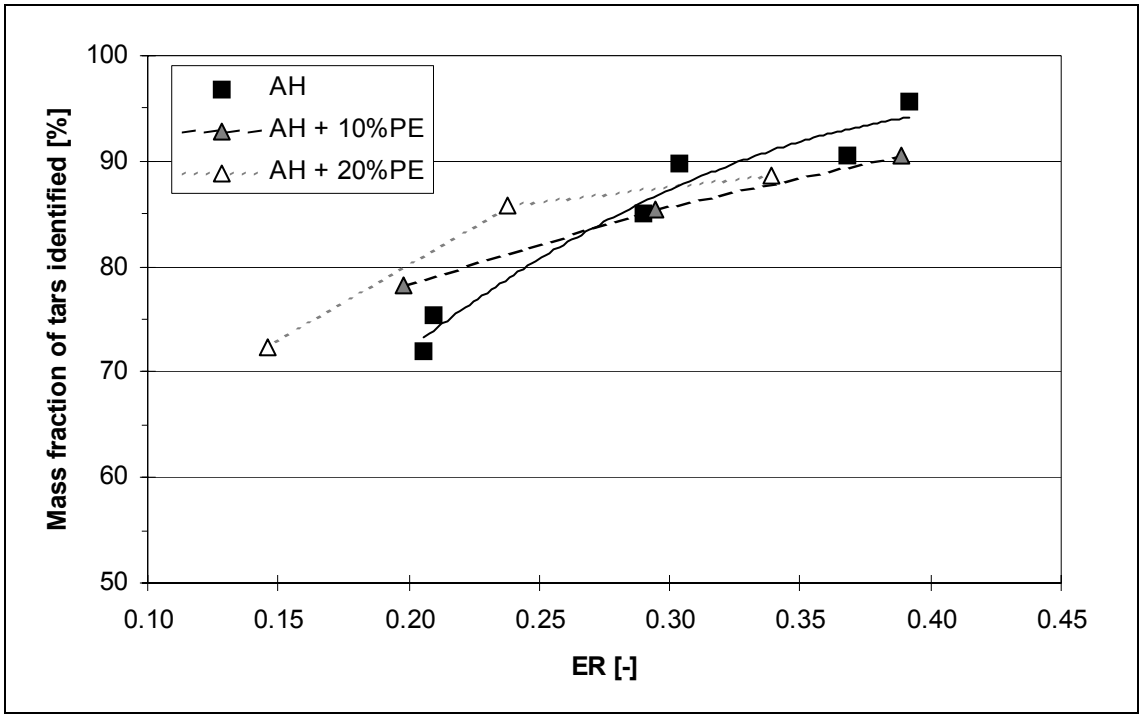

Figure 6.47: Corrected total tar concentration evolution with ER for AH and AH+PE runs.

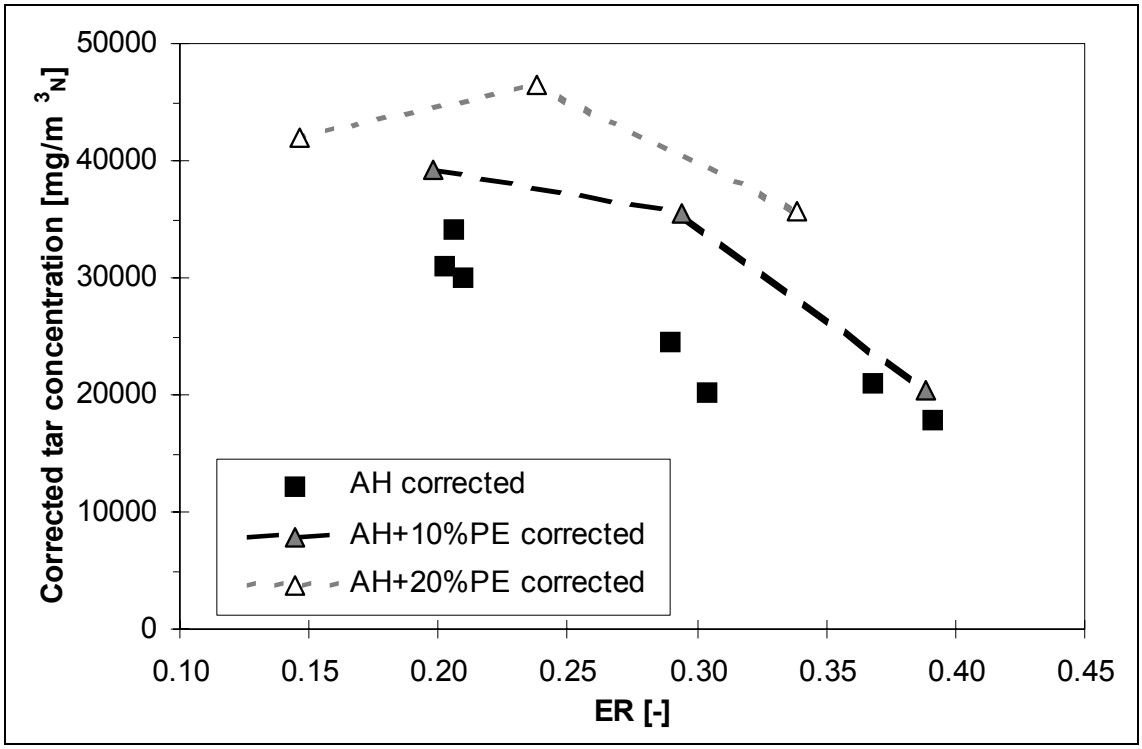

When the total tar concentration is corrected with the fractions of the estimation of the amount of identified tars, the concentration evolution shown in Figure 6.47 is obtained. The curve for the 20% PE mixture is observed to still level off at the lowest ER studied. This could be explained by an even larger fraction of unidentified tars than is estimated by the procedure used, meaning that the true tar concentration for this specific run is probably even higher than reported here.

The evolution of the tar classes concentrations with the ER is shown in Figures 6.48 and 6.49. A marked increase in the benzene concentrations is observed when PE is added to AH. The amount of benzene increases with increasing PE fraction in the fuel. For both mixture levels the benzene concentrations exhibit a maximum, around ER 0.25-0.3. When the ER is raised to 0.4, the benzene concentration for the 10% mixture drops to the same level as for AH.

At 10% mixture level, the 1 ring aromatics are not affected by the addition of PE. Adding 20% PE to AH does however increase the concentration of these compounds. The evolution as a function of ER is similar for all three fuels.

Naphthalene is also increased by the addition of PE. Again the curves exhibit a maximum around ER 0.25-0.3. The amount of PE added does not seem to greatly influence the increase in the naphthalene concentration. As with benzene the naphthalene concentration falls to the same level observed for AH alone at ER = 0.4.

The concentrations of 2 ring aromatics are almost not altered by the addition of PE at ER > 0.3. At ER 0.2 - 0.25 both PE mixtures yield larger concentrations of this tar class, and the increase seems to be dependent on the PE amount in the fuel. For the 20% PE mixture, the 2 ring aromatics decrease at ER = 0.15 below the level measured for ER = 0.25, again suggesting the presence of a maximum in concentration of this tar class.

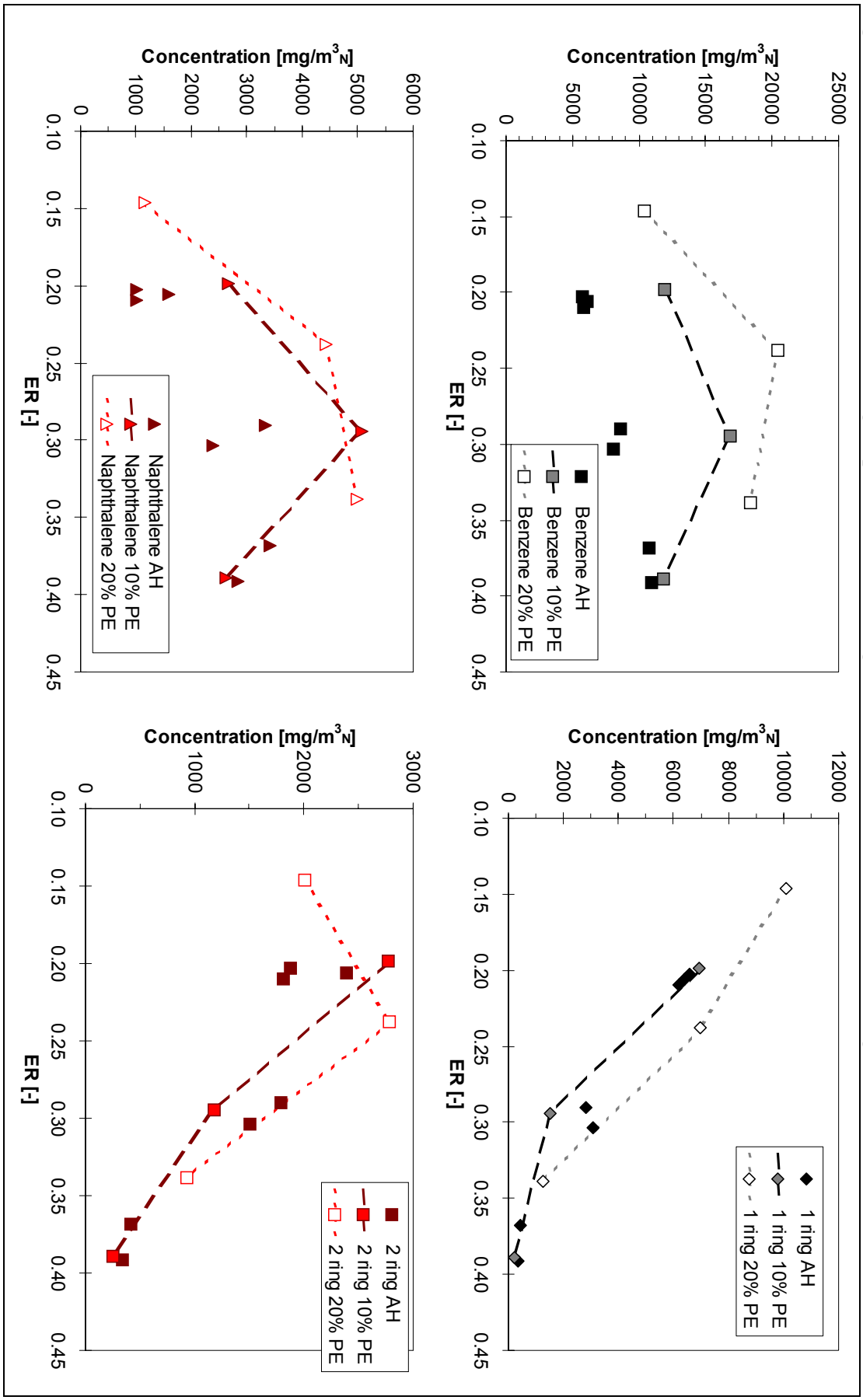

Figure 6.48: Evolution of Benzene, 1 ring, naphthalene and 2 ring classes with ER for AH and AH+PE gasification.

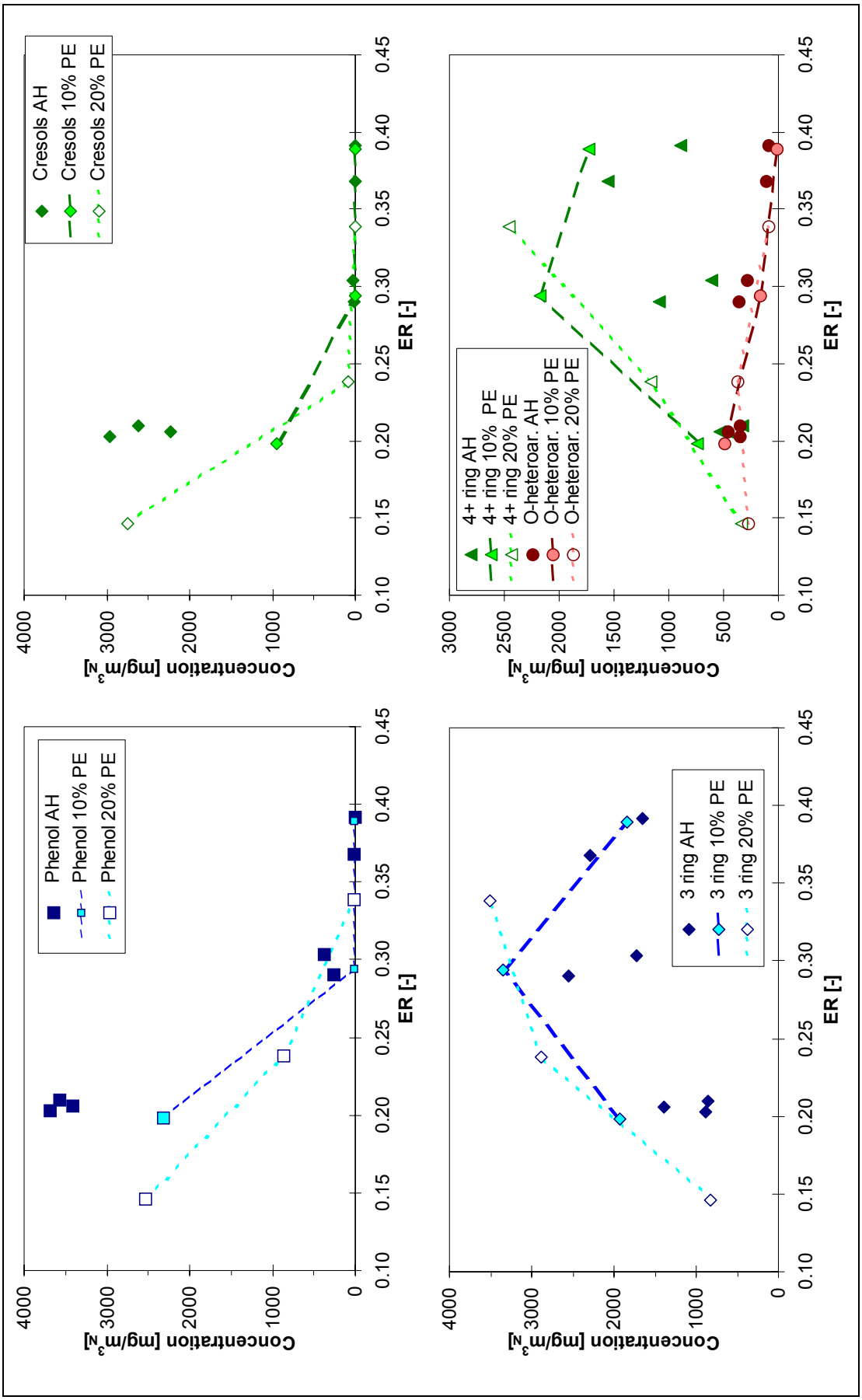

Figure 6.49: Evolution of phenol, cresols,3 ring, 4+ ring and O-heteroaromatic classes with ER for AH and AH+PE gasification.

The concentration of phenol and cresols is lowered by the addition of PE in comparison to AH at the same ER. For all three fuels phenol virtually disappears above ER = 0.3. The reduction in the phenols is stronger for larger PE amounts. The level of PE in the fuel has the same influence in the decrease of cresols concentration and for the 20% PE fuel, cresols disappear from the gas at lower ER than was the case for AH alone.

The concentrations of the 3 and 4+ring tar classes are both increased by the addition of PE. The level of PE added to the AH has no influence on the increase of the concentrations of these tar classes. The behaviour of the 3 ring class in function of the ER is similar for all three fuels, exhibiting a maximum around ER = 0.3. For the 10% PE fuel, this tar class reaches the same concentration as AH alone at ER = 0.4. A maximum is also observed in the 4+ ring tar class for the 10% PE fuel. The data of the 20% PE experiments does not show a maximum, but data at higher ER is missing for this fuel. At high ER, the concentration of the 4+ ring class is somewhat higher for the 10% PE mixture than for AH.

The concentration of O-heteroaromatics is slightly decreased in relation to AH by the addition of PE at high ERs and the amount of PE added has only minor influence in this decrease. At low ERs the concentrations of this tar class for all three fuels is the same.

The tar composition for the AH+PE runs is shown in Figures 6.50 to 6.53. The AH data has been averaged for clarity. The 20%PE results at ER = 0.15 show an increase in both benzene and 1 ringed aromatics. All other tar classes are present in lower amounts in the tars from the 20%PE fuel when compared to the lowest ER data for AH.

At ER 0.2-0.24, the strongest relative influence of the addition of PE on the tars is on benzene. Benzene concentrations in the tars increase strongly compared to AH almost doubling for the 20% PE mixture. The increase in naphthalene concentrations is also about twofold for both mixture levels.The larger PAHs are also increased by PE addition. The 2 ringed aromatics are almost not affected and 1 ringed aromatics decrease at low ER when PE is added to the fuel. The phenolic compounds are strongly reduced by the addition of PE at comparable ER.These differences are seen to depend on the amount of PE added.

Figure 6.50: Normalised tar composition for AH at ER = 0.2 and AH+20%PE at ER = 0.15

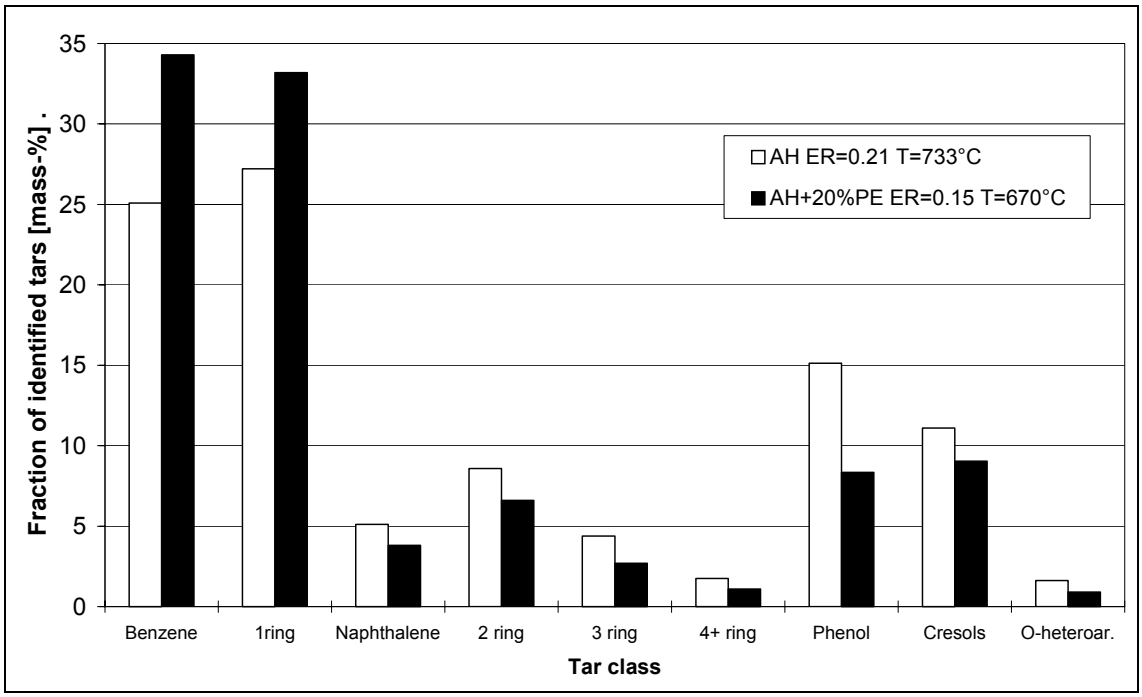

Figure 6.51: Normalised tar composition for AH and AH+PE at 0.2 ≤ ER ≤0.24.

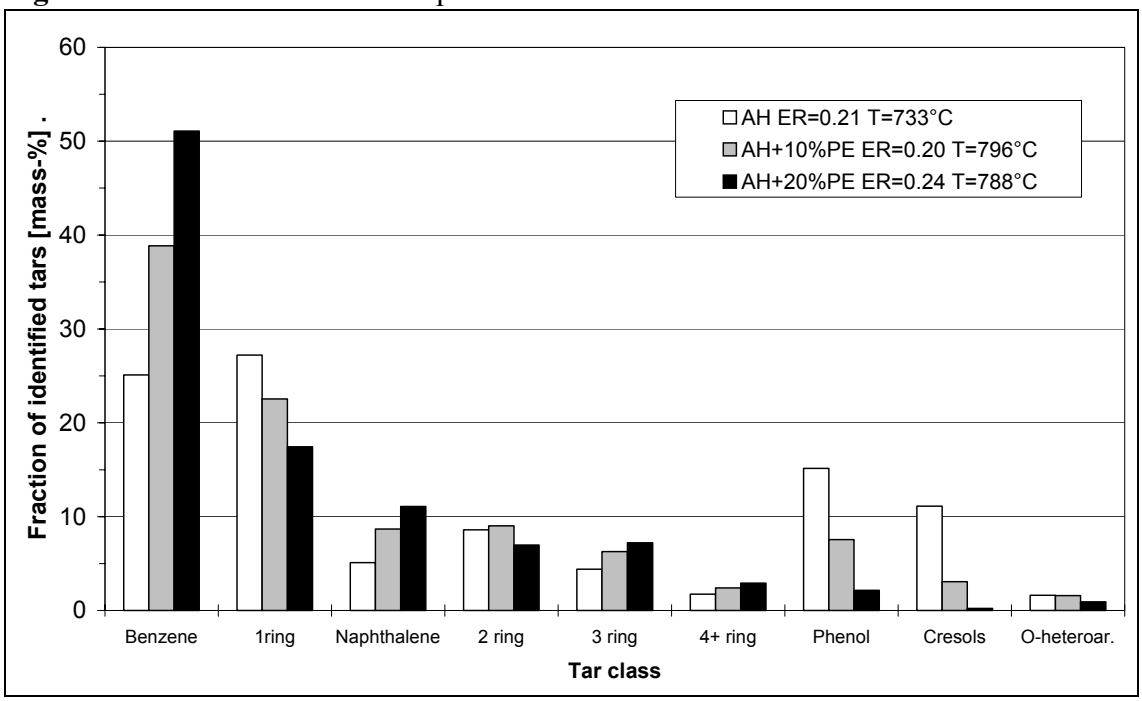

At ER 0.3-0.34, the amount of benzene in the tars is seen to increase by the addition of PE. 1 and 2 ringed aromatics are decreased and so are the phenolic compounds as PE is added. The influence on the amounts of naphthalene and the 3 ringed PAHs is moderate but the larger PAHs (4+ rings) are seen to increase in the tars. Again the differ-

ences are dependent on the amount of PE added, but the influence of the PE mixture level is less pronounced.

Figure 6.52: Normalised tar composition for AH and AH+PE at 0.3 ≤ ER ≤ 0.34.

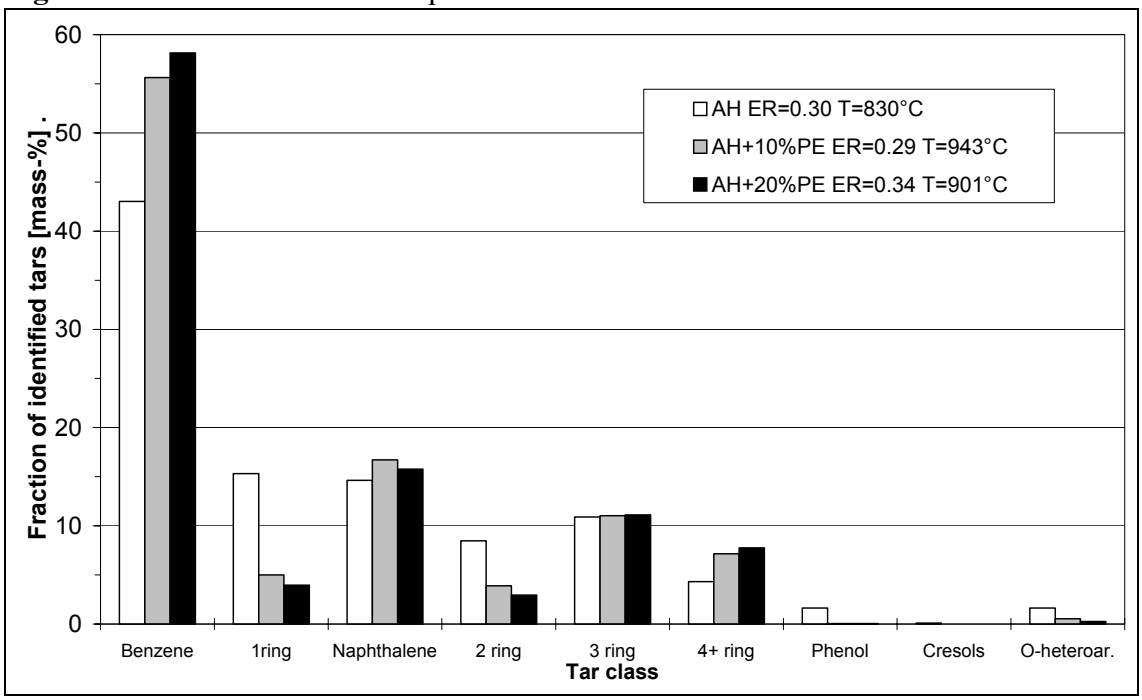

Figure 6.53: Normalised tar composition for AH and AH+PE at ER 0.4.

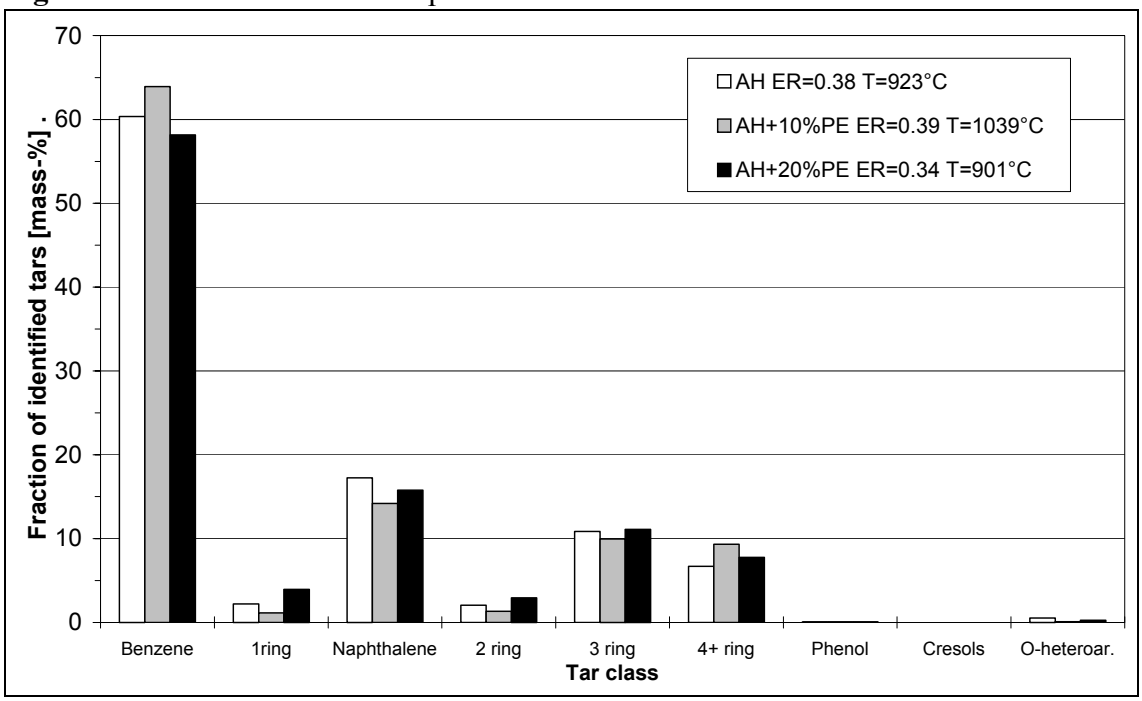

At high ER the tar composition is almost not affected by the addition of PE. The tar composition issued from the 20% PE mixture gasified at ER = 0.34 is almost identical to that of the experiments with AH and 10% PE at higher ER.

When the data from the runs at comparable temperature instead of comparable ER is plotted together as in Figures 6.54 to 6.55, the differences in the tar composition become smaller, especially at high temperatures.

The differences observed in the tar compositions at comparable ER therefore reflect the influence of the different gasification temperatures in the AH and AH+PE experiments. Both parameters influence the tar composition. At ca. 800°C the amount of compounds of "secondary" nature (see Chapter 3), phenols and 1 ringed aromatics, is clearly larger for the experiment at the lowest ER. Inversely, the amount of the remaining tar compounds, which are of a "tertiary" nature, is higher for the experiments at higher ERs. This dependence is also seen in the data for the runs at higher temperature, see Figure 6.55.

The complex interaction of both parameters in the tar chemistry can however not be fully described by the performed experiments. A series of experiments where T_{Bed} and ER could be varied independently would be very useful to establish the influence of each parameter alone, but could not be carried out in the plant used for this study.

Figure 6.54: Normalised tar composition for AH and AH+PE runs at T ≈ 800°C.

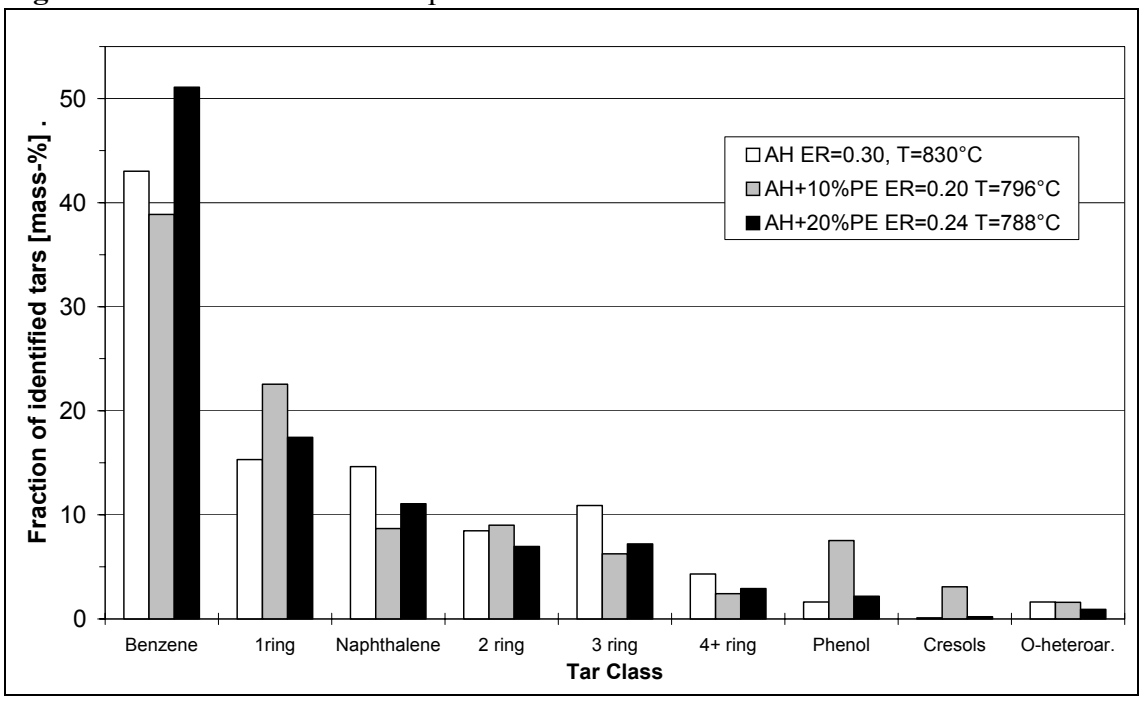

Figure 6.55: Tar composition for AH and AH+PE runs at T > 900°C.

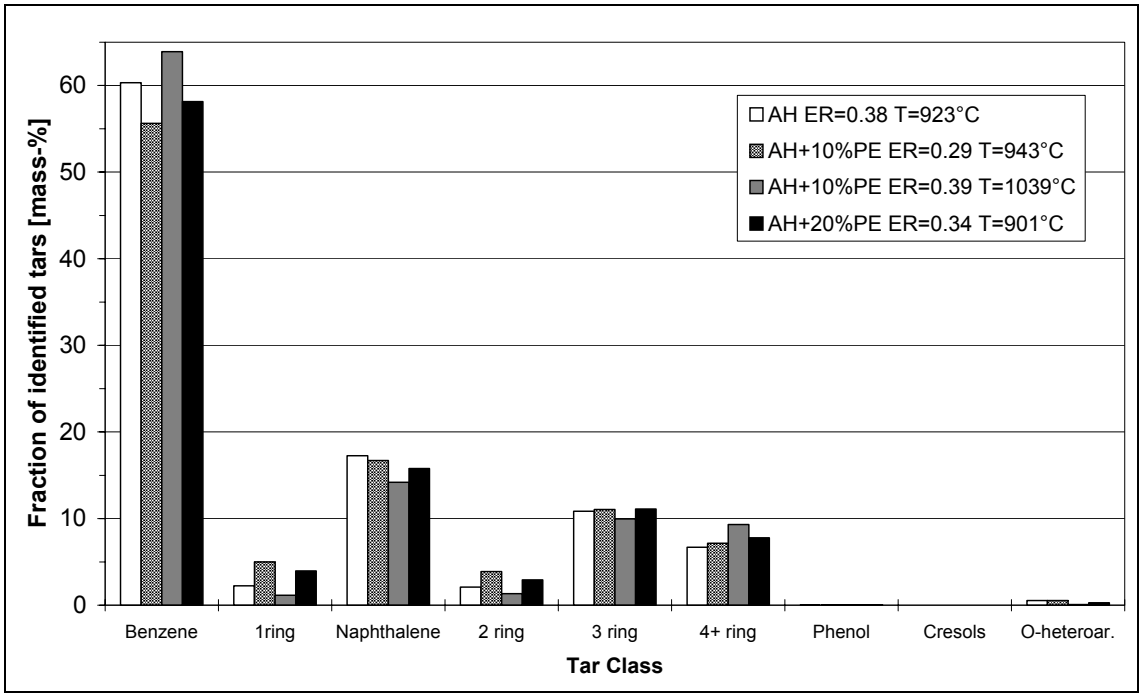

Even if the exact influence of these two, very important parameters in a gasifier on the tar composition cannot be clearly deduced from the data gathered, it is important to emphasise, that at low ER or T_{Bed} the total tar concentration in the gases is considerably higher when PE is added to the fuel as shown in Figure 6.56.

Figure 6.56: Corrected total tar concentration for AH and AH+PE in function of T_{Bed}.

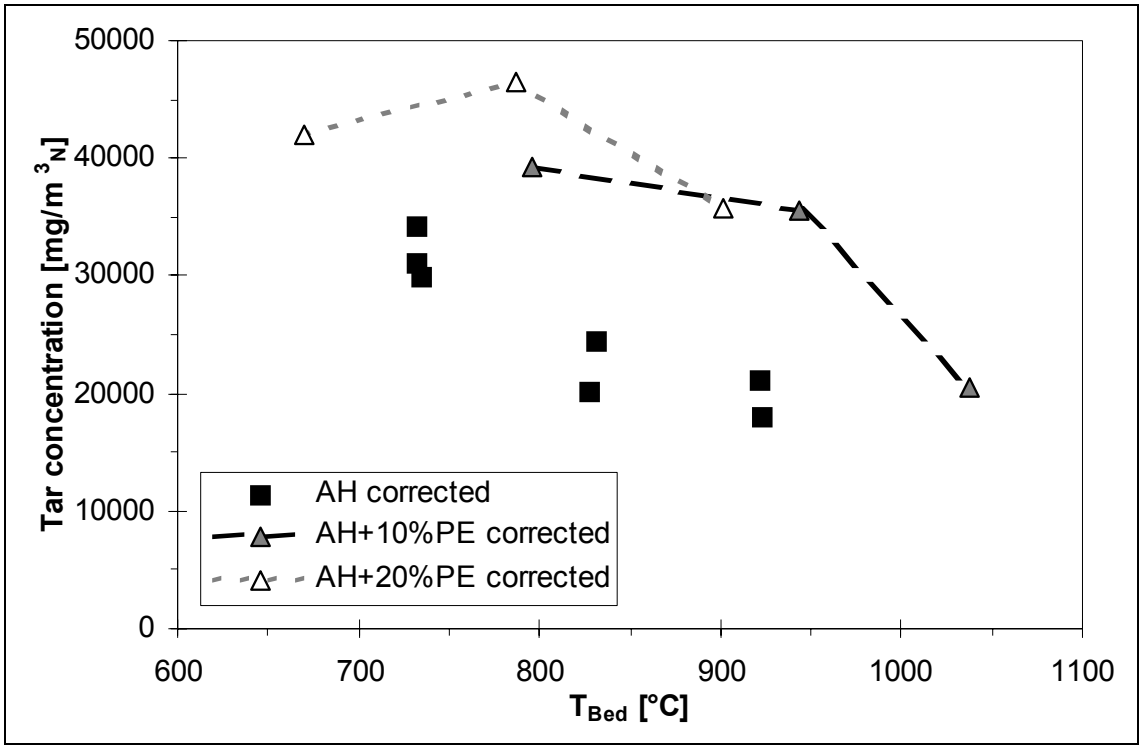

6.2.4 Altholz and Altholz+Polystyrene in steam/oxygen

The temperatures of the reactor were, for both PS mixture levels studied, higher than when AH was gasified, see Figure 6.57. As already shown in Figure 6.41 on page 201 the total power by fuel input for the AH+PS mixtures is the same as in the AH experiments at the equal ER. Also here, the reason for the deviation of the temperatures cannot be traced to diverging operational set-points of the reactor. The differences in temperature are assumed to be a consequence of different heats of reaction involved in the gasification of PS.

Figure 6.57: Bed temperatures for AH and AH+PS experiments.

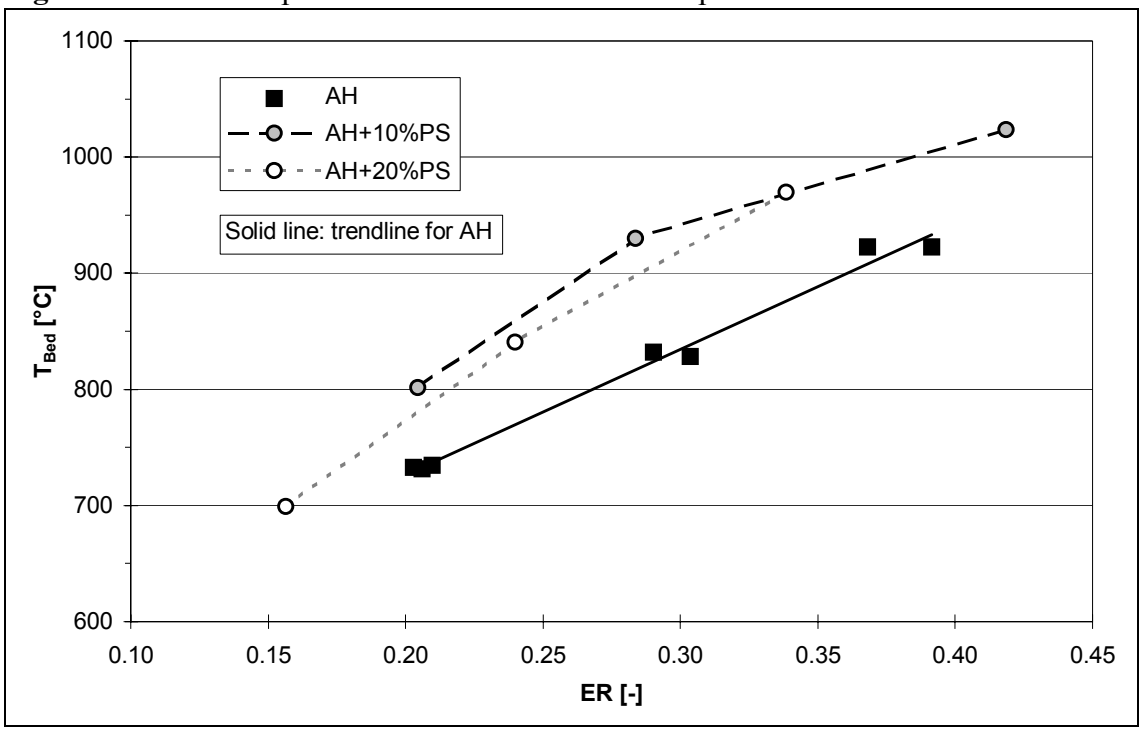

The evolution of gas components as a function of ER is shown in Figure 6.58. All gas components are seen to follow the same trends as ER is increased for all three fuels. The addition of PS to AH has little influence on the CO and CO_2 concentrations at comparable ER, slightly decreasing them in comparison to AH alone. H_2 and CH_4 exhibit almost identical concentrations for the 10% PS mixture compared to AH. H_2 is slightly and CH_4 strongly decreased in the gas from the 20% PS mixture.

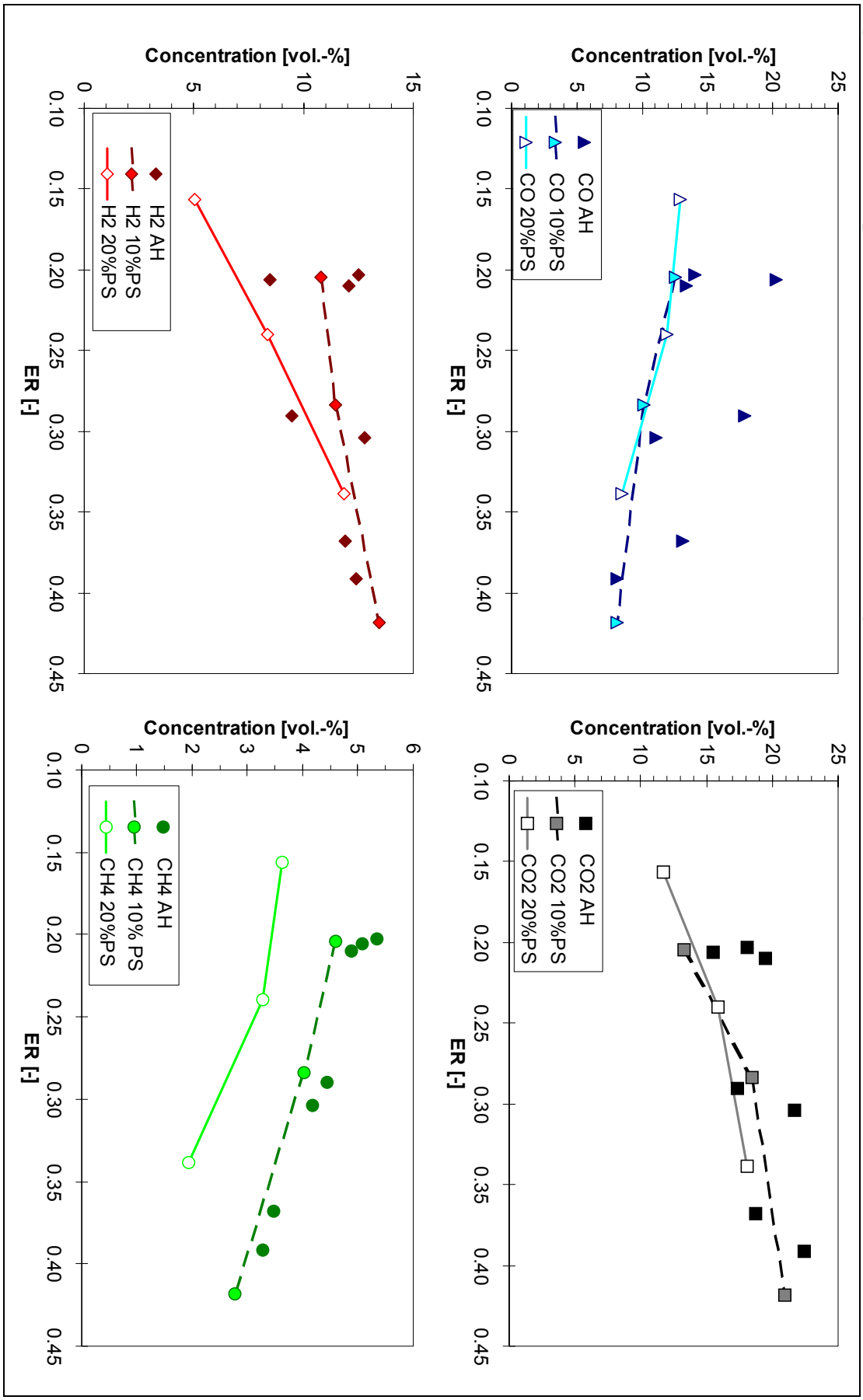

Figure 6.58: Gas composition evolution for AH and AH+PS gasification in function of ER.

Figure 6.59: Total tar concentration in function of ER for AH and AH+PS gasification experiments.

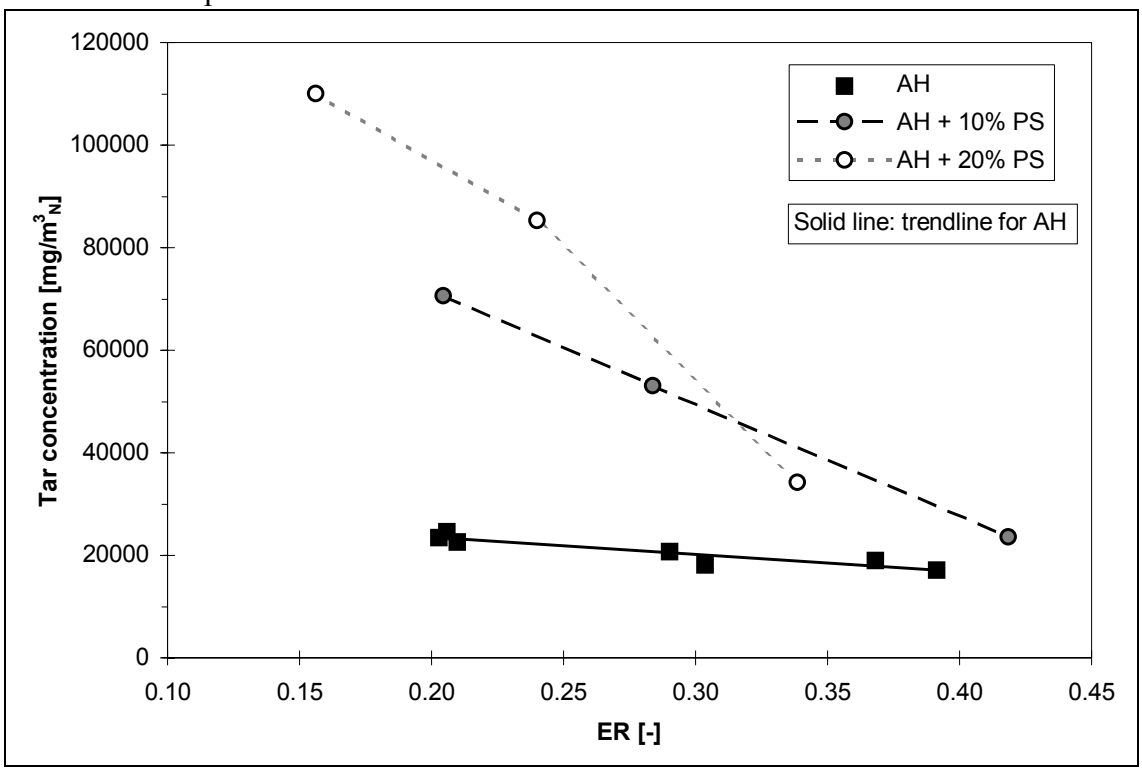

The total tar concentrations measured, displayed in Figure 6.59, clearly show that the total tar concentration is greatly increased by the addition of PS. Even at high ERs larger tar amounts are present in the gas from the PS mixtures. The amount of PS in the fuel seems however only to influence the total tar concentrations at ER < 0.3.

As with previously studied fuels, the fraction of unidentified tar compounds has been estimated for AH+PS. The results are shown in Figure 6.60. For the 10% PS mixture at all ERs and for the 20% PS mixture at ER = 0.34 the amount of identified tars is higher than for AH alone. The explanation for the larger fraction of tars identified is the presence of large amounts of styrene in the tars. However, at lower ER the tars from the gasification of the 20% PS mixture do include a fraction of unidentified compounds larger than that estimated for the AH tars. A possible explanation for this larger fraction of unidentified tar components is the presence of styrene oligomers or other styrene-related compounds. The formation of these compounds is apparently dependent on both, the ER and the amount of PS in the fuel.

The total tar concentration corrected with the results of the above estimation is shown in Figure 6.61, revealing a 3 to 5 fold increase of the tar concentration at low ER.

Figure 6.60: Fraction of tars identified by GC/MSD for AH and AH+PS runs in function of ER.

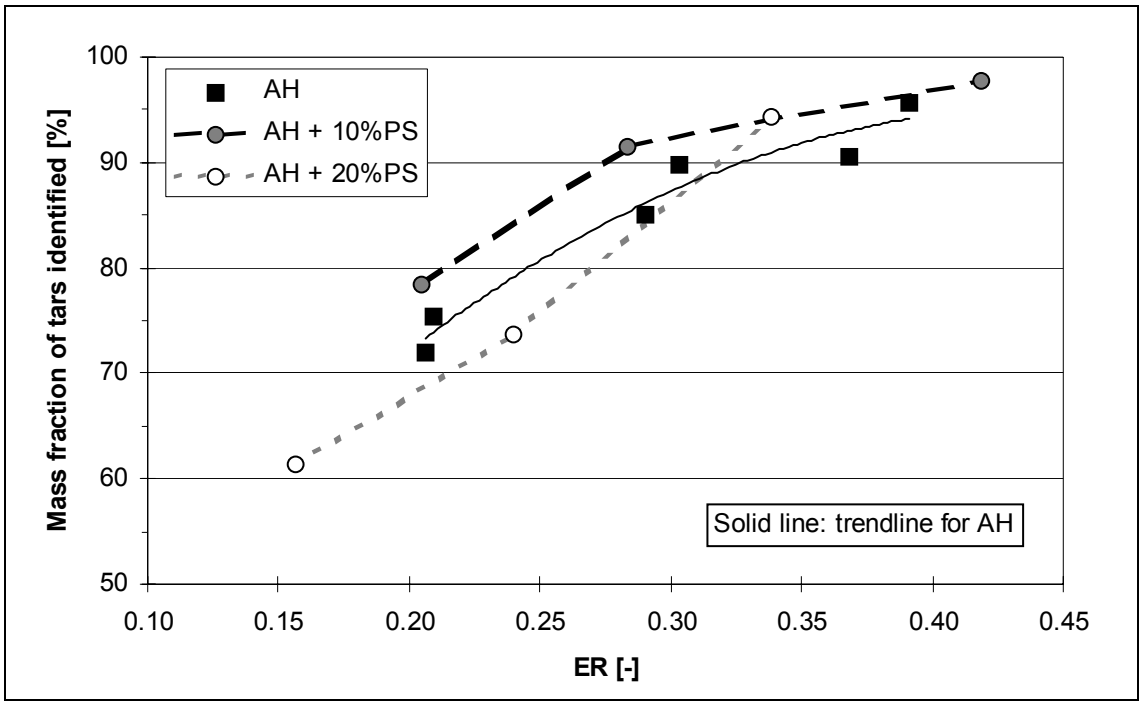

Figure 6.61: Corrected total tar concentration as a function of ER for AH and AH+PS.

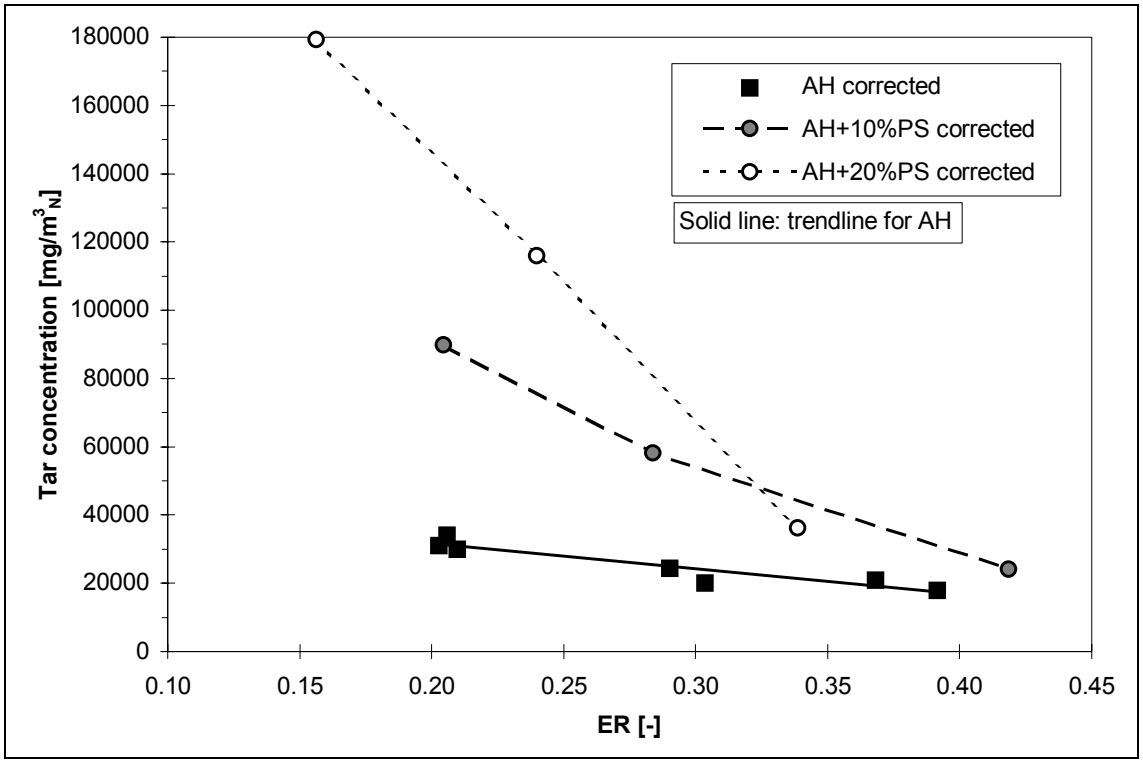

The comparison of the measured gas composition with thermodynamic equilibrium calculations is shown in Figure 6.62.

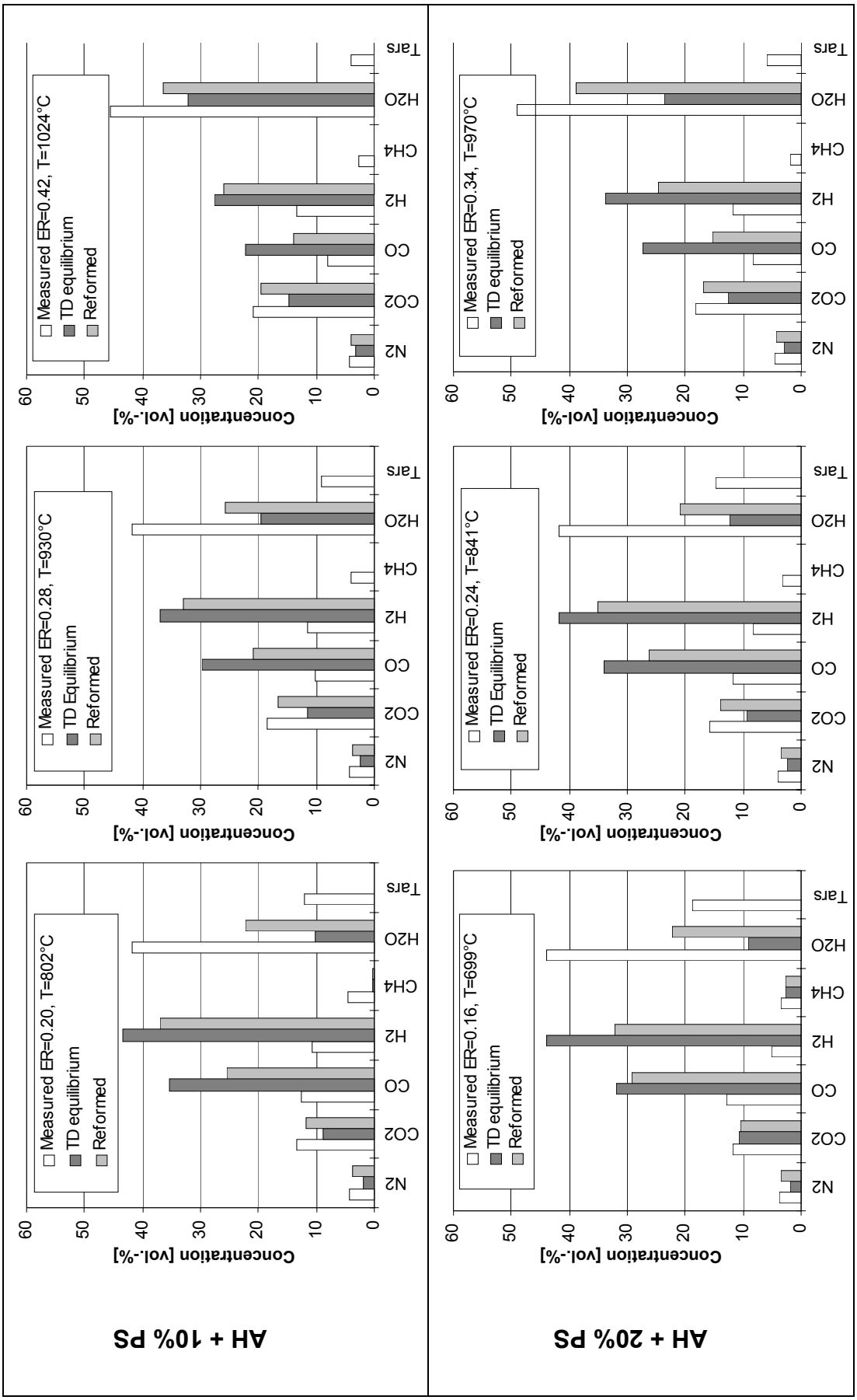

Figure 6.62: Comparison of measured, equilibrium and "reformed" gas composition for AH+PS runs.

Again the gasifier is seen to be operating far from the thermodynamic equilibrium. The equilibrium calculation for the 20% PS mixture at the lowest ER yields 8.4 mole-% of the products in the form of solid carbon. The reforming computation is seen to decrease the differences between measured and equilibrium gas composition but it is again not possible to explain all the deviations this way.

The gas yields for the AH+PS runs are displayed in Figure 6.63. The amount of gases generated is smaller when PS is present in the fuel and the ER is below 0.4. This difference may be attributed to the large fraction of the fuel being converted into tars, as indicated by the very high total tar concentrations measured.

Figure 6.63: Gas yield in function of ER for AH and AH+PS gasification.

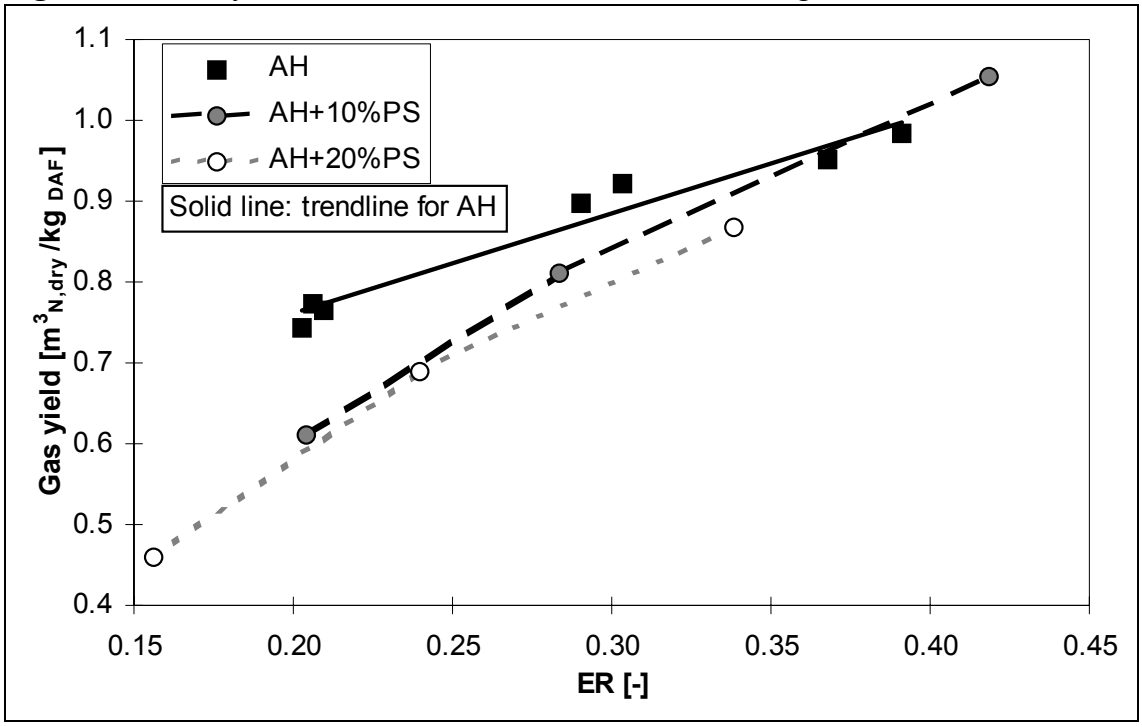

The evolution of the tar classes as a function of the ER for the AH+PS experiments is shown in Figures 6.64 and 6.65. Benzene concentrations are higher for the AH+PS mixtures at all ERs. The increase of this tar class is dependent on the amount of PS present only for ER < 0.3. At high ER the benzene concentration in the AH+PS runs is still much higher than that of AH. Naphthalene concentrations are also increased at low ER in comparison to AH. At high ER the concentrations of naphthalene are identical to those observed in AH gasification.

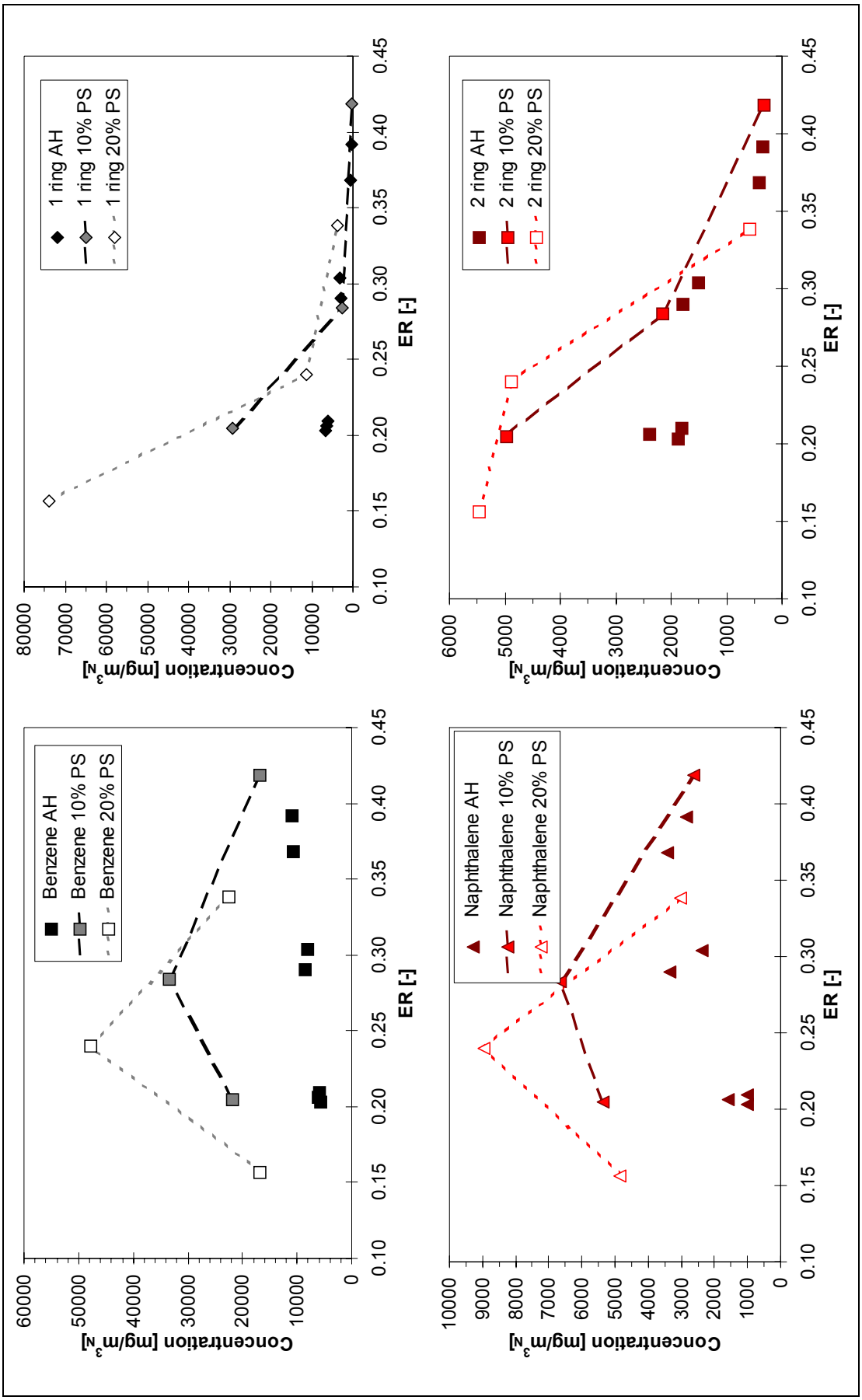

Figure 6.64: Evolution of Benzene, 1 ring, naphthalene and 2 ring classes with ER for AH and AH+PS gasification

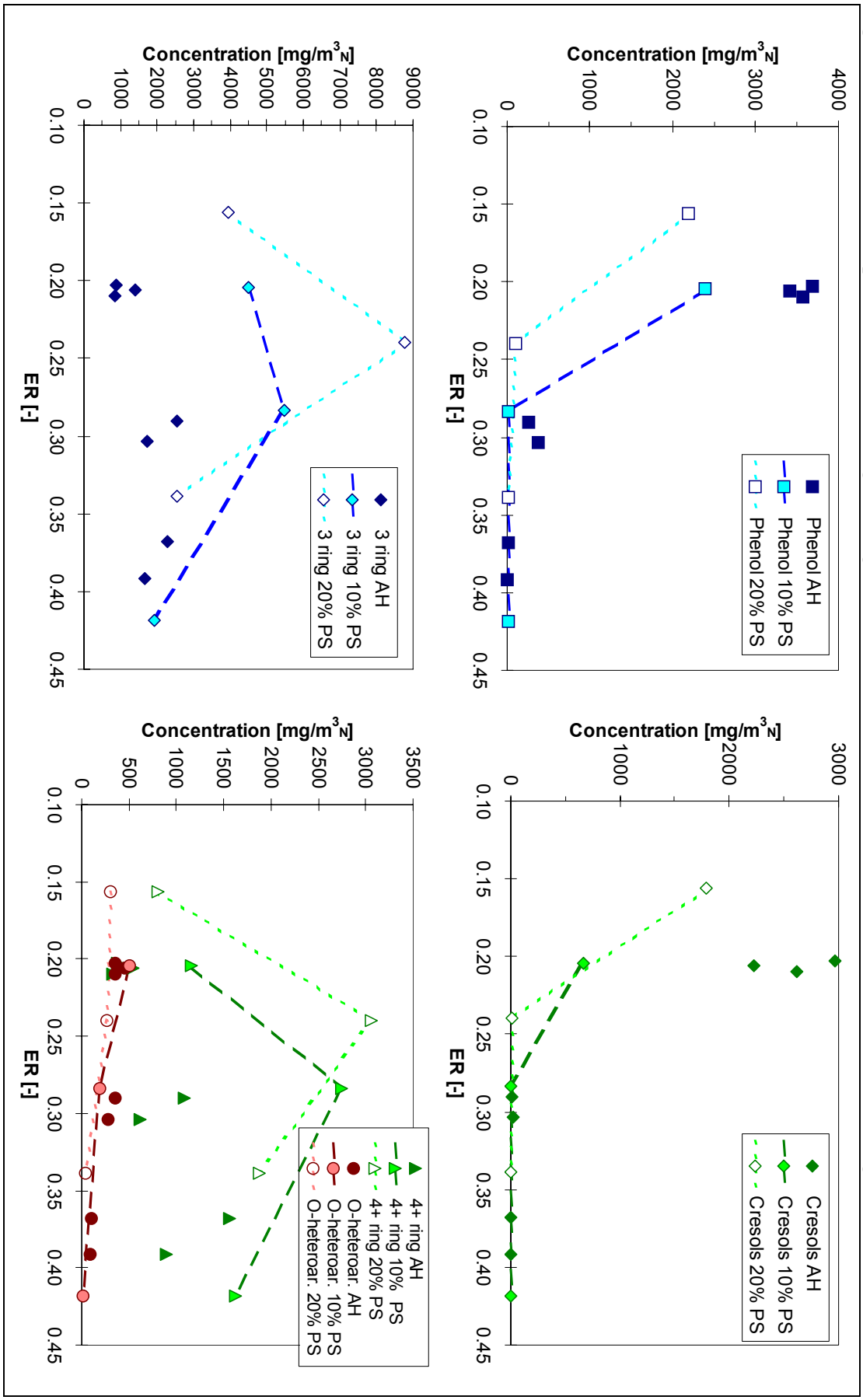

Figure 6.65: Evolution of phenol, cresols,3 ring, 4+ ring and O-heteroaromatic classes with ER for AH and AH+PS gasification.

At low ER the effect of the PS fraction in the fuel on the naphthalene concentrations is similar to that observed for benzene, i.e. a higher PS fraction corresponding to higher concentrations. Both tar classes, benzene and naphthalene exhibit a maximum in their concentrations. The ER value at which this maximum is observed is dependent on the PS fraction in the fuel.

The concentration of 1 ring aromatics is greatly increased by PS addition at low ER. The level of PS in the fuel does not show a large influence in this increase. At ER > 0.3, this tar class shows the same concentration as when no PS is present in the fuel. The concentration of 2 ringed aromatics is also only increased in relation to AH at ER < 0.3. The amount of PS in the fuel has only a minor effect on the concentration of this tar class.

The concentration of phenols and cresols is lower in comparison to AH. Phenol concentration is affected by the fraction of PS in the fuel whereas cresols concentration is seen not to depend on this parameter. These compounds virtually disappear from the tars at lower ER values than is the case for AH alone.

3 ring, 4 ring and larger PAHs show the same behaviour as naphthalene. The 4 and larger ringed PAHs are however present in slightly larger concentrations at high ER than is the case for AH. The presence of PS in the fuel does not seem to influence the oxygen containing heteroaromatic compounds strongly.

A closer look at the composition of the 1 ringed aromatic tars is shown in Figures 6.66 to 6.68. The amount of styrene is strongly increased in the tars for the AH+20% fuel at low ERs. Under these conditions, the composition of this tar class is however not strongly affected when only 10% PS is added to the fuel. At intermediate ERs the situation is similar. As ER is raised above 0.34, a reduction of styrene with an increase in the concentration of toluene is observed for the fuel with 20% PS. Again no large differences are seen between the AH and the 10% PS fuel.

Figure 6.66: Concentration of tar compounds in the 1ring class for AH+PS at ER≤0.21.

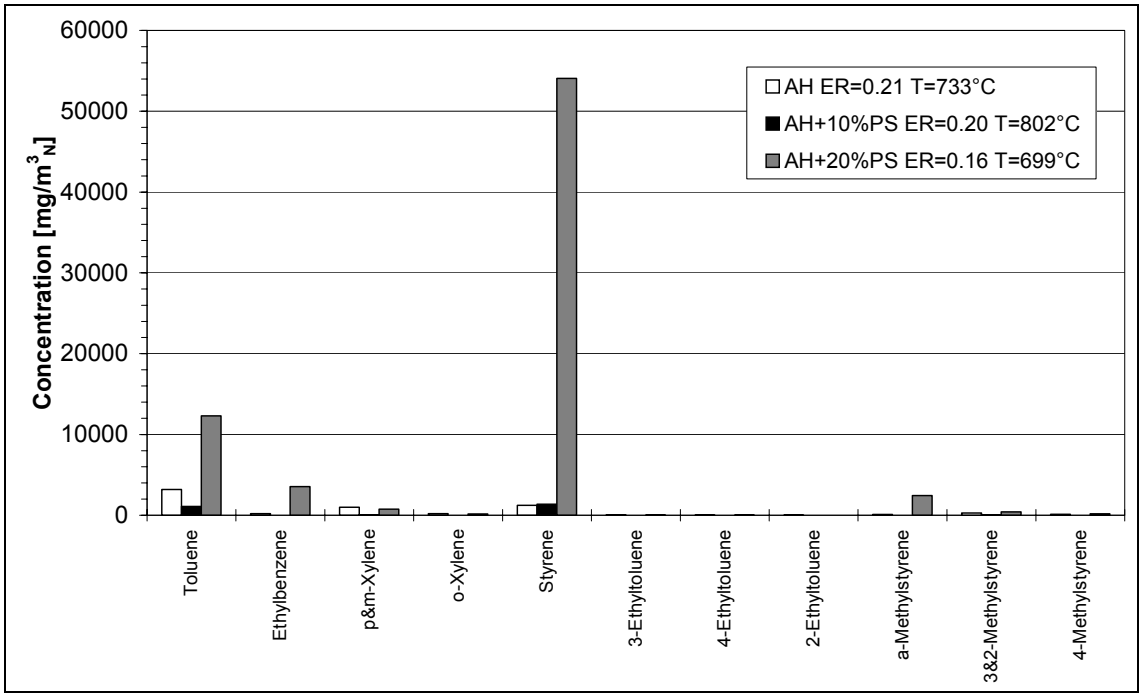

Figure 6.67: Concentration of tar compounds in the 1ring class for AH+PS at ER≤0.3.

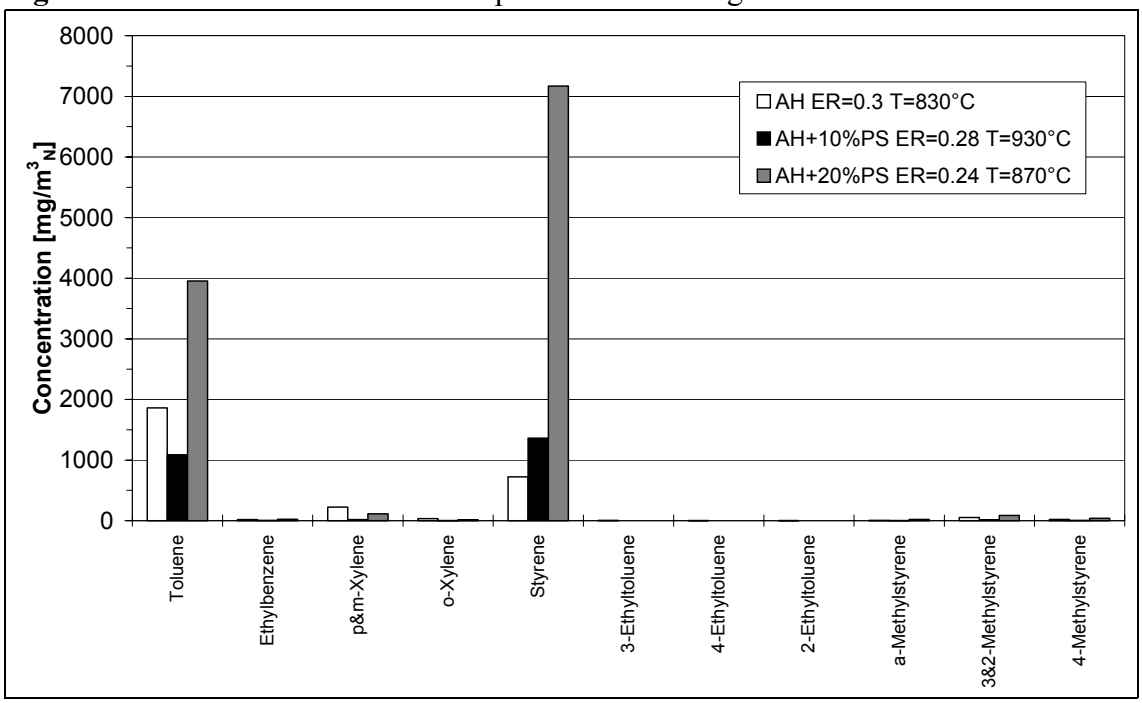

Figure 6.68: Concentration of tar compounds in the 1ring class for AH+PS at ER≥0.34.

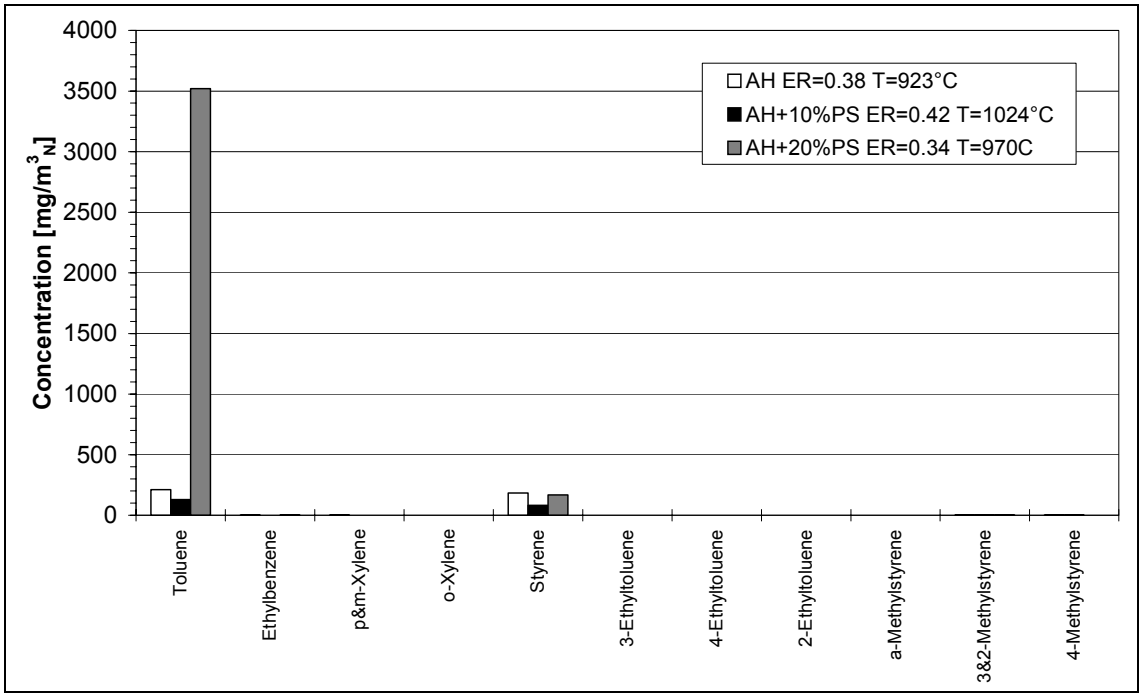

Figure 6.69: Fraction of styrene in tars to polystyrene input as a function of T_{Bed}.

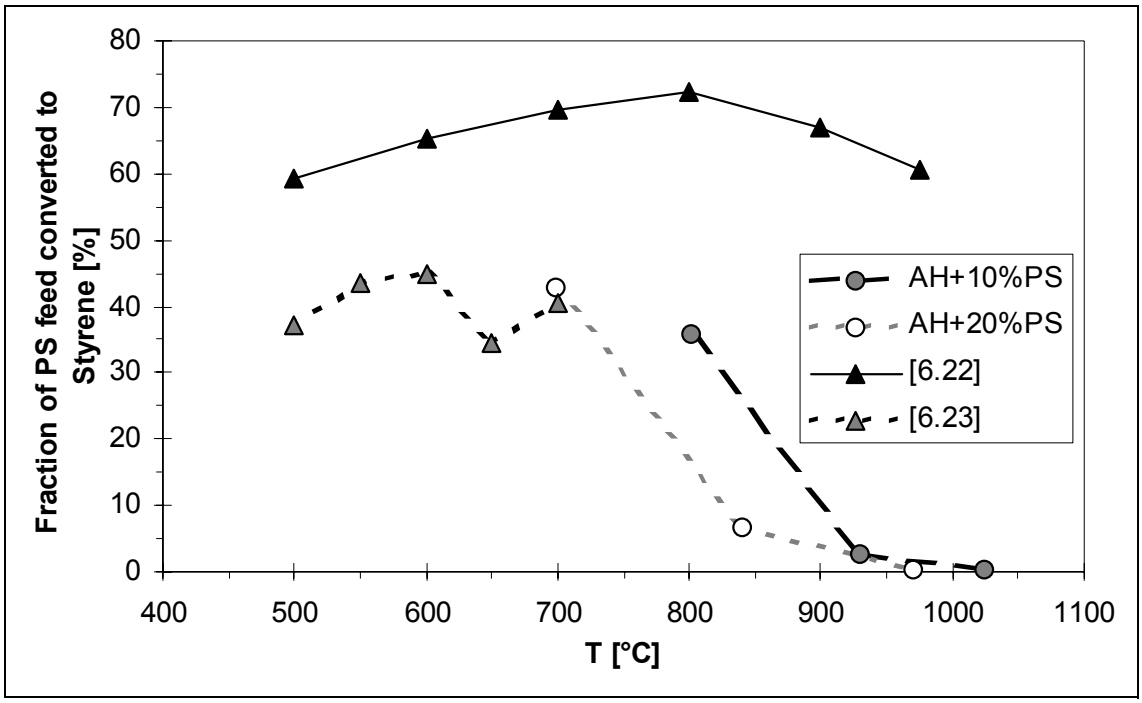

The fraction of the polystyrene converted to styrene monomer is shown in Figure 6.69 as a function of the temperature to enable comparison with literature data [6.23], [6.24]. Note that the results reported in the named references are from pyrolysis experiments, i.e. ER = 0.

The differences in relation to [6.23] depicted in Figure 6.69 might be explained by the experimental set-up used in that study, a pyroprobe pyrolyser. This instrument allows for very short residence times of the products at high temperature, thus minimising secondary reactions. These results indicate, that the main primary product of PS pyrolysis is styrene monomer. The fraction of PS converted to styrene reported in [6.24], where the pyrolysis was conducted in a fluidised bed, seem well comparable to the present results at the lowest temperature achieved in the experiments of the present study. The reduction in the fraction of PS converted to styrene observed at higher temperatures in the current study could be related to both increasing decomposition of the primary product(s) due to the high temperature or to the presence of oxygen, also affecting secondary reactions.

The temperature and ER combination at which gasification of AH+PS mixtures is carried out is in any case seen to be very important in reducing the fraction of primary PS decomposition products and so the amount of tars in the gasification products. Notice how the conversion of the polymer to the monomer appears to be enhanced at low PS levels in the fuel for a given temperature. The 10% PS mixture yields almost as much styrene monomer at T_{Bed} = 802°C and ER = 0.2 as the 20% PS mixture at T_{Bed} = 699°C and ER = 0.16. Both sets of reactor conditions would strongly favour the formation of primary products in biomass gasification, which in the case of PS translates to the preferential formation of monomer. This reaction pathway is also preferred in the case of the AH+PS mixtures, as the observed high conversions to monomer confirm. This reaction pathway is however inhibited by the presence of larger amounts of PS in the fuel, as is suggested by the observed lower conversion to monomer in the results of 20% PS mixture at T_{Bed} = 841°C and ER = 0.24, a set of conditions still favouring primary reaction products in the case of pure biomass. Another hypothesis which could explain this behaviour is a stronger sensitivity of the primary to secondary (or tertiary) conversion reactions to the presence of oxygen (= higher ER) for PS.

The tar composition is shown in Figures 6.70 to 6.72. Both PS mixtures show increased fractions of the 1 ringed components at low ER, reflecting the high conversion of PS to monomer discussed above. The 10% PS mixture does furthermore show a marked increase of the benzene fraction in the tars compared to AH, which is absent in the results of the 20% PS mixture. The difference between the 20% and the 10% mixtures could be explained by the higher ER used in the 10% PS experiment, which could enhance the con-

version of the primary products of the PS pyrolysis to tertiary products. Naphthalene and 3 ringed aromatic compounds have their fractions increased in the 10% PS experiment in relation to AH, but almost no changes are observed for the 20% PS mixture. 2, 4 and larger ringed aromatics are somewhat decreased in the PS mixtures. Phenolic compounds are clearer strongly reduced in the tars from the AH+PS mixtures at low ERs.

Figure 6.70: Normalised tar composition for AH and AH+PS gasification at low ERs (0.16<ER<0.21).

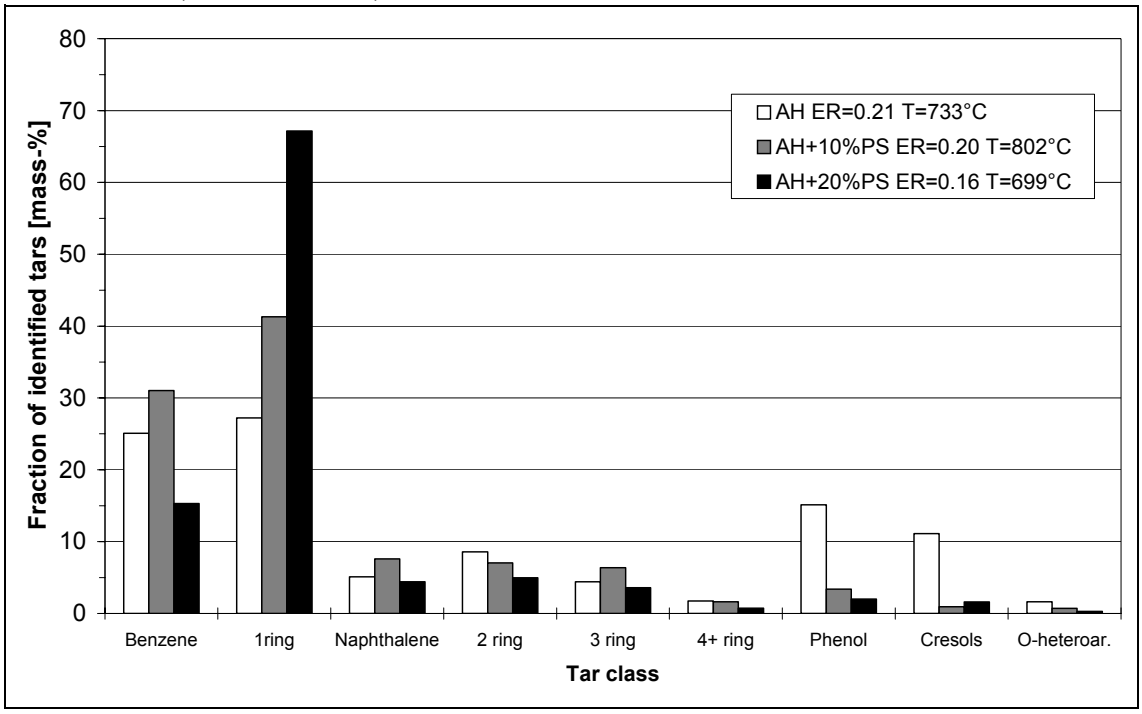

At intermediate ERs both PS mixtures yield tars with a higher fraction of benzene. The 10% PS mixture shows a very low fraction of 1 ringed aromatic compounds compared to the results of the other two fuels. Probably the higher temperature of this particular experiment in comparison to the other two is responsible for the conversion of the primary tar product from PS (styrene) into the thermally more stable benzene. The same situation is observed for the 2 ringed aromatics. Naphthalene is increased in the tars of the AH+PS mixtures in this ER range, as are the 3 ringed aromatics. This increase is seen to be dependent on the fraction of PS present in the fuel. As in the lower ER range, phenolic compounds are strongly reduced in the tars of the AH+PS mixtures.

Figure 6.71: Normalised tar composition for AH and AH+PS gasification at intermediate ERs (0.24<ER<0.30).

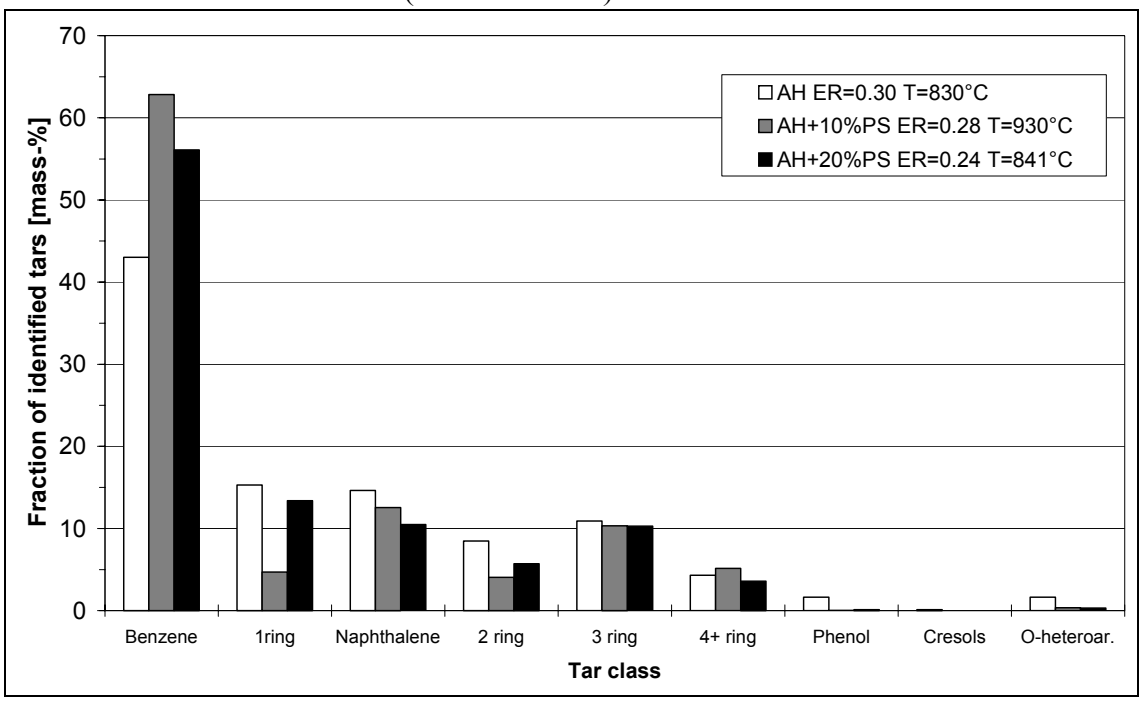

Figure 6.72: Normalised tar composition for AH and AH+PS gasification at high ERs (0.34<ER<0.42).

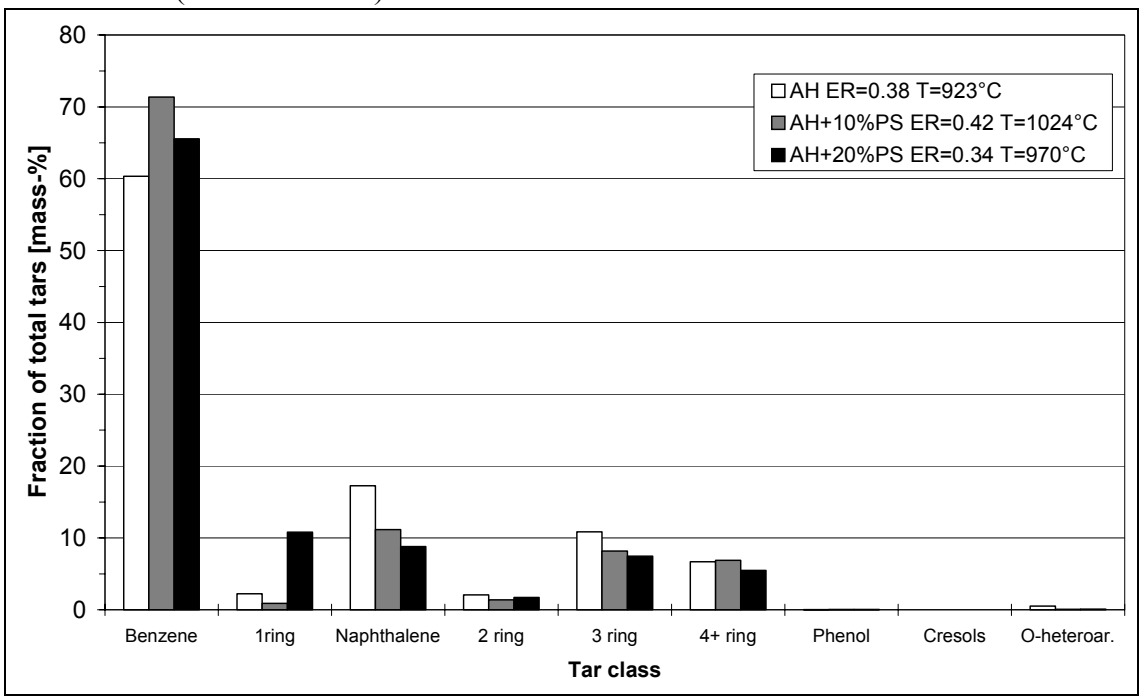

At high ERs, the AH+PS mixtures yield higher benzene fractions in the tars. The 20% PS mixture yields an unexpectedly high 1 ringed aromatics fraction, probably due to the comparatively low ER in that particular experiment. Naphthalene is strongly reduced

in the tars as are the 2 and 3 ringed aromatics. 4 and larger aromatic systems are seen to be almost not influenced by the presence of PS.

6.2.5 Effect of ageing on SCW

The aged SCW was gasified in experiment 000201, at almost the same ERs as the untreated SCW, yielding comparable temperatures as shown in Table 6.9. A discussion of the results can therefore be made for either ER or T_{Bed}.

Table 6.9: ER and T_{Bed} for SCW and aged SCW gasification experiments

SCW		Aged SCW	
ER [-]	**T_{Bed} [°C]**	**ER [-]**	**T_{Bed} [°C]**
0.20	707	0.21	729
0.30	841	0.31	834
0.40	932	0.41	923

Figure 6.73: Gas composition evolution for SCW and aged SCW gasification in steam/ oxygen.

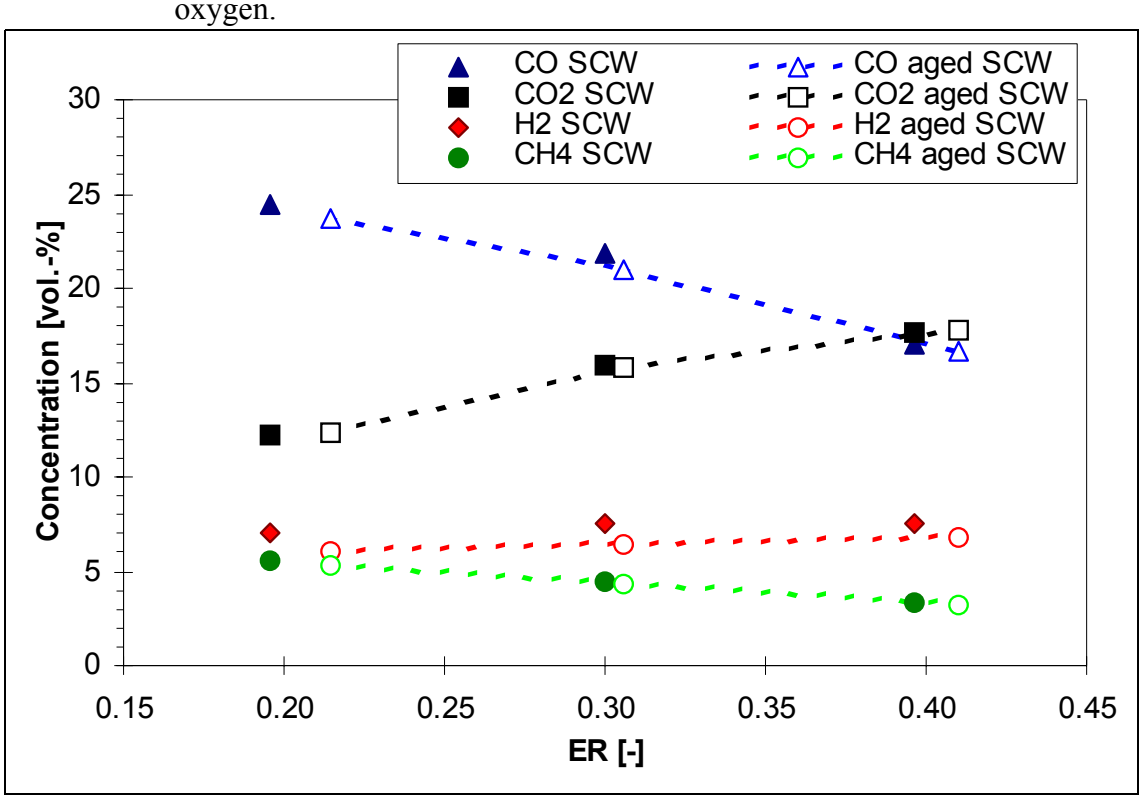

The gas composition evolution with ER for both SCW fuels is shown in Figure 6.73. Almost no differences are observed in the gas composition of both fuels.

A comparison to the thermodynamic equilibrium will not be made. The composition of the aged SCW is assumed to be the same as SCW and the experimental conditions are very similar for both fuels. Therefore the results would be the same for the two fuels and comparable to those shown in Figure 6.29 on page 191.

The gas yield for both types of SCW is shown in Figure 6.74. The aged fuel shows a slightly smaller gas yield at ER < 0.4. The difference is however smaller than that observed between regular SCW and AH. The lower gas amount produced could be due to a lower amount of volatile components in the aged fuel, which can be expected from the treatment (heating over a long time) applied in the preparation of the aged SCW. During this treatment the characteristic smell of light components of coniferous woods (e.g. the fragrant terpene compounds) was detected.

Figure 6.74: Gas yields for SCW and aged SCW gasification in steam/oxygen as a function of the ER.

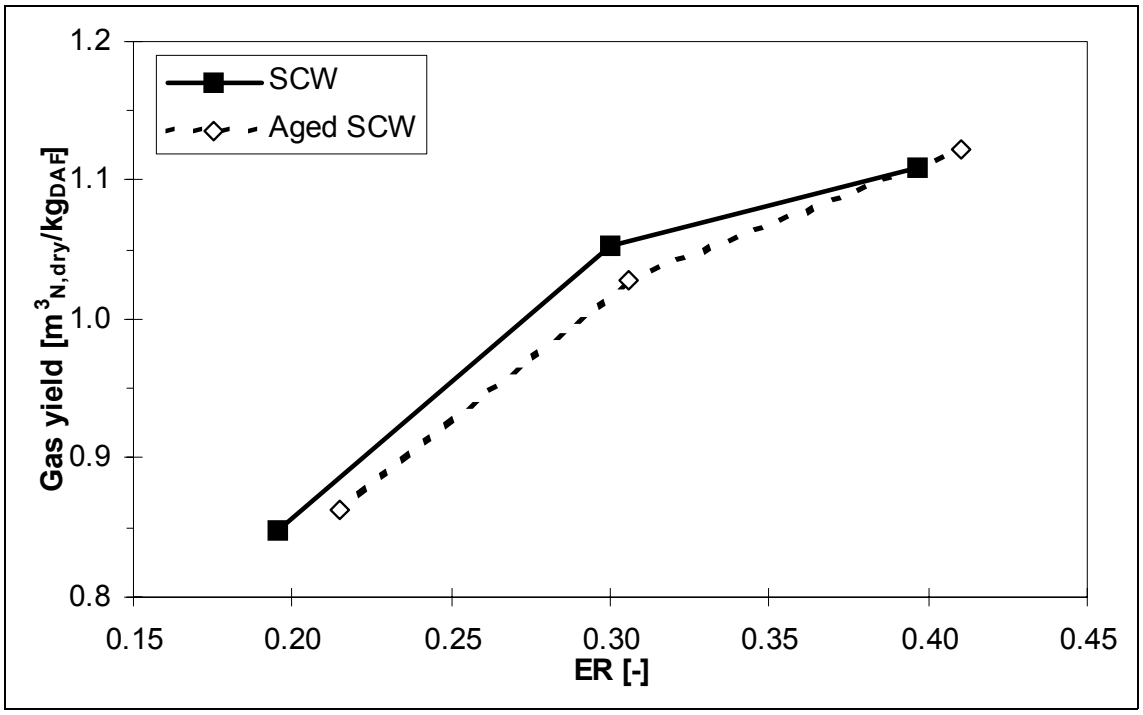

The total tar concentration in the gases of the two SCW variants is shown in Figure 6.75. Apart from some minor differences (at ER = 0.3 the relative deviation is less than 2.5%) both fuels again show practically identical values.

Figure 6.75: Total tar concentration for SCW and aged SCW gasification in steam/ oxygen as a function of ER.

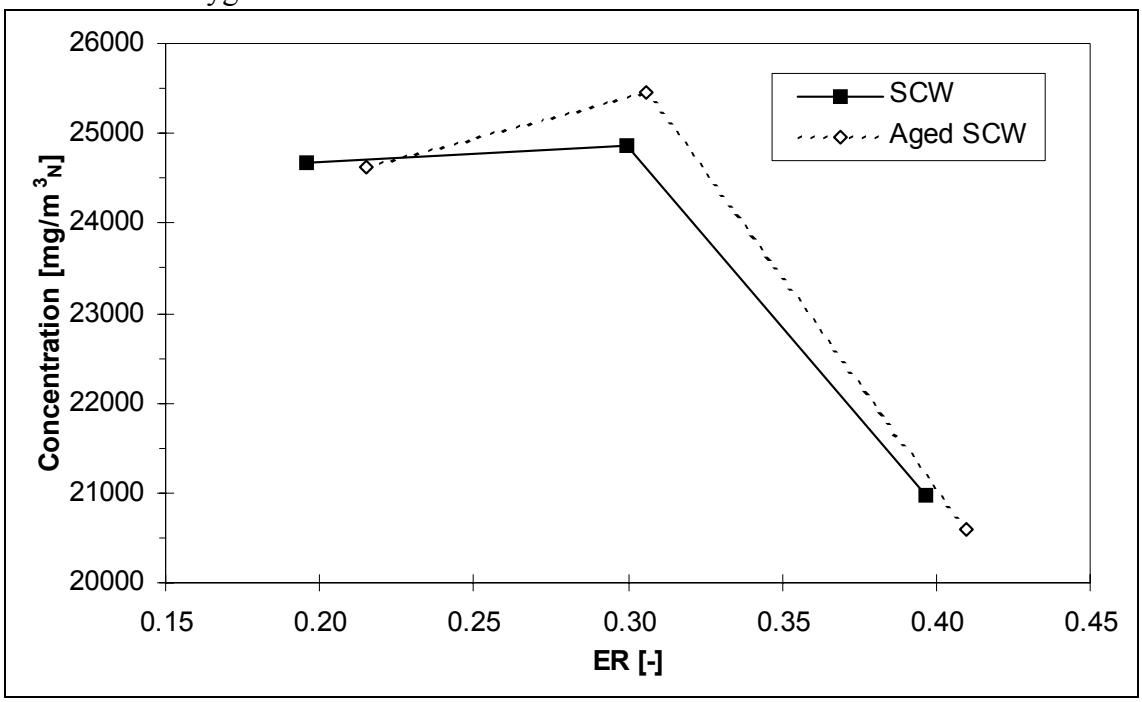

The evolution of the tar classes as a function of the ER is depicted in Figures 6.76 to 6.78.

Figure 6.76: Tar concentration evolution with ER (major aromatics) for regular and aged SCW gasification in steam/oxygen.

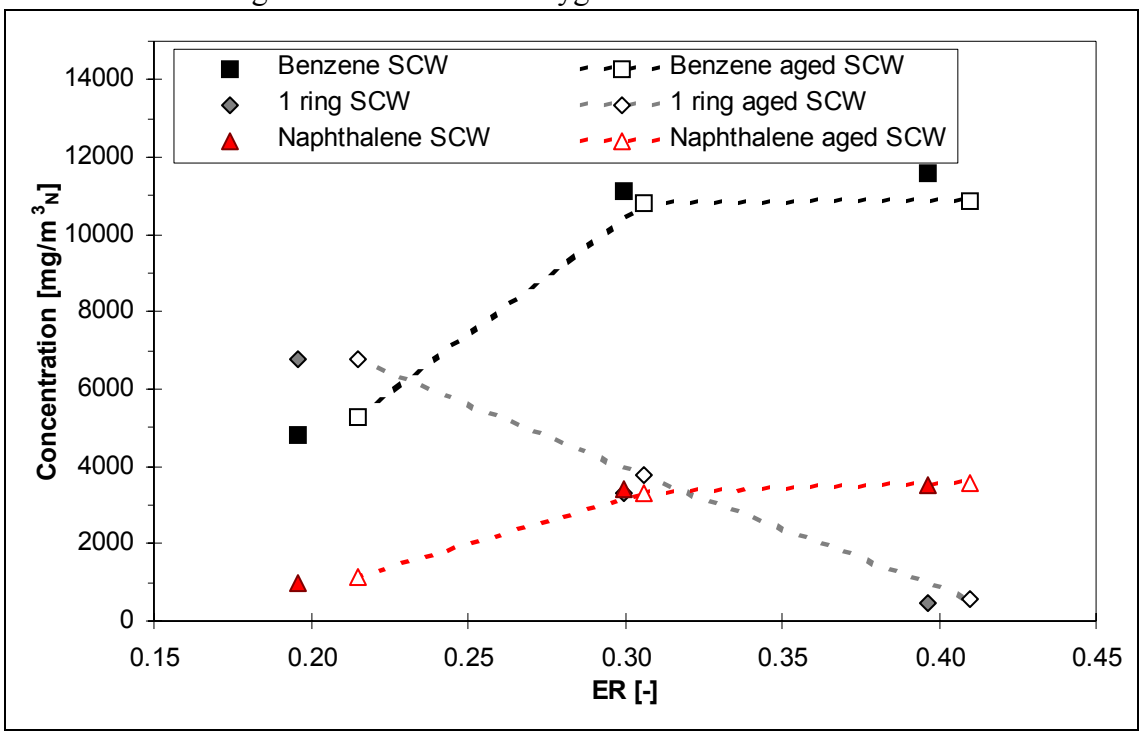

Figure 6.77: Tar concentration evolution with ER (oxygenates) for regular and aged SCW gasification in steam/oxygen.

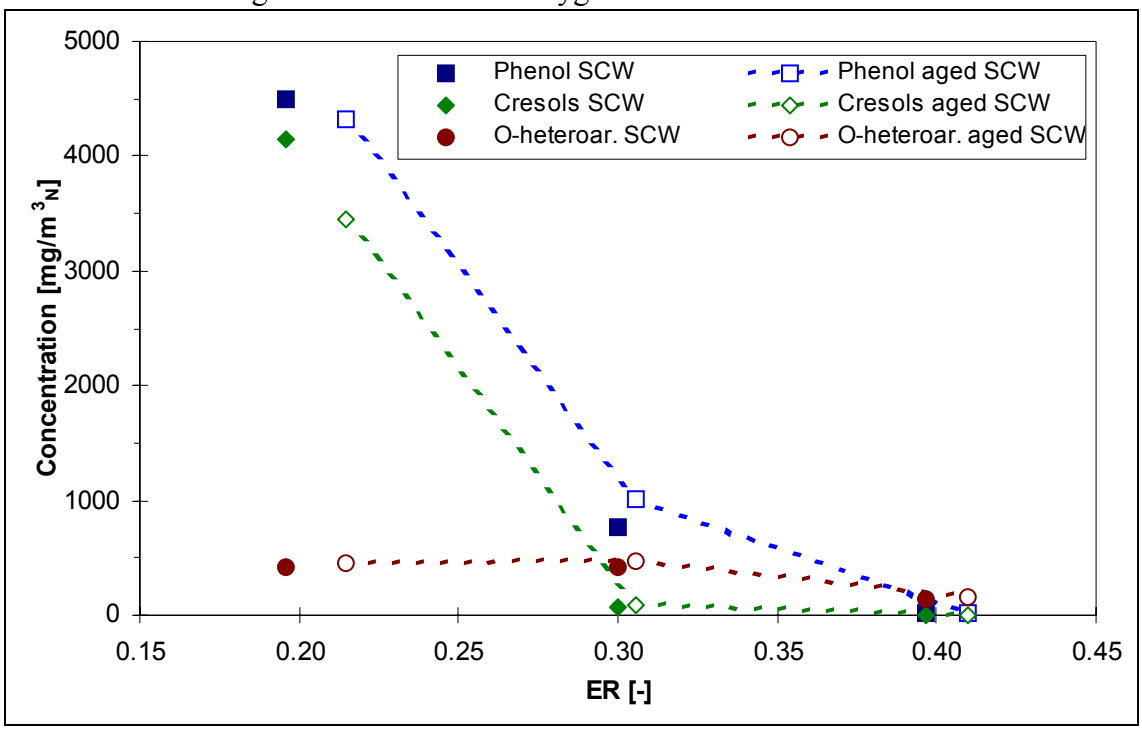

Figure 6.78: Tar concentration evolution with ER (minor aromatics) for regular and aged SCW gasification in steam/oxygen.

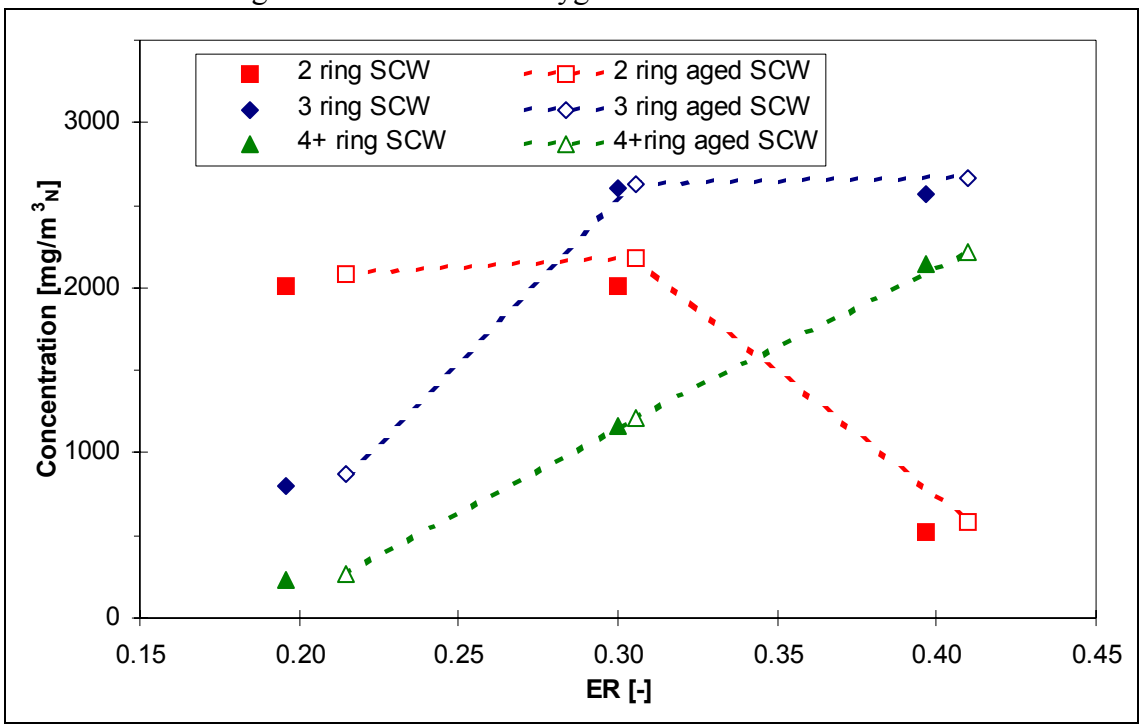

Both fuels show essentially the same evolution and concentrations of the tar classes. Only very small increases in the concentrations of some tar classes are observed.

This identical tar classes evolution means also, that the tar composition for both fuels is practically the same, making a discussion of differences in the tar composition redundant.

Since the tar composition is virtually the same for the standard SCW and the aged variant, the estimation of the identified tar compounds was not carried out for the aged SCW. The results for the regular SCW are assumed to apply to the aged fuel and the corrected total tar concentrations evolution is shown in Figure 6.79. This plot shows, that aged SCW yields a slightly higher tar concentration as the untreated fuel, but again differences are very small and may well be assumed to reflect error margins of the tar measurement method.

Figure 6.79: Corrected total tar concentration for SCW and aged SCW gasification in steam/oxygen as a function of ER.

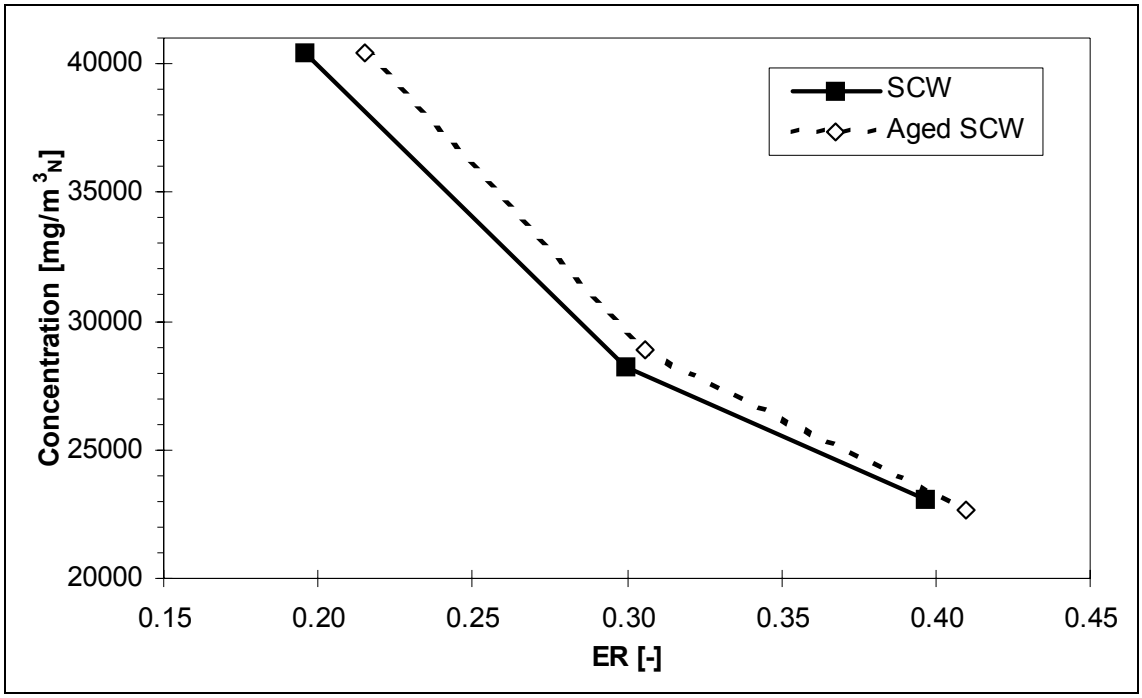

The results presented clearly show, that both fuels behave identically. The simulated ageing had no effect on SCW. Two conclusions are possible: either that the treatment chosen was not the correct one or not applied long enough to simulate the aging process correctly, or that the age of the fuel is not a cause for the observed lower tar concentrations of AH.

6.2.6 Effect of fuel particle size in the gasification of SCW

The milled SCW, with a mean particle size of 220µm was gasified in steam/oxygen in experiment 000330. The original SCW has a mean particle size of approximately 430µm. The temperatures and ERs of the runs in this experiment as well as those for the experiment with the regular SCW are shown in Table 6.10. Again the conditions in the experiment with either fuel are very similar, with the exception of the highest ER for the milled SCW. At the same ER the same T_{Bed} is achieved, making a discussion of the results with respect of either parameter possible.

Table 6.10: ER and T_{Bed} for SCW and milled SCW gasification experiments.

SCW		Milled SCW	
ER [-]	**T_{Bed} [°C]**	**ER [-]**	**T_{Bed} [°C]**
0.20	707	0.19	714
0.30	841	0.31	842
0.40	932	0.46	944

Figure 6.80: Gas composition evolution for SCW and milled SCW gasification in steam/oxygen as a function of ER.

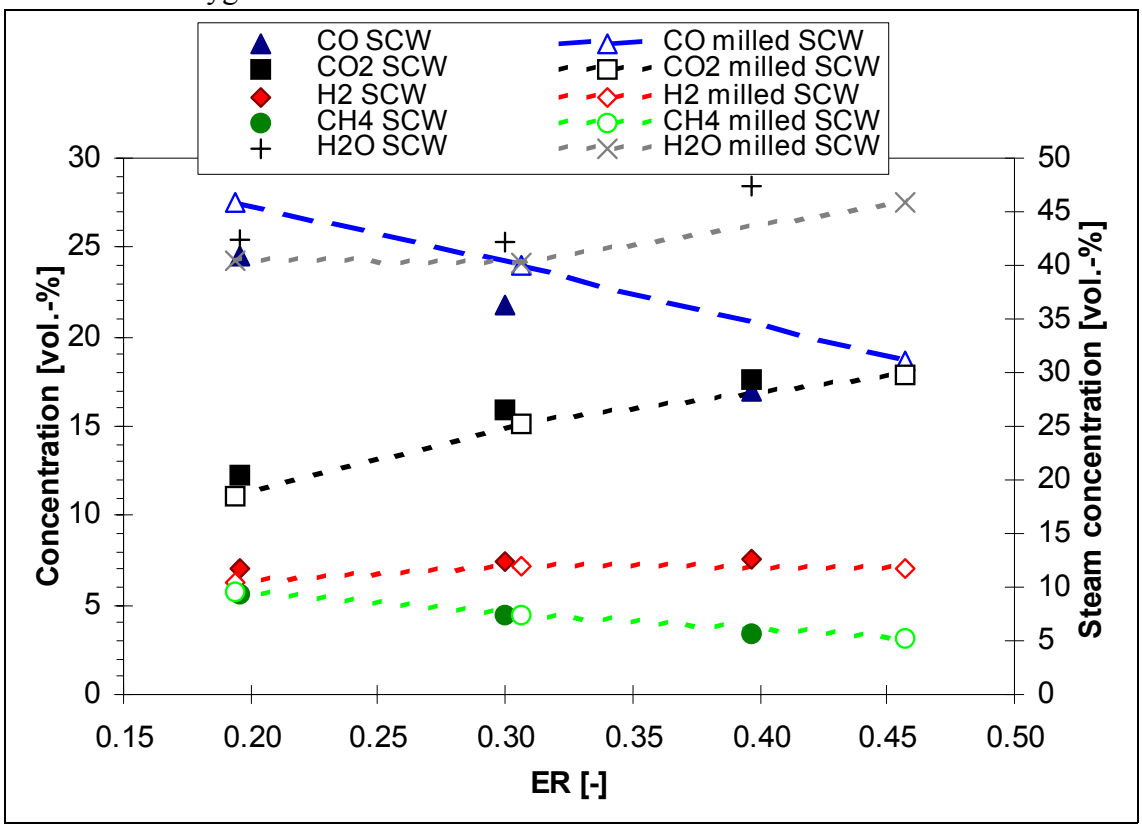

The evolution of gas composition for both fuels, shown in Figure 6.80, reveals only small differences in the gas composition at comparable ER. The CO_2 and H_2 concentrations are slightly lower and the CO concentration is higher for the milled fuel. A hypothesis to explain this higher CO concentration is, that the smaller sized fuel generates char particles with smaller size and therefore larger specific surface. This increase in specific surface of the char could in turn increase the conversion of the char by the Boudouard reaction ($C_{(s)} + CO_2 \rightarrow 2\ CO$), explaining the higher CO and lower CO_2 concentrations observed when the milled fuel is used. The lower solids output with a lower carbon contents observed in the experiment at lowest ER using the milled fuel also supports this hypothesis, see Table 6.11.

Table 6.11: Mass flow, water and carbon content of solids collected in SCW and milled SCW gasification. *: as sampled.

Fuel		**SCW**			**Milled SCW**		
ER	**[-]**	**0.2**	**0.3**	**0.4**	**0.19**	**0.31**	**0.46**
Solids flow	**[kg/h]**	0.411	0.103	0.075	0.141	0.098	0.075
Ash content of solids*	**[mass-%]**	33.7	62.7	58.0	48.1	41.9	30.8
Water content of solids*	**[mass-%]**	1.7	4.9	5.3	2.7	15.5	11.6
Carbon content of dry solids	**[mass-%]**	64.6	32.4	36.7	49.1	42.5	57.6

However, for higher ER, the higher conversion of the char cannot be confirmed by the experimental data. On the contrary, the carbon content of the dry solids (i.e. in the state as they exit the reactor) is higher for the milled fuel in comparison to the regular SCW. The mass flows of solids exiting the reactor is further identical for both fuels. To confirm the hypothesis of the enhanced influence of the heterogeneous water-gas shift reaction, measurements of the solids profile inside the reactor and its carbon content would be necessary. This kind of measurement could unfortunately not be carried out in the present study.

The gas yield for the milled and regular SCW is shown in Figure 6.81 as a function of the ER. The gasification of the milled fuel is seen to yield larger gas amounts compared to the regular SCW. This increase indicates, that better solids conversion occurs when using the milled fuel. This increase could be assigned to the enhanced influence of the heterogeneous water-gas shift reaction put forward in the previous discussion of the gas composition.

Figure 6.81: Gas yield for SCW and milled SCW gasification in steam oxygen.

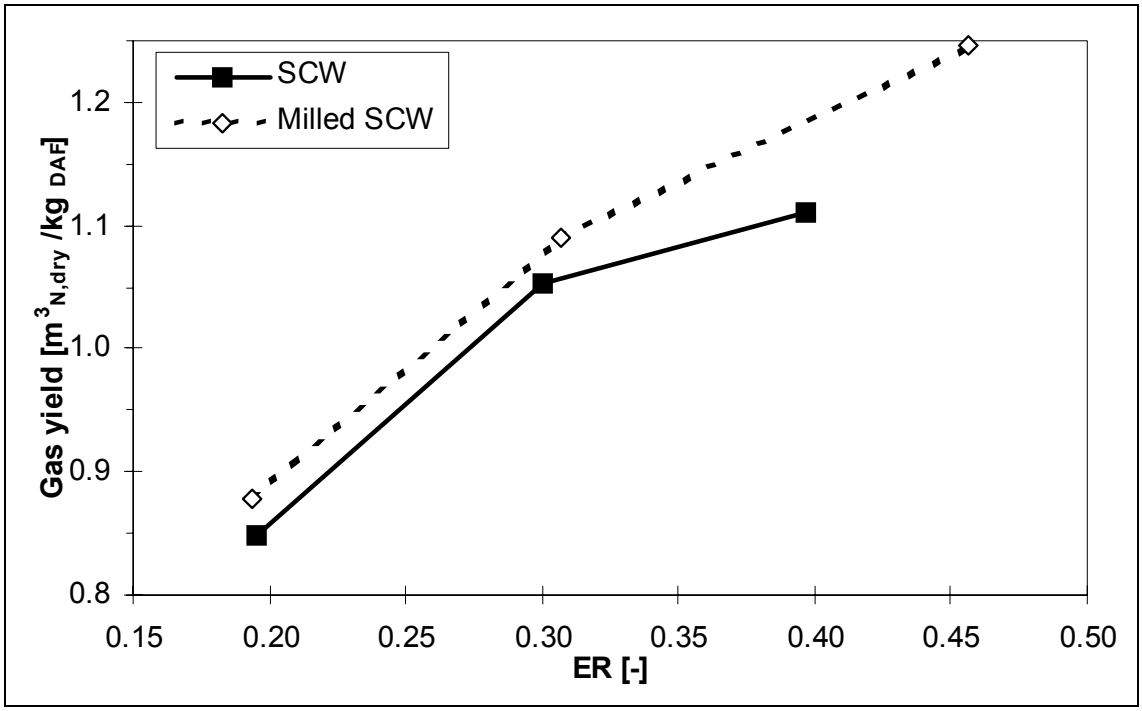

Figure 6.82: Total tar concentration for Altholz, SCW, aged SCW and milled SCW gasification in steam/oxygen.

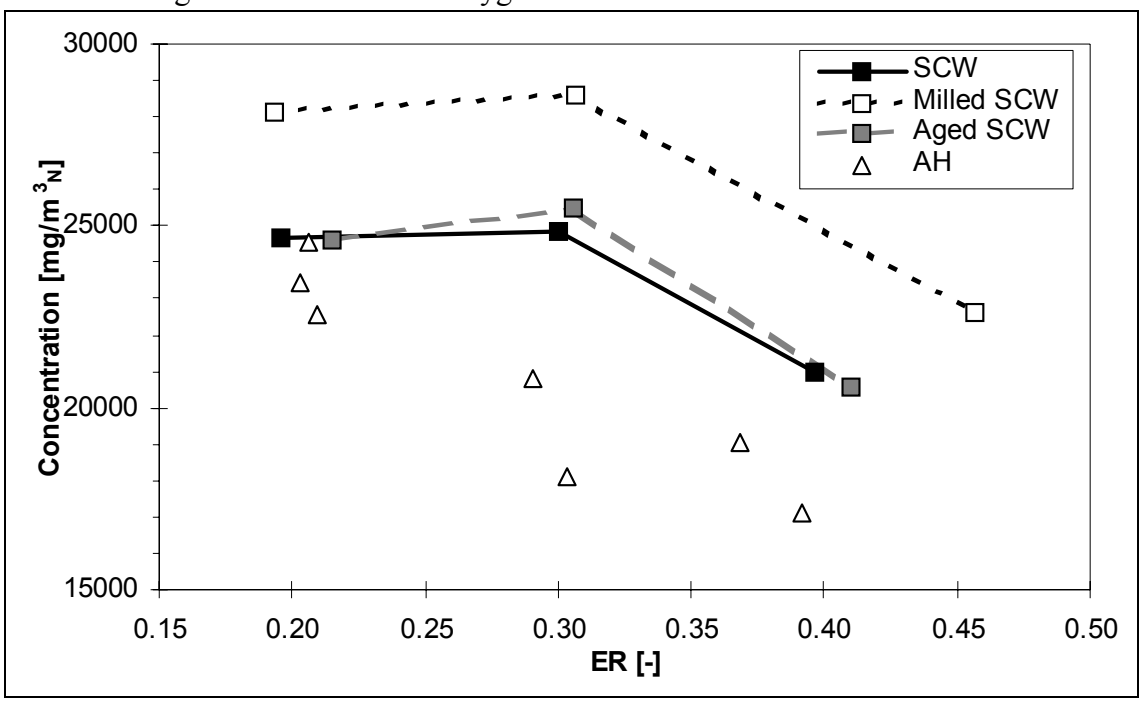

The total tar concentration measured in the gasification of all three SCW variants and of AH is depicted in Figure 6.82 as a function of the ER. The milled SCW is seen to yield higher tar concentrations in the gas than the other two SCW variants. These differences are further seen to be as significant as those observed between regular SCW and

AH. The fuel particle size is therefore seen to have a strong impact on the tar concentrations in the gas, the smaller fuel yielding larger tar concentrations. This experiment had been planned to test whether the lower tar concentrations observed when gasifying AH could be due to the smaller size of the AH fuel (Mean particle diameters: SCW ca. 620μm, AH ca. 330μm). As the results show, smaller fuel particles do on the contrary increase the tar concentrations. Therefore the smaller particle size of the AH is not the cause of the observed lower tar concentrations in the gasification of this fuel.

The higher tar concentrations observed may be explained in the light of the results from pyrolysis experiments (see page 63, Chapter 3). Smaller particles experience higher heat transfer rates. These higher heating rates are known to favour the formation of tars and gases in pyrolysis of biomass. Furthermore, in the smaller particles, lower residence times for the primary pyrolysis products inside the residual carbon matrix can be expected. This decrease in residence time would in turn decrease the interaction of the primary products and the carbon matrix. Increased char/tar interactions are known to reduce the amount of tars in the pyrolysis of biomass. A larger amount of volatilised products would therefore exit the reacting particle because of the two influences described above, explaining the higher tar concentrations measured.

The evolution of the tar classes for SCW and milled SCW is shown in Figures 6.83 to 6.85. The evolution of the tar classes concentrations with ER is the same for both fuels. The milled SCW exhibits markedly higher benzene concentrations over the whole range of ERs studied as well as somewhat higher concentrations of 1 and 2 ringed aromatics. Phenols and cresols as well as the 3 ringed aromatics are also slightly higher for the comminuted fuel. The concentrations of naphthalene and the larger ringed aromatics are seen not to be affected by the particle size. All differences in concentration are, with the exception of benzene relatively small.

Figure 6.83: Tar classes concentration evolution with ER (major aromatics) for regular and milled SCW gasification in steam/oxygen.

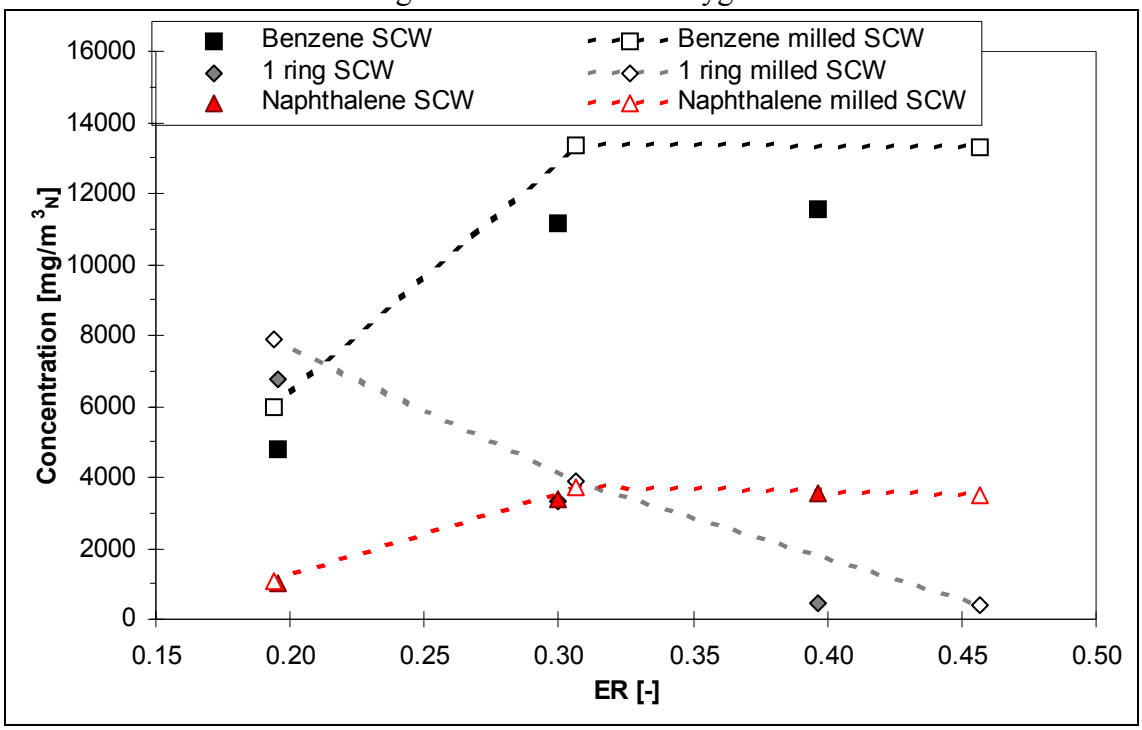

Figure 6.84: Tar classes concentration evolution with ER (oxygenates) for regular and milled SCW gasification in steam/oxygen.

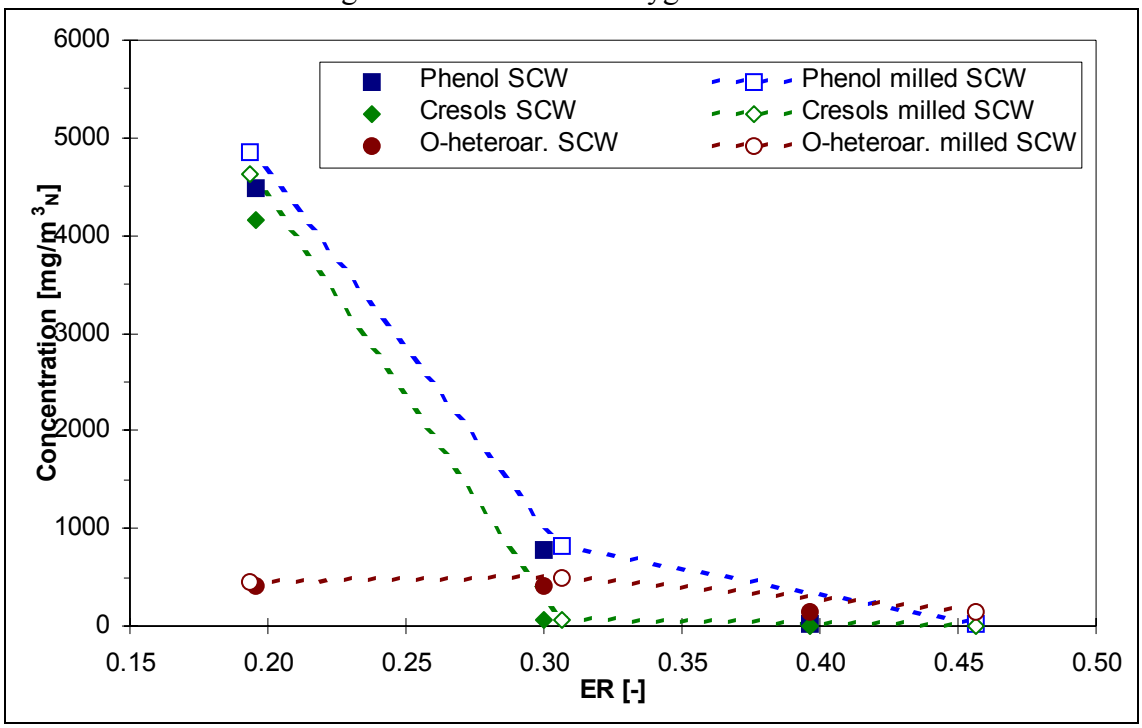

Figure 6.85: Tar classes concentration evolution with ER (minor aromatics) for regular and milled SCW gasification in steam/oxygen.

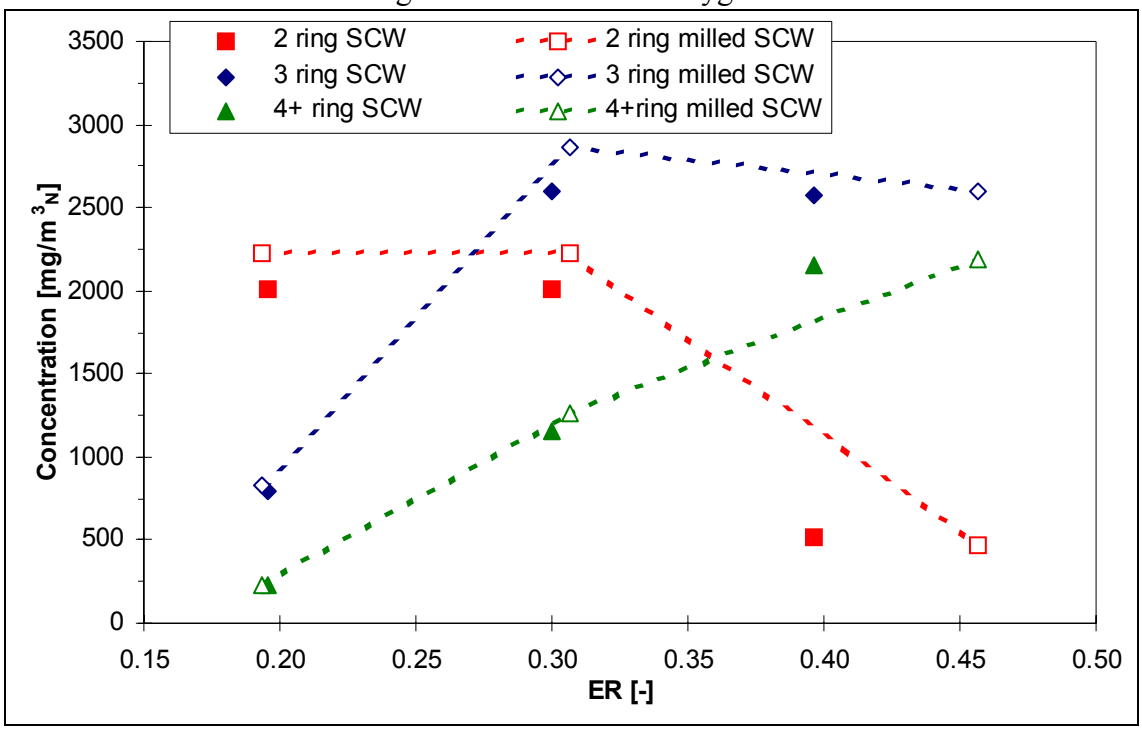

The small differences in the concentrations of the single tar classes are also reflected in the tar composition depicted in Figures 6.86 to 6.88.

Figure 6.86: Normalised tar composition for SCW and milled SCW gasification in steam/oxygen at ER ≈ 0.2.

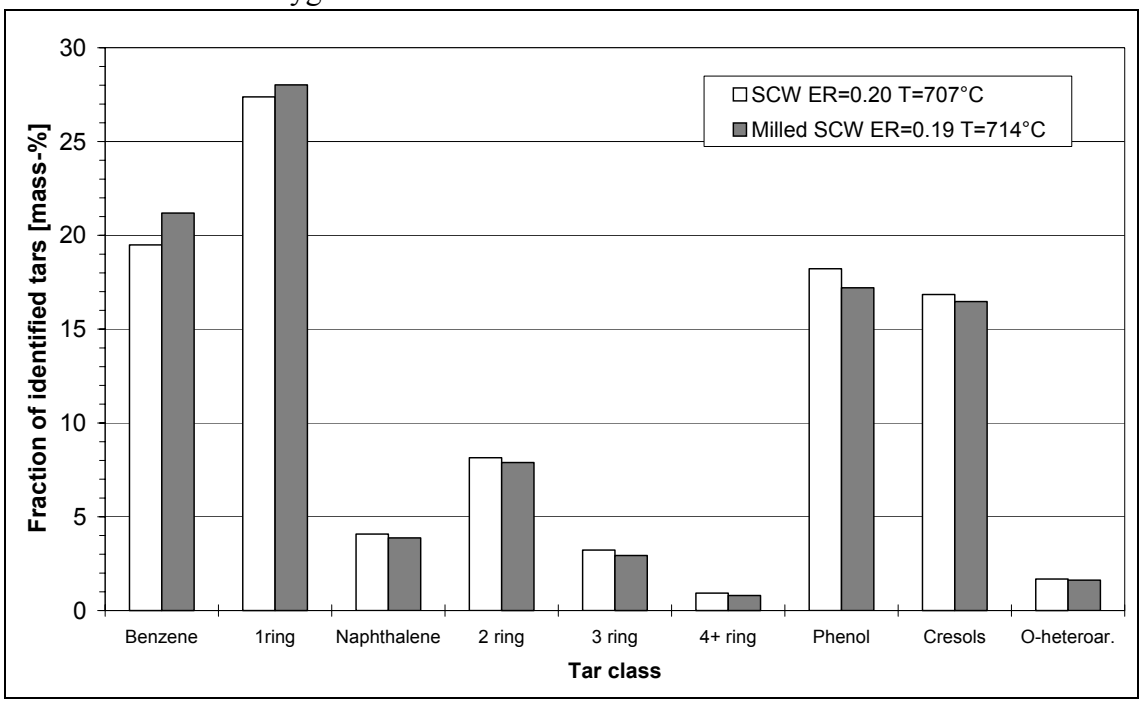

At ER ≈ 0.2 the milled SCW exhibits higher benzene and 1 ringed aromatics content. All other tar classes make up a lesser fraction of the tars of the comminuted fuel, the largest difference is seen in the phenolic compounds.

Figure 6.87: Normalised tar composition for SCW and milled SCW gasification in steam/oxygen at ER≈0.3.

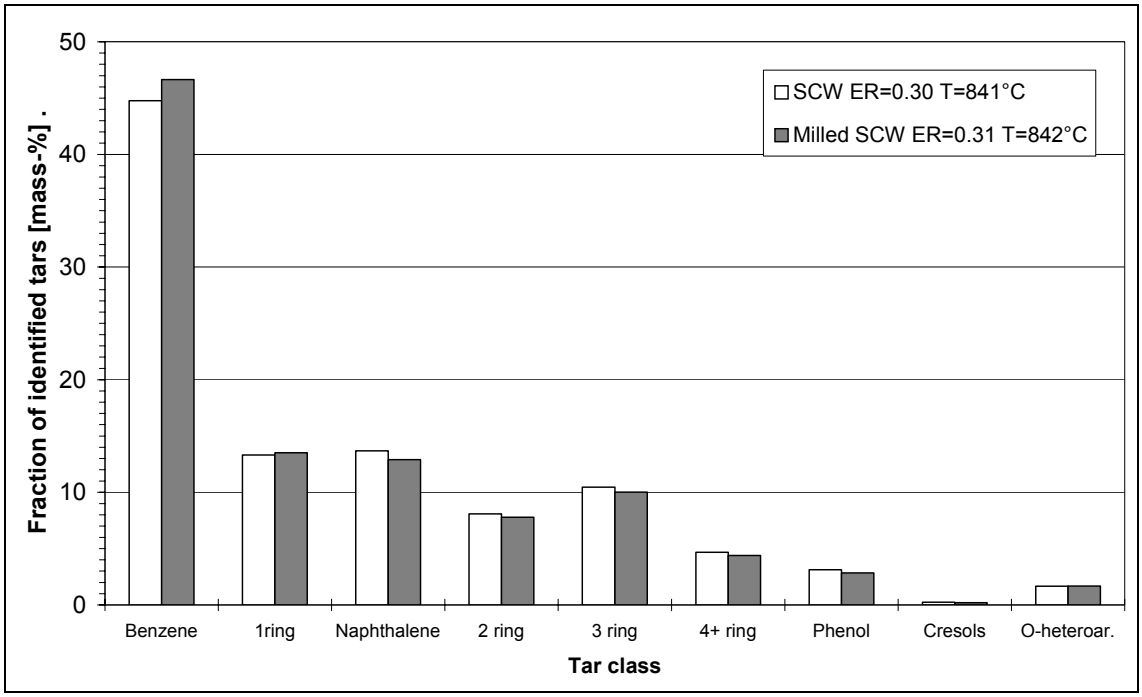

Figure 6.88: Normalised tar composition for SCW and milled SCW gasification in steam/oxygen at ER≥0.4.

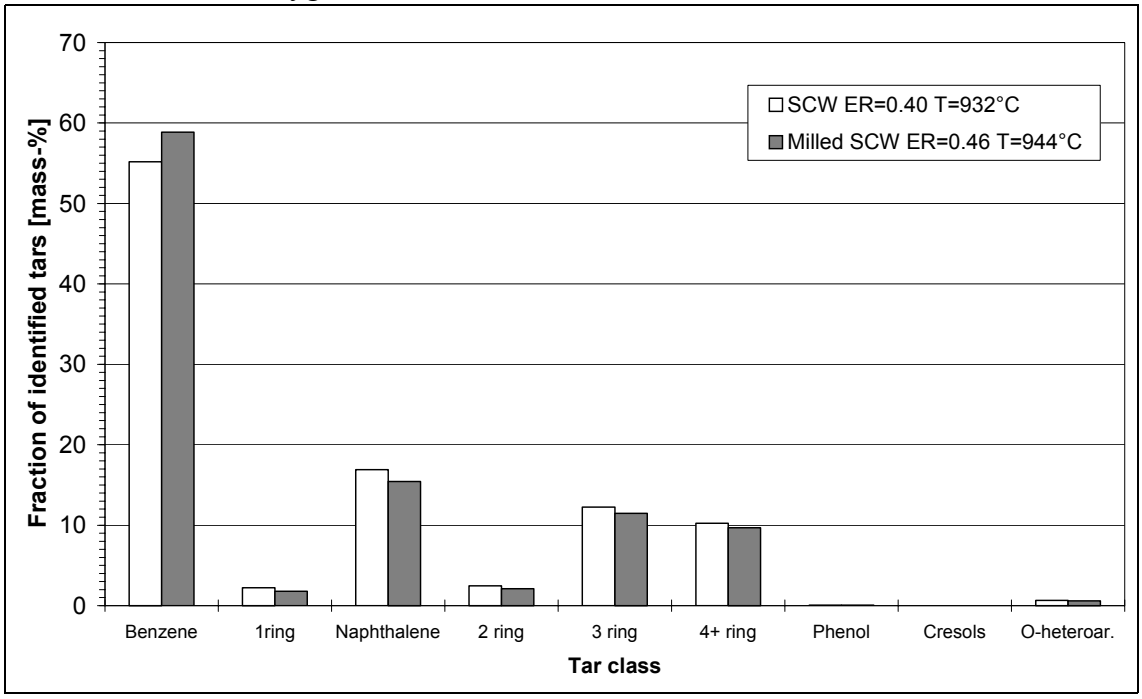

At ER ≈ 0.3, the tars are of very similar composition, with a somewhat higher fraction of benzene present in the tars from the smaller fuel.

The differences in tar composition at ERs higher than 0.4 is very similar to that observed at ER ≈ 0.3. A somewhat greater decrease in the fraction of naphthalene is observed for the milled fuel.

Summarising, the tars issued of both fuels are almost identical in composition at all ERs studied. Only an increase in the benzene contents of the tars is observed when the milled fuel is employed.

6.3 Influence of operational parameters

6.3.1 The gasification agent

With the experimental data gathered in the present study, a comparison of the results obtained with the gasification agents air and steam/oxygen may be carried out for both fuels, AH and SCW, depicting the influence of the gasification agent. The ER setpoints used in the experiments with either gasification agent for either fuel yielded very similar temperatures as shown in Figure 6.89. Either parameter can thus be used for discussion of the results and, as previously, the ER will be used.

The gas composition for these fuel/gasification agent combinations is shown in Figures 6.90 and 6.91. Notice that the gas composition is given on a dry, inert-free basis. The trends in the concentrations of all gas components in function of the ER for both fuels and in either gasification agent are the same.

Figure 6.89: Gasification temperatures as a function of ER for AH and SCW in air and steam/oxygen.

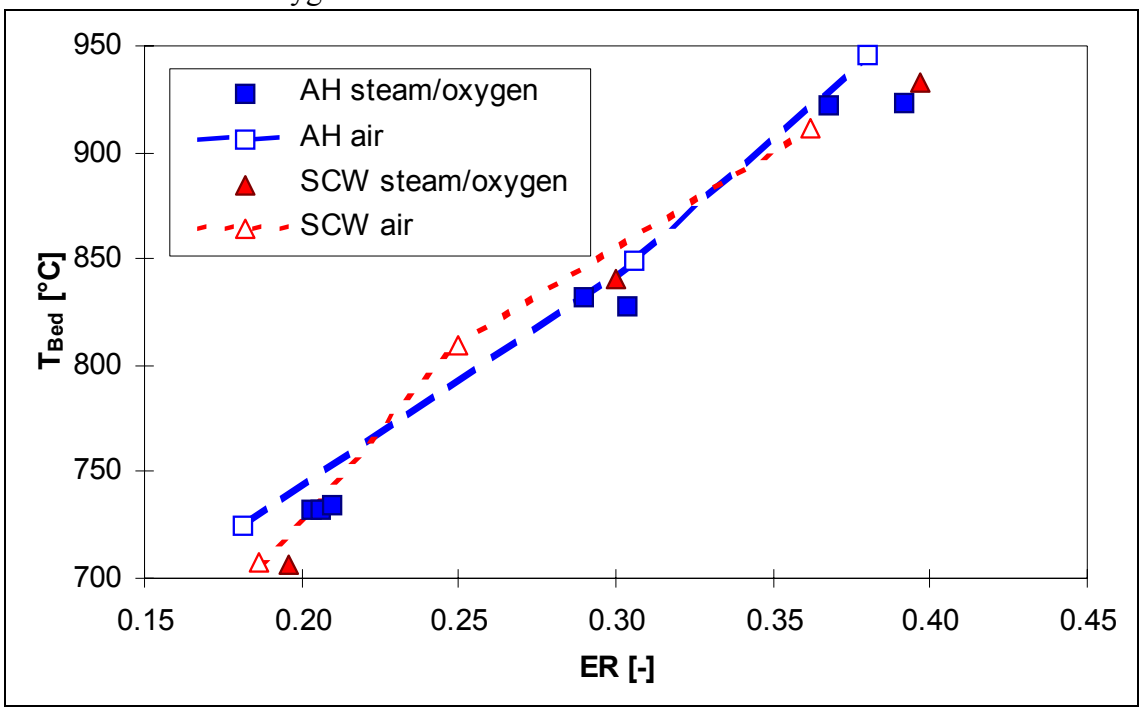

Figure 6.90: Gas composition versus ER for AH gasification in air and steam/oxygen.

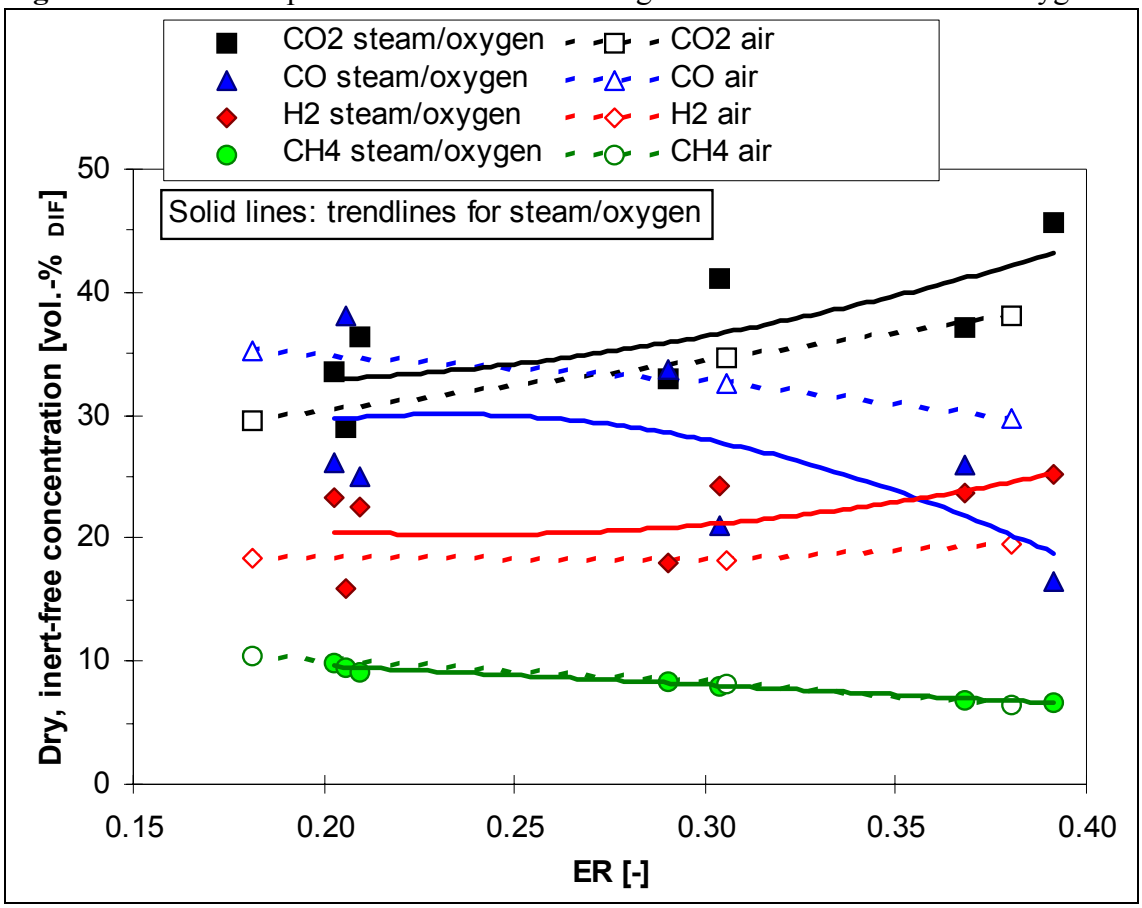

The results of the AH experiments show the marked influence of the homogeneous water-gas shift reaction ($CO + H_2O \rightarrow CO_2 + H_2$) on the gas composition when this fuel is gasified in steam/oxygen mixtures. The CO_2 and H_2 concentrations are higher in this gasification agent when compared to the results in air and at the same time the CO concentration is lower. CH_4 is not affected by the gasification agent.

Figure 6.91: Gas composition versus ER for SCW gasification in air and steam/oxygen.

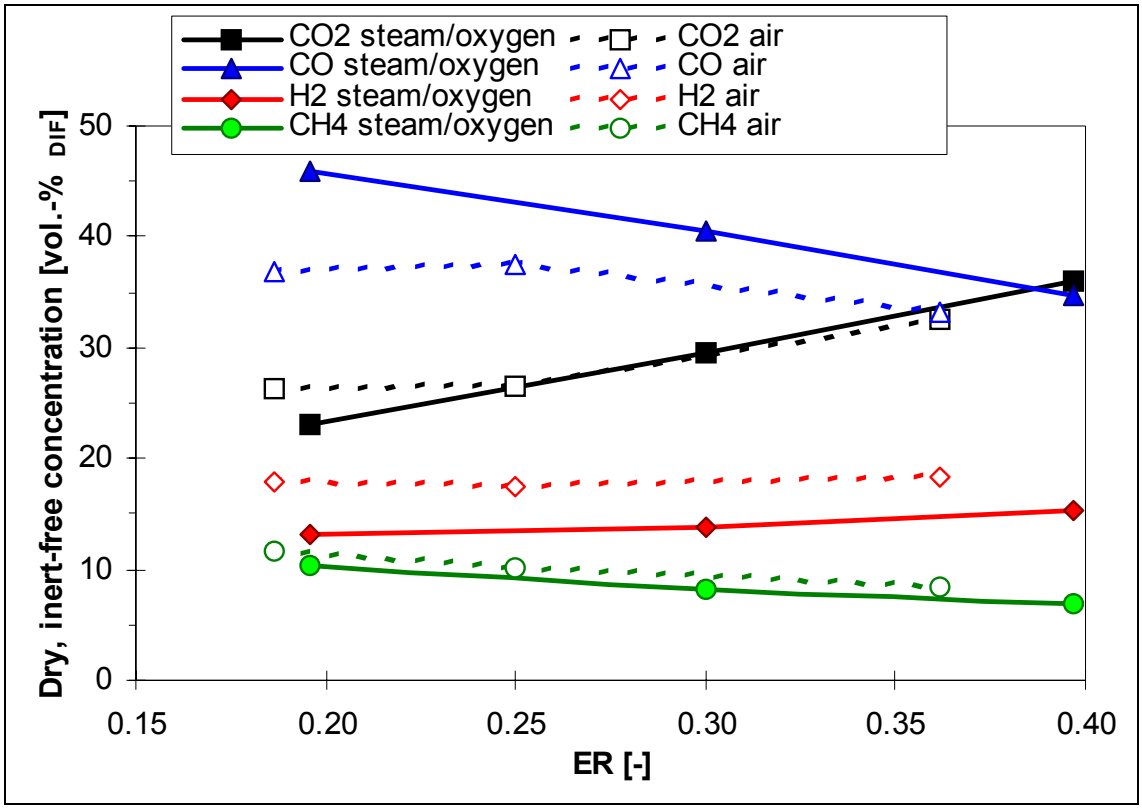

This influence cannot be determined for SCW. Here CO concentrations are higher in steam/oxygen, CO_2 does not seem to be influenced by the gasification agent and H_2 is clearly present in lower concentrations in the steam/oxygen results when compared to the gasification in air. A higher CO concentration could be tentatively explained by the heterogeneous water-gas shift reaction ($C_{(s)} + H_2O \rightarrow CO + H_2$) but the accompanying increase in H_2 concentration is not observed. The use of steam/oxygen mixtures as gasification agent for SCW affects the CH_4 concentration only marginally, lowering it slightly in comparison to the air results. The influence of the gasification agent on SCW observed in the present study is very similar to literature data [6.17]. In this reference the gas com-

position is however given on a dry basis, which enhances the differences between air and steam/oxygen due to the diluting effect of the N_2 in the air results.

The gas yields for both fuels and either gasification agent are plotted in Figure 6.92, again on a dry, inert-free basis. Air gasification clearly yields a larger amount of product gases compared to steam/oxygen gasification. This difference in the gasification agents is again similar to that reported in reference [6.17]. However, in this reference the ER is reported not to influence the gas yield in the case of steam/oxygen gasification as observed in the present study. The reason for this discrepancy is unclear.

Figure 6.92: Gas yield (dry, inert-free basis) for AH and SCW gasification in air and steam/oxygen mixtures.

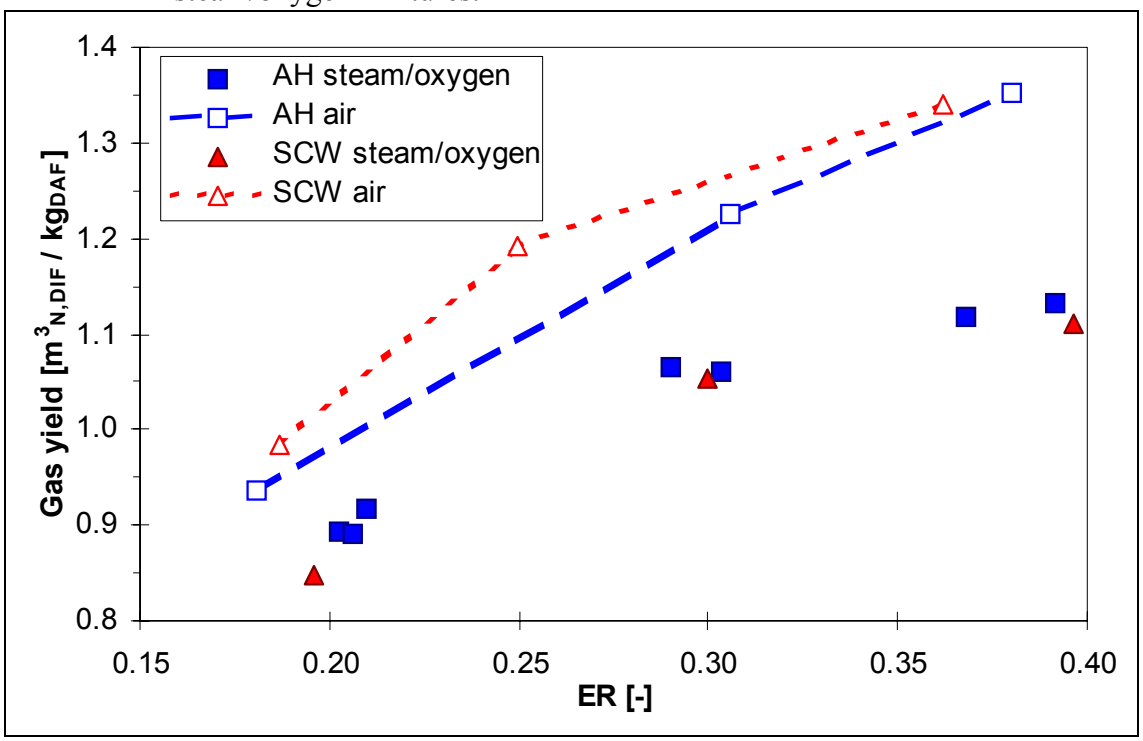

The total tar concentrations corrected with the fraction of tars identified (see page 178) are given in Figure 6.93 for all four combinations of fuel and gasification agent on a dry, inert-free basis. AH is seen to yield lower tar amounts than SCW, but the difference is less marked as in the previously used raw gas basis. The gasification agent does not appear to strongly influence the tar amount in the gases for either fuel with the exception of the result obtained gasifying SCW in steam/oxygen at low ER. The higher tar concentrations for steam/oxygen gasification compared to air reported in the literature (e.g. [6.17]), must therefore be assigned to the dilution of the gases by nitrogen in the air case.

The reason for the higher tar concentration for the SCW in steam/oxygen could be attributed to the more secondary nature of the tars indicated by the lower fraction of tars detected by the measurement method employed in the present study, see Figure 6.35 on page 196.

Figure 6.93: Corrected total tar concentrations for AH and SCW gasification in air and steam/oxygen mixtures on dry, inert-free basis

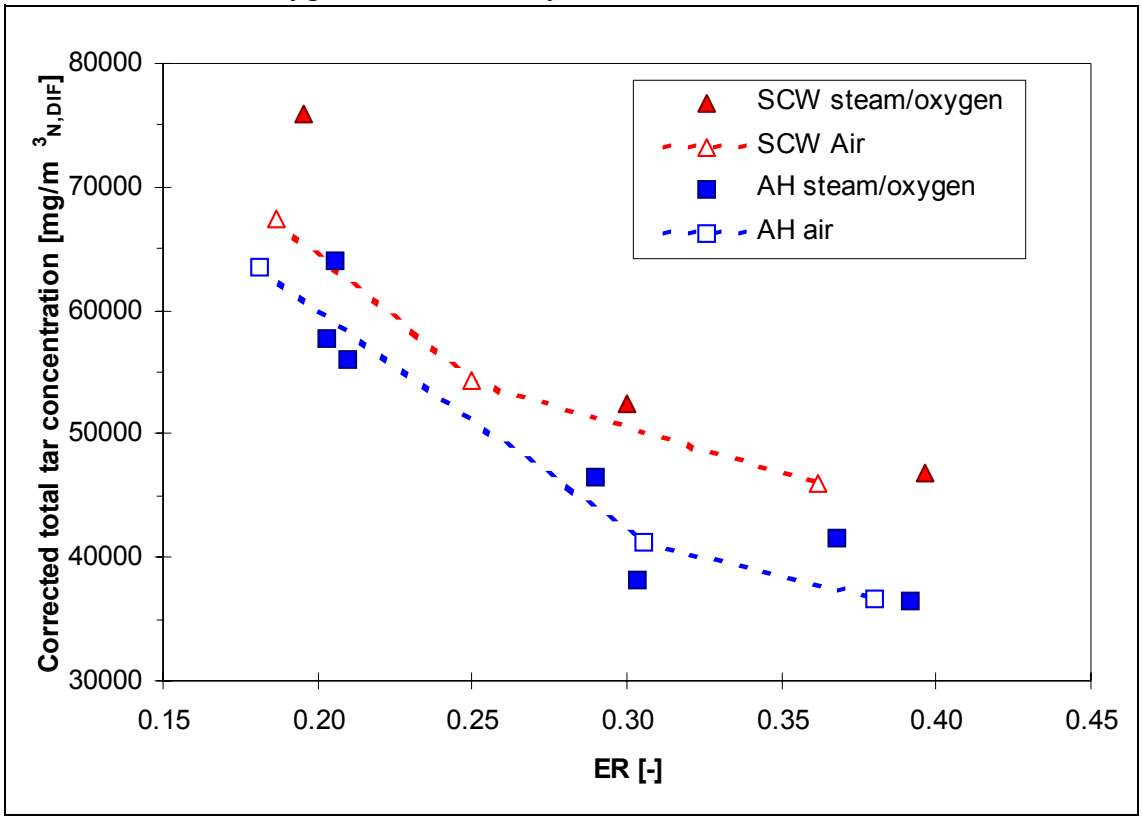

The evolution of the tar classes on a dry, inert-free basis is shown in Figures 6.94 to 6.96 for SCW in both gasification agents. For SCW the influence of the gasification agent is almost negligible. Benzene concentrations are lowered slightly in steam/oxygen compared to air. All other tar classes exhibit the same concentrations independently of the gasification agent.

Figure 6.94: Tar classes concentration evolution (major aromatics, dry, inert-free basis) with ER for SCW gasification in air and steam/oxygen.

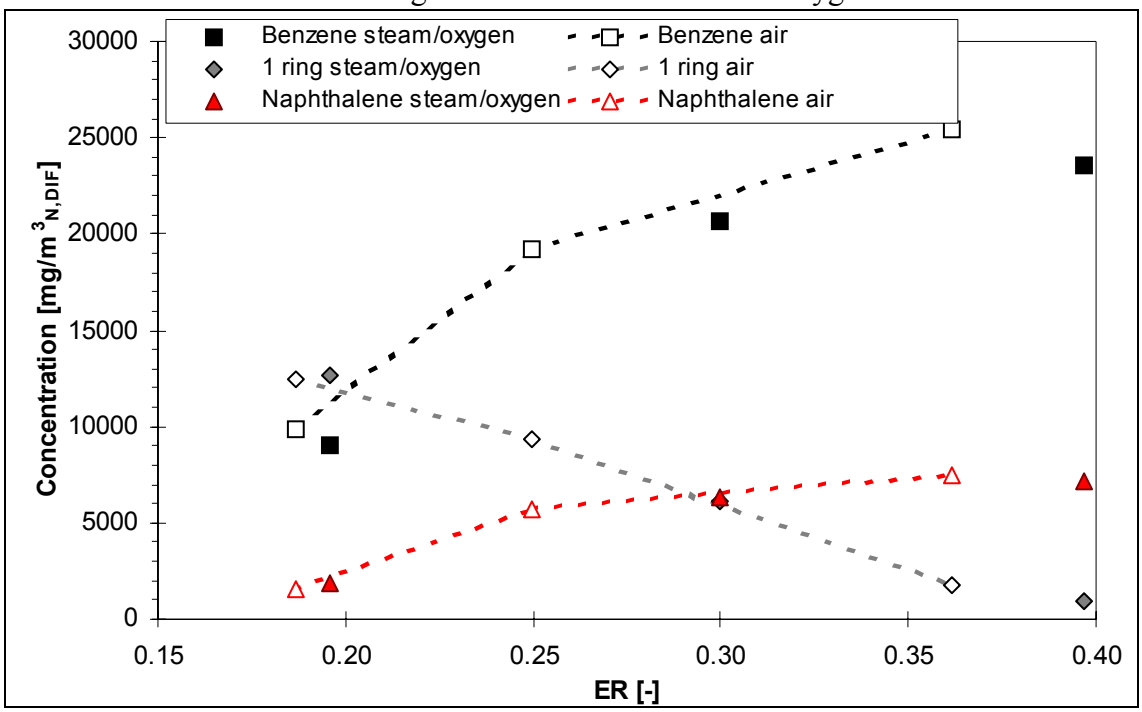

Figure 6.95: Tar classes concentration evolution (oxygenates, dry, inert-free basis) with ER for SCW gasification in air and steam/oxygen.

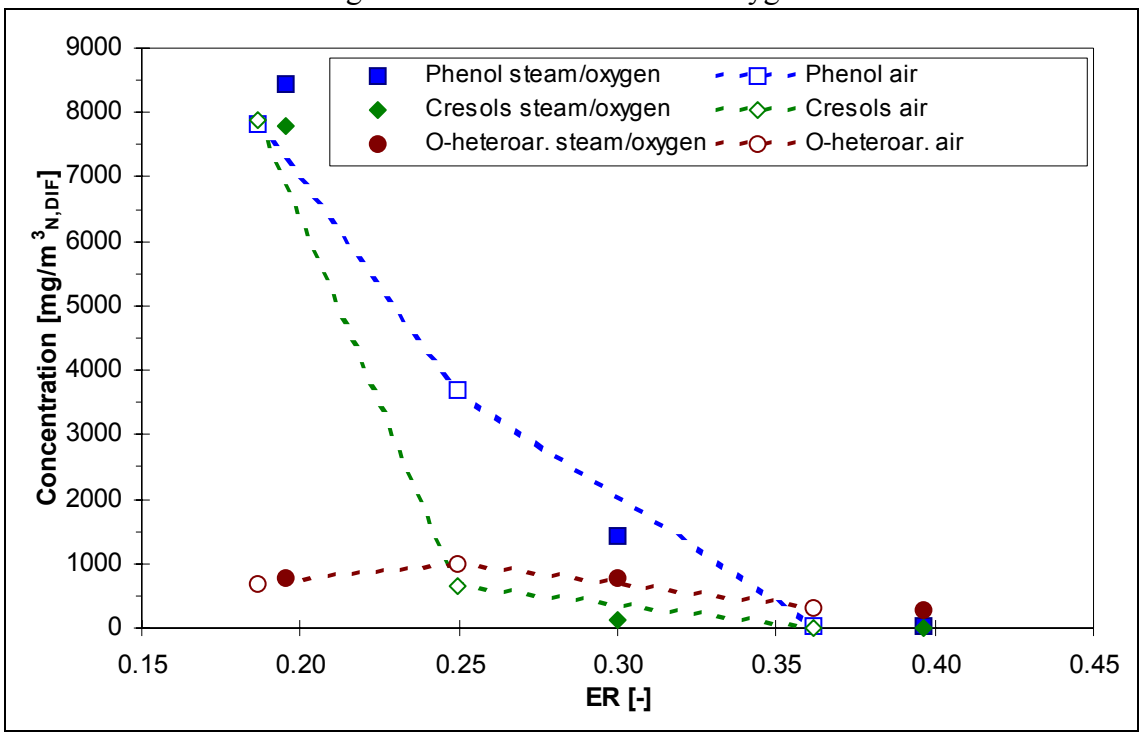

Figure 6.96: Tar classes concentration evolution (minor aromatics, dry, inert-free basis) with ER for SCW gasification in air and steam/oxygen.

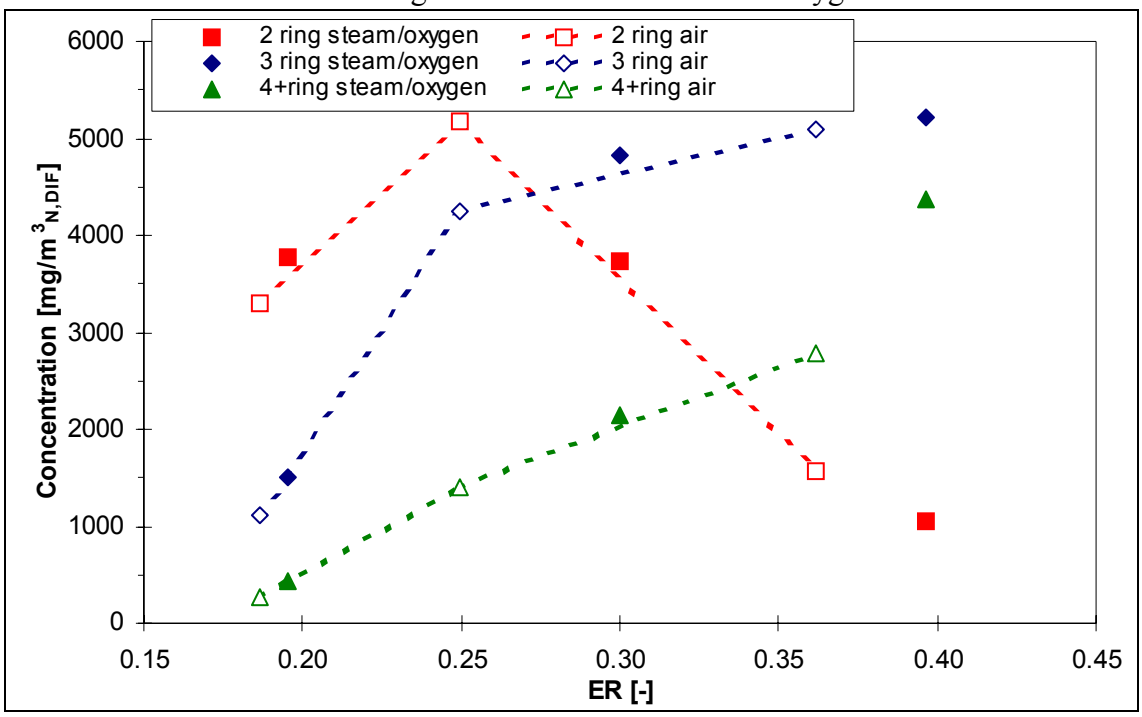

Figures 6.97 to 6.99 show the evolution of the tar classes concentrations for AH in both gasification agents.

Figure 6.97: Tar classes concentration evolution (major aromatics, dry, inert-free basis) with ER for AH gasification in air and steam/oxygen.

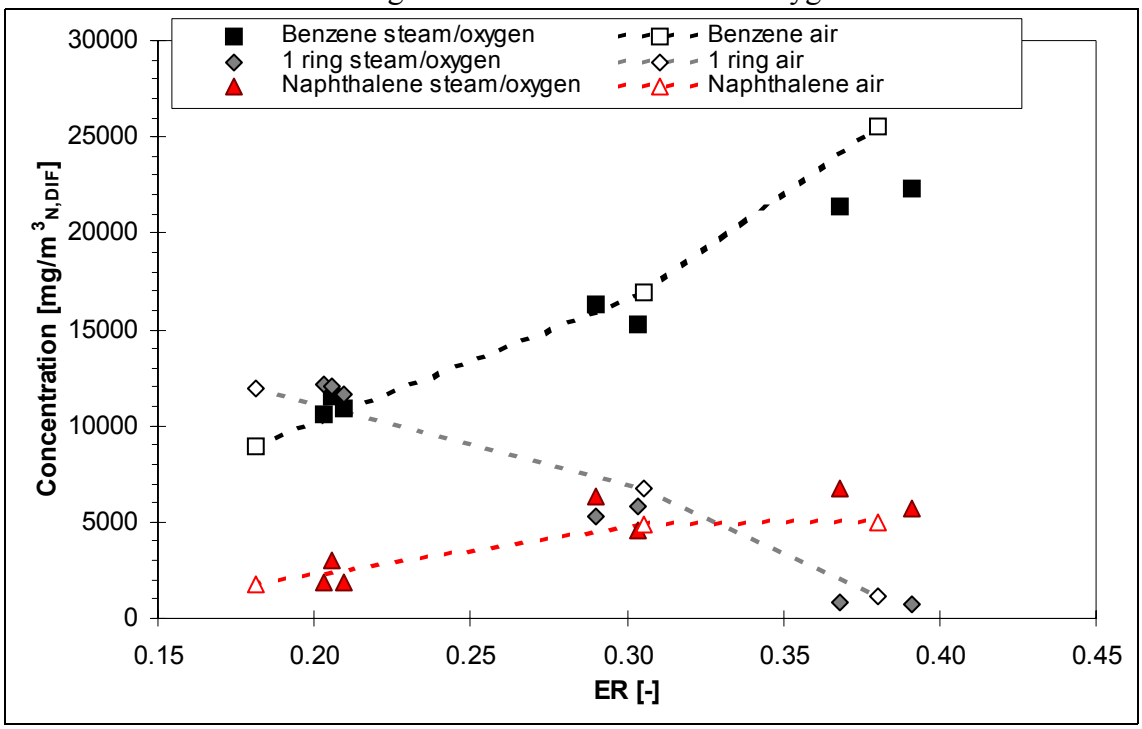

Figure 6.98: Tar classes concentration evolution (oxygenates, dry, inert-free basis) with ER for AH gasification in air and steam/oxygen.

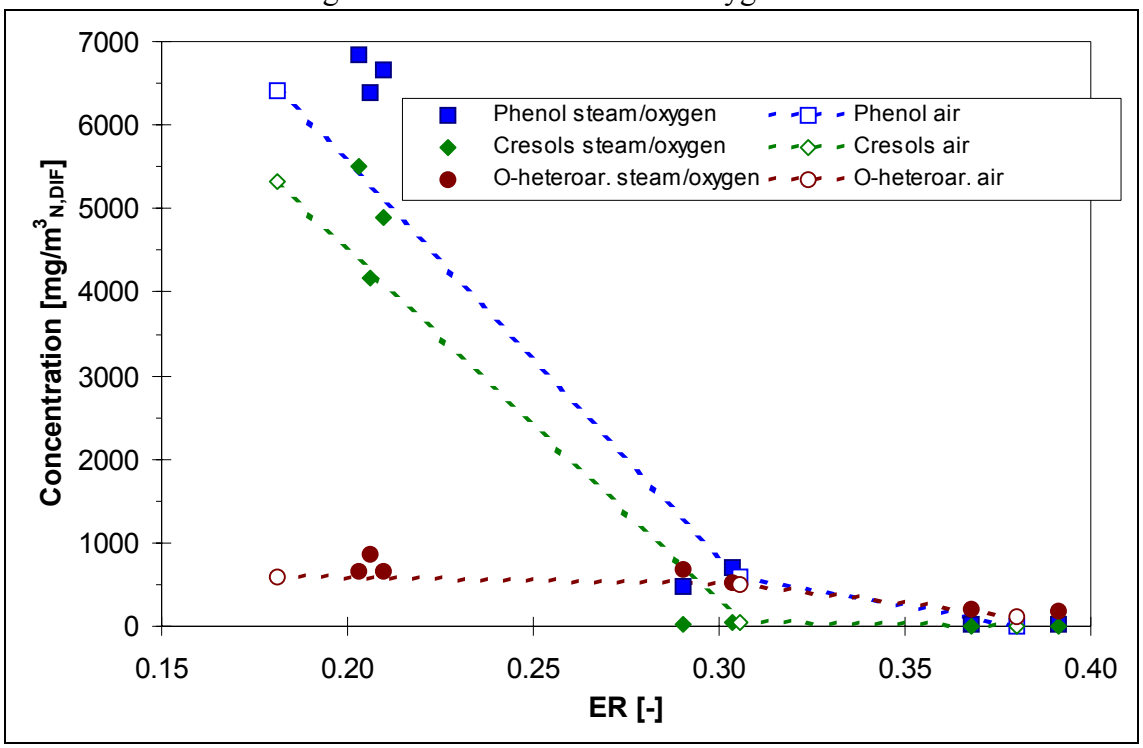

Figure 6.99: Tar classes concentration evolution (minor aromatics, dry, inert-free basis) with ER for AH gasification in air and steam/oxygen.

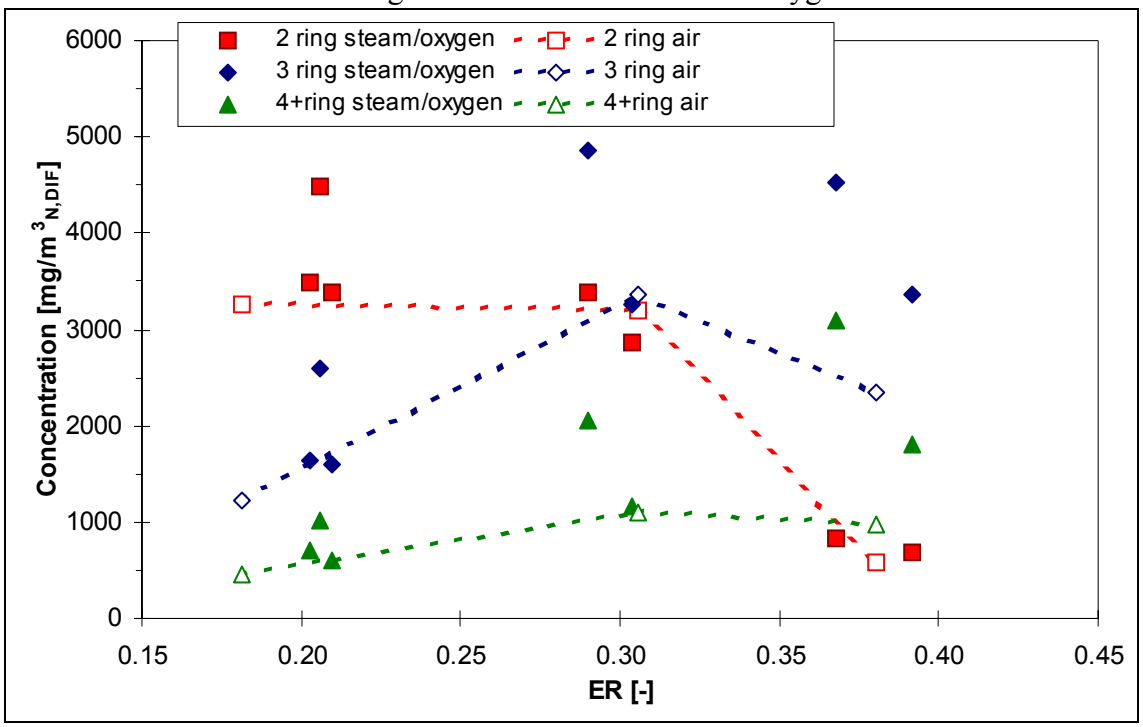

For AH the gasification agent is seen to also have only a minor influence on the tar concentrations of most tar components. The largest aromatic compounds (3 and more

rings) are however observed in larger concentrations in the steam/oxygen products at high ER. In summary, the tars from both fuels are seen to behave similarly, if not identically, in either gasification agent.

The tar composition for either fuel and both gasification agents is shown in Figures 6.100 to 6.105 for the different ER ranges studied. The tar composition at a given ER is seen to be largely independent of gasification agent. The comparatively large differences for SCW at intermediate ER in Figure 6.101 are probably due to the relatively large difference in ER in the two runs involving this fuel in the different gasification agents (0.25 in air and 0.3 in steam/oxygen).

Figure 6.100: Normalised tar composition for SCW gasification in air and steam/oxygen at ER≈0.2.

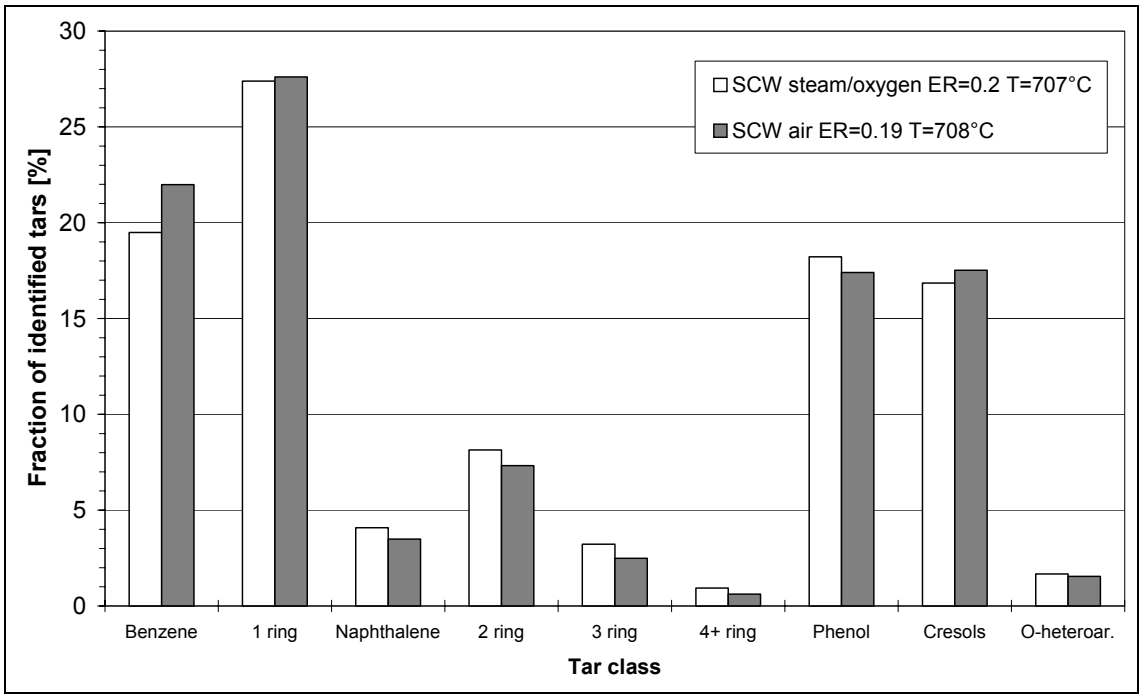

Figure 6.101: Normalised tar composition for SCW gasification in air and steam/oxygen at ER≈0.3.

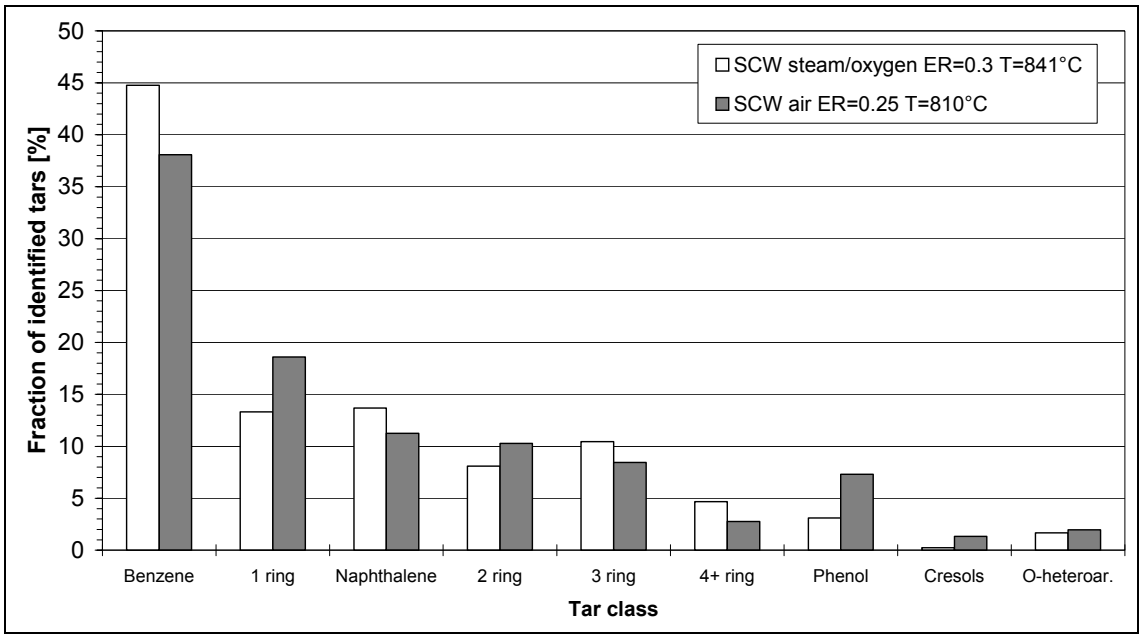

Figure 6.102: Normalised tar composition for SCW gasification in air and steam/oxygen at ER≈0.4.

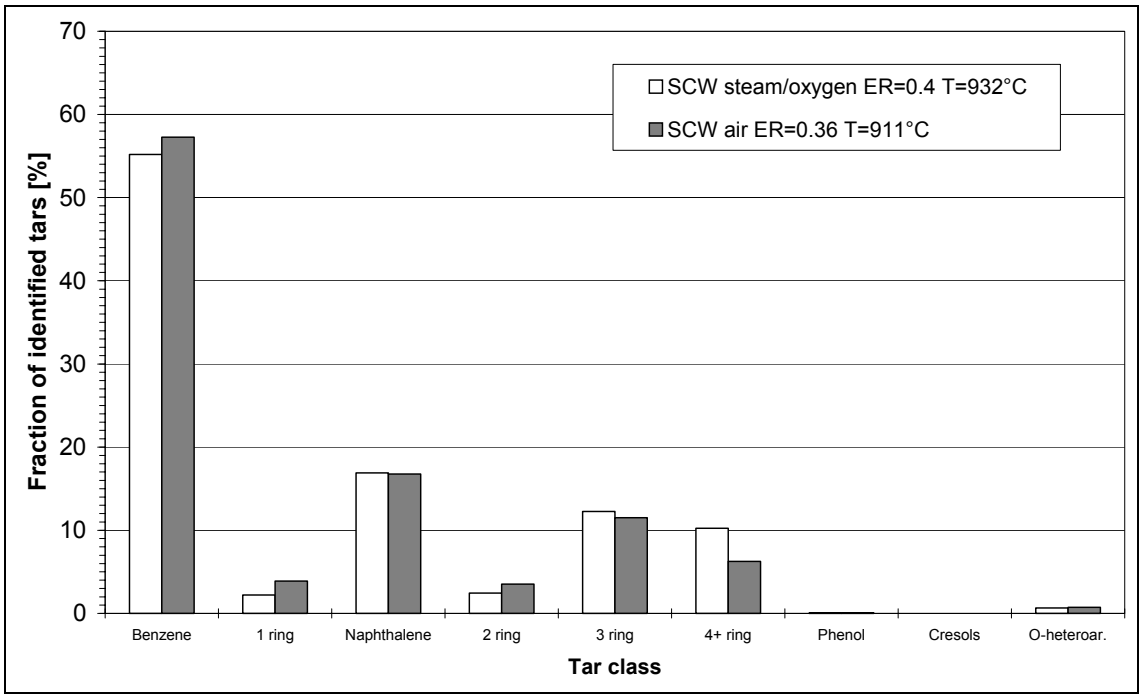

Figure 6.103: Normalised tar composition for AH gasification in air and steam/oxygen at ER≈0.2.

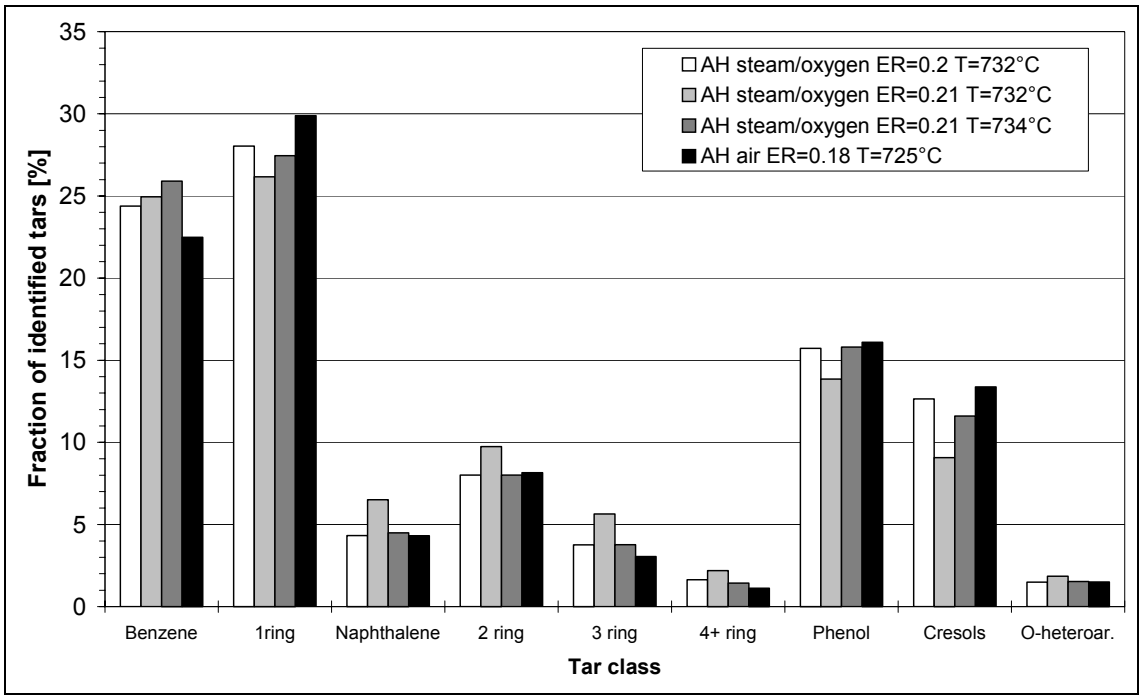

Figure 6.104: Tar composition for AH gasification in air and steam/oxygen at ER≈0.3.

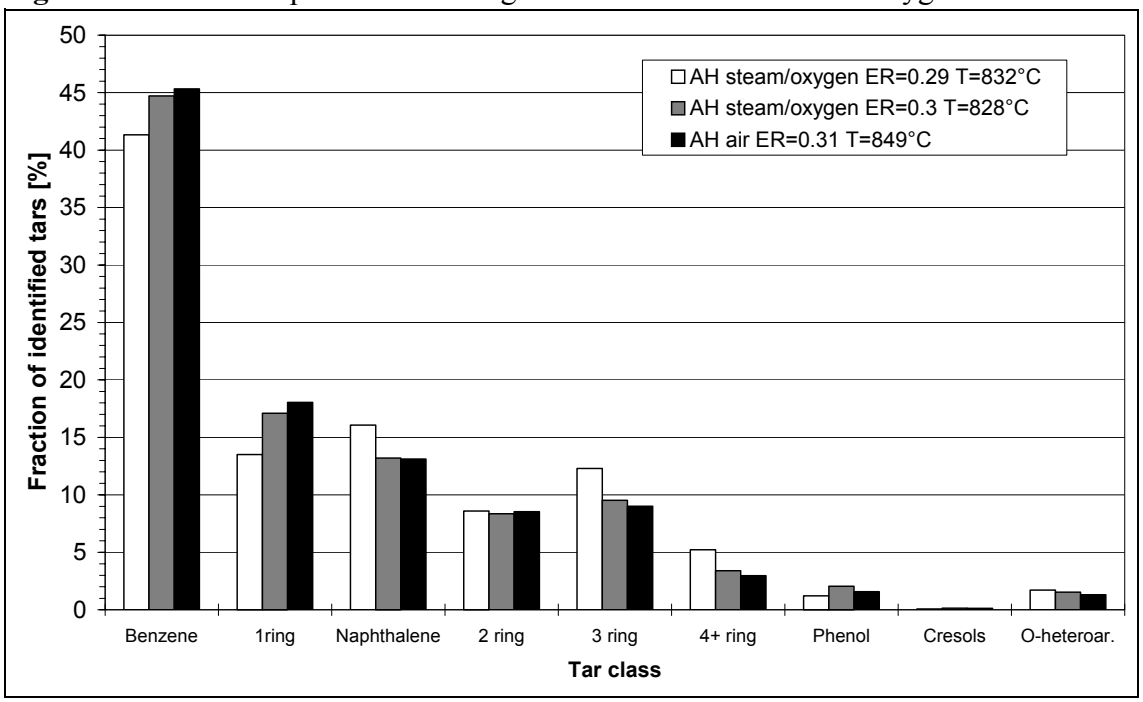

Figure 6.105: Normalised tar composition for AH gasification in air and steam/oxygen at ER ≈ 0.4.

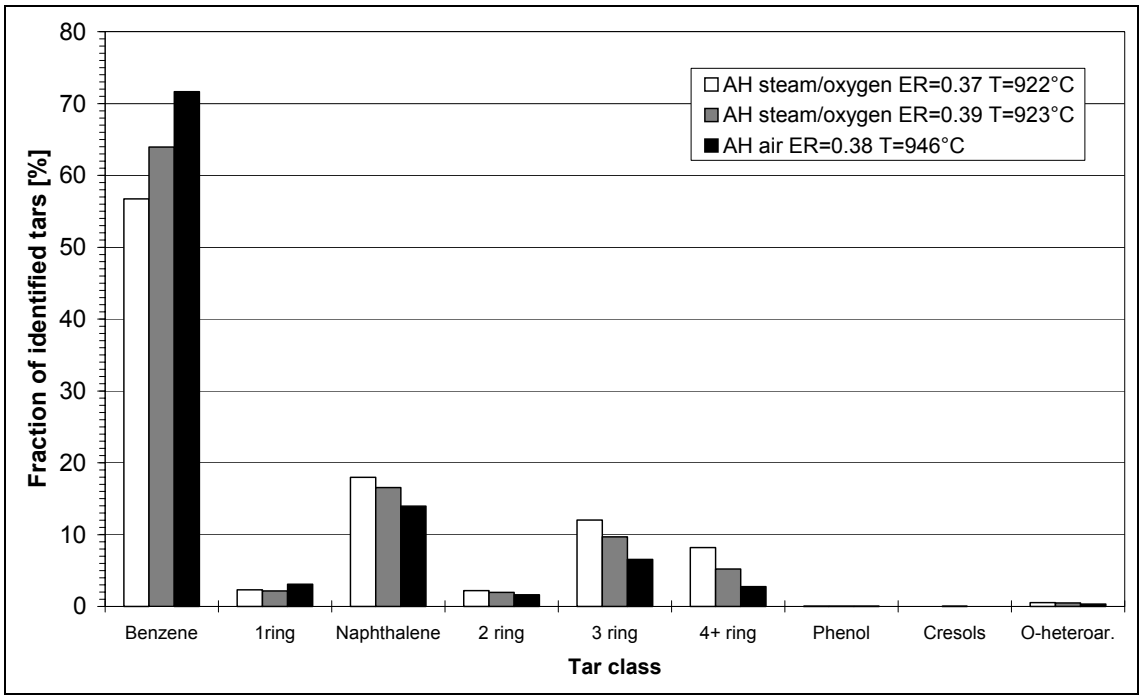

6.3.2 Steam to biomass ratio

To test for the influence of the relative amount of steam added (the so-called steam to biomass ratio), experiments 990706 and 990729 were carried out using twice the "normal" steam input to the reactor, or 11.6 kg/h. Experiment 990706 had to be aborted after the second ER set-point. A large and potentially dangerous gas leak was detected due to a defective gasket between the flanges of two freeboard modules. The tar and water measurement during run A must be discarded, as a large leak in the sampling train was observed. Due to these reasons only the data generated in 990706B is considered meaningful and therefore only this data is presented in the appendix and discussed in this chapter.

The bed temperatures were ca. 30°C lower at comparable ER set-points for the experiments at higher steam input as shown in Figure 6.106. This difference is probably due to a larger energy output from the bed due to the higher gas mass flow exiting this part of the reactor. Nevertheless, the discussion of the results will be made in function of the ER.

Figure 6.106: Bed temperatures for AH gasification at different steam input mass flows.

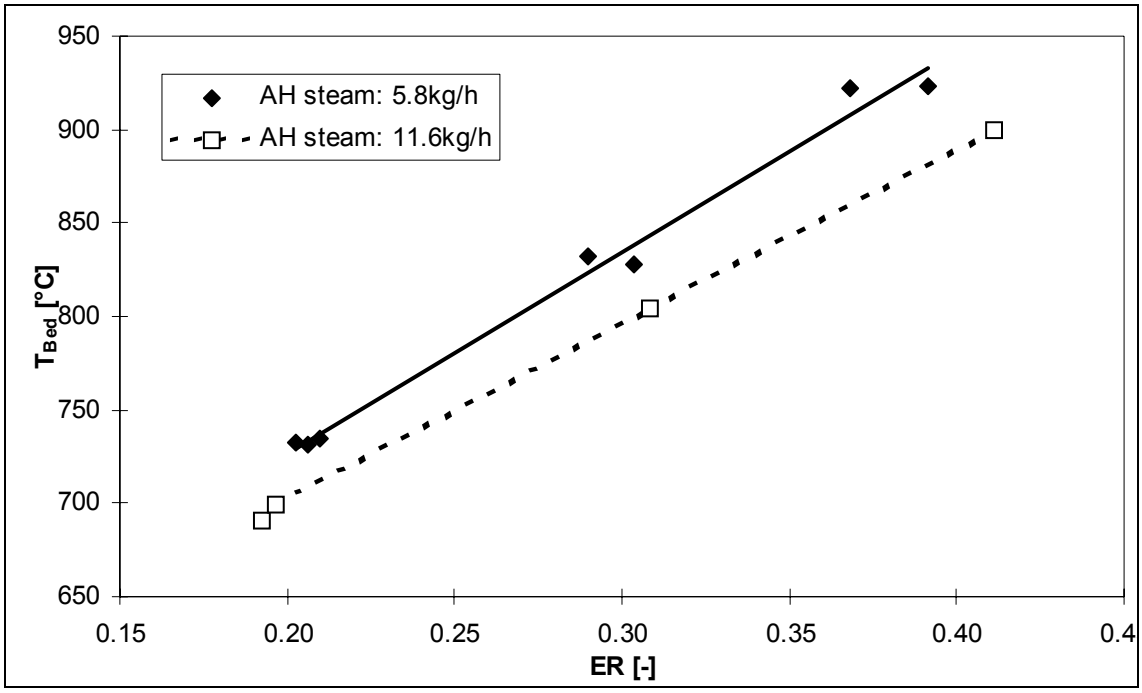

Figure 6.107: Steam concentration for AH gasification experiments at different steam input to the reactor.

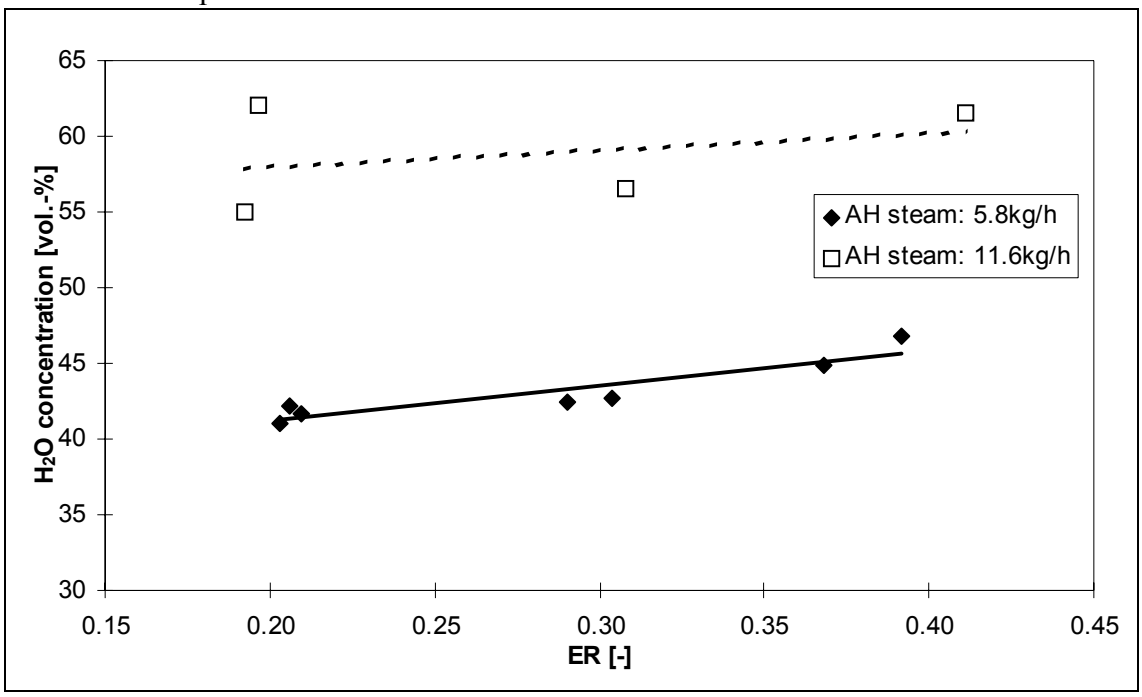

As shown in Figure 6.107 the higher steam input to the reactor yields higher steam concentrations in the gas. Even though the operational procedure of the reactor implies a change in the steam to biomass ratio in an experiment with constant steam input,

Figure 6.108 clearly shows that in these experiments at higher steam input this value was dramatically changed for a given ER.

Figure 6.108: Steam to biomass ratio for AH gasification experiments at different steam input to the reactor.

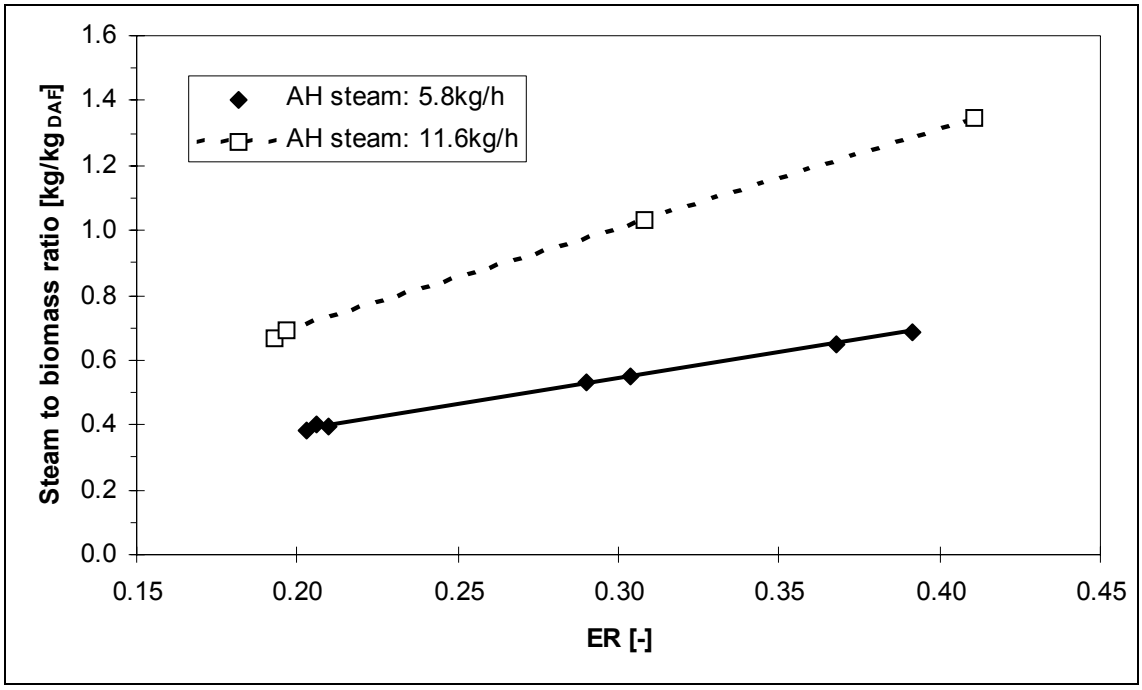

Figure 6.109: Dry, inert-free gas composition versus ER for AH experiments at different steam input mass flows.

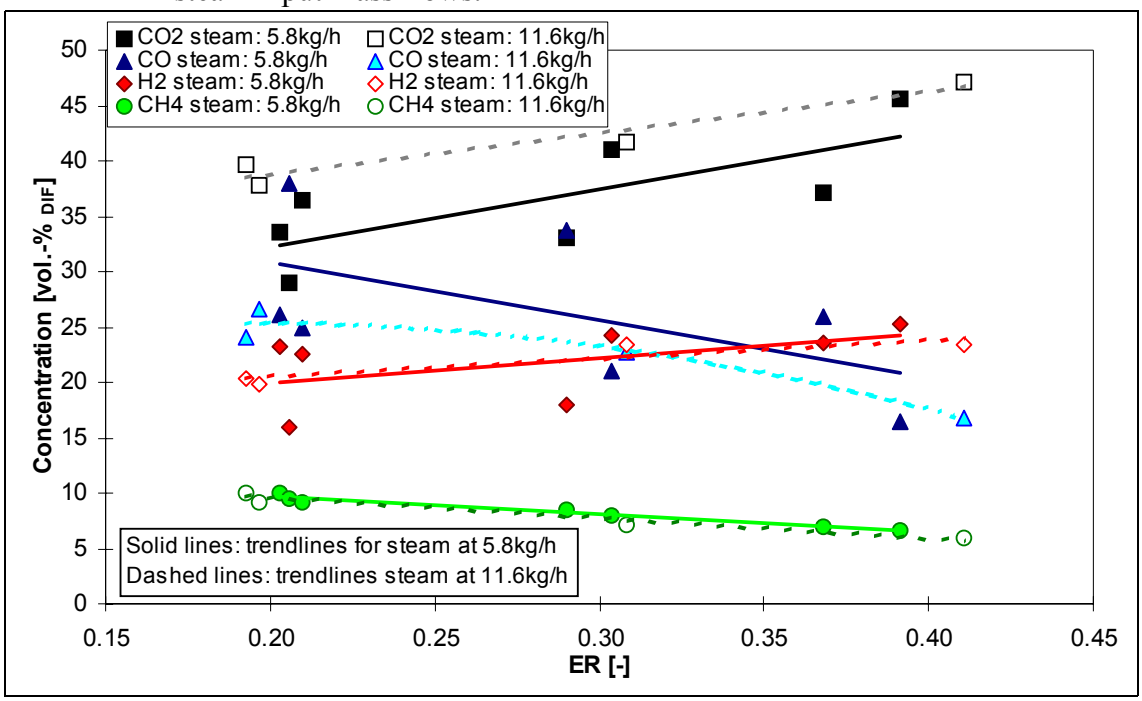

The gas composition is given in Figure 6.109 on a dry, inert-free basis to suppress the effect of dilution by the larger steam amount present in the gas. H_2 and CH_4 are seen not to be affected by the larger steam to biomass ratio. On the other hand, CO is lowered and CO_2 is increased in the experiments at higher steam input. The explanation at hand would be an increased conversion of the CO according to the homogeneous water-gas shift reaction $CO + H_2O \rightarrow CO_2 + H_2$. The increase in H_2 predicted by this hypothesis is however only detected when the equivalence ratio is properly redefined.

The ER definition used so far only accounts for the oxygen input by either fuel, air or oxygen. If the above data is plotted against a "total" ER (TER), which includes the oxygen input by the steam, Figure 6.110 is obtained.

Figure 6.110: Dry, inert-free gas composition evolution versus "total" ER for AH experiments at different steam input mass flows.

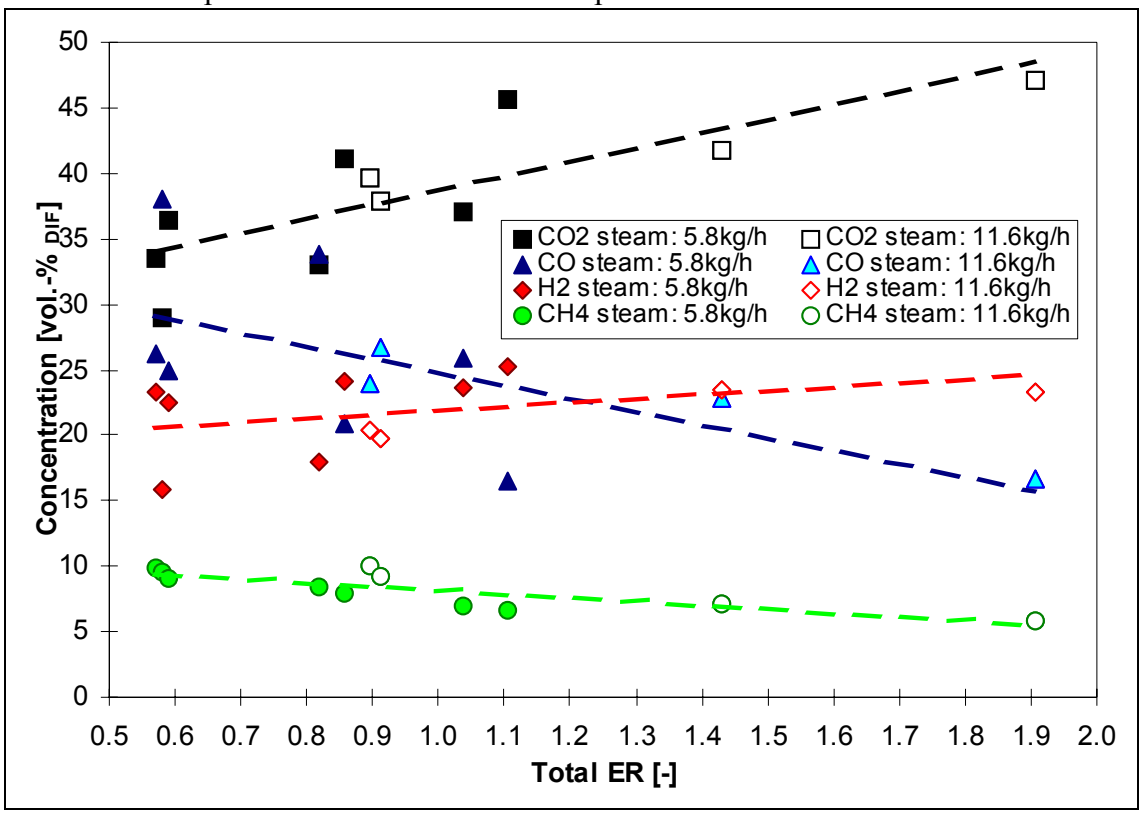

The oxidising effect of the larger steam input is clearly seen from this plot. The gas composition evolution of all components from all experiments is seen to follow approximately the same trend. As TER is increased the gas composition obtained is seen to become stronger influenced by the above mentioned homogeneous water-gas shift reaction.

A similar influence on the heterogeneous water-gas shift reaction ($C_{(s)} + H_2O \rightarrow CO + H_2$) could be expected. If the increased steam input increases the conversion of solid carbon, lower carbon content in the solids exiting the reactor may be expected. Figure 6.111 does however show, that the carbon content of the solids in the experiments at higher steam input is higher. This effect may be attributed to the lower residence times resulting from the increased gas throughput through the reactor. The particles carried out of the bed exit the reactor in a shorter time in the experiment at higher steam mass flow. These particles have therefore less time to react and exhibit thus a higher carbon content.

Figure 6.111: Carbon content of solids for AH gasification experiments at different steam input mass flows.

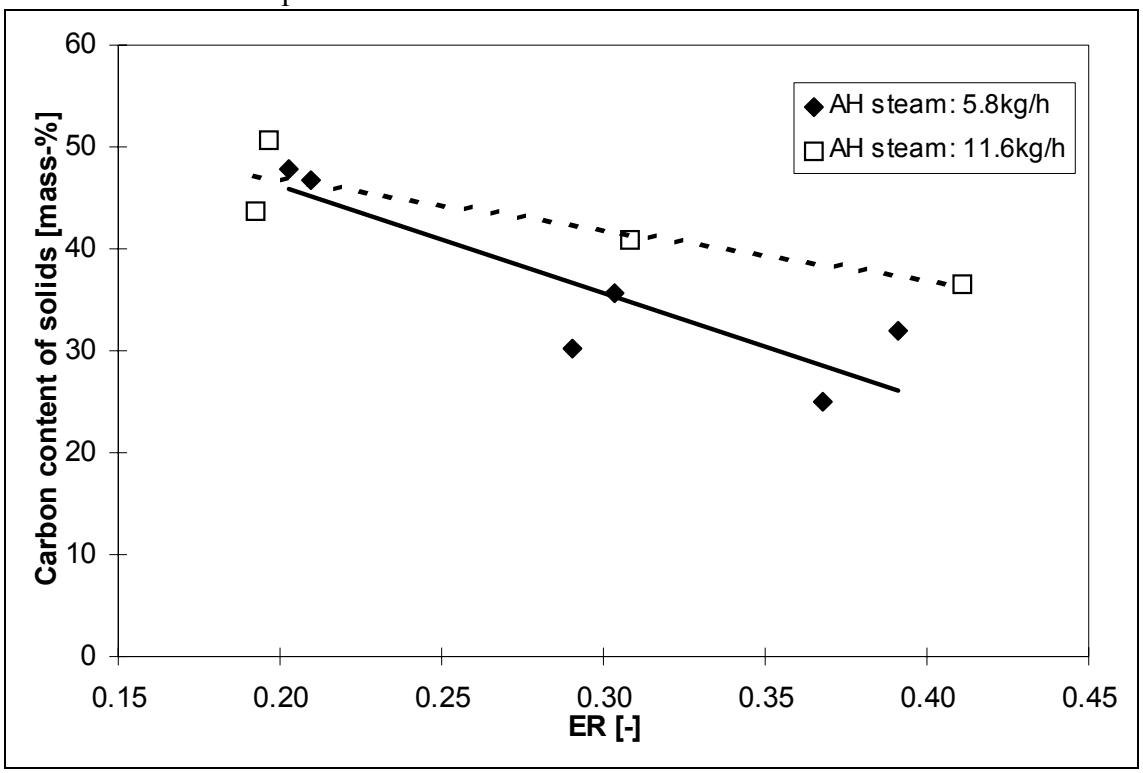

A comparison with the gas composition predicted by thermodynamic equilibrium calculations is shown in Figure 6.112. The thermodynamic equilibrium is clearly not attained. It is interesting to note that the CO_2 concentrations measured do however match those predicted by the calculations quite closely.

Figure 6.112: Measured, thermodynamic equilibrium and reformed gas composition for AH gasification at a steam input mass flow of ca. 11.6 kg/h

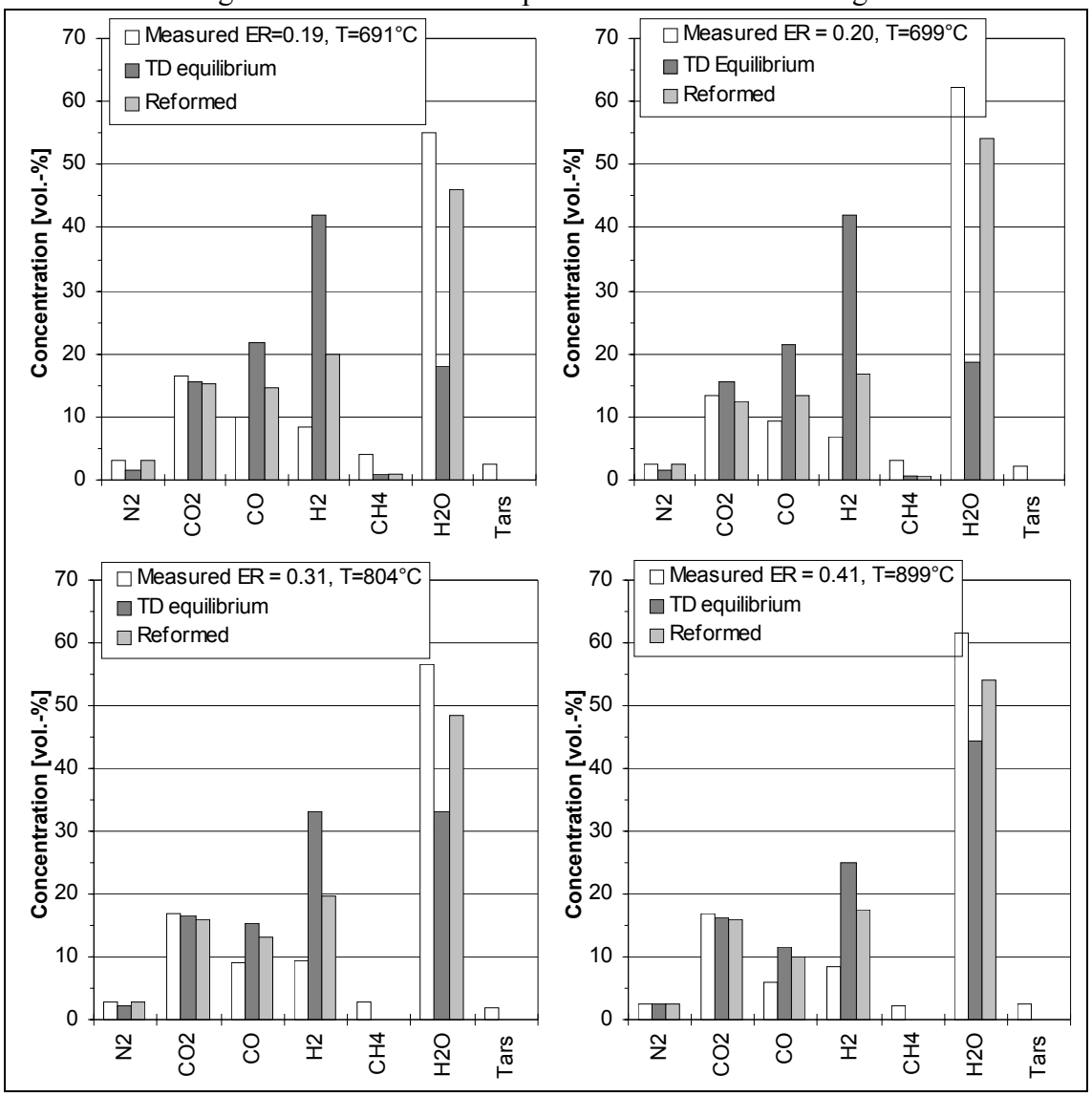

The total tar concentrations measured are displayed in Figure 6.113 on a dry, inert-free basis to cancel the dilution effect of the higher steam content and of the nitrogen in the gas. At low ER the higher steam input to the reactor appears to reduce the total tar concentration in the gases. The tar concentration does exhibit an unexpected minimum at ER ≈ 0.3.

Figure 6.113: Total tar concentration (DIF basis) for AH gasification at different steam input mass flow versus ER.

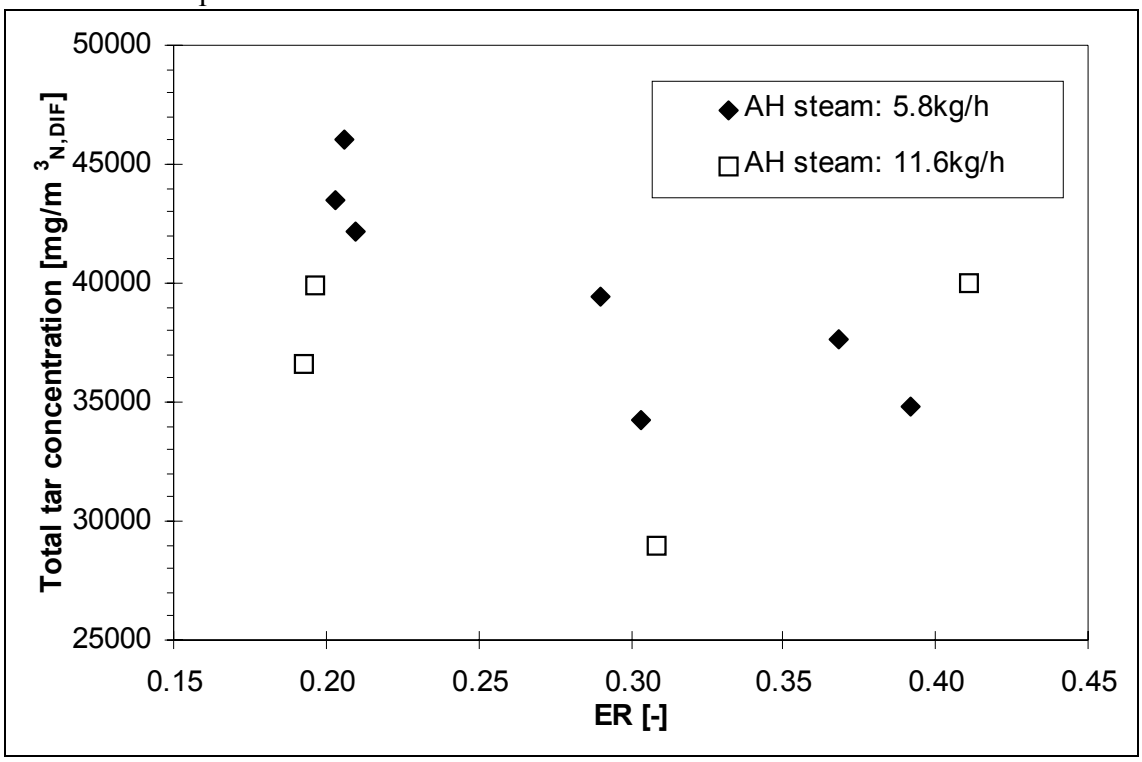

Figure 6.114: Estimated fraction of tar components identified by GC/MSD method for AH gasification with different steam input mass flows.

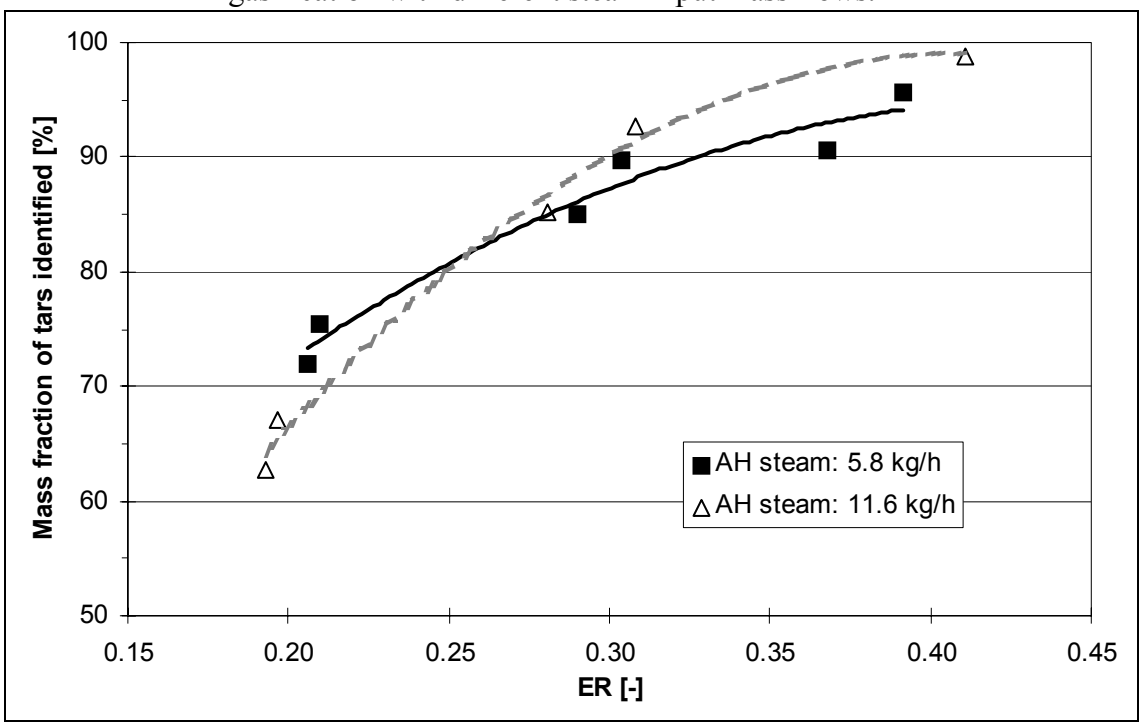

The estimation of the identified tar components has again been done for these experiments at higher steam input mass flow and the results are shown in Figure 6.114. For

the high ER experiments with high steam throughput a very small increase in the amount of identified tar components is observed. For the low ER runs on the other hand the fraction of unidentified tars is markedly higher than that observed in the runs using a lower steam throughput.

Figure 6.115: Corrected total tar concentrations (DIF basis) for AH gasification at different steam input mass flows.

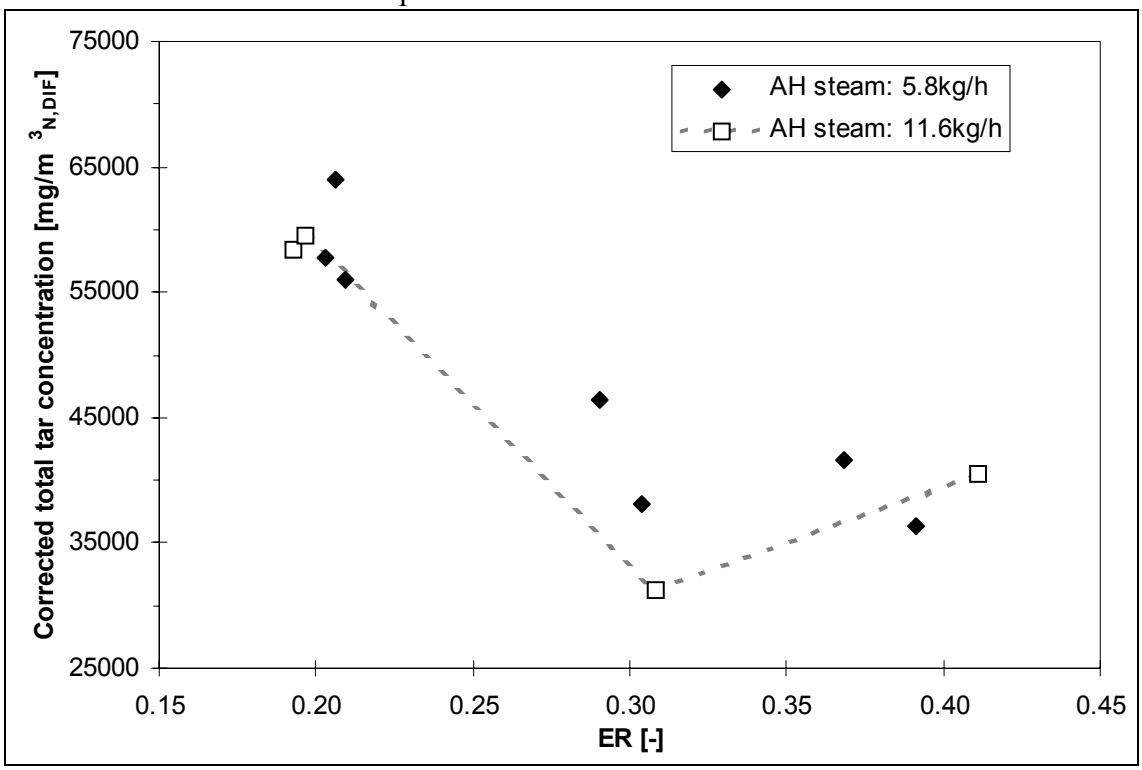

The corrected total tar concentration, taking into account the fraction of identified tar species is shown in Figure 6.115. In this plot the differences between the low and high steam throughput experiments diminish. This observation is however not in line with data published in the literature (e.g [6.19]). An increase in the steam-to-biomass (S/B) ratio should bring about a reduction in the tar concentrations. It is possible that this discrepancy may be assigned to differences in the tar measurement methods employed, or that the range of S/B ratios used in the present study is not large enough to allow the observation of a reduction in the tar concentrations.

The tar classes evolution is shown in Figures 6.116, 6.117 and 6.118. The higher steam content affects the benzene and naphthalene concentrations, lowering both at low ER. However, benzene concentrations are similar in both steam environments at comparable high ER.

Figure 6.116: Tar classes evolution (major aromatics, DIF basis) for AH gasification at different steam input mass flows.

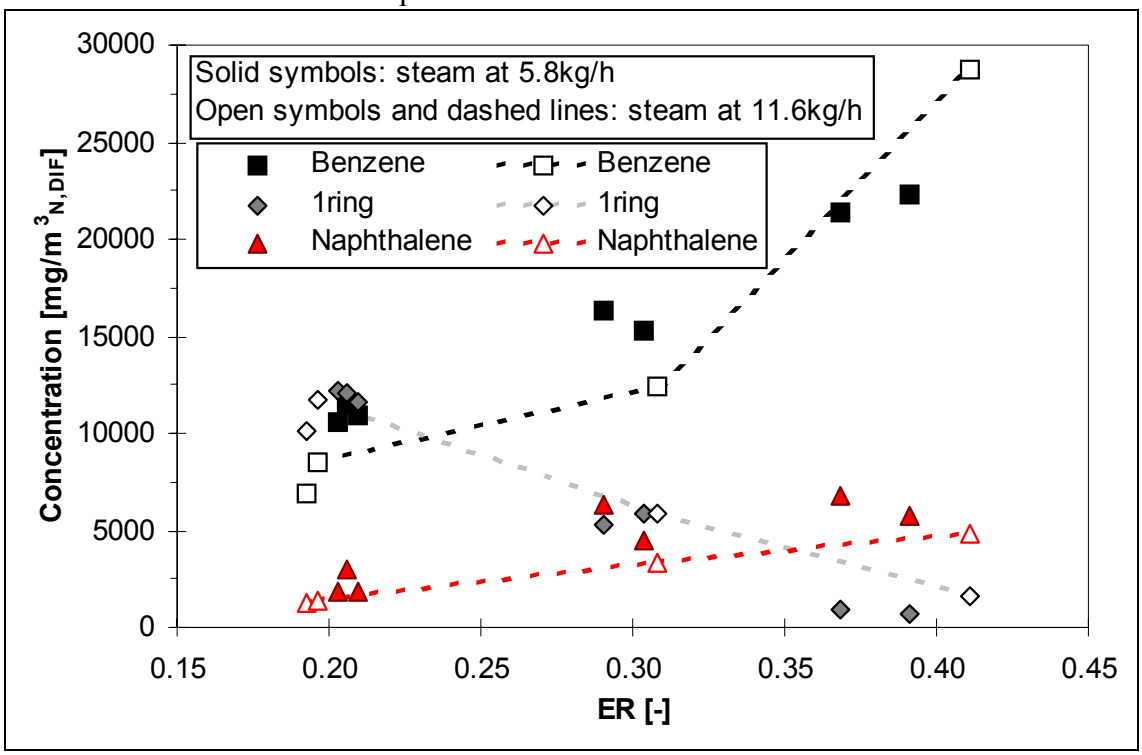

Figure 6.117: Tar classes evolution (oxygenates, DIF basis) for AH gasification at different steam input mass flows.

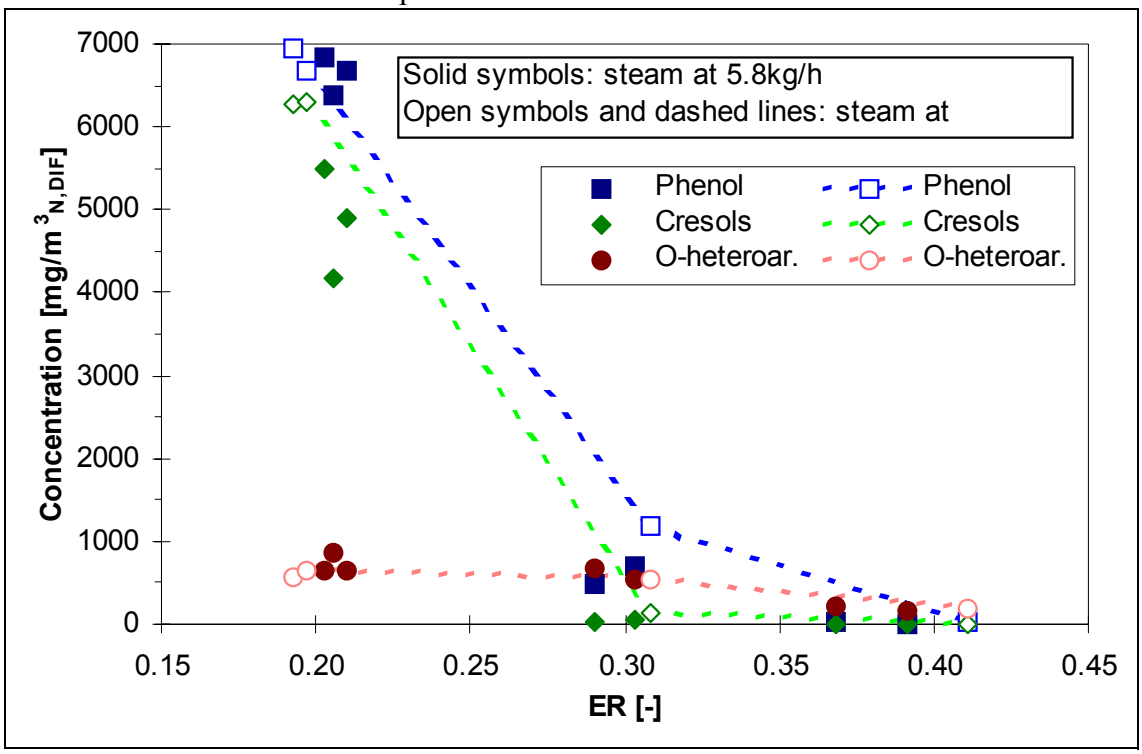

Figure 6.118: Tar classes evolution (minor aromatics, DIF basis) for AH gasification at different steam input mass flows.

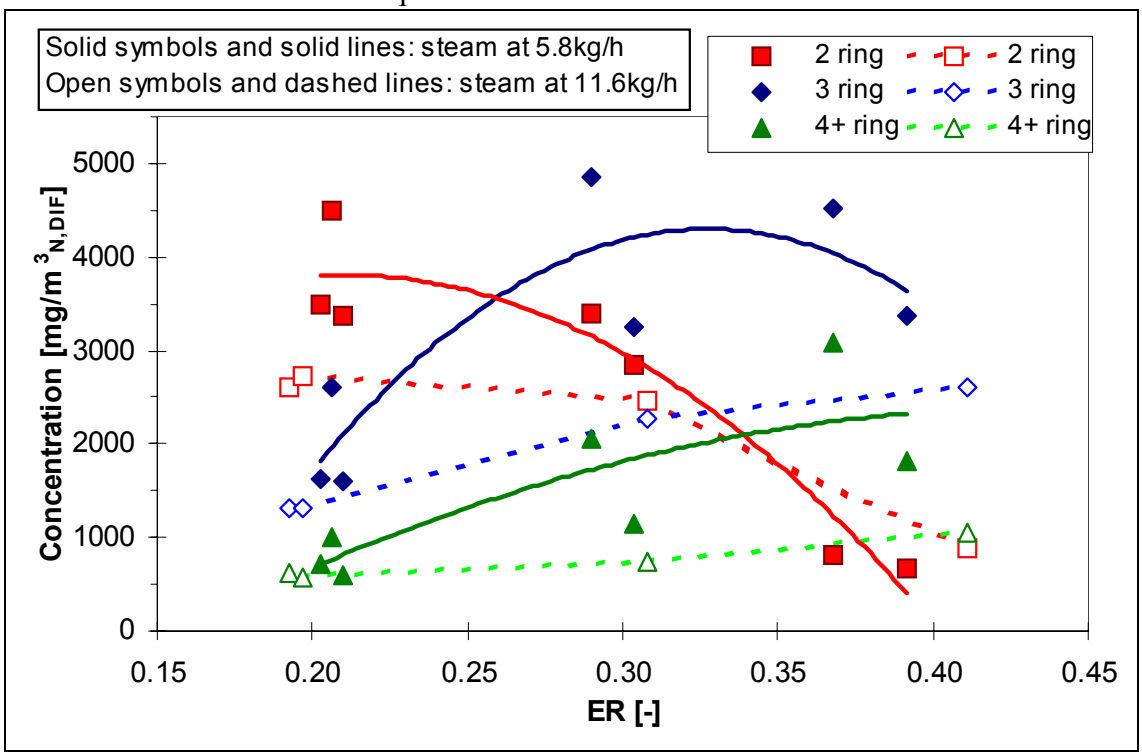

The oxygenated compounds are not affected by the higher steam content of the gas. Large differences are observed in the concentrations of the larger ring systems. 2-ringed aromatics are found in lower concentrations at low ER, and as ER is increased the differences between the two steam environments become smaller.

The 3 and 4+ ring tar classes do however exhibit a different behaviour. At low ER the concentrations of these two tar classes are the same for both steam throughput experiments. As ER is increased, the concentrations for the high steam case are seen to be markedly lower in comparison to the standard steam throughput. This difference is clear despite the large scatter of the data. An exact explanation for this situation cannot be given, but it appears that the reforming reactions of the higher ring systems proceed faster that those of the 2-ringed systems. This observation would be consistent with the fact, that one of the most stable molecules present in the tars is the 2-ringed naphthalene [6.20].

The oxygen containing heteroaromatic compounds are not affected by the larger steam fraction in the gas at all ERs studied.

The tar composition is depicted in Figures 6.119 to 6.121 for the different ER ranges covered by the experiments. At ER ≈ 0.2 the tar fraction of benzene in the tars is strongly reduced by the presence of larger amounts of steam in the gas as are the 2 ringed

PAHs (naphthalene **and** 2 ring) but in a less dramatic manner. The fraction of larger PAHs is not affected by the increase in the steam. Phenol and especially Cresols on the other hand make up a larger fraction of the tars in the case of higher steam amount in the gas.

Figure 6.119: Normalised tar composition for AH gasification at ER ≈ 0.2 and different steam mass flows.

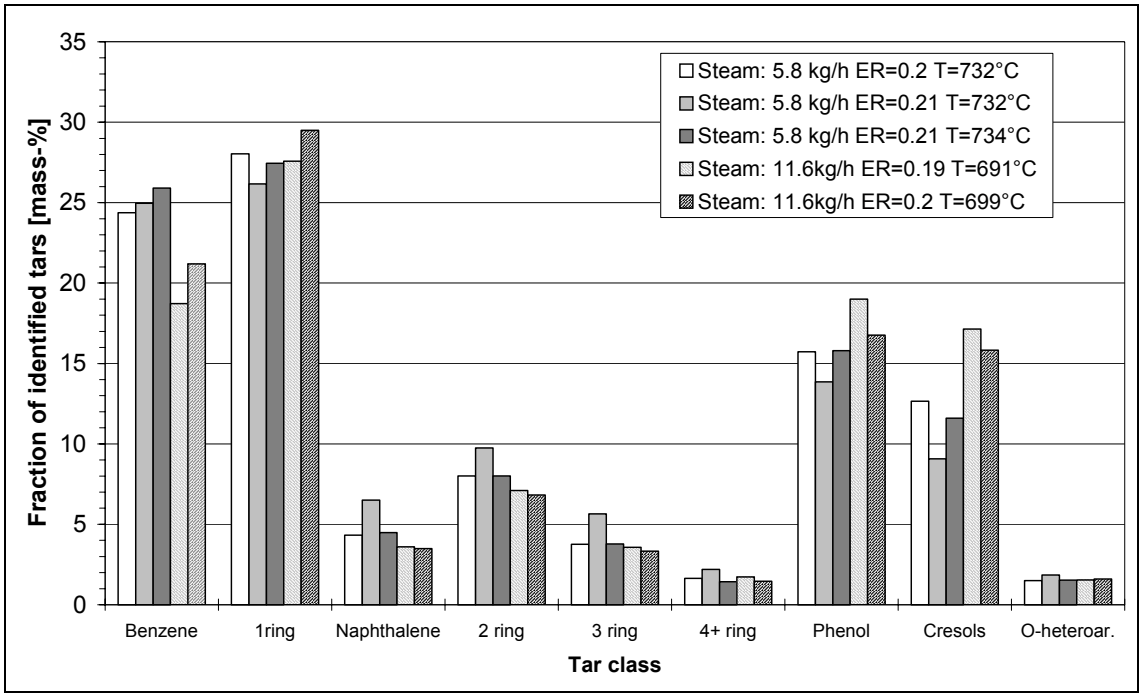

Figure 6.120: Normalised tar composition for AH gasification at ER ≈ 0.3 and different steam mass flows.

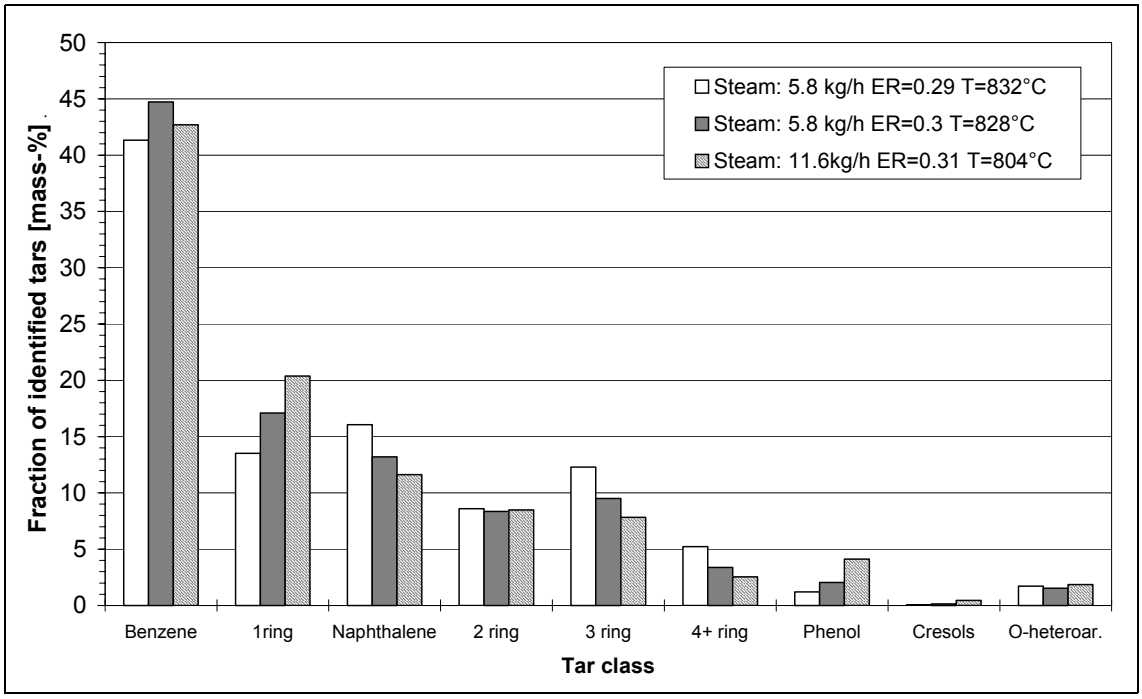

At ER ≈ 0.3 a higher fraction of the phenolic compounds as well as the 1 ring aromatics result form the increase in the steam amount fed to the reactor. Benzene and the 2 ringed aromatics are not strongly affected whereas all other PAHs exhibit a decrease in their fraction of the total tars.

Figure 6.121: Normalised tar composition for AH gasification at ER ≈ 0.4 and different steam mass flows.

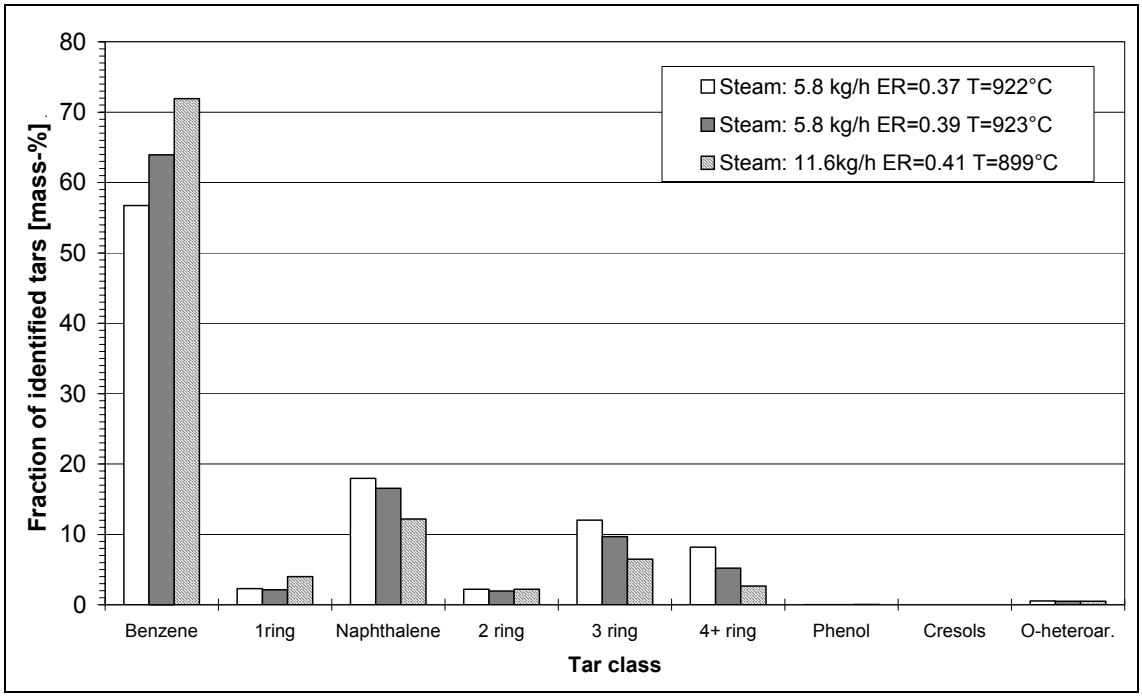

At ER ≈ 0.4 a net increase in the fractions of benzene and 1 ringed aromatics is caused by the higher steam amount in the gas caused by the higher input of steam to the reactor. All PAHs with the exception of the 2 ringed class are lowered as the steam content of the gas rises.

6.3.3 Reactor load

To test the effect of the reactor load, in experiment 991005 the fuel feed rate was kept constant and the variation in ER was achieved by adjusting the oxygen input to the reactor. Altholz was used as fuel and it was chosen to use the fuel feed rate corresponding to ER = 0.3 for the regular experimental procedures (i.e. ca. 14-15 kg/h fuel input). This in turn means, that compared to the regular experimental procedure at ER = 0.2, a smaller and, at ER = 0.4, a larger fuel mass flow will be used. The primary objective of this experiment was to test if differences in e.g. the residence time of the gases (the amount of

which is directly dependent on the fuel mass flow) would influence the gasification procedure.

As the steam mass flow was kept at the regular value of 5.8kg/h, the constant fuel feed rate yields an almost constant steam to biomass ratio in the runs of this experiment, in contrast to the varying steam to biomass ratio in the experiments performed using the regular procedure.

Figure 6.122: T_{Bed} versus ER for AH gasification in steam/oxygen according to the normal operational procedure and at constant fuel feed rate.

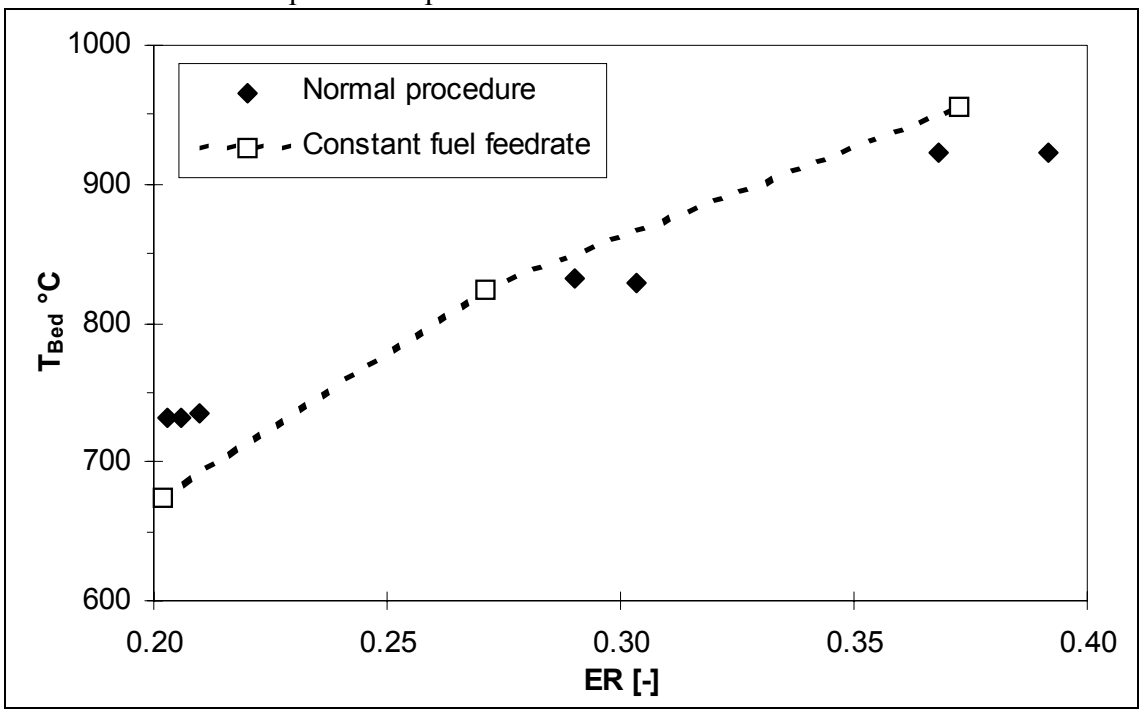

As illustrated in Figure 6.122, the heat management of the reactor is another parameter which is unwillingly altered in relation to the regular procedure. The smaller fuel input at ER = 0.2 compared to the regular experiments yields a lower reactor temperature whereas at ER = 0.4 a higher mass flow of fuel will generate a higher reactor temperature. The discussion of the results will still be made for ER.

The evolution of the gas composition at the top and bottom gas sampling points depicted in Figure 6.123 shows that during run 991005A a large leak was observed in the gas sampling system of the top sampling point. As soon as the leak was corrected (by thightening the lid of the bottle containing the bentonite, solid tar absorbent see page 30), the gas composition values stabilised at similar values to those prior of the start of the

sampling period. The gas composition for this part of the experiment is therefore taken as the average of the values after the suppression of the leak.

Figure 6.123: Gas composition evolution for experiment 991005.

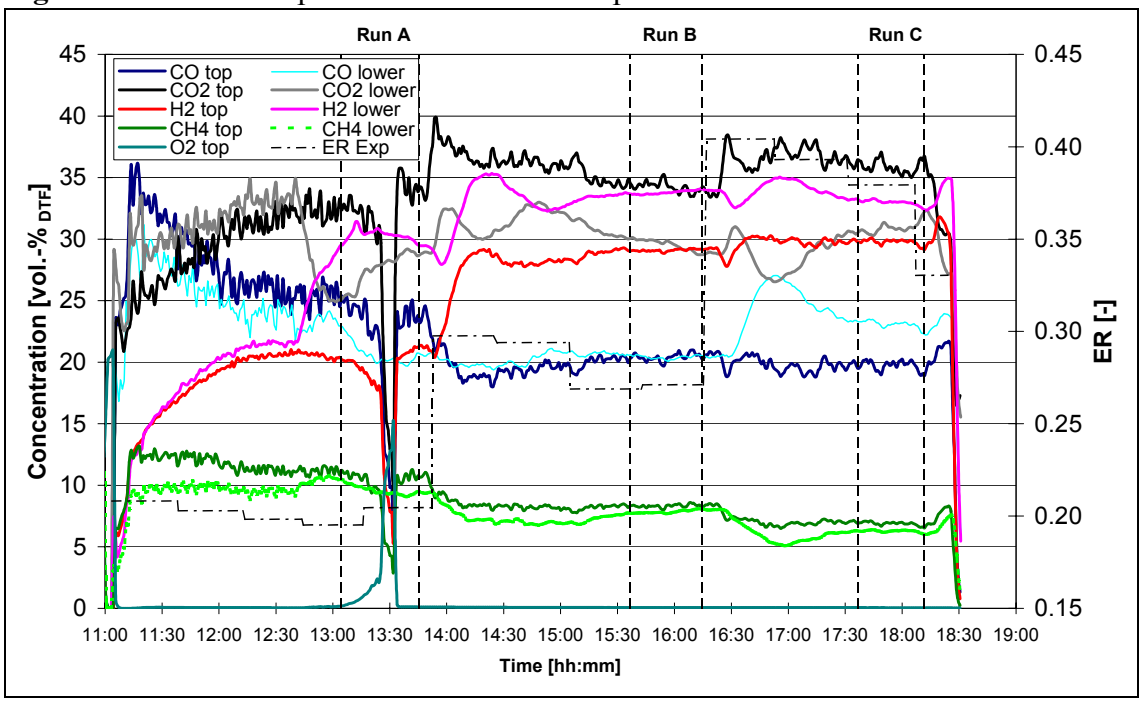

The gas composition evolution with ER is depicted in Figure 6.124. The CO_2 and CH_4 concentrations are unaffected by the change in the fuel feed rate. Under identical conditions at ER = 0.3 (the fuel feed rate experiment 991005 was chosen as the same value used previously for the regular AH experiments at ER = 0.3) the concentrations of these two gas components are seen to be identical for both experiments. However, large differences are observed for the CO and H_2 concentrations, even at ER = 0.3. Furthermore at ER = 0.38, the H2 concentration measured in the experiment at constant fuel feed rate is much higher than that of the experiment under regular conditions. An unambiguous explanation for this behaviour cannot be found, but variations in the fuel composition could be the cause for this strange behaviour. From the (very poor) fuel composition data available, the ash and water content of the fuel used in each period, no differences can be seen as Table 6.12 shows.

Figure 6.124: Gas composition evolution with ER for AH gasification in steam/oxygen according to the normal operational procedure and at constant fuel feed rate.

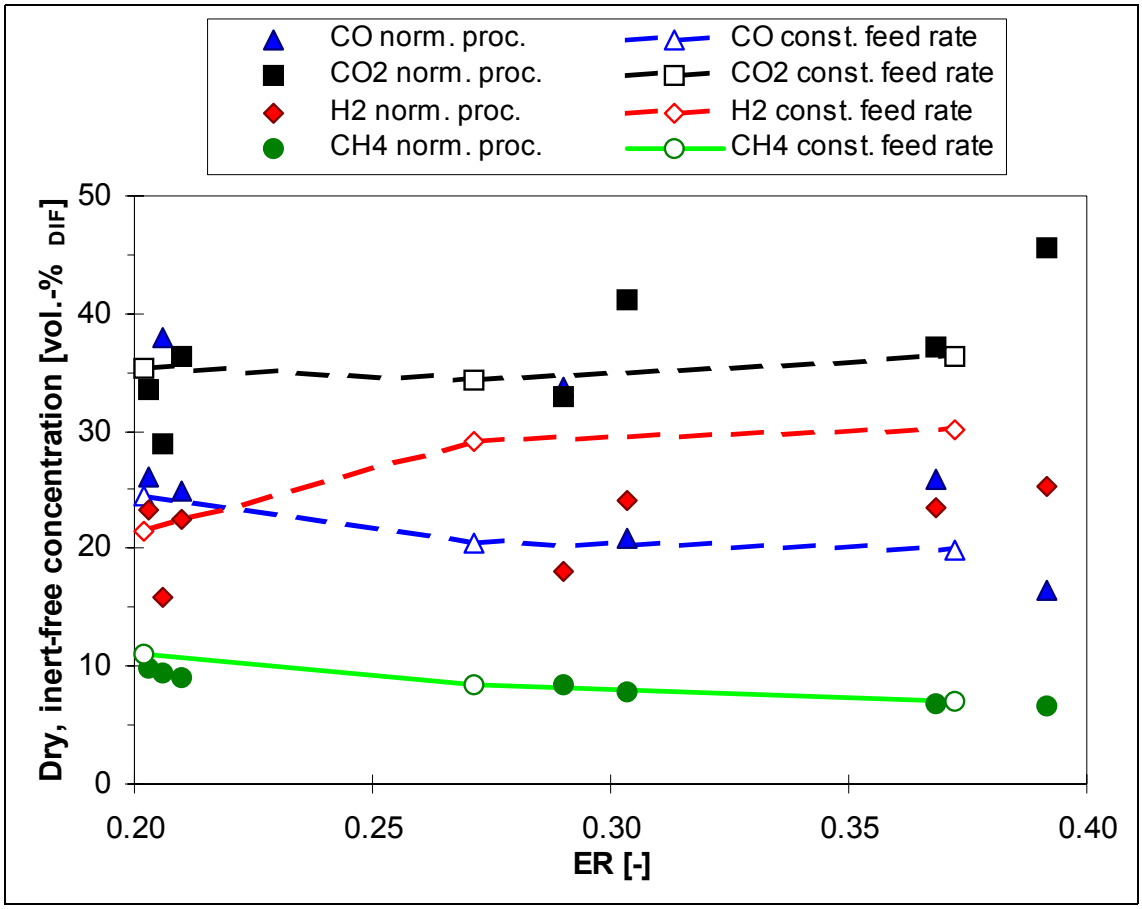

Table 6.12: Ash and water content of fuel used in experiment 991005.

Run	991005A	991005B	991005C
Humidity [mass $\%_{RAW}$]	7.21	7.16	7.17
Ash content [mass $\%_{RAW}$]	5.19	4.79	5.18

The gas yield given in Figure 6.125 shows that under a constant fuel feed rate less gas is generated at all conditions, detailing further discrepancies between the experiments at almost identical conditions (ER = 0.3). The reason for the lower gas yields observed at the two extreme ER set-points is unclear.

Figure 6.125: Gas yield of AH gasification for constant fuel feed rate and regular experiments in steam/oxygen.

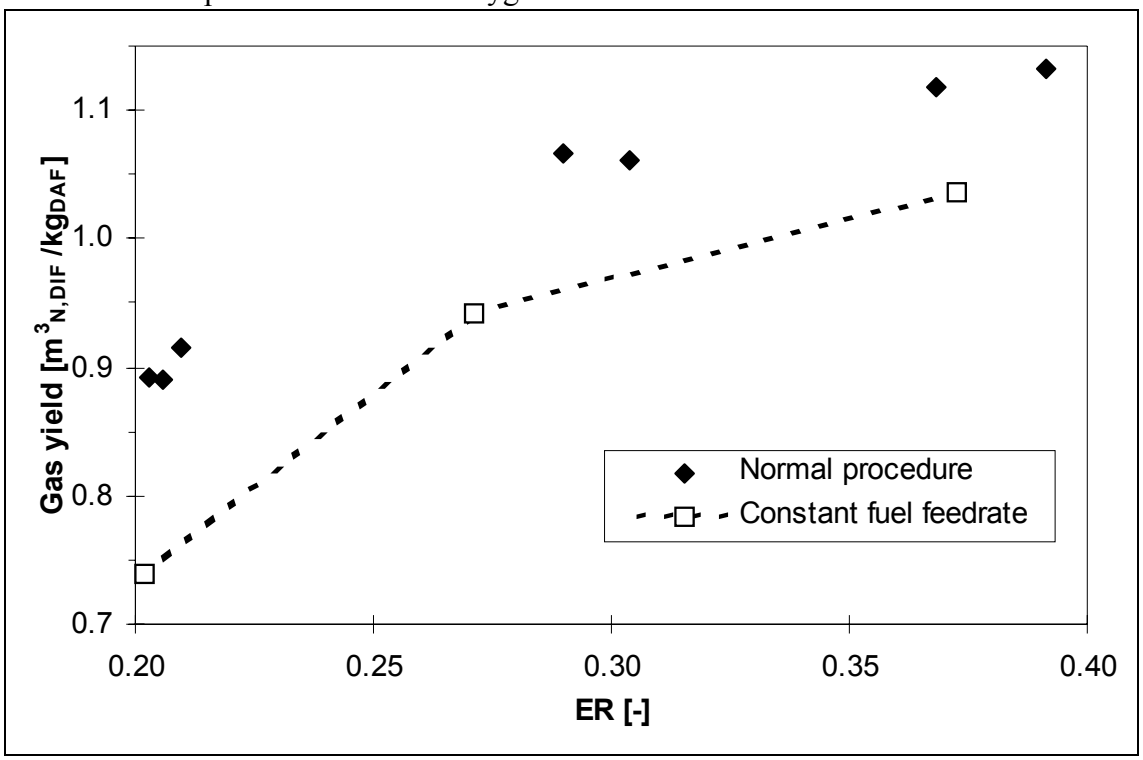

The total tar concentration shown in Figure 6.126 on a dry basis illustrates yet another discrepancy between the experiments: the tar concentrations for the constant fuel feed rate experiment at ER = 0.3 and 0.4 are seen to lie well above the range previously measured using the standard experimental procedure. At ER = 0.2 on the other hand the tar concentration is well below the values measured at regular conditions. No estimation of the fraction of identified tar components was carried out for the experiment at constant fuel feed rate, but using the averages at similar ER obtained for the experiments using the regular experimental procedure (i.e. with a variation of the fuel input mass flows), the corrected total tar concentrations also shown in Figure 6.126 are obtained. The discrepancy observed still persists in the corrected values, and again large disparities are observed at the same experimental conditions at ER = 0.3.

Figure 6.126: Total tar concentration for AH gasification for constant fuel feed rate and regular experiments in steam/oxygen.

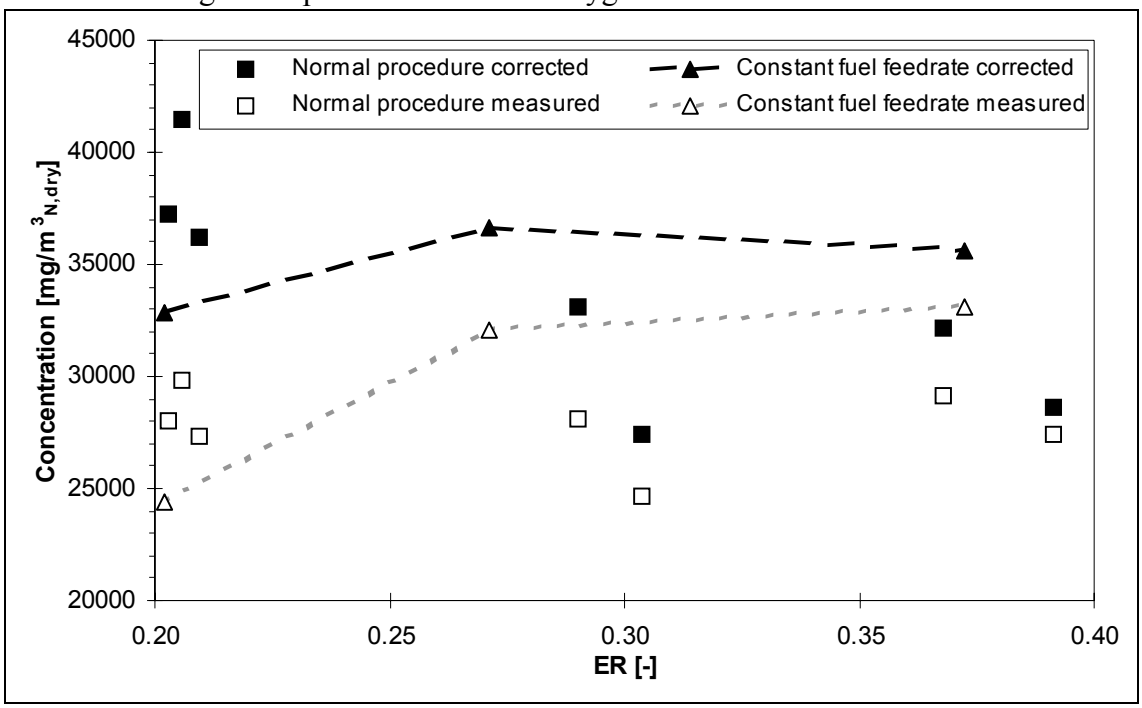

The evolution of the tar classes with the ER is shown in Figures 6.127, 6.128 and 6.129.

Figure 6.127: Tar classes evolution (major aromatics, DIF basis) for AH gasification at different fuel input mass flows.

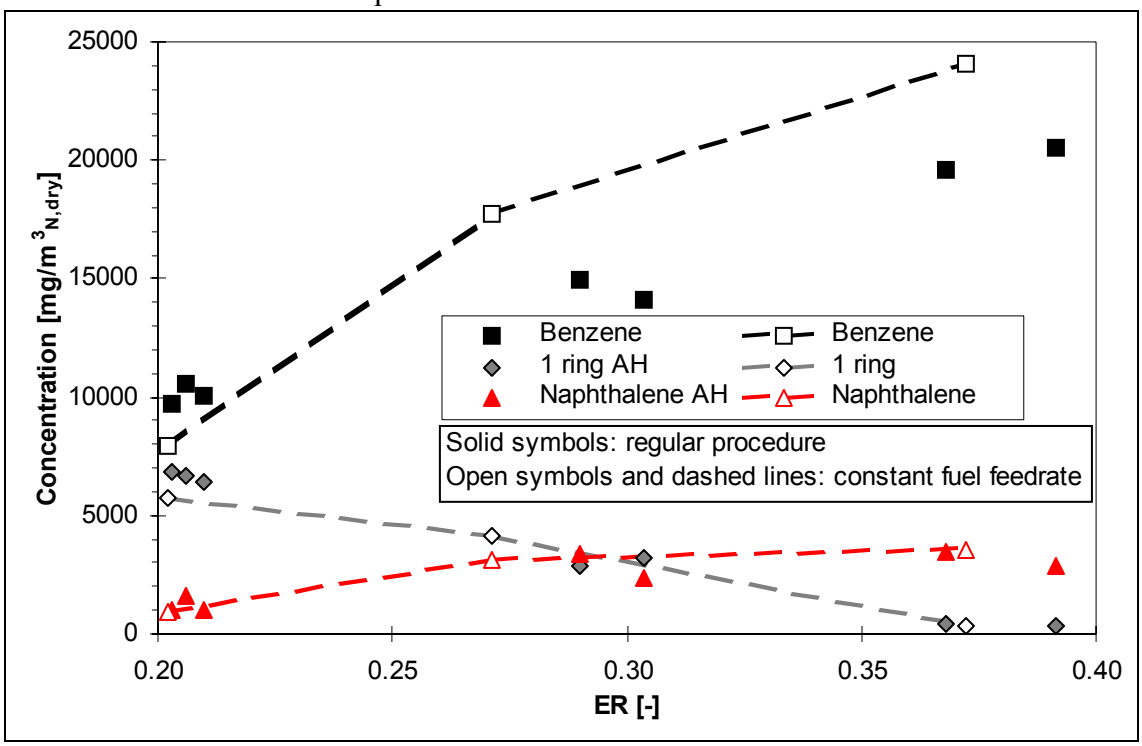

Figure 6.128: Tar classes evolution (oxygenates, DIF basis) for AH gasification at different fuel input mass flows.

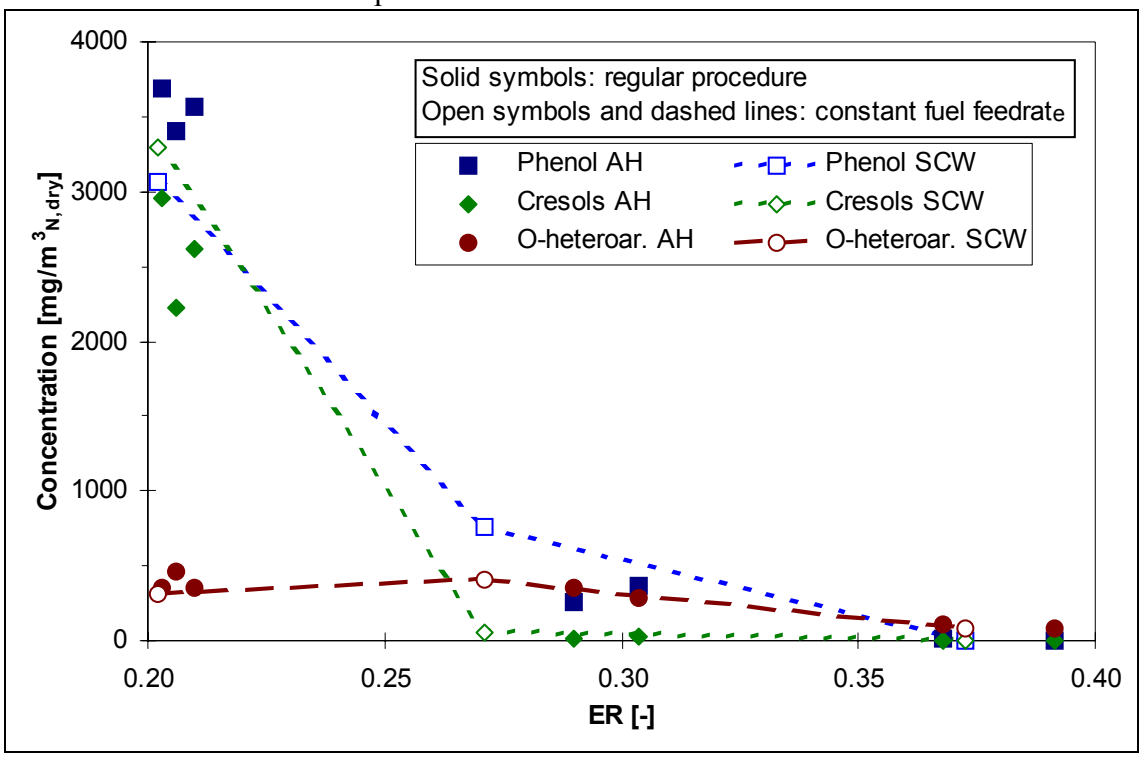

Figure 6.129: Tar classes evolution (minor aromatics, DIF basis) for AH gasification at different fuel input mass flows.

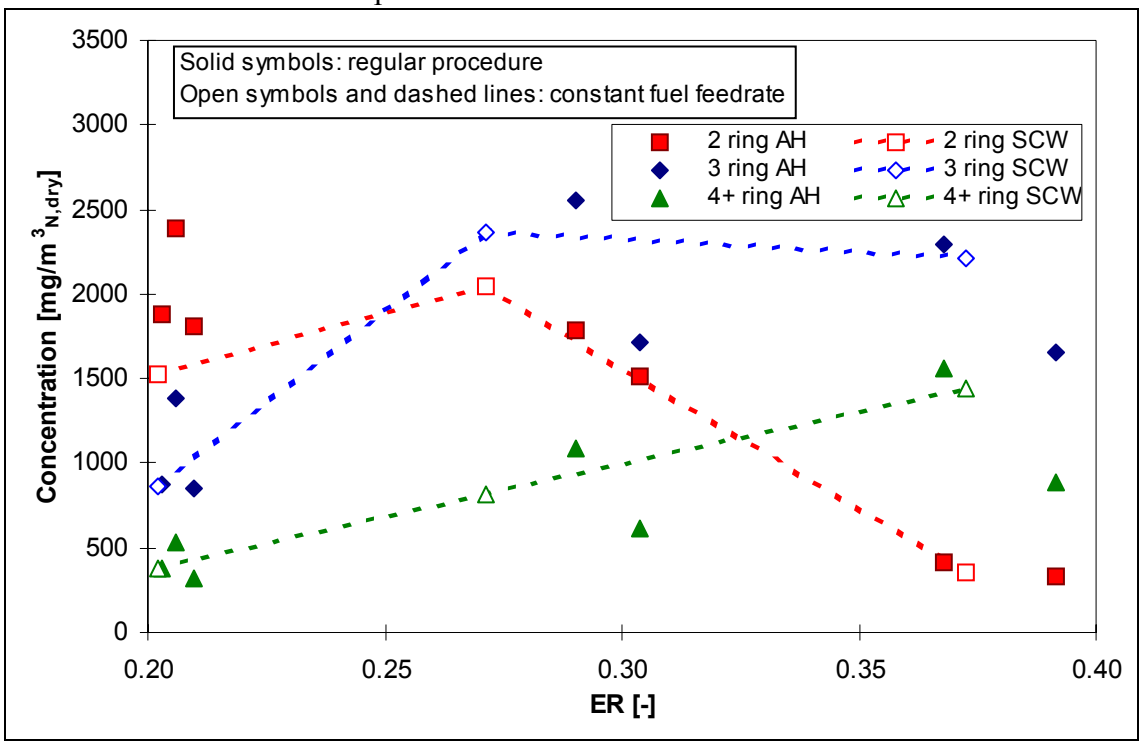

Significant differences are only observed for benzene over the whole ER range and for 1 ringed aromatics, phenol, cresols the 2 ringed aromatics at low ER. At low ER

all 5 tar classes but the cresols are observed in lower concentration in the experiment at constant fuel input mass flow. The cresols concentration is higher for the constant reactor load experiment. These differences disappear at higher ER for all tar classes but for benzene. This tar class is detected in higher concentrations in the gas from the experiment at constant reactor load. The high cresol concentration could be interpreted as a consequence of the relatively low temperature of run 991005A, 674°C. At this relatively low temperature conversion of secondary tar products into tertiary products occurs to a lesser extent, allowing a larger amount of cresols to subsist in the gas.

The tar composition for the experiment at constant reactor load is shown in Figures 6.130 to 6.132 together with the tar composition for the experiments performed according to the regular experimental procedure. The tar composition resulting from the two experimental procedures is quite similar. Only at ER = 0.2 a lower benzene and higher cresols fraction in the tars is observed. As mentioned before this differences could be assigned to the low temperature of the experiment at ER =0.2 and constant reactor load, which would be favourable to the formation of tar products of secondary tar nature, which could not be detected by the tar analysis method employed in the present study.

Figure 6.130: Normalised tar composition for AH gasification experiments at constant fuel input and under regular experimental procedures at ER ≈ 0.2.

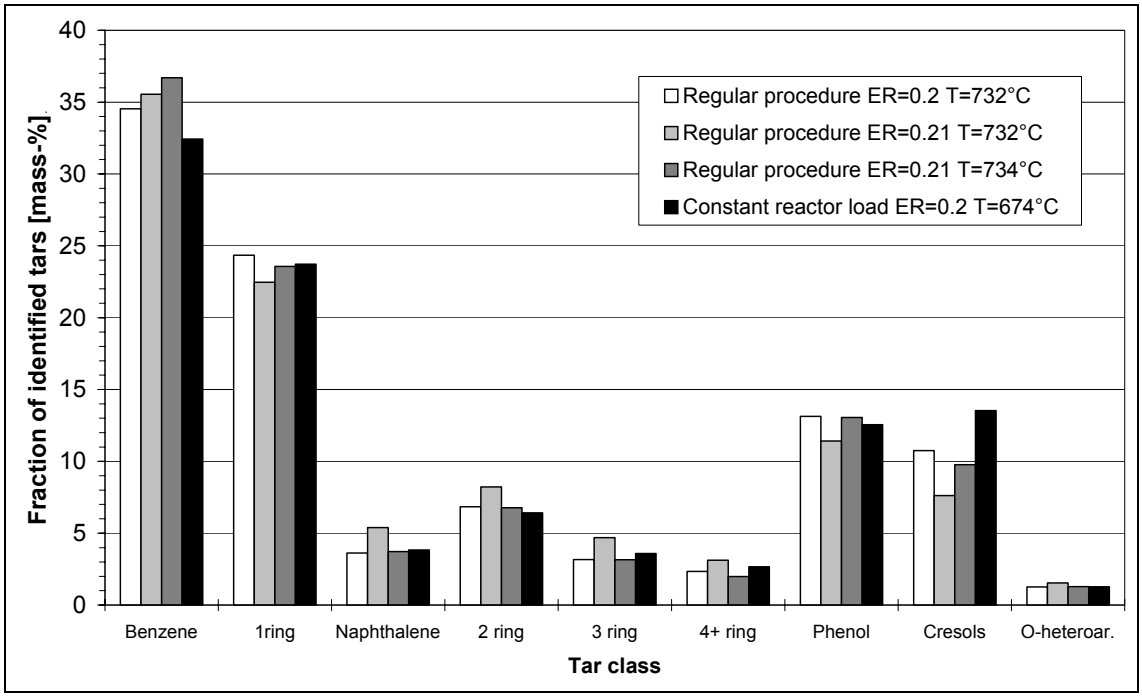

Figure 6.131: Tar composition for AH gasification experiments at constant fuel input and under regular experimental procedures at ER ≈ 0.3.

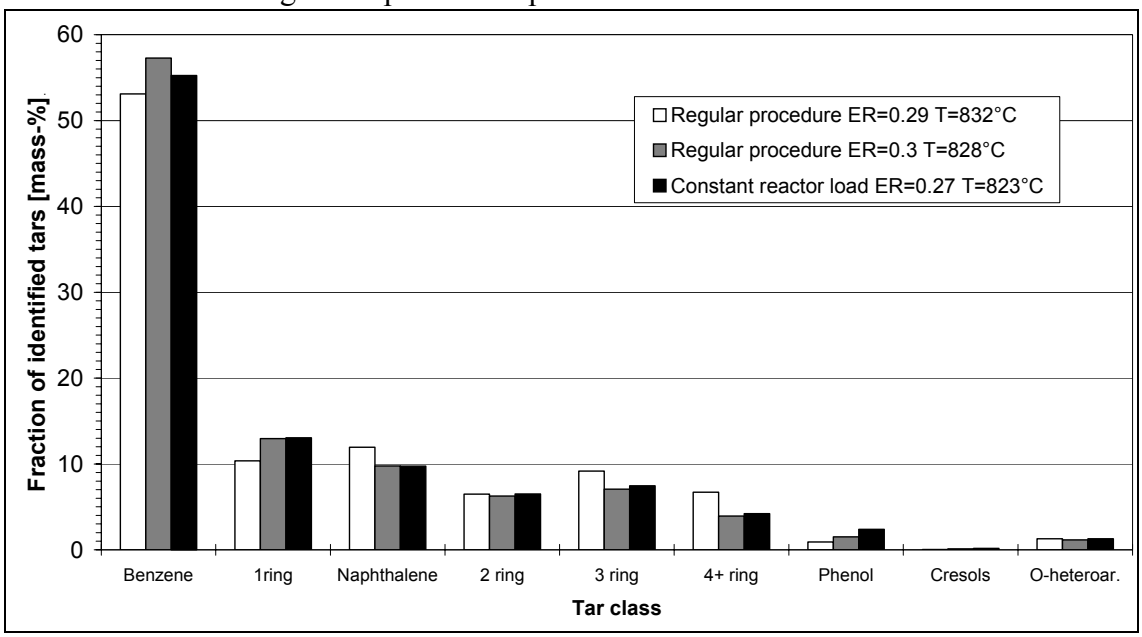

Figure 6.132: Normalised tar composition for AH gasification experiments at constant fuel input and under regular experimental procedures at ER ≈ 0.4.

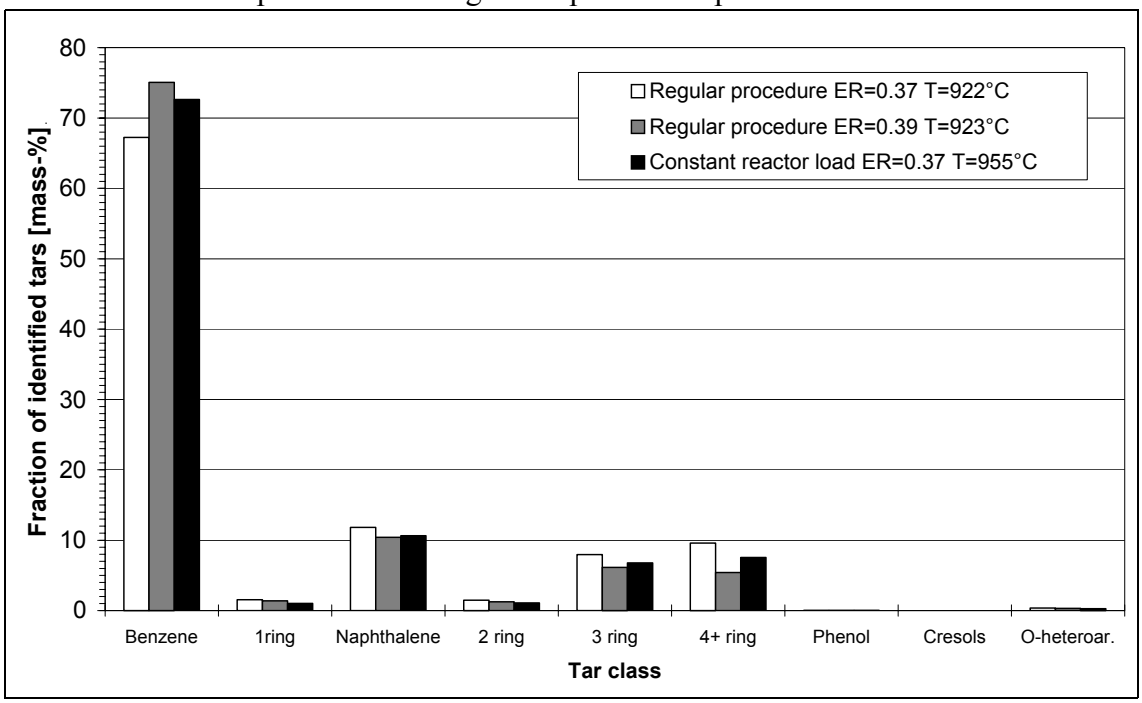

6.4 References

[6.1] E.G. Baker, L.K. Mudge, *Catalysis in Biomass Gasification,* Pacific Northwest Laboratory report PNL-5030, Pacific Northwest Laboratory, Richmond, USA, 1984

[6.2] E.G. Baker, L.K. Mudge, M.D. Brown, *Steam Gasification of Biomass with Nickel Secondary Catalysts*, Industrial Engineering Chemistry Research, 1987, **26**, pp.1335-1339

[6.3] E.G. Baker, L.K. Mudge, W.A. Wilcox, *Catalysis of Gas-Phase Reactions in Steam Gasification of Biomass*, in Fundamentals of Thermochemical Biomass Conversion, R.P. Overend, T.A. Milne and L.K. Mudge (eds.), Elsevier Applied Science Publishers Ltd., London, 1985, pp.863-874

[6.4] C. Eckström, N. Lindman, R. Peterson, *Catalytic Conversion of Tars, Carbon Black and Methane from Pyrolysis/Gasification of Biomass*, in Fundamentals of Thermochemical Biomass Conversion, R.P. Overend, T.A. Milne and L.K. Mudge (eds.), Elsevier Applied Science Publishers Ltd., London, 1985, pp.601-618

[6.5] P. A. Simell, J.B-son. Bredenberg, *Catalytic Purification of Tarry Fuel Gas*, Fuel, 1990. **69**, pp.1219-1225

[6.6] P.A. Simell, J.K. Leppälahti, J.B-son. Bredenberg, *Catalytic Purification of Tarry Fuel Gas with Carbonate Rocks and Ferrous Materials*, Fuel, 1992, **71**, pp.211-218

[6.7] S. Czernik, P.G. Koeberle, P. Jollez, J.F. Bilodeau, E. Chornet, *Gasification of Residual Biomass via the Biosyn Fluidized Bed Technology*, in Advances in Thermochemical Biomass Conversion, A.V. Bridgwater (ed.), Blackie Academic & Professional, Glasgow, 1994, **1**, pp. 423-437

[6.8] K. Maniatis, A.V. Bridgwater, A. Buekens, *Fluidized Bed Gasification of wood*, in Research in Thermochemical Biomass Conversion, A.V. Bridgwater, J.L. Kuester (eds.), Elsevier Applied Science, London, 1988, pp1094-1105

[6.9] I. Navárez, A. Orío, M.P. Aznar, J. Corella, *Biomass Gasification with Air in an Atmospheric Bubbling Fluidized Bed. Effect of Six Operational Variables on the Quality of the Produced Raw Gas*, Industrial and Engineering Chemistry Research, 1996, **35**, pp.2110-2120

[6.10] S. Gordon B.J. McBride, *Computer Program for Calculation of Complex Chemical Equilibrium Composition, Rocket Performance, Incident and Reflected Shocks and Chapman-Jouget Detonations*, National Aeronautics and Space Administration, NASA Report SP-273, 1976

[6.11] C.M. Kinoshita, Y. Wang, J. Zhou, *Effect of Reformer Conditions on Catalytic Reforming of Biomass Gasification Tars*, Industrial and Engineering Chemistry Research, 1995, **34**, pp.2949-2954

[6.12] E. Kurkela, P. Ståhlberg, J. Laatikainen, *Pressurised Fluidized-Bed Gasification Experiments with Wood, Peat and Coal at VTT in 1991-1992 Part 1. Test Facilities and Gasification Experiments with Sawdust*, Technical Research Centre of Finland, VTT Publications 161, Espoo, 1993

[6.13] E. Kurkela, P. Ståhlberg, *Air Gasification of Peat, Wood and Brown Coal in a Pressurised Fluidized-Bed Reactor. I. Carbon Conversion, Gas Yields and Tar Formation*, Fuel Processing Technology, 1992, **31**, pp.1-21

[6.14] O. Moersch, H. Spliethoff, K.R.G. Hein, *Influence of Temperature and Stoichiometry on Gas Quality and Conversion Rate in Fluidized Bed Gasification of Biomass*, in Biomass for Energy and the Environment, Proceedings of the 9th European Bioenergy Conference, Copenhagen, Denmark 24-27 June 1996, P. Chartier et. al. (eds.), Elsevier Science, Oxford, 1996, Volume 2, pp.1398-1403

[6.15] C.M. Kinoshita, Y. Wang, J. Zhou, *Tar Formation under Different Biomass Gasification Conditions*, Journal of Analytical an Applied Pyrolysis, 1994, **29**, pp.169-181

[6.16] A. Aldén, P. Hagström, A. Hallgren, L. Waldheim, *Investigations in High Temperature Catalytic Gas Cleaning for Pressurised Gasification Processes*, in Developments in Thermochemical Biomass Conversion, A.V. Bridgwater, D.G.B. Boocock (eds.), Blackie Academic & Professional, London, 1997, Volume 2, pp.1131-1143

[6.17] J. Gil, J. Corella, M.P. Aznar, M.A. Caballero, *Biomass Gasification in Atmospheric Bubbling Fluidized Bed: Effect of Type of Gasifying agent on the Product Distribution*, Biomass and Bioenergy, 1999, **17**, pp.389-403

[6.18] C.M. Kinoshita, Y. Wang, P.K. Takahashi, *Chemical Equilibrium Computations for Gasification of Biomass to Produce Methanol*, Energy Sources, 1991, **13**, pp.361-368

[6.19] J. Gil, M.P. Aznar, M.A. Caballero, E. Francés, J. Corella, *Biomass Gasification in Fluidized Bed at Pilot Scale with Steam-Oxygen Mixtures. Product Distribution for Very Different Operating Conditions*, Energy & Fuels, 1997, **11**, (6), pp.1109-1118

[6.20] H. Aldén, E. Björkman, M. Carlsson, L. Waldheim, *Catalytic Cracking of Naphthalene on Dolomite*, in Advances in Thermochemical Biomass Conversion, A.V. Bridgwater (ed.), Blackie Academic & Professional, Glasgow, 1994, (Vol. 1), pp.216-232

[6.21] K. Weissermehl, H.-J. Arpe, *Industrielle Organische Chemie: bedeutende Vor- und Zwischenprodukte*, 3. überarbeitete und erweiterte Auflage, VCH Verlagsgesellschaft, Weinheim, Germany, 1988

[6.22] F. Pinto, I. Gulyurtlu, C. Fracnco I. Cabrita, *Optimisation of Gasification Experimental Conditions of Mixtures of Biomass with Plastic Wastes*, in Biomass, A

Growth Opportunity in Green Energy and Value-Added Products, Proc. of the 4th Biomass Conference of the Americas, August 29-September 2 1999, Oakland, USA, R.P. Overend, E. Chornet, (eds.), Elsevier Science, 1999, pp.1041-1046

[6.23] C. Bouster, P. Vermande, J. Veron, *Evolution of the Product Yield with Temperature and Molecular Weight in the Pyrolysis of Polystyrene*, Journal of Analytical and Applied Pyrolysis, 1989, **15**, pp.249-259

[6.24] P.T. Williams, E.A. Williams, *Product Composition from the Fast Pyrolysis of Polystyrene*, Environmental Technology, 1999, **20**, pp.1109-1118

7 CONCLUSIONS

7.1 Summary of conclusions

The conclusions from the discussion of the results in Chapter 6 are presented in the following in summarised form.

7.1.1 General

- The gas composition in Altholz gasification is subject to catalytic effects. Both heterogeneous as well as homogeneous reactions seem to be influenced. This catalysis may lead to considerable differences in gas composition under otherwise identical reactor operational conditions.
- The reproducibility of the results should be ascertained using a fuel with constant composition and free of potentially catalytic active contaminants, i.e. SCW. Altholz is

unsuitable to establish reproducibility as the contaminants present in this fuel influence the results, especially the gas composition.

- Reactions are seen to occur in the reactor's freeboard. Gas composition differences are observed at different locations in the freeboard for low as well as high ER (or temperature) set-points. These differences are furthermore a function of the type of fuel (SCW or AH) used.
- Experimental evidence exists suggesting that reforming type reactions occur in the freeboard region of the gasifier. The concentration of tars in the gases could therefore be influenced by the residence time of the products in the reactor. This difference could however not be correctly ascertained by the experiments carried out in this study.
- The gas composition and tar amount and composition results obtained are well comparable to literature data in either gasification agent.
- As already reported in the literature, the gasifier delivers a gas with a composition very different from that predicted by thermodynamic equilibrium calculations. This difference is observed for all fuels and gasification agents studied. These differences can however not fully be explained by the presence of products of "incomplete" gasification, CH_4 and tars, as the results of the theoretical reforming to CO, CO_2 and H_2 suggest.
- The CO_2 concentration is for most of the experiments performed higher than that predicted by the thermodynamic equilibrium. The concentrations of H_2 and CO are on the other hand consistently lower than this theoretical forecast. A gas with lower energy contents or heating value is the result indicating that energy has been lost in the gasification. This apparent loss may be explained by:
  a) the presence of light hydrocarbons in the gas which remain unaccounted for by the gas analysis method used and contain considerable chemical energy (i.e. heating value);
  b) the fact that some of the fuel's energy must be converted to heat to compensate for the energy losses in the reactor which is operated in autothermal and not adiabatic mode as assumed for the thermodynamic calcualtions.

- For all fuels studied, an evolution of the tar composition towards a composition made up solely of benzene and unsubstituted PAHs is observed as ER is increased. Phenolic compounds virtually disappear above ER = 0.3.

7.1.2 Tar measurement method

- The tar measurement method used in this study yields reproducible results, even with the inhomogeneous Altholz as fuel.
- The manpower and instrumental effort involved in the present method is considerable, but yields very detailed information on tar composition. For research purposes such a method is justifiable, but for process control or other applications simpler methods yielding fast results must be developed.
- The fraction of the tars correctly quantified by the method used in the present study is primarily a function of the ER. Fractions above 85% are correctly quantified at ER > 0.3. This fraction drops to 60-70% at low ER, still the majority of the tar components present. To increase the fraction of correctly quantifiable compounds a very large number of substances should be included in the GC/MSD method. The manpower and instrumental effort required for this amelioration should not be underestimated.

7.1.3 SCW versus AH as fuel

- The gas composition for both fuels is very similar when gasification is performed in air. However, in steam/oxygen mixtures, the AH gas composition shows a marked effect of the water-gas shift reaction, yielding comparably lower CO and higher CO_2 and H_2 concentrations.
- Both fuels SCW and AH yield essentially the same gas amount in either gasification agent. Their thermal behaviour is furthermore the same (i.e. same T_{Bed} for a given ER).
- Under the same experimental conditions (ER/T_{Bed}), Altholz yields lower tar concentrations in the gas than SCW. This observation is true for both gasification agents studied here, air and steam/oxygen mixtures.
- Using air as gasification agent, the concentrations of all tar classes are lower for AH in comparison to SCW at ER > 0.3. At low ER (ca 0.2) all tar classes show similar

concentrations for both fuels, with the exception of much higher concentrations of phenolic compounds for SCW.

- In steam/oxygen mixtures the evolution of the tar components concentrations in function of the ER for both fuels is even more alike. An exception are benzene and phenolic compounds observed in higher concentrations for the gasification of SCW, the latter however only at low ERs.

7.1.4 Gasification agent

- The thermal behaviour of the wood fuels (AH and SCW) is not influenced by the gasification agent.
- In the case of AH, a clear influence of the homogeneous water-gas shift reaction on the gas composition is observed when gasification is carried out in steam/oxygen mixtures.
- Air gasification results in larger product gas volumes.
- Tar concentrations are identical for either gasification agent (separetely for both woody fuels studied) if the dilution effect by N_2 and H_2O is compensated, i.e. when the dry, inert-free concentrations are considered.
- The tar composition is not influenced by the gasification agent used.

7.1.5 Steam to biomass ratio

- Higher steam input to the reactor results in lower operating temperatures.
- The gas composition is affected by higher amounts of steam in the gasification agent. Additional steam shows an oxidative behaviour on the gas components.
- On a dry, inert-free basis the tar amounts remain the same when increasing the steam to biomass ratio. On a raw basis of course smaller tar concentrations will be measured due to the dilution by larger steam amounts.
- Higher steam to biomass ratios do only marginally reduce the concentrations of the main tar components (benzene and naphthalene) but do reduce the concentrations of larger PAH significantly.

7.1.6 Plastics admixture to the AH fuel

- The thermal behaviour of AH/plastics mixtures is observed to diverge from that of AH alone in autothermal gasification in steam/oxygen mixtures. The exact cause of this diversion cannot clearly be established from the data gathered in this study.
- Only minor differences are observed in the concentration of the gas components CO and CO_2 with PE admixture to the fuel. A decrease in H_2 concentration at high PE level and a very small increase in CH_4 concentrations can be established. The presence of light hydrocarbons in the gas could however not properly be determined, and these could contain a significant amount of both hydrogen and carbon.
- In the case of PS admixture, CO and CO_2 are also not strongly affected. Again a decrease of H2 concentrations for high plastic level in the fuel is observed. CH_4 concentrations are lowered by the presence of PS in the fuel, in contrast to PE admixture.
- No large influence of the PE in the fuel on the amount of gas produced could be registered. However the presence of light hydrocarbons could change this observation. The PS admixture lowers the amount of gas produced.
- Total tar amounts are increased by the addition of PE to the fuel. The increase is a function of the PE level in the fuel. At high ER and low PE level in the fuel the tar concentrations do however become almost identical.
- PS admixture does drastically increase the tar amounts in the products and the increase is a function of the amount of PS in the fuel. This increase could explain the lower gas amounts produced by this mixture. Also here the increase in tar concentration is observed to become less pronounced with increasing ER.
- The concentrations of benzene and PAHs are increased by the addition of PE for a given ER. Phenolic compounds are reduced by PE admixture.
- For PS an increase is observed in the concentrations of all aromatic compounds. Benzene and larger unsubstituted PAHs are present in larger concentrations at all ERs. 1 ringed and 2 ringed aromatics are drastically increased at low ERs only and under these conditions phenolic compounds are present in lower concentrations.

7.1.7 Effect of aging/particle size

- The aging simulation process applied to SCW yielded results identical to the original SCW fuel. Most probably the procedure employed was not appropriate to simulate the

aging process. The hypothesis of the influence of the age of the AH on the tar amounts can neither be confirmed nor rejected by the results obtained.

- Smaller fuel particle size does only marginally influence the gas composition and gas yields.
- The tar concentrations are increased when smaller fuel is gasified. Notably benzene concentrations are increased at a given ER when the smaller fuel is used. The hypothesis that the smaller particle size of AH could explain the lower tar amounts is clearly rejected.

7.2 Recommendations for further research

Some interesting study points and recommendations for future research based on the author's experience and the results obtained in the present study are presented below.

- Systematic study of the influence of heavy metals (and other) AH contaminants on the gas composition and tar amounts. This study should be carried out by selectively adding heavy metals to SCW. In-depth elemental analysis of the fuels used in this study should precede these experiments.
- Proper study of the freeboard phenomena. Tar and solids concentrations should be studied at different locations of the gasifier's freeboard.
- Study of the influence of ER and T_{bed} *separately* on tar amount and composition is recommended. The fuel moisture is an important operational parameter for an autothermal full-scale gasifier and in turn influences the combination ER/T_{Bed}.
- Light hydrocarbons in the gas should be included in a gas composition measurement method. The concentration of these components is of interest when gasification is carried out in steam/oxygen mixtures (as required for synthesis gas generation) and especially when potential precursors such as polyethylene are present in the fuel (as would be the case in a BIOMETH plant).
- The combined influence of different plastic types in the fuel should be studied. Literature data on the co-pyrolysis of PE and PS suggests that the composition (and possibly also the amount) of tar components cannot simply be deduced from the results of gasifying single plastics.
- The study of industrial waste plastics (i.e. such as they will be encountered in the Biometh plant) should be considered. Just as differences are observed between the ideal biomass "SCW" and the waste wood fuel "AH", a diverse behaviour can be expected between ideal, clean plastics and waste plastics.
- The thermochemistry of the gasification of AH or SCW and plastics mixtures should be studied. The presence of the plastics in the fuel may lead to dangerous, diverging operational conditions (too high temperatures) in a full-scale autothermal gasifier.

APPENDIX A: TAR DATA

The raw tar data from all experiments according to the final experimental plan (see page 128) is reported in this appendix. The concentration data is given in milligrams tar compound per normal cubic meter (m^3_N) of wet, tar containing product gas.

Table A.1: Concentrations of tar compounds for experiment 990903.

Tar species	990903A	990903B	990903C
Benzene	4228	8281	9584
Toluene	2632	2360	328
Ethylbenzene	214	9	1
p&m-Xylene	860	387	10
o-Xylene	202	66	1
Styrene	863	1030	300
3-Ethyltoluene	54	2	0
4-Ethyltoluene	27	1	0
2-Ethyltoluene	23	0	0
Phenol	3348	1590	13
α-Methylstyrene	72	15	1
3&2-Methylstyrene	246	117	7
4-Methylstyrene	117	55	4
2,3-Benzofuran	255	272	8
o-Cresol	1029	52	0
Indene	823	1443	358
p-Cresol	1240	77	0
m-Cresol	1102	159	0
Naphthalene	673	2445	2804
2-Methylnaphthalene	308	368	58
1-Methylnaphthalene	221	251	35
Biphenyl	58	173	137
Acenaphthylene	216	807	874
Acenaphthene	38	33	11
Dibenzofuran	43	153	115
Fluorene	75	307	163
Phenanthrene	101	478	690
Anthracene	50	209	186
Fluoranthene	30	160	308
Pyrene	33	162	288
Benz[a]anthracene	16	74	87
Chrysene	10	56	95
Benz[e]acephenanthrylene	5	24	39
Benzo[k]fluoranthene	4	32	53
Benzo[a]pyrene	9	48	79
Perylene	2	6	13
Dibenzo[ah]anthracene	2	6	12
Indeno[1,2,3-cd]pyrene	5	18	40
Benzo[ghi]perylene	3	14	34

Table A.2: Concentrations of tar compounds for experiment 000125.

Tar species	000125A	000125B	000125C
Benzene	4806	11134	11568
Toluene	3138	2055	188
Ethylbenzene	255	4	0
p&m-Xylene	1180	221	3
o-Xylene	269	32	1
Styrene	1169	898	267
3-Ethyltoluene	65	1	0
4-Ethyltoluene	34	0	0
2-Ethyltoluene	24	0	0
Phenol	4493	775	14
α-Methylstyrene	96	5	1
3&2-Methylstyrene	359	66	3
4-Methylstyrene	165	29	1
2,3-Benzofuran	342	188	2
o-Cresol	1243	8	0
Indene	1138	1246	294
p-Cresol	1563	11	1
m-Cresol	1348	42	0
Naphthalene	1007	3403	3540
2-Methylnaphthalene	455	314	48
1-Methylnaphthalene	322	196	35
Biphenyl	93	254	138
Acenaphthylene	362	1051	1112
Acenaphthene	58	29	16
Dibenzofuran	71	225	139
Fluorene	122	373	172
Phenanthrene	174	848	1035
Anthracene	80	300	233
Fluoranthene	56	314	606
Pyrene	62	291	584
Benz[a]anthracene	30	135	140
Chrysene	20	112	164
Benz[e]acephenanthrylene	11	57	98
Benzo[k]fluoranthene	9	69	107
Benzo[a]pyrene	18	86	184
Perylene	4	13	36
Dibenzo[ah]anthracene	3	14	25
Indeno[1,2,3-cd]pyrene	9	41	105
Benzo[ghi]perylene	6	30	100

Table A.3: Concentrations of tar compounds for experiment 000201.

Tar species	000201A	000201B	000201C
Benzene	5265	10792	10840
Toluene	3179	2306	237
Ethylbenzene	264	6	1
p&m-Xylene	1102	270	4
o-Xylene	256	42	1
Styrene	1270	1010	302
3-Ethyltoluene	58	1	0
4-Ethyltoluene	29	0	0
2-Ethyltoluene	22	0	0
Phenol	4317	1007	17
α-Methylstyrene	93	7	1
3&2-Methylstyrene	360	80	3
4-Methylstyrene	157	36	1
2,3-Benzofuran	368	242	3
o-Cresol	1085	13	0
Indene	1171	1347	339
p-Cresol	1274	19	1
m-Cresol	1092	59	0
Naphthalene	1129	3330	3558
2-Methylnaphthalene	463	344	55
1-Methylnaphthalene	333	225	40
Biphenyl	111	261	150
Acenaphthylene	387	1048	1117
Acenaphthene	62	33	17
Dibenzofuran	81	229	156
Fluorene	130	372	190
Phenanthrene	203	870	1085
Anthracene	92	305	253
Fluoranthene	67	319	628
Pyrene	75	304	598
Benz[a]anthracene	37	147	158
Chrysene	24	130	184
Benz[e]acephenanthrylene	13	58	99
Benzo[k]fluoranthene	11	69	112
Benzo[a]pyrene	21	90	188
Perylene	4	12	33
Dibenzo[ah]anthracene	3	12	24
Indeno[1,2,3-cd]pyrene	9	40	102
Benzo[ghi]perylene	6	28	92

Table A.4: Concentrations of tar compounds for experiment 000330.

Tar species	000330A	000330B	000330C
Benzene	5966	13343	13314
Toluene	3637	2393	151
Ethylbenzene	319	4	0
p&m-Xylene	1346	249	2
o-Xylene	309	36	0
Styrene	1412	1070	248
3-Ethyltoluene	78	0	0
4-Ethyltoluene	41	0	0
2-Ethyltoluene	29	0	0
Phenol	4843	814	13
α-Methylstyrene	114	6	1
3&2-Methylstyrene	416	74	2
4-Methylstyrene	188	32	1
2,3-Benzofuran	375	216	1
o-Cresol	1441	9	0
Indene	1288	1387	268
p-Cresol	1805	10	0
m-Cresol	1391	37	0
Naphthalene	1090	3690	3489
2-Methylnaphthalene	486	343	42
1-Methylnaphthalene	345	216	31
Biphenyl	103	285	134
Acenaphthylene	380	1165	1186
Acenaphthene	63	33	15
Dibenzofuran	81	265	133
Fluorene	126	393	152
Phenanthrene	178	957	1038
Anthracene	79	320	206
Fluoranthene	55	336	615
Pyrene	62	310	592
Benz[a]anthracene	30	154	140
Chrysene	19	123	168
Benz[e]acephenanthrylene	11	65	99
Benzo[k]fluoranthene	9	77	118
Benzo[a]pyrene	18	93	193
Perylene	3	13	35
Dibenzo[ah]anthracene	3	14	23
Indeno[1,2,3-cd]pyrene	9	43	107
Benzo[ghi]perylene	6	30	103

Table A.5: Concentrations of tar compounds for experiment 981029.

Tar species	981029A	981029B	981029C
Benzene	3572	6199	8731
Toluene	2210	1485	207
Ethylbenzene	213	1	2
p&m-Xylene	773	197	3
o-Xylene	170	32	1
Styrene	923	679	159
3-Ethyltoluene	48	0	0
4-Ethyltoluene	22	0	0
2-Ethyltoluene	20	0	0
Phenol	2556	215	3
α-Methylstyrene	72	5	0
3&2-Methylstyrene	211	49	6
4-Methylstyrene	84	22	2
2,3-Benzofuran	202	98	1
o-Cresol	763	0	0
Indene	733	715	102
p-Cresol	656	8	0
m-Cresol	703	10	0
Naphthalene	685	1794	1700
2-Methylnaphthalene	286	197	18
1-Methylnaphthalene	213	132	12
Biphenyl	63	123	64
Acenaphthylene	200	556	391
Acenaphthene	34	14	5
Dibenzofuran	37	81	40
Fluorene	55	161	32
Phenanthrene	155	397	322
Anthracene	41	104	49
Fluoranthene	55	108	110
Pyrene	49	108	99
Benz[a]anthracene	17	39	21
Chrysene	16	43	30
Benz[e]acephenanthrylene	7	17	13
Benzo[k]fluoranthene	7	22	15
Benzo[a]pyrene	11	31	20
Perylene	2	4	4
Dibenzo[ah]anthracene	2	5	3
Indeno[1,2,3-cd]pyrene	7	15	12
Benzo[ghi]perylene	5	12	11

Table A.6: Concentrations of tar compounds for experiment 990615.

Tar species	990615A	990615B
Benzene	5710	5844
Toluene	3227	3100
Ethylbenzene	239	218
p&m-Xylene	1048	985
o-Xylene	229	214
Styrene	1242	1142
3-Ethyltoluene	51	46
4-Ethyltoluene	22	21
2-Ethyltoluene	18	15
Phenol	3684	3564
α-Methylstyrene	88	82
3&2-Methylstyrene	290	266
4-Methylstyrene	112	105
2,3-Benzofuran	279	274
o-Cresol	1040	901
Indene	1070	1028
p-Cresol	905	793
m-Cresol	1017	923
Naphthalene	1012	1012
2-Methylnaphthalene	412	397
1-Methylnaphthalene	296	283
Biphenyl	97	98
Acenaphthylene	336	320
Acenaphthene	45	42
Dibenzofuran	71	73
Fluorene	138	148
Phenanthrene	290	279
Anthracene	71	65
Fluoranthene	125	111
Pyrene	102	87
Benz[a]anthracene	36	29
Chrysene	34	29
Benz[e]acephenanthrylene	17	14
Benzo[k]fluoranthene	16	13
Benzo[a]pyrene	23	17
Perylene	4	4
Dibenzo[ah]anthracene	3	2
Indeno[1,2,3-cd]pyrene	13	10
Benzo[ghi]perylene	10	7

Table A.7: Concentrations of tar compounds for experiment 990722.

Tar species	990722A	990722B	990722C
Benzene	3440	8083	10945
Toluene	2091	1930	200
Ethylbenzene	167	32	2
p&m-Xylene	731	270	2
o-Xylene	161	40	1
Styrene	824	717	157
3-Ethyltoluene	40	12	0
4-Ethyltoluene	18	5	0
2-Ethyltoluene	14	3	0
Phenol	2597	370	6
α-Methylstyrene	60	6	0
3&2-Methylstyrene	199	51	2
4-Methylstyrene	80	24	2
2,3-Benzofuran	193	134	1
o-Cresol	732	6	1
Indene	690	894	182
p-Cresol	663	6	1
m-Cresol	756	13	0
Naphthalene	684	2388	2831
2-Methylnaphthalene	294	267	31
1-Methylnaphthalene	207	166	21
Biphenyl	70	182	101
Acenaphthylene	227	677	648
Acenaphthene	31	17	35
Dibenzofuran	54	145	83
Fluorene	98	225	79
Phenanthrene	207	647	780
Anthracene	46	155	115
Fluoranthene	86	193	316
Pyrene	63	165	272
Benz[a]anthracene	22	55	42
Chrysene	22	66	71
Benz[e]acephenanthrylene	10	25	34
Benzo[k]fluoranthene	9	30	39
Benzo[a]pyrene	12	35	46
Perylene	3	5	9
Dibenzo[ah]anthracene	3	7	7
Indeno[1,2,3-cd]pyrene	8	19	27
Benzo[ghi]perylene	5	13	27

Table A.8: Concentrations of tar compounds for experiment 991214.

Tar species	991214A	991214B	991214C
Benzene	6127	8588	10796
Toluene	3248	1792	222
Ethylbenzene	132	4	0
p&m-Xylene	994	181	2
o-Xylene	206	26	0
Styrene	1328	729	211
3-Ethyltoluene	27	2	0
4-Ethyltoluene	11	0	0
2-Ethyltoluene	7	0	0
Phenol	3403	252	7
α-Methylstyrene	73	3	0
3&2-Methylstyrene	281	49	2
4-Methylstyrene	116	21	1
2,3-Benzofuran	347	158	1
o-Cresol	715	2	0
Indene	1388	1135	234
p-Cresol	687	4	1
m-Cresol	825	8	0
Naphthalene	1598	3339	3419
2-Methylnaphthalene	504	269	38
1-Methylnaphthalene	358	167	28
Biphenyl	144	215	117
Acenaphthylene	566	1026	1063
Acenaphthene	56	21	13
Dibenzofuran	108	197	104
Fluorene	204	366	121
Phenanthrene	420	873	910
Anthracene	141	269	182
Fluoranthene	175	320	481
Pyrene	148	286	451
Benz[a]anthracene	63	113	94
Chrysene	49	112	122
Benz[e]acephenanthrylene	21	46	65
Benzo[k]fluoranthene	21	55	68
Benzo[a]pyrene	31	78	113
Perylene	5	10	24
Dibenzo[ah]anthracene	4	10	13
Indeno[1,2,3-cd]pyrene	13	31	66
Benzo[ghi]perylene	9	24	62

Table A.9: Concentrations of tar compounds for run 990706B.

Tar species	990706B
Benzene	2842
Toluene	1934
Ethylbenzene	191
p&m-Xylene	726
o-Xylene	161
Styrene	746
3-Ethyltoluene	48
4-Ethyltoluene	23
2-Ethyltoluene	19
Phenol	2884
α-Methylstyrene	62
3&2-Methylstyrene	200
4-Methylstyrene	76
2,3-Benzofuran	177
o-Cresol	856
Indene	568
p-Cresol	829
m-Cresol	918
Naphthalene	546
2-Methylnaphthalene	260
1-Methylnaphthalene	184
Biphenyl	66
Acenaphthylene	182
Acenaphthene	29
Dibenzofuran	58
Fluorene	77
Phenanthrene	209
Anthracene	46
Fluoranthene	95
Pyrene	67
Benz[a]anthracene	25
Chrysene	25
Benz[e]acephenanthrylene	11
Benzo[k]fluoranthene	9
Benzo[a]pyrene	12
Perylene	3
Dibenzo[ah]anthracene	3
Indeno[1,2,3-cd]pyrene	7
Benzo[ghi]perylene	5

For the reasons why the data of only this one run of experiment 990706 is presented see page 254 in Chapter 6

Table A.10: Concentrations of tar compounds for experiment 990729.

Tar species	990729A	990729B	990729C
Benzene	2977	4994	10267
Toluene	1935	1355	405
Ethylbenzene	190	8	2
p&m-Xylene	732	252	8
o-Xylene	159	41	1
Styrene	711	630	150
3-Ethyltoluene	43	2	0
4-Ethyltoluene	20	1	0
2-Ethyltoluene	18	0	0
Phenol	2355	482	6
α-Methylstyrene	68	10	0
3&2-Methylstyrene	194	58	3
4-Methylstyrene	73	26	1
2,3-Benzofuran	174	125	5
o-Cresol	730	8	1
Indene	525	565	187
p-Cresol	747	13	1
m-Cresol	745	33	0
Naphthalene	490	1359	1739
2-Methylnaphthalene	218	183	29
1-Methylnaphthalene	159	123	17
Biphenyl	57	120	80
Acenaphthylene	161	391	378
Acenaphthene	23	11	24
Dibenzofuran	51	93	66
Fluorene	64	100	58
Phenanthrene	178	335	397
Anthracene	40	78	71
Fluoranthene	75	106	143
Pyrene	57	80	117
Benz[a]anthracene	20	28	24
Chrysene	18	30	32
Benz[e]acephenanthrylene	8	11	12
Benzo[k]fluoranthene	7	12	14
Benzo[a]pyrene	9	14	15
Perylene	2	2	3
Dibenzo[ah]anthracene	2	3	3
Indeno[1,2,3-cd]pyrene	5	6	9
Benzo[ghi]perylene	4	5	8

Table A.11: Concentrations of tar compounds for experiment 991005.

Tar species	991005A	991005B	991005C
Benzene	4617	10167	13031
Toluene	2880	2645	153
Ethylbenzene	188	8	1
p&m-Xylene	908	325	2
o-Xylene	197	50	0
Styrene	871	879	171
3-Ethyltoluene	46	1	0
4-Ethyltoluene	21	1	0
2-Ethyltoluene	16	0	0
Phenol	3061	763	7
α-Methylstyrene	78	9	1
3&2-Methylstyrene	253	81	2
4-Methylstyrene	101	36	1
2,3-Benzofuran	235	223	1
o-Cresol	1116	8	0
Indene	823	1206	190
p-Cresol	1055	9	0
m-Cresol	1128	35	0
Naphthalene	929	3105	3503
2-Methylnaphthalene	356	396	33
1-Methylnaphthalene	260	222	23
Biphenyl	90	219	110
Acenaphthylene	334	989	1065
Acenaphthene	40	23	19
Dibenzofuran	74	186	84
Fluorene	116	359	97
Phenanthrene	293	759	877
Anthracene	86	236	154
Fluoranthene	135	252	496
Pyrene	100	219	457
Benz[a]anthracene	44	90	74
Chrysene	36	85	97
Benz[e]acephenanthrylene	15	31	49
Benzo[k]fluoranthene	12	38	55
Benzo[a]pyrene	18	53	88
Perylene	3	6	20
Dibenzo[ah]anthracene	3	7	11
Indeno[1,2,3-cd]pyrene	8	19	51
Benzo[ghi]perylene	6	14	50

Table A.12: Concentrations of tar compounds for experiment 991123.

Tar species	991123A	991123B	991123C
Benzene	11931	16889	11837
Toluene	3692	615	99
Ethylbenzene	101	3	0
p&m-Xylene	751	20	1
o-Xylene	153	4	0
Styrene	1765	852	109
3-Ethyltoluene	14	1	0
4-Ethyltoluene	7	0	0
2-Ethyltoluene	4	0	0
Phenol	2314	13	9
α-Methylstyrene	55	2	1
3&2-Methylstyrene	271	13	2
4-Methylstyrene	112	5	1
2,3-Benzofuran	363	15	0
o-Cresol	279	0	0
Indene	1597	724	121
p-Cresol	286	1	0
m-Cresol	383	1	0
Naphthalene	2666	5074	2628
2-Methylnaphthalene	542	115	22
1-Methylnaphthalene	405	86	18
Biphenyl	223	257	86
Acenaphthylene	786	1385	980
Acenaphthene	70	37	13
Dibenzofuran	127	144	15
Fluorene	247	303	63
Phenanthrene	614	1310	696
Anthracene	206	314	94
Fluoranthene	201	619	496
Pyrene	221	658	585
Benz[a]anthracene	87	159	53
Chrysene	72	177	82
Benz[e]acephenanthrylene	28	81	59
Benzo[k]fluoranthene	32	99	56
Benzo[a]pyrene	53	166	130
Perylene	7	25	34
Dibenzo[ah]anthracene	6	19	9
Indeno[1,2,3-cd]pyrene	19	85	92
Benzo[ghi]perylene	15	81	129

Table A.13: Concentrations of tar compounds for experiment 000215.

Tar species	000215A	000215B	000215C
Benzene	10417	20393	18392
Toluene	5169	3757	383
Ethylbenzene	506	24	2
p&m-Xylene	1478	483	9
o-Xylene	408	85	2
Styrene	1592	2301	843
3-Ethyltoluene	96	4	0
4-Ethyltoluene	49	1	0
2-Ethyltoluene	56	1	0
Phenol	2537	864	13
α-Methylstyrene	111	23	1
3&2-Methylstyrene	457	202	8
4-Methylstyrene	163	81	3
2,3-Benzofuran	219	245	3
o-Cresol	982	17	0
Indene	1051	1625	511
p-Cresol	900	16	1
m-Cresol	865	52	0
Naphthalene	1157	4420	4990
2-Methylnaphthalene	471	496	87
1-Methylnaphthalene	373	351	64
Biphenyl	114	310	266
Acenaphthylene	286	1133	1575
Acenaphthene	50	62	32
Dibenzofuran	56	124	83
Fluorene	123	345	234
Phenanthrene	282	1036	1394
Anthracene	77	304	279
Fluoranthene	111	280	683
Pyrene	94	351	757
Benz[a]anthracene	39	128	153
Chrysene	31	124	186
Benz[e]acephenanthrylene	13	45	86
Benzo[k]fluoranthene	9	51	119
Benzo[a]pyrene	16	100	198
Perylene	3	10	30
Dibenzo[ah]anthracene	2	11	20
Indeno[1,2,3-cd]pyrene	8	35	108
Benzo[ghi]perylene	6	29	114

Table A.14: Concentrations of tar compounds for experiment 991126.

Tar species	991126A	991126B	991126C
Benzene	21905	33407	16888
Toluene	6315	1088	129
Ethylbenzene	333	5	0
p&m-Xylene	599	18	0
o-Xylene	112	2	0
Styrene	20912	1364	82
3-Ethyltoluene	7	1	0
4-Ethyltoluene	4	0	0
2-Ethyltoluene	1	0	0
Phenol	2394	13	10
α-Methylstyrene	487	2	1
3&2-Methylstyrene	268	16	2
4-Methylstyrene	121	7	1
2,3-Benzofuran	347	15	0
o-Cresol	180	0	0
Indene	2977	948	103
p-Cresol	192	1	0
m-Cresol	296	0	0
Naphthalene	5361	6663	2638
2-Methylnaphthalene	641	134	18
1-Methylnaphthalene	506	90	14
Biphenyl	840	983	193
Acenaphthylene	875	1432	746
Acenaphthene	66	32	10
Dibenzofuran	156	175	18
Fluorene	676	423	56
Phenanthrene	2492	3181	1019
Anthracene	391	422	103
Fluoranthene	317	880	544
Pyrene	257	585	428
Benz[a]anthracene	151	242	66
Chrysene	177	325	109
Benz[e]acephenanthrylene	59	184	97
Benzo[k]fluoranthene	50	119	53
Benzo[a]pyrene	71	169	112
Perylene	9	29	35
Dibenzo[ah]anthracene	22	46	15
Indeno[1,2,3-cd]pyrene	27	96	91
Benzo[ghi]perylene	18	64	78

Table A.15: Concentrations of tar compounds for experiment 991207.

Tar species	991207A	991207B	991207C
Benzene	16831	47841	22415
Toluene	12285	3954	3521
Ethylbenzene	3541	24	1
p&m-Xylene	747	113	0
o-Xylene	151	16	0
Styrene	54065	7169	169
3-Ethyltoluene	34	1	0
4-Ethyltoluene	16	0	0
2-Ethyltoluene	10	0	0
Phenol	2187	100	17
α-Methylstyrene	2442	22	1
3&2-Methylstyrene	401	89	1
4-Methylstyrene	176	39	1
2,3-Benzofuran	226	103	1
o-Cresol	606	1	0
Indene	3324	2162	144
p-Cresol	565	3	1
m-Cresol	614	3	0
Naphthalene	4841	8942	3013
2-Methylnaphthalene	705	324	23
1-Methylnaphthalene	552	229	18
Biphenyl	887	2158	402
Acenaphthylene	448	1238	752
Acenaphthene	67	48	11
Dibenzofuran	74	158	39
Fluorene	654	933	88
Phenanthrene	2419	5933	1563
Anthracene	344	622	142
Fluoranthene	247	841	639
Pyrene	158	506	385
Benz[a]anthracene	129	390	104
Chrysene	129	534	168
Benz[e]acephenanthrylene	35	236	143
Benzo[k]fluoranthene	26	134	75
Benzo[a]pyrene	40	170	120
Perylene	5	24	35
Dibenzo[ah]anthracene	17	84	31
Indeno[1,2,3-cd]pyrene	14	89	102
Benzo[ghi]perylene	9	51	70

APPENDIX B: EXPERIMENTAL DATA

In this appendix the data collected in the experiments according to the final experimental plan is given in summarised form. The data is be presented in the same order as in Table 5.4 on page 131.

Table B.1: Data for experiment 990903.

Fuel: SCW		**Gasification agent: Air**		
Run		**990903A**	**990903B**	**990903C**
Input				
Fuel	[kg/h]	22.402	16.407	11.602
$w_{H2O,Fuel}$	[mass-%$_{Raw}$]	5.1	5.5	5.5
$w_{Ash,Fuel}$	[mass-%$_{Raw}$]	0.22	0.30	0.30
LHV_{Fuel}	[kJ/kg$_{Raw}$]	17.971	17.886	17.886
Air	[kg/h]	24.513	24.513	24.492
Oxygen	[kg/h]	0	0	0
Steam	[kg/h]	0	0	0
Argon	[kg/h]	0.304	0.304	0.304
ER	[-]	0.19	0.25	0.36
S/F	[kg/kg$_{Fuel,DAF}$]	0.05	0.06	0.06
T_{Bed}	[°C]	708	810	911
T_{FB}	[°C]	700	800	900
Output				
Solids	[kg/h]	0.514	0.287	0.187
$w_{C,Solids}$	[mass-%$_{Raw}$]	77.7	48.6	56.1
$w_{H2O,Solids}$	[mass-%$_{Raw}$]	0.9	0.6	1.5
Argon loss	[kg/h]	0.183	0.279	0.295
Gas + Tars	[kg/h]	46.521	40.658	35.916
Gas composition $y_{i,PG}$ [vol.-%]				
N_2		41.1	44.7	49.7
CO_2		11.3	11.4	12.3
CO		15.8	16.2	12.5
H_2		7.6	7.5	6.9
CH_4		5.0	4.4	3.1
Ar		0.6	0.6	0.6
H_2O		15.5	11.6	11.9
Tars		3.1	3.7	2.9
ρ_N	[kg/m^3_N]	1.130	1.148	1.171
Y_{Gas}	[m$^3_{N,DIF}$/kg$_{Fuel,DAF}$]]	0.983	1.191	1.340
LHV_{Gas}	[kJ/m^3_N]	4599	4421	3451

Table B.1: Data for experiment 990903.

Fuel: SCW		**Gasification agent: Air**		
Run		**990903A**	**990903B**	**990903C**
$C_{Tar\ class}$	[mg/m^3_N]			
Benzene		4228	8281	9584
1 ring		5311	4041	652
Naphthalene		673	2445	2804
2 ring		1409	2235	588
3 ring		479	1835	1924
4+ ring		119	601	1048
Phenol		3348	1590	13
Cresols		3371	287	0
O-heteroar.		298	425	123
$C_{Tars,Total}$	[mg/m^3_N]	19235	21740	16735
Y_{Tar}	[$g/kg_{Fuel,DAF}$]	37.34	49.83	46.97
LHV_{Tars}	[MJ/kg]	37.107	38.906	39.524
M_{Tars}	[kg/kmol]	13.854	13.195	12.950
Tar elemental composition [mass-%]				
C		86.7	91.0	92.7
H		7.5	7.2	7.0
O		5.8	1.7	0.2
η_{CG}	[%]	46.2	52.4	50.3
η_{Tars}	[%]	7.3	10.2	9.8
Balances	[%]			
C		76.0	88.2	93.4
H		85.9	85.9	94.0
O		100.8	94.8	98.3
N		114.1	106.9	103.0

Table B.2: Data for experiment 000125.

Fuel: SCW		**Gasification agent: steam/oxygen**		
Run		**000125A**	**000125B**	**000125C**
Input				
Fuel	[kg/h]	21.873	14.248	10.786
$w_{H2O,Fuel}$	[mass-%$_{Raw}$]	7.8	7.7	7.8
$w_{Ash,Fuel}$	[mass-%$_{Raw}$]	0.13	0.12	0.12
LHV_{Fuel}	[kJ/kg$_{Raw}$]	17.527	17.527	17.527
Air	[kg/h]	1.273	1.263	1.269
Oxygen	[kg/h]	5.375	5.374	5.381
Steam	[kg/h]	5.810	5.807	5.811
Argon	[kg/h]	0.304	0.304	0.304
ER	[-]	0.20	0.30	0.40
S/F	[kg/kg$_{Fuel,DAF}$]	0.37	0.53	0.67
T_{Bed}	[°C]	707	841	932
T_{FB}	[°C]	700	800	900
Output				
Solids	[kg/h]	0.411	0.103	0.075
$w_{C,Solids}$	[mass-%$_{Raw}$]	66.3	37.3	42.0
$w_{H2O,Solids}$	[mass-%$_{Raw}$]	1.7	4.9	5.3
Argon loss	[kg/h]	0.042	0.085	0.140
Gas + Tars	[kg/h]	34.181	26.809	23.336
Gas composition $y_{i,PG}$ [vol.-%]				
N_2		3.8	3.4	3.0
CO_2		12.2	16.0	17.7
CO		24.5	21.8	17.0
H_2		7.0	7.5	7.5
CH_4		5.6	4.4	3.3
Ar		0.5	0.5	0.5
H_2O		42.4	42.1	47.4
Tars		4.0	4.3	3.6
ρ_N	[kg/m^3_N]	1.014	1.040	1.037
Y_{Gas}	[m$^3_{N,DIF}$/kg$_{Fuel,DAF}$]	0.848	1.053	1.110
LHV_{Gas}	[kJ/m^3_N]	5838	5132	4158

Table B.2: Data for experiment 000125.

Fuel: SCW		**Gasification agent: steam/oxygen**		
Run		**000125A**	**000125B**	**000125C**
$C_{Tar\ class}$	[mg/m^3_N]			
Benzene		4806	11134	11568
1 ring		6753	3312	465
Naphthalene		1007	3403	3540
2 ring		2008	2010	515
3 ring		796	2601	2568
4+ ring		230	1160	2149
Phenol		4493	775	14
Cresols		4154	61	2
O-heteroar.		413	413	141
$C_{Tars,Total}$	[mg/m^3_N]	24660	24869	20962
Y_{Tar}	[$g/kg_{Fuel,DAF}$]	41.27	48.82	47.48
LHV_{Tars}	[MJ/kg]	37.043	39.269	39.419
M_{Tars}	[kg/kmol]	13.855	13.053	12.941
Tar elemental composition [mass-%]				
C		86.7	92.0	92.8
H		7.5	7.1	6.9
O		5.8	0.8	0.3
η_{CG}	[%]	50.1	51.7	48.5
η_{Tars}	[%]	8.0	10.1	9.8
Balances	[%]			
C		84.6	96.9	100.3
H		88.7	86.4	92.3
O		105.1	101.3	101.1
N		164.9	115.6	87.8

Table B.3: Data for experiment 000201.

Fuel: Aged SCW		**Gasification agent: steam/oxygen**		
Run		**000201A**	**000201B**	**000201C**
Input				
Fuel	[kg/h]	20.316	14.215	10.688
$w_{H2O,Fuel}$	[mass-%$_{Raw}$]	9.6	9.2	10.0
$w_{Ash,Fuel}$	[mass-%$_{Raw}$]	0.19	0.20	0.18
LHV_{Fuel}	[kJ/kg$_{Raw}$]	17.527	17.527	17.527
Air	[kg/h]	1.271	1.268	1.267
Oxygen	[kg/h]	5.382	5.386	5.386
Steam	[kg/h]	5.799	5.809	5.809
Argon	[kg/h]	0.304	0.304	0.304
ER	[-]	0.21	0.31	0.41
S/F	[kg/kg$_{Fuel,DAF}$]	0.42	0.55	0.72
T_{Bed}	[°C]	729	834	923
T_{FB}	[°C]	700	800	900
Output				
Solids	[kg/h]	0.183	0.092	0.064
$w_{C,Solids}$	[mass-%$_{Raw}$]	64.6	53.8	55.9
$w_{H2O,Solids}$	[mass-%$_{Raw}$]	4.5	7.6	4.6
Argon loss	[kg/h]	0.046	0.104	0.113
Gas + Tars	[kg/h]	32.842	26.785	23.278
Gas composition $y_{i,PG}$ [vol.-%]				
N_2		4.0	3.6	3.1
CO_2		12.3	15.8	17.7
CO		23.7	21.0	16.6
H_2		6.0	6.4	6.8
CH_4		5.3	4.3	3.2
Ar		0.5	0.5	0.5
H_2O		44.3	44.1	48.4
Tars		4.0	4.4	3.6
ρ_N	[kg/m^3_N]	1.020	1.042	1.043
Y_{Gas}	[m$^3_{N,DIF}$/kg$_{Fuel,DAF}$]	0.862	1.029	1.122
LHV_{Gas}	[kJ/m^3_N]	5517	4873	3989

Table B.3: Data for experiment 000201.

Fuel: Aged SCW		**Gasification agent: steam/oxygen**		
Run		**000201A**	**000201B**	**000201C**
$C_{Tar\ class}$	[mg/m^3_N]			
Benzene		5265	10792	10840
1 ring		6791	3758	549
Naphthalene		1129	3330	3558
2 ring		2078	2177	583
3 ring		875	2628	2662
4+ ring		270	1210	2220
Phenol		4317	1007	17
Cresols		3451	91	1
O-heteroar.		449	471	159
$C_{Tars,Total}$	[mg/m^3_N]	24625	25463	20588
Y_{Tar}	[$g/kg_{Fuel,DAF}$]	43.26	50.81	47.86
LHV_{Tars}	[MJ/kg]	37.290	39.182	39.382
M_{Tars}	[kg/kmol]	13.771	13.080	12.939
Tar elemental composition [mass-%]				
C		87.2	91.8	92.8
H		7.5	7.1	6.9
O		5.3	1.0	0.3
η_{CG}	[%]	48.7	49.0	46.6
η_{Tars}	[%]	8.3	10.3	9.7
Balances	[%]			
C		85.3	96.6	101.8
H		88.8	86.7	91.5
O		104.5	101.3	100.8
N		166.6	120.7	89.7

Table B.4: Data for experiment 000330.

Fuel: Milled SCW		**Gasification agent: steam/oxygen**		
Run		**000330A**	**000330B**	**000330C**
Input				
Fuel	[kg/h]	21.997	13.885	9.327
$w_{H2O,Fuel}$	[mass-%$_{Raw}$]	7.0	7.0	7.0
$w_{Ash,Fuel}$	[mass-%$_{Raw}$]	0.50	0.50	0.50
LHV_{Fuel}	[kJ/kg$_{Raw}$]	17.527	17.527	17.527
Air	[kg/h]	1.266	1.259	1.262
Oxygen	[kg/h]	5.391	5.387	5.388
Steam	[kg/h]	5.806	5.814	5.814
Argon	[kg/h]	0.304	0.761	0.761
ER	[-]	0.19	0.31	0.46
S/F	[kg/kg$_{Fuel,DAF}$]	0.36	0.53	0.75
T_{Bed}	[°C]	714	842	944
T_{FB}	[°C]	700	800	900
Output				
Solids	[kg/h]	0.141	0.098	0.075
$w_{C,Solids}$	[mass-%$_{Raw}$]	51.9	58.1	69.2
$w_{H2O,Solids}$	[mass-%$_{Raw}$]	2.7	15.5	11.6
Argon loss	[kg/h]	-0.007	0.522	0.531
Gas + Tars	[kg/h]	34.631	26.487	21.946
Gas composition $y_{i,PG}$ [vol.-%]				
N_2		4.0	3.5	2.8
CO_2		11.1	15.1	17.8
CO		27.5	24.0	18.6
H_2		6.3	7.1	7.1
CH_4		5.8	4.4	3.2
Ar		0.5	0.6	0.7
H_2O		40.4	40.3	45.9
Tars		4.6	4.9	3.9
ρ_N	[kg/m^3_N]	1.020	1.042	1.050
Y_{Gas}	[m$^3_{N,DIF}$/kg$_{Fuel,DAF}$]	0.878	1.090	1.247
LHV_{Gas}	[kJ/m^3_N]	6206	5390	4252

Table B.4: Data for experiment 000330.

Fuel: Milled SCW		**Gasification agent: steam/oxygen**		
Run		**000330A**	**000330B**	**000330C**
$C_{Tar\ class}$	[mg/m^3_N]			
Benzene		5966	13343	13314
1 ring		7888	3866	404
Naphthalene		1090	3690	3489
2 ring		2222	2230	475
3 ring		826	2866	2596
4+ ring		226	1258	2193
Phenol		4843	814	13
Cresols		4637	56	0
O-heteroar.		456	481	134
$C_{Tars,Total}$	[mg/m^3_N]	28154	28606	22618
Y_{Tar}	[$g/kg_{Fuel,DAF}$]	47.00	56.62	54.78
LHV_{Tars}	[MJ/kg]	37.183	39.322	39.471
M_{Tars}	[kg/kmol]	13.823	13.050	12.945
Tar elemental composition [mass-%]				
C		86.9	92.0	92.8
H		7.5	7.2	7.0
O		5.6	0.8	0.3
η_{CG}	[%]	53.2	54.8	53.2
η_{Tars}	[%]	9.2	11.8	11.4
Balances	[%]			
C		87.0	102.2	112.6
H		86.5	84.3	89.6
O		104.5	99.8	98.9
N		173.9	116.6	76.3

Table B.5: Data for experiment 981029.

Fuel: AH		**Gasification agent: air**		
Run		**981029A**	**981029B**	**981029C**
Input				
Fuel	[kg/h]	23.920	14.170	11.388
$w_{H2O,Fuel}$	[mass-%$_{Raw}$]	4.4	4.4	4.4
$w_{Ash,Fuel}$	[mass-%$_{Raw}$]	7.69	7.69	7.69
LHV_{Fuel}	[kJ/kg$_{Raw}$]	18.217	18.217	18.217
Air	[kg/h]	24.524	24.519	24.522
Oxygen	[kg/h]	0.000	0.000	0.000
Steam	[kg/h]	0.000	0.000	0.000
Argon	[kg/h]	0.304	0.304	0.304
ER	[-]	0.18	0.31	0.38
S/F	[kg/kg$_{Fuel,DAF}$]	0.05	0.05	0.05
T_{Bed}	[°C]	725	849	946
T_{FB}	[°C]	700	800	900
Output				
Solids	[kg/h]	2.041	0.859	0.462
$w_{C,Solids}$	[mass-%$_{Raw}$]	44.2	34.1	24.3
$w_{H2O,Solids}$	[mass-%$_{Raw}$]	0.4	0.6	0.6
Argon loss	[kg/h]	0.155	0.249	0.259
Gas + Tars	[kg/h]	46.552	37.885	35.493
Gas composition $y_{i,PG}$ [vol.-%]				
N_2		42.2	49.6	53.2
CO_2		11.8	12.7	13.0
CO		14.0	11.9	10.2
H_2		7.3	6.6	6.7
CH_4		4.1	3.0	2.2
Ar		0.7	0.7	0.7
H_2O		17.3	13.1	12.0
Tars		2.6	2.4	2.1
ρ_N	[kg/m^3_N]	1.137	1.177	1.190
Y_{Gas}	[m$^3_{N,DIF}$/kg$_{Fuel,DAF}$]	0.937	1.226	1.352
LHV_{Gas}	[kJ/m^3_N]	4035	3286	2791

Table B.5: Data for experiment 981029.

Fuel: AH		**Gasification agent: air**		
Run		**981029A**	**981029B**	**981029C**
$C_{Tar\ class}$	[mg/m^3_N]			
Benzene		3572	6199	8731
1 ring		4746	2469	378
Naphthalene		685	1794	1700
2 ring		1295	1168	196
3 ring		484	1232	799
4+ ring		179	404	336
Phenol		2556	215	3
Cresols		2123	17	0
O-heteroar.		239	180	40
$C_{Tars,Total}$	[mg/m^3_N]	15877	13679	12184
Y_{Tar}	[$g/kg_{Fuel,DAF}$]	30.93	35.36	36.32
LHV_{Tars}	[MJ/kg]	37.516	39.530	39.761
M_{Tars}	[kg/kmol]	13.723	13.025	12.972
Tar elemental composition [mass-%]				
C		87.5	92.2	92.6
H		7.5	7.3	7.3
O		4.9	0.5	0.1
η_{CG}	[%]	37.4	40.5	39.7
η_{Tars}	[%]	5.6	6.7	7.0
Balances	[%]			
C		73.9	84.7	87.0
H		84.5	87.8	90.7
O		105.9	102.5	100.5
N		115.5	107.2	106.6

Table B.6: Data for experiment 990615.

Fuel: AH		**Gasification agent: steam/oxygen**	
Run		**990615A**	**990615B**
Input			
Fuel	[kg/h]	22.400	21.669
$w_{H2O,Fuel}$	[mass-%$_{Raw}$]	6.2	6.2
$w_{Ash,Fuel}$	[mass-%$_{Raw}$]	10.46	10.46
LHV_{Fuel}	[kJ/kg$_{Raw}$]	18.217	18.434
Air	[kg/h]	1.268	1.265
Oxygen	[kg/h]	5.370	5.371
Steam	[kg/h]	5.808	5.808
Argon	[kg/h]	0.304	0.304
ER	[-]	0.20	0.21
S/F	[kg/kg$_{Fuel,DAF}$]	0.39	0.40
T_{Bed}	[°C]	732	734
T_{FB}	[°C]	700	800
Output			
Solids	[kg/h]	1.707	1.588
$w_{C,Solids}$	[mass-%$_{Raw}$]	47.9	46.8
$w_{H2O,Solids}$	[mass-%$_{Raw}$]	0.0	0.0
Argon loss	[kg/h]	0.080	0.101
Gas + Tars	[kg/h]	33.364	32.728
Gas composition $y_{i,PG}$ [vol.-%]			
N_2		4.7	4.5
CO_2		18.1	19.5
CO		14.1	13.4
H_2		12.5	12.0
CH_4		5.3	4.9
Ar		0.4	0.4
H_2O		41.1	41.6
Tars		3.8	3.7
ρ_N	[kg/m^3_N]	0.999	1.016
Y_{Gas}	[m$^3_{N,DIF}$/kg$_{Fuel,DAF}$]	0.893	0.916
LHV_{Gas}	[kJ/m^3_N]	5041	4734

Table B.6: Data for experiment 990615.

Fuel: AH		**Gasification agent: steam/oxygen**	
Run		**990615A**	**990615B**
$C_{Tar\ class}$	[mg/m^3_N]		
Benzene		5710	5844
1 ring		6566	6191
Naphthalene		1012	1012
2 ring		1874	1807
3 ring		880	852
4+ ring		382	323
Phenol		3684	3564
Cresols		2962	2617
O-heteroar.		350	347
$C_{Tars,Total}$	[mg/m^3_N]	23420	22558
Y_{Tar}	[$g/kg_{Fuel,DAF}$]	41.87	40.24
LHV_{Tars}	[MJ/kg]	37.572	37.641
M_{Tars}	[kg/kmol]	13.691	13.669
Tar elemental composition [mass-%]			
C		87.7	87.9
H		7.5	7.5
O		4.8	4.6
η_{CG}	[%]	40.3	37.3
η_{Tars}	[%]	7.2	6.8
Balances	[%]		
C		84.9	84.4
H		98.2	95.6
O		110.8	111.7
N		176.4	164.3

Table B.7: Data for experiment 990722.

Fuel: AH		**Gasification agent: steam/oxygen**	
Run		**990722B**	**990722C**
Input			
Fuel	[kg/h]	14.350	11.130
$w_{H2O,Fuel}$	[mass-%$_{Raw}$]	7.6	7.6
$w_{Ash,Fuel}$	[mass-%$_{Raw}$]	5.50	5.50
LHV_{Fuel}	[kJ/kg$_{Raw}$]	18.124	18.124
Air	[kg/h]	1.252	1.250
Oxygen	[kg/h]	5.368	5.365
Steam	[kg/h]	5.806	5.807
Argon	[kg/h]	0.304	0.304
ER	[-]	0.30	0.39
S/F	[kg/kg$_{Fuel,DAF}$]	0.55	0.69
T_{Bed}	[°C]	828	923
T_{FB}	[°C]	800	900
Output			
Solids	[kg/h]	0.927	0.491
$w_{C,Solids}$	[mass-%$_{Raw}$]	36.8	33.7
$w_{H2O,Solids}$	[mass-%$_{Raw}$]	1.6	2.6
Argon loss	[kg/h]	0.173	0.175
Gas + Tars	[kg/h]	25.980	23.190
Gas composition $y_{i,PG}$ [vol.-%]			
N_2		4.2	3.8
CO_2		21.7	22.4
CO		11.1	8.1
H_2		12.8	12.4
CH_4		4.2	3.3
Ar		0.3	0.4
H_2O		42.7	46.7
Tars		3.1	3.0
ρ_N	[kg/m^3_N]	1.025	1.022
Y_{Gas}	[m$^3_{N,DIF}$/kg$_{Fuel,DAF}$]	1.061	1.132
LHV_{Gas}	[kJ/m^3_N]	4274	3530

Table B.7: Data for experiment 990722.

Fuel: AH		**Gasification agent: steam/oxygen**	
Run		**990722B**	**990722C**
$C_{Tar\ class}$	[mg/m^3_N]		
Benzene		8083	10945
1 ring		3091	366
Naphthalene		2388	2831
2 ring		1509	335
3 ring		1720	1657
4+ ring		612	888
Phenol		370	6
Cresols		25	2
O-heteroar.		279	85
$C_{Tars,Total}$	[mg/m^3_N]	18078	17115
Y_{Tar}	[$g/kg_{Fuel,DAF}$]	36.74	40.13
LHV_{Tars}	[MJ/kg]	39.447	39.599
M_{Tars}	[kg/kmol]	13.039	12.958
Tar elemental composition [mass-%]			
C		92.1	92.7
H		7.3	7.1
O		0.6	0.2
η_{CG}	[%]	40.9	39.0
η_{Tars}	[%]	7.0	7.6
Balances	[%]		
C		89.6	92.3
H		93.8	99.4
O		104.3	104.1
N		125.8	104.1

Table B.8: Data for experiment 991214.

Fuel: AH		**Gasification agent: steam/oxygen**		
Run		**991214A**	**991214B**	**991214C**
Input				
Fuel	[kg/h]	21.147	15.492	12.092
$w_{H2O,Fuel}$	[mass-%$_{Raw}$]	7.3	7.2	7.3
$w_{Ash,Fuel}$	[mass-%$_{Raw}$]	5.74	8.51	7.59
LHV_{Fuel}	[kJ/kg$_{Raw}$]	18.217	18.217	18.217
Air	[kg/h]	1.259	1.261	1.257
Oxygen	[kg/h]	5.375	5.376	5.377
Steam	[kg/h]	5.812	5.813	5.813
Argon	[kg/h]	0.304	0.304	0.456
ER	[-]	0.21	0.29	0.37
S/F	[kg/kg$_{Fuel,DAF}$]	0.40	0.53	0.65
T_{Bed}	[°C]	732	832	922
T_{FB}	[°C]	700	800	900
Output				
Solids	[kg/h]	1.444	0.796	0.712
$w_{C,Solids}$	[mass-%$_{Raw}$]	94.3	30.9	25.5
$w_{H2O,Solids}$	[mass-%$_{Raw}$]	0.3	1.0	0.7
Argon loss	[kg/h]	0.017	-0.036	0.134
Gas + Tars	[kg/h]	32.437	27.487	24.150
Gas composition $y_{i,PG}$ [vol.-%]				
N_2		4.0	4.1	3.7
CO_2		15.5	17.4	18.7
CO		20.3	17.8	13.1
H_2		8.5	9.5	11.9
CH_4		5.1	4.4	3.5
Ar		0.5	0.8	0.8
H_2O		42.1	42.5	44.9
Tars		4.1	3.6	3.3
ρ_N	[kg/m^3_N]	1.024	1.031	1.008
Y_{Gas}	[m$^3_{N,DIF}$/kg$_{Fuel,DAF}$]	0.890	1.066	1.118
LHV_{Gas}	[kJ/m^3_N]	5289	4857	4187

Table B.8: Data for experiment 991214.

Fuel: AH		**Gasification agent: steam/oxygen**		
Run		**991214A**	**991214B**	**991214C**
$C_{Tar\ class}$	[mg/m^3_N]			
Benzene		6127	8588	10796
1 ring		6424	2807	438
Naphthalene		1598	3339	3419
2 ring		2393	1786	417
3 ring		1386	2555	2289
4+ ring		538	1086	1560
Phenol		3403	252	7
Cresols		2228	14	1
O-heteroar.		455	356	105
$C_{Tars,Total}$	[mg/m^3_N]	24553	20782	19031
Y_{Tar}	[$g/kg_{Fuel,DAF}$]	42.31	42.45	44.30
LHV_{Tars}	[MJ/kg]	37.892	39.376	39.470
M_{Tars}	[kg/kmol]	13.552	12.998	12.942
Tar elemental composition [mass-%]				
C		88.6	92.4	92.8
H		7.4	7.1	7.0
O		4.0	0.5	0.2
η_{CG}	[%]	42.5	45.0	44.7
η_{Tars}	[%]	7.7	7.7	8.2
Balances	[%]			
C		94.3	95.0	96.5
H		88.4	91.9	98.9
O		107.4	105.5	103.3
N		142.6	129.0	107.9

Table B.9: Data for experiment 990729.

Fuel: AH		**Gasification agent: steam/oxygen**		
Run		**990729A**	**990729B**	**990729C**
Input				
Fuel	[kg/h]	22.153	14.135	10.603
$w_{H2O,Fuel}$	[mass-%$_{Raw}$]	7.6	7.6	7.6
$w_{Ash,Fuel}$	[mass-%$_{Raw}$]	5.50	5.50	5.50
LHV_{Fuel}	[kJ/kg$_{Raw}$]	18.124	18.124	18.124
Air	[kg/h]	1.260	1.261	1.268
Oxygen	[kg/h]	5.373	5.369	5.375
Steam	[kg/h]	11.601	11.601	11.610
Argon	[kg/h]	0.304	0.304	0.304
ER	[-]	0.20	0.31	0.41
S/F	[kg/kg$_{Fuel,DAF}$]	0.69	1.03	1.35
T_{Bed}	[°C]	699	804	899
T_{FB}	[°C]	700	800	900
Output				
Solids	[kg/h]	2.435	1.207	0.692
$w_{C,Solids}$	[mass-%$_{Raw}$]	50.7	41.5	38.6
$w_{H2O,Solids}$	[mass-%$_{Raw}$]	0.0	1.1	3.4
Argon loss	[kg/h]	0.175	0.217	0.213
Gas + Tars	[kg/h]	38.082	31.247	28.255
Gas composition $y_{i,PG}$ [vol.-%]				
N_2		2.5	2.9	2.6
CO_2		13.3	16.8	16.8
CO		9.4	9.2	6.0
H_2		7.0	9.5	8.3
CH_4		3.2	2.9	2.1
Ar		0.2	0.2	0.2
H_2O		62.1	56.5	61.5
Tars		2.3	2.0	2.5
ρ_N	[kg/m^3_N]	0.957	0.981	0.972
Y_{Gas}	[m$^3_{N,DIF}$/kg$_{Fuel,DAF}$]	0.623	0.957	0.990
LHV_{Gas}	[kJ/m^3_N]	3098	3211	2403

Table B.9: Data for experiment 990729.

Fuel: AH		**Gasification agent: steam/oxygen**		
Run		**990729A**	**990729B**	**990729C**
$C_{Tar\ class}$	[mg/m^3_N]			
Benzene		2977	4994	10267
1 ring		4142	2383	569
Naphthalene		490	1359	1739
2 ring		958	991	314
3 ring		467	915	927
4+ ring		206	298	379
Phenol		2355	482	6
Cresols		2222	54	1
O-heteroar.		225	218	71
$C_{Tars,Total}$	[mg/m^3_N]	14042	11696	14274
Y_{Tar}	[$g/kg_{Fuel,DAF}$]	29.03	30.33	45.01
LHV_{Tars}	[MJ/kg]	37.269	39.291	39.776
M_{Tars}	[kg/kmol]	13.801	13.110	12.981
Tar elemental composition [mass-%]				
C		87.0	91.6	92.5
H		7.5	7.3	7.3
O		5.4	1.1	0.1
η_{CG}	[%]	30.3	39.5	35.8
η_{Tars}	[%]	5.2	5.7	8.6
Balances	[%]			
C		72.8	90.6	94.4
H		100.1	93.8	98.8
O		110.3	103.1	102.7
N		112.2	111.4	89.7

Table B.10: Data for run 990706B.

Fuel: AH		**Gasification agent: steam/oxygen**	
Run		**990706B**	
Input			For the reasons why the data of only this one run of experiment 990706 is presented see page 254 in Chapter 6
Fuel	[kg/h]	22.340	
$w_{H2O,Fuel}$	[mass-%$_{Raw}$]	6.6	
$w_{Ash,Fuel}$	[mass-%$_{Raw}$]	5.38	
LHV_{Fuel}	[kJ/kg$_{Raw}$]	18.330	
Air	[kg/h]	1.268	
Oxygen	[kg/h]	5.374	
Steam	[kg/h]	11.620	
Argon	[kg/h]	0.304	
ER	[-]	0.19	
S/F	[kg/kg$_{Fuel,DAF}$]	0.67	
T_{Bed}	[°C]	691	
T_{FB}	[°C]	800	
Output			
Solids	[kg/h]	2.428	
$w_{C,Solids}$	[mass-%$_{Raw}$]	43.8	
$w_{H2O,Solids}$	[mass-%$_{Raw}$]	0.0	
Argon loss	[kg/h]	0.129	
Gas + Tars	[kg/h]	38.349	
Gas composition $y_{i,PG}$ [vol.-%]			
N_2		3.2	
CO_2		16.5	
CO		10.0	
H_2		8.4	
CH_4		4.2	
Ar		0.3	
H_2O		55.0	
Tars		2.5	
ρ_N	[kg/m^3_N]	0.988	
Y_{Gas}	[m$^3_{N,DIF}$/kg$_{Fuel,DAF}$]	0.753	
LHV_{Gas}	[kJ/m^3_N]	3662	

Table B.10: Data for run 990706B.

Fuel: AH		**Gasification agent: steam/oxygen**
Run		**990706B**
$C_{Tar\ class}$	[mg/m^3_N]	
Benzene		2842
1 ring		4186
Naphthalene		546
2 ring		1078
3 ring		542
4+ ring		262
Phenol		2884
Cresols		2603
O-heteroar.		234
$C_{Tars,Total}$	[mg/m^3_N]	15178
Y_{Tar}	[$g/kg_{Fuel,DAF}$]	29.98
LHV_{Tars}	[MJ/kg]	36.947
M_{Tars}	[kg/kmol]	13.882
Tar elemental composition [mass-%]		
C		86.5
H		7.5
O		6.0
η_{CG}	[%]	34.2
η_{Tars}	[%]	5.3
Balances	[%]	
C		78.1
H		92.8
O		107.4
N		138.0

Table B.11: Data for experiment 991005.

Fuel: AH		**Gasification agent: steam/oxygen**		
Run		**991005A**	**991005B**	**991005C**
Input				
Fuel	[kg/h]	14.254	15.899	15.473
$w_{H2O,Fuel}$	[mass-%$_{Raw}$]	7.2	7.2	7.2
$w_{Ash,Fuel}$	[mass-%$_{Raw}$]	5.19	4.79	5.18
LHV_{Fuel}	[kJ/kg$_{Raw}$]	18.204	18.214	18.213
Air	[kg/h]	1.243	1.240	1.241
Oxygen	[kg/h]	3.476	5.364	7.244
Steam	[kg/h]	5.810	5.808	5.812
Argon	[kg/h]	0.304	0.304	0.304
ER	[-]	0.20	0.27	0.37
S/F	[kg/kg$_{Fuel,DAF}$]	0.55	0.50	0.51
T_{Bed}	[°C]	674	823	955
T_{FB}	[°C]	700	800	900
Output				
Solids	[kg/h]	1.249	1.043	1.288
$w_{C,Solids}$	[mass-%$_{Raw}$]	58.1	36.6	37.8
$w_{H2O,Solids}$	[mass-%$_{Raw}$]	0.1	1.3	3.0
Argon loss	[kg/h]	0.241	0.222	0.214
Gas + Tars	[kg/h]	23.595	27.351	28.572
Gas composition $y_{i,PG}$ [vol.-%]				
N_2		4.5	4.1	4.0
CO_2		15.4	18.6	19.7
CO		10.6	11.1	10.8
H_2		9.3	15.8	16.3
CH_4		4.8	4.5	3.8
Ar		0.2	0.2	0.2
H_2O		51.8	41.7	41.5
Tars		3.4	4.1	3.6
ρ_N	[kg/m^3_N]	0.974	0.963	0.972
Y_{Gas}	[m$^3_{N,DIF}$/kg$_{Fuel,DAF}$]	0.739	0.941	1.037
LHV_{Gas}	[kJ/m^3_N]	4066	4718	4485

Table B.11: Data for experiment 991005.

Fuel: AH		**Gasification agent: steam/oxygen**		
Run		**991005A**	**991005B**	**991005C**
$C_{Tar\ class}$	[mg/m^3_N]			
Benzene		4617	10167	13031
1 ring		5561	4037	331
Naphthalene		929	3105	3503
2 ring		1528	2042	356
3 ring		868	2365	2212
4+ ring		380	814	1447
Phenol		3061	763	7
Cresols		3299	52	0
O-heteroar.		309	409	84
$C_{Tars,Total}$	[mg/m^3_N]	20553	23754	20972
Y_{Tar}	[$g/kg_{Fuel,DAF}$]	39.87	48.20	45.46
LHV_{Tars}	[MJ/kg]	37.374	39.314	39.552
M_{Tars}	[kg/kmol]	13.747	13.068	12.951
Tar elemental composition [mass-%]				
C		87.4	91.9	92.7
H		7.5	7.2	7.0
O		5.1	0.9	0.2
η_{CG}	[%]	37.2	45.1	45.8
η_{Tars}	[%]	7.2	9.2	8.7
Balances	[%]			
C		79.8	85.6	91.5
H		99.9	103.3	106.8
O		108.2	104.1	100.2
N		130.1	137.1	140.4

Table B.12: Data for experiment 991123.

Fuel: AH + 10% PE		**Gasification agent:**		
Run		**991123A**	**991123B**	**991123C**
Input				
Fuel	[kg/h]	19.214	12.836	9.739
$w_{H2O,Fuel}$	[mass-%$_{Raw}$]	6.3	6.7	6.5
$w_{Ash,Fuel}$	[mass-%$_{Raw}$]	5.71	4.58	4.98
LHV_{Fuel}	[kJ/kg$_{Raw}$]	20.398	20.398	20.398
Air	[kg/h]	1.261	1.259	1.258
Oxygen	[kg/h]	5.368	5.368	5.369
Steam	[kg/h]	5.816	5.807	5.811
Argon	[kg/h]	0.304	0.304	0.304
ER	[-]	0.20	0.29	0.39
S/F	[kg/kg$_{Fuel,DAF}$]	0.42	0.58	0.75
T_{Bed}	[°C]	796	943	1038
T_{FB}	[°C]	700	800	900
Output				
Solids	[kg/h]	0.908	0.545	0.273
$w_{C,Solids}$	[mass-%$_{Raw}$]	36.5	29.5	30.9
$w_{H2O,Solids}$	[mass-%$_{Raw}$]	0.6	1.7	1.5
Argon loss	[kg/h]	0.068	0.099	0.137
Gas + Tars	[kg/h]	30.987	24.930	22.072
Gas composition $y_{i,PG}$ [vol.-%]				
N_2		5.4	4.6	3.7
CO_2		13.7	18.1	18.6
CO		13.7	11.8	8.8
H_2		8.9	11.6	16.0
CH_4		5.7	5.1	3.5
Ar		0.4	0.5	0.4
H_2O		46.9	43.0	45.8
Tars		5.2	5.3	3.2
ρ_N	[kg/m^3_N]	0.973	0.992	0.955
Y_{Gas}	[m$^3_{N,DIF}$/kg$_{Fuel,DAF}$]	0.659	0.899	1.014
LHV_{Gas}	[kJ/m^3_N]	4714	4574	4081

Table B.12: Data for experiment 991123.

Fuel: AH + 10% PE		**Gasification agent:**		
Run		**991123A**	**991123B**	**991123C**
$C_{Tar\ class}$	[mg/m^3_N]			
Benzene		11931	16889	11837
1 ring		6924	1516	212
Naphthalene		2666	5074	2628
2 ring		2766	1180	246
3 ring		1924	3349	1846
4+ ring		743	2170	1726
Phenol		2314	13	9
Cresols		948	2	0
O-heteroar.		489	160	15
$C_{Tars,Total}$	[mg/m^3_N]	30706	30353	18520
Y_{Tar}	[$g/kg_{Fuel,DAF}$]	57.84	66.92	49.67
LHV_{Tars}	[MJ/kg]	38.877	39.528	39.556
M_{Tars}	[kg/kmol]	13.254	12.948	12.948
Tar elemental composition [mass-%]				
C		90.6	92.8	92.8
H		7.4	7.0	7.0
O		2.0	0.2	0.2
η_{CG}	[%]	37.1	42.5	46.6
η_{Tars}	[%]	9.7	11.5	8.5
Balances	[%]			
C		73.6	88.7	90.5
H		98.6	96.1	108.0
O		110.7	103.6	104.2
N		199.9	140.0	104.2

Table B.13: Data for experiment 000215.

Fuel: AH + 20% PE		**Gasification agent: steam/oxygen**		
Run		**000125A**	**000125B**	**000125C**
Input				
Fuel	[kg/h]	23.178	14.412	9.938
$w_{H2O,Fuel}$	[mass-%$_{Raw}$]	5.5	6.1	5.7
$w_{Ash,Fuel}$	[mass-%$_{Raw}$]	5.69	6.20	4.86
LHV_{Fuel}	[kJ/kg$_{Raw}$]	22.578	22.578	22.578
Air	[kg/h]	1.269	1.267	1.263
Oxygen	[kg/h]	5.390	5.398	5.395
Steam	[kg/h]	5.810	5.801	5.803
Argon	[kg/h]	1.521	1.521	1.521
ER	[-]	0.15	0.24	0.34
S/F	[kg/kg$_{Fuel,DAF}$]	0.34	0.53	0.72
T_{Bed}	[°C]	670	788	901
T_{FB}	[°C]	700	800	900
Output				
Solids	[kg/h]	1.247	0.553	0.383
$w_{C,Solids}$	[mass-%$_{Raw}$]	54.1	35.5	26.5
$w_{H2O,Solids}$	[mass-%$_{Raw}$]	0.6	1.4	0.8
Argon loss	[kg/h]	0.625	1.046	1.062
Gas + Tars	[kg/h]	35.296	26.800	22.476
Gas composition $y_{i,PG}$ [vol.-%]				
N_2		7.1	6.1	5.2
CO_2		12.4	14.4	16.7
CO		19.3	17.4	14.0
H_2		5.3	6.0	6.9
CH_4		6.6	5.7	4.5
Ar		1.5	1.1	1.2
H_2O		42.8	42.5	46.0
Tars		5.1	6.9	5.5
ρ_N	[kg/m^3_N]	1.026	1.023	1.029
Y_{Gas}	[m$^3_{N,DIF}$/kg$_{Fuel,DAF}$]	0.681	0.828	0.981
LHV_{Gas}	[kJ/m^3_N]	5383	4875	4135

Table B.13: Data for experiment 000215.

Fuel: AH + 20% PE		**Gasification agent: steam/oxygen**		
Run		**000125A**	**000125B**	**000125C**
$C_{Tar\ class}$	[mg/m^3_N]			
Benzene		10417	20393	18392
1 ring		10085	6962	1252
Naphthalene		1157	4420	4990
2 ring		2009	2782	928
3 ring		819	2881	3513
4+ ring		332	1163	2455
Phenol		2537	864	13
Cresols		2748	84	1
O-heteroar.		276	369	85
$C_{Tars,Total}$	[mg/m^3_N]	30380	39920	31630
Y_{Tar}	[$g/kg_{Fuel,DAF}$]	50.82	82.77	77.75
LHV_{Tars}	[MJ/kg]	38.629	39.558	39.542
M_{Tars}	[kg/kmol]	13.442	13.045	12.945
Tar elemental composition [mass-%]				
C		89.4	92.1	92.8
H		7.7	7.4	7.0
O		2.9	0.6	0.2
η_{CG}	[%]	34.4	37.7	39.0
η_{Tars}	[%]	7.7	12.7	12.2
Balances	[%]			
C		72.0	86.7	93.5
H		80.5	83.9	88.2
O		114.3	105.4	102.2
N		277.2	192.2	139.4

Table B.14: Data for experiment 991126.

Fuel: AH + 10% PS		**Gasification agent: steam/oxygen**		
Run		**991126A**	**991126B**	**991126C**
Input				
Fuel	[kg/h]	19.760	13.777	9.310
$w_{H2O,Fuel}$	[mass-%$_{Raw}$]	6.1	6.1	4.4
$w_{Ash,Fuel}$	[mass-%$_{Raw}$]	9.14	6.33	7.69
LHV_{Fuel}	[kJ/kg$_{Raw}$]	20.034	20.034	20.034
Air	[kg/h]	1.264	1.260	1.259
Oxygen	[kg/h]	5.367	5.368	5.282
Steam	[kg/h]	5.803	5.812	5.820
Argon	[kg/h]	0.761	0.761	0.761
ER	[-]	0.20	0.28	0.42
S/F	[kg/kg$_{Fuel,DAF}$]	0.42	0.55	0.76
T_{Bed}	[°C]	802	930	1024
T_{FB}	[°C]	700	800	900
Output				
Solids	[kg/h]	1.227	0.814	0.375
$w_{C,Solids}$	[mass-%$_{Raw}$]	33.2	24.1	22.4
$w_{H2O,Solids}$	[mass-%$_{Raw}$]	0.3	0.0	1.0
Argon loss	[kg/h]	0.293	0.411	0.400
Gas + Tars	[kg/h]	31.434	25.753	21.658
Gas composition $y_{i,PG}$ [vol.-%]				
N_2		4.2	4.3	4.2
CO_2		13.3	18.4	20.9
CO		12.6	10.2	8.1
H_2		10.8	11.4	13.4
CH_4		4.6	4.0	2.8
Ar		0.8	0.8	1.0
H_2O		41.7	41.7	45.5
Tars		12.1	9.2	4.1
ρ_N	[kg/m^3_N]	0.933	0.984	1.003
Y_{Gas}	[m$^3_{N,DIF}$/kg$_{Fuel,DAF}$]	0.612	0.810	1.055
LHV_{Gas}	[kJ/m^3_N]	4400	3954	3466

Table B.14: Data for experiment 991126.

Fuel: AH + 10% PS		**Gasification agent: steam/oxygen**		
Run		**991126A**	**991126B**	**991126C**
$C_{Tar\ class}$	[mg/m^3_N]			
Benzene		21905	33407	16888
1 ring		29159	2501	214
Naphthalene		5361	6663	2638
2 ring		4963	2154	329
3 ring		4501	5490	1934
4+ ring		1158	2740	1627
Phenol		2394	13	10
Cresols		668	1	0
O-heteroar.		503	190	18
$C_{Tars,Total}$	[mg/m^3_N]	70613	53159	23657
Y_{Tar}	[$g/kg_{Fuel,DAF}$]	142.04	115.33	62.44
LHV_{Tars}	[MJ/kg]	39.583	39.643	39.679
M_{Tars}	[kg/kmol]	13.098	12.960	12.966
Tar elemental composition [mass-%]				
C		91.7	92.7	92.6
H		7.5	7.2	7.2
O		0.8	0.2	0.2
η_{CG}	[%]	34.6	35.5	39.2
η_{Tars}	[%]	23.8	20.0	10.9
Balances	[%]			
C		86.5	90.0	92.7
H		107.8	99.5	103.8
O		107.9	103.7	104.2
N		163.8	133.6	111.9

Table B.15: Data for experiment 991207.

Fuel: AH + 20% PE		**Gasification agent: steam/oxygen**		
Run		**991207A**	**991207B**	**991207C**
Input				
Fuel	[kg/h]	22.971	14.438	10.108
$w_{H2O,Fuel}$	[mass-%$_{Raw}$]	5.8	5.9	5.5
$w_{Ash,Fuel}$	[mass-%$_{Raw}$]	7.16	3.83	3.20
LHV_{Fuel}	[kJ/kg$_{Raw}$]	21.850	21.850	21.850
Air	[kg/h]	1.263	1.260	1.249
Oxygen	[kg/h]	5.378	5.377	5.385
Steam	[kg/h]	5.811	5.801	5.810
Argon	[kg/h]	0.304	0.304	0.304
ER	[-]	0.16	0.24	0.34
S/F	[kg/kg$_{Fuel,DAF}$]	0.36	0.51	0.69
T_{Bed}	[°C]	699	841	970
T_{FB}	[°C]	700	800	900
Output				
Solids	[kg/h]	1.567	0.717	0.235
$w_{C,Solids}$	[mass-%$_{Raw}$]	40.7	27.5	28.0
$w_{H2O,Solids}$	[mass-%$_{Raw}$]	0.4	0.5	1.6
Argon loss	[kg/h]	0.211	0.274	0.285
Gas + Tars	[kg/h]	33.950	26.189	22.337
Gas composition $y_{i,PG}$ [vol.-%]				
N_2		3.7	4.1	4.6
CO_2		11.7	15.9	18.1
CO		12.9	11.9	8.4
H_2		5.0	8.4	11.8
CH_4		3.6	3.3	1.9
Ar		0.2	0.1	0.1
H_2O		44.1	41.7	49.1
Tars		18.8	14.7	5.9
ρ_N	[kg/m^3_N]	0.935	0.964	0.973
Y_{Gas}	[m$^3_{N,DIF}$/kg$_{Fuel,DAF}$]	0.460	0.689	0.866
LHV_{Gas}	[kJ/m^3_N]	3464	3575	3030

Table B.15: Data for experiment 991207.

Fuel: AH + 20% PE		**Gasification agent: steam/oxygen**		
Run		**991207A**	**991207B**	**991207C**
$C_{Tar\ class}$	[mg/m^3_N]			
Benzene		16831	47841	22415
1 ring		73868	11428	3694
Naphthalene		4841	8942	3013
2 ring		5469	4874	588
3 ring		3932	8774	2556
4+ ring		809	3059	1872
Phenol		2187	100	17
Cresols		1785	6	1
O-heteroar.		300	261	39
$C_{Tars,Total}$	[mg/m^3_N]	110022	85284	34195
Y_{Tar}	[$g/kg_{Fuel,DAF}$]	199.76	177.84	85.05
LHV_{Tars}	[MJ/kg]	39.926	39.719	39.785
M_{Tars}	[kg/kmol]	13.107	12.969	12.989
Tar elemental composition [mass-%]				
C		91.6	92.6	92.5
H		7.7	7.3	7.4
O		0.6	0.1	0.2
η_{CG}	[%]	22.1	28.1	30.4
η_{Tars}	[%]	31.8	29.2	14.1
Balances	[%]			
C		81.8	87.9	77.6
H		99.7	95.3	104.3
O		112.5	104.6	107.1
N		155.1	132.7	132.0

Curriculum Vitae

Name:	Luiz Carlos Reichenbach de Sousa
Date of Birth:	27 October 1966
Place of Birth:	São Paulo, Brazil
Citizenship:	Portuguese and Brazilian

Education:

1972 - 1977	Elementary and primary school at the Schweizerschule São Paulo, Brazil.
1978 - 1980	Primary school at the CES Charles Péguy, Le Chesnay and at the Lycée International, St. Germain-en-Laye, France.
1980 - 1984	Secondary school at Schweizerschule São Paulo, Brazil. Studies of French language and literature at the Alliance Française in São Paulo, Brazil with Nancy III diploma.
December 1984	Conclusion of secondary school at the Schweizerschule São Paulo, with Brazilian scientific certificate.
1985 - 1986	Preparatory course for the admission exam (Aufnahmeprüfung) to the Swiss Federal Institute of Technology Zürich (ETH Zürich) in Fribourg, Switzerland.
1986 - 1989	Chemical Engineering studies at the ETH Zürich.
November 1989	Graduation as Dipl. Chem.-Ing. ETH.
1997-2000	Ph.D. thesis at the Paul Scherrer Institute, Switzerland.

Professional experience:

1990-1991	Scientific collaborator to Prof. Dr. L. Reh at the Institute for Cryogenic and Process Engineering, ETH Zürich, Switzerland.
1991 - 1993	Research Engineer for the Combustion Research Department of the Paul Scherrer Institute, Switzerland.
1993 - 1997	Research Engineer for the Element Cycles Department of the Paul Scherrer Institute, Switzerland.
Since October 2000	Project Engineer for Holcim Group Support Ltd, Switzerland.